Dissertation zur Erlangung des Doktorgrades
Der Fakultät für Chemie und Pharmazie
Der Ludwig-Maximilians-Universität München

Reactivity and Basicity: Insight into Organocatalysis by Secondary Amines

Feng An

aus

Rizhao, Shandong, China

2019

Erklärung

Diese Dissertation wurde im Sinne von § 7 der Promotionsordnung von 01. Oktorber. 2013 von Herrn Prof. Dr. Herbert Mayr betreut.

Eidesstattliche Versicherung

Diese Dissertation wurde eigenständig und ohne unerlaubte Hilfe erarbeitet.

München, 14. 02. 2019

Feng An

Feng An

Dissertation eingereicht am 21.02.2019

1. Gutachter: Prof. Dr. Herbert Mayr
2. Gutachter: Prof. Dr. Hendrik Zipse

Mündliche Prüfung am 22.03.2019

...dedicated to my family

Acknowledgements

First of all, I would like to express my deep and sincere gratitude to my supervisor, Professor Dr. Herbert Mayr for offering me the opportunity to experimentally study the mechanism of organic chemistry in his research group, which is always my dream direction when I started to learn chemistry, and especially for allowing me a large degree of creative freedom to explore chemisty with his endless support, trust, and patience.

I would like to thank Professor Dr. Hendrik Zipse for reviewing my thesis.

I am grateful to PD. Dr. Armin R. Ofial for financially supporting me to finish this thesis in the last two years.

My special thanks to Dr. Sami Lakdar for helping me to start the study of mechamism in organocatalytic chemistry. I would like to thank Dr. Biplab Maji for the early exploration in the topic of organocatalyst before leaving Munich. I would also like to thank Dr. Xingwei Guo, Prof. Dr. Sinjiro Kobayashi, Dr. Guillaume Berionni for nice discussions in the time of working together. Many thanks to Frau Hampel Nathalie, Frau Hildegard Lipfert, Frau Brigitte Janker for all kind of helps.

I am grateful to Dr. Alison Levens, Hannes Erdmann, Shyeni Paul for completing the cooperation publications with you.

I would like to thank all past and present colleagues within the group of Professor Dr. Mayr and PD. Dr. Armin R. Ofial. It has been a pleasure to work together with you all.

I am fully indebted to my parents and my wife for their unconditional supports over years, which mentally support me to finish my thesis finally.

Table of contents

Acknowledgements i

Table of contents ii

Chapter 0: Summary 1

0.1 General 1

0.2 Brønsted Basicities and nucleophilic reactivities of pyrrolidines and imidazolidinones 1

0.3 Appendix 1 7

0.4 Appendix 2 7

0.5 Appendix 3 8

0.6 Appendix 4 8

Chapter 1: Introduction and Objective 10

1.1 Secondary Amines as Organocatalysts 10

1.2 Goals of this Work 14

Chapter 2: Synthesis of the secondary Amines A1–A32 15

2.1 Synthesis of Pyrrolidines from L-Proline 15

2.2 Synthesis of Pyrrolidines from other Precursors 19

2.3 Synthesis of the Imidazolidinones A29–A32 20

2.4 ^{13}C Spectra of Secondary Amines 21

Chapter 3: Brønsted Basicities of Substituted Pyrrolidines and Imidazolidinones 23

3.1 General 23

3.2 Titration Method 24

3.3 Synthesis of the Indicators 25

3.4 Results 26

Chapter 4: Nucleophilic Reactivities of substituted Pyrrolidines and Imidazolidinones 29

4.1 General 29

4.2 Kinetic Method 31

4.3 Reaction Mechanism 32

4.4 Kinetics in the Presence of Sterically Shielded Pyridines 36

4.5 Kinetic Measurements of the Reactions of Imidazolidinones A29–A32 39

4.6 Correlation Analysis 41

Chapter 5: Discussion 48

Chapter 6: Conclusion 60

Chapter 7 Experiment 61

7.1 Synthesis and Analytics 61

7.1.1 General 61

7.1.2 Syntheses of Secondary Amines 62

7.1.3 Preparation of Indicators 79

7.1.4 Copies of NMR and IR spectra 81

7.2 Experimental Section for Kinetic Measurements 130

7.2.1 General 130

7.2.2 Kinetics in Acetonitrile 131

7.2.3 Kinetics in Dichloromethane 213

7.3 Experimental Section for pK_{aH} Measurements 215

References 295

Appendix 1 Published work 1 299

Appendix 2 Published work 2 322

Appendix 3 Published work 3 335

Appendix 4 Published work 4 349

Appendix 5 Correlation between the change of activation energy and free energy change 368

Chapter 0: Summary

0.1 General

The purpose of this thesis is to provide a physical basis for the design of organocatalytic reactions using secondary amines. For that reason the Brønsted basicities and nucleophilic reactivities of pyrrolidines and imidazolidinones substituted by groups with different steric and electronic effects, which are the main classes of secondary amine organocatalysts, have been investigated.

In addition, I have contributed to several related collaboration projects (Appendices 1–4), where my contributions are shown in the Experimental Sections.

0.2 Brønsted Basicities and nucleophilic reactivities of pyrrolidines and imidazolidinones

Equilibrium constants (K) for the proton transfer reactions from the CH acids (indicator acids with known pK_a values) to pyrrolidines and imidazolidinones were determined by spectrophotometric titration in acetonitrile at 20 °C (Scheme 0-1).

Scheme 0-1. Proton transfer reaction of secondary amines with CH acids

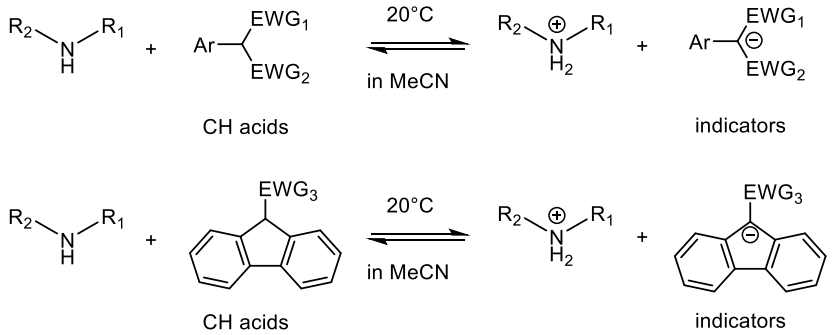

Ar = p-NO_2-C_6H_4, C_6F_5, p-Cl-C_6F_4; EWG = CN, COOEt, COOMe

The Brønsted basicities of most pyrrolidines vary within 4 orders of magnitude (pK_{aH} from 16 to 20). However, prolinate **A1** is a much stronger Brønsted base and the imidazolium and trifluoromethyl substituted pyrrolidines **A14** and **A21** are much weaker bases. The imdazolidinones **A29**–**A32** are weaker Brønsted bases than substituted pyrrolidines (Figure 0-1).

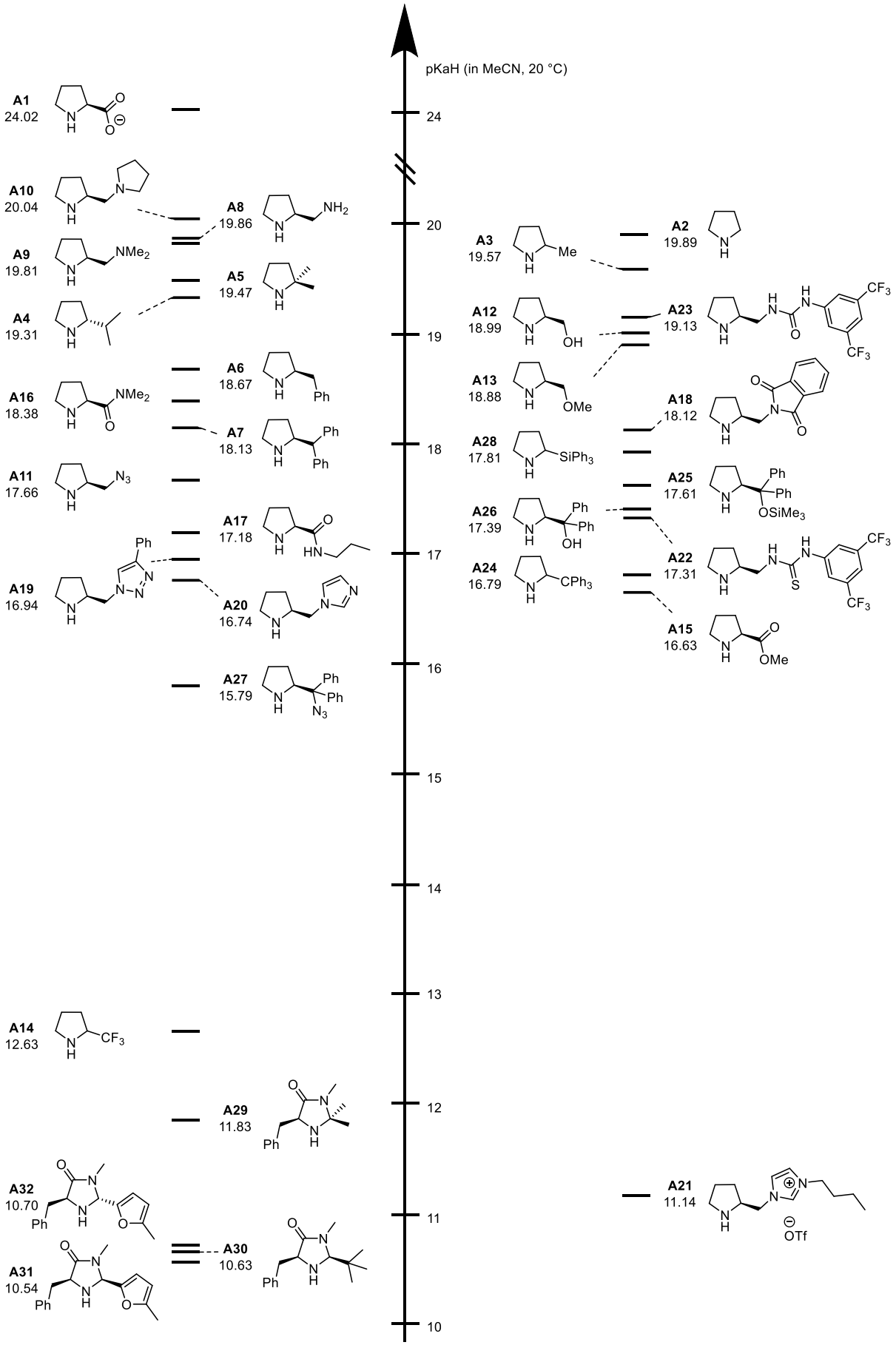

Figure 0-1. pK_{aH} values of pyrrolidines and imidazolidinones in acetonitrile (20 °C)

Benzhydrylium ions (Ar_2CH^+) and structurally related quinone methides were employed as reference electrophiles for comparing the nucleophilic reactivities of pyrrolidines and imidazolidinones by measuring the second-order rate constants for their reactions with these amines in acetonitrile.

Scheme 0-2. Reactions of secondary amines with benzhydrylium ions and quinone methides in acetonitrile at 20 °C

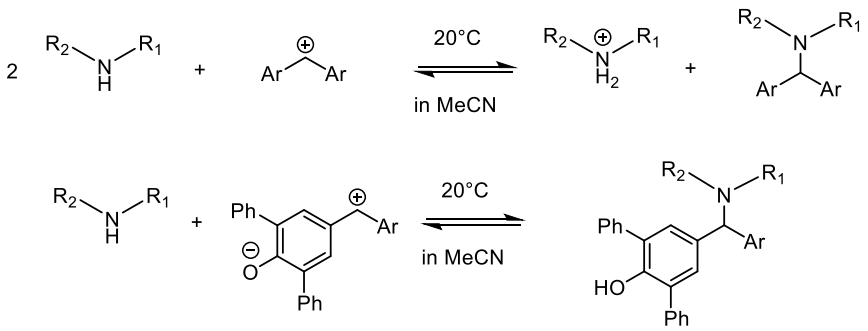

The linear-free-energy relationship $\lg k_2$ (20 °C) = $s_N(N + E)$, where s_N and N are nucleophile-specific parameters and E is an electrophile-specific parameter, was employed to define the nucleophilic reactivities of pyrrolidines and imidazolidinones, whereby the slopes of the linear correlations between $\lg k_2$ and E correspond to the nucleophile-specific parameter s_N and the intercepts on the abscissa ($\lg k_2 = 0$) represent the nucleophilicity parameters N of the secondary amines. Figure 0-2 shows the linear correlation between $\lg k_2$ and corresponding E parameters of the reference electrophiles.

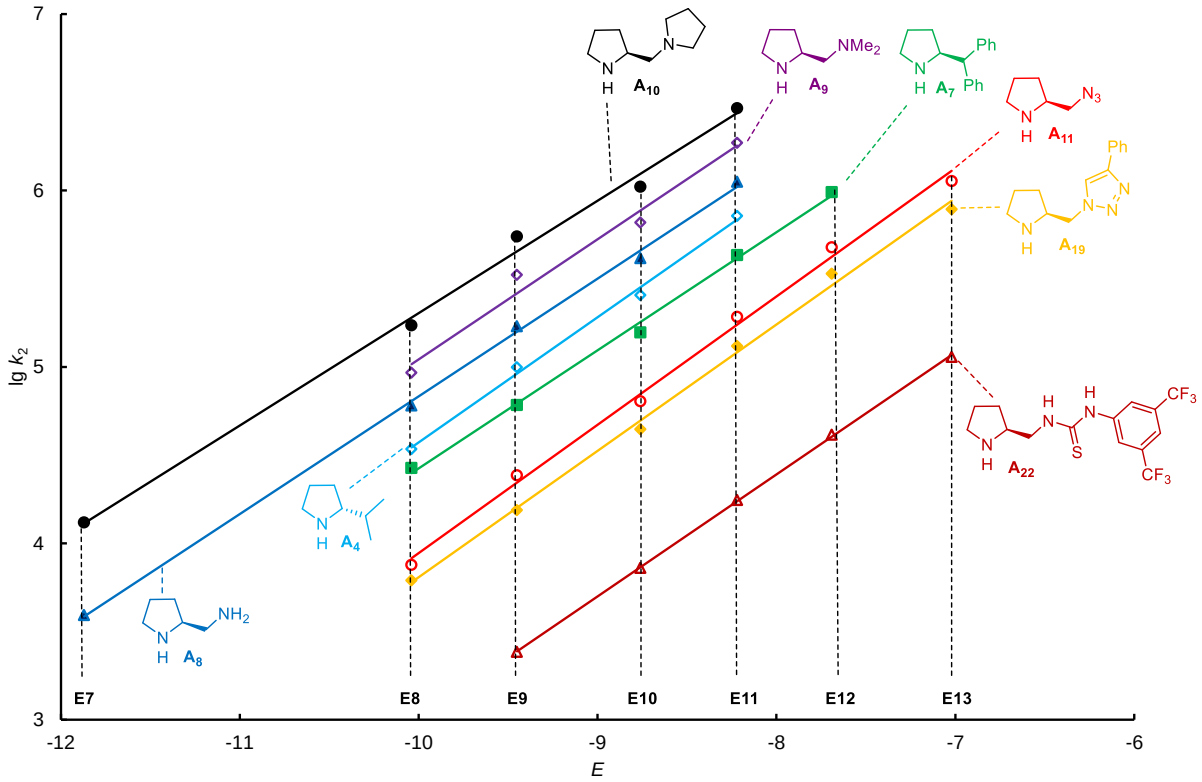

Figure 0-2. Plot of $\lg k_2$ versus the corresponding electrophilicities of the benzhydrylium ions and quinone methides for the reactions of pyrrolidines with reference electrophiles in acetonitrile at 20 °C

The almost parallel correlation lines in Figure 0-2 (numerically expressed by similar s_N values) illustrate that the relative nucleophilicities of these pyrrolidines are independent of the electrophilicity of the reaction partners. Figure 0-3 shows, however, that the slopes (≙ s_N) for the pyrrolidines with bulky substituents in 2-position are steeper, i.e., their reactivities are more affected by variation of the reaction partner than those of ordinary pyrrolidines. All imidazolidinones are less nucleophilic than the investigated pyrrolidines and have s_N values around 1, in between ordinary pyrrolidines ($0.53 < s_N < 0.82$) and pyrrolidines with bulky substituents ($0.98 < s_N < 1.39$).

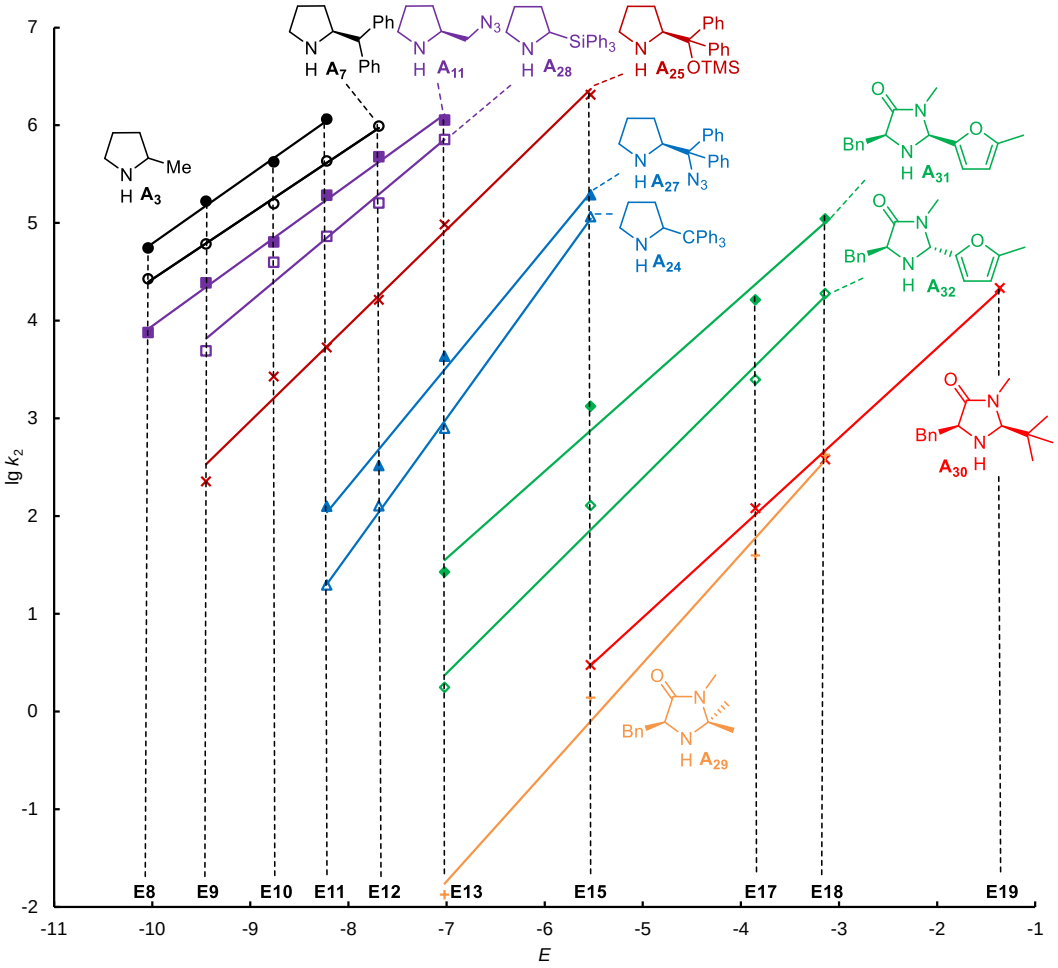

Figure 0-3. Plot of lgk_2 versus the corresponding electrophilicities of the benzhydrylium ions for the reactions of pyrrolidines with reference electrophiles in acetonitrile at 20 °C

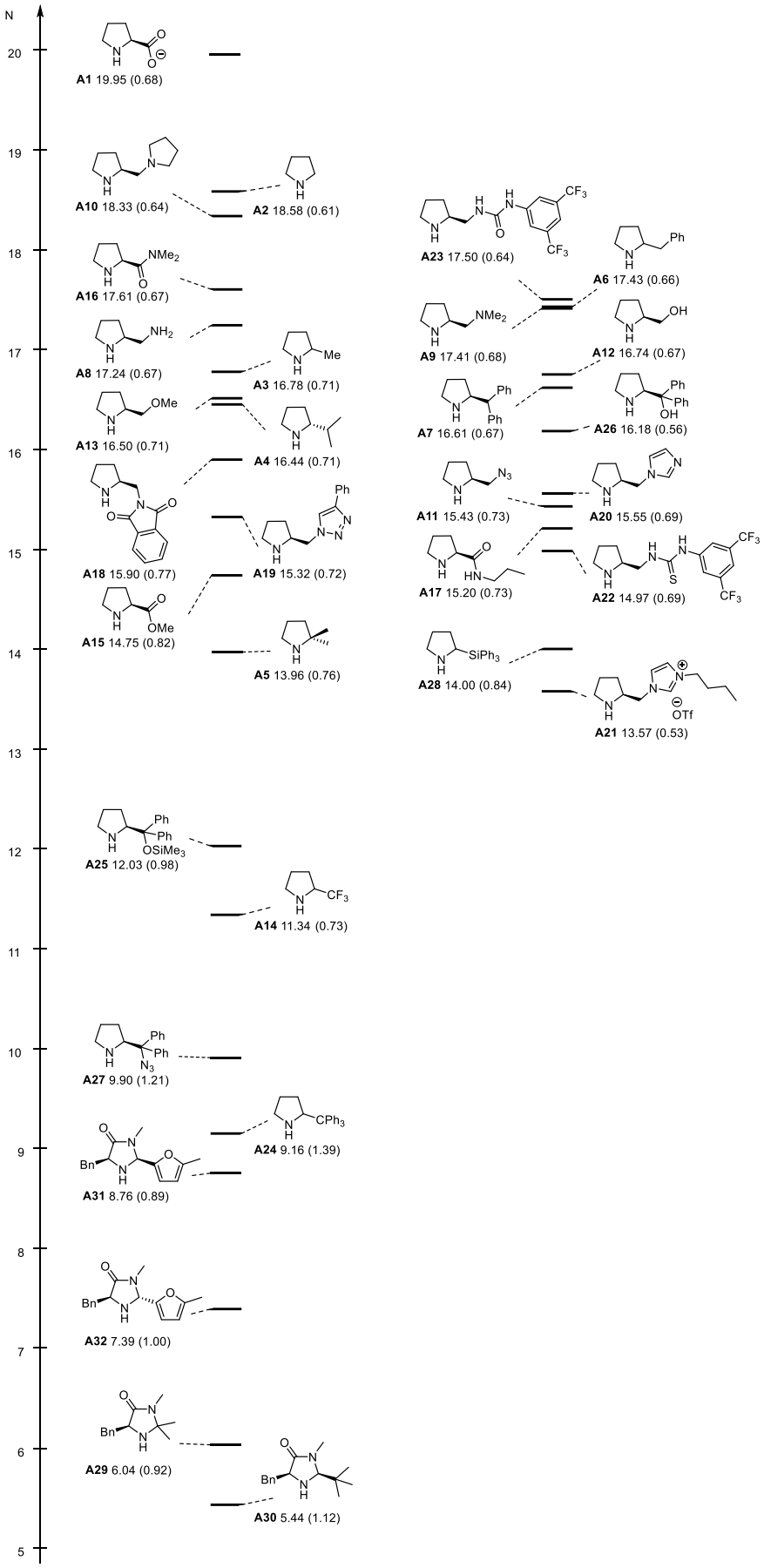

Figure 0-4. Reactivity parameters for 2-substituted pyrrolidines and imidazolidinones in acetonitrile

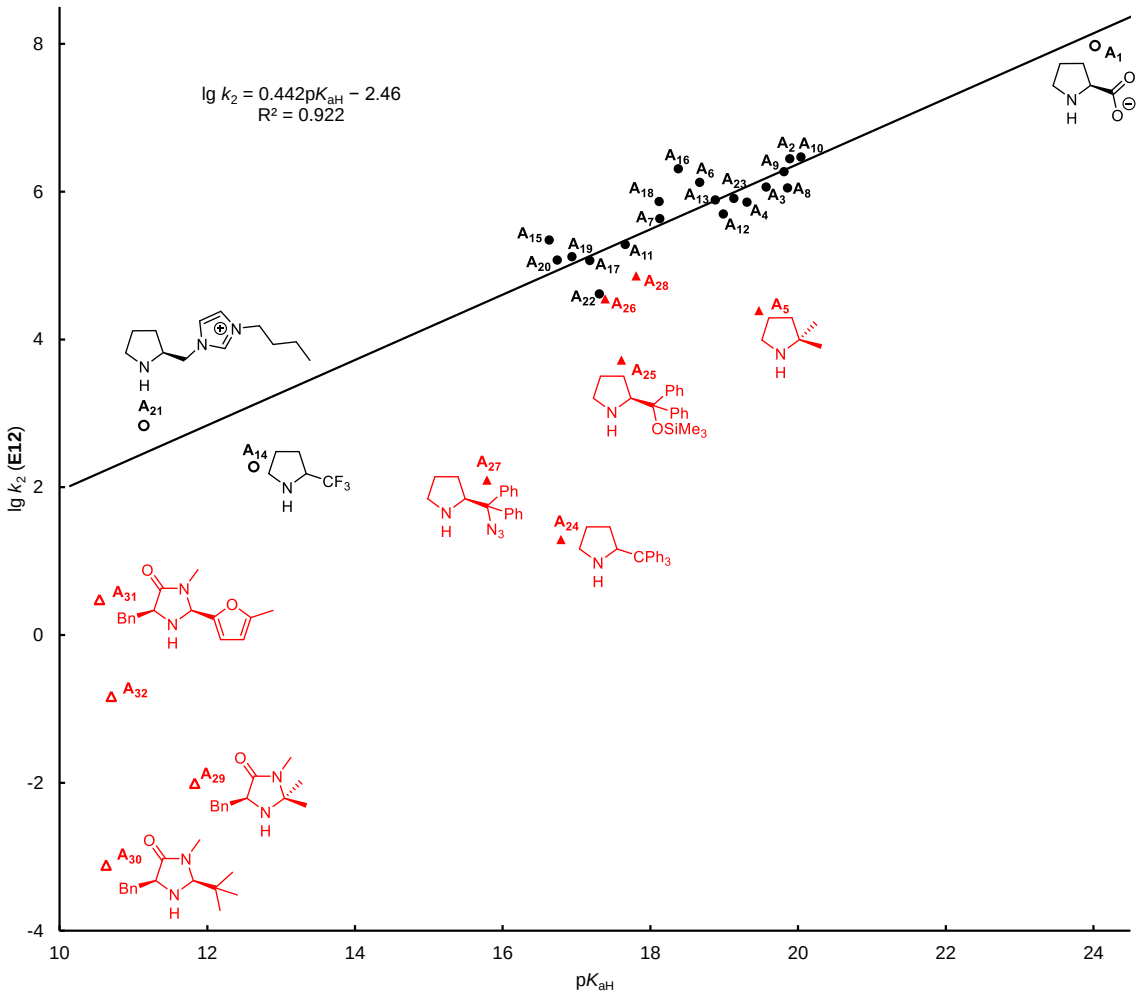

Figure 0-5. Plot of the rate constants for the reactions of secondary amines with benzhydrylium ion **E11** versus their Brønsted basicities; The correlation line is based on the reactivities of pyrrolidines identified by circles (i.e. excludes pyrrolidines with bulky substituents and imidazolidinones); open symbols refer to the rate constants which have not been directly measured but were calculated by the linear-free-energy relationship lgk_2(20 °C) = $s_N(N + E)$

The correlation line drawn in Figure 0-5 shows a fair correlation (R^2 = 0.92) between the rate constants of the reactions of the 2-substituted pyrrolidines represented by circles (pyrrolidines with bulky substituents represented by triangles are excluded) with benzhydrylium ion **E11** versus the Brønsted basicities pK_{aH}. From the Brønsted coefficent of this correlation one can see that 44% of the differences in basicity are reflected in the transition states of their reactions with **E11**. Figure 0-5 furthermore shows that the trityl-(**A24**) and azidodiphenylmethyl-substituted pyrrolidines (**A27**) react 2–3 orders of magnitude more slowly than ordinary pyrrolidines of comparable basicity. Obviously the steric retardation is much smaller for the Hayashi-Jørgensen catalyst **A25**, which is located only by a factor of 40 below the correlation line. The nucleophilicities of the diphenylprolinol **A26** and triphenylsilyl-substituted pyrrolidine **A28** are only marginally smaller than expected from their basicities. The imidazolidinones **A29**–**A32** (represented

by open triangles) react much more slowly than all pyrrolidines included in this investigation.

0.3 Appendix 1

We have synthesized a series of substituted Cinnamaldehyde-derived iminium ions and studied their structures in the solid and liquid phases. The kinetics of the reactions of iminium ions with the ketene acetals allowed us to determine their electrophilicities, which cover almost 5 orders of magnitude, reflecting the strong effect of the substituents at the aromatic ring of the cinnamaldehydes on the electrophilicity of the corresponding iminium ions, which is in line with the substituent effects on the structures of the iminium ions elucidated by the crystal structures.

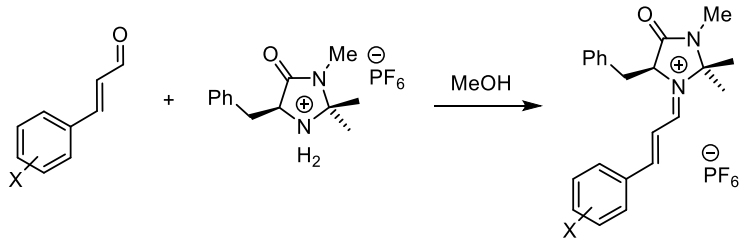

0.4 Appendix 2

Though the trityl group had previously been reported to be an electronically neutral substituent with a Hammett substituent constant of σ ≈ 0, the trityl group behaves as an electron-withdrawing substituent in 2-position of pyrrolidine, which we explain by negative hyperconjugation. This effect rationalizes why the trityl-substituted enamine is 26 times less nucleophilic than the parent analogue and the trityl substituted iminium ion is 8 to 12 times more electrophilic than the parent analogue.

Comparison of the reactivities of the 2-trityl-pyrrolidine-derived enamine and the 2-trityl-pyrrolidine-derived iminium ion with the corresponding Jørgensen-Hayashi pyrrolidine-derived analogues indicates that the CPh_3 group and the CPh_2OSiMe_3 group exert similar electronic effects on the enamine and iminium intermediates of organocatalytic reactions.

Reaction	X	H	CPh_3	$CPh_2(OSiMe_3)$
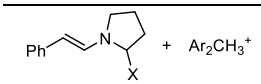	k_{rel}	1.0	1/26	1/28
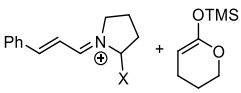	k_{rel}	1.0	12	19

0.5 Appendix 3

The ability to modulate the nucleophilicity and Lewis basicity of N-heterocyclic carbenes is pivotal to their application as organocatalysts. Herein we examine the impact of the N-substituent on nucleophilicity and Lewis basicity. Four N-substituents popular in NHC organocatalysis have been examined, *N*-2,6-$(CH_3O)_2C_6H_3$, *N*-2,4,6-$(CH_3)_3C_6H_2$, *N*-4-$(CH_3O)C_6H_4$, and *N*-*t*-butyl groups. From these studies it is clear that the nucleophilicity is strongly affected by the nature of this substituent, with the *N*-2,6-$(CH_3O)_2C_6H_3$ group giving one of the most nucleophilic imidazolylidene NHCs reported to date and the *t*-butyl one of the least. This difference in nucleophilicity is reflected in the catalyst efficiency observed with a recently reported trienyl ester rearrangement.

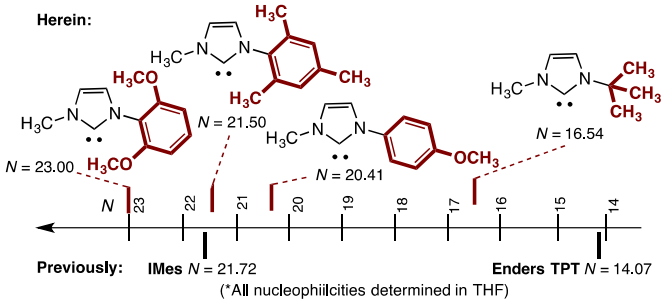

0.6 Appendix 4

2-Cinnamoylimidazolium ions **4** have been synthesized by treatment of 2-cinnamoylimidazoles with methyl triflate. They were characterised by NMR and mass spectroscopy, in one case also by X-ray analysis. The kinetics of their reactions [and also those of cinnamoyl fluoride (**1**)] with stabilized carbanions and silyl ketene acetals (reference nucleophiles) were measured photometrically. The correlation log *k* (20 °C) = $s_N(E + N)$ was used to calculate the electrophilicity parameters *E* of the cinnamoyl azolium ions **4** from the resulting second-order rate constants *k* and the previously reported *N* and s_N parameters of the reference nucleophiles. All 2-cinnamoylimidazolium ions **4** were found to be 2-4 orders of magnitude more electrophilic than cinnamoyl fluoride (**1**) showing that the direct attack of nucleophiles at **1** can be avoided if sufficient concentrations of **4** are produced in the NHC-catalysed reactions of **1** with nucleophiles. From the range of electrophilicity ($-12 < E < -10$) for the cinnamoylimidazolium ions **4** one can derive that only nucleophiles stronger than $N \approx 7$ will react with **4** at 20 °C in

reasonable time, suggesting that in NHC-catalysed reactions of cinnamoyl fluoride (**1**) with silyl enol ethers (typically 4 < *N* < 7), enolate ions, produced by fluoride-induced desilylation of silyl enol ethers, are the active nucleophiles.

Plausible catalytic cycle for the NHC-catalysed reaction of cinnamoyl fluoride with 1-(trimethylsiloxy)-cyclohexene:

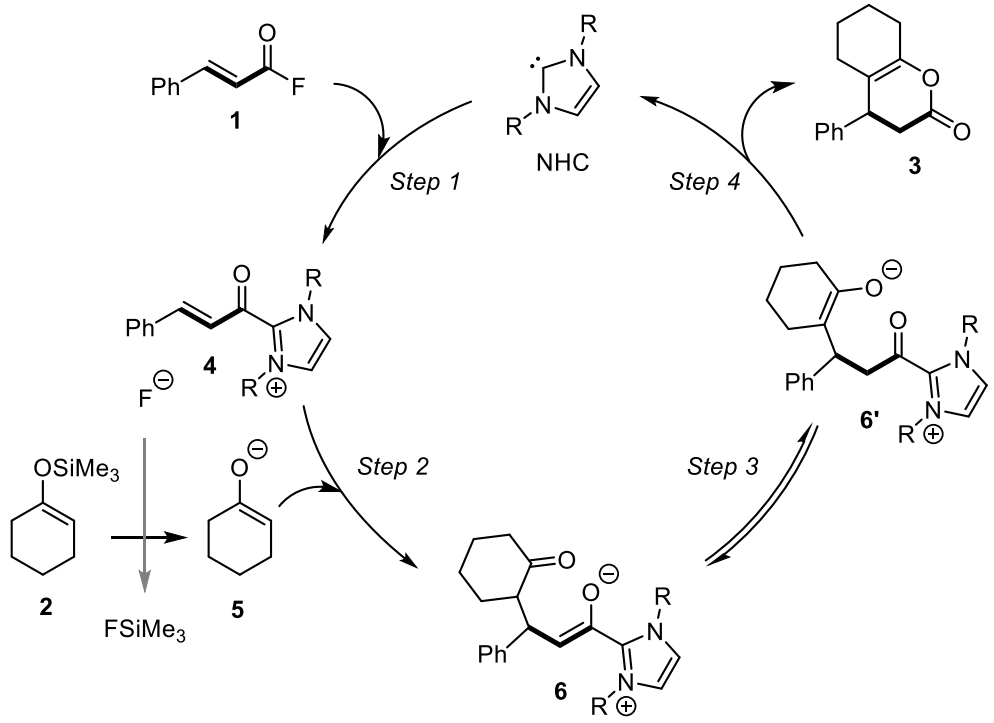

Chapter 1: Introduction and Objective

1.1 Secondary Amines as Organocatalysts

Organocatalysis refers to the acceleration of organic reactions by substoichiometric amounts of organic compounds (organocatalyst), such as amines, carbenes, ylides, and so on. Because of their wide applications for the functionalization of carbonyl compounds, chiral secondary amines are considered as one of the most useful class of organocatalysts. Secondary amine catalysis can be employed for: (a) α–functionalization of ketones or aldehydes through the formation of enamines (enamine activation) or radical cations (SOMO–activation); (b) β–functionalization of enals via the formation of α,β–unsaturated iminium ions or γ–functionalization of enals through the formation of dienamines; (c) ε,β–functionalization of 2,4–dienals via the formation of trienamines, which undergo Diels–Alder reactions with highly polarized electron-deficient olefinic species, such as 3–alkenyl oxindoles, azlactones, and so on.[1]

Enamines have been introduced as reagents in organic synthesis by Stork in the 1950s.[2] As shown in Scheme 1, they were used for α-alkylations of cyclic ketones and Michael additions to acceptor substituted olefins.

Scheme 1. Use of enamines as reagents and reactive intermediates by Stork

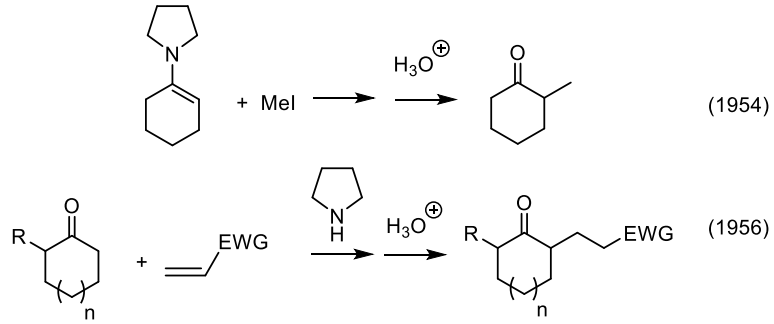

EWG = CN; COR; COOR R = H; Me; CH_2CH_2CN n = 1,2

The L-proline-catalyzed intramolecular aldol-condensation shown in Scheme 2 reported in 1971 known as Hajos–Parrish–Eder–Sauer–Wiechert reaction[3] represents the first asymmetric secondary amine catalyzed reaction.

Scheme 2. The first asymmetric synthesis using secondary amine as organocatalyst

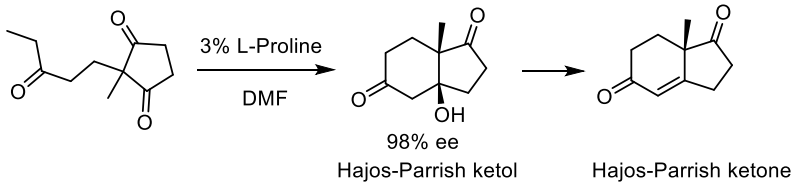

Yamaguchi reported that the lithium prolinate-catalyzed addition of dimethyl malonate to hex-2-enal in methanol led to a racemic adduct, [4a] whereas 59% ee was observed when rubidium prolinate was used as a catalyst in chloroform.[4b]

Scheme 3. The first iminium-activated conjugate addition in 1991 by Yamaguchi

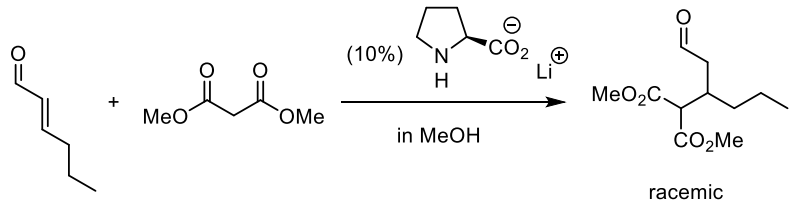

In the last two decades, numerous new types of secondary amines were synthesized and applied as organocatalysts. Among them, the most important classes are substituted pyrrolidines and imidazolidinones.

In the beginning of this century, MacMillan and coworkers reported applications of chiral imidazolidinones as catalysts for enantioselective cycloadditions and electrophilic aromatic substitutions.

Scheme 4. Imidazolidinones as organocatalysts in iminium-activated reactions by MacMillan

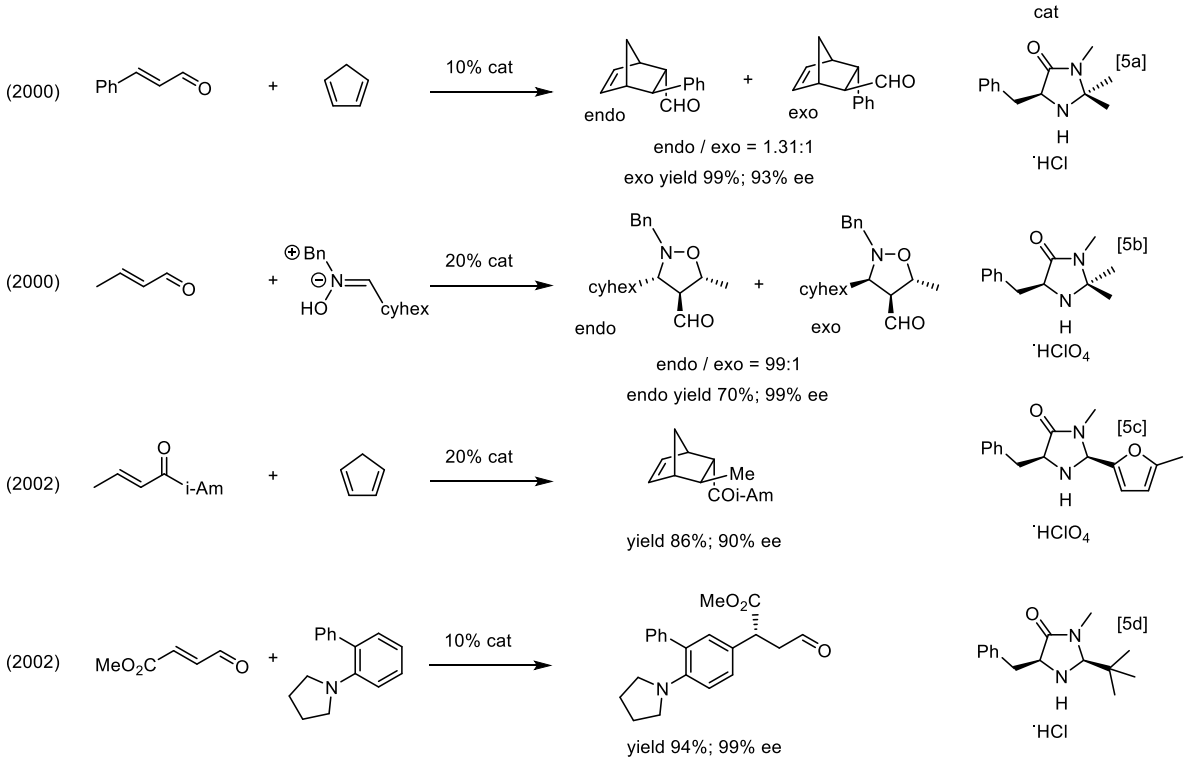

Till today, imidazolidinones have been applied as catalysts in more than two hundred publications (for enamine activated reactions see [6]; for crystal structure and conformation studies of the catalysts and enamine and iminium intermediates see [7]; for SOMO activated reactions see [8]; for reactivity studies of enamine intermediates and iminium ions see [9]; for proton catalysis of iminium formation see [10]).

In 2005, the groups of Jørgensen and Hayashi published the first diarysilylprolinol-catalyzed reactions, illustrated in Scheme 5.

Scheme 5. First application of diarysilylprolinols as organocatalysts

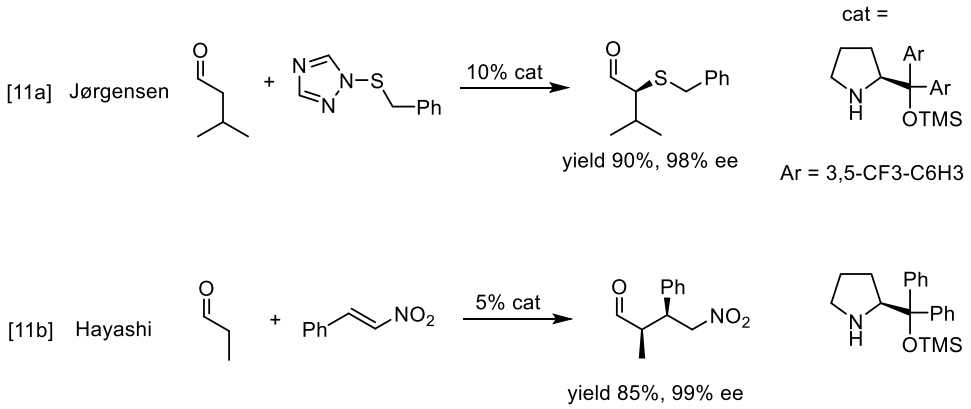

Since then diarysilylprolinols became the most successful catalysts in the pyrrolidine family, which so far were applied in more than four hundred publications (for further enamine mediated reactions see [12]; for iminium mediated reactions see [13]; for single crystal study see [14]; for dienamine activation see [15]; for trienamine activation see [16]; for α,β,γ,δ-conjugate iminium activation see [17]; for reactivity of enamines see [18]; for [2+2] cycloaddition see [19]; mechanistic studies of enamine mediated reactions see [20]; for pH-efficiency relationship study see [21]; for the comparison with imidazolidinones see [22]).

In view of the success of diarysilylprolinol catalysts, some structural analogs were synthesized and applied as organocatalysts. As examples, the use of trityl[23] and triphenylsilyl[24]-substituted pyrrolidines as catalysts is shown in Scheme 6.

Scheme 6. Trityl and triphenylsilyl substituted pyrrolidines as catalysts

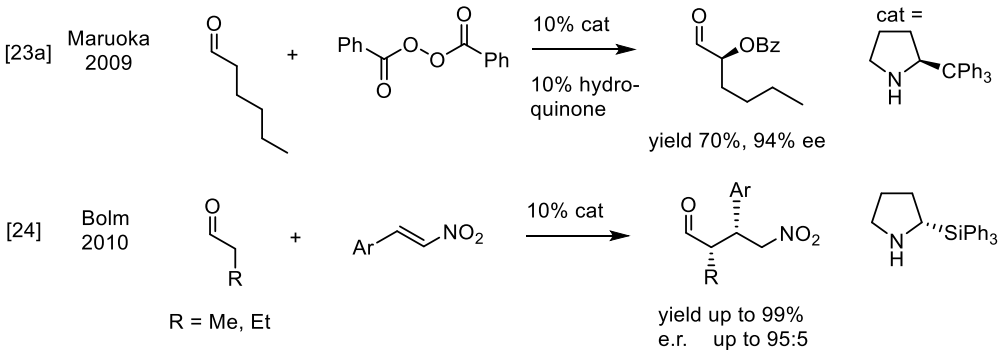

Applications of other substituted pyrrolidines as organocatalysts are shown in Scheme 7.

Scheme 7. Other 2-substituted pyrrolidines as organocatalysts

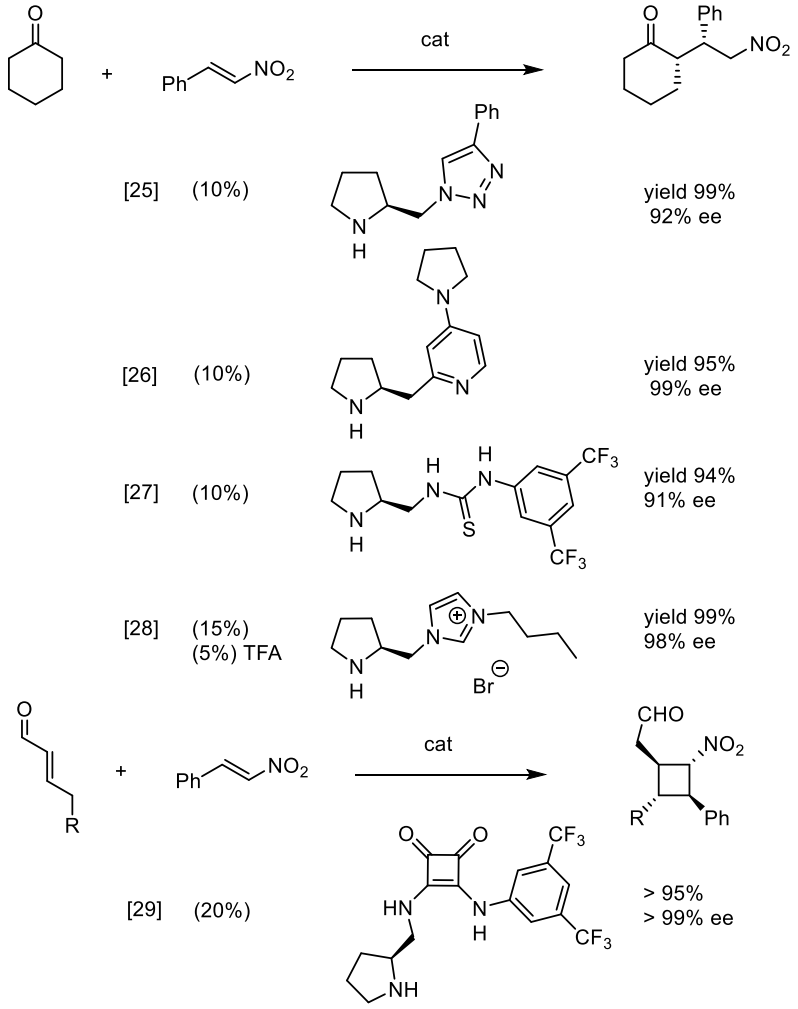

1.2 Goals of this Work

As shown in chapter 1.1, numerous secondary amines as organocatalysts have been applied for a variety of reactions. In order to obtain insights in the relationship between catalytic efficiency and structure of the amines, in this work, basicities and nucleophilicities of pyrrolidines and imidazolidinones substituted by groups with different steric and electronic effects were studied in acetonitrile. These amines are depicted in Figure 1.

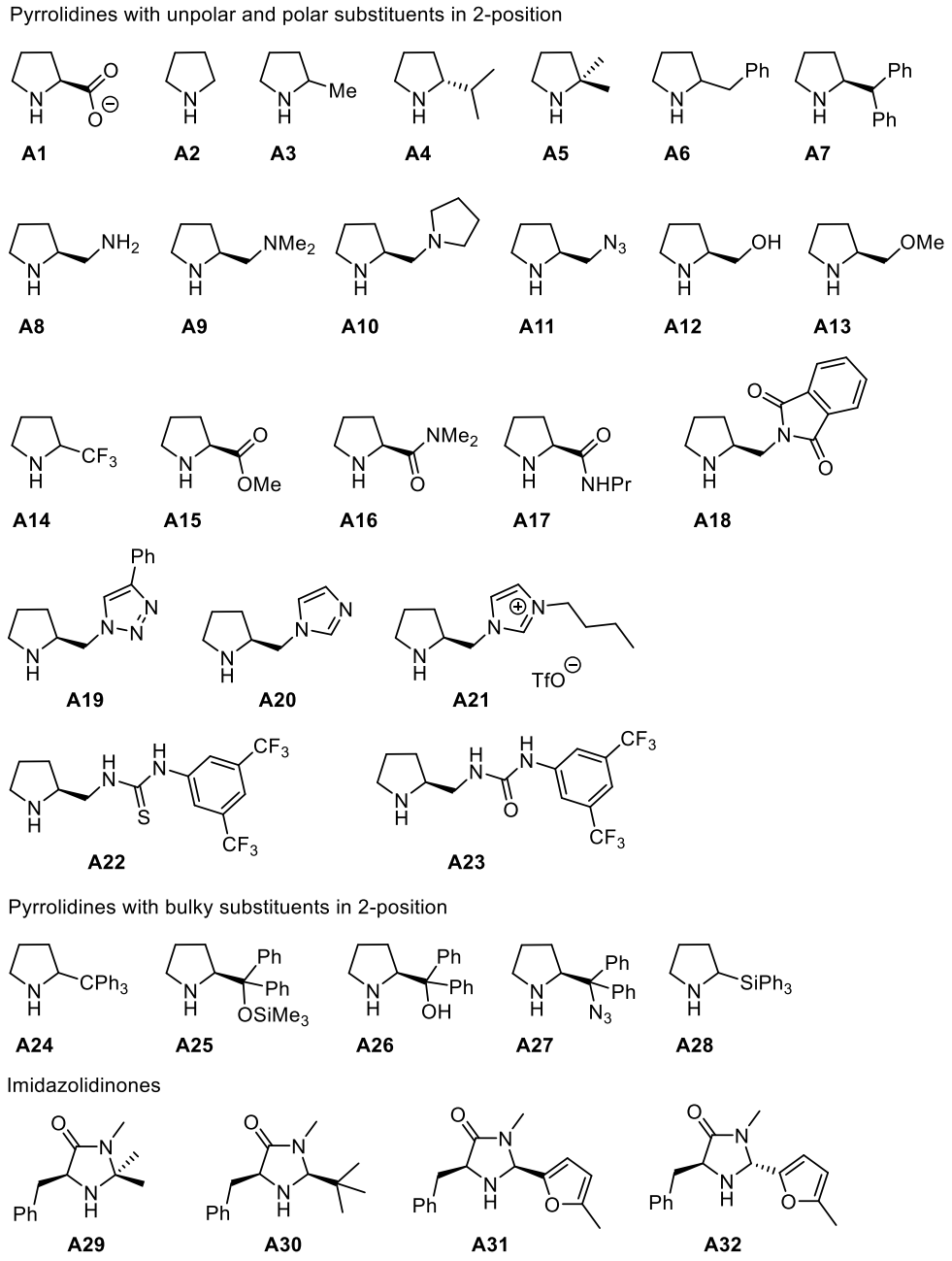

Figure 1. Amines investigated in this research

Chapter 2: Synthesis of the secondary Amines A1–A32

2.1 Synthesis of Pyrrolidines from L-Proline

Most pyrrolidines were synthesized from commercially available L-proline. Esterification with $SOCl_2$/MeOH according to literature procedures [30] gave methyl prolinate **A15**.

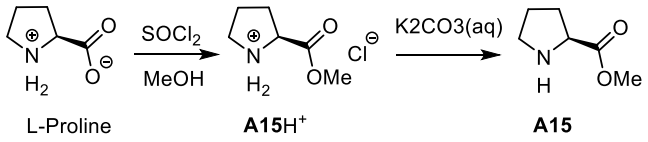

Reduction of proline with LAH gave prolinol **A12**[31], which was Boc protected and methylated with NaH/MeI to give prolinol methyl ether **A13**.[32]

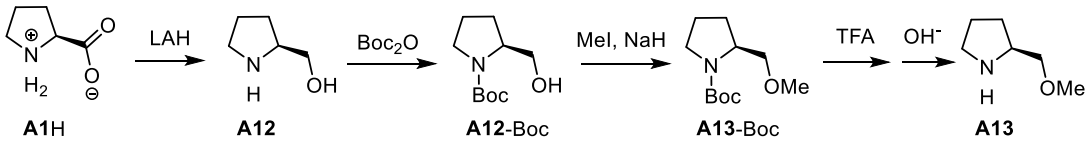

The condensation of *N*-Boc-protected **A12** with phthalimide according to Mitsunobu reaction afforded *N*-Boc **A18**, which was deprotected to give protonated **A18**.[33]

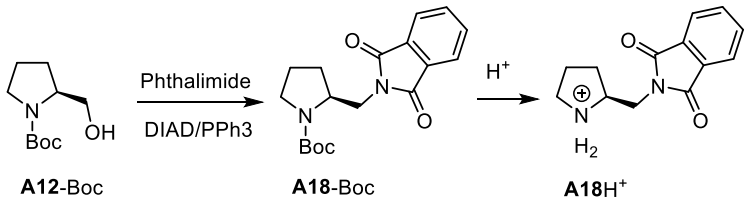

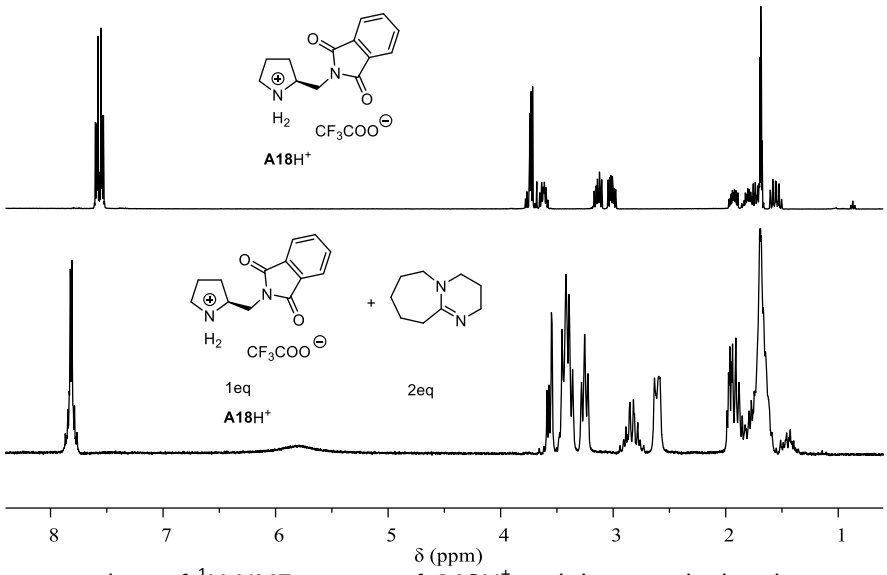

Figure 2. The comparison of ^{1}H NMR spectra of **A18**H$^+$ and the quantitative deprotonation of **A18**H$^+$ with DBU in CD_3CN

The clean quantitative deprotonation of **A18**H$^+$ in acetonitrile was achieved with DBU base (Figure 2). However, the resulting amine **A18** is only stable in highly diluted solution and side reactions turned up during attempts to remove the solvent.

Tosylation of *N*-Boc-protected **A12** gave 1-Boc-2-(*S*)-pyrrolidinylmethyl *p*-toluenesulfonate[34], which reacts with pyrrolidine to give **A10**-Boc[35], with azide anion to give **A11**-Boc[36], and with imidazolide anion to give **A20**-Boc[28]. Deprotection of the Boc group afforded **A10**, **A11**, and **A20**, respectively.

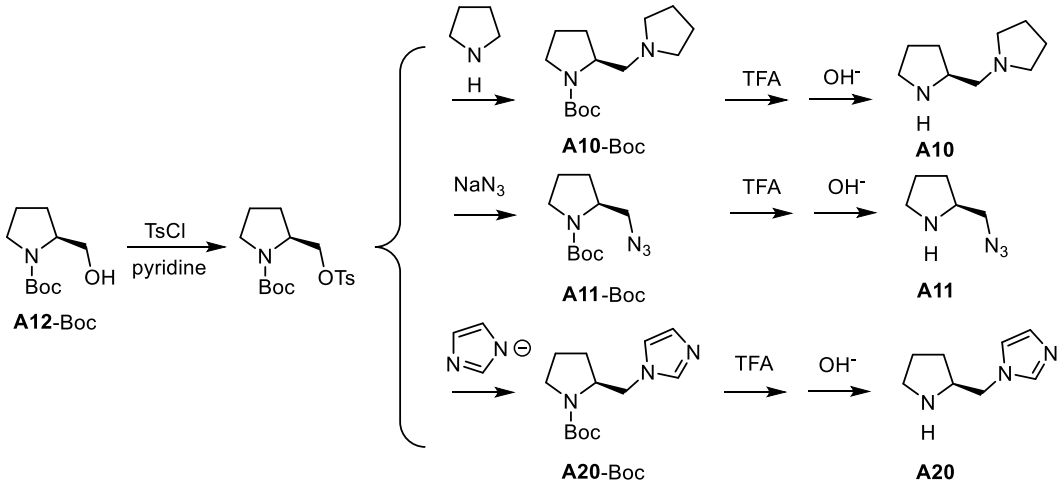

The copper-catalyzed 1,3-dipolar cycloaddition of *N*-Boc-protected **A11** with phenyl acetylene led to the formation of **A19**-Boc[25], which was deprotected to yield **A19**.

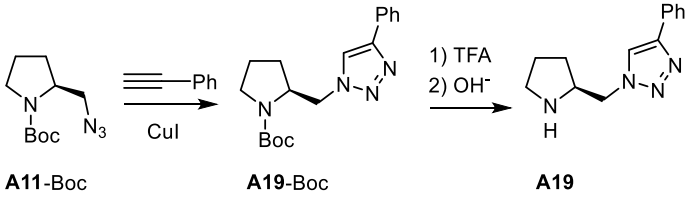

n-Butylation of **A20**-Boc gave **A21**-Boc[28]. The deprotection of the Boc group and counter ion exchange with silver triflate gave **A21-**OTf.

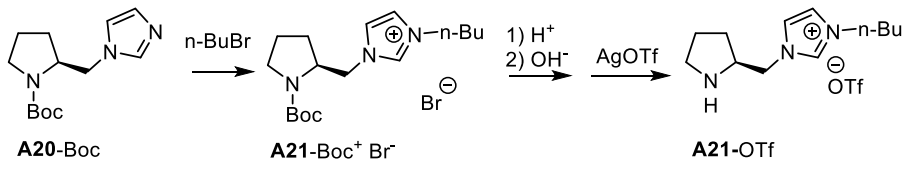

The quantitative deprotonation of **A21**H$^+$ with sodium carbonate in water does not provide the target amine **A21**. When the much weaker basic and less nucleophilic sodium hydrogen carbonate was applied to remove the proton, pure **A21** was obtained whose NMR spectrum is shown in Figure 3. The fact that the full deprotonation of **A21**H$^+$

requires more than 40-equivalents of sodium bicarbonate shows that **A21** is a slightly stronger Brønsted base in water than sodium bicarbonate.

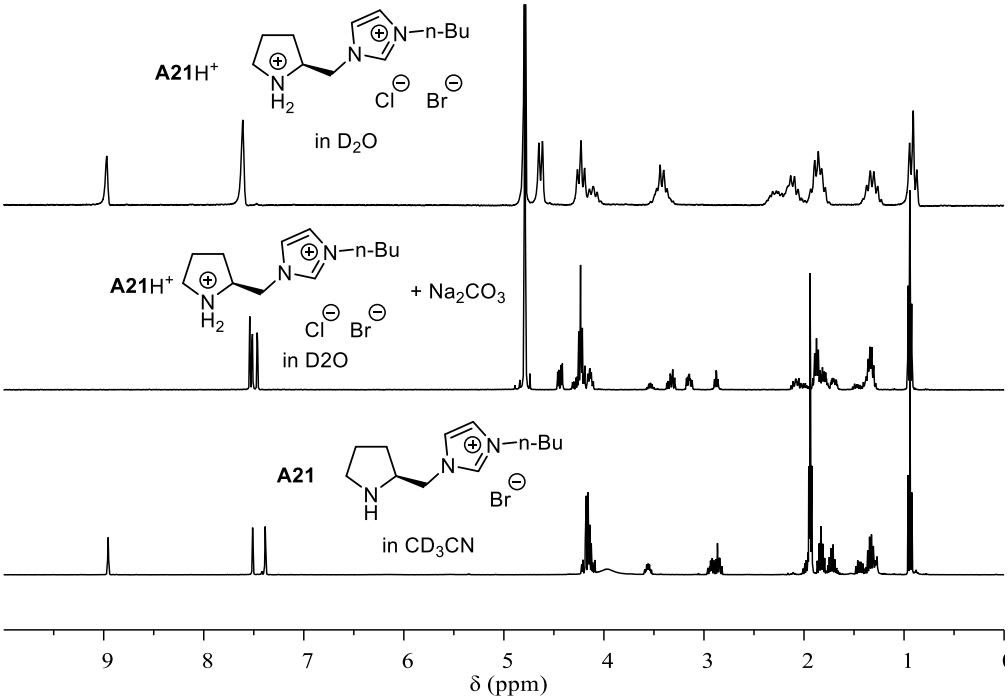

Figure 3. Comparison of ^{1}H NMR spectra of **A21**H^{+} in D_2O, the quantitative deprotonation of **A21**H^{+} with sodium carbonate in D_2O, and **A21** in CD_3CN

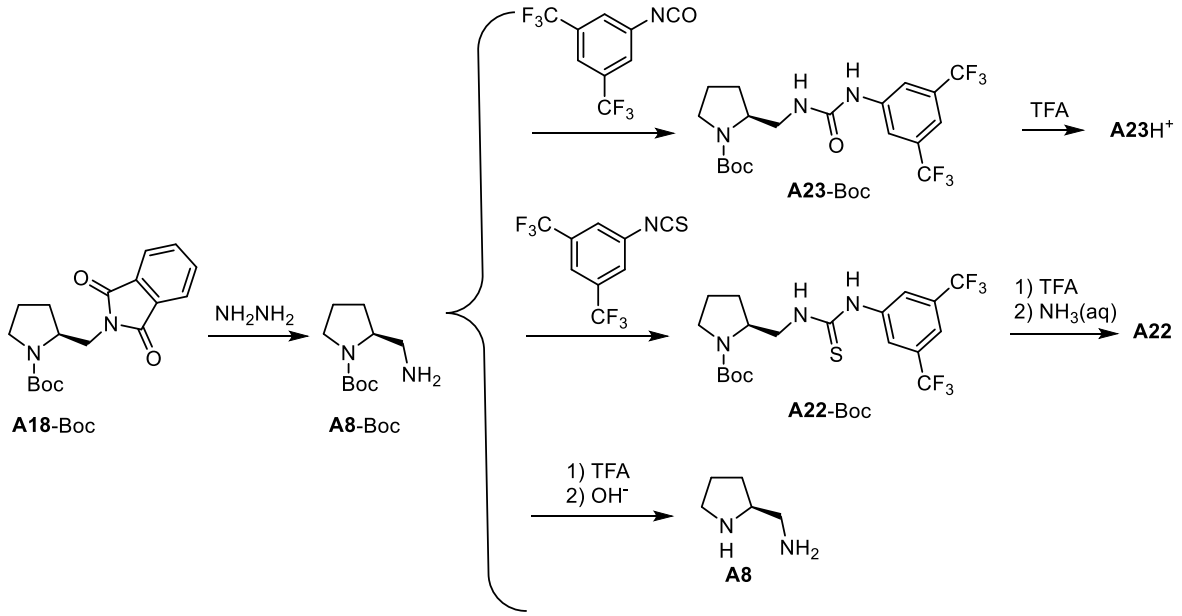

N-Boc protected **A18** reacted with hydrazine to give **A8**-Boc[33], which was combined with 1-isocyanato-3,5-bis(trifluoromethyl) benzene and 1-isothiocyanato-3,5-bis (trifluoromethyl) benzene[37] to give *N*-Boc protected **A23** and **A22**. Removing the Boc group under acidic conditions and subsequent deprotonation gave **A7** and **A22**. Amine **A23** was stored as protonated salt, because it is only stable in highly diluted solution. The clean quantitative deprotonation of **A23**H^{+} in acetonitrile was achieved with DBU base.

The deprotonation of **A23**H$^+$ with saturated aqueous sodium bicarbonate solution as reported in the literature failed.[37,38]

Protection of **A1** with ethyl chloroformate in methanol gave *N*-ethoxycarbonyl-protected **A15**, which was treated with PhMgBr and then deprotected with KOH to give **A26**[39].

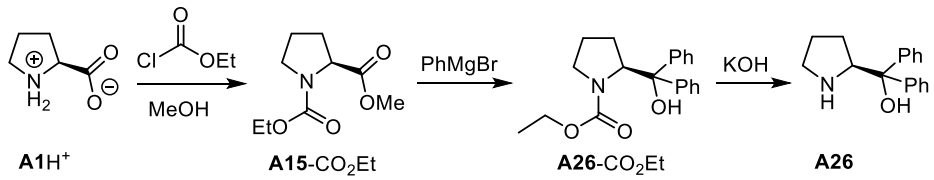

Amine **A26** reacted with TMSOTf/triethylamine to give **A25**[11a], with sodium azide in the presence of trifluoroacetic acid to afford **A27**[40], and with triphosgene and subsequent hydrogenation to yield **A7**[41].

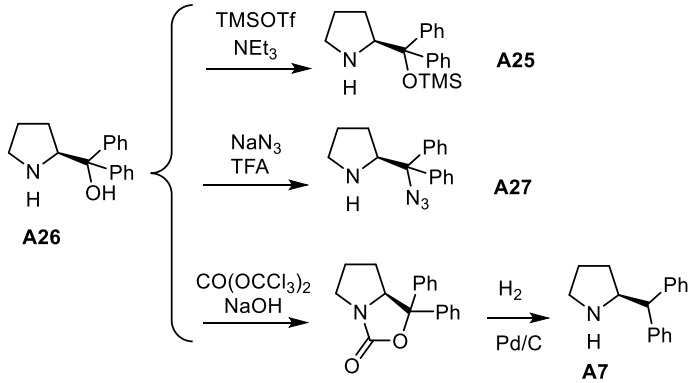

N-Protection of **A1** with benzyl chloroformate and esterfication with 4-nitrophenol gave 1-benzyloxycarbonyl-2-(4-nitrophenyloxycarbonyl)-(*S*)-pyrrolidine, which reacted with dimethylamine and *n*-propylamine to give *N*-Cbz protected **A16** and **A17**[42]. Catalytic hydrogenation of **A16**-Cbz and **A17**-Cbz gave **A16** and **A17**, respectively.

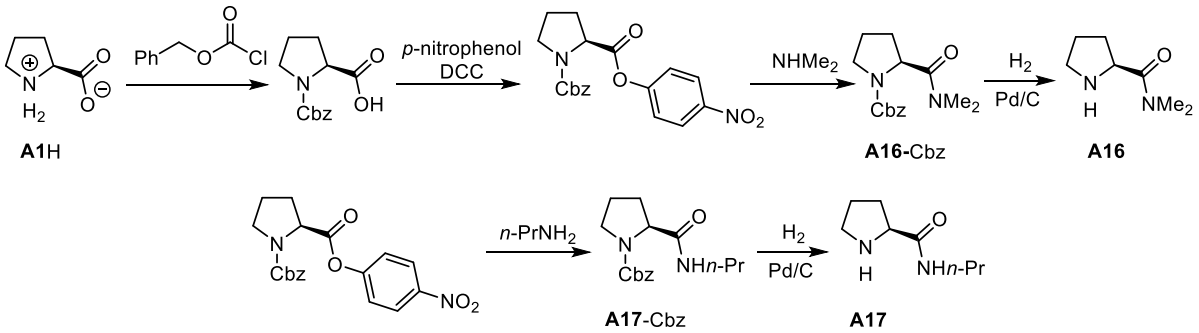

Reduction of **A16** with lithium aluminium hydride gave **A9**[42], which was protonated with triflic acid to give **A9**H.

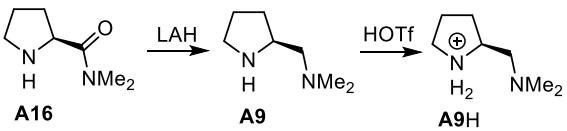

2.2 Synthesis of Pyrrolidines from other Precursors

Racemic **A3** was prepared by catalytic hydrogenation of the cyclic hydroxylamine **A3**-OH, which was obtained by the reaction of hydroxylamine with 1,4-dibromopentane[43].

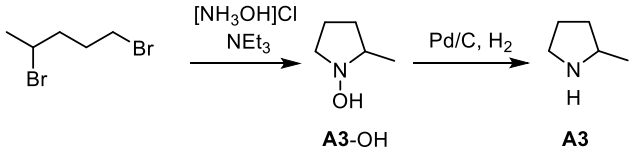

Pyrrolidine **A4** was synthesized from L-valine in six steps. Reduction of L-valine gave L-valinol[44], which was first *N,O*-ditosylated with tosyl chloride and then combined with diethyl malonate. After ester cleavage with concentrated hydrobromic acid and decarboxylation, the protonated amino acid (*R*)-1-carboxy-4-methylpentan-3-aminium bromide was obtained, which cyclized in pyridine to give (*R*)-5-isopropylpyrrolidin-2-one. Its reduction with litium aluminium hydride gave **A4** [45].

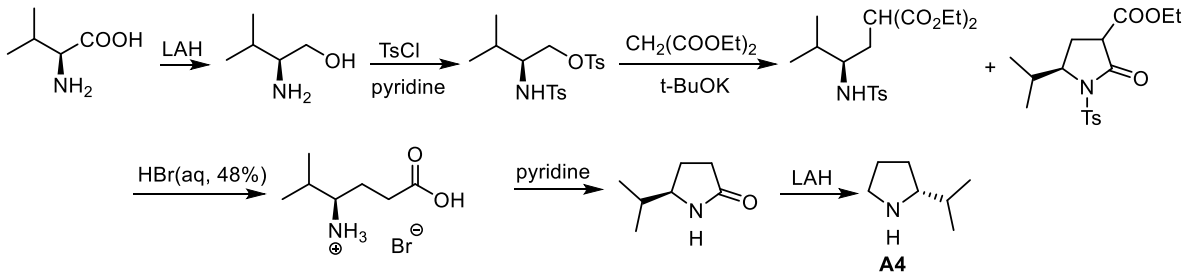

N-Boc-protected pyrrolidine[46] was deprotonated with BuLi/TMEDA and subsequently treated with dimethoxyldiphenylsilane and phenyllithium to give *N*-Boc protected **A28**, which gave **A28** after deprotection of the Boc group[47].

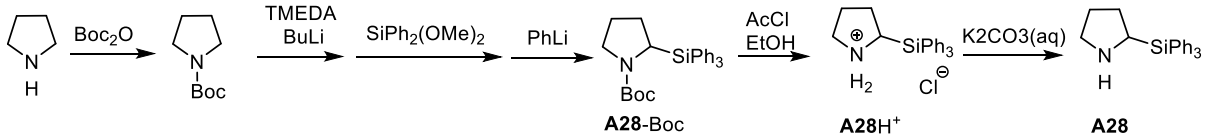

Pyrrolidine **A5** was synthesized in two different ways. Route 1: The Michael adduct from nitromethane and methyl vinyl ketone[48] was reduced with zinc dust and aqueous ammonium chloride solution[49]. The resulting cyclic nitrone was methylated with methylmagnesium bromide and reduced by catalytic hydrogenation to give **A5**[50]. Route 2: The Michael adduct from 2-nitropropane and methyl acrylate[51] was reduced with nickel(II) chloride-sodium borohydride in methanol[52] to yield 5,5-dimethylpyrrolidin-2-one, which was reduced by lithium aluminium hydride to give **A5** [53].

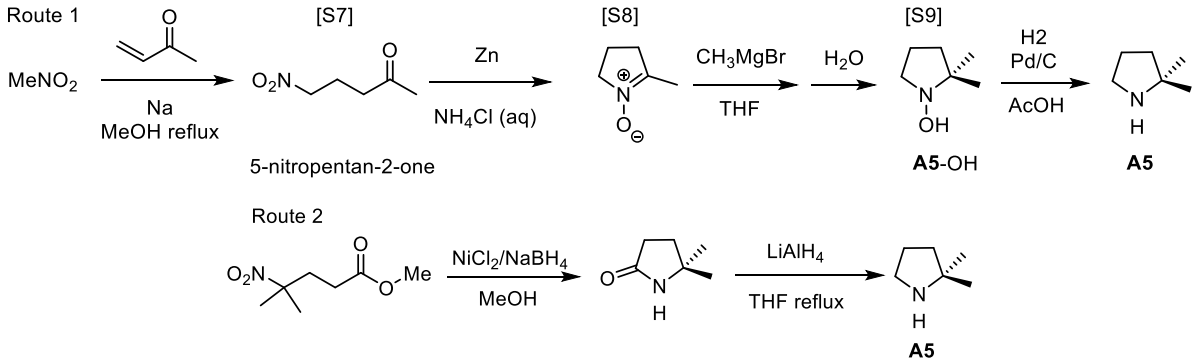

Hydroxylamine was combined with 1,4-dibromobutane to give *N*-hydroxypyrrolidine, which was oxidized by mercury(II) oxide to form a nitrone[54]. Its reaction with trityl anion afforded **A24**-OH, which was reduced by hydrogen to form **A24**[23a].

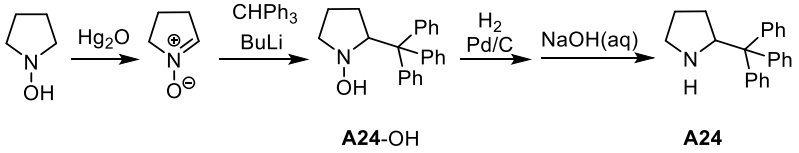

The product from the combination of deprotonated 1-vinyl-2-pyrrolidinone and ethyl trifluoroacetate was treated with hydrochloric acid to give 5-trifluoromethyl-3,4-dihydro-2H-pyrrol, which was hydrogenated to yield **A14**[55].

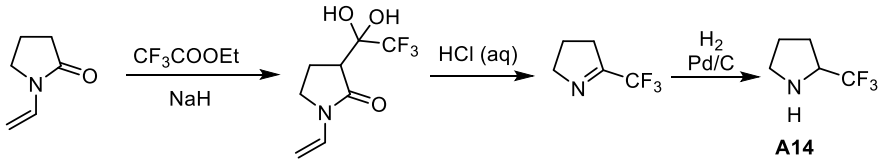

2.3 Synthesis of the Imidazolidinones A29–A32

The imidazolidinones were constructed from (*S*)-(−)-phenylalanine following literature procedures.

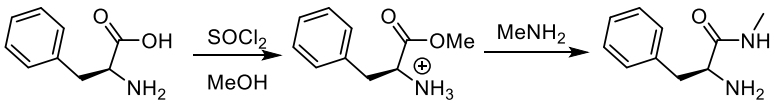

Esterification of phenylalanine with $SOCl_2$/MeOH gave L-phenylalanine methyl ester. Treatment with methyl amine yields in L-phenylalanine methyl amide, which is a key intermediate for the synthesis of **A29**–**A32**.

Under activation of Brønsted acid or Lewis acid, L-phenylalanine methylamide reacted with acetone to give **A29**[5a,5b], with pivalaldehyde to give **A30**[5d] and with 5-methyl-2-fural to give a mixture of **A31** and **A32**[5c], which were separated by column chromatography.

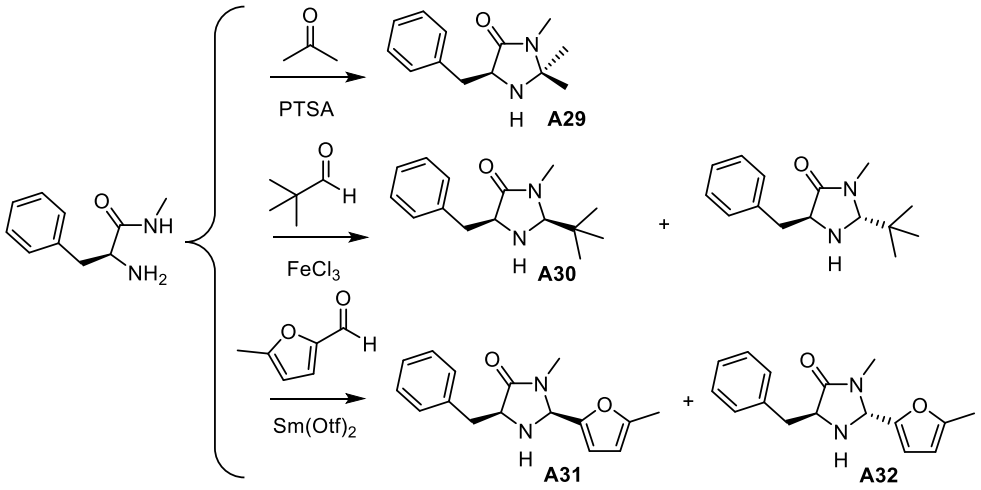

2.4 ^{13}C Spectra of Secondary Amines

As shown in Table 1, the carbon chemical shifts of C4 and C5 of the pyrrolidines **A1**–**A28** generally differ less than 2 ppm and are slightly downfield-shifted from that of the parent compound **A2** [δ(C4) = 25.0 and δ(C5) = 46.5]. The strongest downfield-shift of C4 is observed for the 2,2-dimethyl substituted pyrrolidine **A5** [δ(C4) = 29.0] whereas the strongest downfield-shift of C5 is observed for 2–triphenylsilyl pyrrolidine **A28** [δ(C5) = 49.3]. Analogously δ(C4) and δ(C5) of the imidazolidinones **A29**–**A32** are almost unaffected by variation of the substituents at C2.

Table 1. ^{13}C NMR chemical shifts of pyrrolidine ring and imidazolidinone ring in $CDCl_3$

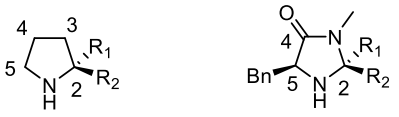

δ / ppm	C2	C3	C4	C5
A1[*]	62.8	31.3	26.2	47.1
A2[56]	46.5	25.0	25.0	46.5
A3	54.7	33.8	25.9	46.9
A4	66.2	29.9	25.7	47.0
A5	59.0	39.7	29.0	46.2
A7[**]	62.7	31.7	26.0	47.1
A8	61.3	29.3	26.0	46.8
A9[**]	57.1	30.8	25.8	46.8
A10	57.6	30.3	25.2	46.3
A11	57.9	29.2	25.7	46.8
A12	59.3	27.8	26.3	46.6

A13	57.8	27.9	25.4	46.6
A14	58.8	26.0	25.7	47.3
A15**	60.5	30.8	26.4	47.7
A16	58.3	30.8	26.6	47.9
A17	60.7	30.8	26.2	47.3
A19	58.1	29.2	25.6	46.7
A20	59.0	29.2	25.3	46.6
A21**	60.0	29.0	25.0	48.1
A22	59.6	28.6	27.4	46.3
A24	64.1	29.2	25.9	46.8
A25**	65.4	27.6	25.3	47.5
A26	64.6	26.4	25.7	46.9
A27	65.4	28.1	26.2	47.3
A28	46.8	29.2	26.9	49.3
A29**	76.3	−	174.0	60.3
A30	82.6	−	175.4	59.6
A31	71.1	−	174.0	60.3
A32	71.1	−	173.9	59.8

*: measurement in DMSO-*d*6; **: measurement in CD_3CN

Chapter 3: Brønsted Basicities of Substituted Pyrrolidines and Imidazolidinones

3.1 General

In order to correlate the nucleophilic reactivities of the pyrrolidines and imidazolidinones, which are measured in acetonitrile, with their basicities, the pK_a values of their conjugate ammonium ions (also defined as pK_{aH} values of secondary amines) were determined in acetonitrile. For that purpose, the CH acids **C1**H–**C6**H were used as indicators, since their pK_a values have previously been reported by Leito and coworkers (Figure 4). Compared to colored OH and NH acids, carbon acids have particular advantages as indicators. Because of the highly delocalized charge in the colored carbanions, traces of water or other ions in the medium do not disturb the measurements [57]. The pK_a values of the carbon acid used as indicators cover the whole range of the basicities of investigated amines.

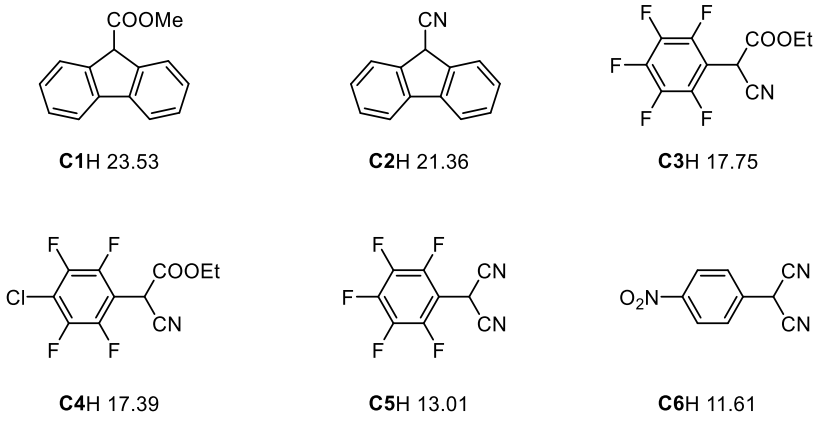

C1H 23.53 **C2**H 21.36 **C3**H 17.75

C4H 17.39 **C5**H 13.01 **C6**H 11.61

Figure 4. pK_a values of indicator acids in acetonitrile[58]

3.2 Titration Method

The basicities of the secondary amines **A** were measured by spectrophotometric titration using indicators **C**H, the anions of which ($\mathbf{C}^-$) have UV-Vis absorptions in the range of 300–600 nm, while the amines **A**, the ammonium ions $\mathbf{A}H^+$ and the indicators **C**H are transparent in this region.

(Titration Method) $\mathbf{A} + \mathbf{C}H \rightleftarrows \mathbf{A}H^+ + \mathbf{C}^-$:

Solutions containing the indicator acids **C**H were titrated with stock solutions of amine **A**, while the spectra in the range of 300–600 nm were recorded. The number of titration points per experiment ranged from 5 to 10. Full quantitative deprotonation of the carbon acids **C**H was subsequently achieved by adding the strong bases 1,5,7-triazabicyclo[4.4.0]dec-5-ene (TBD) or 1,8-diazabicyclo[5.4.0]undec-7-ene (DBU) after titration. The absorption (A) of the solutions at a specific wavelength during the titration and after quantitative deprotonation (A_f) was recorded.

For each step of the titration, the equilibrium constant K can be calculated by equation (1).

$$\boldsymbol{K} = \frac{[\mathbf{A}H^+][\mathbf{C}^-]}{[\mathbf{A}][\mathbf{C}H]} \tag{1}$$

Since

$$[\mathbf{A}H^+] = [\mathbf{C}^-] = [\mathbf{C}H]_0 \cdot A/A_f$$

$$[\mathbf{A}] = [\mathbf{A}]_0 - [\mathbf{C}H]_0 \cdot A/A_f$$

$$[\mathbf{C}H] = [\mathbf{C}H]_0 - [\mathbf{C}H]_0 \cdot A/A_f$$

Then the equilibrium constant K can be expressed by equation (2).

$$K = \frac{[\mathrm{C}^-]^2}{([\mathrm{A}]_0 - [\mathbf{C}^-])([\mathbf{C}H]_0 - [\mathrm{C}^-])} \tag{2}$$

According to equation (1), the individual equilibrium constants lg K were then determined from the slopes of a linear plot of [**A**][**C**H] vs $[\mathbf{C}^-]^2$. The basicity of amine **A** (pK_{aH}) is then given by equation (3):

$$\mathrm{p}K_{\mathrm{aH}}(\mathbf{A}) = \mathrm{p}K_{\mathrm{a}}(\mathbf{C}H) + \lg K \tag{3}$$

Since the free amines **A18** and **A23** are only stable in highly diluted solution, their basicities were determined by titration of their ammonium salts $\mathbf{A18}H^+$ and $\mathbf{A23}H^+$ with the colored anions of the indicators ($\mathbf{C}^-$)

3.3 Synthesis of the Indicators

The indicators **C1**H and **C2**H were synthesized by former members of the group. The indicators **C3**H–**C6**H were synthesized by nucleophilic aromatic substitutions of electron deficient fluorobenzenes with secondary carbanions following literature procedures (Figure 5).

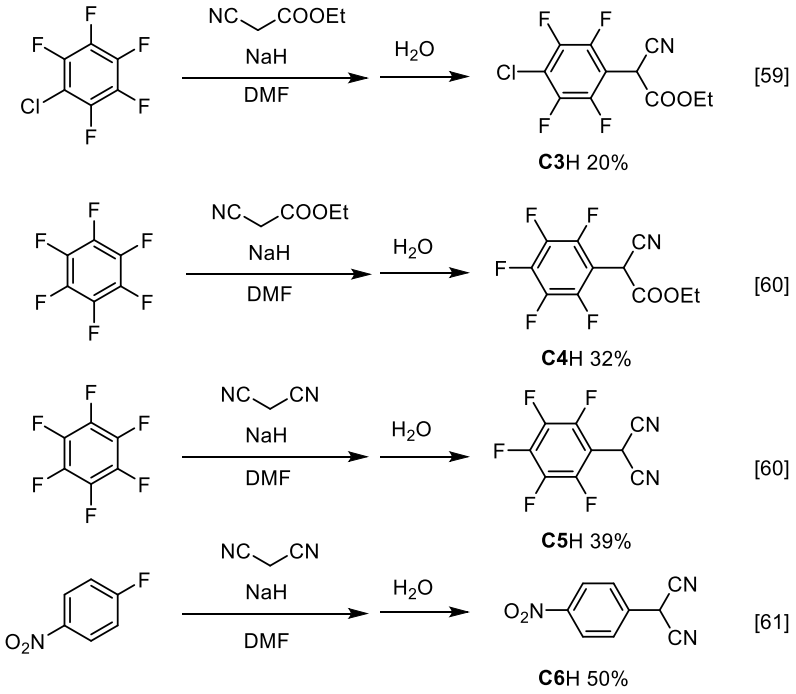

Figure 5. Synthesis of indicators by nucleophilic aromatic substitutions

The crude products were recrystallized several times (details see experimental part in Chapter 7) to get pure crystalline products, which were used as indicators.

3.4 Results

Though the pK_a values of the used indicators were measured at 25 °C by Leito and coworkers, all proton transfer equilibria were measured at 20 °C, the temperature used for the kinetic measurements.[58] In order to avoid almost quantitative deprotonation of the indicator acid **C**H, the basicity of the amine should at maximum be one pK_a unit higher than that of the indicator. On the other side, pK_{aH} (**A**) should not be too low to achieve sufficient deprotonation of the catalyst, which led to the range (pK_{aH} (**C**) –3 < pK_{aH} (**A**) < pK_{aH} (**C**) + 1) for the equilibrium measurements.

As shown in Table 2, the indicator acids covered an acidity range from 11.6 < pK_a < 23.5, which allowed us to compare amines of widely differing basicity. In several cases (**A7**, **A11**, **A15**–**A20**, **A22**–**A29**) basicities were determined with two different indicators, and the agreement was typically within 0.03 pK_a units, and never deviated by more than 0.1 pK_a units.

Table 2. Acid dissociation measurement results of amines **A** in acetonitrile at 20°C

Amine	Indicator	K^a	Individual pK_{aH}	Averaged pK_{aH}
A1	**C1**H	3.07	24.02	24.02
A2	**C2**H	3.35×10^{-2}	19.89	19.89
A3	**C2**H	1.62×10^{-2}	19.57	19.57
A4	**C2**H	8.92×10^{-3}	19.31	19.31
A5	**C2**H	1.30×10^{-2}	19.47	19.47
A6	**C2**H	2.04×10^{-3}	18.67	18.67
A7	**C2**H	5.59×10^{-4}	18.11	18.13
	C3H	2.47	18.14	
A8	**C2**H	3.19×10^{-2}	19.86	19.86
A9	**C2**H	2.82×10^{-2}	19.81	19.81
A9H$^+$	**C6**H	3.46×10^{-4}	8.15	8.15
A10	**C2**H	4.81×10^{-2}	20.04	20.04
A11	**C3**H	7.65×10^{-1}	17.63	17.66
	C4H	1.93	17.68	
A12	**C2**H	4.28×10^{-3}	18.99	18.99
A13	**C2**H	3.28×10^{-3}	18.88	18.88
A14	**C5**H	4.21×10^{-1}	12.63	12.63
A15	**C3**H	7.56×10^{-2}	16.63	16.63
	C4H	1.72×10^{-1}	16.63	
A16	**C2**H	1.14×10^{-3}	18.42	18.38
	C3H	6.11	18.34	
A17	**C3**H	2.72×10^{-1}	17.18	17.18
	C4H	6.19×10^{-1}	17.18	
A18	**C3**$^-$	2.28 [b]	18.11	18.12

	C4$^-$	5.53 [b]	18.13	
A19	**C3**H	1.72×10^{-1}	16.99	16.94
	C4H	3.13×10^{-1}	16.89	
A20	**C3**H	9.78×10^{-2}	16.74	16.74
	C4H	2.26×10^{-1}	16.75	
A21	**C6**H	3.38×10^{-1}	11.14	11.14
A22	**C3**H	3.97×10^{-1}	17.35	17.31
	C4H	7.64×10^{-1}	17.27	
A22$^-$	—[c]	7.04	25.16	25.16
A23	**C3**$^-$	2.14×10^{1} [b]	19.08	19.13
	C4$^-$	6.12×10^{1} [b]	19.18	
A24	**C3**H	1.12×10^{-1}	16.80	16.79
	C4H	2.47×10^{-1}	16.78	
A25	**C3**H	7.21×10^{-1}	17.61	17.61
	C4H	1.68	17.62	
A26	**C3**H	4.36×10^{-1}	17.39	17.39
	C4H	9.82×10^{-1}	17.38	
A27	**C3**H	1.14×10^{-2}	15.81	15.79
	C4H	2.46×10^{-2}	15.78	
A28	**C3**H	1.17	17.82	17.81
	C4H	2.57	17.80	
A29	**C5**H	6.72×10^{-2}	11.84	11.83
	C6H	1.64	11.83	
A30	**C6**H	1.06×10^{-1}	10.63	10.63
A31	**C6**H	8.61×10^{-2}	10.54	10.54
A32	**C6**H	1.22×10^{-1}	10.70	10.70

[a] K as defined in equation 3; [b] Obtained by titrating $\mathbf{A}H^+$ into solutions of deprotonated indicators $\mathbf{C}^-$. [c] By following the absorbance of $\mathbf{A22}^-$ in the titration with DBU (pK_{aH} = 24.31)[62].

The basicity constants in Figure 6 show that the basicity scale in acetonitrile covers the range from 10–24, where most pyrrolidines are in the range 16 < pK_{aH} < 20 and the imidazolidinones are in the range 10 < pK_{aH} < 12. Thus, steric and electronic effects of the 2-substituents generally reduce the basicity of the parent compound **A2** by less than 4 pK_a units. If one disregards the slightly higher basicity of the diamine **A10**, 2-trifluoromethylpyrrolidine **A14** is the only neutral pyrrolidine outside this range with a basicity constant which is 7 pK_a units smaller than that of the parent pyrrolidine. On the other hand, charged substituents have a large effect on the basicity. Thus, the negative charge of the carboxylate group in **A1** increases the basicity of the pyrrolidine by 4 orders of magnitude, while the positive charge of the imidazolium group in **A21** reduces the basicity by almost 9 pK_{aH} units.

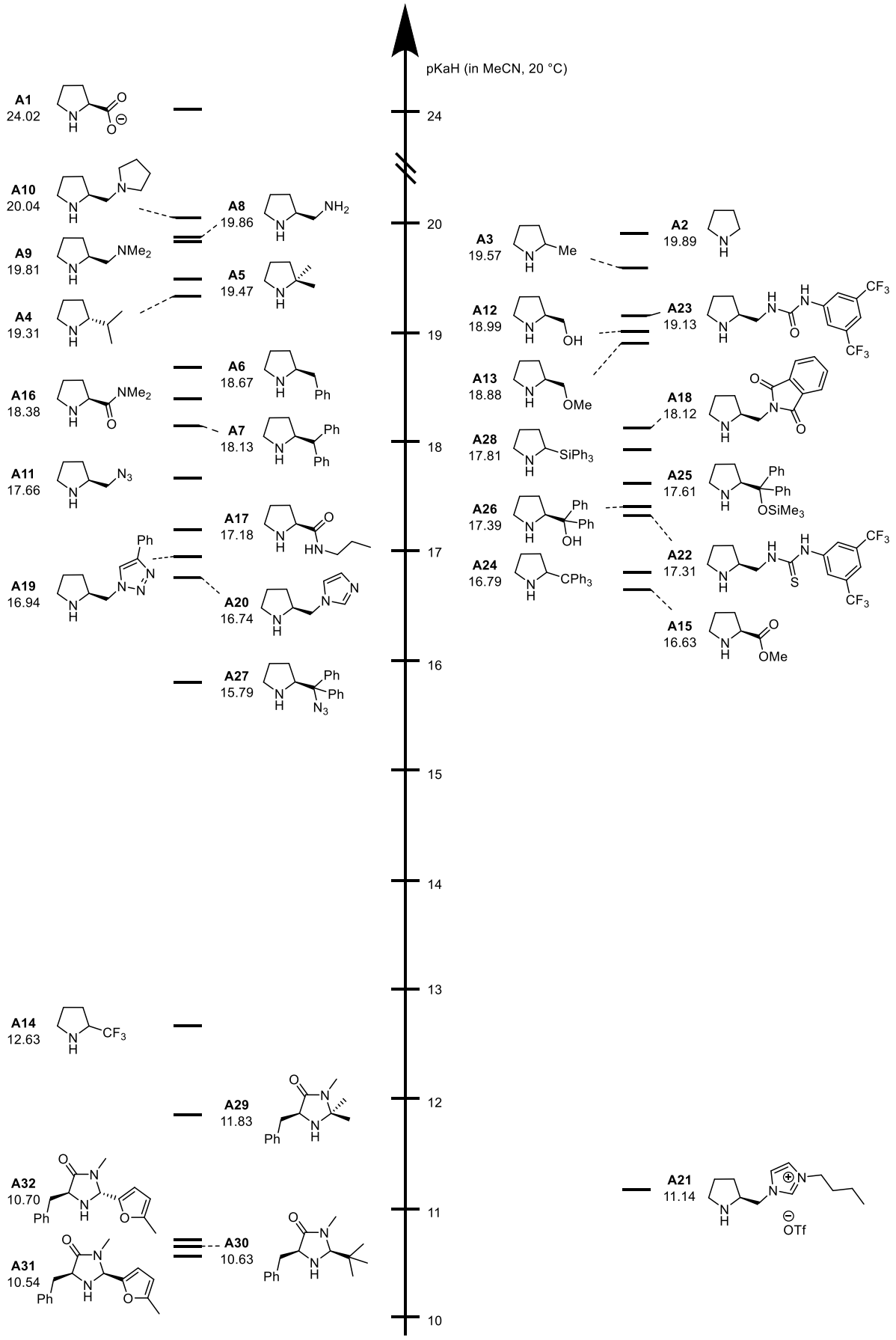

Figure 6. pK_{aH} values of secondary amines in acetonitrile (20 °C)

Chapter 4: Nucleophilic Reactivities of substituted Pyrrolidines and Imidazolidinones

4.1 General

Mayr and coworkers demonstrated that the linear free energy relationship (equation 4)[63] can be used to describe the rate constants for the reactions of carbocations and Michael acceptors with π-, σ-, and n-nucleophiles .

$$\lg k_2(20\ °\mathrm{C}) = s_\mathrm{N}(N + E) \qquad (4)$$

In equation (4), the solvent-independent electrophilicity parameter *E* characterizes the strengths of electrophiles; the solvent-dependent nucleophilicity parameter *N* characterizes the strengths of the nucleophiles and the sensitivity parameter s_N is a nucleophile-dependent slope parameter. More than 1100 nucleophiles and 300 electrophiles are summarized in the freely accessible database: http://www.cup.uni-muenchen.de/oc/mayr/DBintro.html.

Following earlier strategies in the Mayr group, the nucleophilic reactivities of the amines **A1**–**A32** (Figure 7) were calculated by equation (4) from the second order rate constants of their reactions with benzhydrylium ions and quinone methides of known electrophilicities.

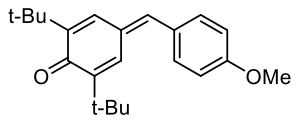

E1 (*E* = –16.11)

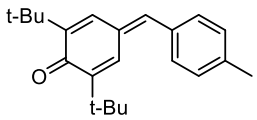

E2 (*E* = –15.83)

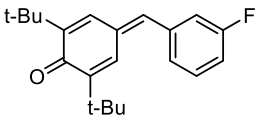

E3 (*E* = –15.03)

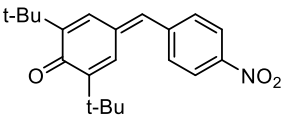

E4 (*E* = –14.36)

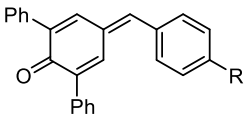

R = NMe_2, **E5** (*E* = –13.39)
OMe, **E6** (*E* = –12.18)
H, **E7** (*E* = –11.87)

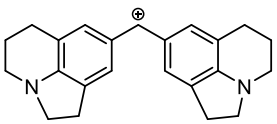

E8 (*E* = –10.04)

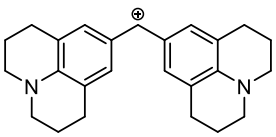

E9 (*E* = –9.45)

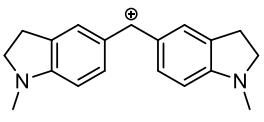

E10 (*E* = –8.76)

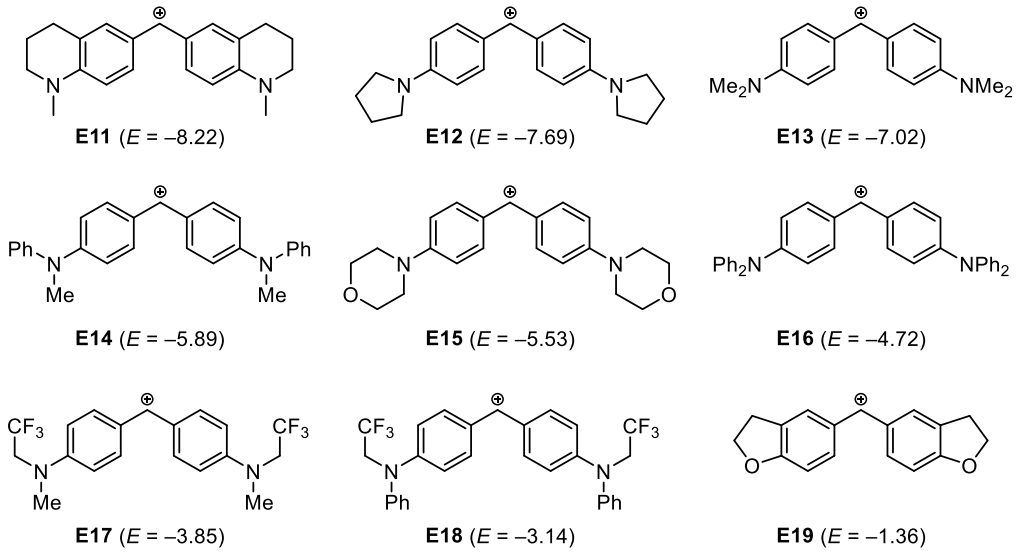

Figure 7. Electrophilicity parameters of benzhydrylium ions and quinone methides

4.2 Kinetic Method

The kinetics of the reactions of the amines **A1**–**A32** with the quinone methides **E3**–**E7** and benzhydrylium ions **E8**–**E19** were determined photometrically in acetonitrile at 20 °C. The disappearance of the colored electrophiles (346 nm ≤ λ_{max} ≥ 646 nm) was monitored by time-resolved UV-Vis spectroscopy.

The kinetic investigations of all reactions were performed with a high excess of the amines over the electrophiles (≥ 10 equivalents) resulting in pseudo-first-order kinetics. As a consequence, a mono-exponential decay of the absorbances of the electrophiles was observed, from which the first-order rate constants k_{obs} (s^{-1}) were derived by a least squares fitting of the function $A_t = A_0\exp(-k_{obs}t) + C$ to the observed time-dependent absorbances. According to the relation $k_{obs} = k_2[Nu]$, the first-order rate constants k_{obs} were linearly dependent on the nucleophile concentrations [**A**], and the slopes correspond to the second-order rate constants k_2 (M^{-1} s^{-1}), as illustrated for the reaction of amine **A13** with **E9** in figure 8.

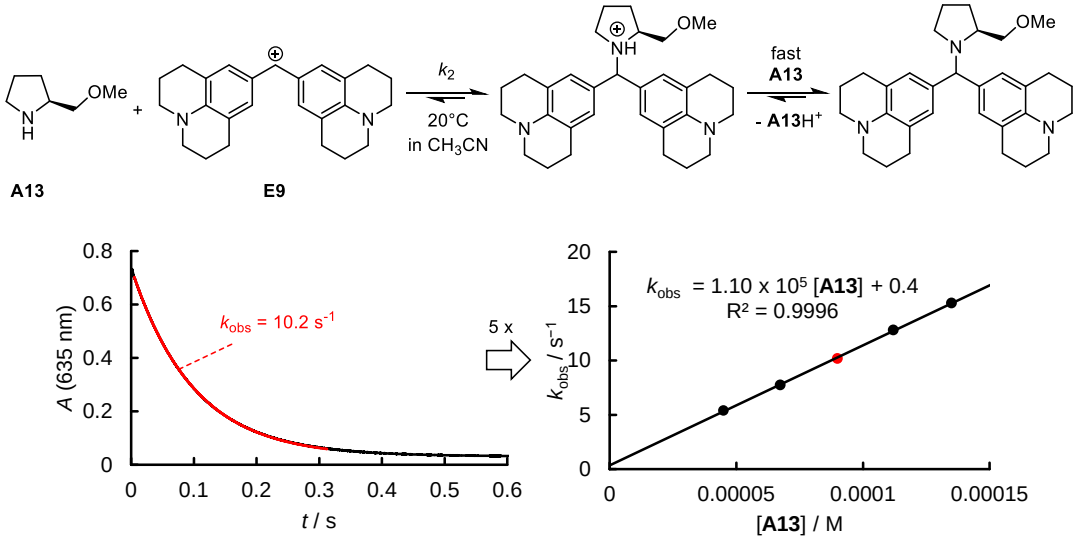

Figure 8. left: Determination of the pseudo-first-order rate constant for the reaction of **A13 (**4.49 x 10^{-5} mol·L^{-1}) with **E9** (4.28 x 10^{-6} mol·L^{-1}); right: determination of the second order rate constant for reaction of **A13** with **E9**

The second order rate constants for the reactions of **A1, A3**–**A13**, **A15**–**A23** and **A26** with electrophiles were determined by this method. In all these measurements, a linear correlation between the concentrations of the amines **A** and the observed rate constants k_{obs} was observed, which allowed us to determine the second-order rate constants for the reactions of amines with electrophiles. More complex kinetics were observed for the other amines as discussed below.

4.3 Reaction Mechanism

The mechanism for the reactions of amines **A** with benzhydrylium ions is described in Scheme 8:

Scheme 8. Mechanism for the reactions of amines **A** with benzhydrylium ions

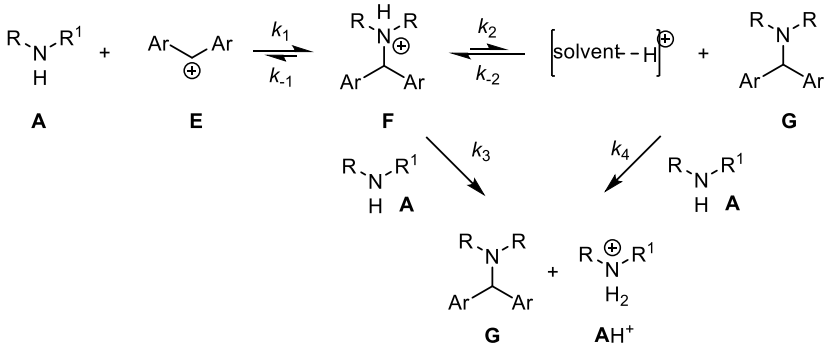

The reaction of **A** with **E** initially generates ammonium ion **F**, which may either directly transfer a proton to amine **A** (k_3) used in large excess, or undergo proton transfer to the solvent (k_2). Though the latter step will be usually be endergonic due to the lower basicity of most solvents compared to the amines **F**, reversibility of this step can be neglected since proton transfer from the protonated solvent to **a** (k_4[**A**]) will be faster than the reverse reaction (k_{-2}[**F**]). There are three different cases which have to be considered:

Case 1: If $k_{-1} < k_2$ or k_3[**A**], the NC-bond formation (k_1) is rate-determining. The reaction follows second order kinetics, first order in **A** and first order in **E**. Under pseudo first-order-conditions ([**A**] >> [**E**]), a linear increase of the first-order rate constants with the concentration of the amine **A** should be observed. The free energy diagrams for the reactions in case 1 are shown in Scheme 9.

Scheme 9. Free energy diagrams for the reaction in case 1. Please note that the heights of the barriers in this scheme do not directly correlate with the rates of the individual reactions, since k_1 and k_3 are second-order rate constants, whereas k_{-1} and k_2 are first-order rate constants.

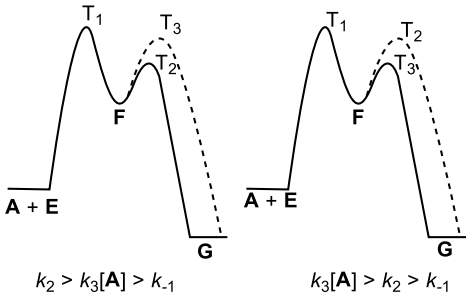

$k_2 > k_3$[**A**] > k_{-1} k_3[**A**] > $k_2 > k_{-1}$

Case 2: If $k_{-1} > k_2 > k_3$[**A**], the proton transfer from **F** to the solvent to give **G** is rate-determining. Under pseudo first-order-conditions, the first-order rate constants will depend on the concentration of **F** and the protophilicity of the solvent (Scheme 10). This

case should only be encountered in highly basic solvents and results in second-order kinetics, first order in **A** and first order in **E**.

Case 3: If $k_{-1} > k_3[\mathbf{A}] > k_2$, the proton transfer from **F** to **A** to give **G** is the rate-determining step. The reaction follows third-order kinetics, second order in **A** and first order in **E**. Under pseudo first-order-conditions ([**A**] >> [**E**]), the first-order rate constants increase with the square of the concentration of the amine **A** (Scheme 10).

Scheme 10. Free energy diagrams for the reaction in cases 2 and 3

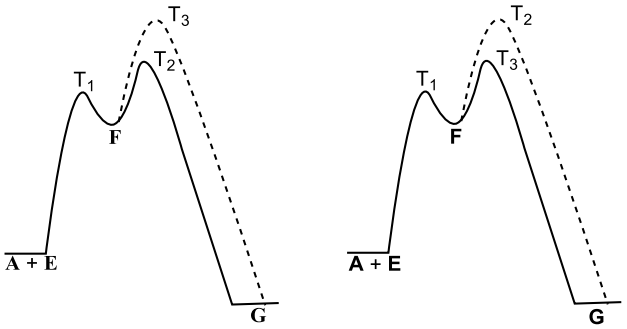

Case 2: $k_{-1} > k_2 > k_3[\mathbf{A}]$ Case 3: $k_{-1} > k_3[\mathbf{A}] > k_2$

The reactions of amines **A** with quinone methides can be expected to proceed in a similar way as the reactions with benzhydrylium ions (Scheme 11). Since the isomerization **F**→**G** cannot proceed intramolecularly, either the solvent or another amine must serve as a proton shuttle.

Scheme 11. Mechanism for the reactions of amines **A** with quinone methides **E1**–**E7**

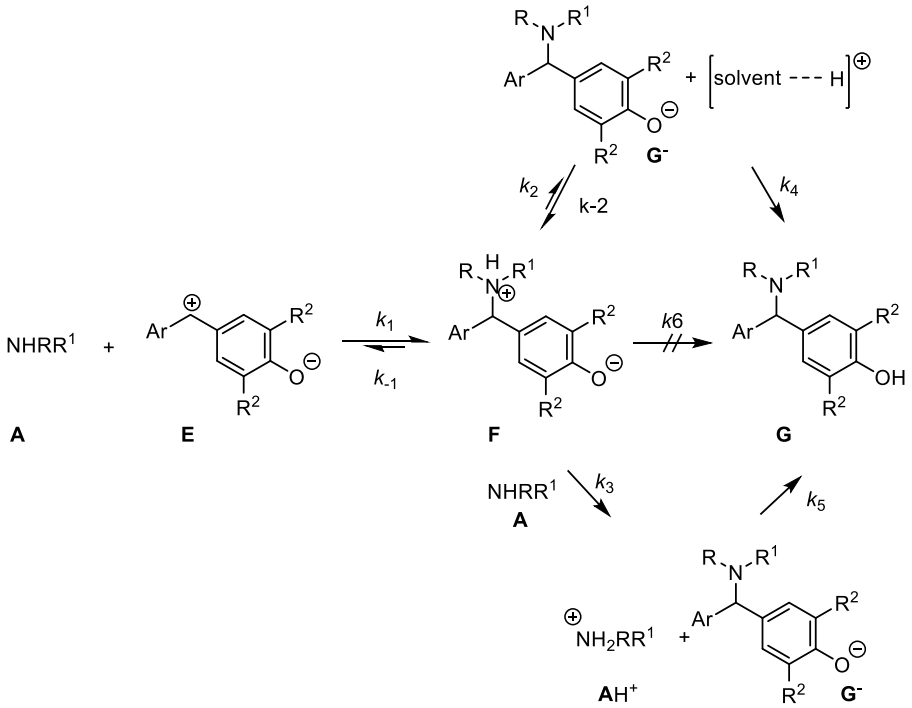

Figure 9 shows that the pseudo-first order rate constants for the reactions of pyrrolidine (**A2**) with the benzhydrylium ions **E8** and **E9** in dichloromethane do not increase linearly

with the concentration of pyrrolidine, indicating operation of mechanism case 2 with a transition state which involves more than one pyrrolidine molecule.

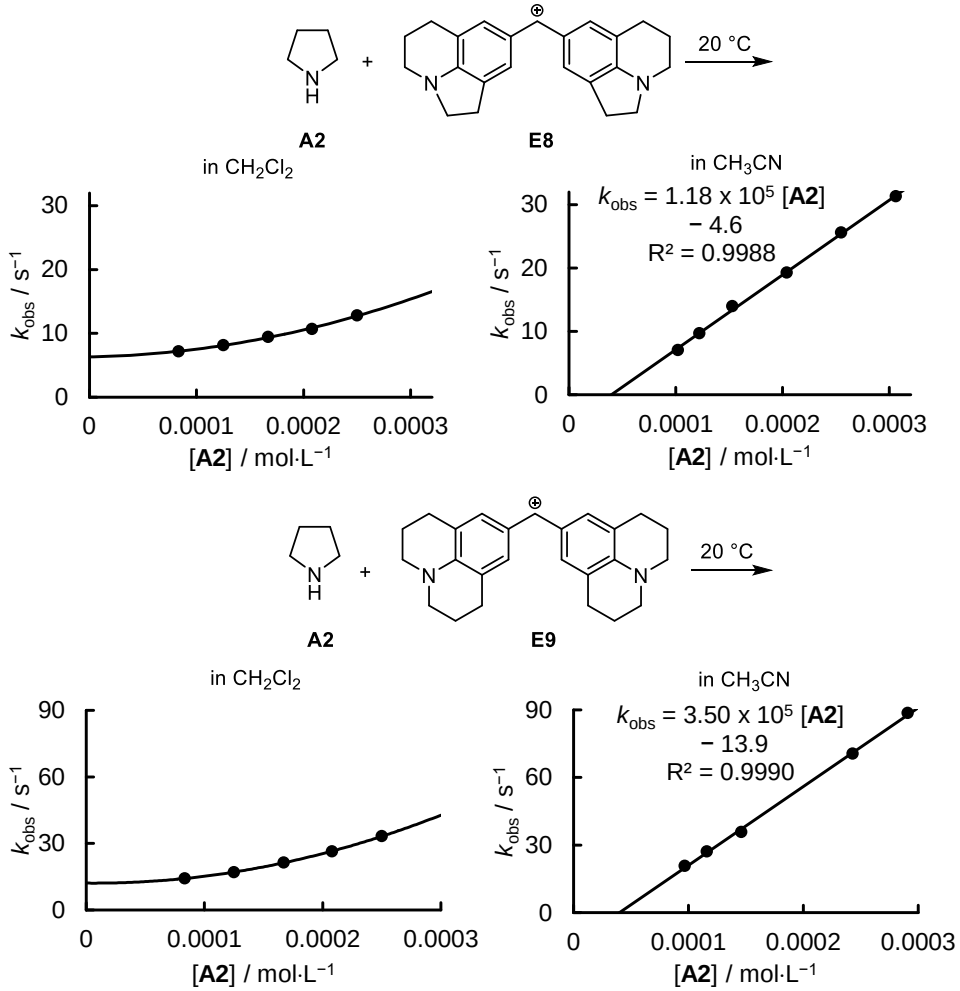

Figure 9. Kinetics of the reactions of pyrrolidine **A2** with electrophiles **E8** (top) and **E9** (bottom) in dichloromethane (left) and acetonitrile (right) [64]

On the contrary, in acetonitrile the reactions follow second order kinetics. Due to the higher basicity of acetonitrile compared to dichloromethane, the proton transfer rate constant k_2 becomes greater than k_{-1}, and k_{obs} increases linearly with the concentration of **A2** (Figure 9).

For that reason, acetonitrile was used for all kinetic investigations. However, also in acetonitrile, not all reactions of amines with the reference electrophiles followed second-order kinetics.

As exemplified in Figure 10 for the reaction of **A27** with the benzhydrylium ion **E13**, deviations from the linear k_{obs} versus [**A**] correlations were generally observed in the reactions of the pyrrolidines **A24**, **A25**, **A27**, and **A28** carrying bulky substituents in

2-position as well as in the reaction of the weakly basic 2-CF_3 substituted pyrrolidine **A14**. Reversibility of the initial attack of the amine at the benzhydrylium ions was thus indicated.

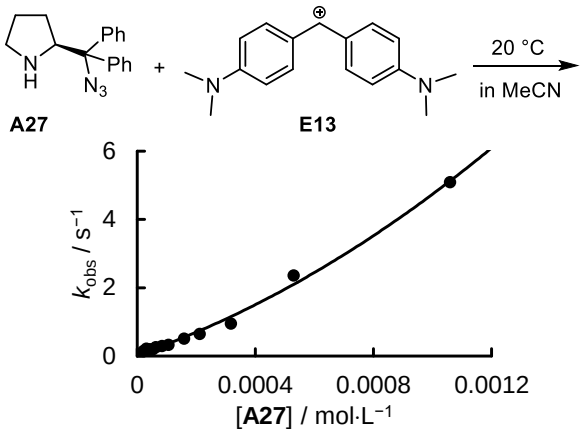

Figure 10. Plot of observed pseudo first order rate constants and the concentration of nucleophile for the reaction between **A27** and **E13** (2.35×10^{-6} M)

Deviations from the linear k_{obs} versus [**A**] correlations were also observed in the reactions of pyrrolidine **A2** with the quinone methides **E3** and **E4**. Thus deprotonation is generally rate determining in the reactions of secondary amines which initially form thermodynamically unstable zwitterions.

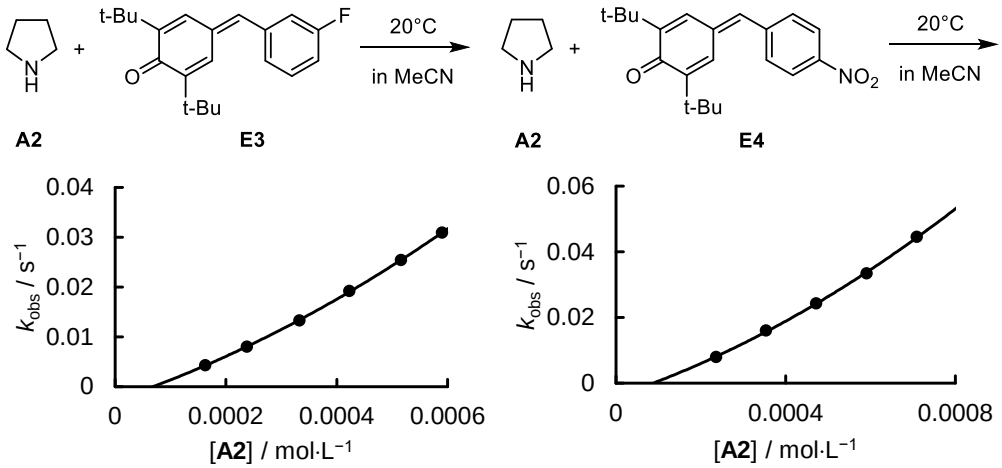

Figure 11. Plot of pseudo first-order rate constants k_{obs} versus the concentration of amines for the reactions of **A2** with **E3** and **E4**

4.4 Kinetics in the Presence of Sterically Shielded Pyridines

The reaction between **A27** and **E13** (Figure 11) follows case 2 type kinetics. A second molecule of amine **A27** was needed to remove the proton from the initially formed ammonium ion. However, the upper line of Figure 12 shows that the benzhydrylium ion **E13** is only consumed to a small extent by 10 equivalents of the sterically shielded pyrrolidine **A27**. Attempts to shift this equilibrium by adding aliphatic tertiary amines (trimethylamine, ethyldimethylamine, ethyldisopropylamine) were unsuccessful, because these amines reacted with **E13** (probably via hydride transfer) with similar rates as **A27**. In contrast, the substituted pyridines **D1** and **D2** did not react with **E13**. As shown by the lower graphs in Figure 12, addition of large quantities of **E2** shifted the reaction of **A27** with **E13** to the product side.

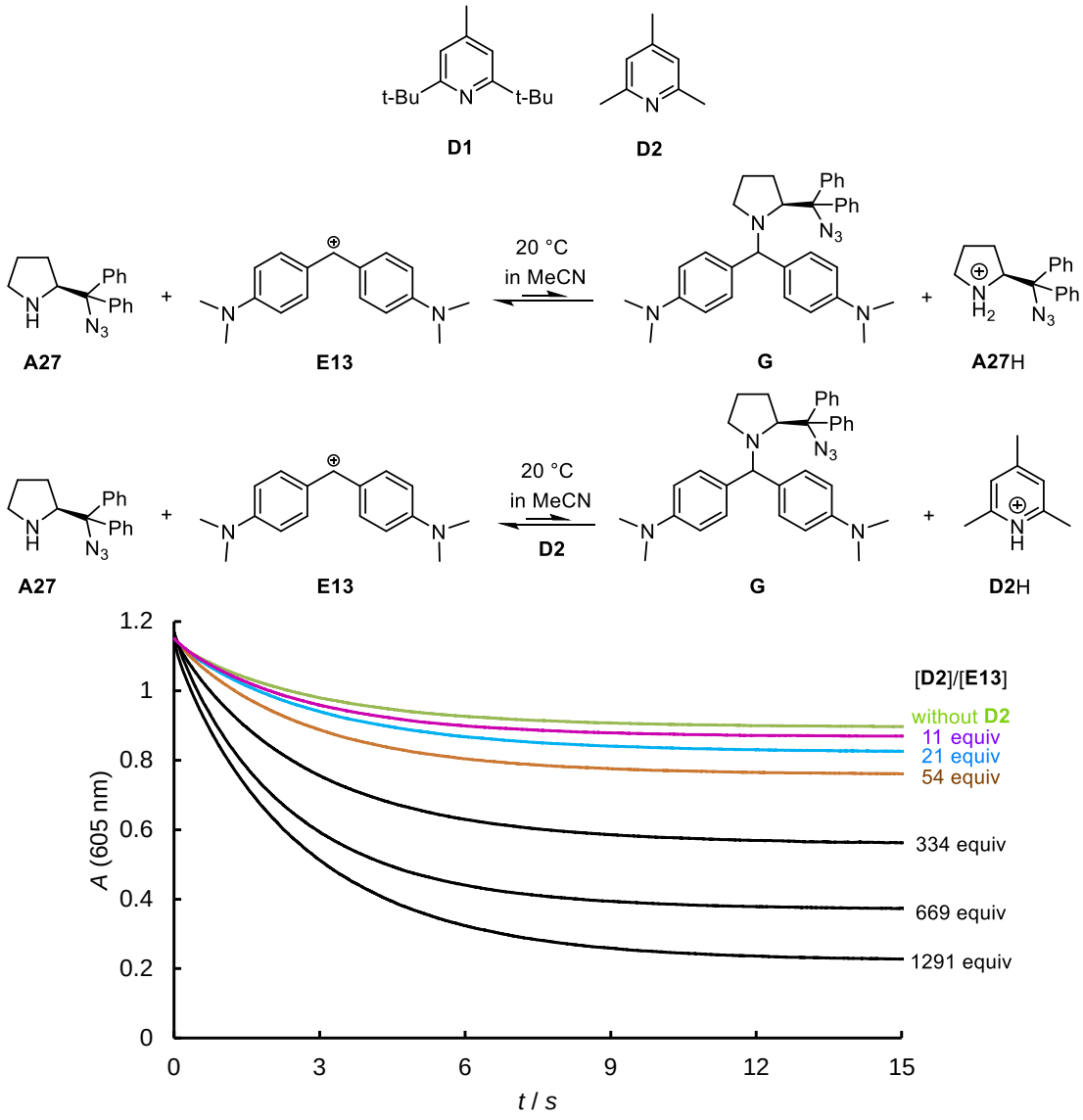

Figure 12. Reaction of **A27** (7.67×10^{-5} mol/L) with **E13** (7.06×10^{-6} mol/L) in presence of different amounts of **D2**.

As depicted in Figure 13, collidine (**D2**) can also suppress the reversibility of the first step of the case 2 (Scheme 8) mechanism resulting in a second-order reaction, first order with respect to **E13** and first order with respect to pyrrolidine **A27**. A confirmation for this interpretation comes from the observation that the same rate constants were obtained when collidine (**D2**) or the *tert*-butyl substituted pyridine **D1** were used as additives (Figure 13).

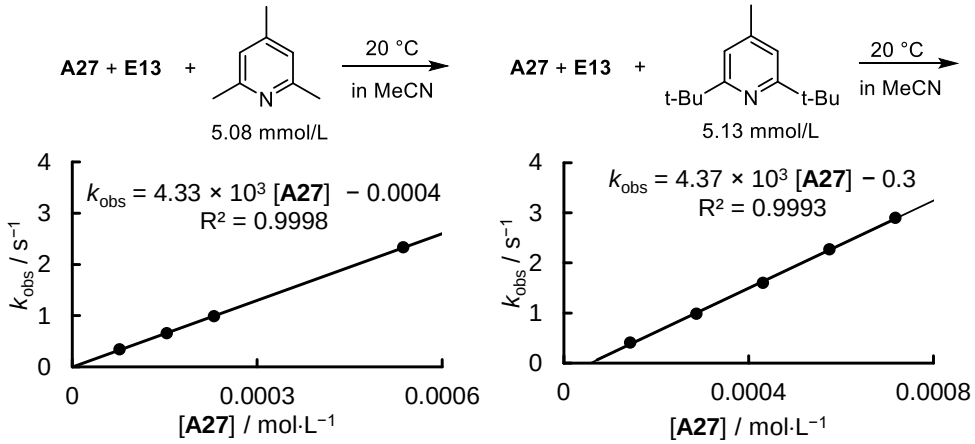

Figure 13. Comparison of the reaction between **A27** and **E13** (left: 5.10 × 10^{-6} M; right: 5.29 × 10^{-6} M) with **D1** and **D2** as additives

Deviations from second-order kinetics were not only observed, however, in reactions of pyrrolidines with low Lewis basicity due to bulky substituents in 2-position, but also in the case of pyrrolidine **A14**, which is a weaker Lewis and Brønsted base due to the electron-withdrawing CF_3 group in 2-position.The kinetics of the reactions between **A14** and **E13** are shown in Figure 14.

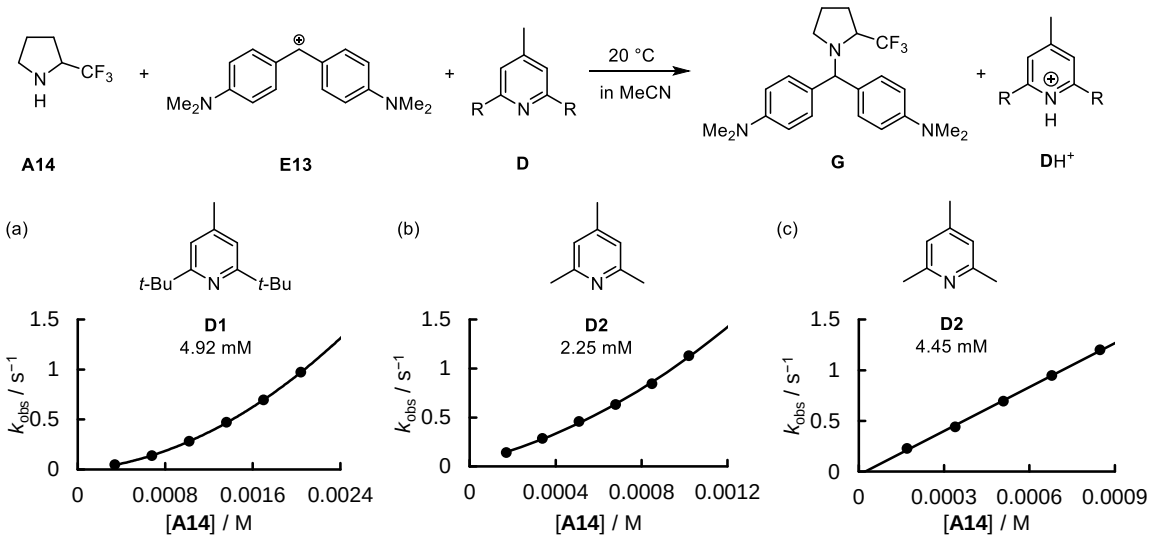

Figure 14. Kinetics of the reactions between **A14** and **E13** (4.85 × 10^{-6} mol/L) with different base additives

The reaction of the CF_3-substituted pyrrolidine **A14** with **E18** the most electrophilic and Lewis-acidic benzhydrylium ion of this series followed second order kinetics (see last column of Table 3). In contrast, the less electrophilic (and less Lewis acidic) benzhydrylium ions **E17** and **E15** only reacted by second-order kinetics, when an additional base was present. In these cases, addition of the di-*tert*-butyl-methyl substituted pyridine **D1** (2.46×10^{-3} mol/L for the reaction with **E15** and 1.23×10^{-3} mol/L for the reaction with **E17**) was found to be sufficient for obtaining pseudo-first order kinetics in the reaction of **E17** and **E15** with more than 10 equivalents of **A14**. Figure 14a shows, however, that k_{obs} for the reaction of the better stabilized benzhydrylium ion **E13** with excess **A14** does not linearly increase with the concentration of **A14**, even in the presence of 4.92×10^{-3} M of **D1**. A concentration of 2.25×10^{-3} M of **D2** was also not sufficient to achieve a linear correlation between k_{obs} with [**A14**] for the reaction of **A14** with **E13** (Fig. 14b). A linear correlation of k_{obs} with [**A14**] was eventually observed in the presence of 4.45×10^{-3} M of **D2** (Fig. 14c). With a pK_{aH} value of 15.00[62], collidine (**D2**) is a stronger base than **A14** (pK_{aH} = 12.63) which explains the observation that second-order kinetics for the reaction of **E13** with **A14** ware obtained in the presence of **D2** at a high concentration 4.45×10^{-3} M. Since pyridine **D1** is less basic (pK_{aH} = 12.8[65]) than **D1** in acetonitrile, one can explain, why **D1** is less efficient as a proton acceptor. A rationalization of the different kinetics in Fig.14a and Fig.14c is shown in Figure 15.

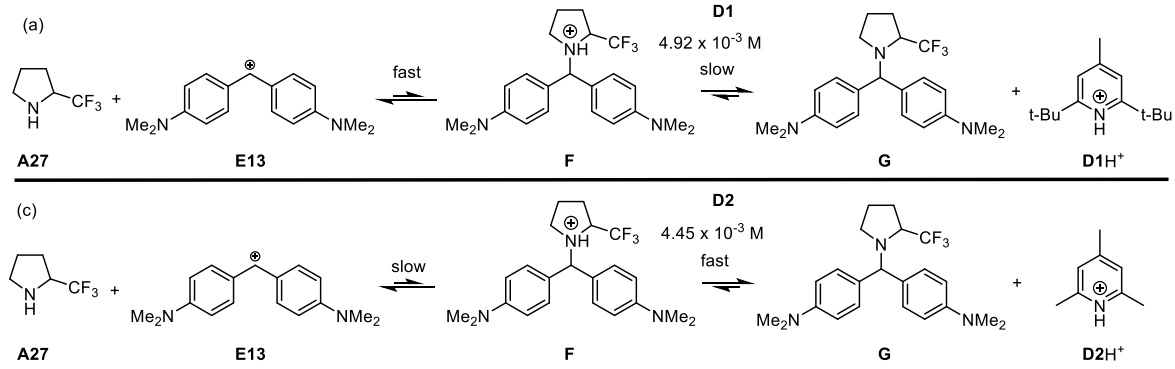

Figure 15. Change of mechanism in the reactions of **A14** with **E13** using **D1** and **D2** as additives

4.5 Kinetic Measurements of the Reactions of Imidazolidinones A29–A32

According to the discussion in 4.4, both steric hindrance and electron withdrawing effects will reduce the Lewis basicity of the amines and lead to kinetics in which deprotonation of the initially formed ammonium ions is rate determining. Imidazolidinones **A29**–**A32** have a sterically hindered reaction center by the substituents neighboring the NH group and are less basic than **A14** (Table 2). As a consequence, even the initial attack of the imidazolidinones at the highly reactive benzhydrylium ions **E17** and **E18** is reversible as illustrated in Figures 16 and 17.

Figure 16a shows traces for three reactions of **A29** with **E18** performed under exactly the same conditions (concentrations etc.), i.e., the kinetics of the reaction of **A30** with **E18** without additives are not reproducible. Figure 16b shows that the benzhydrylium ion **E17** is only consumed to a small extent when combined with 11 equivalents of **A29**.

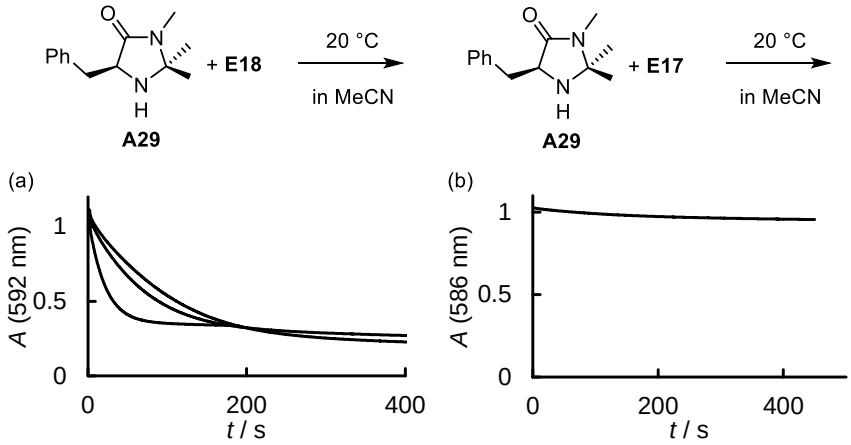

Figure 16. (a) Nonreproducible kinetics of the reactions of **A29** (1.78×10^{-4} M) with **E18** (1.36×10^{-5} M) (b) kinetics of the reaction of **A29** (1.67×10^{-4} M) with **E17** (1.54×10^{-5} M)

In the presence of 9.87×10^{-4} M of **D1**, the reproducibility of the kinetics of the reaction of **A29** with **E18** improved and a linear correlation between k_{obs} and [**A29**] was observed (see 7.2.2). However, in the presence of a similar concentration of **D1** (9.66×10^{-4} M) k_{obs} for the reaction of the better stabilized benzhydrylium ion **E17** with **A29** did not linearly increase with the concentration of **A29** (Fig. 17a). A concentration of 1.18×10^{-3} M of **D2** also was not sufficient to achieve a linear correlation between k_{obs} and [**A29**] for the reaction of **A29** with **E17** (Fig. 17b). Clean second-order kinetics were observed for the reactions of **A29** with **E17**, however, when a high concentration of **D2** (2.33×10^{-3} M) was present (Fig. 17c).

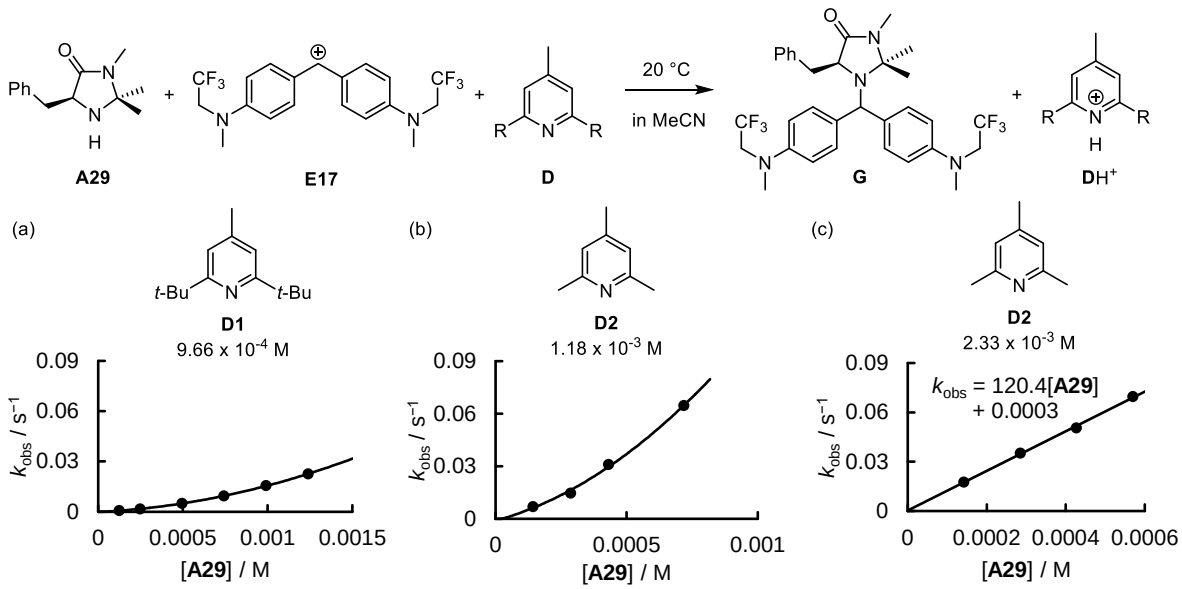

Figure 17. Kinetics of the reactions between **A29** and **E17** (1.01–1.33 × 10^{-5} M) in the presence of the weakly nucleophilic pyridines **D1** and **D2**

4.6 Correlation Analysis

Table 3 summarizes that most reactions of the secondary amines with benzhydrylium ions followed second-order kinetics in acetonitrile in the absence of any additive. As indicated in the last column of Table 3, in several cases 2,4,6-trialkylated pyridines were added in order to get second-order kinetics with rate-determining attack of the amine at the carbenium center.

Figure 18 shows that the second-order rate constants (lgk_2) for the attack of the amines **a** at the electrophiles **E7**–**E13** correlate linearly with the corresponding *E* parameters as required by eq. (3), whereby the slopes correspond to the nucleophile-specific parameter s_N and the intercepts on the abscissa (lgk_2 = 0) represent the nucleophilicity parameters *N* of the secondary amines **A**.

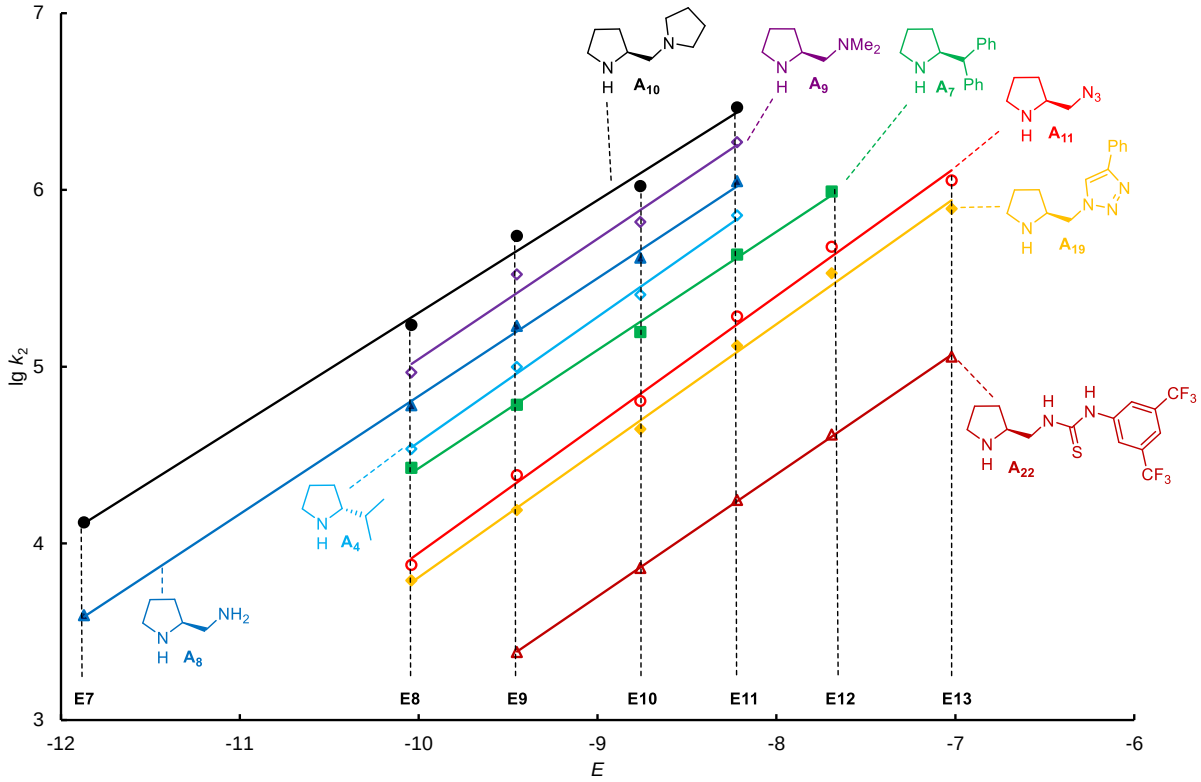

Figure 18. Plot of lgk_2 versus *E* of the reactions of pyrrolidines **A** with reference electrophiles **E** in acetonitrile at 20 °C

The almost parallel correlation lines in Figure 18 (numerically expressed by similar s_N values) illustrates that the relative nucleophilicities of these pyrrolidines are independent of the electrophilicity of the reaction partners. Figure 19 shows, however, that the slopes (≙ s_N) for the pyrrolidines with bulky substituents in 2-position are steeper, i.e. their reactivities are more affected by variation of the reaction partner than the those of ordinary pyrrolidines. All imidazolidinones **A29**–**A32** are less nucleophilic than the

investigated pyrrolidines and have s_N values around 1, in between ordinary pyrrolidines and pyrrolidines with bulky substituents.

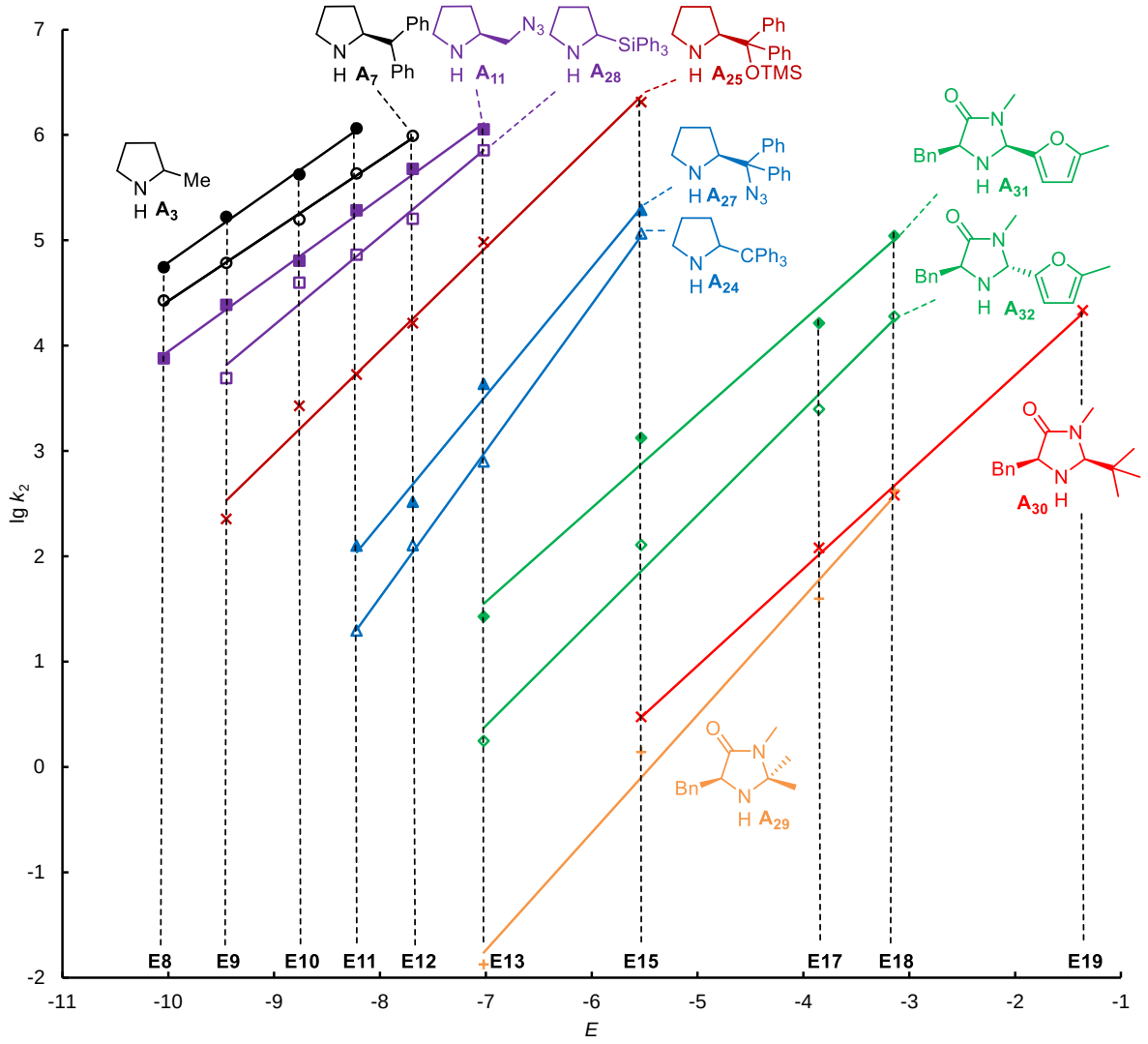

Figure 19. Plot of lgk_2 versus E of the reactions of pyrrolidines carrying bulky substituents in 2-position and imidazolidinones with reference electrophiles **E** in acetonitrile at 20 °C

Table 3. Nucleophilicity determination of the investigated amines A

Amines	Electrophiles	k_2 ($M^{-1}s^{-1}$)	Aditives	N	s_N
A1	**E2**	no reaction		19.95	0.68
	E3	2.53×10^3			
	E4	4.77×10^3			
	E5	4.09×10^4			
	E6	1.39×10^5			
	E7	2.31×10^5			
	E8	6.41×10^6			

 A2	**E1**	3.25 × 10^{1} [a]	18.58	0.61
	E2	4.82 × 10^{1} [a]		
	E3	not linear		
	E4	not linear		
	E5	2.12 × 10^{3}		
	E6	6.31 × 10^{3}		
	E7	1.09 × 10^{4}		
	E8	1.18 × 10^{5} [a]		
	E9	3.50 × 10^{5} [a]		
	E10	1.06 × 10^{6}		
	E11	2.78 × 10^{6}		
 A3	**E8**	5.53 × 10^{4}	16.78	0.71
	E9	1.67 × 10^{5}		
	E10	4.22 × 10^{5}		
	E11	1.15 × 10^{6}		
 A4	**E8**	3.42 × 10^{4}	16.44	0.71
	E9	9.94 × 10^{4}		
	E10	2.55 × 10^{5}		
	E11	7.18 × 10^{5}		
 A5	**E9**	2.72 × 10^{3}	13.96	0.76
	E10	7.89 × 10^{3}		
	E11	2.46 × 10^{4}		
	E12	7.18 × 10^{4}		
	E13	1.78 × 10^{5}		
	E14	1.33 × 10^{6}		
 A6	**E8**	7.21 × 10^{4}	17.43	0.66
	E9	2.29 × 10^{5}		
	E10	4.51 × 10^{5}		
	E11	1.33 × 10^{6}		
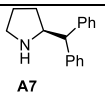 A7	**E8**	2.67 × 10^{4}	16.61	0.67
	E9	6.08 × 10^{4}		
	E10	1.57 × 10^{5}		
	E11	4.30 × 10^{5}		
	E12	9.80 × 10^{5}		
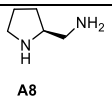 A8	**E7**	3.92 × 10^{3}	17.24	0.67
	E8	6.03 × 10^{4}		
	E9	1.70 × 10^{5}		
	E10	4.14 × 10^{5}		
	E11	1.12 × 10^{6}		
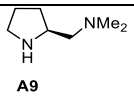 A9	**E8**	9.25 × 10^{4}	17.41	0.68
	E9	3.32 × 10^{5}		
	E10	6.58 × 10^{5}		
	E11	1.86 × 10^{6}		

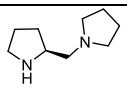 A10	**E7**	1.31×10^4		18.33	0.64
	E8	1.72×10^5			
	E9	5.48×10^5			
	E10	1.05×10^6			
	E11	2.93×10^6			
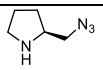 A11	**E8**	7.54×10^3		15.43	0.73
	E9	2.43×10^4			
	E10	6.38×10^4			
	E11	1.92×10^5			
	E12	4.76×10^5			
	E13	1.13×10^6			
 A12	**E8**	2.90×10^4		16.74	0.67
	E9	7.89×10^4			
	E10	2.02×10^5			
	E11	4.98×10^5			
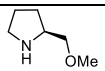 A13	**E8**	3.60×10^4		16.50	0.71
	E9	1.10×10^5			
	E10	2.63×10^5			
	E11	7.69×10^5			
 A14	**E13**	1.45×10^3	D2	11.34	0.73
	E15	1.91×10^4	D1		
	E17	2.27×10^5	D1		
	E18	1.21×10^6			
 A15	**E8**	6.57×10^3		14.75	0.82
	E9	2.47×10^4			
	E10	7.00×10^4			
	E11	2.21×10^5			
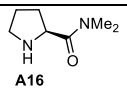 A16	**E8**	1.08×10^5		17.61	0.67
	E9	3.70×10^5			
	E10	7.67×10^5			
	E11	2.04×10^6			
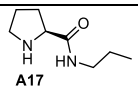 A17	**E9**	1.68×10^4		15.20	0.73
	E10	3.87×10^4			
	E11	1.17×10^5			
	E12	3.04×10^5			
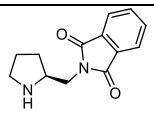 A18	**E8**	3.33×10^4		15.90	0.77
	E9	8.06×10^4			
	E10	2.77×10^5			
	E11	7.35×10^5			
	E12	2.06×10^6			
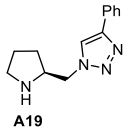 A19	**E8**	6.16×10^3		15.32	0.72
	E9	1.54×10^4			
	E10	4.42×10^4			
	E11	1.31×10^5			
	E12	3.37×10^5			
	E13	7.81×10^5			

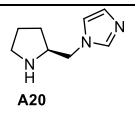 A20	**E8**	5.39×10^3		15.55	0.69
	E9	1.83×10^4			
	E10	3.66×10^4			
	E11	1.18×10^5			
	E12	2.77×10^5			
	E13	6.28×10^5			
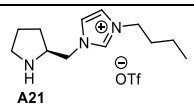 A21	**E13**	2.97×10^3		13.57	0.53
	E14	$2.11 \times 10^{4\,b}$			
	E15	1.49×10^4			
	E16	$1.20 \times 10^{5\,b}$			
	E17	1.33×10^5			
	E18	3.09×10^5			
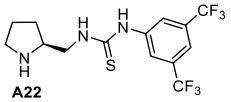 A22	**E8**	2.42×10^3		14.97	0.69
	E9	7.25×10^3			
	E10	1.76×10^4			
	E11	4.11×10^4			
	E12	1.14×10^5			
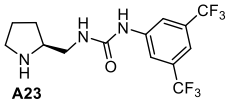 A23	**E8**	5.44×10^4		17.50	0.64
	E9	1.45×10^5			
	E10	3.68×10^5			
	E11	8.11×10^5			
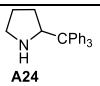 A24	**E11**	1.97×10^1	**D1**	9.16	1.39
	E12	1.27×10^2	**D1**		
	E13	7.92×10^2	**D1**		
	E15	1.16×10^5	**D1**		
	E15	$1.14 \times 10^{5\,c}$			
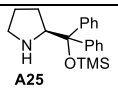 A25	**E9**	2.26×10^2	**D1**	12.03	0.98
	E10	2.67×10^3	**D1**		
	E11	5.30×10^3	**D1**		
	E12	1.63×10^4	**D1**		
	E13	9.65×10^4			
	E15	2.05×10^6			
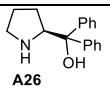 A26	**E9**	5.48×10^3		16.18	0.56
	E10	1.22×10^4			
	E11	3.57×10^4			
	E12	7.50×10^4			
	E13	1.72×10^5			
	E15	$7.64 \times 10^{5\,c}$			
	E15	8.02×10^5	**D1**		
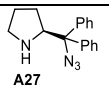 A27	**E11**	1.26×10^2	**D2**	9.90	1.22
	E12	3.29×10^2	**D2**		
	E13	4.33×10^3	**D2**		
	E13	$4.37 \times 10^{3\,c}$	**D1**		
	E15	1.94×10^5			

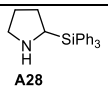 A28	**E9**	4.90×10^{3}	**D1**	14.00	0.84
	E10	3.96×10^{4}	**D1**		
	E10	4.14×10^{4} [c]			
	E10	4.02×10^{4} [c]	**D1**		
	E11	7.29×10^{4}			
	E12	1.60×10^{5}			
	E13	7.15×10^{5}			
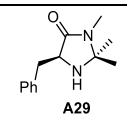 A29	**E15**	2.99	**D2**	6.04	0.92
	E17	1.20×10^{2}	**D2**		
	E18	3.79×10^{2}	**D1**		
	E19	2.16×10^{4}			
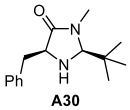 A30	**E13**	1.33×10^{-2}	**D2**	5.44	1.12
	E15	1.38	**D2**		
	E17	3.94×10^{1}	**D2**		
	E18	4.24×10^{2}	**D1**		
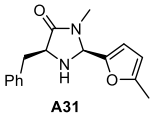 A31	**E13**	2.68×10^{1}	**D2**	8.76	0.89
	E15	1.33×10^{3}	**D2**		
	E17	1.63×10^{4}	**D2**		
	E18	1.10×10^{5}	**D1**		
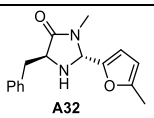 A32	**E13**	1.76	**D2**	7.39	1.00
	E15	1.28×10^{2}	**D2**		
	E17	2.48×10^{3}	**D2**		
	E18	1.89×10^{4}	**D1**		

[a]: literature reported date[63] [b]: Second-order rate constants k_2 for the reactions of **A21** with **E14** and **E16** were not used for the determination of the N and sN parameters. [c]: Comparative measurements of the Second-order rate constants k_2 under different conditions of additives (concentrations of additives see 7.2).

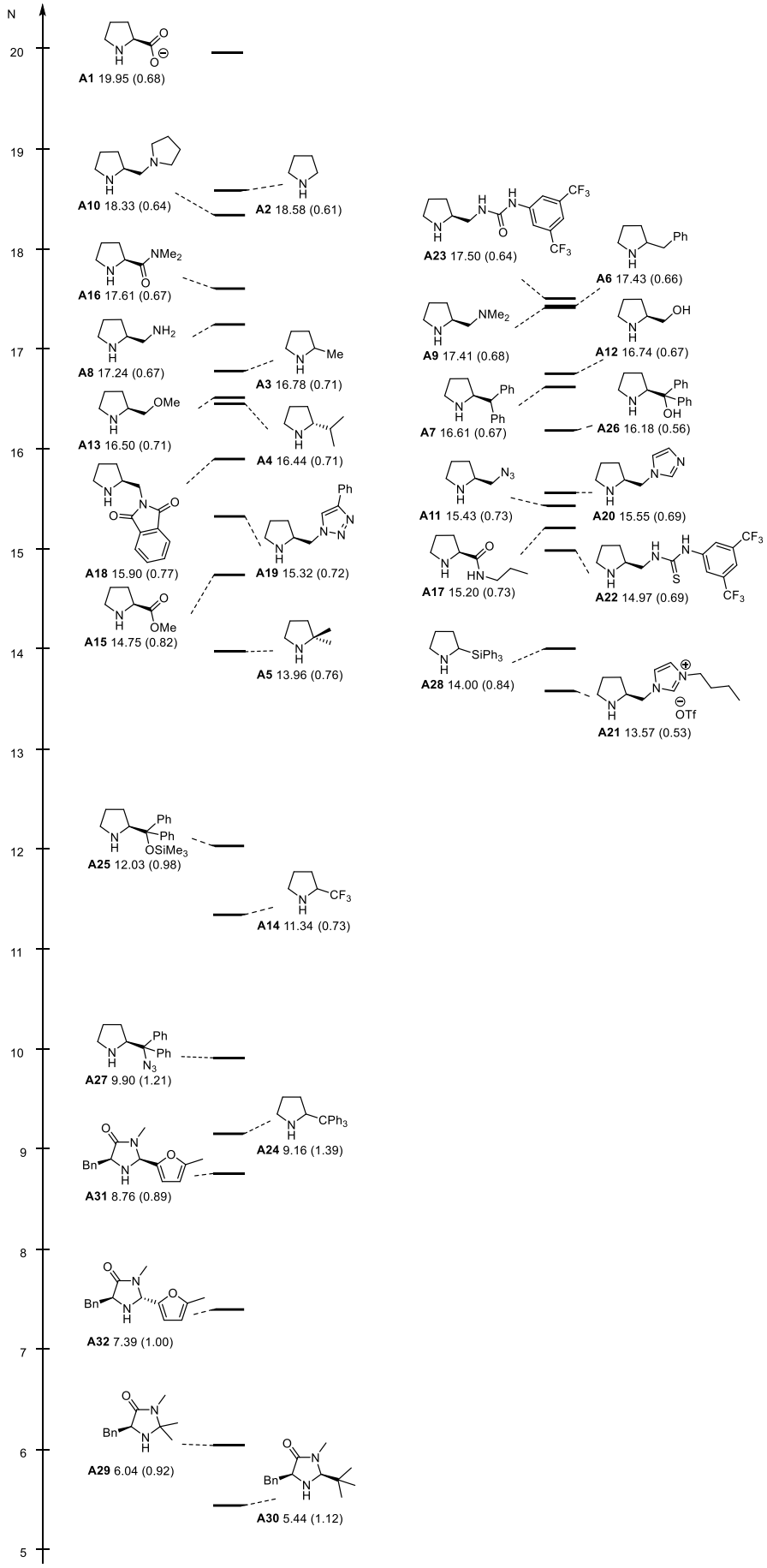

Figure 20. Reactivity parameters for 2-substituted pyrrolidines and imidazolidinones in acetonitrile

Chapter 5: Discussion

Correlations between nucleophilic reactivities and Brønsted basicities (so-called Brønsted correlations) have been a main topic of Physical Organic Chemistry since the 1930s. It is well known that seperate lg*k* vs. pK_{aH} correlations are obtained when the nature of the central atom of the nucleophiles is varied.[66] However, in recent work we reported that lg*k* vs. pK_{aH} correlations are even very poor when only *N*-centered nucleophiles of different structures are considered.[63, 67]

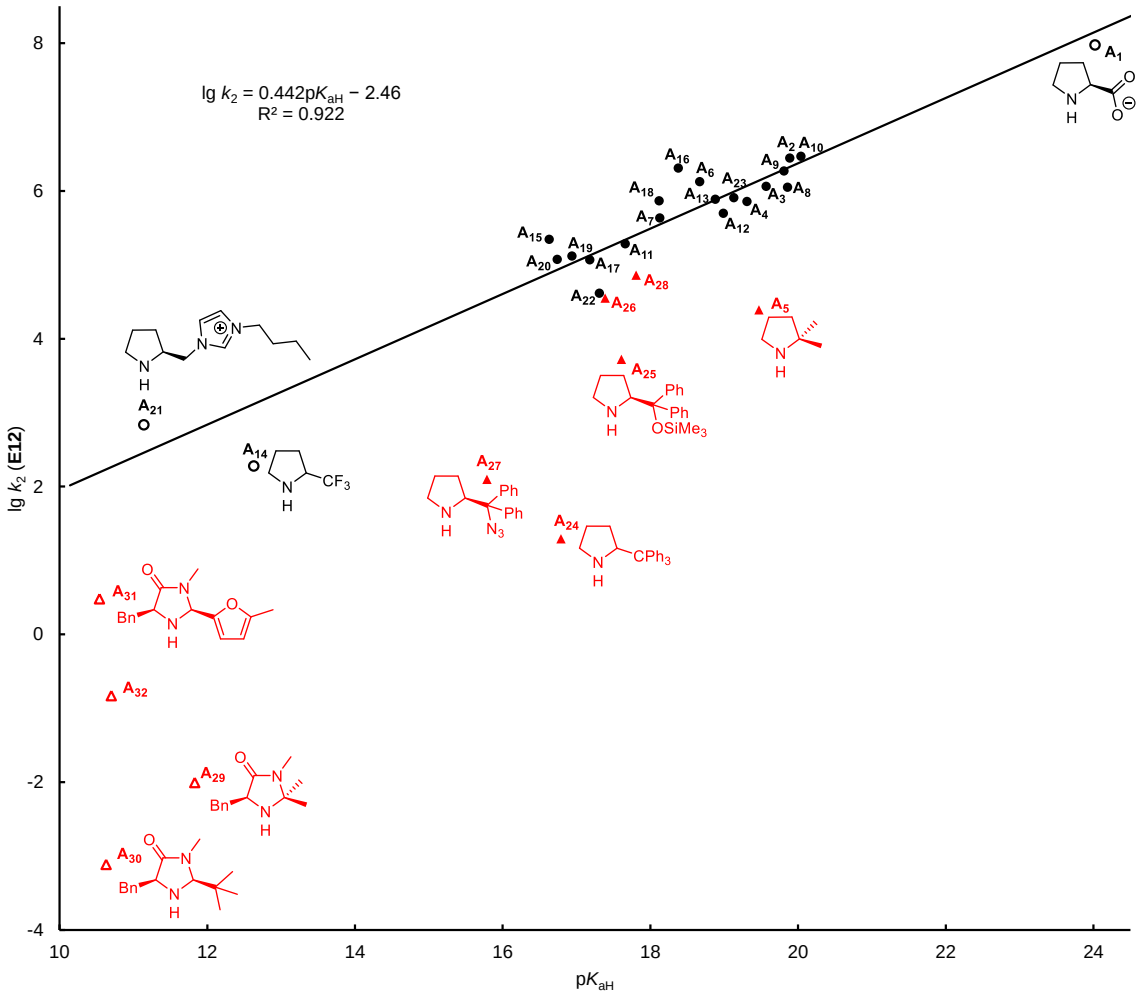

Figure 21. Plot of the rate constants for the reactions of **A** with **E11** versus their Brønsted basicities The correlation line is based on the reactivities of pyrrolidines identified by circles (i.e. excludes pyrrolidines with bulky substituents and imidazolidinones). Rate constants characterized by open symbols were calculated by eq. (3) because their direct measurement is not possible due to the lacking thermodynamic driving force or their extremely high speed (**A1**).

Because of the wide structural variation of the pyrrolidines (**A1**–**A28**) and imidazolidinones (**A29**–**A32**), it is not possible to select a single reference electrophile for the characterization of the nucleophilic reactivities of all investigated amines (**A1**–**A32**). In order to compare nucleophiles of widely differing reactivities, we have generally regarded

the nucleophilicity parameter *N* as defined by eq. (3). Table 2 shows, however, that several of the secondary amines have widely differing s_N values with the consequence that their *N* values may differ significantly even if similar rate constants have been measured in reactions with certain electrophiles. For that reason, we have plotted the rate constants for the reactions of the amines **A1**–**A32** with benzhydrylium ion **E11** against the corresponding pK_{aH} values in Figure 21. The open symbols in Figure 21 refer to the rate constants which have not been directly measured but were calculated by eq. (3). The reliability of these extrapolations is justified by the high quality of the correlations in Figures 18 and 19.

The correlation line drawn in Figure 21 shows a fair correlation (R^2 = 0.92) between the rate constants of the reactions of the 2-substituted pyrrolidines represented by circles with benzhydrylium ion **E11**, while pyrrolidines with bulky substituents (represented by triangles) are excluded. From the Brønsted coeffient of this correlation one can see that 44% of the differences in basicity are reflected in the transition states of their reactions with **E11**. Figure 21 furthermore shows that the trityl-(**A24**) and azidodiphenylmethyl-substituted pyrrolidines (**A27**) react 2–3 orders of magnitude more slowly than ordinary pyrrolidines of comparable basicity. Obviously the steric retardation is much smaller for the Hayashi-Jørgensen catalyst **A25**, which is located only by a factor of 40 below the correlation line. The nucleophilicities of the diphenylprolinol **A26** and triphenylsilyl-substituted pyrrolidine **A28** are only marginally smaller than expected from their basicities.

The imidazolidinones **A29**–**A32** (represented by open triangles) react much more slowly than all pyrrolidines included in this investigation. This can only partially be due to their lower basicity, since the pyrrolidine **A21**, which has a similar basicity reacts much faster. Obviously, steric retardation is most effective in the reactions of MacMillan generation 2 catalyst **A31**, followed by MacMillan generation 1 catalyst **A29**. Steric effects also retard the reactions of the 2-furyl substituted imidazolidinones **A30** and **A31**, among which the trans-isomer is 20-times less reactive because there is a substituent on both faces of the 5-membered ring.

A different analysis of steric effects on nucleophilic reactivities can be based on the comparison of pyrrolidines **A2, A3,** and **A5**. Table 4 and Figure 22 show that one 2-methyl group reduces Brønsted basicity and nucleophilic reactivity by a factor of 2, which may be assigned to a statistical effect. While the second 2-CH_3 group has almost

no effect on basicity, the nucleophilic reactivity towards benzhydrylium ions is reduced by approximately two orders of magnitude.

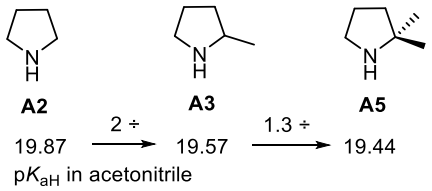

Figure 22. Comparison of the Brønsted basicities of **A2, A3**, and **A5**

Table 4. Comparison of the second order rate constants k_2 ($M^{-1}s^{-1}$) for the reactions of **A2, A3** and **A5** with electrophiles **E8**-**E11**

k_2	**A2**	**A3**	**A5**
E8	1.18×10^5	5.53×10^4	-
E9	3.50×10^5	1.67×10^5	2.72×10^3
E10	1.06×10^6	4.22×10^5	7.89×10^3
E11	2.78×10^6	1.15×10^6	2.46×10^4

Since 2-methyl-pyrrolidine **A3** and 2-isopropyl-pyrrolidine **A4** have similar basicities and nucleophilicities, we can conclude that the differences between the 2-monosubstituted pyrrolidines characterized by circles in Figure 21 are predominantly due to electronic effects.

As a consequence, the basicities (Figures 23 and 24 left) as well as the rate constants for the reactions of these pyrrolidines (systems with bulky substituents in 2-position excluded) with reference electrophile **E11** (Figures 23 and 24 right) correlate fairly with the Hammett σ_m parameters[68] of the 2-substituents.

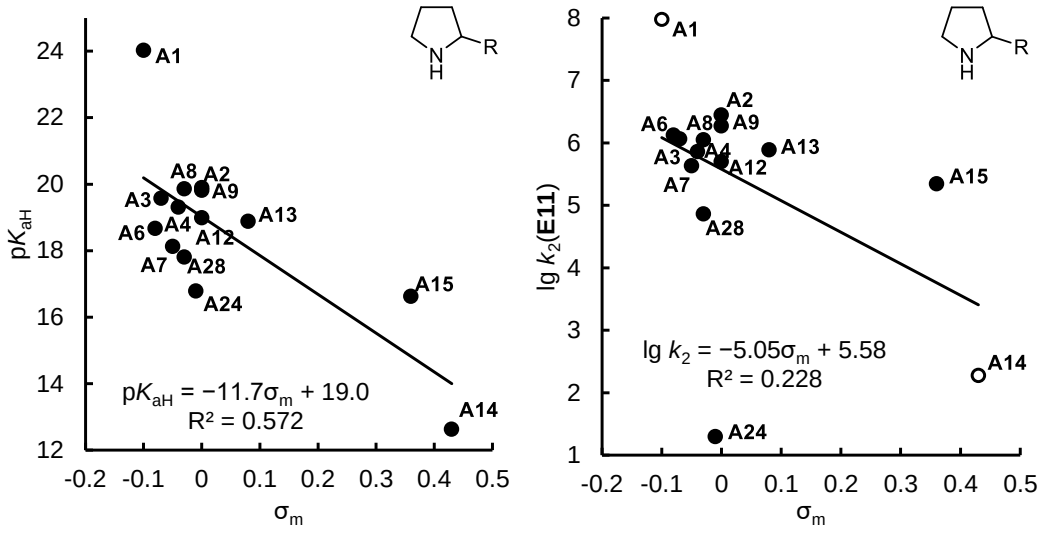

Figure 23. Hammett plot between pK_{aH} and σ_m of substituents at C-2 positon of pyrrolidine ring (left); Hammett plot between the rate constants for the reactions of **A** with **E11** and σ_m of substituents at C-2 positon of pyrrolidine ring (right).

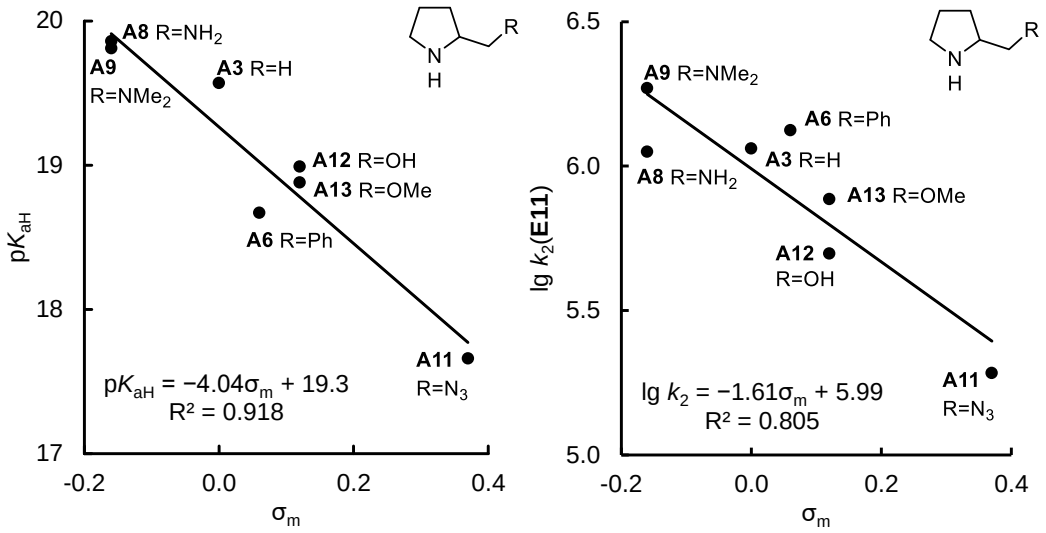

Figure 24. Hammett plot between pK_{aH} and σ_m of substituents at pyrrolidin-2-ylmethyl positon (left); Hammett plot between the rate constants for the reactions of **A** with **E11** and σ_m of substituents at pyrrolidin-2-ylmethyl positon (right)

The corresponding Hammett ρ values for the rate constants (−5.05 in Fig. 23 and −1.61 in Fig. 24) are somewhat smaller than those for the correlations of pK_{aH} with σ_m (−11.7 in Fig. 23 and −4.04 in Fig. 24). The much lower quality of the correlations for the pyrrolidines with substituents at C-2 position of pyrrolidine ring (Fig. 23) compared to the plots in Fig. 24 indicates that other effects (steric effect, etc.) beyond electric effect play a more important role when the substituents are located closer to the react center nitrogen atom. We have also analyzed to corresponding correlations with Taft's aliphatic substituent constants σ^{*}[68b]. Figures 25 and 26 show that these correlations are of similar quality, we have not pursued these correlations further.

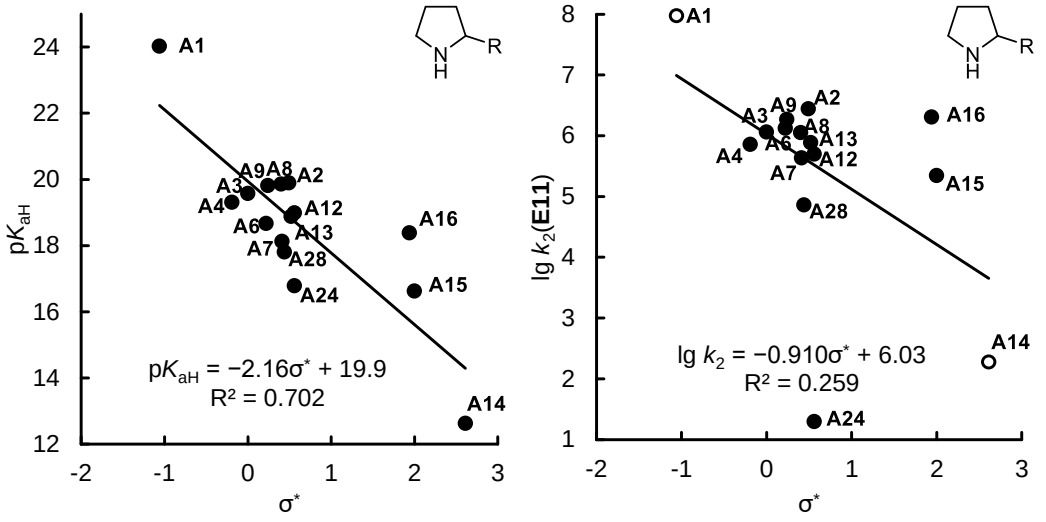

Figure 25. Taft plot between pK_{aH} and σ^{*} of substituents at C-2 positon of pyrrolidine ring (left); Taft plot between the rate constants for the reactions of **A** with **E11** and σ^{*} of substituents at C-2 positon of pyrrolidine ring (right)

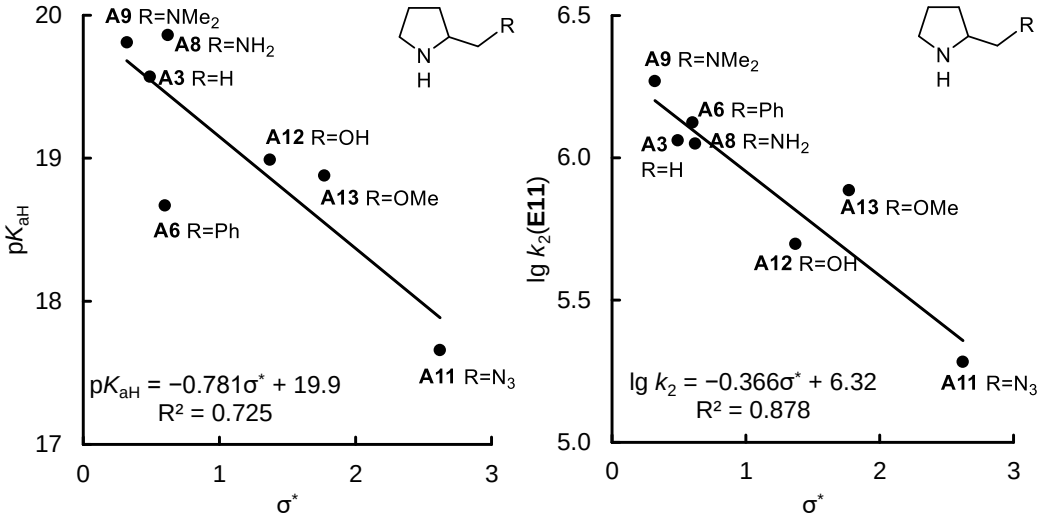

Figure 26. Taft plot between pK_{aH} and σ^* of substituents at pyrrolidin-2-ylmethyl positon (left); Taft plot between the rate constants for the reactions of **A** with **E11** and σ^* of substituents at pyrrolidin-2-ylmethyl positon (right)

Though alkyl carboxylates are stronger bases in acetonitrile [pK_a(CH_3CO_2H) = 23.51] than 2-substituted pyrrolidine **A3** [pK_a(**A3**H^+) = 19.57] (Fig. 27), protonation of **A1** occurs at nitrogen to give a zwitterion, as shown in the crystal structure of 4-hydroxyproline*[69]. The short distance between H1 and O1 marked in Figure 28 stabilizes the zwitterion and explains, why the prolinate anion **A1** is a stronger Brønsted base as well as a stronger nucleophile than the parent pyrrolidine.

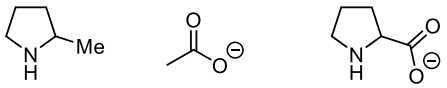

	A3		**A1**
pK_{aH}	19.57	23.51	24.02
$N(s_N)$	16.78(0.71)	16.90(0.75)*	19.95(0.68)
k_{rel}	1.0	2.8	82

Figure 27. Comparison of the Brønsted Basicity and Nucleophilicity (k_{rel} vs **E11**) of the Prolinate Anion and its Building Blocks (Acetonitrile, 20 °C)[58,70] *measured at 25 °C

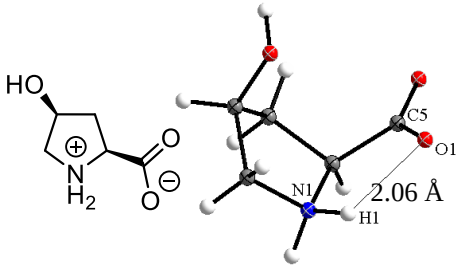

Figure 28. Single crystal structure of 4-hydroxyproline[69]

As shown in Figure 29, the amino-substituted pyrrolidines **A8–A10** are slightly stronger Brønsted bases than 2-methyl pyrrolidine (**A3**), whereas the hydroxyl and

* Crystal structure of the parent proline generally include an additional HCl molecule.[71]

methoxyl-substituted pyrrolidine **A12** and **A13** are slightly weaker Brønsted bases. Their reactivities toward electrophile **E11** differ only slightly. While the aminomethyl-substituted pyrrolidine **A8** is a marginally stronger Brønsted base than the dimethylaminomethyl-substituted pyrrolidine **A9**, the nucleophilic reactivity of **A8** is smaller than that of **A9**. Analogonsly, the hydroxylmethyl-substituted pyrrolidine **A12** is a stronger Brønsted base than methoxylmethyl-substituted pyrrolidine **A13**, whereas the nucleophilic reactivity of **A12** is smaller than that of **A13**.

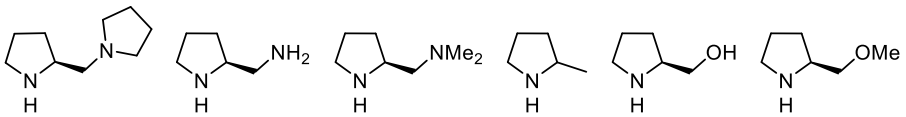

	A10	**A8**	**A9**	**A3**	**A12**	**A13**
pK_{aH}	20.04	19.86	19.81	19.57	18.99	18.88
k_{rel}	2.5	0.97	1.6	1.0	0.43	0.67

Figure 29. Comparison of Brønsted basicities and rate constants for the reactions of 2-substituted pyrrolidines with **E11** in acetonitrile at 20 °C

The unexpected observation that the less basic *N,N*-dimethylamino-substituted pyrrolidine **A16** has a similar nucleophilic reactivity as the *N,N*-dimethylaminomethyl substituted pyrrolidine **A9** (Figure 30) can be assigned to intramolecular hydrogen bridge in the ammonium ion initially formed during electrophilic attack at **A16**. This bond is marked in the structurally related tripeptide in Figure 31. The corresponding interactions with the secondary amide in **A17** and the ester **A15** are obviously less important.

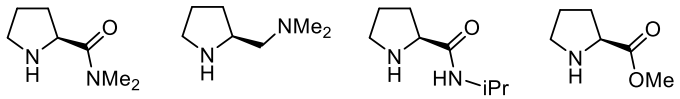

	A16	**A9**	**A17**	**A15**
pK_{aH}	18.38	19.81	17.18	16.63
k_2(with **E11**, $M^{-1}s^{-1}$)	2.04×10^6	1.86×10^6	1.17×10^5	2.21×10^5

Figure 30. Comparison of basicities and nucleophilic reactivities towards **E11** of **A15–A17** and **A9**

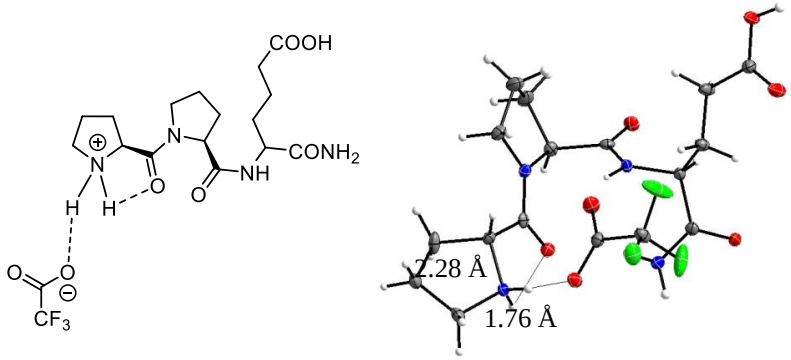

Figure 31. Single crystal structure of tripeptide[72]

Figure 32 shows that the aryl urea-substituted pyrrolidine **A23** has a slightly weaker Brønsted basicity and nucleophilic reactivity than 2-methyl-pyrrolidine (**A3**), whereas the

change from the urea to the thiourea derivative **A22** reduces the Brønsted basicity and nucleophilic reactivity by two orders of magnitude. The phthalimidyl-substituted pyrrolidine **A18** is one order of magnitude less basic than **A23**, while their nucleophilic reactivity is similar. 1,2,3-Triazole- and 1-imidazole-substituted pyrrolidines **A19** and **A20** have similar Brønsted basicities and nucleophilic reactivities, whereas butylation of imidazole (**A21**) reduces the Brønsted basicity by 5.6 orders of magnitude and the nucleophilic reactivity by a factor of 172. Trifluoromethyl-substituted pyrrolidine **A14** is 31 times more basic but 4 times less nucleophilic than **A21**.

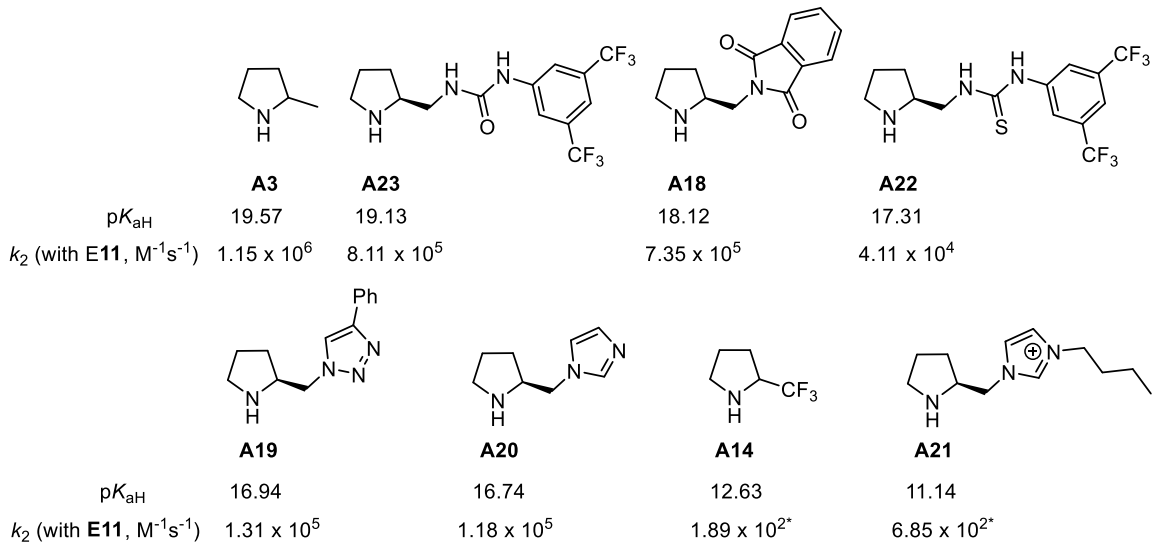

Figure 32. Comparison of the Brønsted basicities of pyrrolidines **A3**, **A14** and **A18**–**A23** the rate constants of their reactions with **E11** in acetonitrile at 20 °C

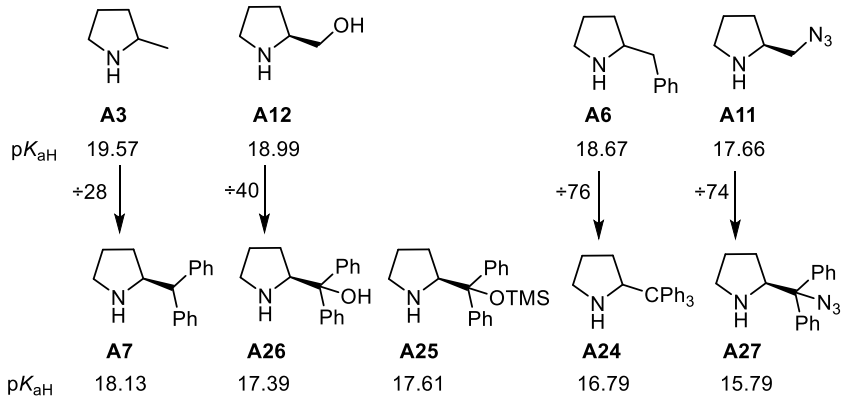

Figure 33. Comparison for the Brønsted basicity decrease (in acetonitrile) by introduction of two phenyl groups

Comparison of the Brønsted basicities of the pyrrolidines in the upper line of Figure 33 with those in the bottom line shows that introduction of two phenyl groups in the side chain reduces the basicity by one to two orders of magnitude. Comparison of **A6** and **A7** shows that the change from benzyl to benzhydryl substitution reduces the basicity by a

factor of three, whereas the trityl group reduces the basicity by fast 2 orders of magnitude relative to **A6**.

The analogous substituent effects on nucleophilic reactivities are shown in Figure 34 for the reactions of amines **a** with electrophile **E11**. The benzhydryl-substituted pyrrolidine **A7** is 2.7 times less nucleophilic than 2-methylpyrrolidine (**A3**), whereas the diphenylhydroxymethyl group reduces the reactivity by one order of magnitude more than hydroxylmethyl group (**A26** vs **A12**). Large steric effects on nucleophilic reactivities are found in the comparison **A24**/**A6** (factor 6750) and **A27**/**A11** (factor 1520).

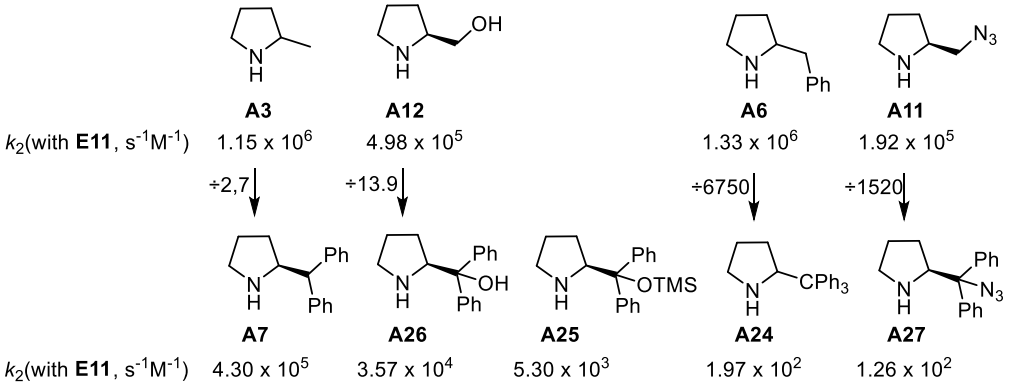

Figure 34. Comparison for the second order rate constants of the reactions of **A** with **E11** by introduction of two phenyl groups

Figure 35 shows that the basicities of the 2-alkyl-substituted pyrrolidines correlate fairly with Taft's steric parameters E_s.[68b]

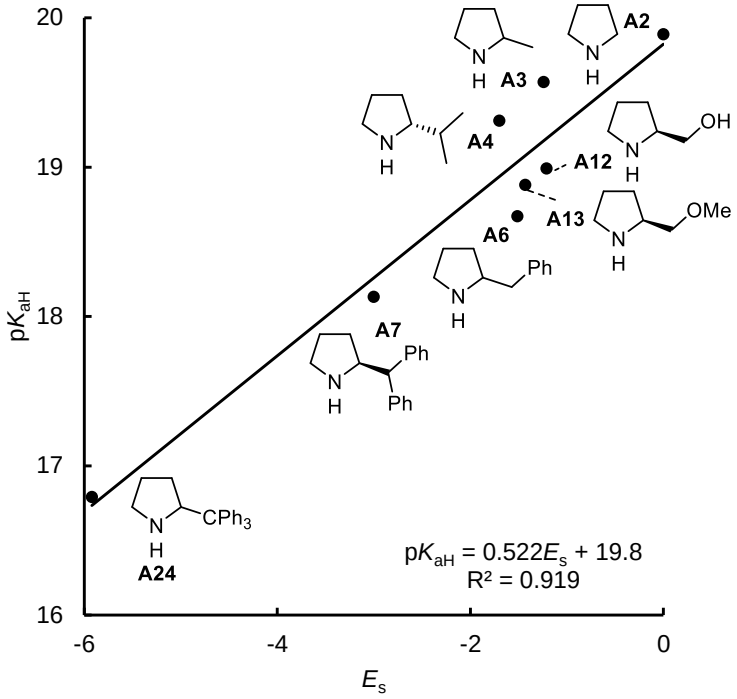

Figure 35. Correlation between pK_{aH} and E_s of substituted pyrrolidines

Figure 36 shows crystal structures of pyrrolidines with bulky groups in 2-position.

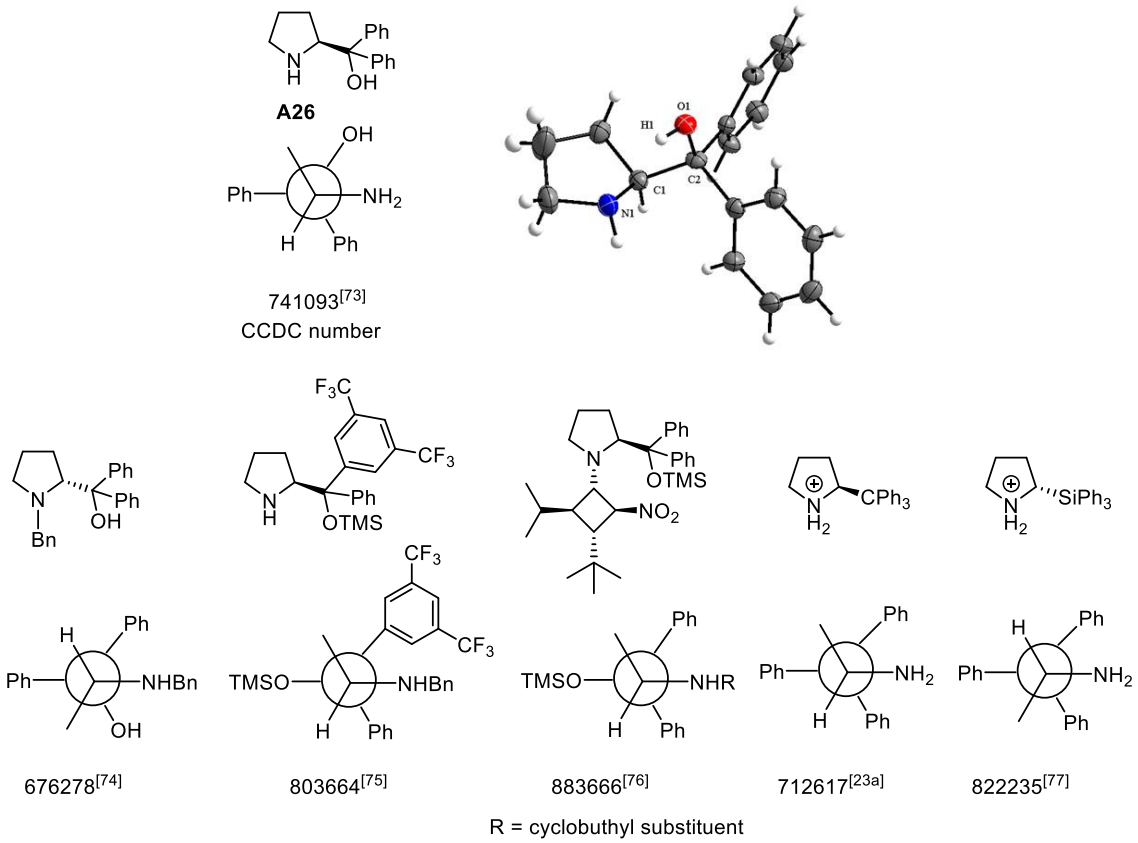

Figure 36. Crystal structures (with CCDC numbers) of pyrrolidines with bulky substituents in 2-position

Whereas the amino group in the four structures on the right is schielded by two gauche aryl groups, the intramolecular hydrogen bridge (N1–H1–O1) fixes the OH-group in gauche position to the amno group and thus accounts for the weaker reduction of nucleophilic reactivity of **A26** (Fig. 34).

The imidazolidinones **A29**–**A32** can be looked at as 2-amido substituted pyrrolidines (Scheme 12).

Scheme 12. Comparison of Brønsted basicities and rate constants ($M^{-1}s^{-1}$) of the reactions of **A16** and **A29**–**A32** with **E11** in acetonitrile at 20 °C

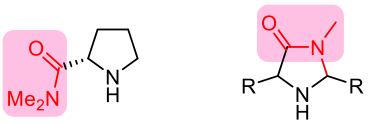

	A16	**A29–A32**
pK_{aH}	18.38	10.5 to 11.8
log k_2(with **E11**)	6.31	–3.10 to +0.48

Scheme 12 illustrates that the marked in-plane dialkylamido group in the imidazolidinones **A29**–**A32** reduces basicity by 7–8 pK_a units and nucleophilic reactivity by 6–9 orders of magnitude compared to **A16**, which indicates that the in plane *N,N*-dialkylamido group in the imidazolidinones is a much stronger electron acceptor than the *N,N*-dialkylamido group in 2-position of the pyrrolidine **A16.**

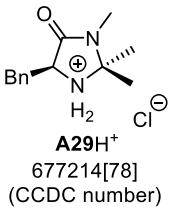

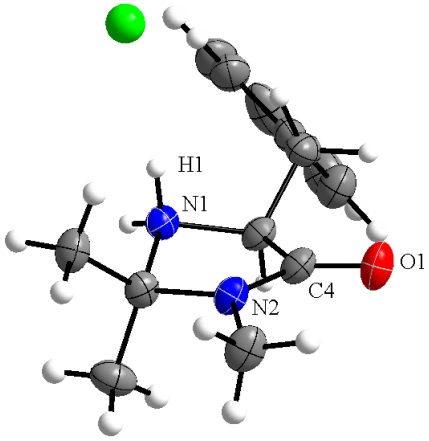

Figure 37. Crystal structure of protonated **A29**

The planar arrangement of the amido group may lead to an interaction of the nitrogen lone pair of the NH group with the π* orbital of the carbonyl group and thus reduce basicity and nucleophilicity of imidazolidinones (Crystal structure of **A29**H^+ in Fig. 37 shows the angle between N1–H1 and the plane N2–C4–O1 is 88.7° and the distance from N1 to N2–C4 is 2.2 Å). In addition, the two nitrogen atoms in **A29**–**A32** are in geminal position and may undergo different anomeric interactions in the nonprotonated and protonated imidazolidinones.

Figure 38 shows the intersection of the extrapolated correlation lines of Figure 19 with the horizontal line at lgk_2 = 9, i.e. where the reactions become diffusion–controlled (called E_{diff}). One can see that the ordering of these intersections reflects the relative pK_{aH} values of the amines.

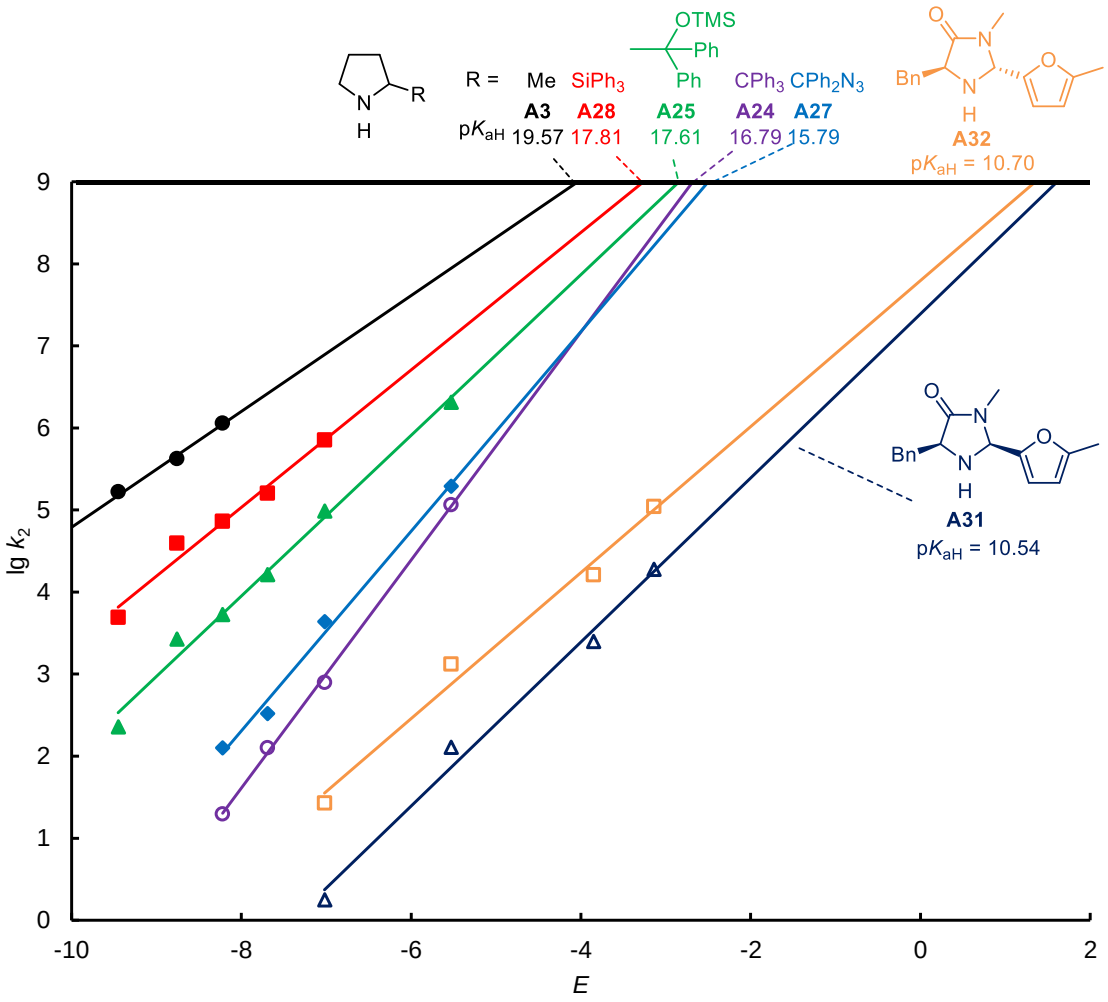

Figure 38. Extrapolations of the lgk_2 vs E correlations to the diffusion limit (k_2 = 10^9 Lmol^{-1}s^{-1})

A plot of these intersections (E_{diff}) against the Brønsted basicities of pyrrolidines and imidazolidinones (Fig. 39) shows a much better correlation than the analogous plot in Figure 21, from which only C2-disubstituted compounds (**A5**, **A29**) and the amines with small s_N parameter (0.56 for **A26**, 0.53 for **A21**) deviate. The origin of this correlation has so far not been understood.

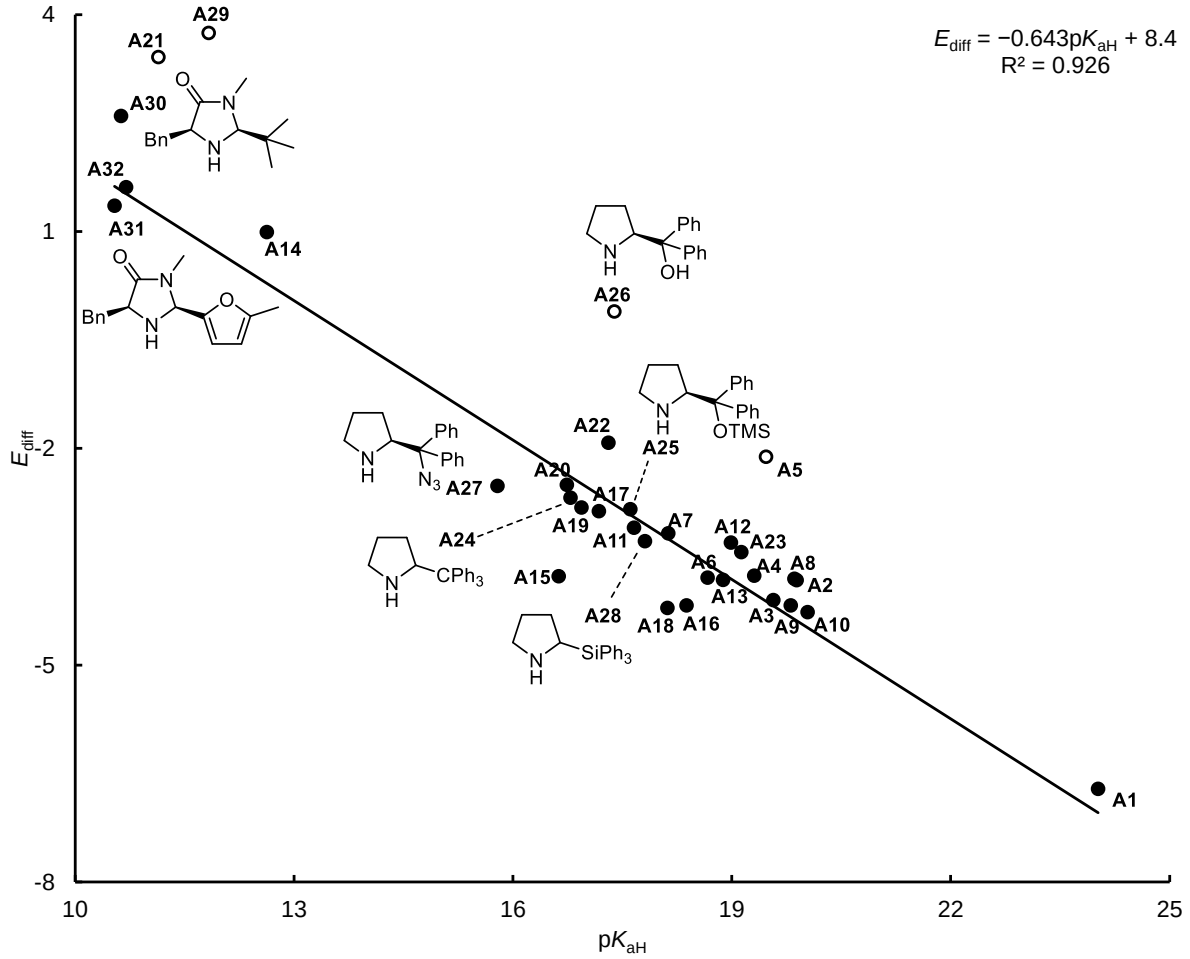

Figure 39. Correlation between Brønsted basicity of secondary amines and their E_{diff} values

Chapter 6: Conclusion

The kinetic and thermodynamic data presented in this investigation can be used for optimizing the conditions for reactions catalyzed by secondary amines. The low nucleophilicities of the imidazolidinones, shown in Fig. 20 explain, for example, why they generally do not react with nonactivated carbonyl groups and require the presence of Brønsted acids, most commonly trifluoroacetic acid. Fine-tuning of the Brønsted acids is now possible by consideration of the pK_a values of the cocatalyzing Brønsted acids and the electrophilicity of the carbonyl substrate. On the other hand, many pyrrolidines are much more nucleophilic than the imidazolidinones and may react with carbonyl compounds without Brønsted acid activation. Brønsted acids may even be detrimental because they deactivate the pyrrolidines by protonation.

The analysis of steric and electronic substituent effects on nucleophilicity and basicity presented in this work can furthermore be used as a guide for designing organocatalysts with new structural motives.

Chapter 7 Experiment

7.1 Synthesis and Analytics

7.1.1 General

7.1.1.1 Analytics

^{1}H NMR and ^{13}C NMR spectra were measured on Bruker Avance 400 MHz, Varian 600 MHz, or Bruker Avance 800 MHz spectrometers. The ^{1}H and ^{13}C NMR chemical shifts (δ) are given in ppm and calibrated to residual solvent peaks. Coupling constants are given in Hz. Multiplicities are abbreviated as follows: s = singlet, d = doublet, t = triplet, q = quartet, pent = pentet, sext = sextet, m = multiplet and br = broad. The assignments of individual NMR signals were based on additional 2D-NMR experiments (gHSQC, gHMBC, and NOESY). HRMS spectra were determined on a Finnigan MAT 95 mass spectrometer. IR spectra were recorded on a FTIR Spectrometer SPECTRUM BX II (Perkin Elmer).

7.1.1.2 Synthesis

Flash column chromatography was performed on Merck silica gel 60 (0.040–0.063 mm) or Sigma-Aldrich aluminium oxide 90 active neutral (0.063–0.200 mm) using compressed air. Thin layer chromatography (TLC) was performed using Merck silica gel 60 F254 aluminum plates. Eluted plates were visualized using a 254 nm UV lamp and/or by treatment with a suitable stain followed by heating. Concentration under reduced pressure was performed on a rotary evaporator with a water bath temperature of 40 °C. Starting materials and reagents were purchased from Sigma-Aldrich or ABCR and were used as supplied or, in the case of some liquids, distilled. Solvents were distilled or dried prior to use over appropriate drying agents: dichloromethane (calcium hydride), diethyl ether (sodium/benzophenone), tetrahydrofuran (sodium/benzophenone), toluene (sodium hydride), and acetonitrile (phosphorus pentoxide). Solvents for filtration, chromatography, and recrystallization were purchased from Fisher and used as received.

Pyrrolidine (**A2**) was purchased (ABCR) and freshly distillated over calcium hydride. Pyrrolidine **A6** was purchased (ABCR) and used as received.

L-Valinol was synthesized by a procedure reported by Mckennon.[44]

N-Boc-L-prolinol and 1-Boc-2-(*S*)-pyrrolidinylmethyl *p*-toluenesulfonate were prepared according to a literature procedure.[34]

1-Benzyl 2-(4-nitrophenyl) (*S*)-pyrrolidine-1,2-dicarboxylate was synthesized by a procedure reported by Diakos.[42]

tert-Butyl pyrrolidine-1-carboxylate (*N*-Boc pyrrolidine) was prepared following the literature procedure by Kerrick.[46]

7.1.2 Syntheses of Secondary Amines

Preparation of Potassium L-prolinate (A1)

L-Proline (0.890 g, 7.73 mmol) was loaded into a 25 ml Schlenk flask, which was subsequently dried by high vacuum, filled with nitrogen atmosphere and cooled with ice bath. A saturated solution of potassium *tert*-butoxide (1.30 g, 11.6 mmol) in anhydrous tetrahydrofuran was added. The mixture was intensely stirred for 2 hrs at 45 °C. The suspension was filtrated and the residue was washed with anhydrous tetrahydrofuran under nitrogen atmosphere. 1.07 g white solid (93%, decomposed at 214 °C) as product was obtained after high-vacuum drying.

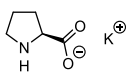

^{1}H NMR (400 MHz, DMSO-d_6) δ 2.96 (dd, J = 8.5, 5.7 Hz, 1H), 2.88 (ddd, J = 10.4, 7.1, 5.0 Hz, 1H), 2.46 (dt, J = 10.3, 7.0 Hz, 1H), 1.72 (dq, J = 12.0, 7.6 Hz, 1H), 1.57 (ddt, J = 11.8, 8.1, 5.7 Hz, 1H), 1.54–1.40 (m, 1H), 1.44–1.31 (m, 1H).

^{13}C NMR (101 MHz, DMSO-*d*6) δ 176.8, 62.8, 47.1, 31.3, 26.2.

Preparation of 2-Methylpyrrolidine (A3)

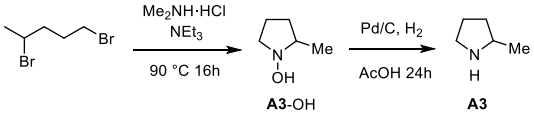

A3-OH **A3**

Compound **A3**-OH was prepared according to the modified procedure by Cicchi.[43] 1,4-Dibromopentane (5.25 ml, 38.5 mmol) and dimethylamine hydrochloride (14.6 g, 179 mmol) were dissolved in 180ml trimethylamine. The solution was refluxed for 16 h at 90 °C. The residue, from removing the solvent under vacuum, was purified by column chromatography on silica gel (EtOAc/MeOH 10:1) to afford **A3**-OH, which was mixed with palladium on carbon (1.70 g) in 160 ml of acetic acid under hydrogen atmosphere. The suspension was kept stirring for 24 h at ambient temperature and then filtrated through celite. The filtrate was mixed with 20 ml of trifluoroacetic acid and the whole was concentrated. The residue was dissolved in 55 ml of 6 M NaOH solution. The aqueous phase was extracted with diethyl ether (2 × 60 ml) and dichloromethane (2 × 60 ml). The organic phases were combined and the solvent was removed under reduced pressure to

provide the crude product, which was distilled (1 bar, 88–90 °C) to afford **A3** (2.43 g, 28.5 mmol, 74.1%) as a colorless oil.

^{1}H NMR (300 MHz, $CDCl_3$) δ 3.08–2.94 (m, 2H), 2.85–2.72 (m, 1H), 1.91–1.62 (m, 3H), 1.24–1.13 (m, 1H), 1.11 (d, *J* = 6.3 Hz, 3H).

^{13}C NMR (75 MHz, $CDCl_3$) δ 54.7, 46.9, 33.8, 25.9, 21.4.

HRMS (EI): m/z calculated for $C_5H_{12}N^+$ ($M + H^+$): 86.0964, found: 86.0964.

Preparation of (*R*)-2-Isopropylpyrrolidine (A4)

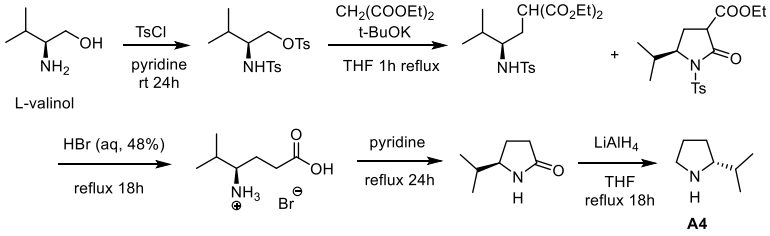

Amine **A4** was prepared by a modified procedure described by Tseng.[45] L-Valinol (11.8 g, 114 mmol) was dissolved in 200 ml of pyridine. *p*-Toluenesulfonyl chloride (87.5 g, 459 mmol) was added in portions under ice cooling bath. The mixture was stirred at ambient temperature for 24 h and then was poured onto an ice-water mixture (300 ml). The aqueous phase was extracted with dichloromethane (4 × 200 ml). The combined organic phase was successively with 10% HCl (3 × 200 ml), saturated copper sulfate solution (2 × 200 ml), water (1 × 200 ml), saturated bicarbonate solution (2 × 200 ml) and brine (4 × 100 ml). After drying ($MgSO_4$) and removal of the solvent under vacuum, the residue was purified by column chromatography on silica gel (pentane/ethyl acetate 2:1 to 3:2). The obtained compound (S)-3-methyl-2-((4-methylphenyl)sulfonamido)butyl *p*-tosylate (26.0 g, 63.2mmol) was mixed with diethyl malonate (30.4 g, 190mmol) and potassium *tert*-butoxide (21.3 g, 190mmol) in 600 ml of tetrahydrofuran. The solution was refluxed for 1 h and the solvent was removed under vacuum. The residue was mixed with 100 ml of brine. The aqueous phase was extracted with ethyl acetate. The combined organic phase was concentrated.

The residual mixture was mixed with 100 ml of 48% HBr aqueous solution and the whole mixture was refluxed for 18 h.

After removal of the solvent under reduced pressure, the residue was dissolved in 250 ml of pyridine. The solution was refluxed for 24 h and the concentrated to provide the crude product of (*R*)-5-isopropylpyrrolidin-2-one, which was first purified by column chromatography on silica gel (chloroform/methanol 5:1) and then by a quick distillation (2 × 10^{-3} mbar, 120 °C) as a colorless oil.

The obtained (*R*)-5-isopropylpyrrolidin-2-one (4.90 g, 38.5 mmol) was mixed with lithium aluminium hydride (2.20 g, 58.0 mmol) in 70 ml of anhydrous tetrahyrofuran. After 18 h refluxing, 10 ml of 20% KOH solution was dropped into the mixture under ice cooling bath. The suspension was filtrated and the filtrate was dried and concentrated to afford the crude product, which was distilled (48 mbar, 62 °C) to provide **A4** (1.89 g, 16.7 mmol, 14.6%) as a colorless oil.

^{1}H NMR (400 MHz, $CDCl_3$) δ 2.99 (ddd, *J* = 10.2, 7.3, 5.4 Hz, 1H), 2.81 (dt, *J* = 10.2, 7.4 Hz, 1H), 2.60 (td, *J* = 8.4, 6.8 Hz, 1H), 1.88–1.78 (m, 1H), 1.77–1.64 (m, 2H), 1.56 (br, 1H), 1.57–1.40 (m, 1H), 1.27 (dtd, *J* = 12.0, 9.1, 7.6 Hz, 1H), 0.96 (d, *J* = 6.6 Hz, 3H), 0.89 (d, *J* = 6.7 Hz, 3H).

^{13}C NMR (101 MHz, $CDCl_3$) δ 66.2, 47.0, 34.2, 29.9, 25.7, 20.8, 20.1.

HRMS (EI): m/z calculated for $C_7H_{16}N^+$ (M + H^+): 114.1277, found: 114.1278.

Preparation of 2,2-Dimethylpyrrolidine (A5)

Method 1

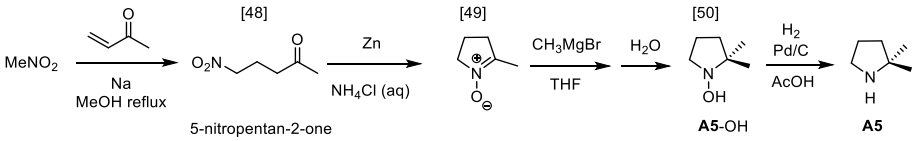

5-Nitropentan-2-one was synthesized following the procedure by Alderson.[48] 5-Methyl-3,4-dihydro-2H-pyrrole 1-oxide was prepared from 5-nitropentan-2-one according to the procedure by Pou.[49] Compound **A5**-OH was synthesized by treatment of nitrone with methylmagnesium bromide following the procedure by Ali.[50]

The obtained **A5**-OH (4.50 g, 39.1 mmol) and palladium on carbon (450 mg) were mixed in 60.0 ml of acetic acid. The mixture was stirred overnight under hydrogen atmosphere at ambient temperature, filtrated through celite and concentrated. The residue was dissolved in 3.00 ml of water. The solution was dropped into 200 g potassium hydroxide in a closed 250 ml flask. Amine **A5** was collected by a quick distillation (1 × 10^{-3} mbar, rt, distillate condensed under liquid nitrogen cooling bath) to afford **A5** (810 mg, 8.17 mmol, 20.9%) as a colorless oil.

Method 2

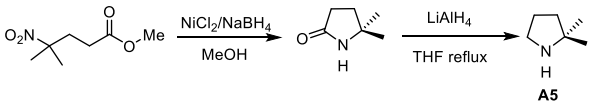

Methyl 4-nitropentanoate was synthesized following the procedure by Leinisch.[51] 5,5-Dimethylpyrrolidin-2-one was prepared from methyl 4-nitropentanoate according to the procedure by Osby.[52] 5,5-Mimethylpyrrolidin-2-one was reduced by lithium aluminium hydride following the procedure by Moffett.[53]

^{1}H NMR (400 MHz, $CDCl_3$) δ 3.00–2.94 (m, 2H), 1.85–1.73 (m, 2H), 1.56–1.45 (m, 2H), 1.14 (s, 6H).

^{13}C NMR (101 MHz, $CDCl_3$) δ 59.0, 46.2, 39.7, 29.0, 26.3.

HRMS (EI): m/z calculated for $C_6H_{13}N^{\bullet+}$ ($M^{\bullet+}$): 99.1043, found: 99.1043.

Preparation of (*S*)-2-Benzhydrylpyrrolidine (A7)

Amine **A7** was prepared according to the procedure by Claudio.[41]

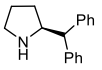

^{1}H NMR (400 MHz, CD_3CN) δ 7.40–7.32 (m, 4H), 7.31–7.24 (m, 4H), 7.19–7.13 (m, 2H), 3.91–3.84 (m, 1H), 3.72 (d, *J* = 10.3 Hz, 1H), 2.90 (dtd, *J* = 10.0, 5.1, 2.4 Hz, 1H), 2.82–2.75 (m, 1H), 1.85 (br, 2H), 1.78–1.58 (m, 3H), 1.34–1.20 (m, 1H).

^{13}C NMR (101 MHz, CD_3CN) δ 145.7, 145.5, 129.4, 129.3, 129.1, 129.0, 127.1, 127.0, 62.7, 59.4, 47.1, 31.7, 26.0.

HRMS (EI): m/z calculated for $C_{17}H_{20}N^+$ ($M + H^+$): 238.1590, found: 238.1589.

Preparation of (*S*)-Pyrrolidin-2-ylmethanamine (A8)

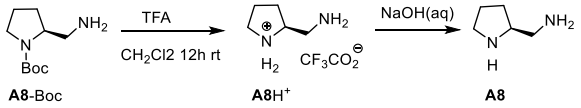

A8-Boc **A8**H$^+$ **A8**

Compound **A8**-Boc was synthesized following the procedure reported by Cao.[33] Compound **A8**-Boc (2.90 g, 14.5 mmol) was dissolved in a mixture of trifluoroacetic acid (10 ml) and dichloromethane (20 ml). The solution was stirred overnight at ambient temperature. The residue, from removing the solvent under reduced pressure, was mixed at 0 °C with 20 ml NaOH solution (6 M). The aqueous phase was extracted with dichloromethane (5 × 20 ml). The combined organic phases were dried ($MgSO_4$) and concentrated. The crude product was distilled (20 mbar, 73–75 °C) to provide **A8** (500 mg, 4.99 mmol, 34.4%) as a colorless oil.

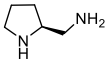

^{1}H NMR (400 MHz, $CDCl_3$) δ 3.06 (m, 1H), 2.96–2.82 (m, 2H), 2.68 (ddd, *J* = 12.4, 4.9, 0.9 Hz, 1H), 2.59 (ddd, *J* = 12.4, 7.5, 0.9 Hz, 1H), 1.90–1.58 (m, 3H), 1.35 (br, 2H), 1.35–1.21 (m, 1H).

^{13}C NMR (101 MHz, $CDCl_3$) δ 61.3, 47.4, 46.8, 29.3, 26.0.

Preparation of (*S*)-*N*,*N*-Dimethyl-1-(pyrrolidin-2-yl)methanamine (A9)

The crude product of Amine **A9** was synthesized following the procedure reported by Diakos,[42] which was kept in vacuum (1.1 mbar) for 1 h at 0 °C. A quick distillation (rt, 1×10^{-3} mbar, distillate condensed under liquid nitrogen cooling bath) was proceeded to provide **A9** as a colorless oil.

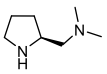

^{1}H NMR (400 MHz, CD_3CN) δ 3.10 (p, *J* = 6.9 Hz, 1H), 2.86 (ddd, *J* = 10.0, 7.2, 5.8 Hz, 1H), 2.72 (dt, *J* = 9.9, 7.2 Hz, 1H), 2.23–2.16 (m, 1H), 2.16 (s, 6H), 2.10 (dd, *J* = 11.9, 5.8 Hz, 1H), 1.83–1.57 (m, 3H), 1.27 (ddt, *J* = 12.0, 8.6, 6.8 Hz, 1H).

^{13}C NMR (101 MHz, CD_3CN) δ 66.4, 57.1, 46.8, 46.2, 30.8, 25.8.

IR (neat, ATR probe, cm^{-1}): 3335, 2945, 2864, 2823, 2774, 1633, 1530, 1458, 1396, 1342, 1261, 1195, 1168, 1149, 1100, 1033, 908, 841, 812, 731.

HRMS (EI): m/z calculated for $C_7H_{17}N_2^+$ ($M + H^+$): 129.1386, found: 129.1385.

Preparation of (*S*)-2-((Dimethylamino)methyl)pyrrolidin-1-ium trifluoromethanesulfonate (A9H$^+$OTf$^-$)

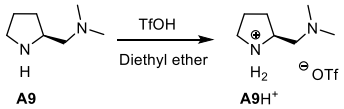

Amine **A9** (0.236 g, 1.84 mmol) was dissolved in 5 ml of anhydrous diethyl ether. Triflic acid (0.207 g, 1.38 mmol) was dissolved in 5 ml of anhydrous diethyl ether. The triflic acid solution was dropped into the solution of **A9** under ice cooling bath. The precipitate was filtrated and dried under vacuum to afford product **A9**H$^+$ with quantitative yield as a colorless solid (mp 107.0–109.0 °C).

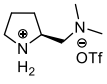

^{1}H NMR (400 MHz, $CDCl_3$) δ 7.49 (br, 2H), 3.94–3.81 (m, 1H), 3.40 (tt, *J* = 8.4, 4.2 Hz, 2H), 2.62–2.39 (m, 2H), 2.27–2.14 (m, 1H), 2.14–2.01 (m, 2H), 1.68 (ddt, *J* = 12.5, 7.2, 6.1 Hz, 1H).

^{13}C NMR (101 MHz, $CDCl_3$) δ 59.9, 57.4, 45.6, 45.2, 28.1, 23.8.

Preparation of (*S*)-1-(Pyrrolidin-2-ylmethyl)pyrrolidine (A10)

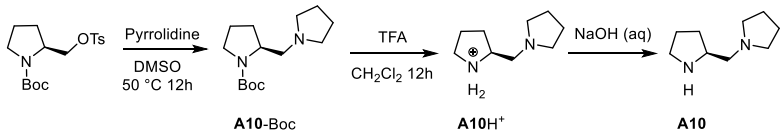

Compound **A10**-Boc was synthesized in analogy to the reported procedure by Hendrie.[35] 1-BOC-2-(S)-pyrrolidinylmethyl *p*-toluenesulfonate (3.04 g, 8.55 mmol) and pyrrolidine (2.67 g, 37.5 mmol) were dissolved in 30 ml of anhydrous DMSO. The solution was kept

overnight at 50 °C. After mixing with 50 ml of water, the mixture was extracted with diethyl ether (3 × 50 ml). The residue, resulting from removal of the solvent in vacuo, was purified by column chromatography on silica gel (EtOAc/MeOH 4:1) to afford **A10**-Boc (2.14 g, 8.41 mmol, 98.4%). The obtained **A10**-Boc (2.14 g, 8.41 mmol) was dissolved in a mixture of dichloromethane (30 ml) and 10 ml of trifluoroacetic acid. The solution was stirred overnight at ambient temperature. After removing the solvent under reduced pressure, diethyl ether was added into the residue. The mixture was filtrated and the residue was washed with diethyl ether to provide **A10**H^+ with quantitative yield, which was dissolved in 10 ml of 1M NaOH solution at 0 °C. The aqueous phase was extracted with dichloromethane (5 × 30 ml). The combined organic phase was dried ($MgSO_4$) and concentrated. The residue was first kept under vacuum (1 mbar) at 0 °C for 1 h and then a quick distillation (60 °C, 4 × 10^{-3} mbar, distillate condensed under liquid nitrogen cooling bath) was proceeded to provide **A10** (725 mg, 4.70 mmol, 58.1%) as a colorless oil.

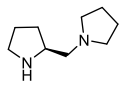

^{1}H NMR (400 MHz, $CDCl_3$) δ 3.20 (dtd, *J* = 8.3, 7.0, 5.2 Hz, 1H), 2.97 (ddd, *J* = 10.1, 7.3, 5.9 Hz, 1H), 2.83 (ddd, *J* = 10.1, 7.7, 6.6 Hz, 1H), 2.59–2.43 (m, 5H), 2.37–2.29 (m, 1H), 1.95 (br, 1H), 1.87 (dddd, *J* = 12.4, 8.6, 7.3, 5.5 Hz, 1H), 1.80–1.63 (m, 6H), 1.32 (ddt, *J* = 12.2, 8.7, 6.9 Hz, 1H).

^{13}C NMR (101 MHz, $CDCl_3$) δ 62.4, 57.6, 54.8, 46.3, 30.3, 25.2, 23.6.

Preparation of (*S*)-2-(Azidomethyl)pyrrolidine (A11)

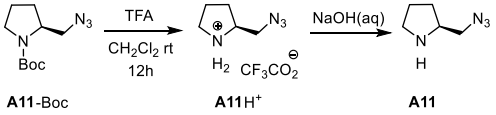

A11-Boc **A11**H^+ **A11**

Following the procedure by Dahlin crude **A11**-Boc was prepared,[36] which was purified by column chromatography on silica gel (*n*-pentane/ethyl acetate 10:1). Ammonium **A11**H^+ was synthesized from **A11**-Boc according to the reported method by Luo.[25] The obtained **A11**H^+ (1.85 g, 7.70 mmol) was mixed with 25 ml of 6 M NaOH solution under ice cooling bath. The aqueous phase was extracted with dichloromethane (3 × 30 ml). The organic phase was dried and concentrated. The residue was purified by a quick distillation (4 × 10^{-3} mbar, rt, distillate condensed under liquid nitrogen cooling bath) to afford **A11** (560 mg, 4.44 mmol, 57.6%) as a colorless oil.

^{1}H NMR (400 MHz, $CDCl_3$) δ 3.35–3.12 (m, 3H), 3.02–2.85 (m, 2H), 1.95 – 1.64 (m, 4H), 1.42 (ddt, *J* = 12.2, 8.6, 6.5 Hz, 1H).

^{13}C NMR (101 MHz, $CDCl_3$) δ 57.9, 56.4, 46.8, 29.2, 25.7.

HRMS (EI): m/z calculated for $C_5H_{11}N_4^+$ (M + H^+): 127.0978, found: 127.0980.

Preparation of (*S*)-Pyrrolidin-2-ylmethanol (A12)

Amine **A12** was synthesized by direct reduction of L-proline with lithium aluminium hydride as a colorless oil, which was pioneered by Vogl.[31]

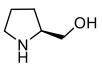

^{1}H NMR (400 MHz, CD_3CN) δ 3.38 (dd, *J* = 10.7, 4.7 Hz, 1H), 3.30 (br, 2H), 3.27 (dd, *J* = 10.8, 6.9 Hz, 1H), 3.09 (qd, *J* = 7.0, 4.8 Hz, 1H), 2.90–2.71 (m, 2H), 1.82–1.54 (m, 3H), 1.33 (ddt, *J* = 11.9, 8.5, 6.9 Hz, 1H).

^{13}C NMR (101 MHz, $CDCl_3$) δ 65.4, 60.9, 47.0, 28.5, 26.4.

^{1}H NMR (599 MHz, $CDCl_3$) δ 3.51 (dd, *J* = 9.9, 3.7 Hz, 1H), 3.34–3.26 (m, 2H), 2.99–2.92 (m, 1H), 2.86 (dt, *J* = 10.5, 6.7 Hz, 1H), 2.20 (br, 2H), 1.88–1.74 (m, 2H), 1.74–1.64 (m, 1H), 1.48–1.40 (m, 1H).

^{13}C NMR (151 MHz, $CDCl_3$) δ 64.9, 59.3, 46.6, 27.8, 26.3.

Preparation of (*S*)-2-(Methoxymethyl)pyrrolidine (A13)

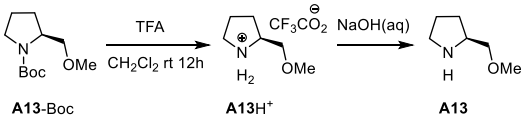

The preparation of **A13**-Boc from *N*-Boc-L-Prolinol follows the procedure described by Krishna.[32] Compound **A13**-Boc (11.6 g, 53.9 mmol) was mixed with 10 ml of trifluoroacetic acid and 100 ml of dichloromethane. The solution was stirred overnight at ambient temperature and concentrated. The residue was mixed with 20 ml of 2.5 M HCl solution. The aqueous phase was washed with diethyl ether (2 × 30 ml) and neutralized with 4 M NaOH solution till pH value of the solution was above 10. The aqueous phase was then extracted with dichloromethane (5 × 30 ml). The combined organic phase was dried (Na_2SO_4) and concentrated. The rude product was distilled (52 mbar, 70–80 °C) to afford **A13** (4.47 g, 40.2 mmol, 74.6%) as a colorless oil.

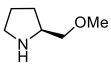

^{1}H NMR (400 MHz, $CDCl_3$) δ 3.35–3.25 (m, 1H), 3.31 (s, 3H), 3.26–3.18 (m, 2H), 2.91 (ddd, *J* = 10.2, 7.1, 5.8 Hz, 1H), 2.82 (ddd, *J* = 9.9, 7.4, 6.4 Hz, 1H), 1.93 (br, 1H), 1.83–1.58 (m, 3H), 1.41–1.27 (m, 1H).

^{13}C NMR (101 MHz, $CDCl_3$) δ 76.4, 59.0, 57.8, 46.6, 27.9, 25.4.

^{1}H NMR (400 MHz, CD_3CN) δ 3.28 (s, 3H), 3.26–3.09 (m, 3H), 2.84 (ddd, *J* = 9.8, 7.0, 5.7 Hz, 1H), 2.76 (ddd, *J* = 9.9, 7.3, 6.6 Hz, 1H), 1.82 (br, 1H), 1.80–1.55 (m, 3H), 1.38–1.24 (m, 1H).

^{13}C NMR (101 MHz, CD_3CN) δ 77.5, 58.9, 58.5, 47.1, 29.0, 26.0.

Preparation of 2-(Trifluoromethyl)pyrrolidine (A14)

The preparation of **A14** was following the procedure by Schevchenko.[56]

^{1}H NMR (400 MHz, CD_3Cl) δ 3.70–3.59 (m, 1H), 3.05–2.97 (m, 2H), 2.08–1.82 (m, 4H), 1.81–1.68 (m, 1H).

^{13}C NMR (101 MHz, CD_3Cl) δ 127.1 (q, *J* = 279.2 Hz), 58.8 (q, *J* = 29.6 Hz), 47.3, 26.0 (q, *J* = 1.8 Hz), 25.7.

^{19}F NMR (376 MHz, Chloroform-*d*) δ −76.90 (d, *J* = 8.1 Hz).

Preparation of Methyl L-prolinate (A15)

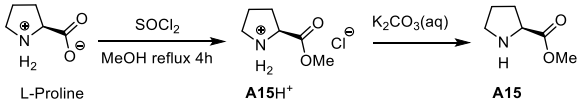

Amine **A15** was synthesized through direct esterification of amino acid in analogy to the documented method by Brenner.[30] Thionylchloride (2.50 ml, 34.5 mmol) was dropped into a solution of L-proline (2.48 g, 21.5 mmol) in 20 ml of MeOH under ice cooling bath. The mixture was refluxed for 4 h and concentrated under vacuum. The residue was neutralized with saturated K_2CO_3 solution, and the aqueous phase was extracted with chloroform. The organic phase was concentrated to afford the crude product, which was first purified by column chromatography on silica gel (chloroform/methanol 10:1) and then by a quick distillation (1×10^{-3} mbar, rt, distillate condensed under liquid nitrogen cooling bath) to afford **A15** (1.65 g, 12.8 mmol, 59.4%) as a colorless oil.

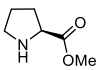

^{1}H NMR (400 MHz, CD_3CN) δ 3.66 (dd, *J* = 8.6, 5.6 Hz, 1H), 3.65 (s, 3H), 2.95 (dt, *J* = 9.9, 6.6 Hz, 1H), 2.80 (dt, *J* = 10.1, 6.6 Hz, 1H), 2.27 (s, 1H), 2.08–1.97 (m, 1H), 1.82–1.64 (m, 3H).

^{13}C NMR (101 MHz, CD_3CN) δ 176.7, 60.5, 52.3, 47.7, 30.8, 26.4.

Preparation of (*S*)-*N*,*N*-Dimethylpyrrolidine-2-carboxamide (A16)

The crude product of **A16** was synthesized by the procedure reported by Diakos,[42] which was kept in vacuum (1×10^{-3} mbar) at 0 °C for 30 mins. A quick distillation (60 °C, 1×10^{-3} mbar, distillate condensed under liquid nitrogen cooling bath) was proceeded to provide **A16** (2.85 g, 20.0 mmol, 71.2%) as a colorless oil.

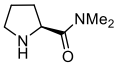

^{1}H NMR (400 MHz, $CDCl_3$) δ 3.83 (dd, *J* = 8.5, 6.1 Hz, 1H), 3.13 (ddd, *J* = 10.7, 7.1, 5.3 Hz, 1H), 2.98 (s, 3H), 2.92 (s, 3H), 2.85–2.75 (m, 1H), 2.75 (br, 1H),

2.10–1.99 (m, 1H), 1.80–1.52 (m, 3H).

^{13}C NMR (101 MHz, $CDCl_3$) δ 174.3, 58.3, 47.9 36.5, 35.8, 30.8, 26.6.

IR (neat, ATR probe, cm^{-1}): 3410, 2950, 2874, 1624, 1504, 1394, 1257, 1153, 1086, 1059, 883.

HRMS (EI): m/z calculated for $C_7H_{14}N_2O^{\bullet+}$ ($M^{\bullet+}$): 142.1101, found: 142.1099.

HRMS (ESI): m/z calculated for $C_7H_{15}N_2O^+$ ($M + H^+$): 143.1179, found: 143.1178.

Preparation of (*S*)-*N*-propylpyrrolidine-2-carboxamide (A17)

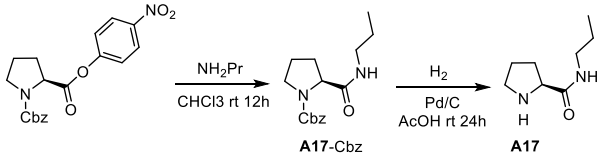

Amine **A17** was synthesized in analogy to the procedure reported by Diakos.[42] 1-Benzyl 2-(4-nitrophenyl) (S)-pyrrolidine-1,2-dicarboxylate (2.00 g, 5.40 mmol) and propylamine (1.00 g, 12.2 mmol) were dissolved in 30 ml chloroform. TLC was used to monitor the reaction till no starting material was left. The solvent was removed under reduced pressure. The residue was purified by column chromatography on aluminium oxide with chloroform (1% NEt_3) as eluent to afford **A17**-Cbz as a colourless solid. The obtained **A17**-Cbz and palladium on carbon (330 mg) were mixed in 25 ml of acetic acid under hydrogen atmosphere. The suspension was stirred for 24 h at ambient temperature and then was filtrated through celite. The filtrate was concentrated and the residue was dissolved in 20 ml of 6 M HCl solution, which was firstly washed with ethyl acetate and then neutralized with 8 M NaOH to pH > 10. The aqueous phase was extracted with chloroform (3 × 30 ml) and ethyl acetate (2 × 30 ml). The combined organic phase was dried ($MgSO_4$) and concentrated. The residue was kept in vacuum (1×10^{-3} mbar) at 0 °C for 30 mins. A quick distillation (110 °C, 1×10^{-3} mbar, distillate condensed under liquid nitrogen cooling bath) was proceeded to provide **A17** (700 mg, 4.48 mmol, 83.0%) as a colorless oil.

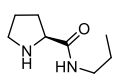

^{1}H NMR (300 MHz, $CDCl_3$) δ 7.59 (br, 1H), 3.66 (dd, *J* = 9.1, 5.3 Hz, 1H), 3.14 (dtd, *J* = 8.3, 6.7, 1.3 Hz, 2H), 2.96 (dt, *J* = 10.2, 6.8 Hz, 1H), 2.84 (dt, *J* = 10.1, 6.3 Hz, 1H), 2.11 (br, 1H), 2.16–1.98 (m, 1H), 1.84 (dt, *J* = 12.5, 6.1 Hz, 1H), 1.72–1.58 (m, 2H), 1.47 (h, *J* = 7.4 Hz, 2H), 0.86 (td, *J* = 7.4, 0.7 Hz, 3H).

^{13}C NMR (75 MHz, $CDCl_3$) δ 175.0, 60.7, 47.3, 40.5, 30.8, 26.2, 22.9, 11.4.

IR (neat, ATR probe, cm^{-1}): 3301, 3080, 2960, 2933, 2873, 2363, 1643, 1523, 1458, 1439, 1381, 1344, 1254, 1150, 1100, 905, 816.

HRMS (EI): m/z calculated for $C_8H_{17}N_2O^+$ (M + H^+): 157.1335, found: 157.1334.
HRMS (ESI): m/z calculated for $C_8H_{17}N_2O^+$ (M + H^+): 157.13354, found: 157.13350.

Preparation of (*S*)-2-((1,3-Dioxoisoindolin-2-yl)methyl)pyrrolidin-1-ium 2,2,2-trifluoroacetate (A18H$^+$)

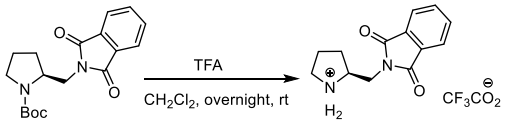

A18-Boc **A18**H$^+$

Compound **A18**-Boc was synthesized following the reported method by Cao.[33] **A18**-Boc (3.00 g, 9.08 mmol) was dissolved in a mixture of 10 ml trifluoroacetic aced and 25 ml of dichloromethane. The solution was stirred overnight at ambient temperature. The residue, from removing the solvent under reduced pressure, was mixed with 15ml diethyl ether. A colorless crystalline solid was formed, which was filtrated and dried under vacuum to provide **A18**H$^+$ with quantitative yield (mp 181.3–182.4 °C).

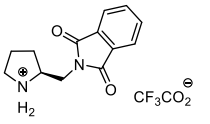

^{1}H NMR (400 MHz, CD_3CN) δ 7.88–7.76 (m, 4H), 4.05–3.92 (m, 3H), 3.87 (dtd, *J* = 9.9, 6.9, 5.2 Hz, 1H), 3.39 (ddd, *J* = 11.7, 8.2, 6.9 Hz, 1H), 3.26 (ddd, *J* = 11.7, 9.0, 6.0 Hz, 1H), 2.24–2.13 (m, 1H), 2.13–1.89 (m, 2H), 1.81 (ddt, *J* = 12.8, 9.8, 8.7 Hz, 1H).

^{13}C NMR (101 MHz, CD_3CN) δ 169.5, 161.4 (q, $J_{C,F}$ = 33.3 Hz, CO_2), 135.3, 133.0, 124.1, 118.0 (q, $J_{C,F}$ = 295.0 Hz, CF_3), 60.5, 46.1, 39.2, 28.4, 23.6.

Preparation of (*S*)-4-Phenyl-1-(pyrrolidin-2-ylmethyl)-1H-1,2,3-triazole (A19)

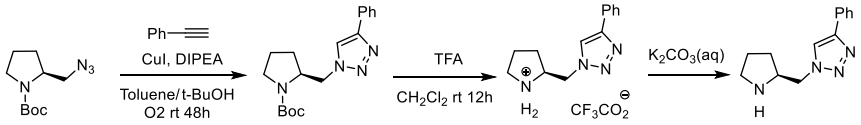

A11-Boc **A19**-Boc **A19**H$^+$ **A19**

Amine **A19** was synthesized according to a modified procedure by Luo.[25] Compound **A11**-Boc (1.00 g, 4.42 mmol), phenylacetylene (600 mg, 5.87 mmol), copper (I) iodide (130 mg, 0.683 mmol) and DIPEA (0.77 ml, 4.53 mmol) were dissolved in a mixture of 40 ml of toluene and 20 ml of *tert*-buthanol. The mixture was stirred under oxygen atmosphere for 48 h at ambient temperature. The suspension was filtrated and the filtrate was concentrated. The residue was purified by column chromatography on silica gel (*n*-penthane/ethyl acetate 3:1 to 2:3).

The obtained **A19**-Boc was dissolved in a mixture of 4.6 ml of trifluoroacetic acid and 16 ml of dichloromethane. The solution was stirred overnight at ambient temperature. After

removal of the solvent under vacuum, the residue was neutralized with saturated K_2CO_3 solution (20 ml) and extracted with ethyl acetate (3 × 40 ml). The combined organic phases were dried ($NaSO_4$) and concentrated to provide crude **A19**, which was purified by column chromatography on silica gel (methanol/ethyl acetate 1:10 to 1:1) to afford **A19** (500 mg, 2.19 mmol, 49.6%) as a white solid.

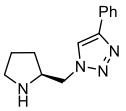

^{1}H NMR (599 MHz, $CDCl_3$) δ 7.93 (s, 1H), 7.86–7.80 (m, 2H), 7.47–7.38 (m, 2H), 7.35–7.29 (m, 1H), 4.46 (dd, *J* = 13.6, 4.5 Hz, 1H), 4.24 (dd, *J* = 13.6, 7.9 Hz, 1H), 3.65 (m, 1H), 2.96 (t, *J* = 6.8 Hz, 2H), 2.69 (br, 1H), 1.97 (dddd, *J* = 12.9, 8.5, 7.5, 5.4 Hz, 1H), 1.85–1.66 (m, 2H), 1.51 (ddt, *J* = 12.7, 8.7, 7.0 Hz, 1H).

^{13}C NMR (151 MHz, $CDCl_3$) δ 147.7, 130.9, 128.9, 128.2, 125.8, 120.7, 58.1, 55.5, 46.7, 29.2, 25.6.

IR (neat, ATR probe, cm^{-1}): 3329, 3130, 2959, 2871, 1609, 1555, 1483, 1464, 1439, 1403, 1367, 1225, 1189, 1076, 1047, 973, 916, 810, 765, 695.

HRMS (ESI): m/z calculated for $C_{13}H_{17}N_4^+$ ($M + H^+$): 229.1448, found: 229.1446.

Preparation of (*S*)-1-(Pyrrolidin-2-ylmethyl)-1H-imidazole (A20)

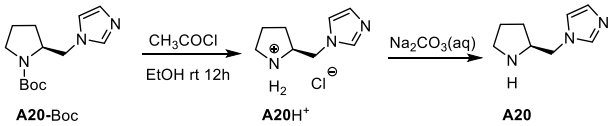

A20-Boc **A20**H$^+$ **A20**

The crude product of **A20**-Boc was synthesized following the reported method by Luo[28], which was purified by column chromatography on silica gel (ethyl acetate/methanol/trimethylamine 10:1:0.01). The obtained **A20**-Boc (1.00 g, 3.98 mmol) was added into a mixture of 10 ml of ethyl acetate, 1.2 ml of ethanol (20.3 mmol) and acetyl chloride (0.85 ml, 12.0 mmol). The solution was stirred overnight at ambient temperature. The formed precipitate was filtrated and dissolved in 20 ml of saturated Na_2CO_3 solution. The aqueous phase was extracted with chloroform (5 × 30 ml). The combined organic phase was concentrated to afford **A20** (200 mg, 1.32 mmol, 33.2%) as a slightly yellow oil.

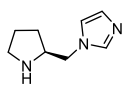

^{1}H NMR (599 MHz, $CDCl_3$) δ 7.51 (s, 1H), 7.03 (s, 1H), 6.97 (s, 1H), 3.94 (dd, *J* = 13.7, 5.0 Hz, 1H), 3.84 (dd, *J* = 13.8, 7.8 Hz, 1H), 3.38 (m, 1H), 2.98–2.87 (m, 2H), 1.89 (dddd, *J* = 12.5, 8.6, 7.4, 5.2 Hz, 1H), 1.83–1.68 (m, 2H), 1.40 (ddt, *J* = 12.6, 9.0, 7.2 Hz, 1H).

^{13}C NMR (151 MHz, $CDCl_3$) δ 137.5, 129.5, 119.4, 59.0, 52.7, 46.6, 29.2, 25.3.

IR (neat, ATR probe, cm^{-1}): 3303, 3112, 2962, 2872, 2190, 1646, 1552, 1507, 1443, 1402, 1365, 1284, 1231, 1107, 1077, 1030, 910, 814, 725, 662.

HRMS (ESI): m/z calculated for $C_8H_{14}N_3^+$ (M + H^+): 152.11822, found: 152.11822.

Preparation of (*S*)-3-Butyl-1-(pyrrolidin-2-ylmethyl)-1H-imidazol-3-ium trifluoromethanesulfonate (A21 OTf^-)

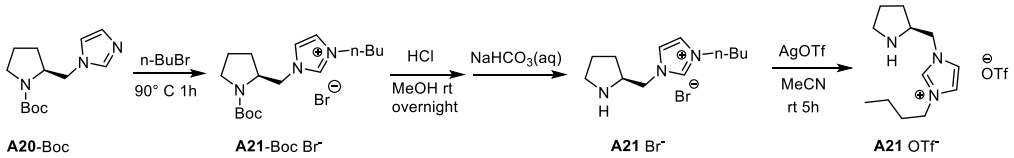

A20-Boc **A21**-Boc Br^- **A21** Br^- **A21** OTf^-

The mixture of **A20**-Boc (1.00 g, 3.98 mmol) and *n*-butyl bromide (3.70 g, 27.0 mmol) was stirred for 1 h at 90 °C. The residue from removal of volatiles under vacuum was dissolved in 20.0 ml of 0.6 M HCl solution in methanol. The solution was stirred overnight at ambient temperature and concentrated. The residue was diluted with 100 ml saturated sodium bicarbonate solution under ice cooling bath. The mixture was stirred for 2 h at 0 °C. The volatiles were removed under reduced pressure. 150 ml of acetonitrile was added into the residue. The suspension was filtrated and the filtrate was concentrated. The residue was mixed with 50 ml of dichloromethane. The whole mixture was filtrated and the solvent was removed under reduced pressure to afford **A21** Br^-.

The obtained **A21** Br^- (200 mg, 0.694 mmol) was mixed with silver tosylate (200 mg, 0.778 mmol) in 8.00 ml of acetonitrile. The mixture was stirred for 5 h at ambient temperature, filtrated and concentrated. The residue was mixed with 10.0 ml dichloromethane. The mixture was filtrated and concentrated to afford **A21** OTf^- (255 mg, 0.714 mmol, 17.9%) as brown oil.

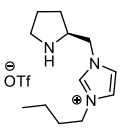

^{1}H NMR (400 MHz, CD_3CN) δ 8.65 (s, 1H), 7.48 (t, *J* = 1.8 Hz, 1H), 7.43 (t, *J* = 1.8 Hz, 1H), 4.27 (qd, *J* = 14.3, 6.7 Hz, 2H), 4.15 (t, *J* = 7.3 Hz, 2H), 3.71 (qd, *J* = 7.8, 5.2 Hz, 1H), 3.19–3.03 (m, 2H), 2.15 – 2.00 (m, 1H), 1.91–1.79 (m, 4H), 1.57 (dq, *J* = 12.8, 8.0 Hz, 1H), 1.34 (dq, *J* = 14.8, 7.4 Hz, 2H), 0.94 (t, *J* = 7.4 Hz, 3H).

^{13}C NMR (101 MHz, CD_3CN) δ 136.8, 123.8, 123.5, 121.3 (q, *J* = 320.3 Hz), 60.0, 52.7, 50.4, 48.1, 32.4, 29.0, 25.0, 19.9, 13.6.

IR (neat, ATR probe, cm^{-1}): 3471, 3142, 2961, 2922, 2852, 1632, 1565, 1467, 1251, 1225, 1162, 1028, 758.

HRMS (ESI): m/z calculated for $C_{12}H_{22}N_3^+$ (M): 208.18082, found: 208.18077; calculated for $CF_3O_3S^-$ (OTf^-): 148.95257, found: 148.95237.

Preparation of

(*S*)-1-(3,5-Bis(trifluoromethyl)phenyl)-3-(pyrrolidin-2-ylmethyl)thiourea (A22)

Compound **A22**$H^+CF_3CO_2^-$ was synthesized following the procedure described by Cao.[37] The obtained **A22**$H^+CF_3CO_2^-$ was deprotonated with 25% ammoniac solution and extracted with ethyl acetate. The crude product from removal of the solvent was purified by column chromatography on silica gel (methanol) to provide **A22** as a white solid.

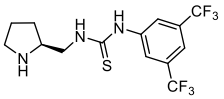

^{1}H NMR (599 MHz, $CDCl_3$) δ 8.04 (s, 2H), 7.57 (s, 1H), 7.40 (br, 1H), 3.59–3.52 (m, 1H), 3.45–3.36 (m, 1H), 3.35–3.26 (m, 1H), 3.16–3.09 (m, 1H), 2.92–2.81 (m, 1H), 2.01–1.87 (m, 2H), 1.79–1.68 (m, 1H), 1.65–1.55 (m, 1H).

^{13}C NMR (151 MHz, $CDCl_3$) δ 183.8, 142.3, 131.7 (q, J = 35.8 Hz), 123.4 (q, J = 272.7 Hz), 122.7, 117.4, 59.6, 51.0, 46.3, 28.6, 27.4.

IR (neat, ATR probe, cm^{-1}): 3241, 2966, 2877, 1610, 1538, 1472, 1381, 1273, 1169, 1125, 1107, 1005, 949, 908, 883, 847, 727, 699, 682.

HRMS (EI): m/z calculated for $C_{14}H_{15}N_3F_6S^{\bullet+}$ ($M^{\bullet+}$): 371.0885, found: 371.0885.

HRMS (ESI): m/z calculated for $C_{14}H_{16}N_3F_6S^+$ ($M + H^+$): 372.09636, found: 372.09626; calculated for $C_{14}H_{14}N_3F_6S^-$ ($M - H^+$): 370.08181, found: 370.08222.

Preparation of

(*S*)-2-((3-(3,5-Bis(trifluoromethyl)phenyl)ureido)methyl)pyrrolidin-1-ium 2,2,2-trifluoroacetate (A23H$^+$)

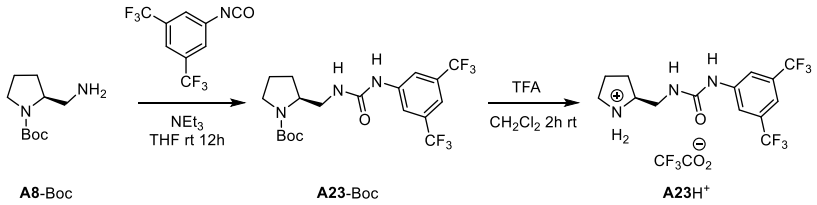

The crude product of **A23**-Boc was prepared following the reported procedure by Cao,[37] which was purified by column chromatography on silica gel (*n*-pentane/ethyl acetate 6:1 to 3:2) to afford **A23**-Boc as a white solid. The obtained **A23**-Boc (1.70 g, 3.73 mmol) was dissolved in a mixture of 10 ml of trifluoroacetic acid and 40 ml of dichloromethane. The mixture was stirred for 2 h at ambient temperature. The crude product after removal of the solvent was recrystallized (ethyl acetate/ dichloromethane) to afford **A23**H^+ (980mg, 2.09 mmol, 56.2%) as a white solid (mp 183.0–184.4 °C).

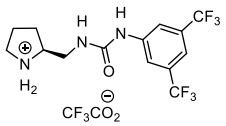

^{1}H NMR (400 MHz, CD_3OD) δ 8.07 (s, 2H), 7.50 (s, 1H), 3.73 (ddt, *J* = 8.9, 7.5, 3.8 Hz, 1H), 3.62–3.44 (m, 2H), 3.42–3.22 (m, 2H), 2.24–1.95 (m, 3H), 1.80 (dq, *J* = 12.6, 8.4 Hz, 1H).

^{13}C NMR (101 MHz, CD_3OD) δ 163.1 (q, *J* = 34.6 Hz, $CF_3\mathbf{C}O_2^-$), 158.5, 143.2, 133.1 (q, *J* = 33.1 Hz), 124.8 (q, *J* = 272.2 Hz), 119.4–119.1 (m), 118.2 (q, *J* = 293.0 Hz, $\mathbf{C}F_3CO_2^-$), 115.8 (t, *J* = 4.0 Hz), 62.8, 46.6, 42.1, 28.3, 24.4.

Preparation of 2-Tritylpyrrolidine (A24)

Amine **A24** was synthesized according to the procedure by Kano.[23a]

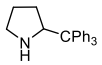

^{1}H NMR (599 MHz, $CDCl_3$) δ 7.36–7.32 (m, 6H), 7.29–7.23 (m, 6H), 7.21–7.16 (m, 3H), 4.73 (dd, *J* = 8.3, 6.7 Hz, 1H), 2.78–2.65 (m, 2H), 2.05 (dtd, *J* = 12.8, 8.2, 6.9 Hz, 1H), 1.63–1.56 (m, 1H), 1.56 – 1.49 (m, 1H), 1.46 (br, 1H), 1.09 (ddt, *J* = 15.8, 11.7, 7.4 Hz, 1H).

^{13}C NMR (151 MHz, $CDCl_3$) δ 146.4 (br), 130.3 (br), 127.7, 126.1, 64.1, 61.4, 46.8, 29.2, 25.9.

Preparation of (*S*)-2-(Diphenyl((trimethylsilyl)oxy)methyl)pyrrolidine (A25)

Amine **A25** was synthesized following the procedure reported by Marigo.[11a]

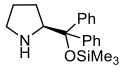

^{1}H NMR (400 MHz, CD_3CN) δ 7.52–7.46 (m, 2H), 7.38–7.33 (m, 2H), 7.32–7.15 (m, 6H), 4.19–4.07 (m, 1H), 2.89 (ddd, *J* = 9.7, 7.8, 6.4 Hz, 1H), 2.77 (ddd, *J* = 9.8, 7.0, 4.9 Hz, 1H), 1.61–1.45 (m, 2H), 1.44–1.31 (m, 2H), −0.08 (s, 9H).

^{13}C NMR (101 MHz, CD_3CN) δ 148.8, 147.6, 128.9, 128.5, 128.4, 127.8, 127.6, 127.4, 83.7, 65.4, 47.5, 27.6, 25.3, 2.6.

Preparation of (*S*)-Diphenyl(pyrrolidin-2-yl)methanol (A26)

Amine **A26** was synthesized according to the method of Kanth.[39]

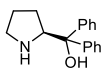

^{1}H NMR (400 MHz, CD_3CN) δ 7.55–7.50 (m, 2H), 7.44–7.37 (m, 2H), 7.37–7.24 (m, 5H), 7.23–7.16 (m, 1H), 4.60–4.52 (m, 1H), 3.06–2.94 (m, 1H), 2.86–2.77 (m, 1H), 2.23 (br, 1H), 1.75–1.54 (m, 3H), 1.52–1.43 (m, 1H).

^{13}C NMR (101 MHz, CD_3CN) δ 144.4, 144.1, 129.5, 129.1, 128.8, 128.2, 127.8, 127.3, 76.2, 65.7, 48.1, 28.9, 27.4.

^{1}H NMR (599 MHz, $CDCl_3$) δ 7.59–7.55 (m, 2H), 7.52–7.48 (m, 2H), 7.32–7.27 (m, 4H), 7.20–7.14 (m, 2H), 4.60 (br, 1H), 4.26 (t, *J* = 7.7 Hz, 1H), 3.04 (ddd, *J* = 9.2, 6.8, 4.8 Hz, 1H), 2.95 (dt, *J* = 9.2, 7.6 Hz, 1H), 1.80–1.53 (m, 5H).

^{13}C NMR (151 MHz, $CDCl_3$) δ 148.3, 145.6, 128.4, 128.1, 126.6, 126.5, 126.0, 125.7, 77.2, 64.6, 46.9, 26.4, 25.7.

Preparation of (*S*)-2-(Azidodiphenylmethyl)pyrrolidine (A27)

Amine **A27** was prepared following the procedure by Shi.[40]

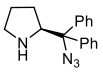

^{1}H NMR (400 MHz, $CDCl_3$) δ 7.53–7.47 (m, 2H), 7.42–7.27 (m, 7H), 7.27–7.21 (m, 1H), 4.35 (t, *J* = 7.1 Hz, 1H), 3.03–2.93 (m, 2H), 2.11 (br, 1H), 1.79–1.55 (m, 4H).

^{13}C NMR (101 MHz, $CDCl_3$) δ 142.8, 142.3, 128.6, 128.3, 128.1, 127.6, 127.3, 127.1, 75.3, 65.4, 47.3, 28.1, 26.2.

HRMS (ESI): m/z calculated for $C_{17}H_{19}N_4^+$ ($M + H^+$): 279.16042, found; 279.16032.

Preparation of 2-(Triphenylsilyl)pyrrolidine (A28)

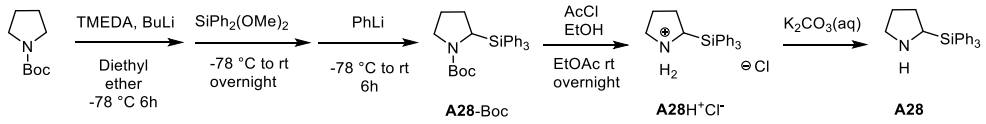

2-(Triphenylsilyl)pyrrolidin-1-ium chloride (**A28**H) was synthesized by the modified procedure reported by Bauer.[47] To a stirred solution of *N*-Boc-pyrrolidine (10.0 g, 58.4 mmol) and freshly distilled TMEDA (10.6 ml, 70.2 mmol) in diethylether (100 ml) at −78 °C was added *s*-BuLi (60.0 ml, 70.2 mmol; 1.17 M solution in cyclohexane). The reaction mixture was stirred for 6 h at −78 °C and then dimethoxydiphenylsilane (17.1 g, 70.0 mmol) was added at −78 °C. The stirring solution was allowed to slowly warm to room temperature overnight. Then, phenyllithium (137 ml, 70.6 mmol; 0.515 M solution in dibutylether) was added at −78 °C. The stirring reaction mixture was warmed to 0 °C over a period of 6 h. After water (80 ml) had been added, the organic layer was separated and the aqueous phase was extracted with diethyl ether (3 × 100 ml). The combined ether extracts were dried (Na_2SO_4) and all volatiles were removed under reduced pressure. The residue was purified by column chromatography on silica gel (*n*-pentane/diethyl ether 9:1) to provide **A28**-Boc (15.0 g, 34.9 mmol, 59.8%) as a white solid.

To a stirred solution of **A28**-Boc (1.00 g, 2.33 mmol) and ethanol (500 µl, 8.56 mmol) in ethyl acetate (10.0 ml) at ambient temperature was added acetyl chloride (560 µl, 7.84 mmol) dropwise. The reaction mixture was then stirred overnight. The precipitate was filtrated and washed with ethyl acetate to provide **A28**H^+Cl^- as a white solid, which was deprotonated with saturated potassium carbonate solution (20 ml) and extracted with

chloroform (3 × 30 ml). The organic phase was dried ($MgSO_4$) and concentrated to afford **A28** (528 mg, 1.35 mmol, 57.7%) as white solid.

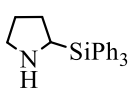

^{1}H NMR (599 MHz, $CDCl_3$) δ 7.6 –7.60 (m, 6H), 7.44–7.40 (m, 3H), 7.39–7.35 (m, 6H), 3.11 (dd, *J* = 10.6, 7.6 Hz, 1H), 3.01 (ddd, *J* = 10.7, 7.6, 4.5 Hz, 1H), 2.76 (dt, *J* = 10.7, 7.7 Hz, 1H), 2.08 (ddt, *J* = 12.5, 8.0, 4.1 Hz, 1H), 1.80–1.65 (m, 2H), 1.60–1.52 (m, 1H), 1.42 (br, 1H).

^{13}C NMR (151 MHz, $CDCl_3$) δ 136.2, 134.1, 129.8, 128.1, 49.3, 46.8, 29.2, 26.9.

Preparation of (*S*)-5-Benzyl-2,2,3-trimethylimidazolidin-4-one (A29)

The crude product of **A29** was prepared following the reported procedure by Ahrendt,[5a,5b] which was purified by column chromatography on silica gel (ethyl acetate) to afford **A29** as a clear oil.

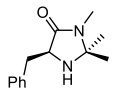

^{1}H NMR (400 MHz, CD_3CN) δ 7.33–7.19 (m, 5H), 3.67 (ddd, *J* = 8.7, 3.9, 0.7 Hz, 1H), 3.11 (dd, *J* = 14.1, 3.9 Hz, 1H), 2.71 (dd, *J* = 14.1, 8.7 Hz, 1H), 2.69 (d, *J* = 0.6 Hz, 3H), 1.21 (s, 6H).

^{13}C NMR (101 MHz, CD_3CN) δ 174.0, 139.8, 130.3, 129.2, 127.2, 76.3, 60.3, 38.8, 27.5, 25.3, 25.2.

Preparation of (2*S*,5*S*)-5-Benzyl-2-(tert-butyl)-3-methylimidazolidin-4-one (A30)

The crude product of **A30** was synthesized according to the procedure by Paras,[5d] which was purified by column chromatography on silica gel (ethyl acetate) to afford **A30** as colorless solid.

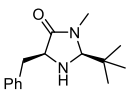

^{1}H NMR (400 MHz, CD_3Cl) δ 7.33–7.16 (m, 5H), 4.06–4.01 (m, 1H), 3.73–3.63 (m, 1H), 3.14 (dd, *J* = 13.7, 4.0 Hz, 1H), 2.92 (dd, *J* = 13.8, 7.7 Hz, 1H), 2.90 (s, 3H), 1.68 (br, 1H), 0.82 (s, 9H).

^{13}C NMR (101 MHz, CD_3Cl) δ 175.4, 138.1, 129.8, 128.7, 126.8, 82.6, 59.6, 38.4, 35.1, 30.8, 25.5.

Preparation of (2*S*,5*S*)-5-Benzyl-3-methyl-2-(5-methylfuran-2-yl)imidazolidin-4-one (A31) and (2*R*,5*S*)-5-Benzyl-3-methyl-2-(5-methylfuran-2-yl)imidazolidin-4-one (A32)

The crude product of the mixture of **A31** and **A32** was prepared following the reported procedure by Northrup,[5c] which was purified by column chromatography on silica gel (ethyl acetate/*n*-pentane 1:1 – 2:1) to afford **A31** as a clear oil and **A32** as a colorless solid.

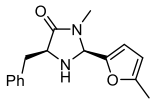

^{1}H NMR (400 MHz, CD_3Cl) δ 7.33–7.19 (m, 5H), 6.09 (d, *J* = 3.2 Hz, 1H), 5.88 (dt, *J* = 3.2, 1.1 Hz, 1H), 5.18 (d, *J* = 1.4 Hz, 1H), 3.78 (dd, *J* = 7.7, 4.3 Hz, 1H), 3.25 (dd, *J* = 14.3, 4.2 Hz, 1H), 3.08 (dd, *J* = 14.3, 7.6 Hz, 1H), 2.63 (s, 3H), 2.20 (s, 3H), 2.08 (br, 1H).

^{13}C NMR (101 MHz, CD_3Cl) δ 174.0, 153.5, 148.7, 137.3, 129.6, 128.8, 126.9, 111.0, 106.6, 71.1, 60.3, 37.6, 27.1, 13.7.

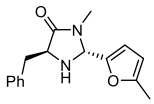

^{1}H NMR (400 MHz, CD_3Cl) δ 7.31–7.17 (m, 5H), 6.16 (d, *J* = 3.1 Hz, 1H), 5.88 – 5.86 (m, 1H), 4.93 (d, *J* = 1.4 Hz, 1H), 4.02 (dd, *J* = 7.7, 4.0 Hz, 1H), 3.13 (dd, *J* = 13.8, 4.0 Hz, 1H), 2.93 (dd, *J* = 13.8, 7.4 Hz, 1H), 2.63 (s, 3H), 2.30 (br, 1H), 2.22 (d, *J* = 1.1 Hz, 3H).

^{13}C NMR (101 MHz, CD_3Cl) δ 173.9, 153.5, 149.3, 137.8, 129.8, 128.6, 126.8, 110.4, 106.4, 71.1, 59.8, 38.4, 27.2, 13.7.

7.1.3 Preparation of Indicators

Preparation of 2-(4-Nitrophenyl)malononitrile (C6H)

C5H was synthesized following the literature procedure.[61]

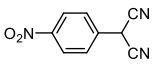

^{1}H NMR (400 MHz, Chloroform-*d*) δ 8.51–8.20 (m, 2H), 7.78–7.64 (m, 2H), 5.26 (s, 1H).

^{13}C NMR (101 MHz, Chloroform-*d*) δ 149.2, 132.8, 128.7, 125.3, 110.8, 28.0.

Preparation of 2-(Perfluorophenyl)malononitrile (C5H)

The Crude product of **C5**H was synthesized following the procedure by Hull,[60] which was purified by recrystallization first from ethanol/water mixture and then from benzene/*n*-Pentane mixture.

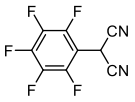

^{1}H NMR (400 MHz, Chloroform-*d*) δ 5.32 (s, 1H).

^{13}C NMR (101 MHz, $CDCl_3$) δ 144.9 (dtdd, *J* = 255.7, 8.5, 5.8, 4.5 Hz), 143.7 (dtt, *J* = 261.9, 13.2, 5.2 Hz), 139.9–136.9 (m), 108.8, 101.9 (td, *J* = 15.7, 4.6 Hz), 16.9–16.7 (m).

^{19}F NMR (377 MHz, $CDCl_3$) δ −138.6–−138.8 (m), −146.3 (tt, *J* = 20.9, 3.9 Hz), −157.2–−157.4 (m).

HRMS (EI): m/z calculated for $C_9H_1N_2F_5^{\bullet+}$ ($M^{\bullet+}$): 232.0054, found: 232.0052.

Preparation of Ethyl 2-(4-chloro-2,3,5,6-tetrafluorophenyl)-2-cyanoacetate (C4H)

C4H was synthesized according to the procedure by Vlasov.[59]

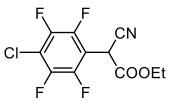

^{1}H NMR (599 MHz, $CDCl_3$) δ 5.10 (s, 1H), 4.42–4.32 (m, 2H), 1.36 (t, *J* = 7.2 Hz, 3H).

^{13}C NMR (151 MHz, $CDCl_3$) δ 162.1, 144.9 (dd, *J* = 253.5, 14.6 Hz), 144.5 (dd, *J* = 252.7, 15.5 Hz), 115.0 (t, *J* = 18.9 Hz), 112.5, 108.9 (t, *J* = 16.4 Hz), 64.7, 32.0, 14.0.

^{19}F NMR (377 MHz, Chloroform-*d*) δ −138.5–−138.6 (m), −139.5–−139.7 (m).

Preparation of Potassium

1-(4-chloro-2,3,5,6-tetrafluorophenyl)-1-cyano-2-ethoxy-2-oxoethan-1-ide (C4K)

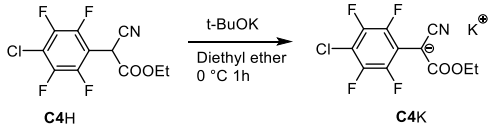

C4H **C4**K

To a stirred saturated solution of *tert*-butoxide (124 mg, 1.11 mmol) in diethyl ether, **C**4H (259 mg, 0.876 mmol) was dropped inside at 0 °C under nitrogen atmosphere. The precipitate was filtrated under nitrogen atmosphere and dried under vacuum to give **C4**K (218 mg, 0.653 mmol, 74.5%) as a white solid.

Preparation of Ethyl 2-cyano-2-(perfluorophenyl)acetate (C3H)

C3H was synthesized following the procedure by Hull.[60]

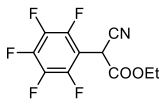

^{1}H NMR (400 MHz, $CDCl_3$) δ 5.09 (s, 1H), 4.39 (qq, *J* = 7.2, 3.6 Hz, 2H), 1.38 (t, *J* = 7.2 Hz, 3H).

^{13}C NMR (101 MHz, $CDCl_3$) δ 162.2, 147.2–136.3 (m, 5C), 112.6, 105.86–105.31 (m, 1C), 64.7, 31.8, 14.0.

^{19}F NMR (376 MHz, Chloroform-*d*) δ −139.91– −140.05 (m), −150.00 (tt, *J* = 20.8, 2.8 Hz), −159.47–−159.67 (m).

Preparation of Potassium 1-cyano-2-ethoxy-2-oxo-1-(perfluorophenyl)ethan-1-ide (C3K)

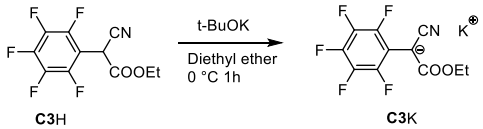

To a stirred saturated solution of *tert*-butoxide (124 mg, 1.11 mmol) in diethyl ether, **C3**H (248 mg, 0.888 mmol) was dropped inside at 0 °C under nitrogen atmosphere. The precipitate was filtrated under nitrogen atmosphere and dried under vacuum to give **C3**K (120 mg, 0.376 mmol, 42.3%) as a white solid.

7.1.4 Copies of NMR and IR spectra

Potassium L-prolinate (A1)

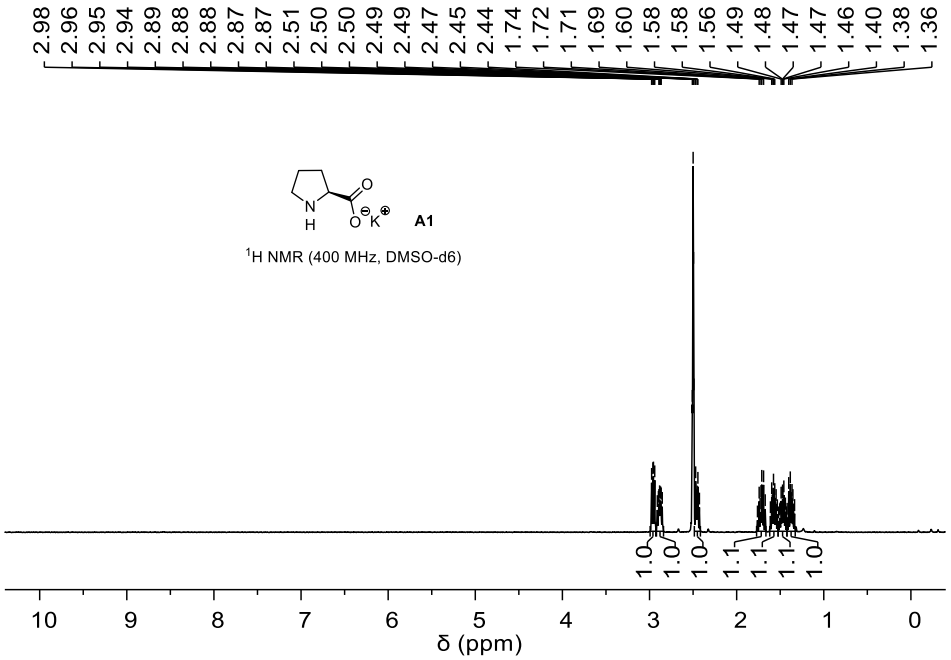

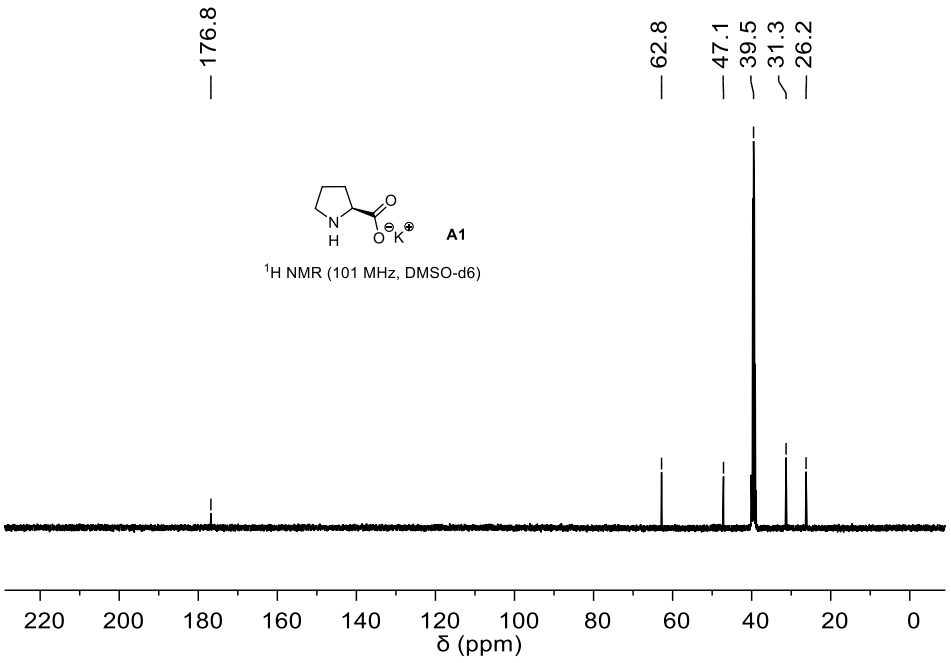

2-Methylpyrrolidine (A3)

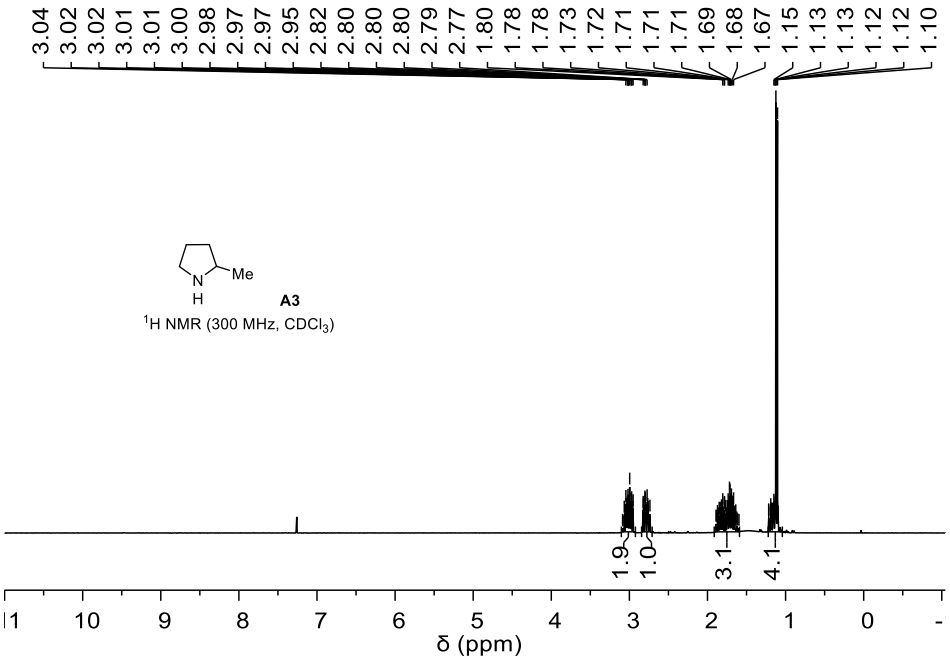

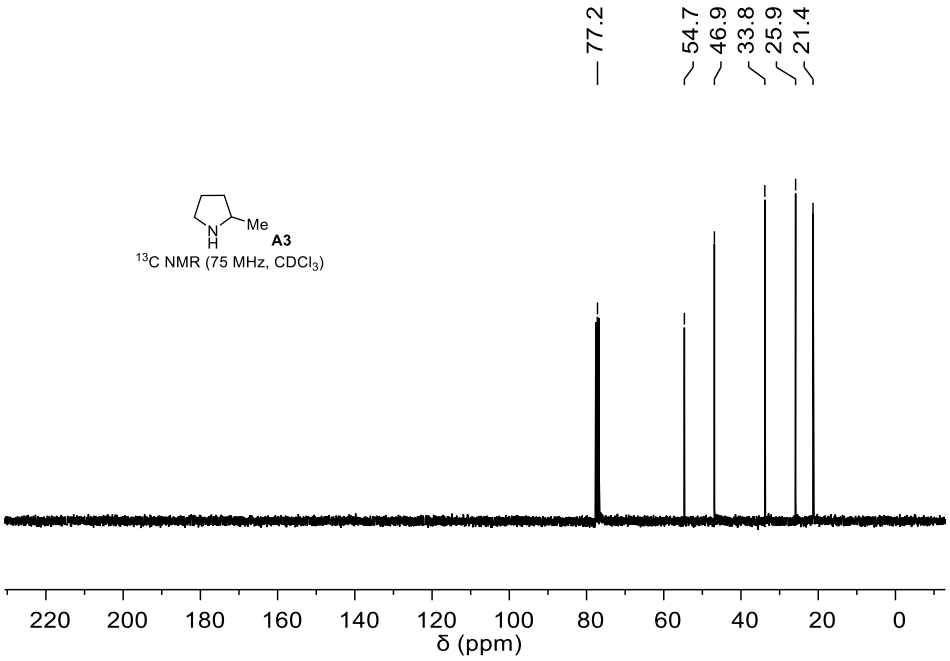

(*R*)-2-Isopropylpyrrolidine (A4)

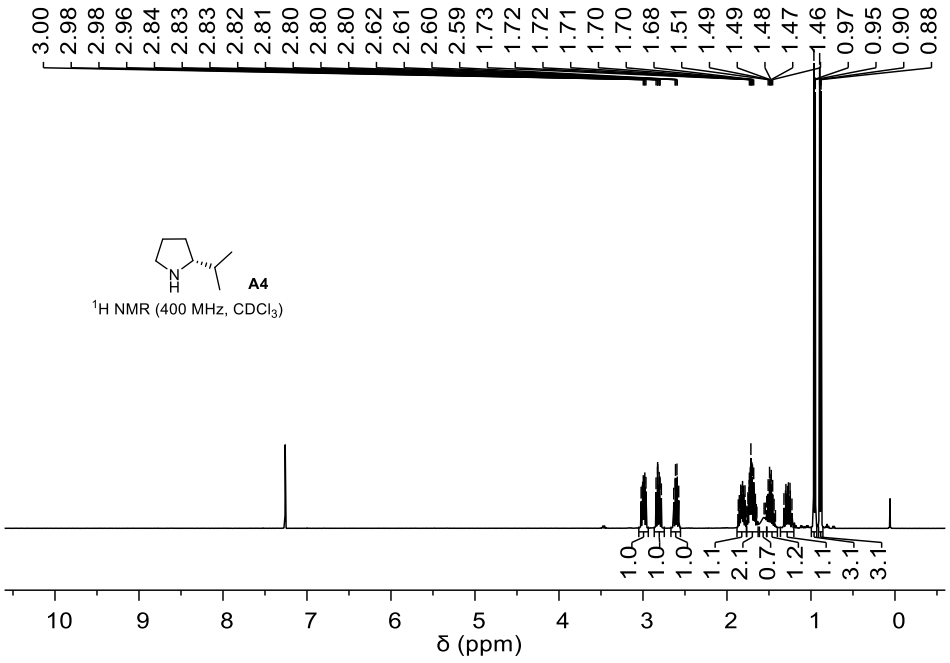

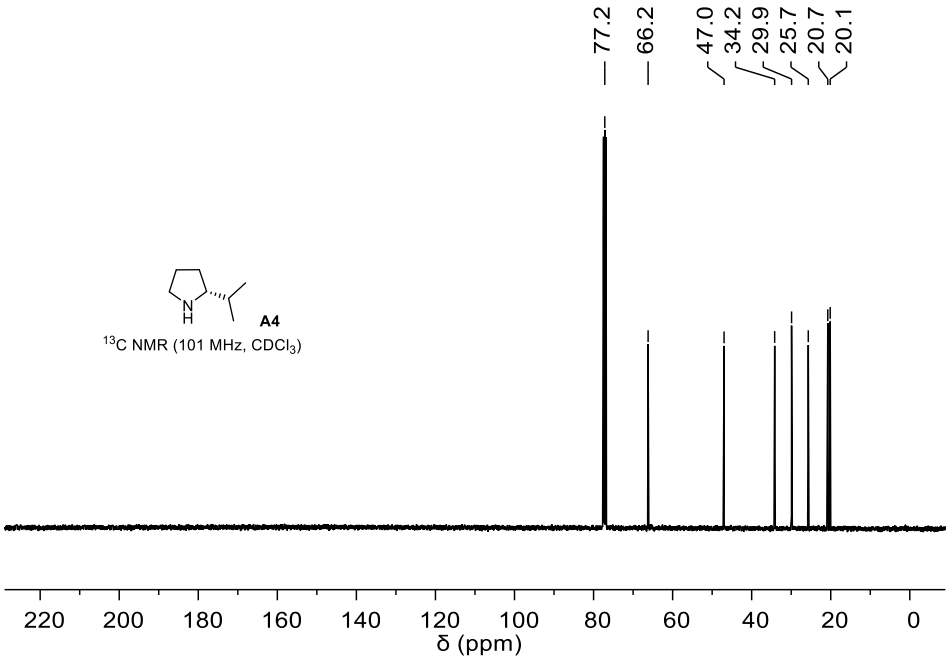

2,2-Dimethylpyrrolidine (A5)

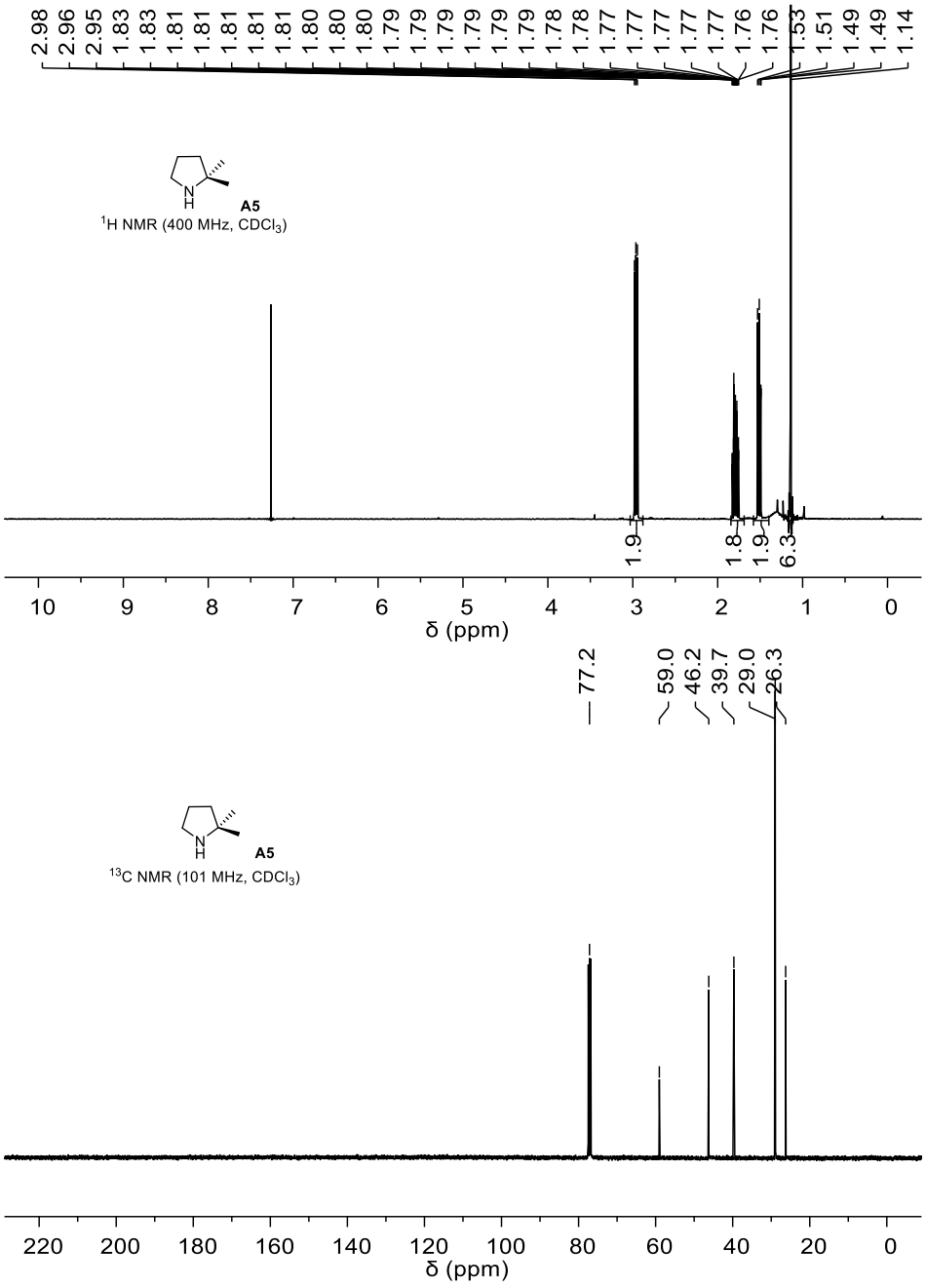

(*S*)-2-Benzhydrylpyrrolidine (A7)

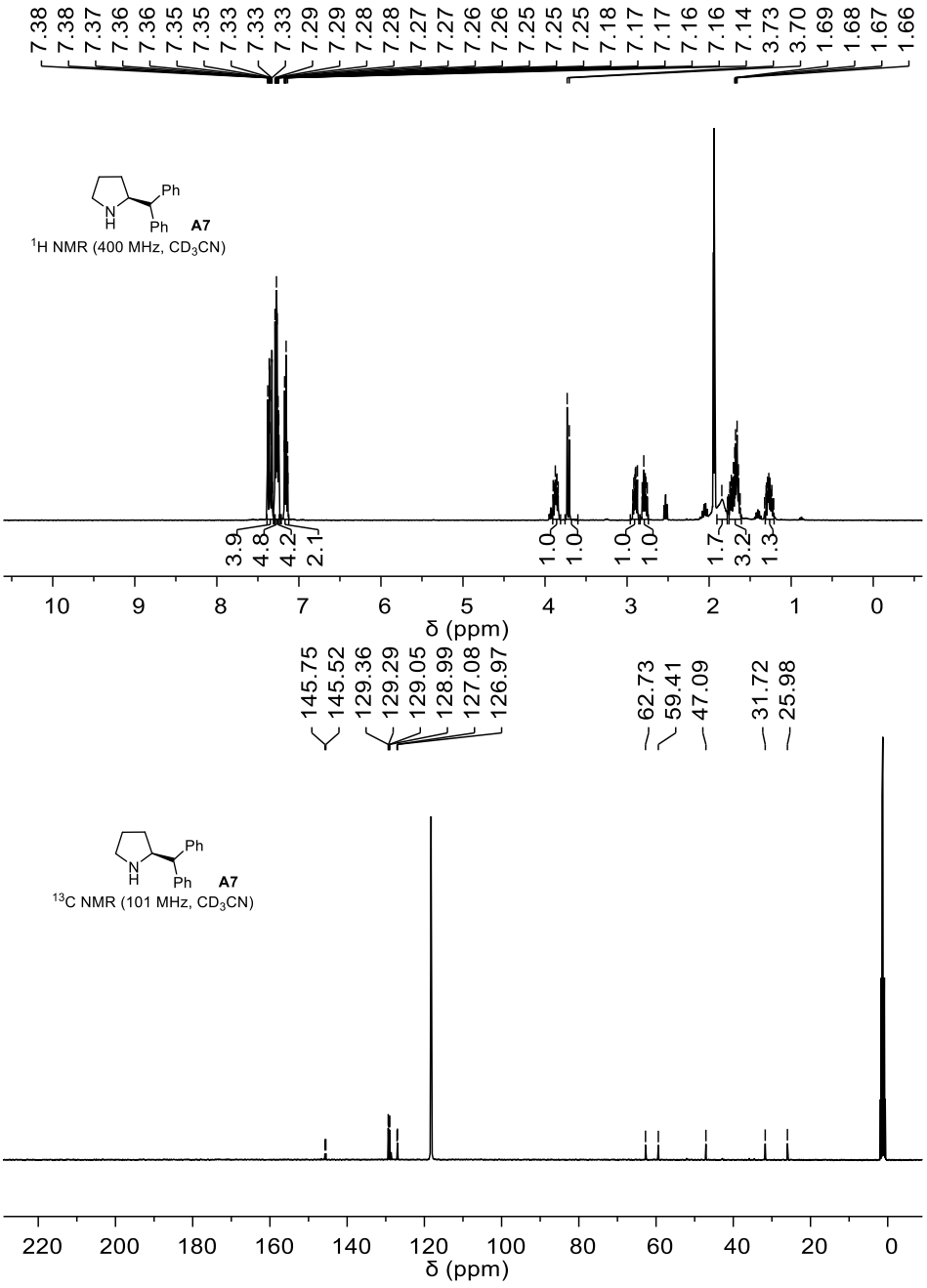

(*S*)-Pyrrolidin-2-ylmethanamine (A8)

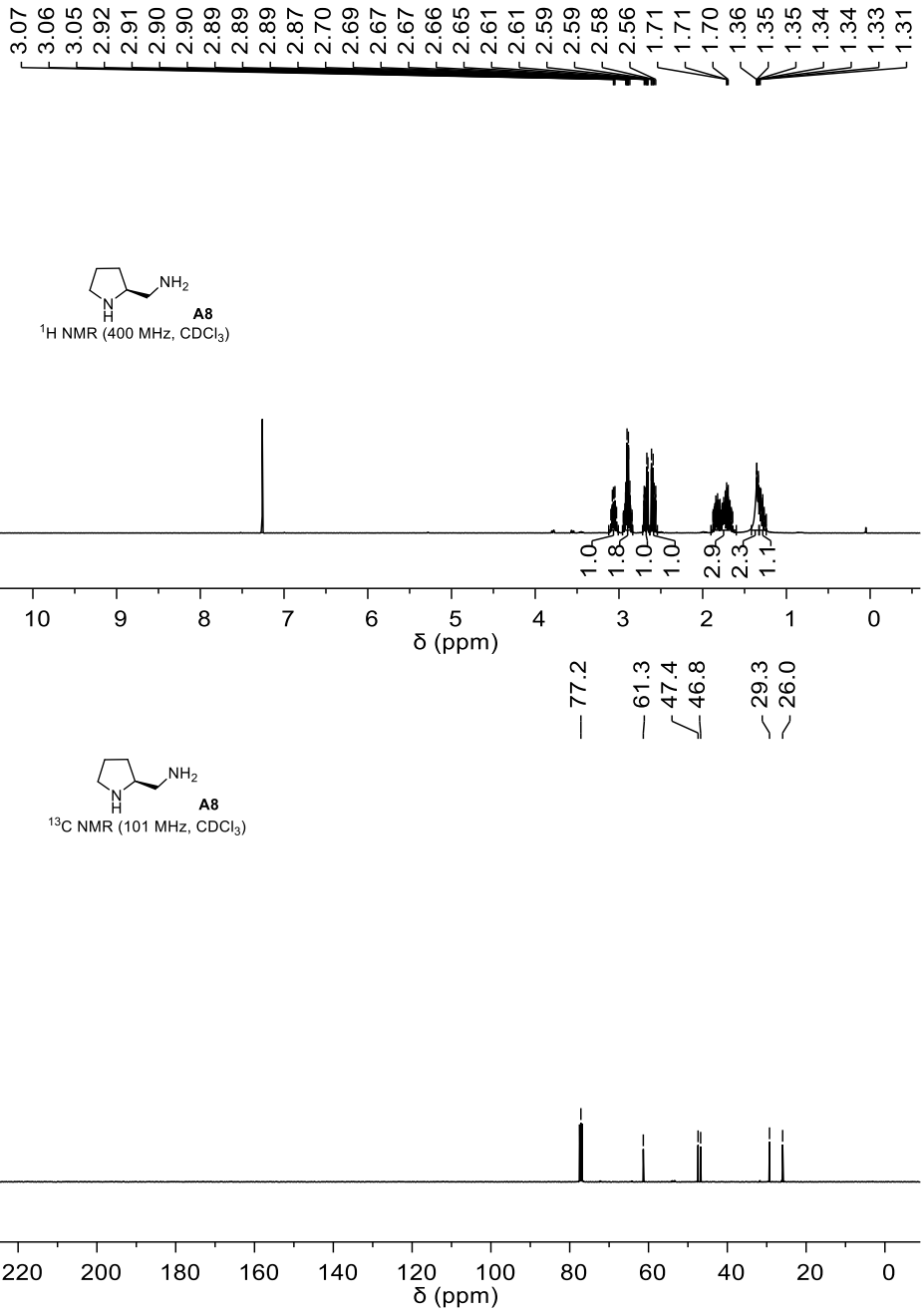

(*S*)-*N*,*N*-Dimethyl-1-(pyrrolidin-2-yl)methanamine (A9)

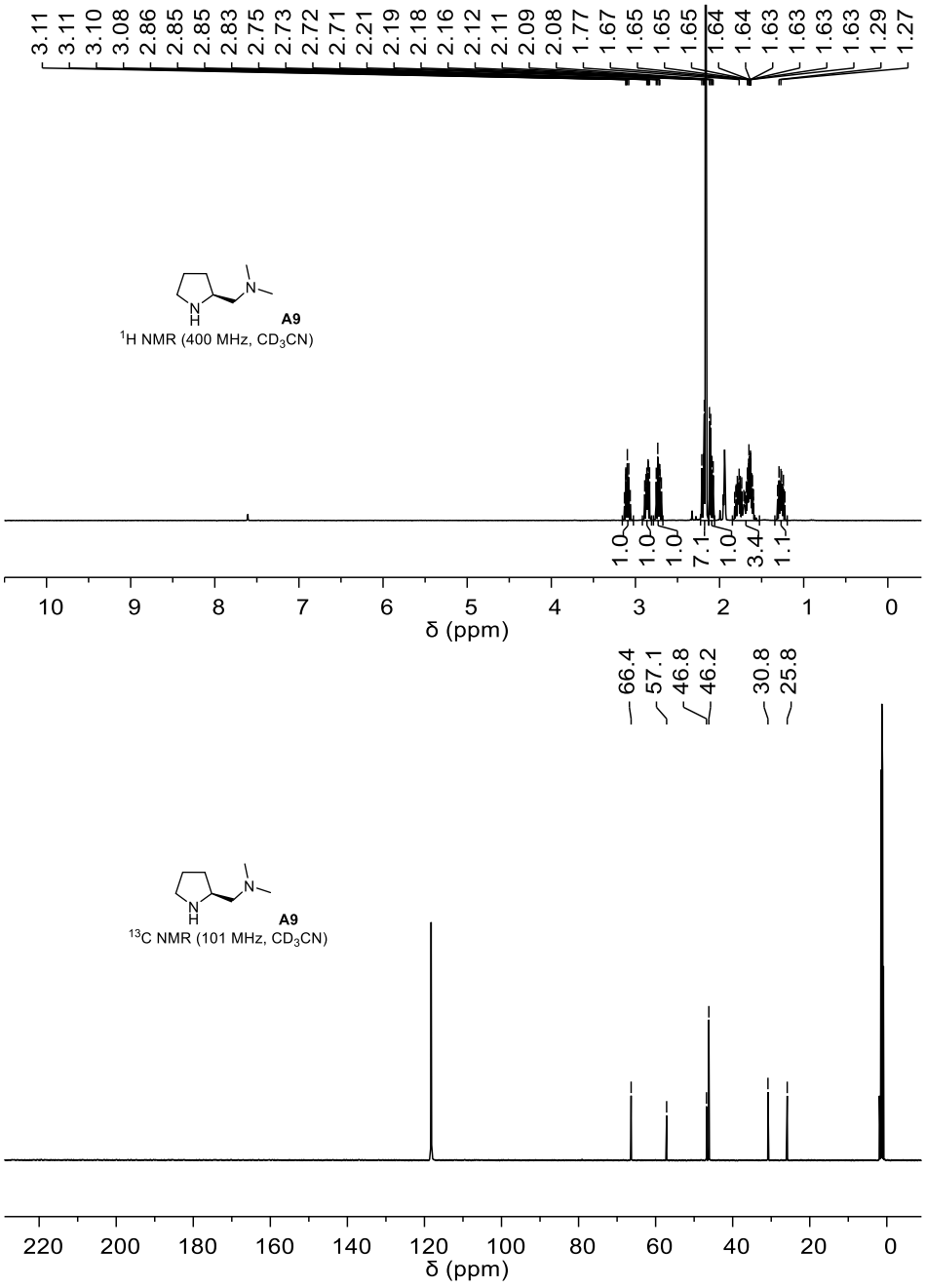

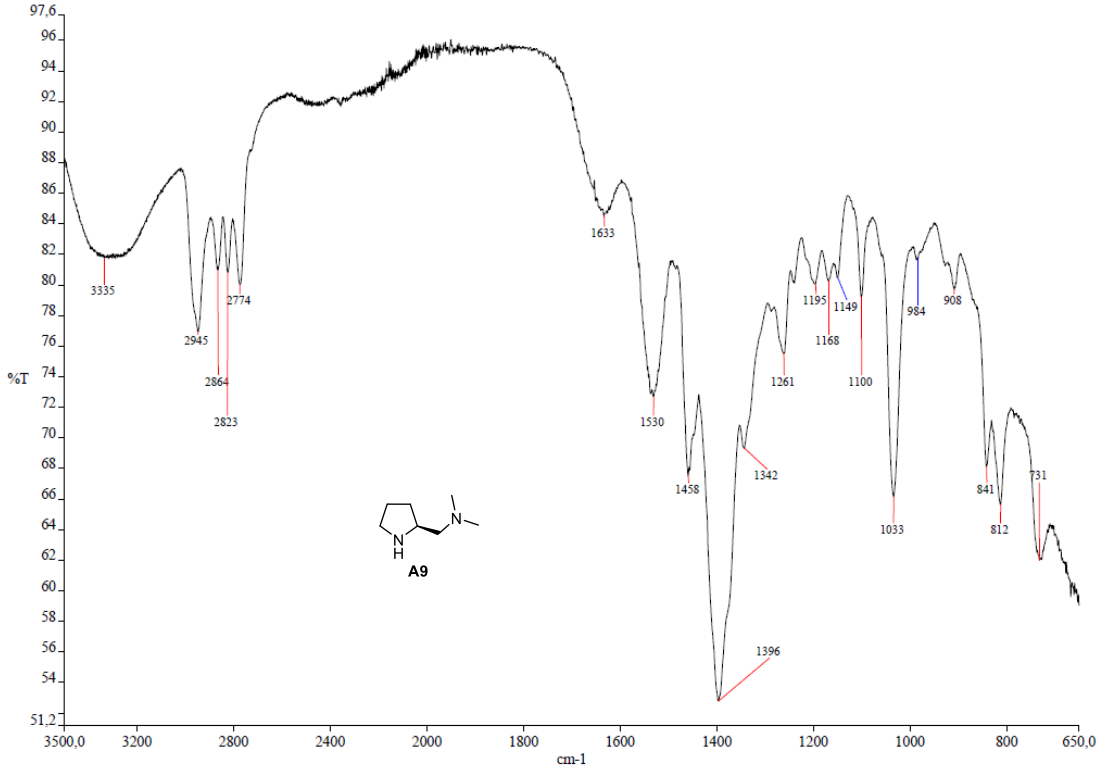
97,6
96
94
92
90
88
86
84
82
80
78
76
74
72
70
68
66
64
62
60
58
56
54
51,2
%T
3500,0
3200
2800
2400
2000
1800
1600
1400
1200
1000
800
650,0
cm-1
3335
2945
2864
2823
2774
1633
1530
1458
1396
1342
1261
1195
1168
1149
1100
1033
984
908
841
812
731
A9

(*S*)-2-((Dimethylamino)methyl)pyrrolidin-1-ium trifluoromethanesulfonate (A9H$^+$OTf$^-$)

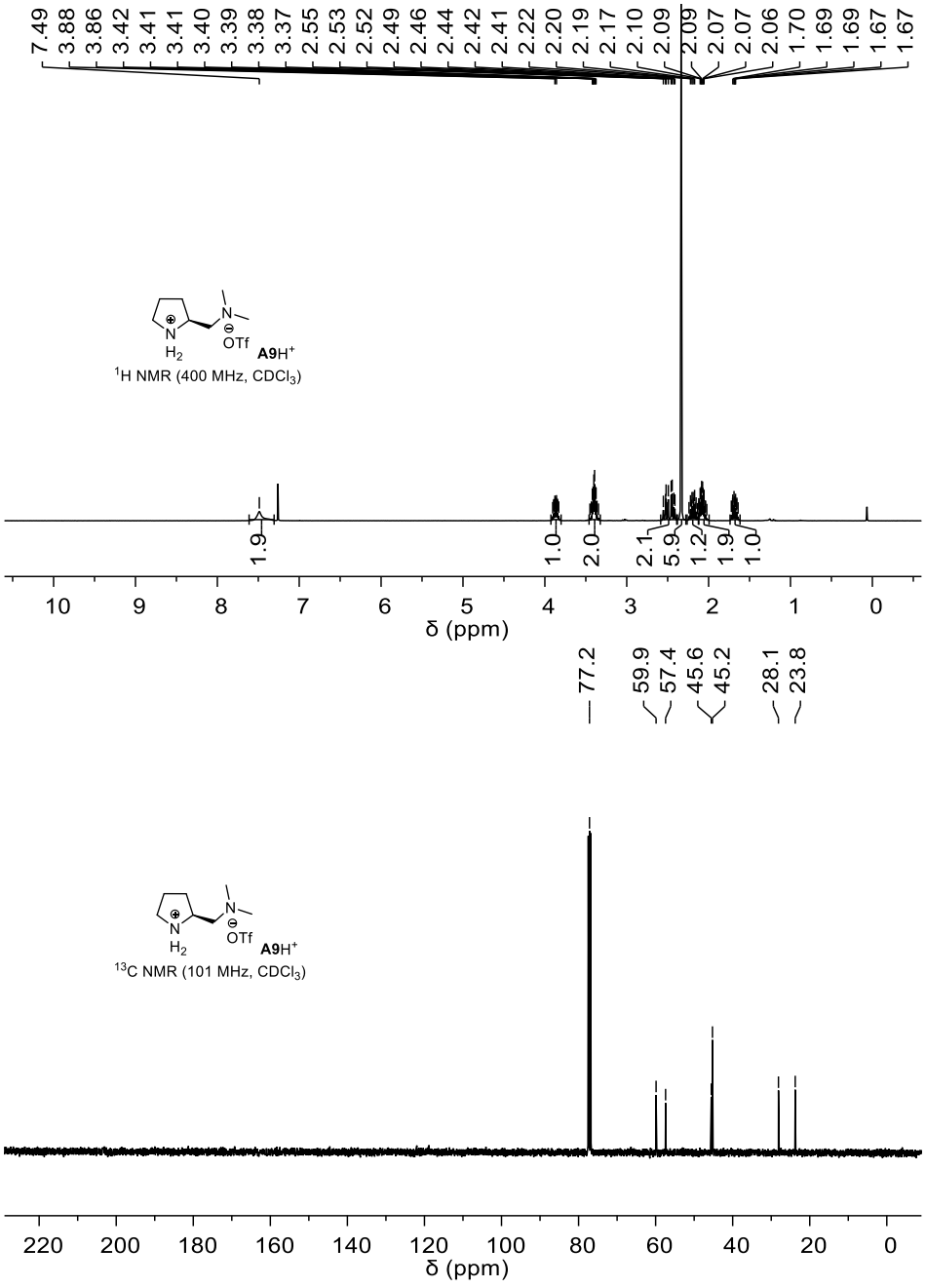

(*S*)-1-(pyrrolidin-2-ylmethyl)pyrrolidine (A10)

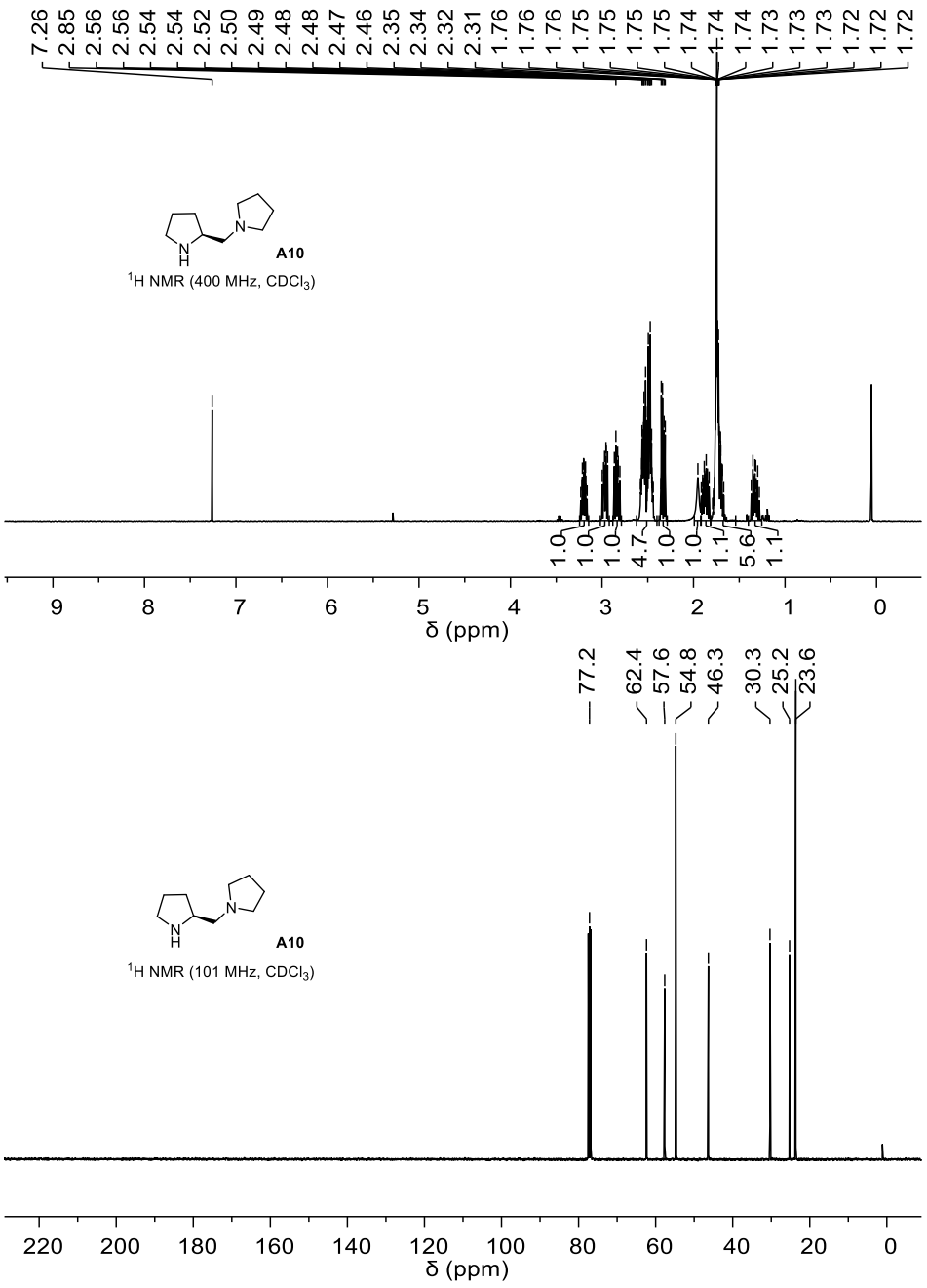

(*S*)-2-(Azidomethyl)pyrrolidine (A11)

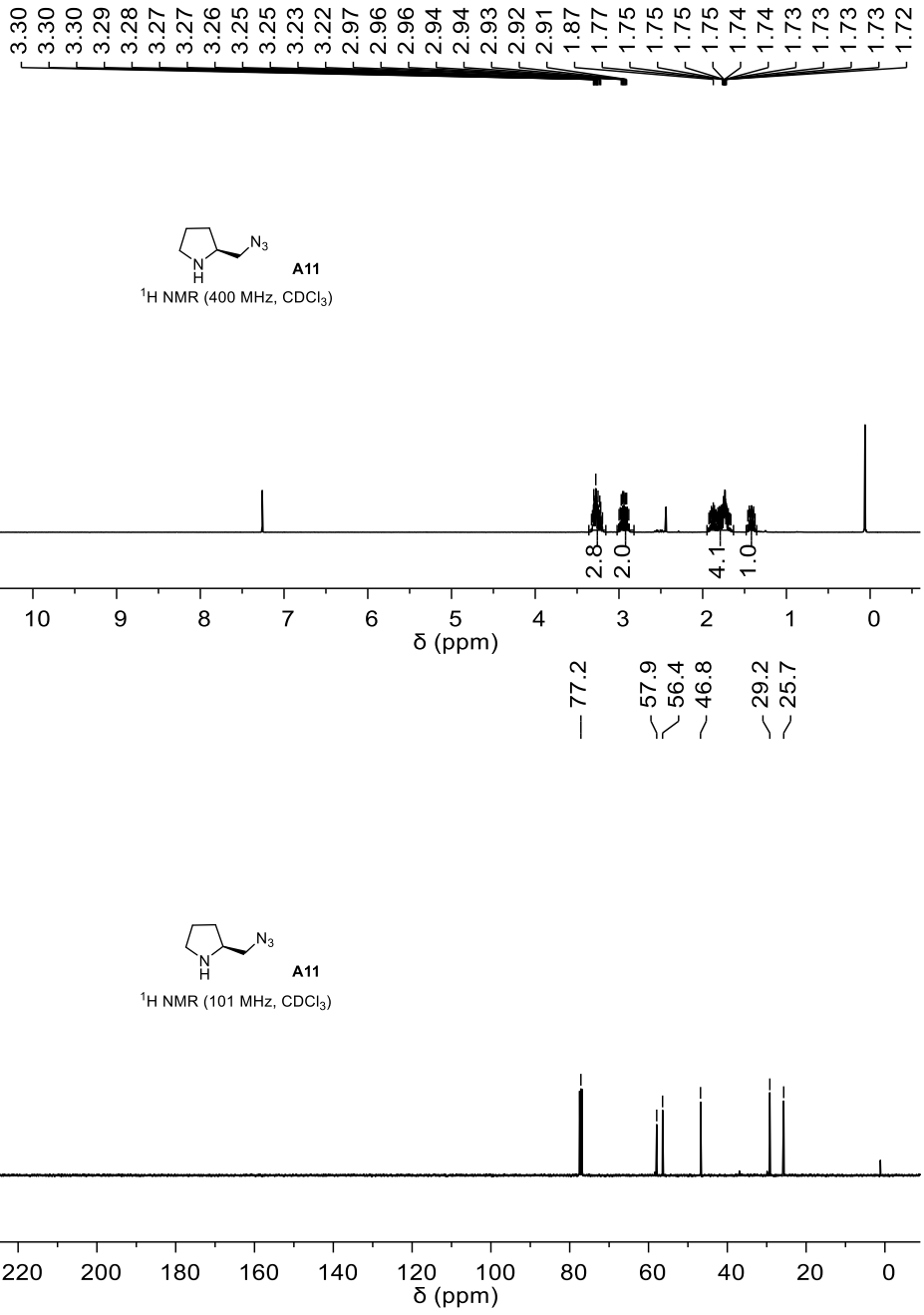

(*S*)-Pyrrolidin-2-ylmethanol (A12)

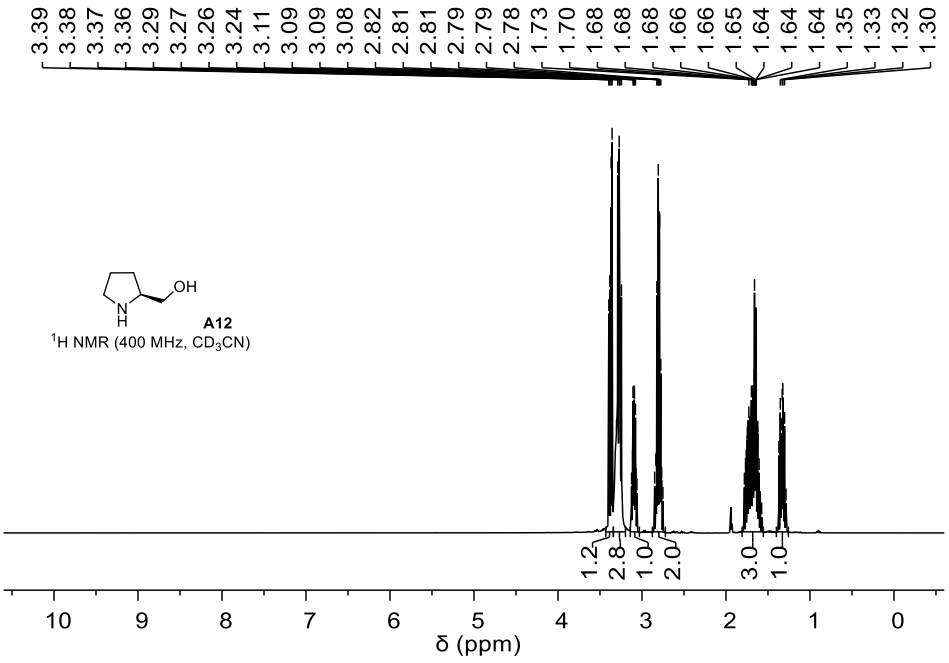

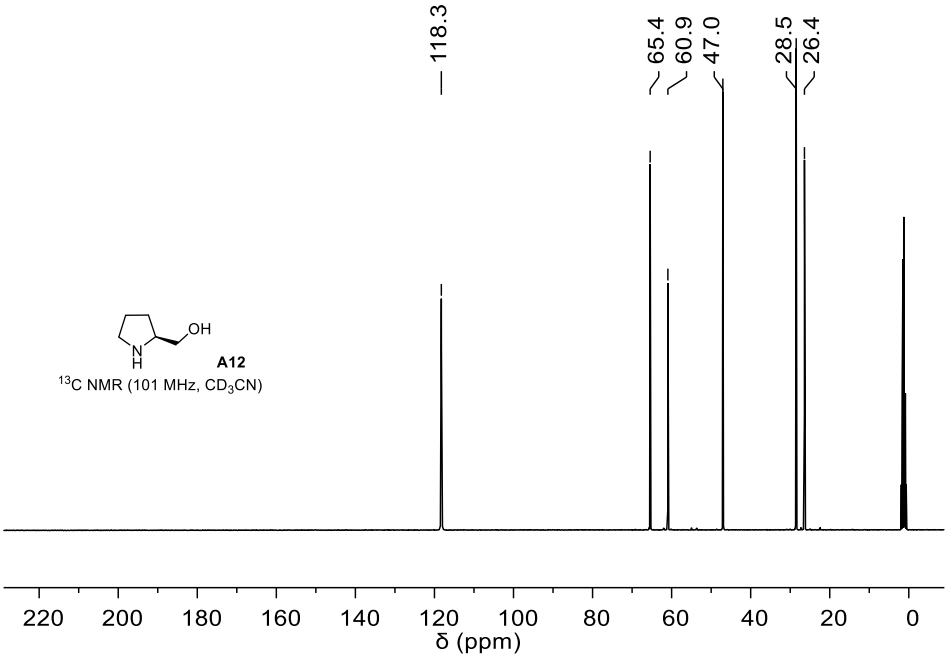

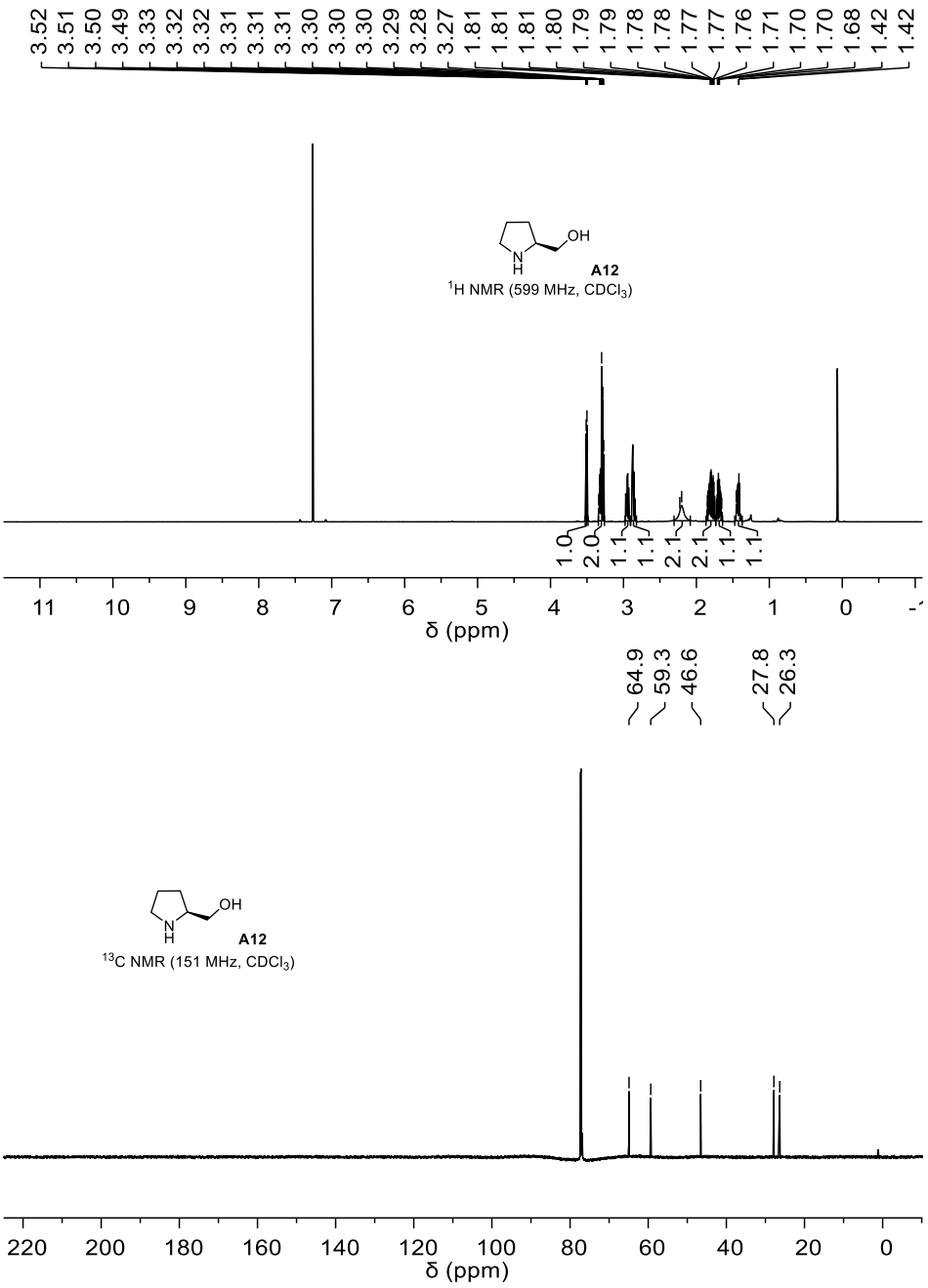
3.52 3.51 3.50 3.49 3.33 3.32 3.32 3.31 3.31 3.31 3.30 3.30 3.30 3.29 3.28 3.27 1.81 1.81 1.81 1.80 1.79 1.79 1.78 1.78 1.77 1.77 1.76 1.71 1.70 1.70 1.68 1.42 1.42
OH
N
H
A12
1H NMR (599 MHz, CDCl3)
1.0 2.0 1.1 1.1 2.1 2.1 1.1 1.1
11 10 9 8 7 6 5 4 3 2 1 0
δ (ppm)
64.9 59.3 46.6 27.8 26.3
OH
N
H
A12
13C NMR (151 MHz, CDCl3)
220 200 180 160 140 120 100 80 60 40 20 0
δ (ppm)

(*S*)-2-(Methoxymethyl)pyrrolidine (A13)

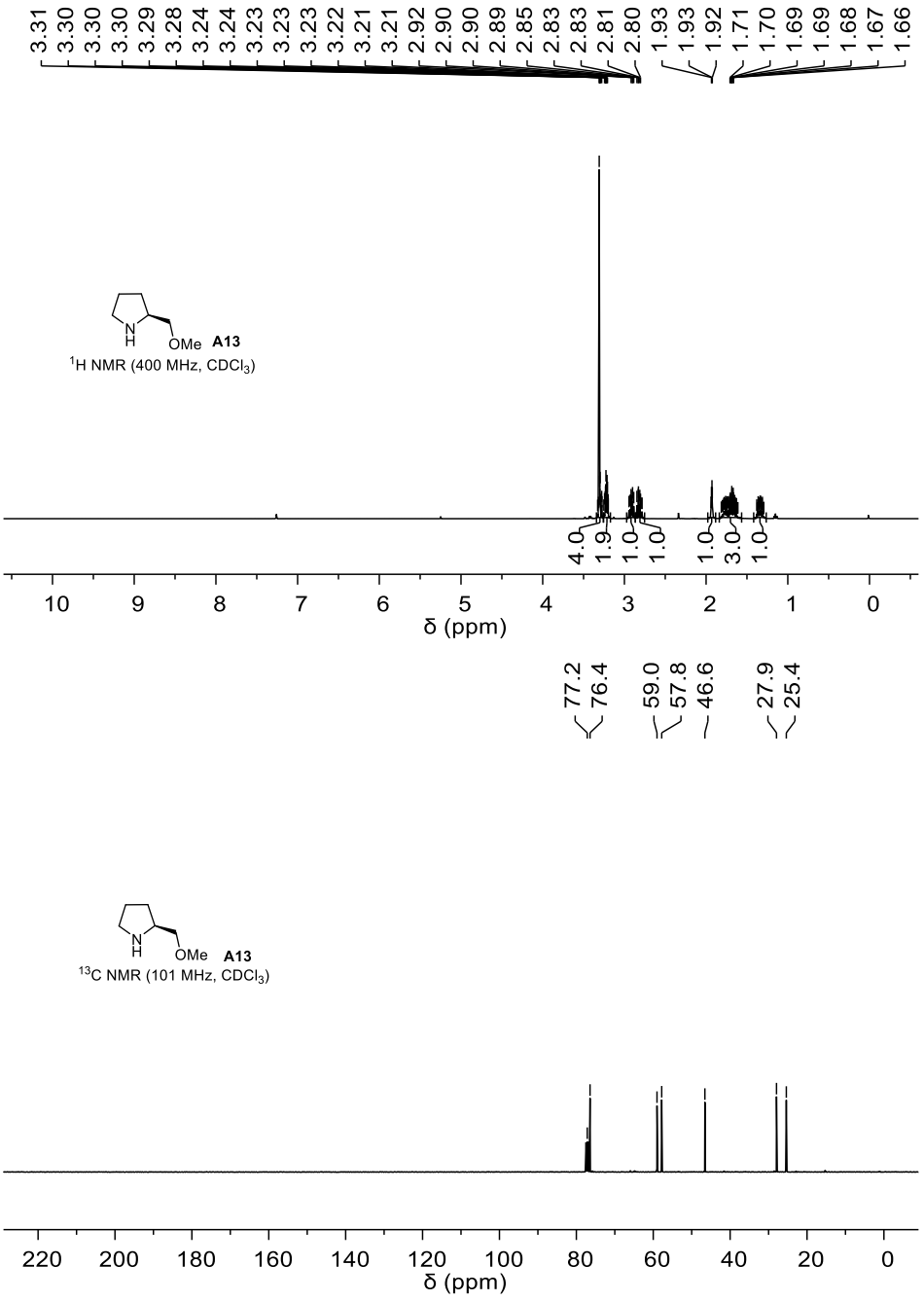

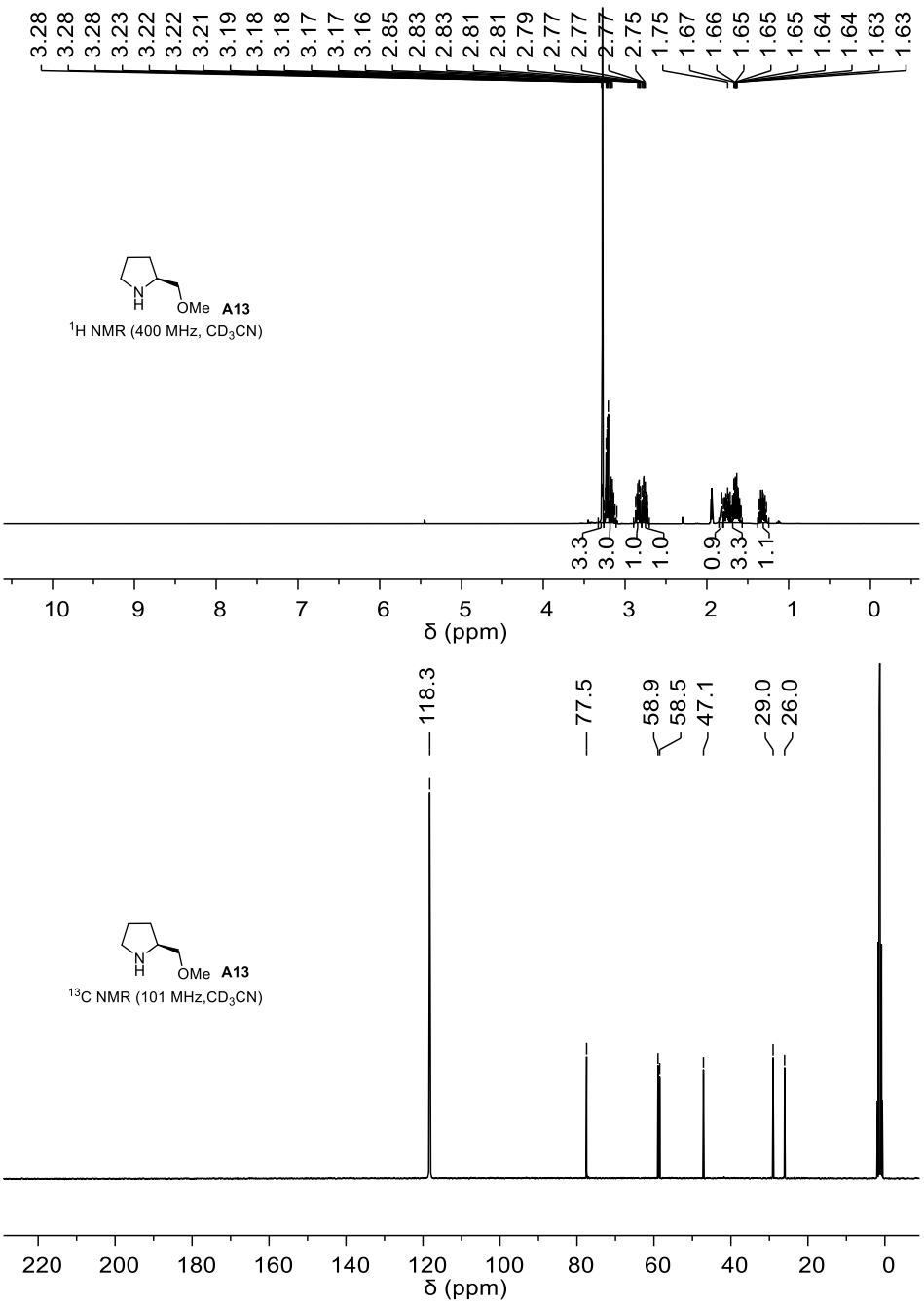
3.28
3.28
3.28
3.23
3.22
3.22
3.21
3.19
3.18
3.18
3.17
3.17
3.16
2.85
2.83
2.83
2.81
2.81
2.79
2.77
2.77
2.77
2.75
1.75
1.67
1.66
1.65
1.65
1.65
1.64
1.64
1.63
1.63
OMe A13
1H NMR (400 MHz, CD3CN)
3.3
3.0
1.0
1.0
0.9
3.3
1.1
10 9 8 7 6 5 4 3 2 1 0
δ (ppm)
118.3
77.5
58.9
58.5
47.1
29.0
26.0
OMe A13
13C NMR (101 MHz,CD3CN)
220 200 180 160 140 120 100 80 60 40 20 0
δ (ppm)

2-(Trifluoromethyl)pyrrolidine (A14)

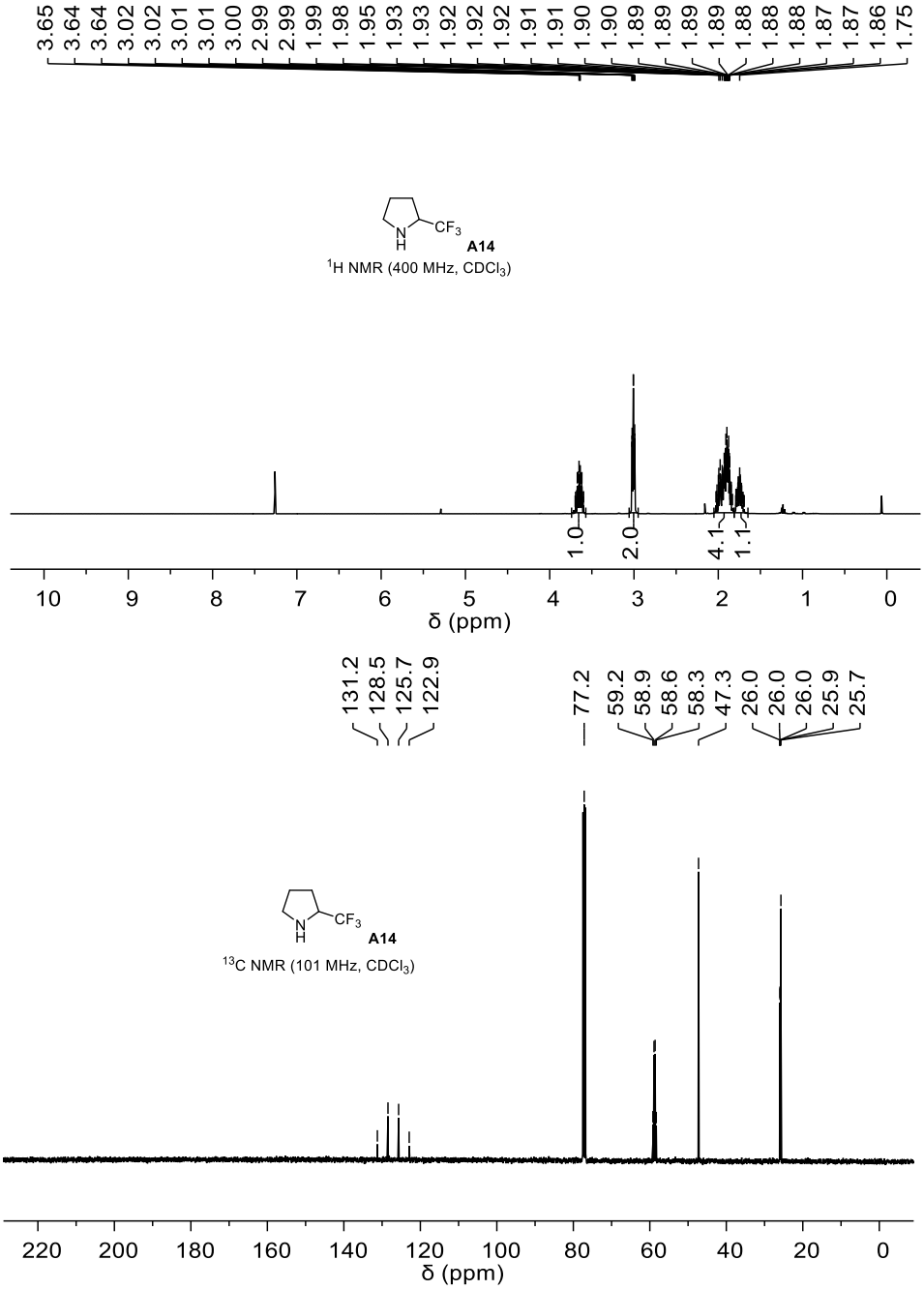

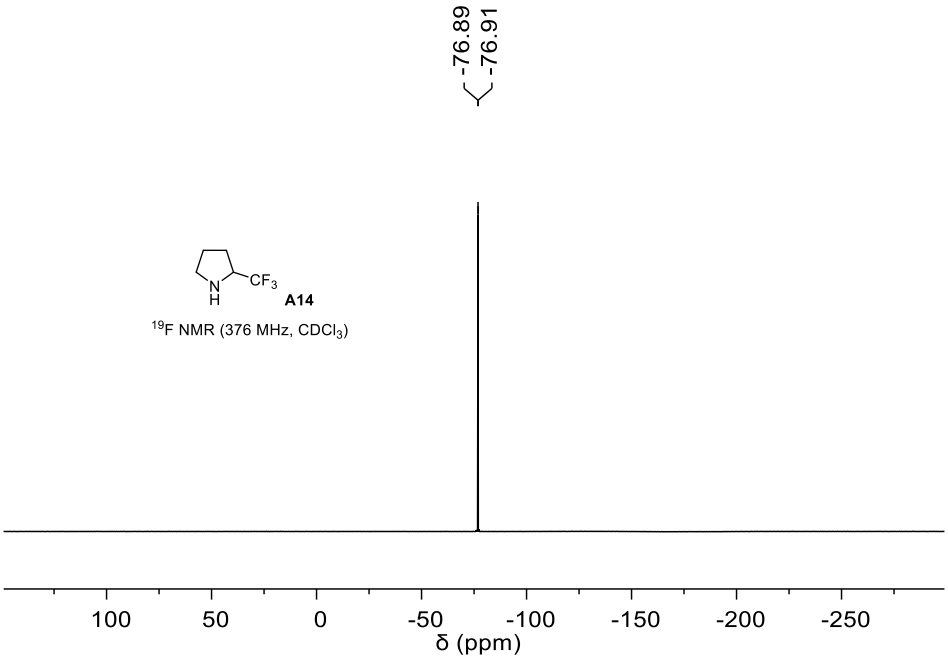
-76.89
-76.91
CF3
N
H
A14
19F NMR (376 MHz, CDCl3)
100
50
0
-50
-100
-150
-200
-250
δ (ppm)

Methyl L-prolinate (A15)

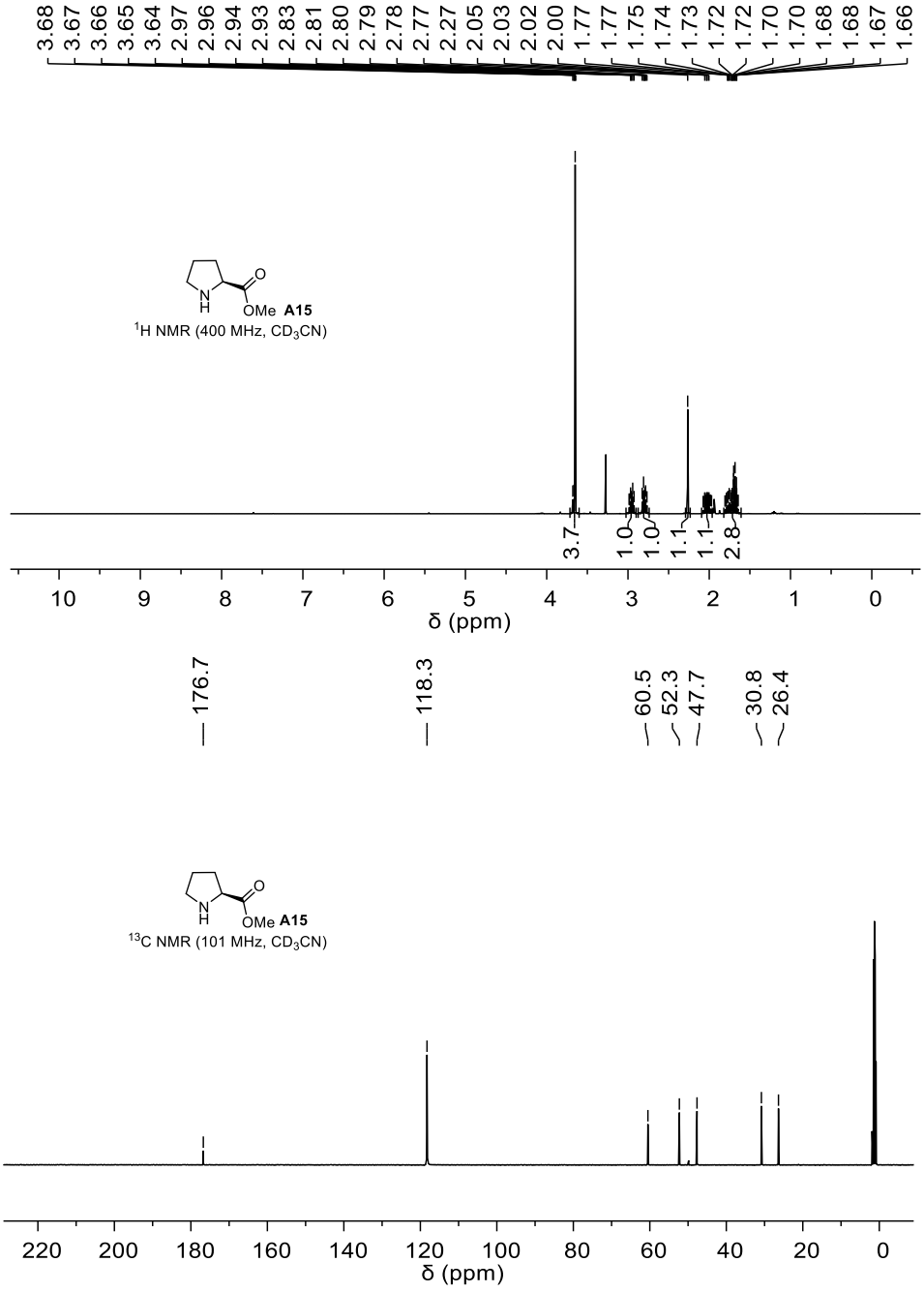

(*S*)-*N*,*N*-Dimethylpyrrolidine-2-carboxamide (A16)

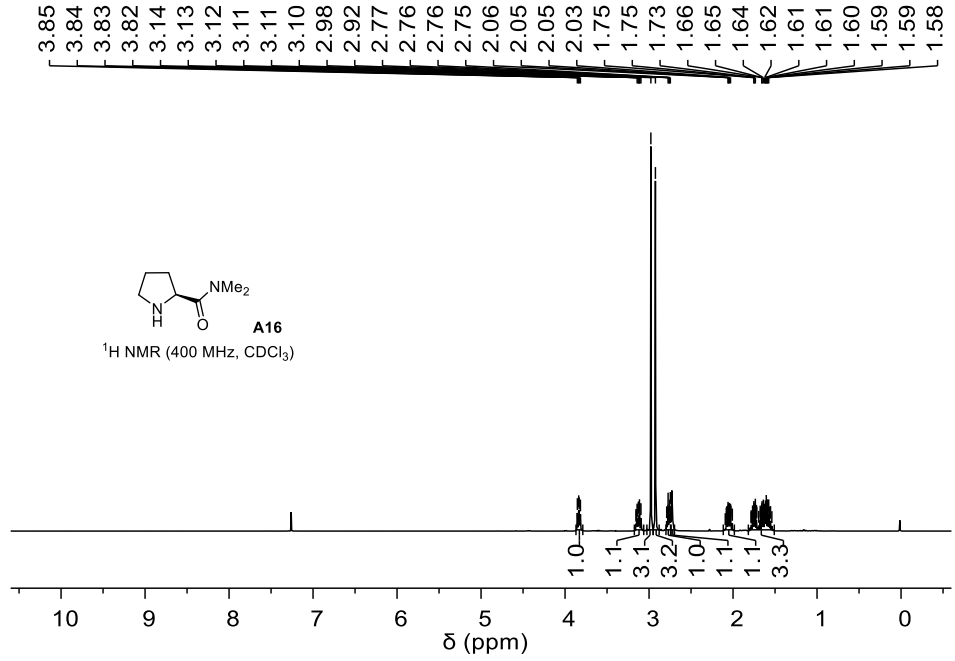

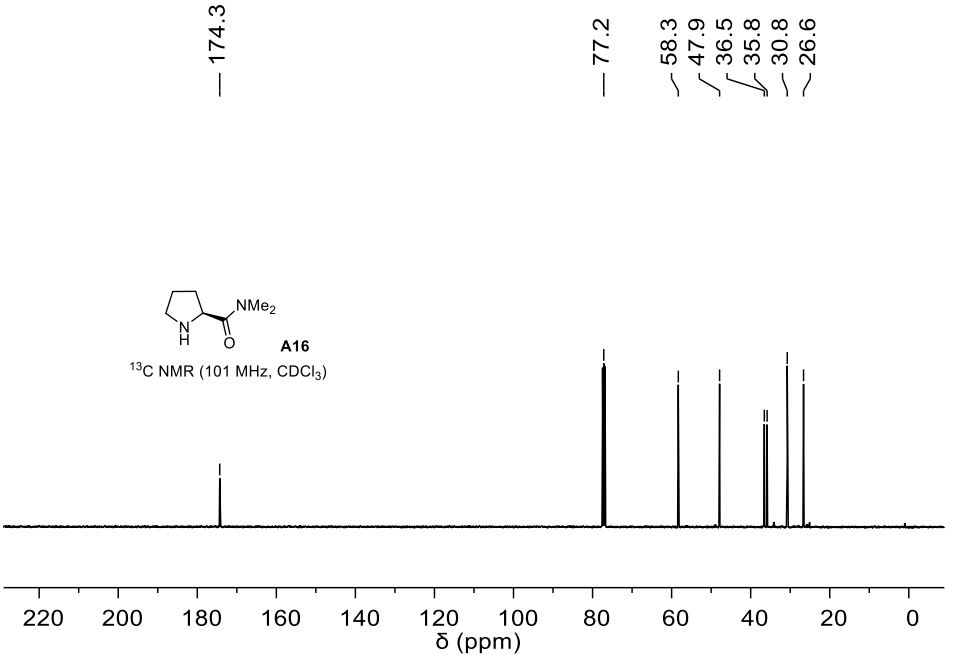

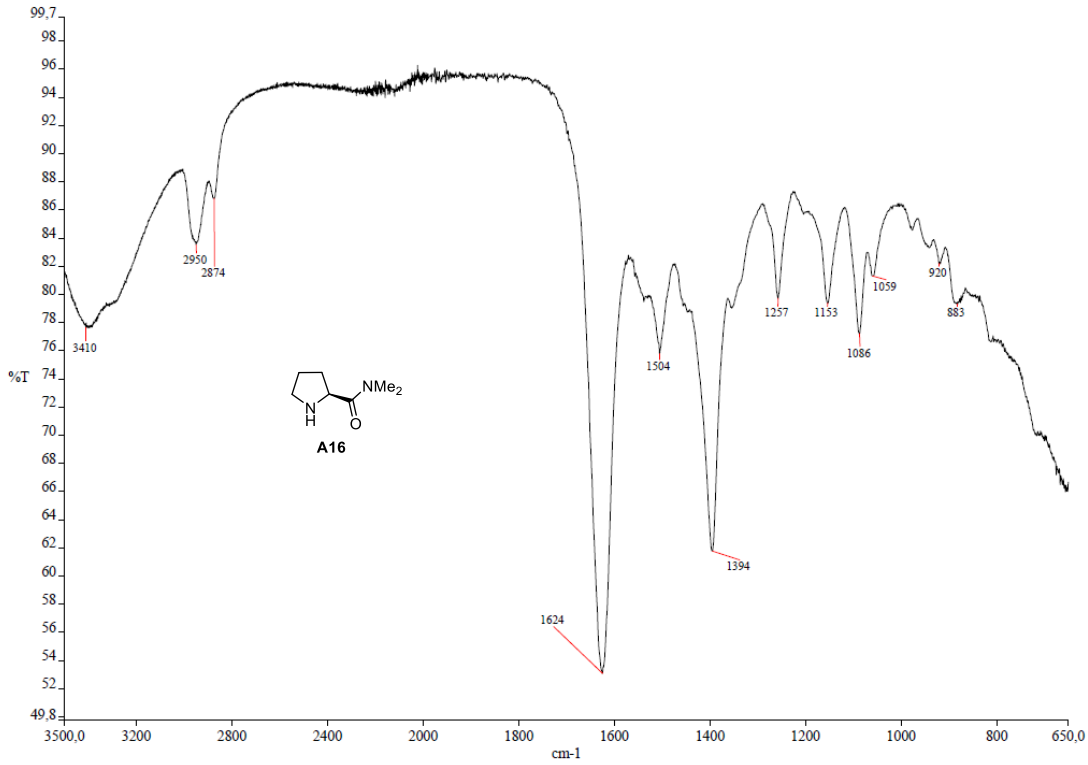
99,7
98
96
94
92
90
88
86
84
82
80
78
76
74
72
70
68
66
64
62
60
58
56
54
52
49,8
%T
3500,0
3200
2800
2400
2000
1800
1600
1400
1200
1000
800
650,0
cm-1
3410
2950
2874
1624
1504
1394
1257
1153
1086
1059
920
883
NMe2
N
H
O
A16

(*S*)-*N*-propylpyrrolidine-2-carboxamide (A17)

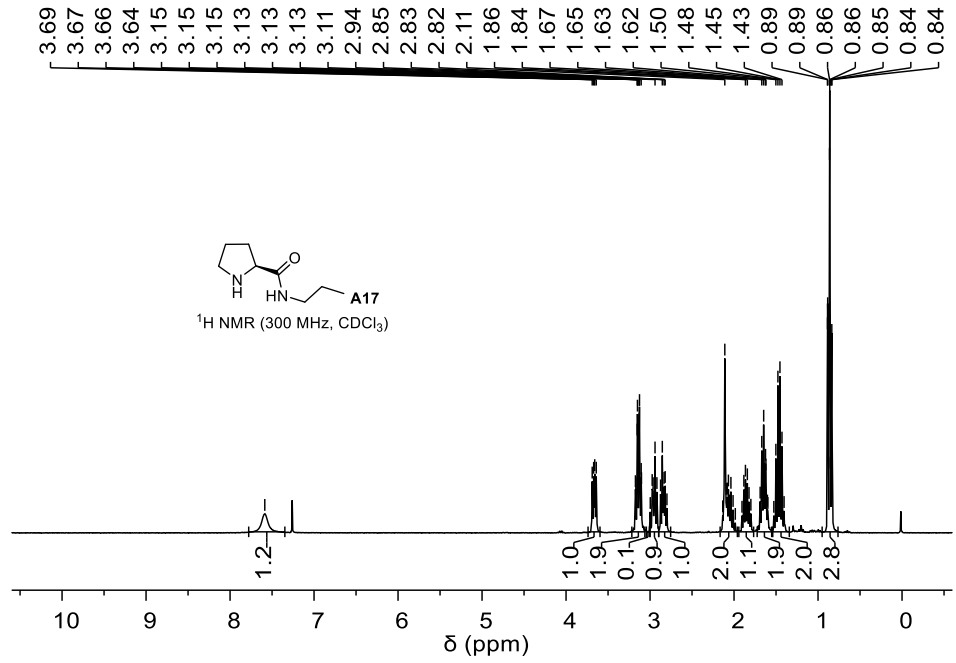

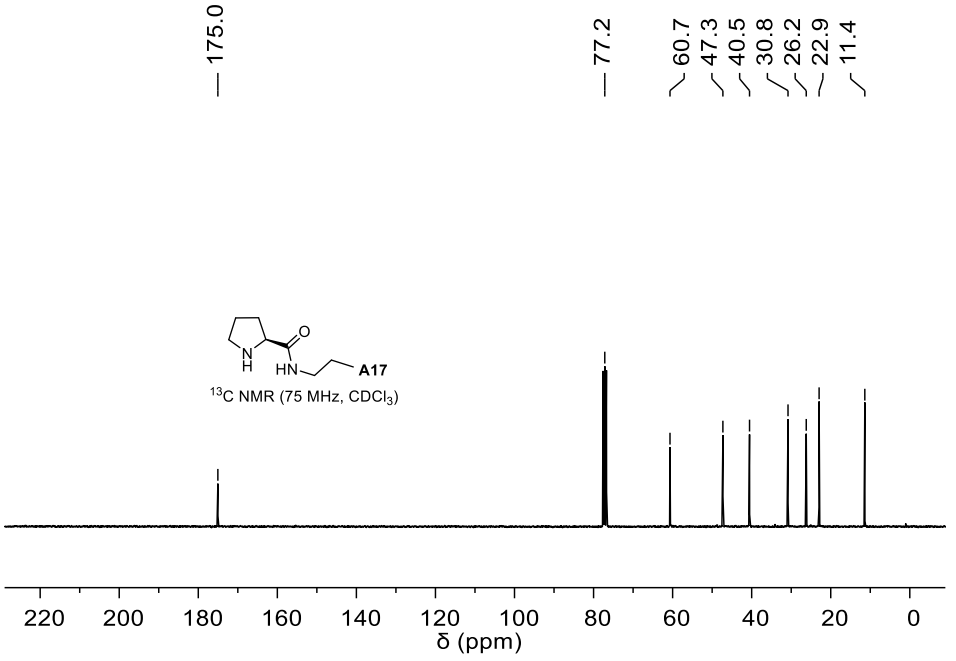

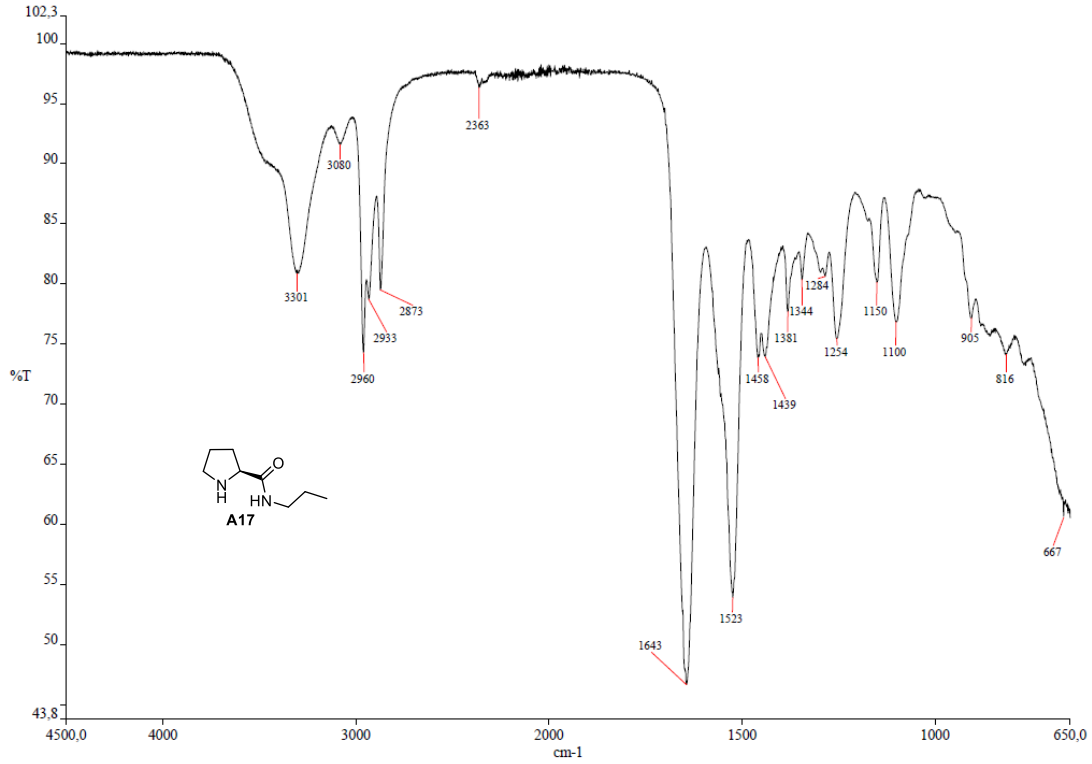
102,3
100
95
90
85
80
75
70
65
60
55
50
43,8
%T
4500,0
4000
3000
2000
1500
1000
650,0
cm-1
3301
3080
2960
2933
2873
2363
1643
1523
1458
1439
1381
1344
1284
1254
1150
1100
905
816
667
A17

(*S*)-2-((1,3-Dioxoisoindolin-2-yl)methyl)pyrrolidin-1-ium 2,2,2-trifluoroacetate (A18H$^+$)

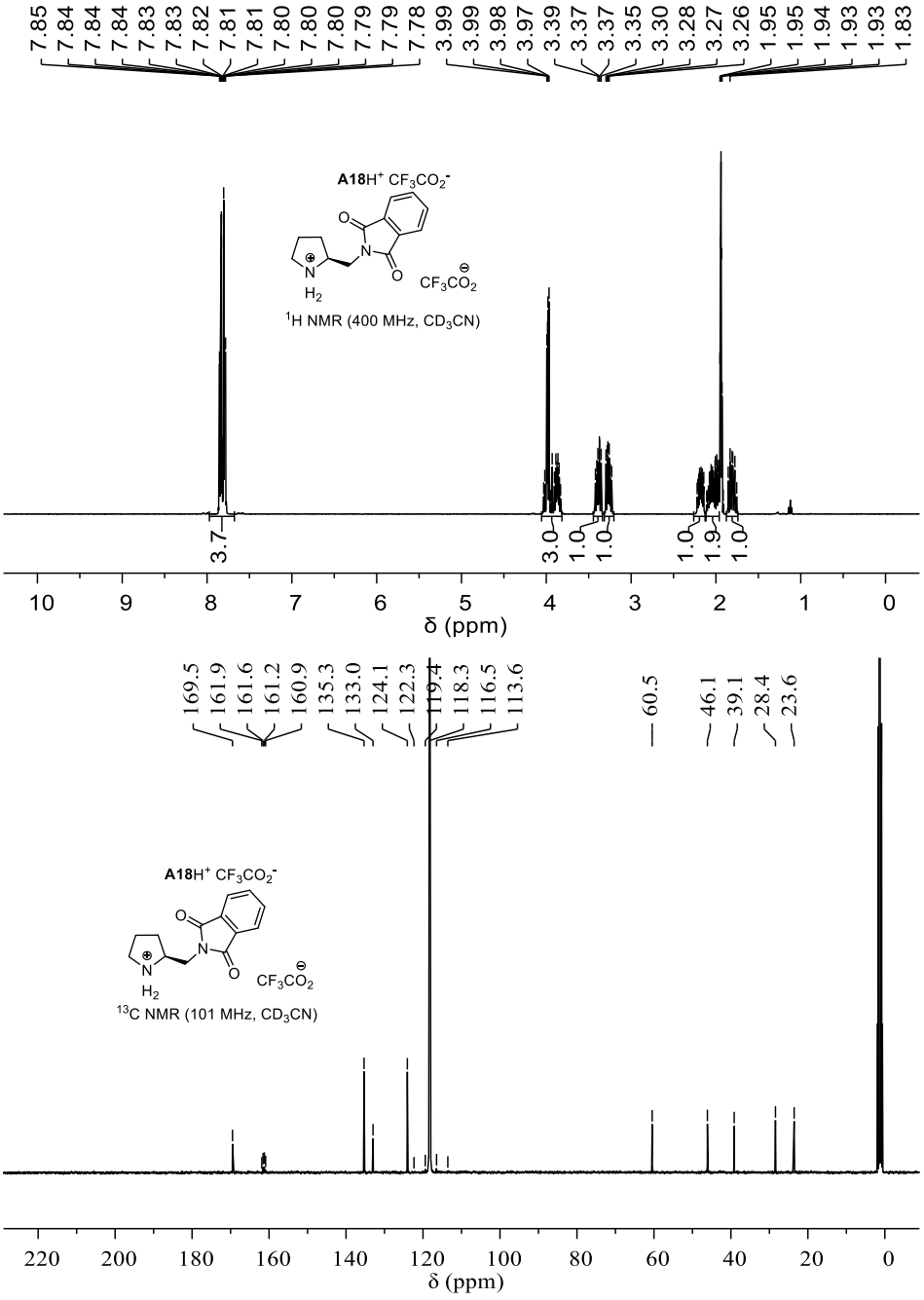

(*S*)-4-Phenyl-1-(pyrrolidin-2-ylmethyl)-1H-1,2,3-triazole (A19)

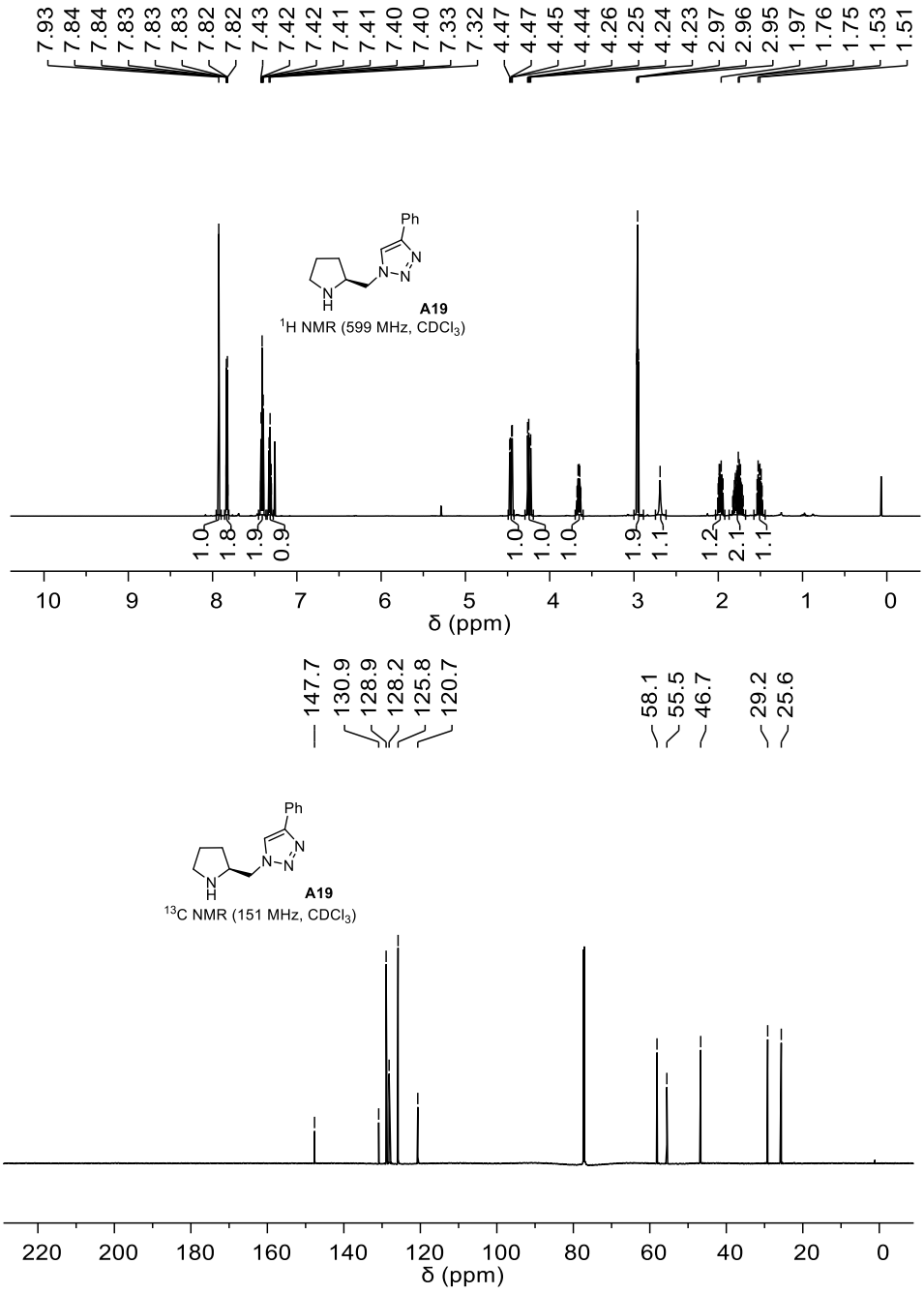

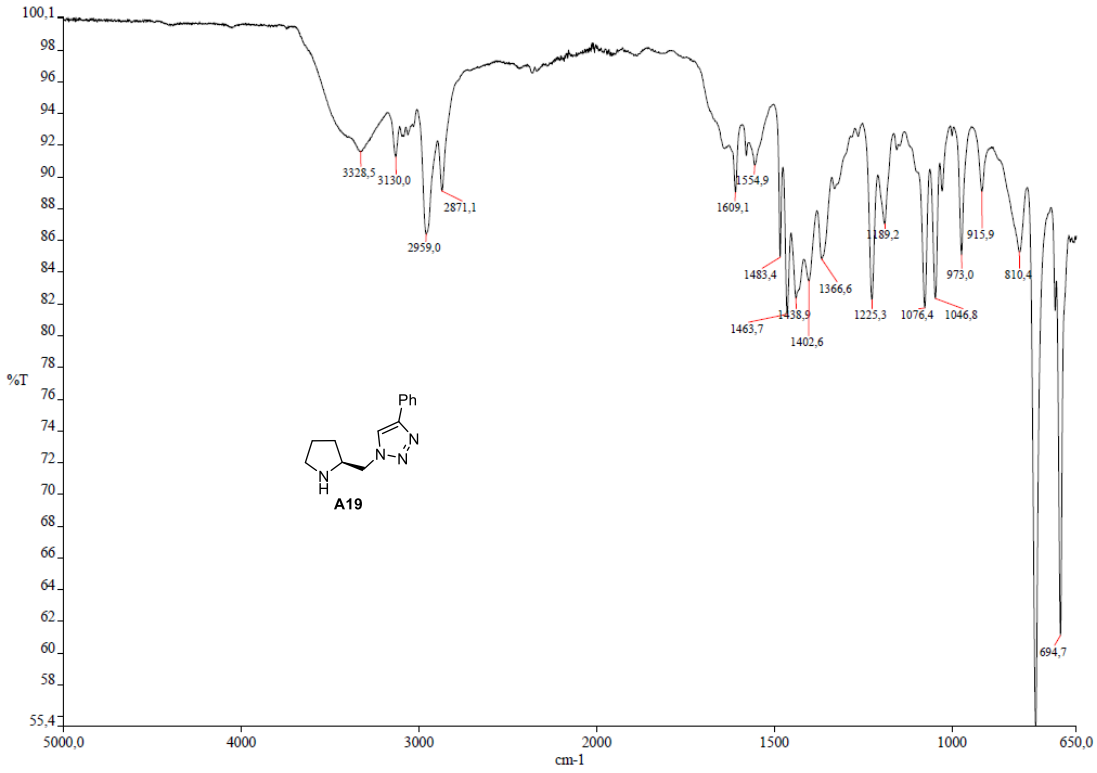
100,1
98
96
94
92
90
88
86
84
82
80
78
76
74
72
70
68
66
64
62
60
58
55,4
%T
5000,0
4000
3000
2000
1500
1000
650,0
cm-1
3328,5
3130,0
2959,0
2871,1
1609,1
1554,9
1483,4
1463,7
1438,9
1402,6
1366,6
1225,3
1189,2
1076,4
1046,8
973,0
915,9
810,4
694,7
Ph
N
N
N
H
A19

(*S*)-1-(Pyrrolidin-2-ylmethyl)-1H-imidazole (A20)

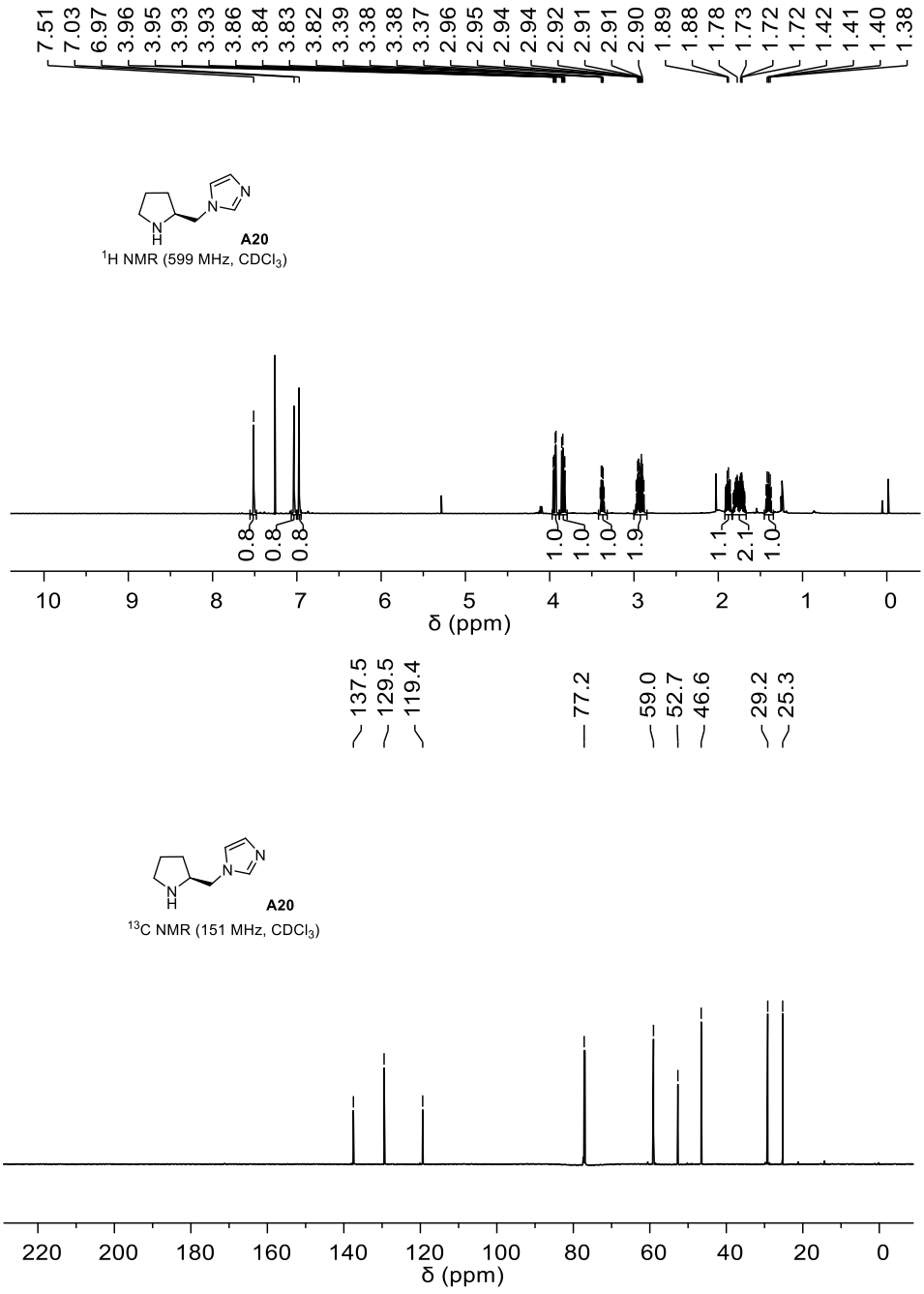

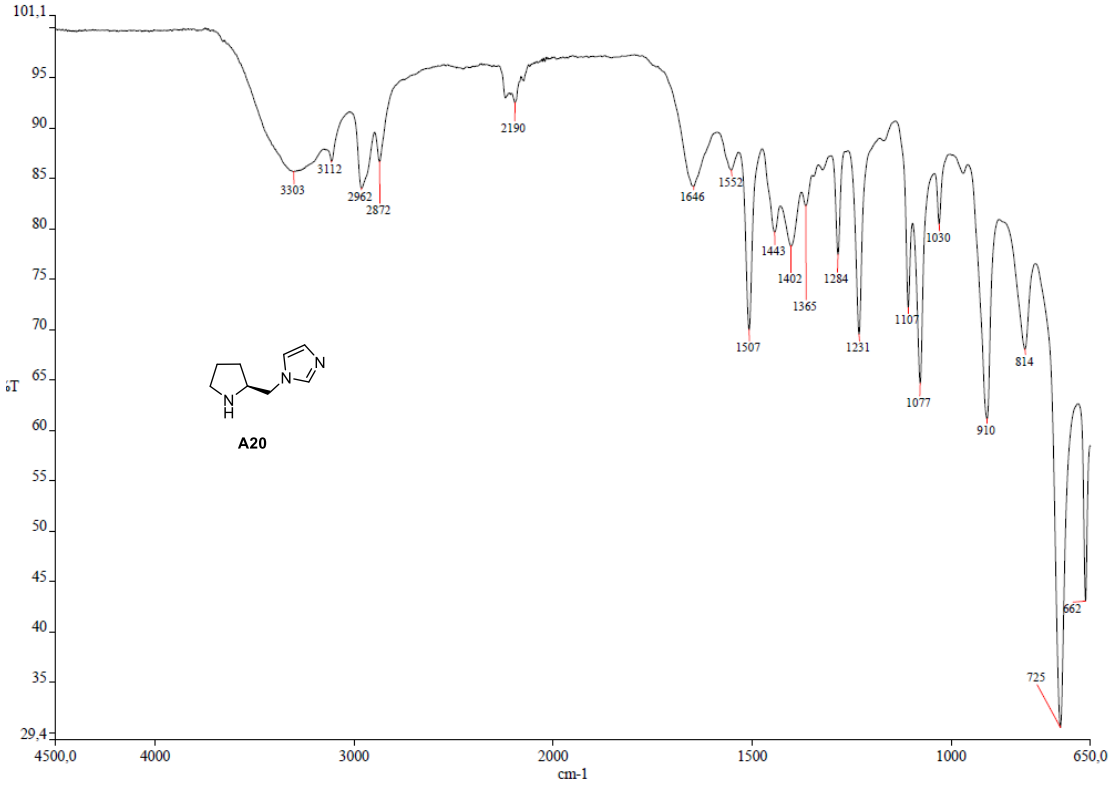
101,1
95
90
85
80
75
70
65
60
55
50
45
40
35
29,4
%T
4500,0
4000
3000
2000
1500
1000
650,0
cm-1
3303
3112
2962
2872
2190
1646
1552
1507
1443
1402
1365
1284
1231
1107
1077
1030
910
814
725
662
A20

(*S*)-3-Butyl-1-(pyrrolidin-2-ylmethyl)-1H-imidazol-3-ium trifluoromethanesulfonate (A21 OTf^-)

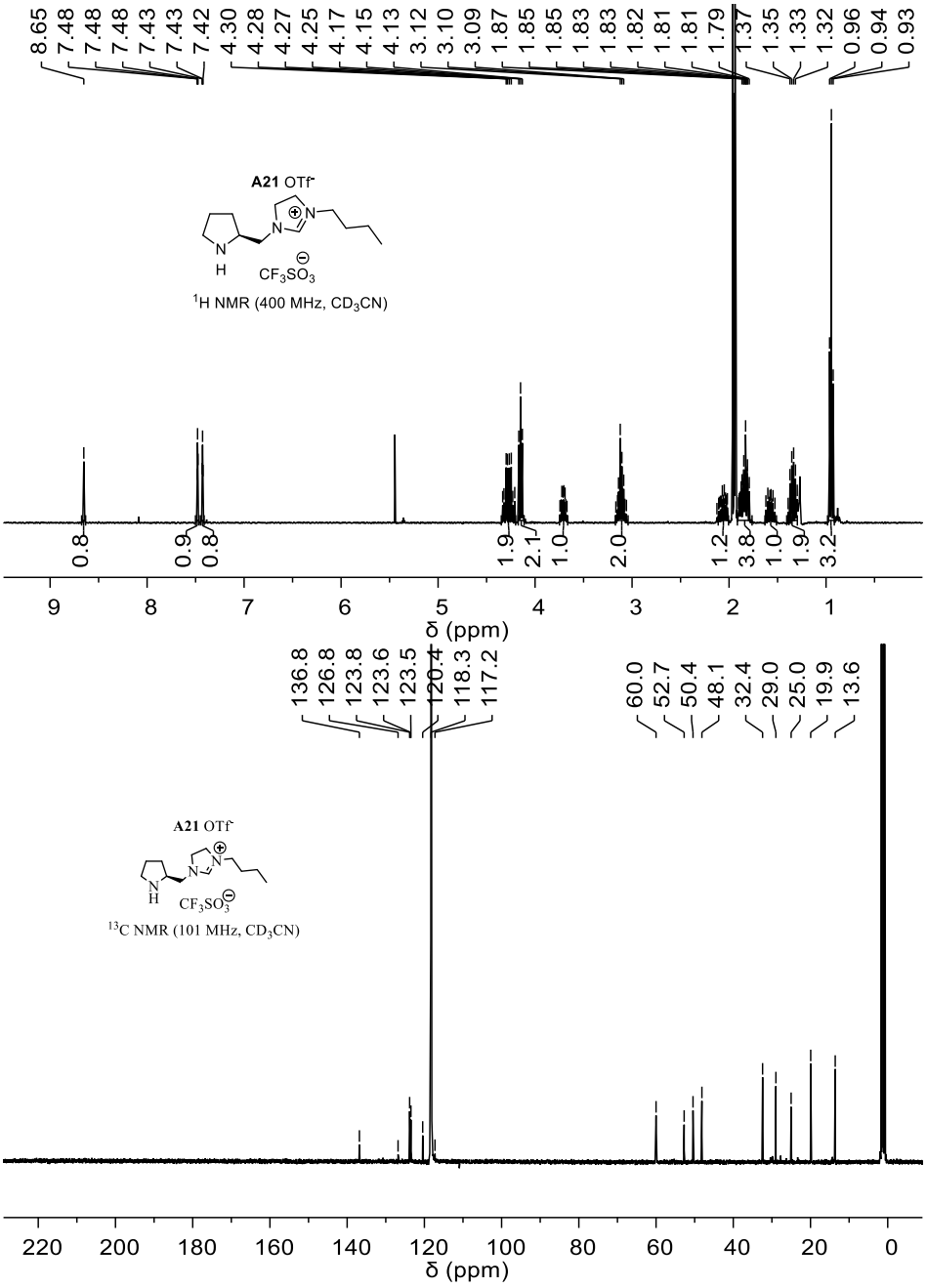

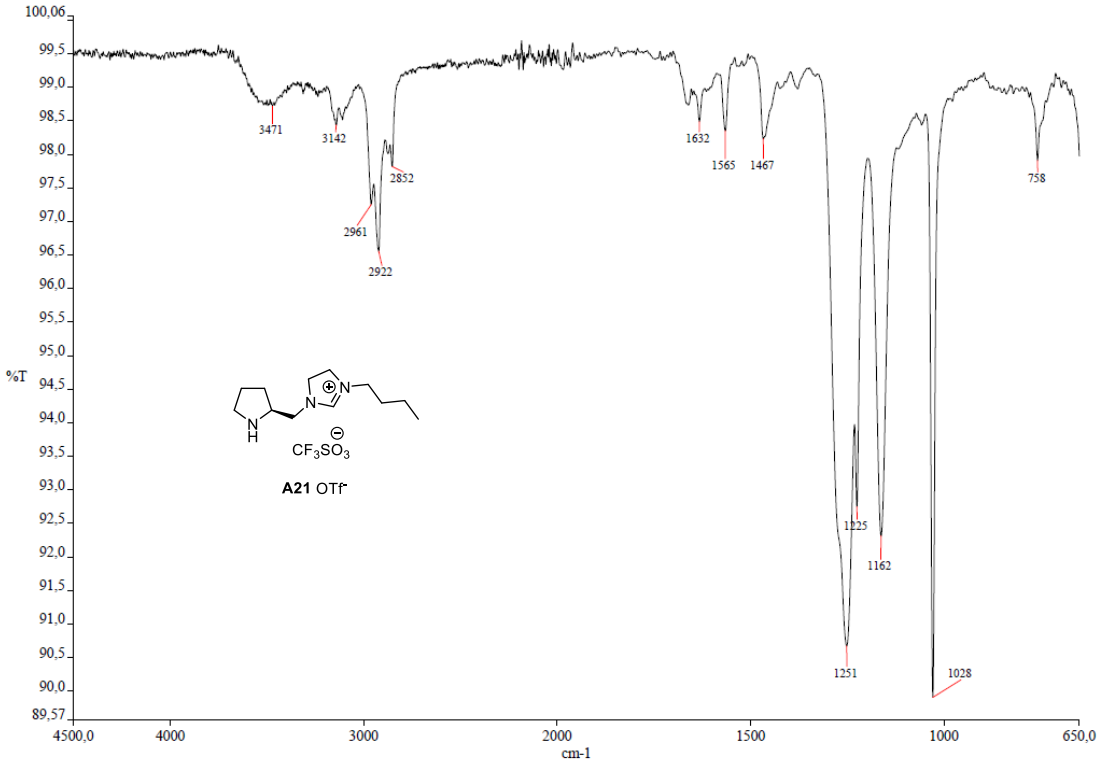
100,06
99,5
99,0
98,5
98,0
97,5
97,0
96,5
96,0
95,5
95,0
94,5
94,0
93,5
93,0
92,5
92,0
91,5
91,0
90,5
90,0
89,57
%T
3471
3142
2961
2922
2852
1632
1565
1467
1251
1225
1162
1028
758
4500,0
4000
3000
2000
1500
1000
650,0
cm-1
A21 OTf

(*S*)-1-(3,5-Bis(trifluoromethyl)phenyl)-3-(pyrrolidin-2-ylmethyl)thiourea (A22)

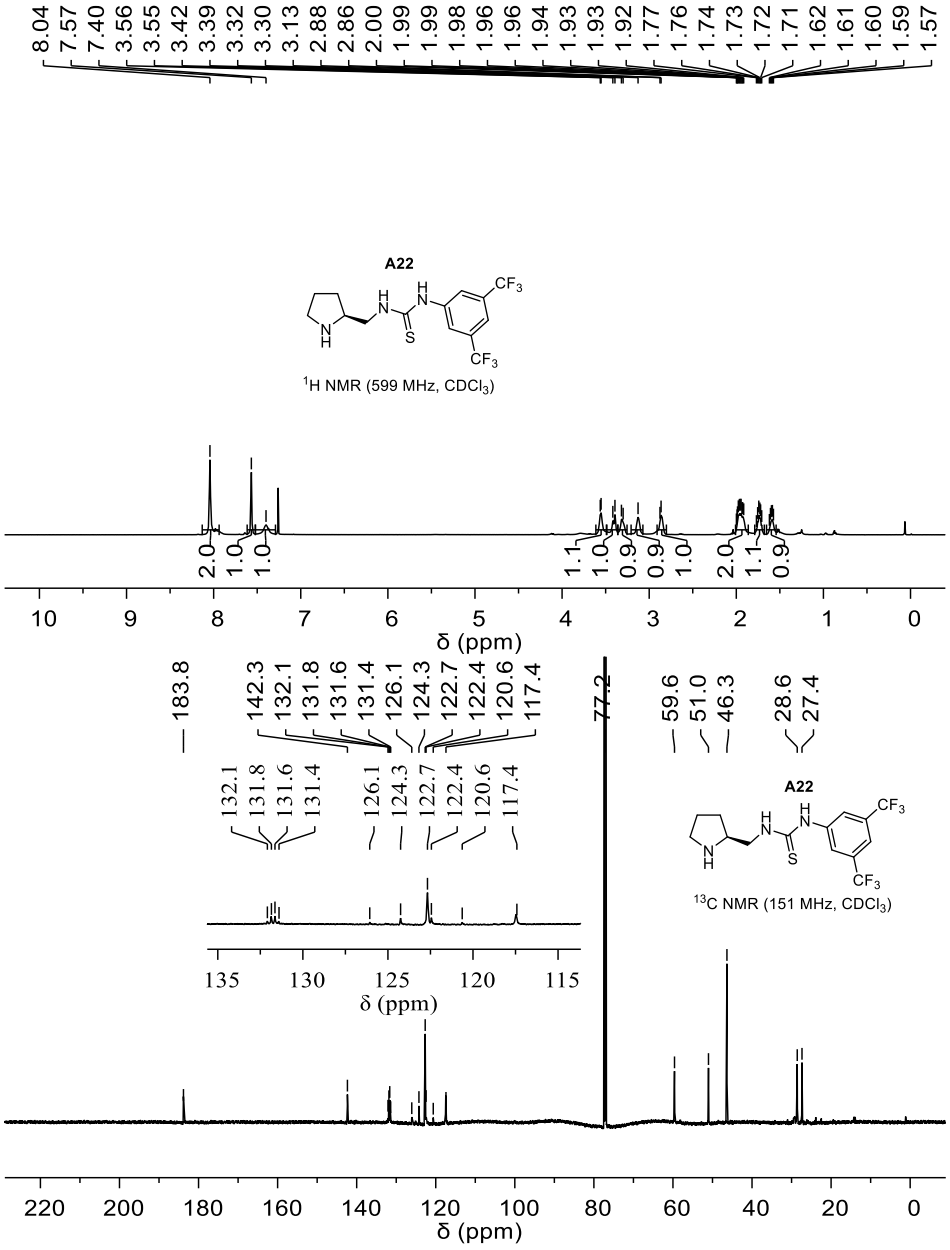

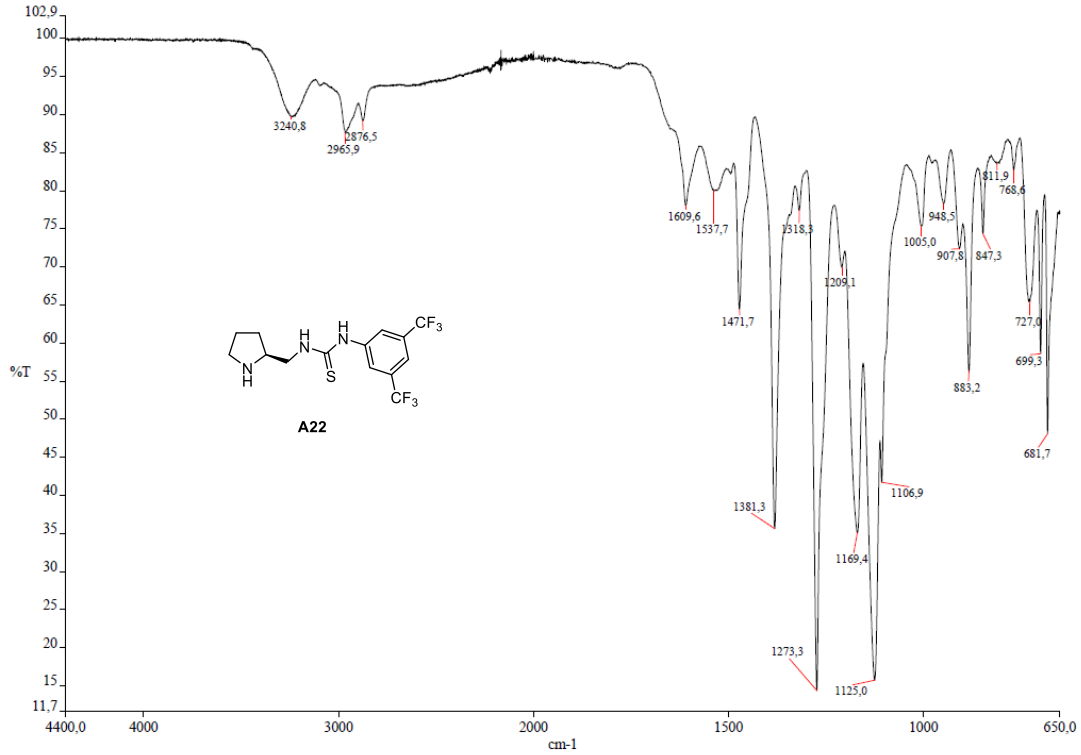
102,9
100
95
90
85
80
75
70
65
60
55
50
45
40
35
30
25
20
15
11,7
%T
4400,0
4000
3000
2000
1500
1000
650,0
cm-1
3240,8
2965,9
2876,5
1609,6
1537,7
1471,7
1381,3
1318,3
1273,3
1209,1
1169,4
1125,0
1106,9
1005,0
948,5
907,8
883,2
847,3
811,9
768,6
727,0
699,3
681,7
A22

(*S*)-2-((3-(3,5-Bis(trifluoromethyl)phenyl)ureido)methyl)pyrrolidin-1-ium 2,2,2-trifluoroacetate (A23H$^+$)

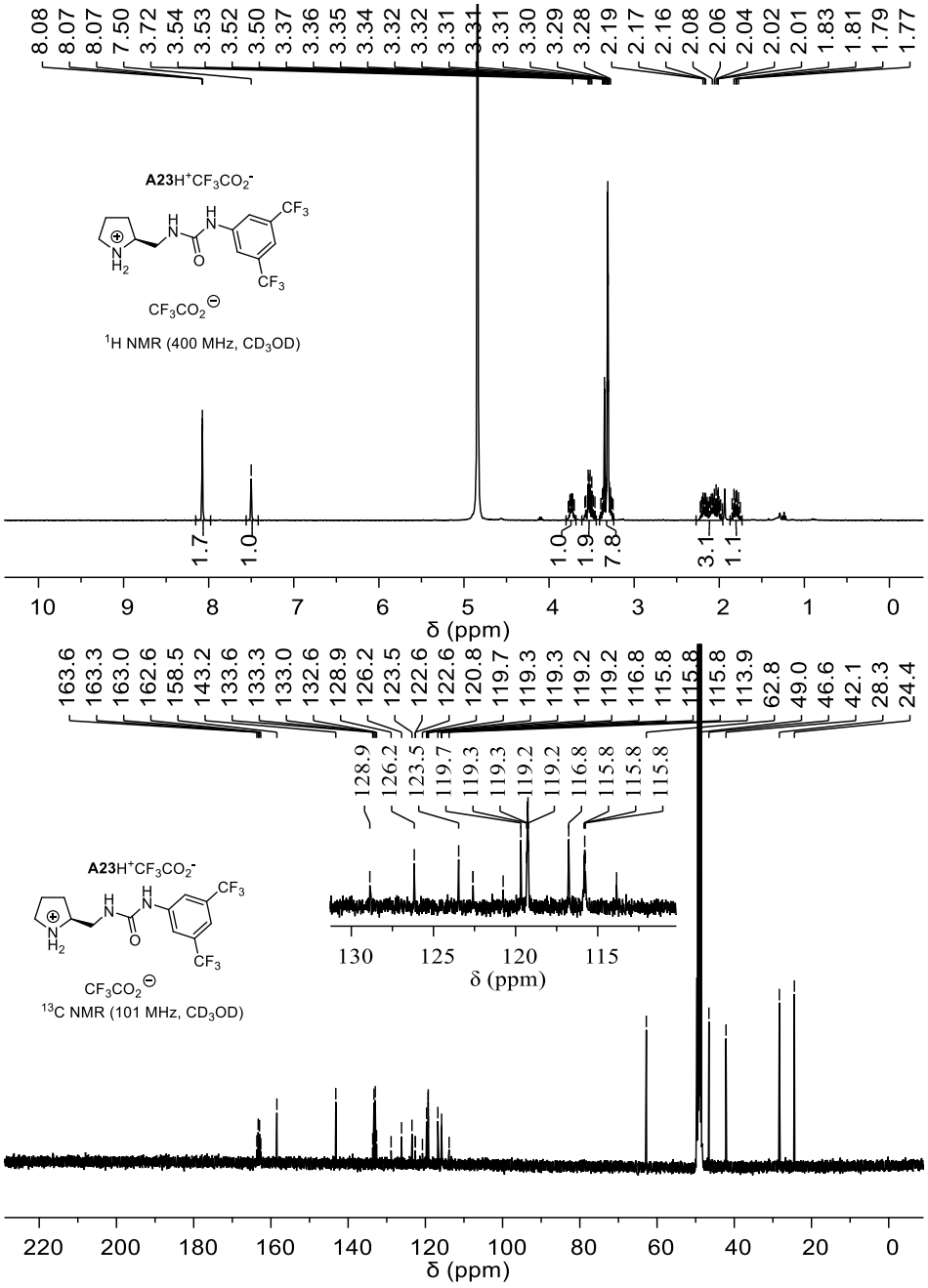

2-Tritylpyrrolidine (A24)

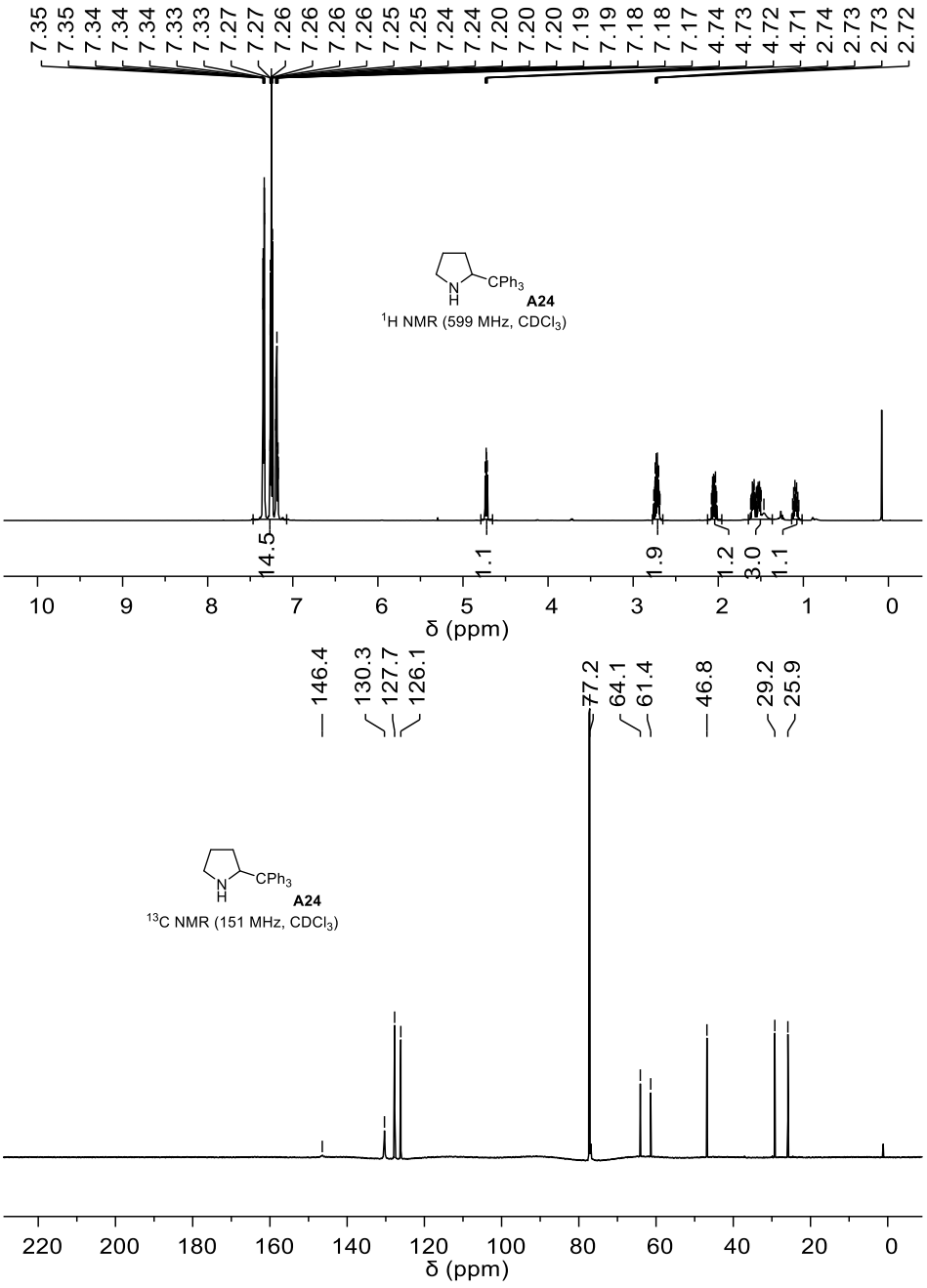

(*S*)-2-(Diphenyl((trimethylsilyl)oxy)methyl)pyrrolidine (A25)

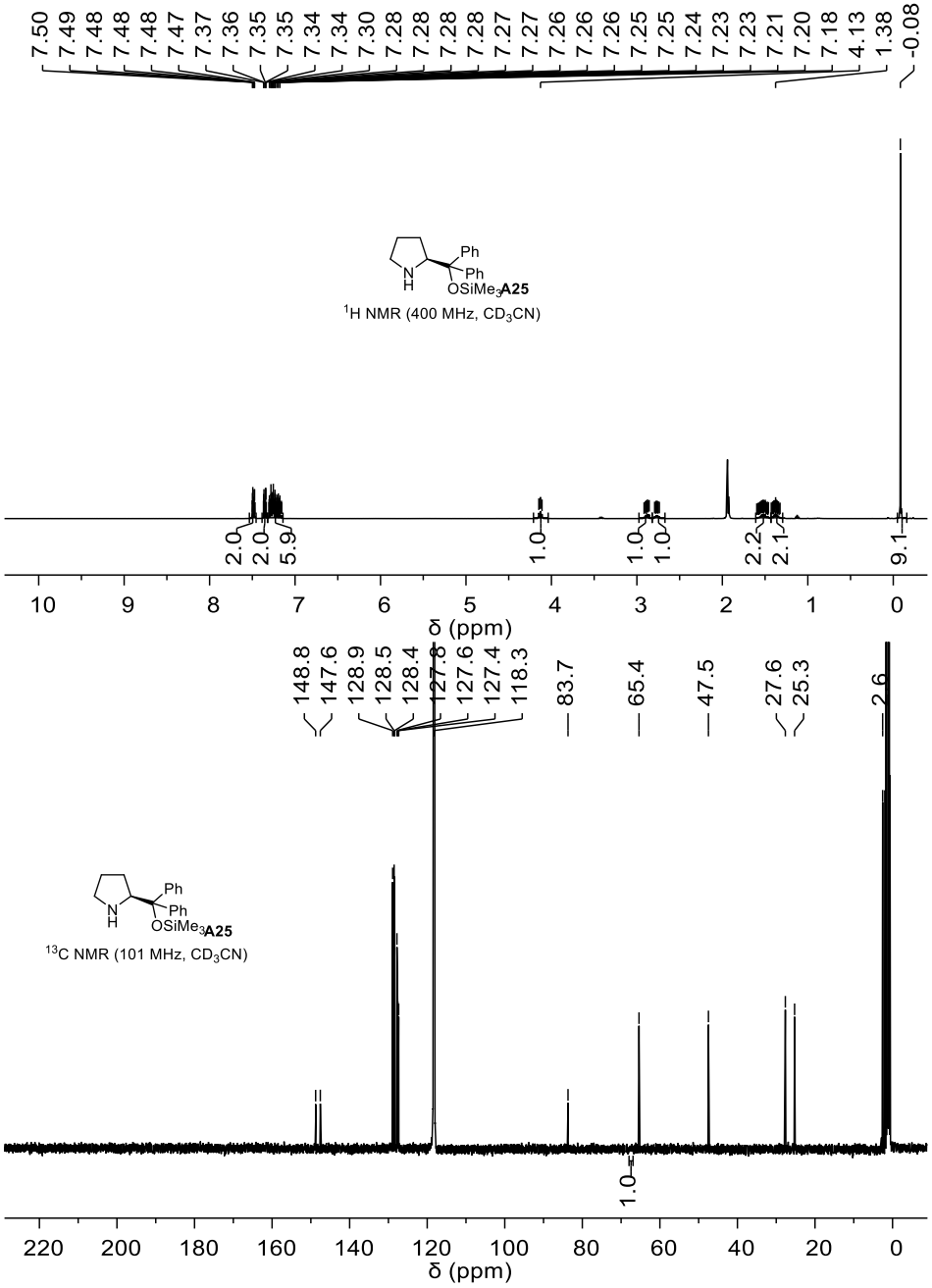

(*S*)-Diphenyl(pyrrolidin-2-yl)methanol (A26)

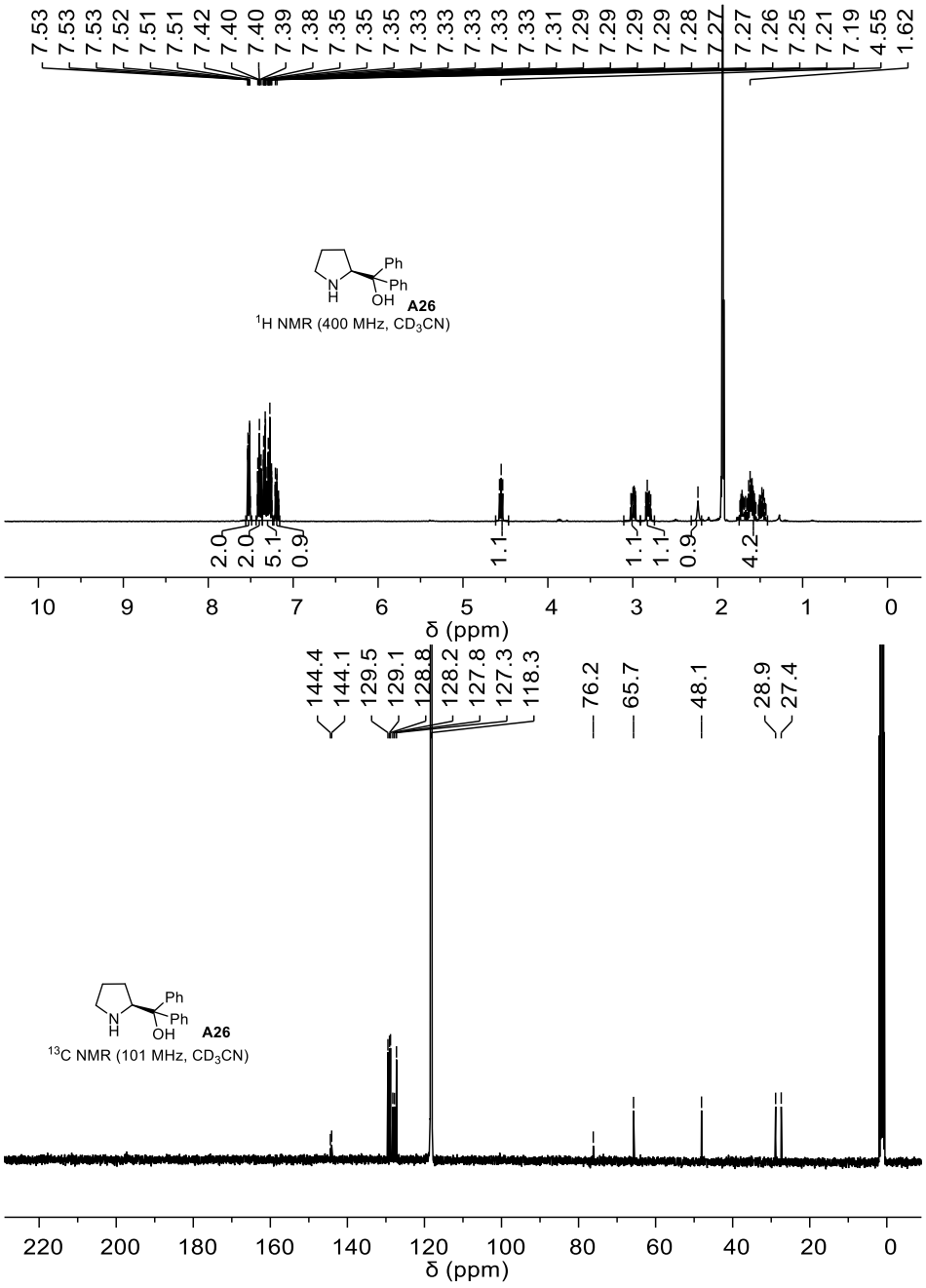

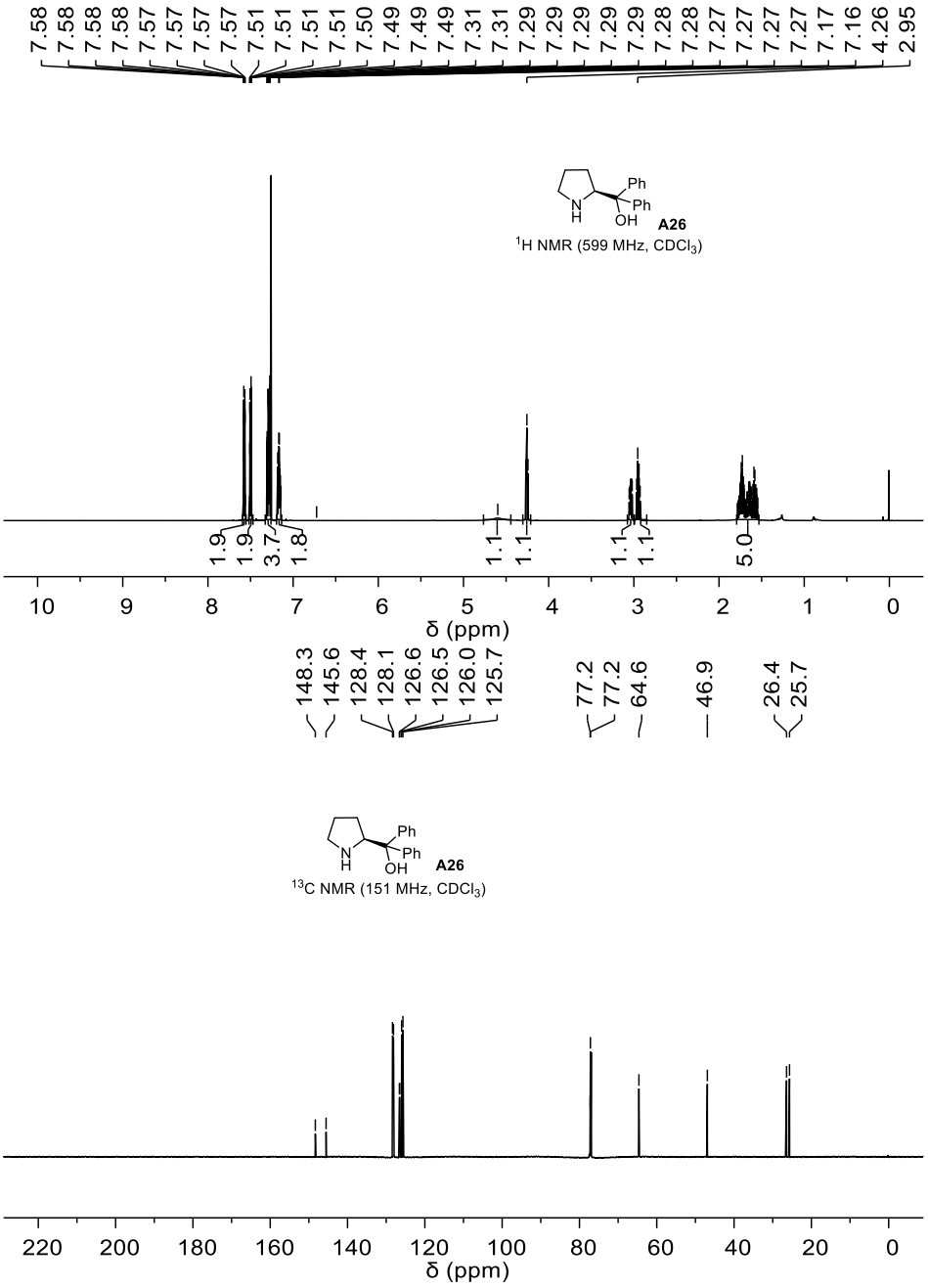
7.58 7.58 7.58 7.58 7.57 7.57 7.57 7.57 7.51 7.51 7.51 7.51 7.50 7.49 7.49 7.49 7.31 7.31 7.29 7.29 7.29 7.29 7.29 7.28 7.28 7.27 7.27 7.27 7.27 7.17 7.16 4.26 2.95
Ph
Ph
OH
N
H
A26
1H NMR (599 MHz, CDCl3)
1.9 1.9 3.7 1.8 1.1 1.1 1.1 1.1 5.0
10 9 8 7 6 5 4 3 2 1 0
δ (ppm)
148.3 145.6 128.4 128.1 126.6 126.5 126.0 125.7 77.2 77.2 64.6 46.9 26.4 25.7
Ph
Ph
OH
N
H
A26
13C NMR (151 MHz, CDCl3)
220 200 180 160 140 120 100 80 60 40 20 0
δ (ppm)

(*S*)-2-(Azidodiphenylmethyl)pyrrolidine (A27)

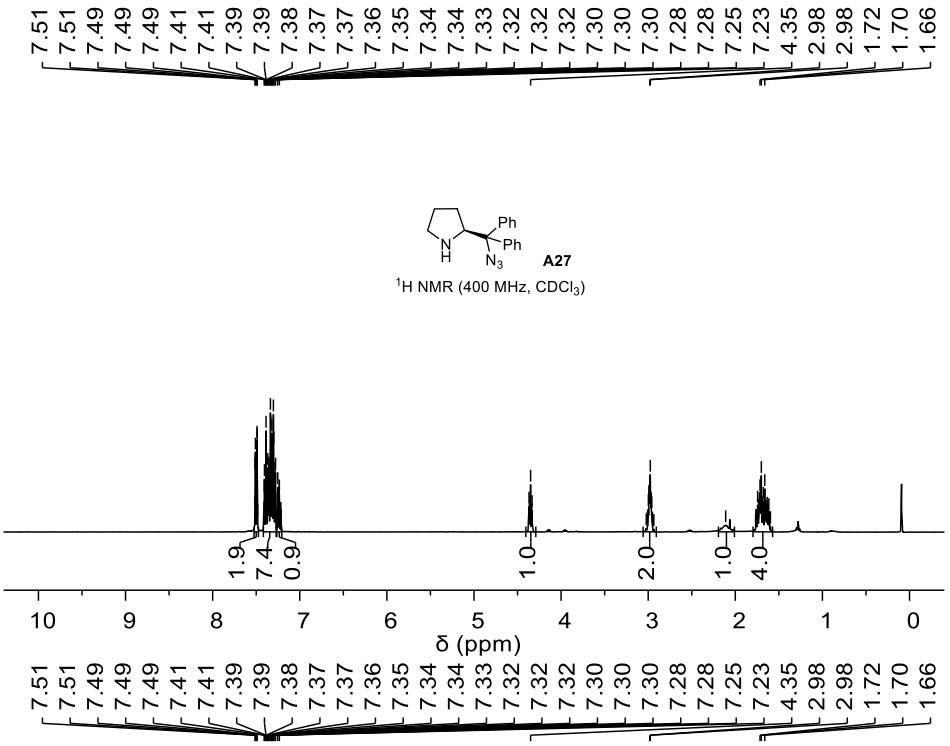

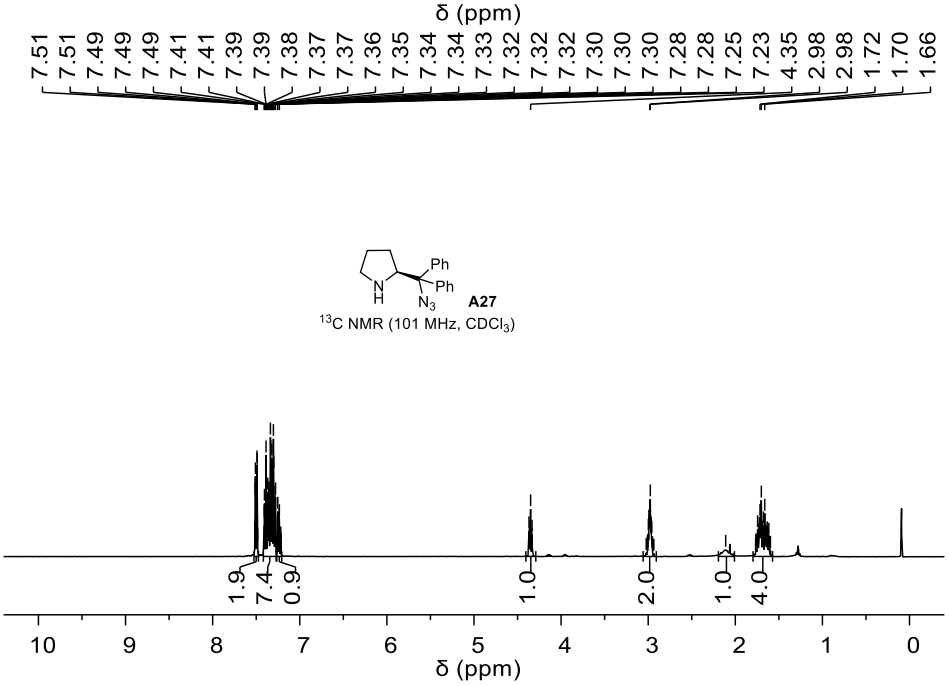

2-(Triphenylsilyl)pyrrolidine (A28)

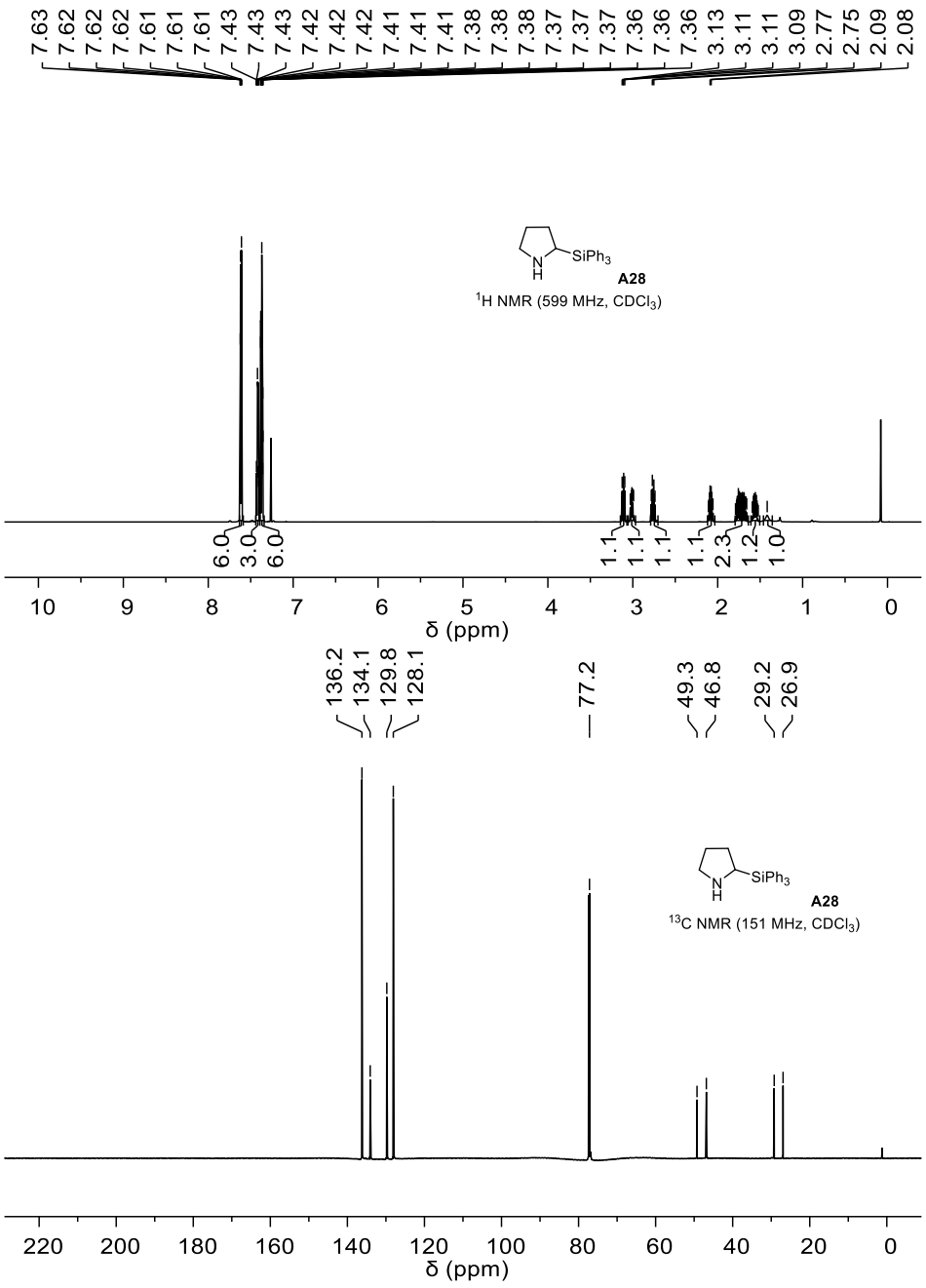

(*S*)-5-Benzyl-2,2,3-trimethylimidazolidin-4-one (A29)

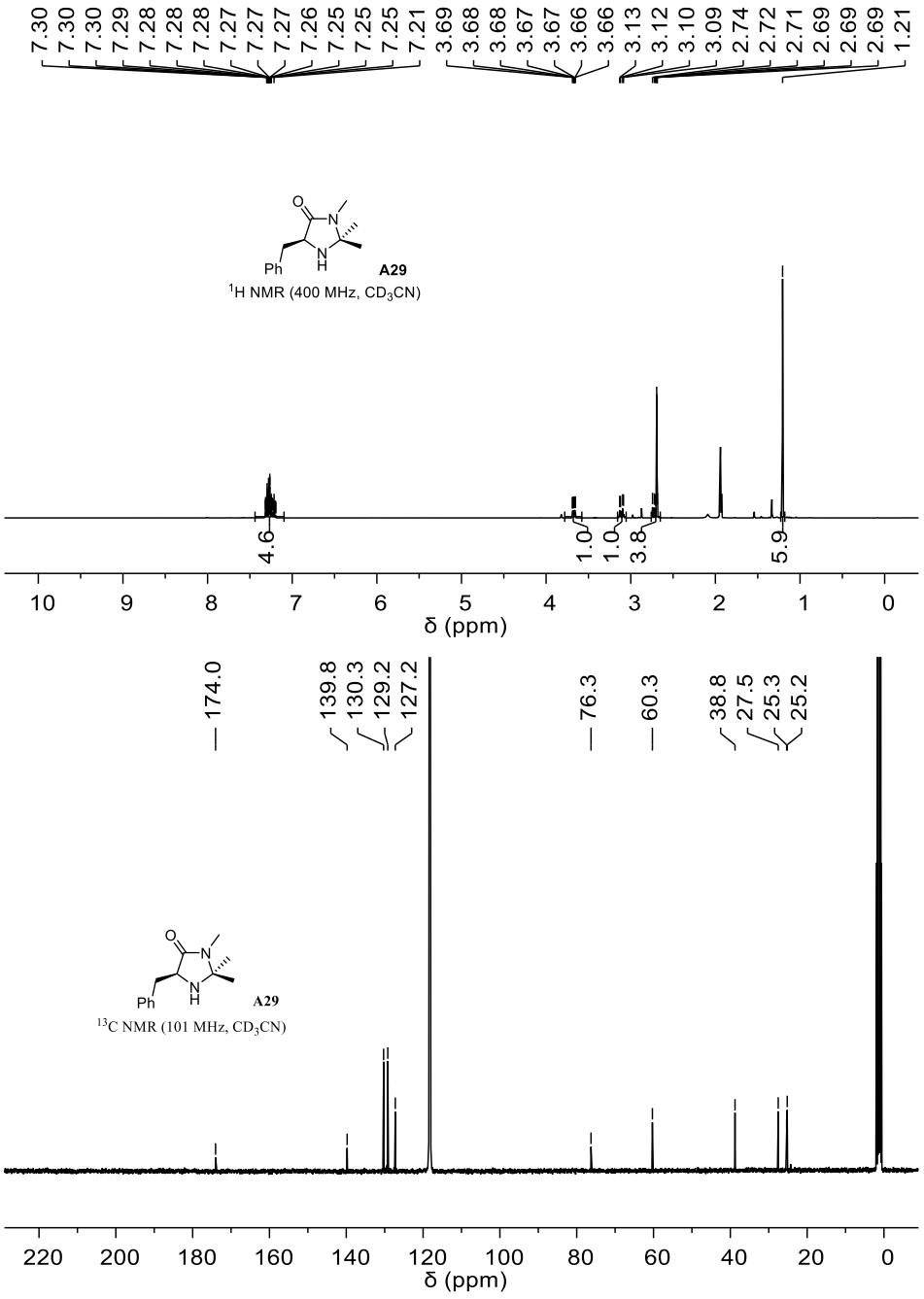

(2*S*,5*S*)-5-Benzyl-2-(tert-butyl)-3-methylimidazolidin-4-one (A30)

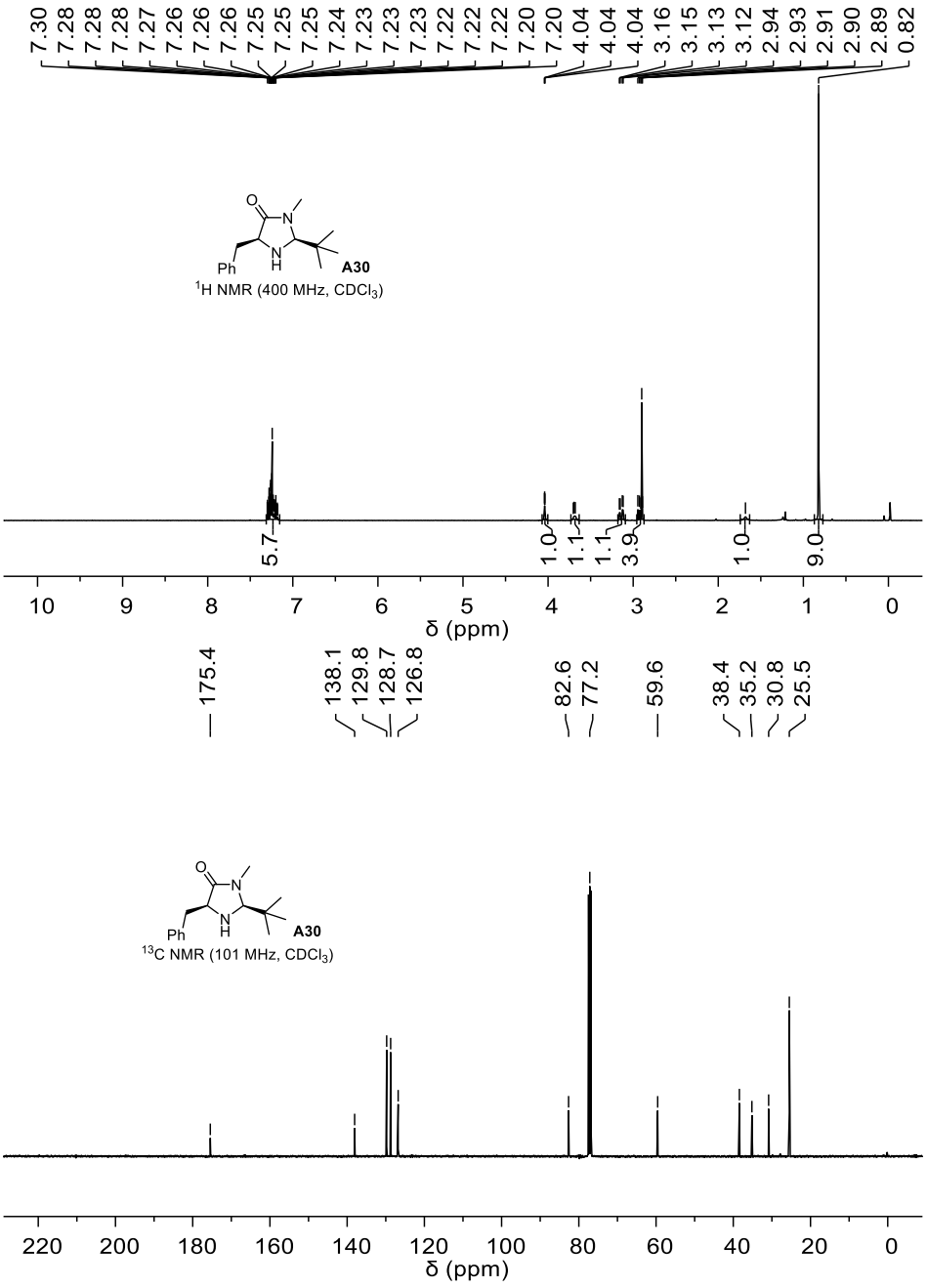

(2*S*,5*S*)-5-Benzyl-3-methyl-2-(5-methylfuran-2-yl)imidazolidin-4-one (A31)

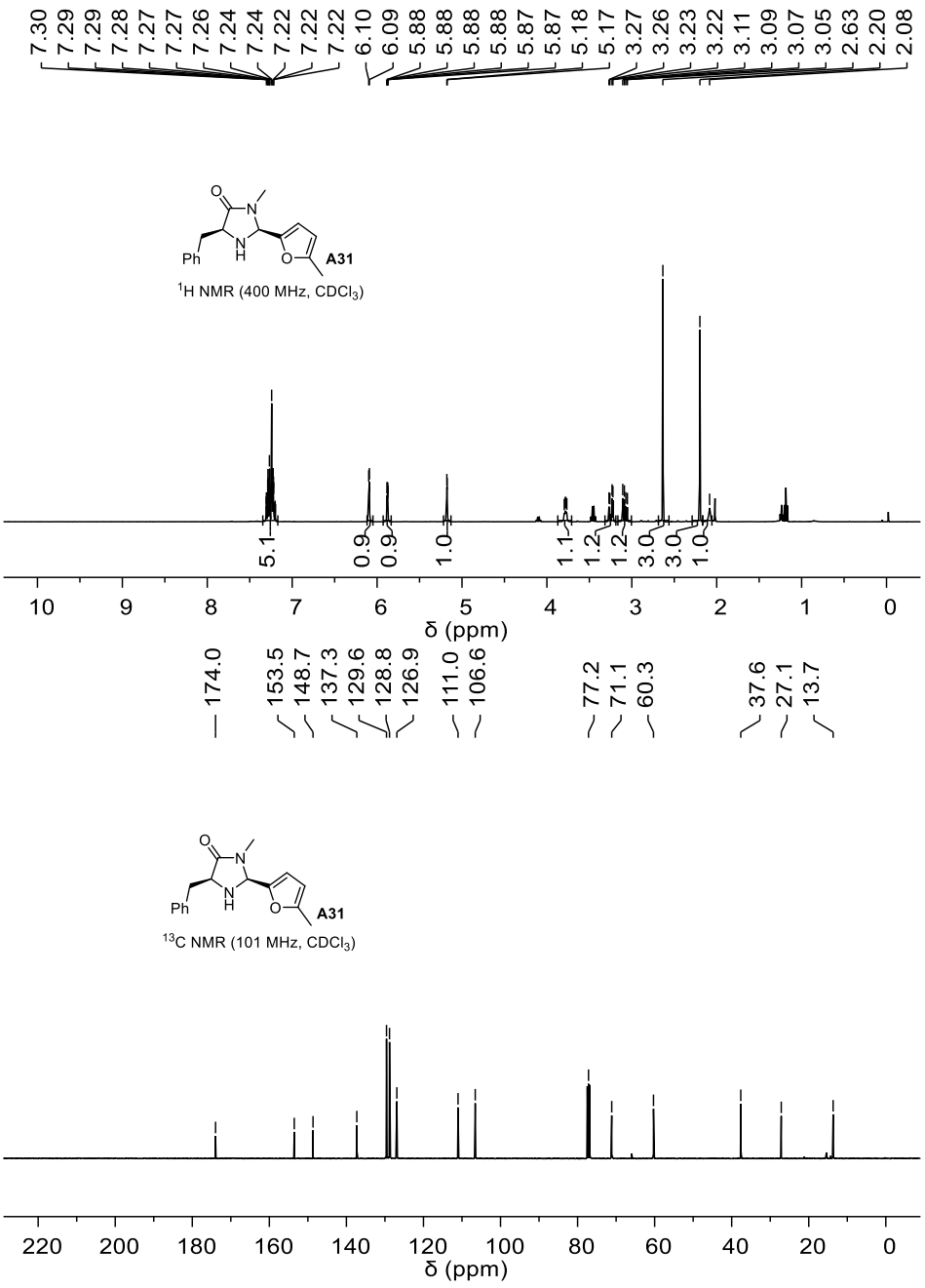

(2*R*,5*S*)-5-Benzyl-3-methyl-2-(5-methylfuran-2-yl)imidazolidin-4-one (A32)

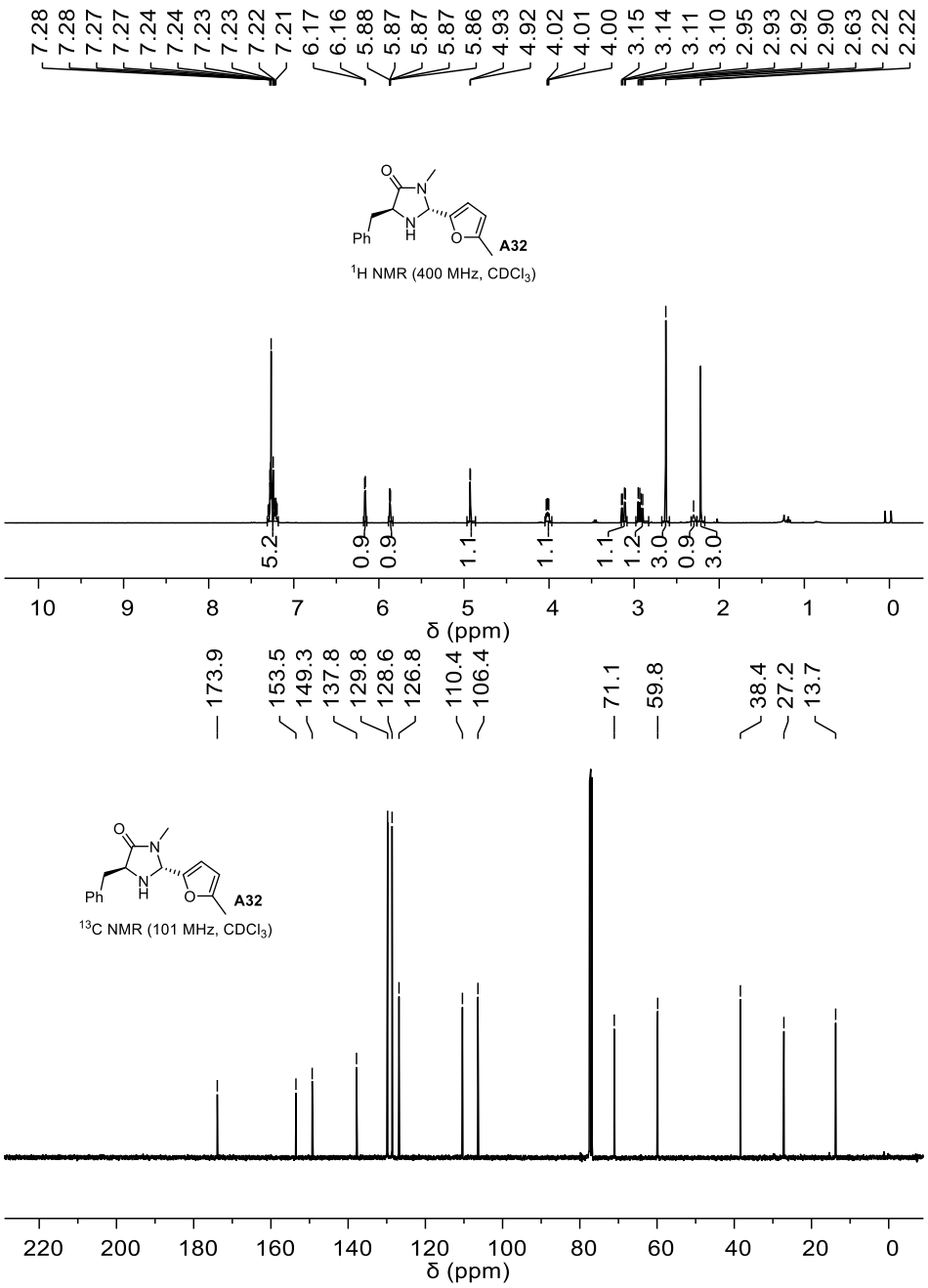

2-(4-Nitrophenyl)malononitrile (C6H)

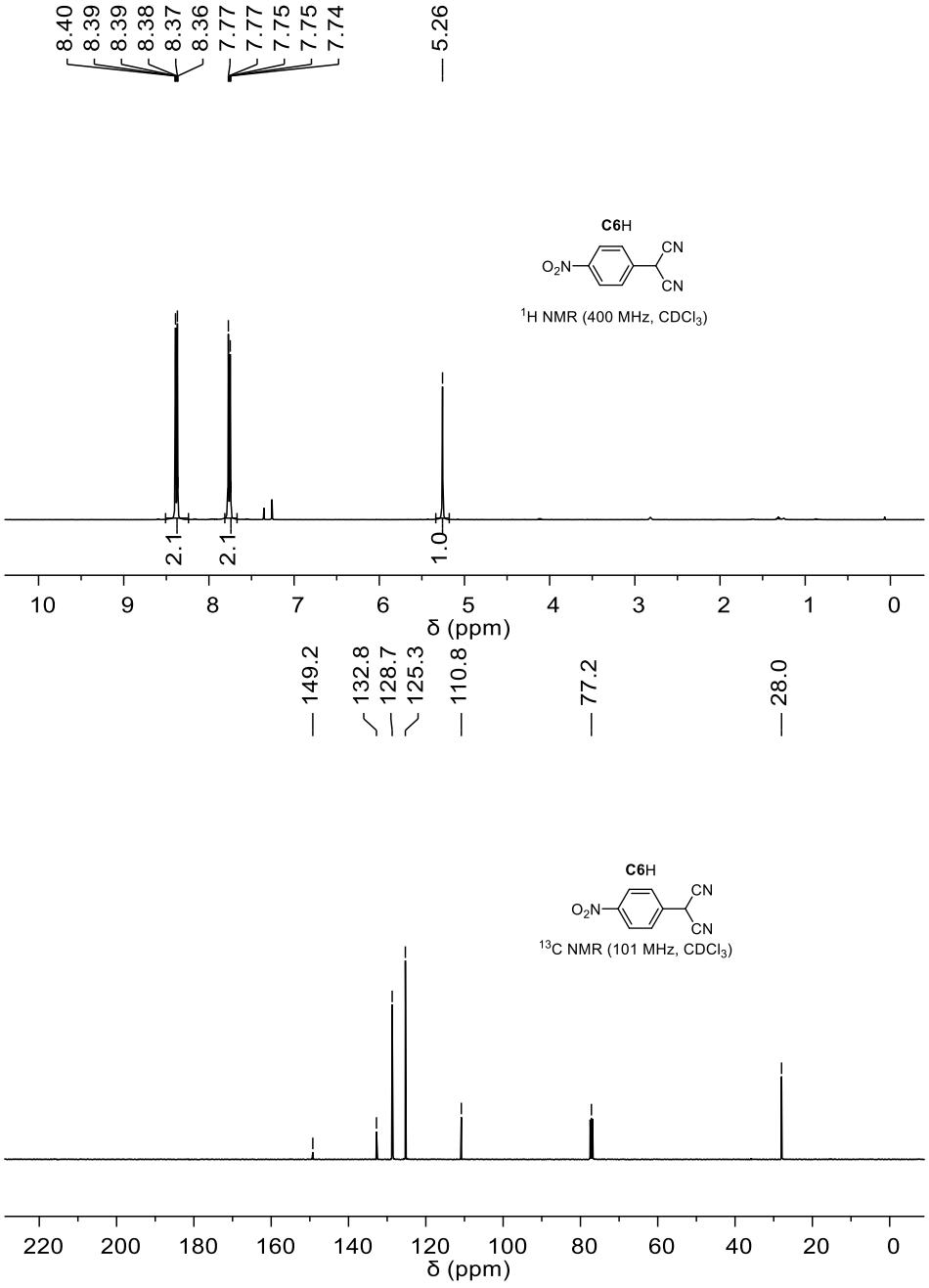

2-(Perfluorophenyl)malononitrile (C5H)

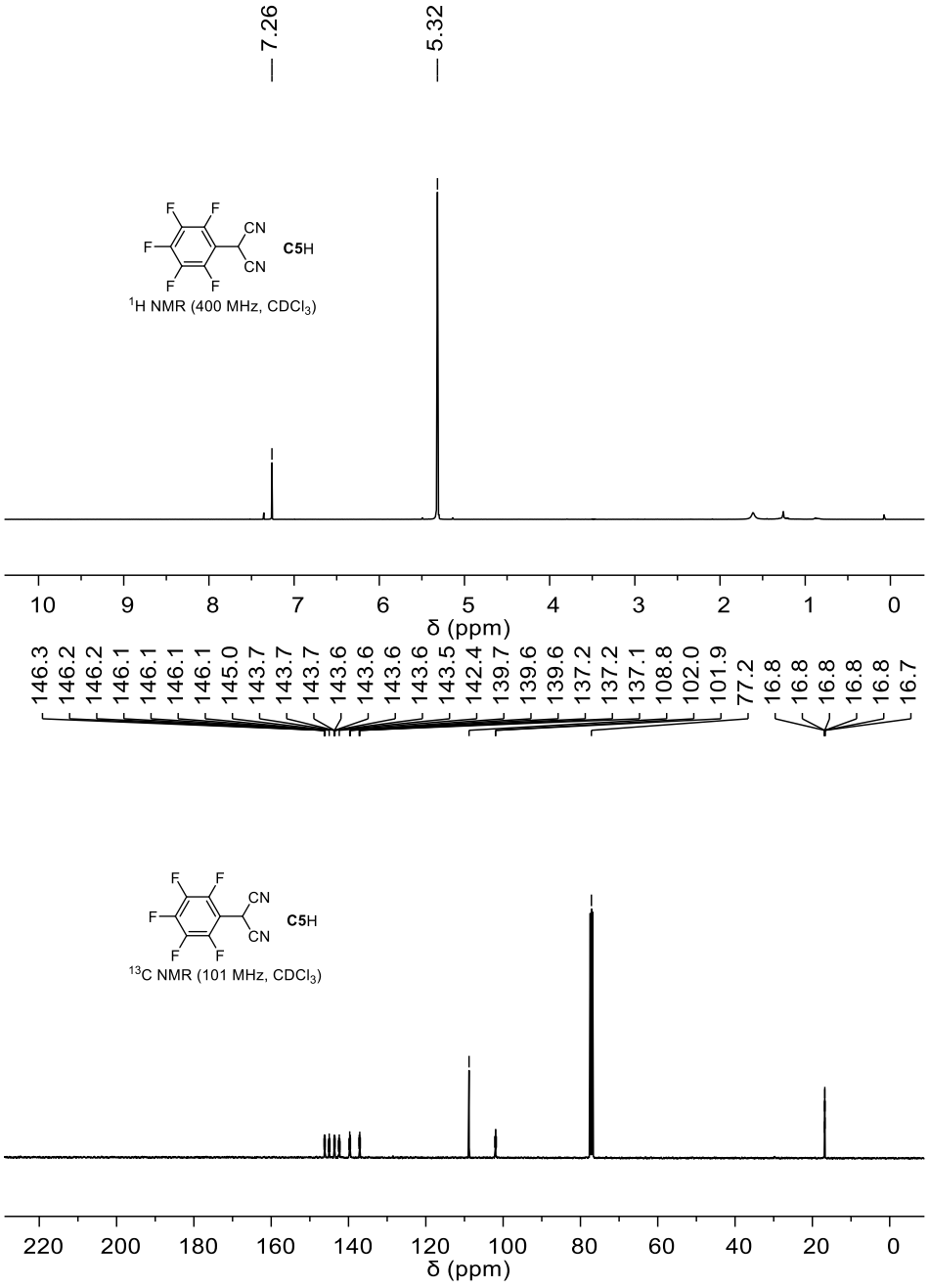

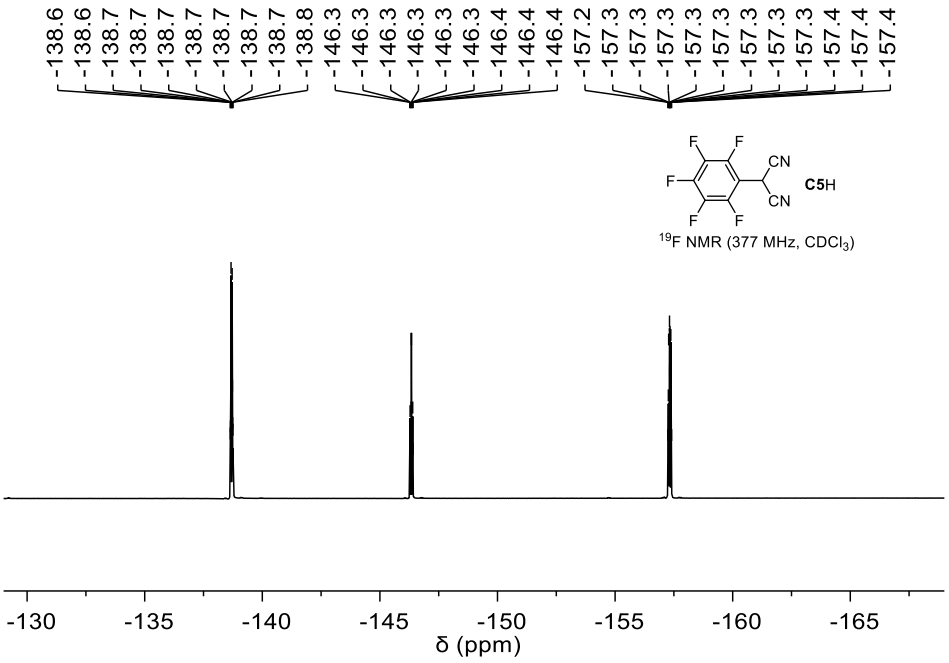
-138.6
-138.6
-138.7
-138.7
-138.7
-138.7
-138.7
-138.7
-138.8
-146.3
-146.3
-146.3
-146.3
-146.3
-146.4
-146.4
-146.4
-157.2
-157.3
-157.3
-157.3
-157.3
-157.3
-157.3
-157.3
-157.3
-157.4
-157.4
-157.4
F
F
F
CN
CN
C5H
F
F
19F NMR (377 MHz, CDCl3)
-130
-135
-140
-145
-150
-155
-160
-165
δ (ppm)

Ethyl 2-(4-chloro-2,3,5,6-tetrafluorophenyl)-2-cyanoacetate (C4H)

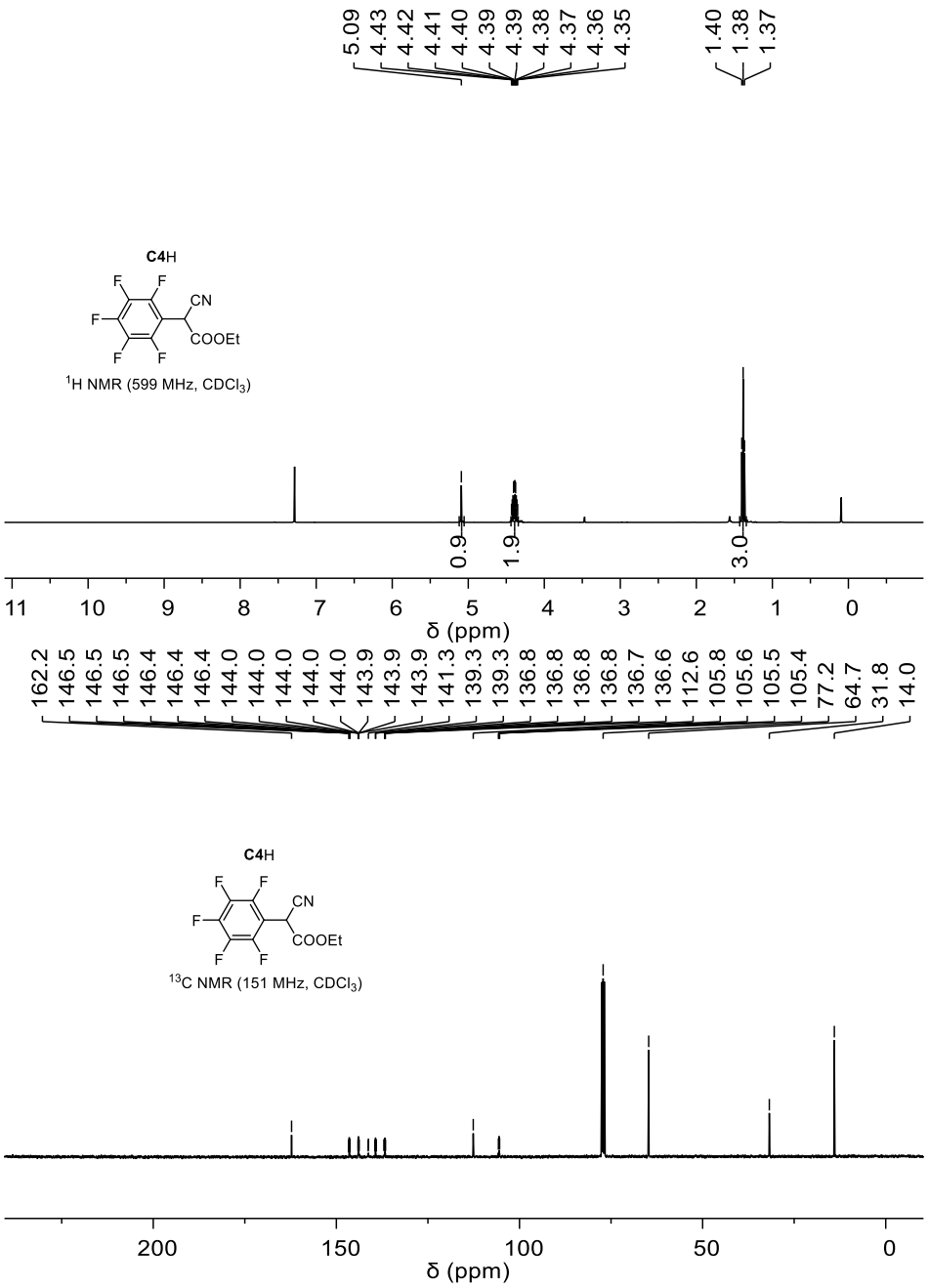

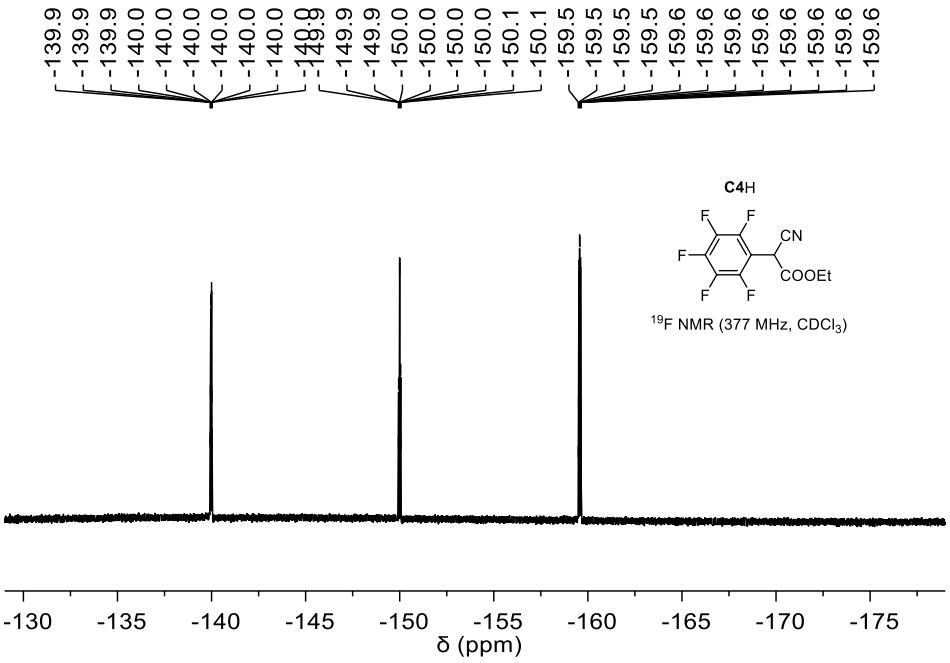
-139.9
-139.9
-139.9
-140.0
-140.0
-140.0
-140.0
-140.0
-140.0
-149.9
-149.9
-150.0
-150.0
-150.0
-150.0
-150.1
-150.1
-159.5
-159.5
-159.5
-159.6
-159.6
-159.6
-159.6
-159.6
-159.6
C4H
F
F
CN
F
COOEt
F
F
19F NMR (377 MHz, CDCl3)
-130
-135
-140
-145
-150
-155
-160
-165
-170
-175
δ (ppm)

Ethyl 2-cyano-2-(perfluorophenyl)acetate (C3H)

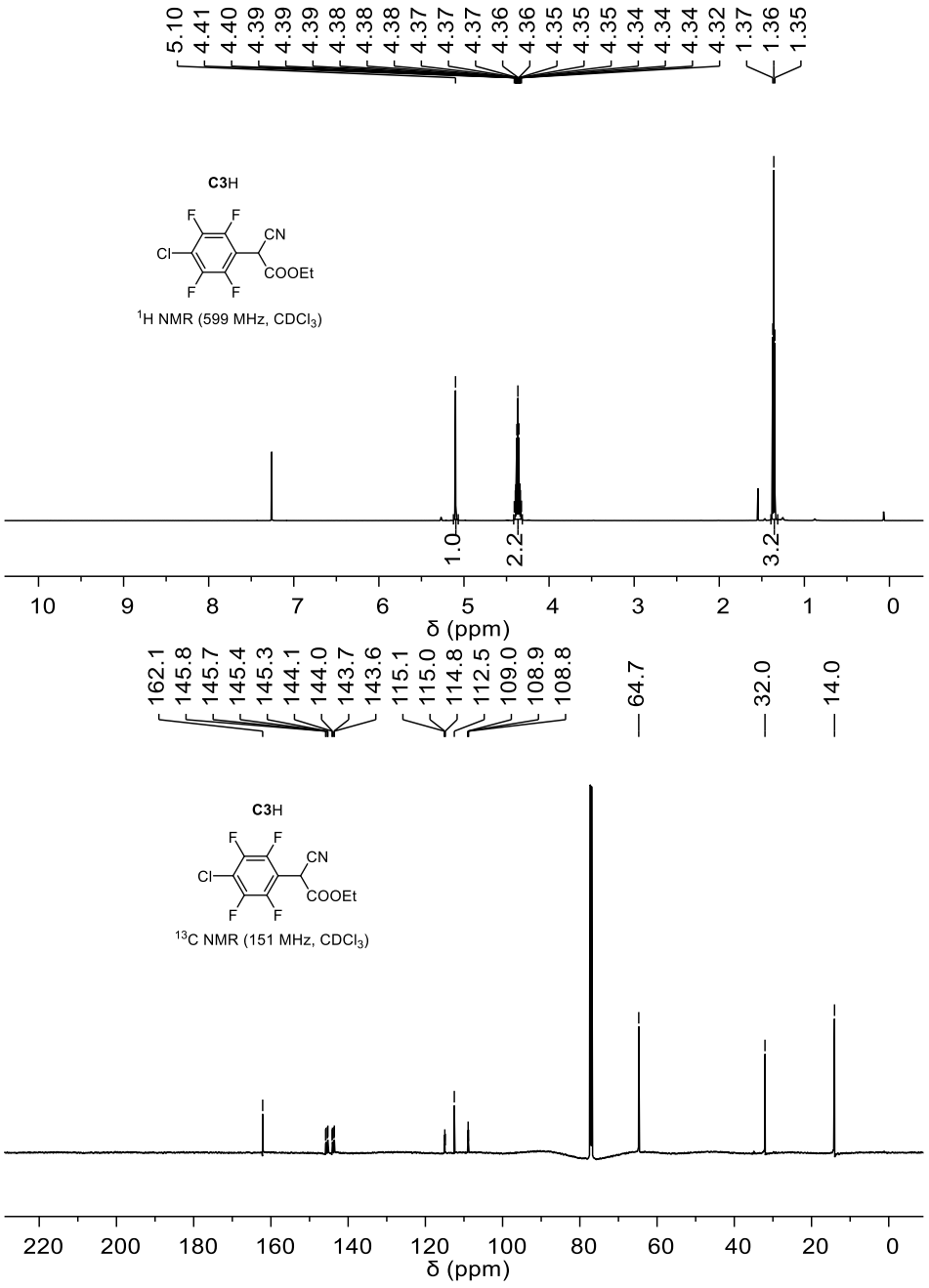

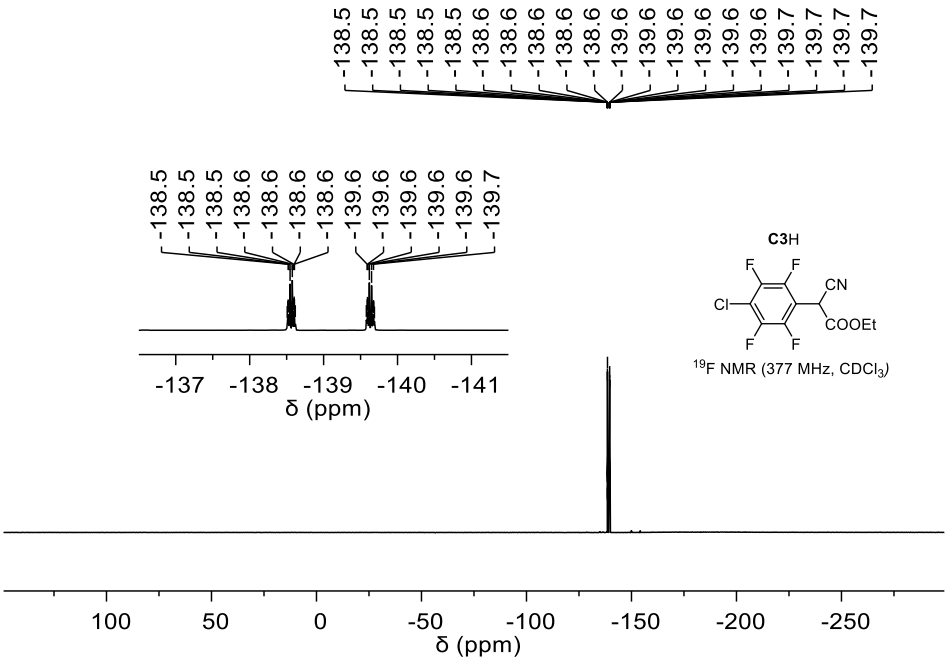
-138.5
-138.5
-138.5
-138.5
-138.5
-138.6
-138.6
-138.6
-138.6
-138.6
-139.6
-139.6
-139.6
-139.6
-139.6
-139.7
-139.7
-139.7
-139.7
-139.7
-138.5
-138.5
-138.5
-138.6
-138.6
-138.6
-138.6
-139.6
-139.6
-139.6
-139.6
-139.6
-139.7
-137
-138
-139
-140
-141
δ (ppm)
C3H
F
F
CN
Cl
COOEt
F
F
19F NMR (377 MHz, CDCl3)
100
50
0
-50
-100
-150
-200
-250
δ (ppm)

7.2 Experimental Section for Kinetic Measurements

7.2.1 General

Measurements with the Stopped-Flow UV-Vis Spectrometer

The kinetics of the fast reactions ($t_{1/2}$ < 40 s) of amines **A** with benzhydrylium ions (**E8**–**E17**) and quinone methides (**E1**–**E7**) were followed by UV/vis spectroscopy by using a stopped-flow spectrophotometer system (Applied Photophysics SX.18MV-R or SX20 Stopped Flow Spectrometers; 5 or 10 mm light path). Stock solutions were prepared in anhydrous acetonitrile, freshly distilled over phosphorus pentoxide. Alternatively, stock solutions in dichloromethane were prepared, which was freshly distilled from calcium hydride. The kinetic runs were initiated by mixing equal volumes of acetonitrile (or dichloromethane) solutions of the amines and the electrophiles. The temperature of the solutions during the kinetic studies was maintained to 20 ± 0.2 °C by using circulating bath cryostats.

Measurement with Conventional UV-Vis Spectroscopy

Anhydrous acetonitrile was freshly distilled from phosphorus pentoxide under an atmosphere of dry nitrogen. The rates of slow reactions of amines **A** with electrophiles **E** ($t_{1/2}$ > 40 s) were determined by using a J&M TIDAS diode array spectrophotometers controlled by Labcontrol Spectacle or TidasDAQ 3.8.1 software and connected to Hellma 661.502-QX quartz Suprasil immersion probe (5 mm light path) via fiber optic cables and standard SMA connectors. The temperature of the solutions during the kinetic studies was maintained to 20 ± 0.1 °C by using circulating bath cryostats.

7.2.2 Kinetics in Acetonitrile

Potassium L-prolinate (A1)

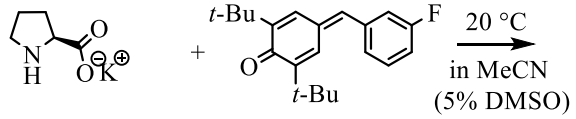

A1 **E3**

Table 5. Kinetics of the reaction of **A1** with **E3** (stopped-flow method, detection at 346 nm)

[**A1**] / M	[**E3**] / M	k_{obs} / s^{-1}
3.84×10^{-4}	2.30×10^{-5}	2.20
5.38×10^{-4}		2.53
6.92×10^{-4}		2.92
8.45×10^{-4}		3.32
9.99×10^{-4}		3.75
$k_2 = 2.53 \times 10^3$ $M^{-1} \cdot s^{-1}$		

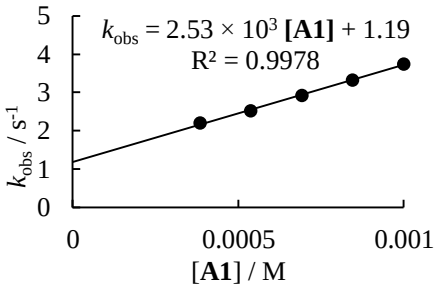

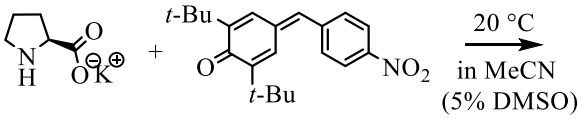

A1 **E4**

Table 6. Kinetics of the reaction of **A1** with **E4** (stopped-flow method, detection at 368 nm)

[**A1**] / M	[**E4**] / M	k_{obs} / s^{-1}
2.56×10^{-4}	1.54×10^{-5}	1.50
3.84×10^{-4}		2.13
7.68×10^{-4}		3.91
8.97×10^{-4}		4.59
$k_2 = 4.77 \times 10^3$ $M^{-1} \cdot s^{-1}$		

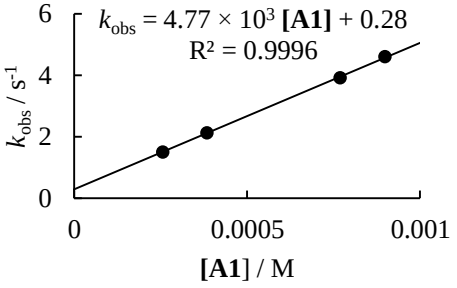

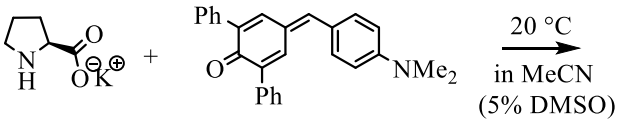

A1 **E5**

Table 7. Kinetics of the reaction of **A1** with **E5** (stopped-flow method, detection at 512 nm)

[**A1**] / M	[**E5**] / M	k_{obs} / s^{-1}
2.05×10^{-4}	1.34×10^{-5}	1.00×10^{1}
3.06×10^{-4}		1.45×10^{1}
4.10×10^{-4}		1.88×10^{1}
5.12×10^{-4}		2.30×10^{1}
6.15×10^{-4}		2.70×10^{1}
7.17×10^{-4}		3.10×10^{1}
$k_2 = 4.09 \times 10^{4}$ $M^{-1} \cdot s^{-1}$		

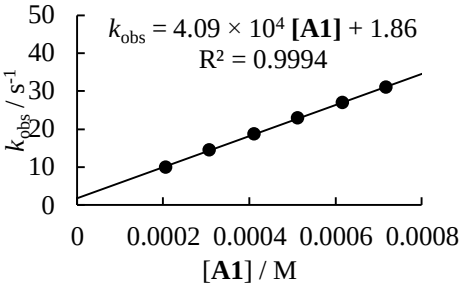

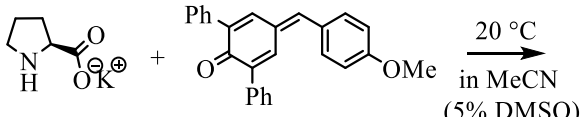

A1 **E6**

Table 8. Kinetics of the reaction of **A1** with **E6** (stopped-flow method, detection at 412 nm)

[**A1**] / M	[**E6**] / M	k_{obs} / s^{-1}
2.05×10^{-4}	1.93×10^{-5}	2.25×10^{1}
3.06×10^{-4}		3.66×10^{1}
4.10×10^{-4}		4.98×10^{1}
5.12×10^{-4}		6.49×10^{1}
6.15×10^{-4}		7.97×10^{1}
7.17×10^{-4}		9.32×10^{1}
$k_2 = 1.39 \times 10^{5}$ $M^{-1} \cdot s^{-1}$		

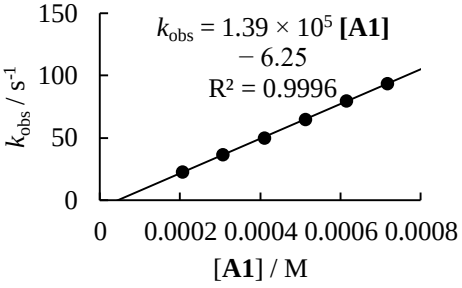

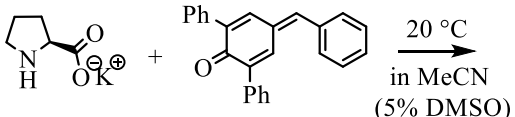

A1 **E7**

Table 9. Kinetics of the reaction of **A1** with **E7** (stopped-flow method, detection at 376 nm)

[**A1**] / M	[**E7**] / M	k_{obs} / s^{-1}
2.05×10^{-4}	2.09×10^{-5}	3.80×10^{1}
3.06×10^{-4}		6.01×10^{1}
4.10×10^{-4}		8.55×10^{1}
5.12×10^{-4}		1.07×10^{2}
6.15×10^{-4}		1.31×10^{2}
7.17×10^{-4}		1.57×10^{2}
$k_2 = 2.31 \times 10^{5}$ $M^{-1} \cdot s^{-1}$		

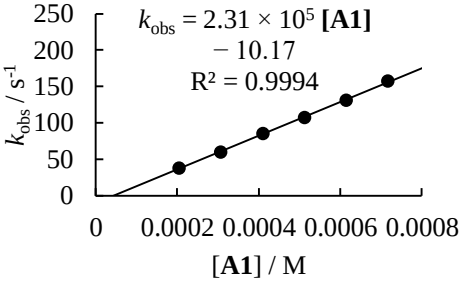

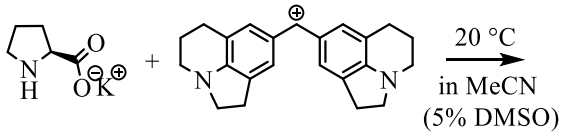

A1 **E8**

Table 10. Kinetics of the reaction of **A1** with **E8** (stopped-flow method, detection at 632 nm)

[**A1**] / M	[**E7**] / M	k_{obs} / s^{-1}
4.16×10^{-5}	4.04×10^{-6}	1.65×10^{2}
6.66×10^{-5}		3.30×10^{2}
9.15×10^{-5}		4.94×10^{2}
1.16×10^{-4}		6.40×10^{2}
$k_2 = 6.41 \times 10^{6}$ $M^{-1} \cdot s^{-1}$		

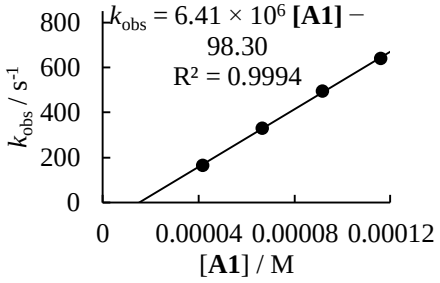

Table 11. Determination of the parameters N and s_N for **A1** in acetonitrile

Electrophile	E	k_2 / $M^{-1} \cdot s^{-1}$
E3	−15.03	2.53×10^{3}
E4	−14.36	4.77×10^{3}
E5	−13.39	4.09×10^{4}
E6	−12.18	1.39×10^{5}
E7	−11.87	2.31×10^{5}
E8	−10.04	6.41×10^{6}
$N = 19.95$ $s_N = 0.68$		

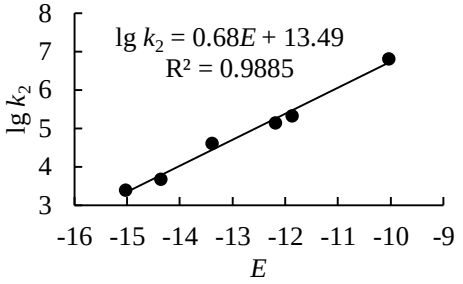

Pyrrolidine (A2)

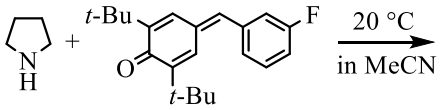

A2 **E3**

Table 12. Kinetics of the reaction of **A2** with **E3** (conventional UV-Vis method, detection at 346 nm)

[**A2**] / M	[**E3**] / M	k_{obs} / s^{-1}
1.63×10^{-4}	1.54×10^{-5}	4.30×10^{-3}
2.38×10^{-4}	1.46×10^{-5}	8.04×10^{-3}
3.33×10^{-4}	1.52×10^{-5}	1.33×10^{-2}
4.23×10^{-4}	1.53×10^{-5}	1.92×10^{-2}
5.16×10^{-4}	1.55×10^{-5}	2.54×10^{-2}
5.90×10^{-4}	1.51×10^{-5}	3.09×10^{-2}

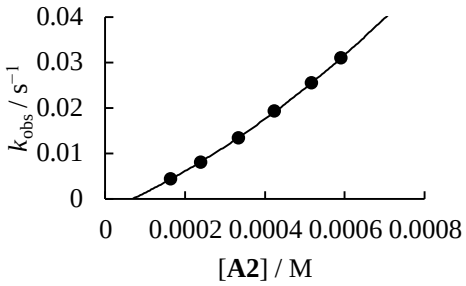

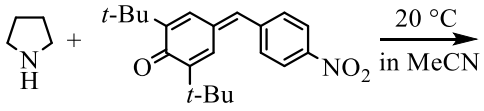

A2 **E4**

Table 13. Kinetics of the reaction of **A2** with **E4** (stopped-flow method, detection at 368 nm)

[**A2**] / M	[**E4**] / M	k_{obs} / s^{-1}
2.36×10^{-4}		7.98×10^{-3}
3.54×10^{-4}		1.60×10^{-2}
4.72×10^{-4}	2.06×10^{-5}	2.43×10^{-2}
5.91×10^{-4}		3.34×10^{-2}
7.09×10^{-4}		4.45×10^{-2}

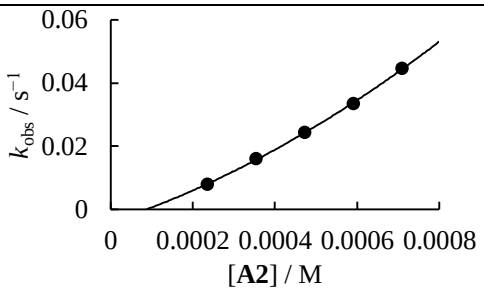

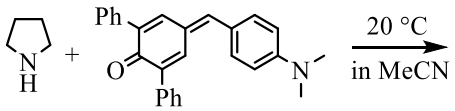

A2 **E5**

Table 14. Kinetics of the reaction of **A2** with **E5** (stopped-flow method, detection at 512 nm)

[**A2**] / M	[**E5**] / M	k_{obs} / s^{-1}
1.65×10^{-4}		2.85×10^{-1}
2.48×10^{-4}		4.59×10^{-1}
3.31×10^{-4}	1.59×10^{-5}	6.23×10^{-1}
4.13×10^{-4}		8.07×10^{-1}
5.31×10^{-4}		1.06
$k_2 = 2.12 \times 10^3$ $M^{-1} \cdot s^{-1}$		

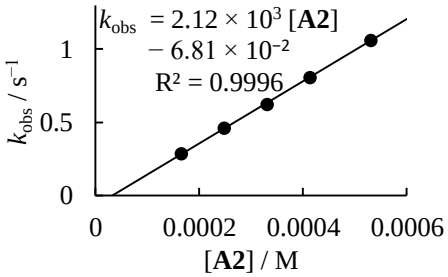

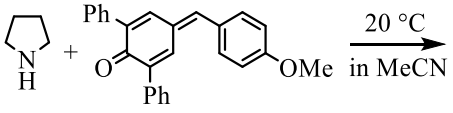

A2 **E6**

Table 15. Kinetics of the reaction of **A2** with **E6** (stopped-flow method, detection at 412 nm)

[**A2**] / M	[**E6**] / M	k_{obs} / s^{-1}
1.65×10^{-4}		9.45×10^{-1}
2.48×10^{-4}		1.48
3.31×10^{-4}	1.65×10^{-5}	2.01
4.13×10^{-4}		2.55
4.96×10^{-4}		3.02
$k_2 = 6.31 \times 10^3$ $M^{-1} \cdot s^{-1}$		

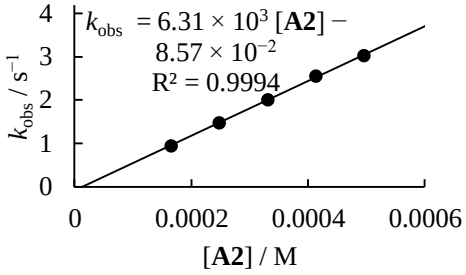

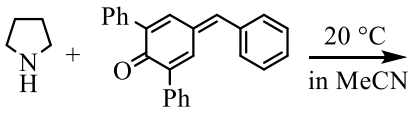

A2 **E7**

Table 16. Kinetics of the reaction of **A2** with **E7** (stopped-flow method, detection at 376 nm)

[**A2**] / M	[**E7**] / M	k_{obs} / s^{-1}
1.65×10^{-4}		1.56
2.48×10^{-4}		2.41
3.31×10^{-4}	1.64×10^{-5}	3.32
4.13×10^{-4}		4.28
4.96×10^{-4}		5.14
$k_2 = 1.09 \times 10^4$ $M^{-1} \cdot s^{-1}$		

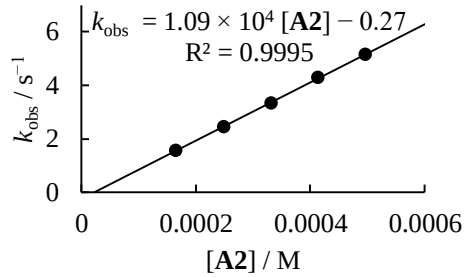

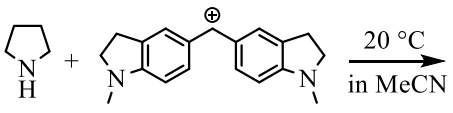

A2 **E10**

Table 17. Kinetics of the reaction of **A2** with **E10** (stopped-flow method, detection at 616 nm)

[**A2**] / M	[**E10**] / M	k_{obs} / s^{-1}
4.72×10^{-5}		4.09×10^1
7.09×10^{-5}		6.63×10^1
9.45×10^{-5}	4.70×10^{-6}	9.08×10^1
1.18×10^{-4}		1.16×10^2
1.42×10^{-4}		1.42×10^2
$k_2 = 1.06 \times 10^6$ $M^{-1} \cdot s^{-1}$		

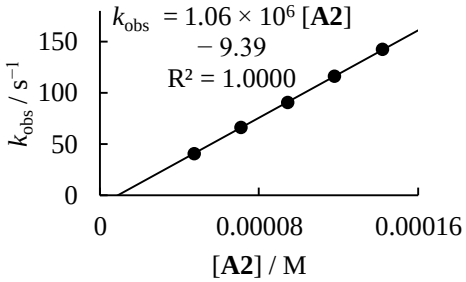

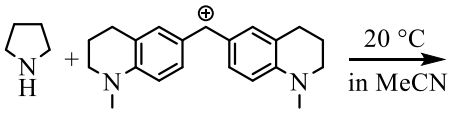

A2 **E11**

Table 18. Kinetics of the reaction of **A2** with **E11** (stopped-flow method, detection at 620 nm)

[**A2**] / M	[**E11**] / M	k_{obs} / s^{-1}
2.36×10^{-5}		5.47×10^{1}
3.54×10^{-5}		8.74×10^{1}
4.72×10^{-5}	2.29×10^{-6}	1.19×10^{2}
5.91×10^{-5}		1.56×10^{2}
7.09×10^{-5}		1.85×10^{2}
$k_2 = 2.78 \times 10^{6}$ $M^{-1} \cdot s^{-1}$		

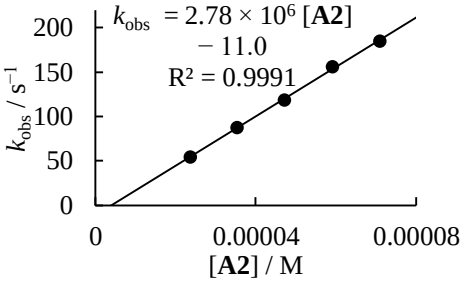

Table 19. Determination of the parameters N and s_N for **A2** in acetonitrile

Electrophile	E	k_2 / $M^{-1} \cdot s^{-1}$
E1	−16.38	3.25×10^{1} [a]
E2	−16.11	4.82×10^{1} [a]
E3	−15.03	-
E4	−14.36	-
E5	−13.39	2.12×10^{3}
E6	−12.18	6.31×10^{4}
E7	−11.87	1.09×10^{4}
E8	−10.04	1.18×10^{5} [a]
E9	−9.45	3.50×10^{5} [a]
E10	−8.76	1.06×10^{6}
E11	−8.22	2.78×10^{6}
N =18.58 s_N = 0.61		

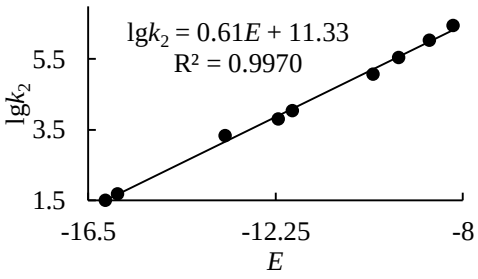

[a] Second-order rate constants k_2 were taken from literature [63]

2-Methylpyrrolidine (A3)

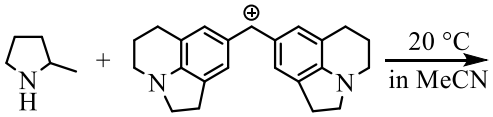

A3 **E8**

Table 20. Kinetics of the reaction of **A3** with **E8** (stopped-flow method, detection at 632 nm)

[**A3**] / M	[**E8**] / M	k_{obs} / s^{-1}
4.49×10^{-4}	1.59×10^{-5}	1.89×10^{1}
8.98×10^{-4}		4.52×10^{1}
1.35×10^{-3}		6.90×10^{1}
1.80×10^{-3}		9.29×10^{1}
2.25×10^{-3}		1.21×10^{2}
2.70×10^{-3}		1.43×10^{2}
$k_2 = 5.53 \times 10^{4}$ $M^{-1} \cdot s^{-1}$		

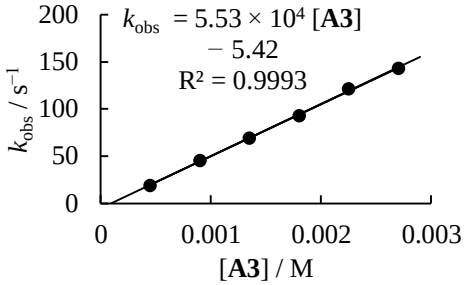

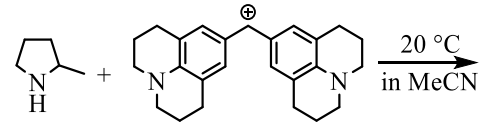

A3 **E9**

Table 21. Kinetics of the reaction of **A3** with **E9** (stopped-flow method, detection at 635 nm)

[**A3**] / M	[**E9**] / M	k_{obs} / s^{-1}
2.25×10^{-4}	1.62×10^{-5}	2.63×10^{1}
4.49×10^{-4}		6.25×10^{1}
6.74×10^{-4}		9.70×10^{1}
8.98×10^{-4}		1.36×10^{2}
1.12×10^{-3}		1.72×10^{2}
1.35×10^{-3}		2.16×10^{2}
$k_2 = 1.67 \times 10^{5}$ $M^{-1} \cdot s^{-1}$		

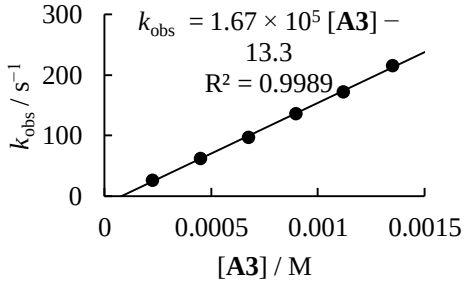

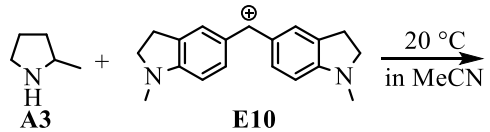

A3 **E10**

Table 22. Kinetics of the reaction of **A3** with **E10** (stopped-flow method, detection at 616 nm)

[**A3**] / M	[**E10**] / M	k_{obs} / s^{-1}
1.35×10^{-4}	1.35×10^{-5}	3.61×10^{1}
2.25×10^{-4}		7.08×10^{1}
3.14×10^{-4}		1.11×10^{2}
4.04×10^{-4}		1.48×10^{2}
4.94×10^{-4}		1.86×10^{2}
5.84×10^{-4}		2.25×10^{2}
$k_2 = 4.22 \times 10^{5}$ $M^{-1} \cdot s^{-1}$		

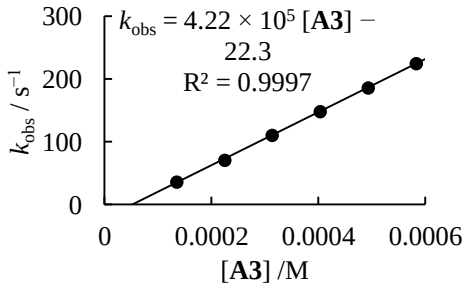

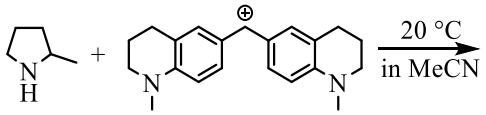

A3 **E11**

Table 23. Kinetics of the reaction of **A3** with **E11** (stopped-flow method, detection at 620 nm)

[**A3**] / M	[**E11**] / M	k_{obs} / s^{-1}
1.35×10^{-4}	5.10×10^{-6}	1.11×10^{2}
2.25×10^{-4}		2.04×10^{2}
3.14×10^{-4}		3.11×10^{2}
4.04×10^{-4}		4.04×10^{2}
4.94×10^{-4}		5.21×10^{2}
5.84×10^{-4}		6.24×10^{2}

$k_2 = 1.15 \times 10^{6}$ $M^{-1} \cdot s^{-1}$

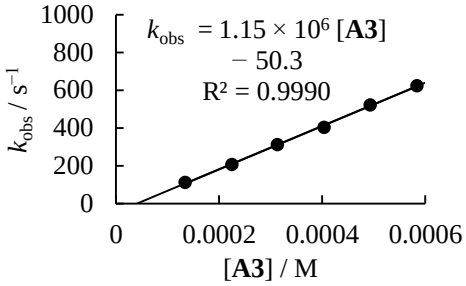

Table 24. Determination of the parameters N and s_N for **A3** in acetonitrile

Electrophile	E	k_2 / $M^{-1} \cdot s^{-1}$
E8	−10.04	5.53×10^{4}
E9	−9.45	1.67×10^{5}
E10	−8.76	4.22×10^{5}
E11	−8.22	1.15×10^{6}

$N = 16.78$ $s_N = 0.71$

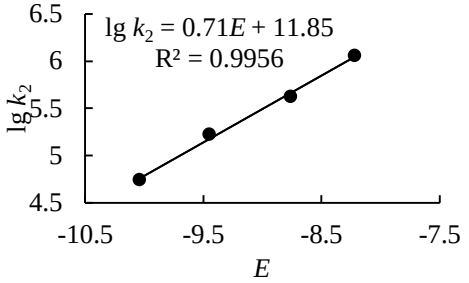

(*R*)-2-Isopropylpyrrolidine (A4)

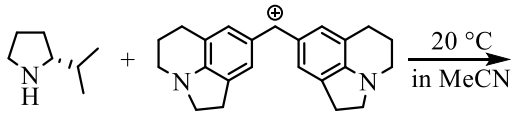

A4 **E8**

Table 25. Kinetics of the reaction of **A4** with **E8** (stopped-flow method, detection at 632 nm)

[**A4**] / M	[**E8**] / M	k_{obs} / s^{-1}
7.47×10^{-5}		2.25
1.12×10^{-4}		3.51
1.49×10^{-4}	5.41×10^{-6}	4.81
1.87×10^{-4}		6.08
2.24×10^{-4}		7.35
$k_2 = 3.42 \times 10^4$ $M^{-1} \cdot s^{-1}$		

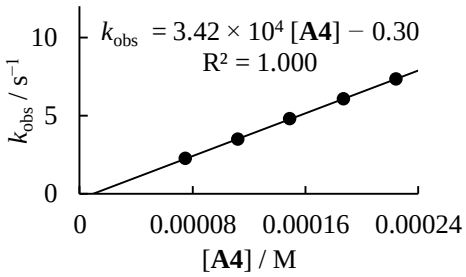

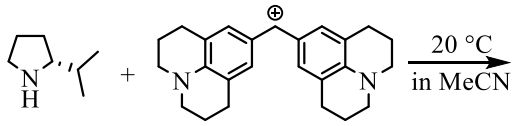

A4 **E9**

Table 26. . Kinetics of the reaction of **A4** with **E9** (stopped-flow method, detection at 635 nm)

[**A4**] / M	[**E9**] / M	k_{obs} / s^{-1}
7.47×10^{-5}		6.29
1.12×10^{-4}		1.01×10^1
1.49×10^{-4}	3.56×10^{-6}	1.33×10^1
1.87×10^{-4}		1.70×10^1
2.24×10^{-4}		2.14×10^1
$k_2 = 9.94 \times 10^4$ $M^{-1} \cdot s^{-1}$		

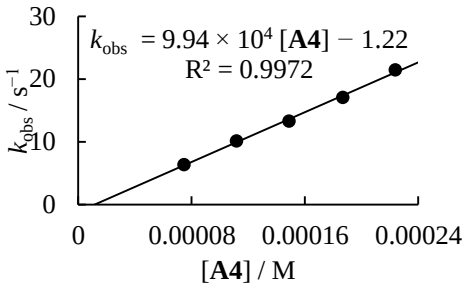

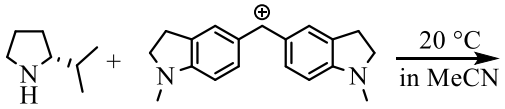

A4 **E10**

Table 27. . Kinetics of the reaction of **A4** with **E10** (stopped-flow method, detection at 616 nm)

[**A4**] / M	[**E10**] / M	k_{obs} / s^{-1}
4.98×10^{-5}		1.01×10^1
7.47×10^{-5}		1.70×10^1
9.96×10^{-5}	5.00×10^{-6}	2.33×10^1
1.25×10^{-4}		2.93×10^1
1.49×10^{-4}		3.56×10^1
$k_2 = 2.55 \times 10^5$ $M^{-1} \cdot s^{-1}$		

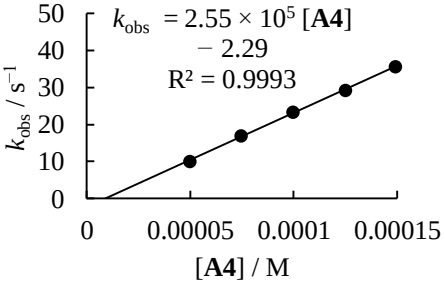

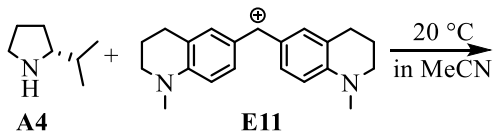

A4 **E11**

Table 28. Kinetics of the reaction of **A4** with **E11** (stopped-flow method, detection at 620 nm)

[**A4**] / M	[**E11**] / M	k_{obs} / s^{-1}
4.98×10^{-5}		2.76×10^{1}
7.47×10^{-5}		4.54×10^{1}
9.96×10^{-5}	5.00×10^{-6}	6.38×10^{1}
1.25×10^{-4}		8.08×10^{1}
1.49×10^{-4}		9.92×10^{1}
$k_2 = 7.18 \times 10^{5}$ $M^{-1} \cdot s^{-1}$		

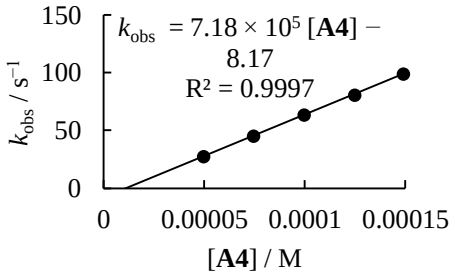

Table 29. Determination of the parameters N and s_N for **A4** in acetonitrile

Electrophile	E	k_2 / $M^{-1} \cdot s^{-1}$
E8	−10.04	3.42×10^{4}
E9	−9.45	9.94×10^{4}
E10	−8.76	2.55×10^{5}
E11	−8.22	7.18×10^{5}
$N = 16.44$ $s_N = 0.71$		

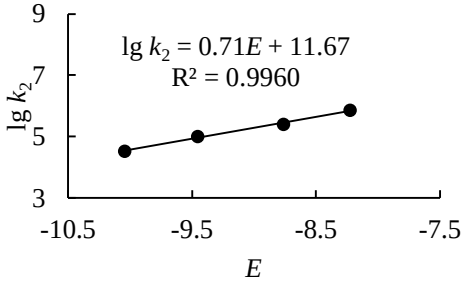

2,2-Dimethylpyrrolidine (A5)

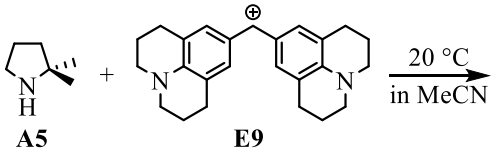

A5 E9

Table 30. Kinetics of the reaction of **A5** with **E9** (stopped-flow method, detection at 635 nm)

[**A5**] / M	[**E9**] / M	k_{obs} / s^{-1}
5.60×10^{-4}	1.52×10^{-5}	1.44
9.33×10^{-4}		2.41
1.31×10^{-3}		3.46
1.68×10^{-3}		4.44
2.05×10^{-3}		5.47
2.43×10^{-3}		6.52
$k_2 = 2.72 \times 10^3$ $M^{-1} \cdot s^{-1}$		

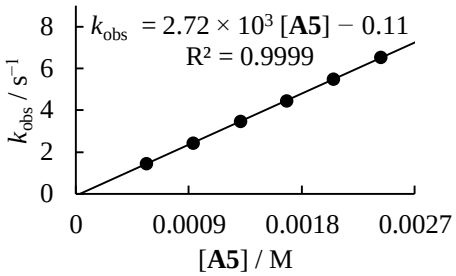

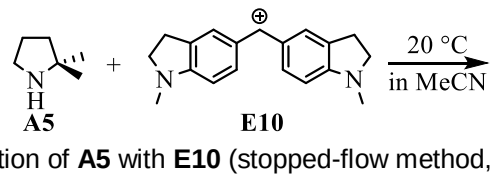

A5 E10

Table 31. Kinetics of the reaction of **A5** with **E10** (stopped-flow method, detection at 616 nm)

[**A5**] / M	[**E10**] / M	k_{obs} / s^{-1}
3.73×10^{-4}	1.93×10^{-5}	2.34
5.60×10^{-4}		4.13
7.46×10^{-4}		5.46
9.33×10^{-4}		6.77
1.12×10^{-3}		8.51
1.31×10^{-3}		9.79
$k_2 = 7.89 \times 10^3$ $M^{-1} \cdot s^{-1}$		

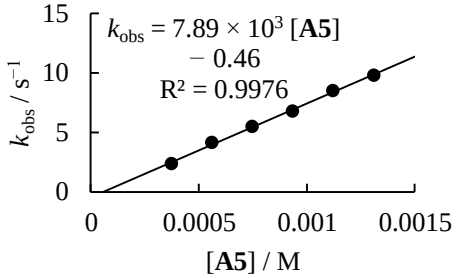

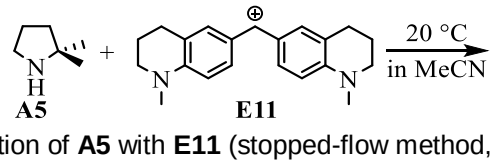

A5 E11

Table 32. Kinetics of the reaction of **A5** with **E11** (stopped-flow method, detection at 620 nm)

[**A5**] / M	[**E11**] / M	k_{obs} / s^{-1}
1.87×10^{-4}	1.28×10^{-5}	3.00
3.36×10^{-4}		6.56
4.85×10^{-4}		1.03×10^1
6.34×10^{-4}		1.37×10^1
7.83×10^{-3}		1.74×10^1
9.33×10^{-3}		2.15×10^1
$k_2 = 2.46 \times 10^4$ $M^{-1} \cdot s^{-1}$		

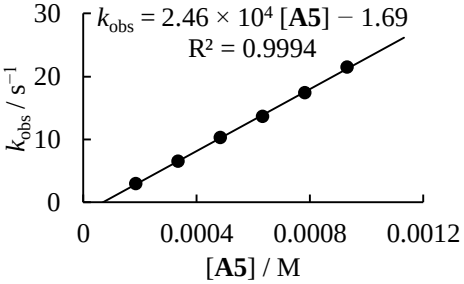

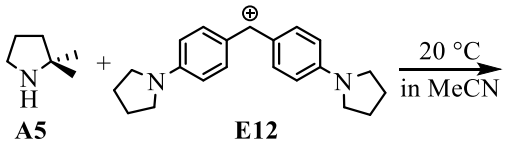

A5 **E12**

Table 33. Kinetics of the reaction of **A5** with **E12** (stopped-flow method, detection at 612 nm)

[**A5**] / M	[**E12**] / M	k_{obs} / s^{-1}
1.87×10^{-4}	1.53×10^{-5}	8.83
3.36×10^{-4}		1.94×10^{1}
4.85×10^{-4}		3.14×10^{1}
6.34×10^{-4}		4.10×10^{1}
7.83×10^{-3}		5.12×10^{1}
9.33×10^{-3}		6.28×10^{1}
$k_2 = 7.18 \times 10^{4}$ $M^{-1} \cdot s^{-1}$		

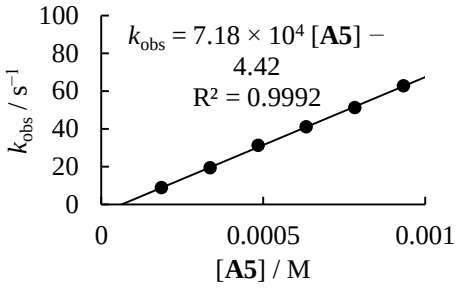

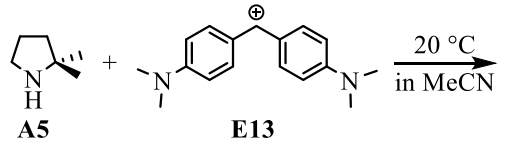

A5 **E13**

Table 34. Kinetics of the reaction of **A5** with **E13** (stopped-flow method, detection at 605 nm)

[**A5**] / M	[**E13**] / M	k_{obs} / s^{-1}
1.87×10^{-4}	9.56×10^{-6}	2.18×10^{1}
3.36×10^{-4}		4.88×10^{1}
4.85×10^{-4}		7.25×10^{1}
6.34×10^{-4}		1.00×10^{2}
7.83×10^{-3}		1.24×10^{2}
9.33×10^{-3}		1.57×10^{2}
$k_2 = 1.78 \times 10^{5}$ $M^{-1} \cdot s^{-1}$		

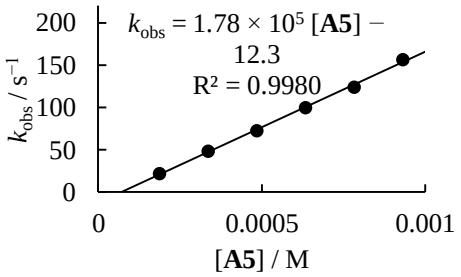

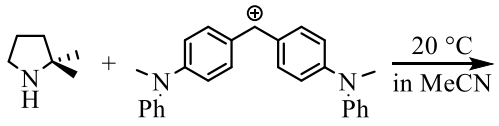

A5 **E14**

Table 35. Kinetics of the reaction of **A5** with **E14** (stopped-flow method, detection at 613 nm)

[**A5**] / M	[**E14**] / M	k_{obs} / s^{-1}
1.12×10^{-4}	1.12×10^{-5}	8.60×10^{1}
1.49×10^{-4}		1.49×10^{2}
1.87×10^{-4}		1.96×10^{2}
2.24×10^{-4}		2.48×10^{2}
2.61×10^{-3}		2.88×10^{2}
2.98×10^{-3}		3.40×10^{2}
$k_2 = 1.33 \times 10^{6}$ $M^{-1} \cdot s^{-1}$		

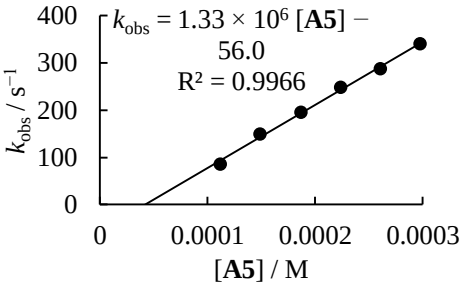

Table 36. Determination of the parameters N and s_N for **A5** in acetonitrile

Electrophile	E	k_2 / $M^{-1} \cdot s^{-1}$
E9	−9.45	2.72×10^{3}
E10	−8.76	7.89×10^{3}
E11	−8.22	2.46×10^{4}
E12	−7.69	7.18×10^{4}
E13	−7.02	1.78×10^{5}
E14	−5.89	1.33×10^{6}
$N = 13.96$ $s_N = 0.76$		

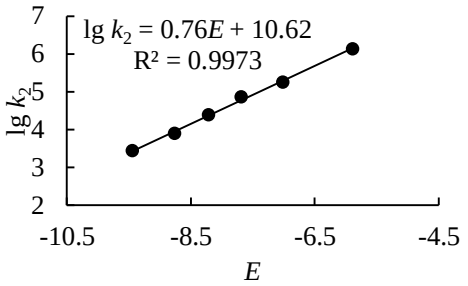

2-Benzylpyrrolidine (A6)

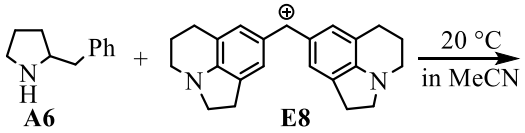

Table 37. Kinetics of the reaction of **A6** with **E8** (stopped-flow method, detection at 632 nm)

[**A6**] / M	[**E8**] / M	k_{obs} / s^{-1}
7.60×10^{-5}	5.29×10^{-6}	5.57
1.52×10^{-4}		1.07×10^{1}
2.28×10^{-4}		1.59×10^{1}
3.04×10^{-4}		2.16×10^{1}
3.80×10^{-4}		2.75×10^{1}
4.56×10^{-4}		3.27×10^{1}
$k_2 = 7.21 \times 10^{4}$ $M^{-1} \cdot s^{-1}$		

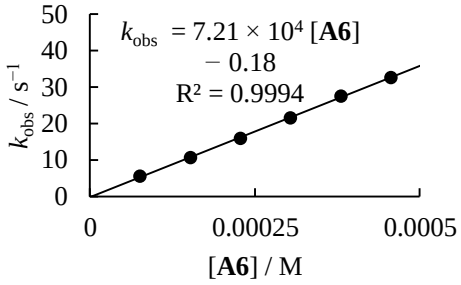

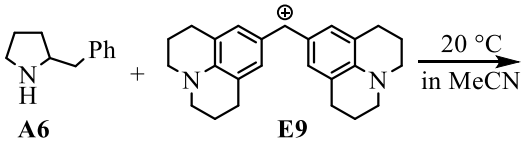

Table 38. Kinetics of the reaction of **A6** with **E9** (stopped-flow method, detection at 635 nm)

[**A6**] / M	[**E9**] / M	k_{obs} / s^{-1}
7.60×10^{-5}	5.06×10^{-6}	1.70×10^{1}
1.52×10^{-4}		3.30×10^{1}
2.28×10^{-4}		5.01×10^{1}
3.04×10^{-4}		6.75×10^{1}
3.80×10^{-4}		8.65×10^{1}
4.56×10^{-4}		1.03×10^{2}
$k_2 = 2.29 \times 10^{5}$ $M^{-1} \cdot s^{-1}$		

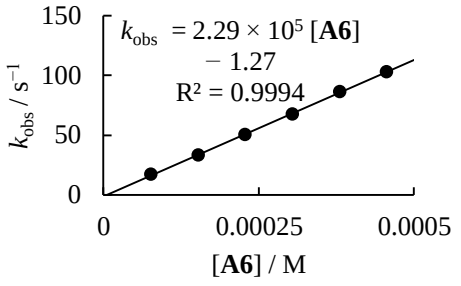

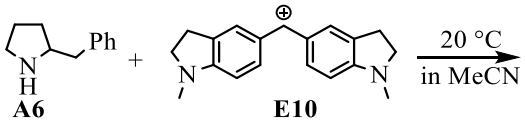

Table 39. Kinetics of the reaction of **A6** with **E10** (stopped-flow method, detection at 616 nm)

[**A6**] / M	[**E10**] / M	k_{obs} / s^{-1}
7.60×10^{-5}	4.67×10^{-6}	2.77×10^{1}
1.52×10^{-4}		6.13×10^{1}
2.28×10^{-4}		9.30×10^{1}
3.04×10^{-4}		1.30×10^{2}
3.80×10^{-4}		1.65×10^{2}
4.56×10^{-4}		1.98×10^{2}
$k_2 = 4.51 \times 10^{5}$ $M^{-1} \cdot s^{-1}$		

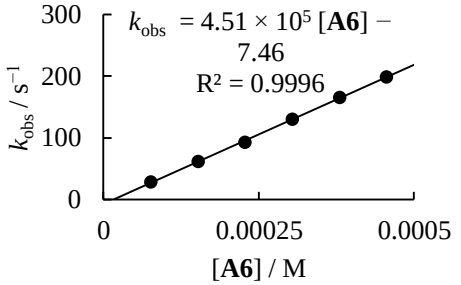

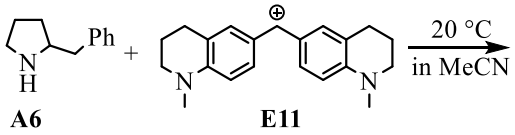

A6 **E11**

Table 40. Kinetics of the reaction of **A6** with **E11** (stopped-flow method, detection at 620 nm)

[**A6**] / M	[**E11**] / M	k_{obs} / s^{-1}
4.75×10^{-5}	4.78×10^{-6}	4.80×10^{1}
7.12×10^{-5}		8.23×10^{1}
9.50×10^{-5}		1.15×10^{2}
1.19×10^{-4}		1.45×10^{2}
1.42×10^{-4}		1.76×10^{2}
1.66×10^{-4}		2.06×10^{2}
$k_2 = 1.33 \times 10^{6}$ $M^{-1} \cdot s^{-1}$		

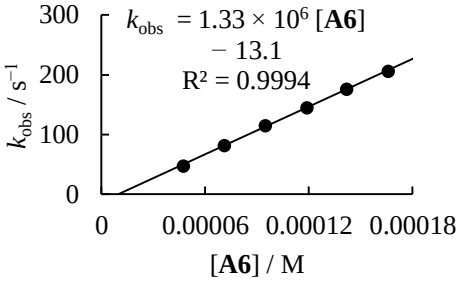

Table 41. Determination of the parameters N and s_N for **A6** in acetonitrile

Electrophile	E	k_2 / $M^{-1} \cdot s^{-1}$
E8	−10.04	7.21×10^{4}
E9	−9.45	2.29×10^{5}
E10	−8.76	4.51×10^{5}
E11	−8.22	1.33×10^{6}
$N = 17.43$ $s_N = 0.66$		

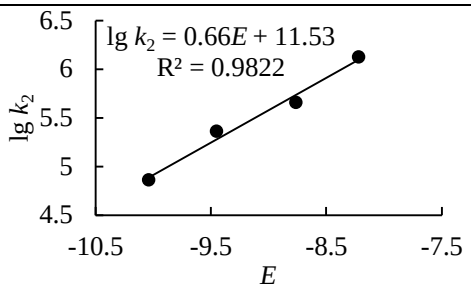

(*S*)-2-Benzhydrylpyrrolidine (A7)

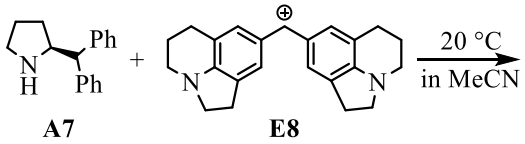

A7 **E8**

Table 42. Kinetics of the reaction of **A7** with **E8** (stopped-flow method, detection at 632 nm)

[**A7**] / M	[**E8**] / M	k_{obs} / s^{-1}
2.70×10^{-4}	4.62×10^{-6}	6.73
4.04×10^{-4}		1.02×10^{1}
5.39×10^{-4}		1.38×10^{1}
8.09×10^{-4}		2.06×10^{1}
1.08×10^{-3}		2.80×10^{1}
1.35×10^{-3}		3.57×10^{1}
$k_2 = 2.67 \times 10^{4}$ $M^{-1} \cdot s^{-1}$		

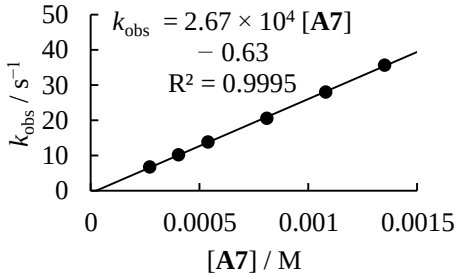

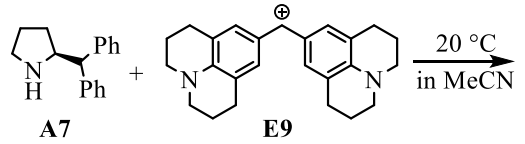

A7 **E9**

Table 43. Kinetics of the reaction of **A7** with **E9** (stopped-flow method, detection at 635 nm)

[**A7**] / M	[**E9**] / M	k_{obs} / s^{-1}
1.35×10^{-4}	4.73×10^{-6}	9.60
2.02×10^{-4}		1.34×10^{1}
2.70×10^{-4}		1.77×10^{1}
3.37×10^{-4}		2.17×10^{1}
4.04×10^{-4}		2.59×10^{1}
$k_2 = 6.08 \times 10^{4}$ $M^{-1} \cdot s^{-1}$		

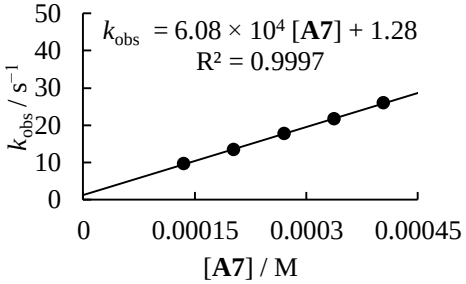

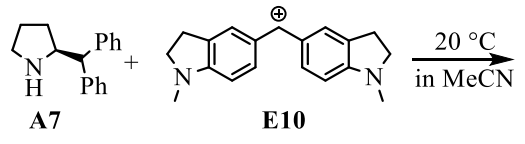

A7 **E10**

Table 44. Kinetics of the reaction of **A7** with **E10** (stopped-flow method, detection at 616 nm)

[**A7**] / M	[**E10**] / M	k_{obs} / s^{-1}
8.09×10^{-5}	6.60×10^{-6}	1.12×10^{1}
1.21×10^{-4}		1.78×10^{1}
1.62×10^{-4}		2.42×10^{1}
2.02×10^{-4}		3.04×10^{1}
2.43×10^{-4}		3.68×10^{1}
2.83×10^{-4}		4.31×10^{1}
$k_2 = 1.57 \times 10^{5}$ $M^{-1} \cdot s^{-1}$		

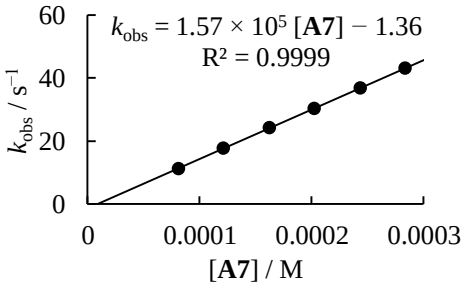

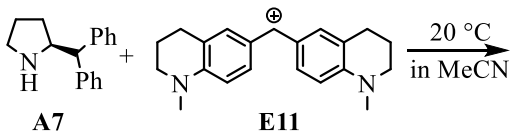

A7 **E11**

Table 45. Kinetics of the reaction of **A7** with **E11** (stopped-flow method, detection at 620 nm)

[**A7**] / M	[**E11**] / M	k_{obs} / s^{-1}
5.39×10^{-5}	4.49×10^{-6}	1.97×10^{1}
8.09×10^{-5}		2.97×10^{1}
1.08×10^{-4}		4.10×10^{1}
1.35×10^{-4}		5.24×10^{1}
1.62×10^{-4}		6.47×10^{1}
1.89×10^{-4}		7.78×10^{1}
$k_2 = 4.30 \times 10^{5}$ $M^{-1} \cdot s^{-1}$		

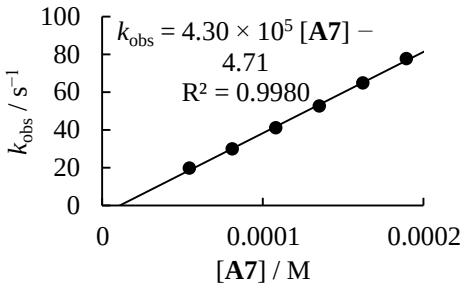

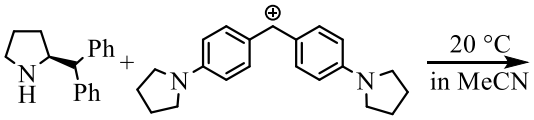

A7 **E12**

Table 46. Kinetics of the reaction of **A7** with **E12** (stopped-flow method, detection at 612 nm)

[**A7**] / M	[**E12**] / M	k_{obs} / s^{-1}
4.04×10^{-5}	4.36×10^{-6}	2.58×10^{1}
6.74×10^{-5}		5.03×10^{1}
9.44×10^{-5}		7.61×10^{1}
1.21×10^{-4}		1.04×10^{2}
1.48×10^{-4}		1.30×10^{2}
1.75×10^{-4}		1.57×10^{2}
$k_2 = 9.80 \times 10^{5}$ $M^{-1} \cdot s^{-1}$		

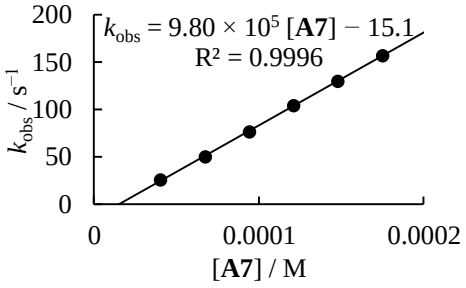

Table 47. Determination of the parameters N and s_N for **A7** in acetonitrile

Electrophile	E	k_2 / $M^{-1} \cdot s^{-1}$
E8	−10.04	2.67×10^{4}
E9	−9.45	6.08×10^{4}
E10	−8.76	1.57×10^{5}
E11	−8.22	4.30×10^{5}
E12	−7.69	9.80×10^{5}
$N = 16.61$ $s_N = 0.67$		

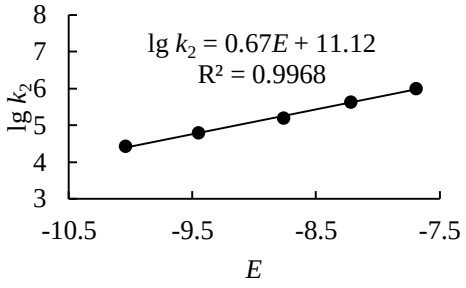

(*S*)-Pyrrolidin-2-ylmethanamine (A8)

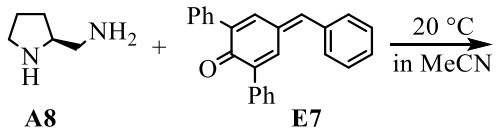

A8 **E7**

Table 48. Kinetics of the reaction of **A8** with **E7** (stopped-flow method, detection at 376 nm)

[**A8**] / M	[**E7**] / M	k_{obs} / s^{-1}
1.93×10^{-4}		6.43×10^{-1}
2.89×10^{-4}		1.07
3.85×10^{-4}	1.61×10^{-5}	1.44
4.82×10^{-4}		1.77
5.78×10^{-4}		2.18
$k_2 = 3.92 \times 10^3$ $M^{-1} \cdot s^{-1}$		

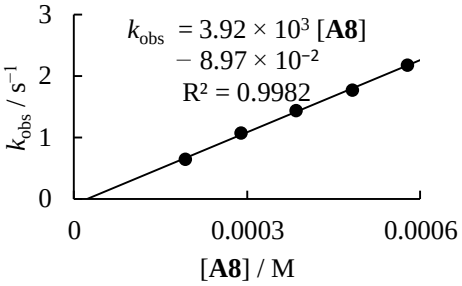

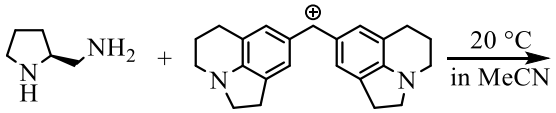

A8 **E8**

Table 49. Kinetics of the reaction of **A8** with **E8** (stopped-flow method, detection at 632 nm)

[**A8**] / M	[**E8**] / M	k_{obs} / s^{-1}
5.78×10^{-5}		2.69
8.67×10^{-5}		4.46
1.16×10^{-4}	5.29×10^{-6}	6.19
1.45×10^{-4}		8.00
1.73×10^{-4}		9.62
$k_2 = 6.03 \times 10^4$ $M^{-1} \cdot s^{-1}$		

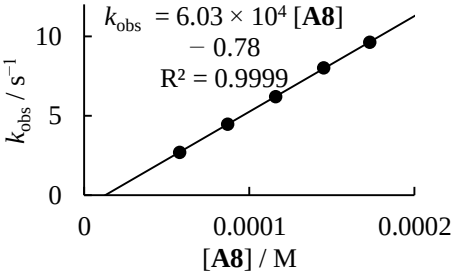

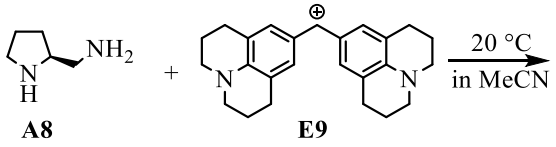

A8 **E9**

Table 50. Kinetics of the reaction of **A8** with **E9** (stopped-flow method, detection at 635 nm)

[**A8**] / M	[**E9**] / M	k_{obs} / s^{-1}
5.78×10^{-5}		8.31
8.67×10^{-5}		1.28×10^1
1.16×10^{-4}	5.67×10^{-6}	1.74×10^1
1.45×10^{-4}		2.29×10^1
1.73×10^{-4}		2.78×10^1
$k_2 = 1.70 \times 10^5$ $M^{-1} \cdot s^{-1}$		

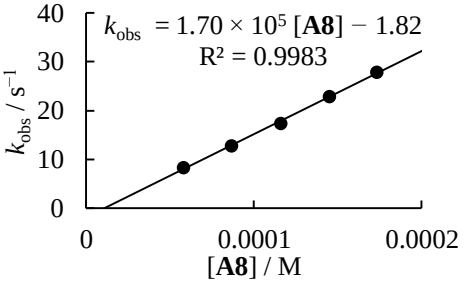

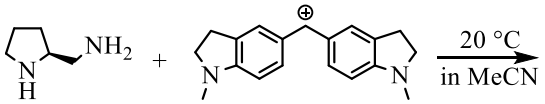

A8 **E10**

Table 51. Kinetics of the reaction of **A8** with **E10** (stopped-flow method, detection at 616 nm)

[**A8**] / M	[**E10**] / M	k_{obs} / s^{-1}
3.85×10^{-5}		1.24×10^{1}
5.78×10^{-5}		2.03×10^{1}
7.71×10^{-5}	3.84×10^{-6}	2.81×10^{1}
9.63×10^{-5}		3.65×10^{1}
1.16×10^{-4}		4.44×10^{1}
$k_2 = 4.14 \times 10^{5}$ $M^{-1} \cdot s^{-1}$		

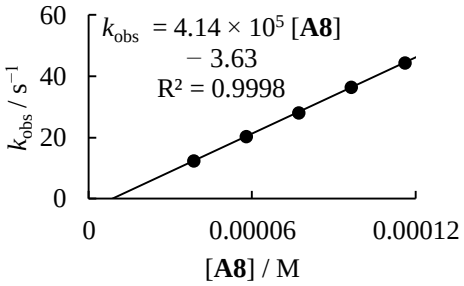

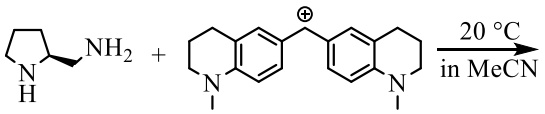

A8 **E11**

Table 52. Kinetics of the reaction of **A8** with **E11** (stopped-flow method, detection at 620 nm)

[**A8**] / M	[**E11**] / M	k_{obs} / s^{-1}
3.85×10^{-5}		3.17×10^{1}
5.78×10^{-5}		5.46×10^{1}
7.71×10^{-5}	3.82×10^{-6}	7.53×10^{1}
9.63×10^{-5}		9.70×10^{1}
1.16×10^{-4}		1.19×10^{2}
$k_2 = 1.12 \times 10^{6}$ $M^{-1} \cdot s^{-1}$		

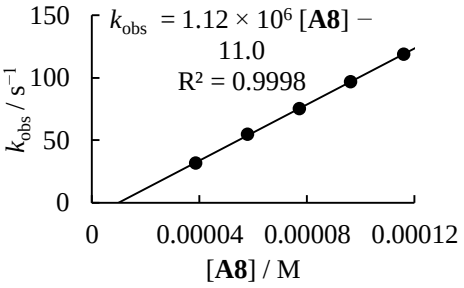

Table 53. Determination of the parameters N and s_N for **A8** in acetonitrile

Electrophile	E	k_2 / $M^{-1} \cdot s^{-1}$
E7	−11.87	3.92×10^{3}
E8	−10.04	6.03×10^{4}
E9	−9.45	1.70×10^{5}
E10	−8.76	4.14×10^{5}
E11	−8.22	1.12×10^{6}
$N = 17.24$ $s_N = 0.67$		

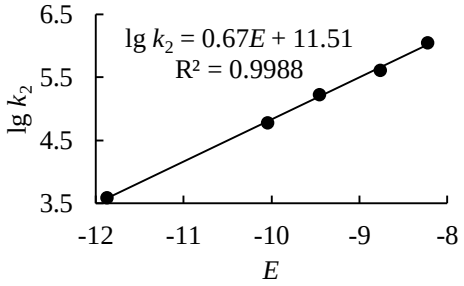

(*S*)-*N*,*N*-Dimethyl-1-(pyrrolidin-2-yl)methanamine (A9)

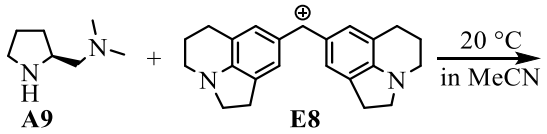

A9 **E8**

Table 54. Kinetics of the reaction of **A9** with **E8** (stopped-flow method, detection at 632 nm)

[**A9**] / M	[**E8**] / M	k_{obs} / s^{-1}
1.04×10^{-4}	8.86×10^{-6}	8.09
1.56×10^{-4}		1.31×10^{1}
2.08×10^{-4}		1.85×10^{1}
3.12×10^{-4}		2.69×10^{1}
4.16×10^{-4}		3.69×10^{1}
5.21×10^{-4}		4.71×10^{1}
$k_2 = 9.25 \times 10^{4}$ $M^{-1} \cdot s^{-1}$		

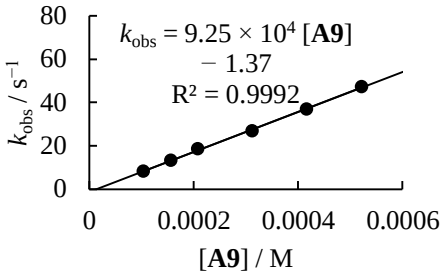

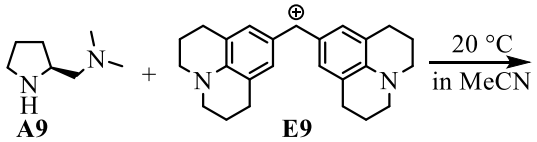

A9 **E9**

Table 55. Kinetics of the reaction of **A9** with **E9** (stopped-flow method, detection at 635 nm)

[**A9**] / M	[**E9**] / M	k_{obs} / s^{-1}
7.81×10^{-5}	6.48×10^{-6}	2.01×10^{1}
1.30×10^{-4}		3.80×10^{1}
1.82×10^{-4}		5.43×10^{1}
2.34×10^{-4}		7.10×10^{1}
3.38×10^{-4}		1.07×10^{2}
$k_2 = 3.32 \times 10^{5}$ $M^{-1} \cdot s^{-1}$		

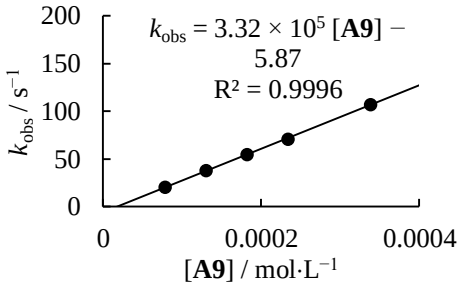

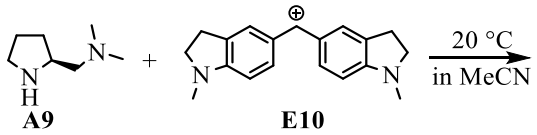

A9 **E10**

Table 56. Kinetics of the reaction of **A9** with E**10** (stopped-flow method, detection at 616 nm)

[**A9**] / M	[**E10**] / M	k_{obs} / s^{-1}
1.04×10^{-4}	5.49×10^{-6}	5.87×10^{1}
1.56×10^{-4}		9.33×10^{1}
2.08×10^{-4}		1.24×10^{2}
2.60×10^{-4}		1.63×10^{2}
3.12×10^{-4}		1.95×10^{2}
$k_2 = 6.58 \times 10^{5}$ $M^{-1} \cdot s^{-1}$		

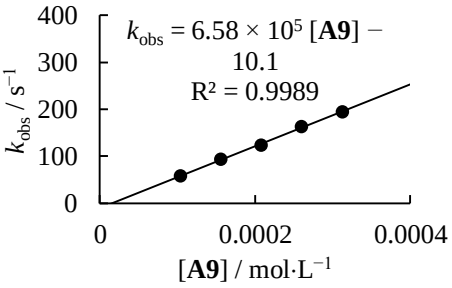

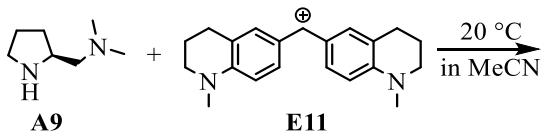

A9 **E11**

Table 57. Kinetics of the reaction of **A9** with E**11** (stopped-flow method, detection at 620 nm)

[**A9**] / M	[**E11**] / M	k_{obs} / s^{-1}
4.16×10^{-5}	4.21×10^{-6}	5.73×10^{1}
5.10×10^{-5}		7.64×10^{1}
6.25×10^{-5}		9.98×10^{1}
8.33×10^{-5}		1.34×10^{2}
1.04×10^{-4}		1.71×10^{2}
1.25×10^{-4}		2.16×10^{2}
$k_2 = 1.86 \times 10^{6}$ $M^{-1} \cdot s^{-1}$		

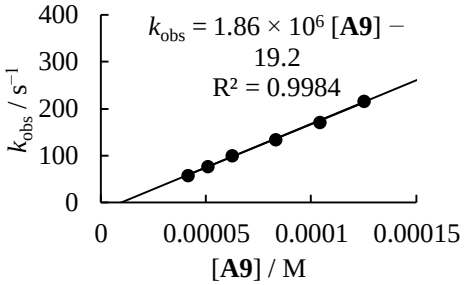

Table 58. Determination of the parameters N and s_N for **A9** in acetonitrile

Electrophile	E	k_2 / $M^{-1} \cdot s^{-1}$
E8	−10.04	9.25×10^{4}
E9	−9.45	3.32×10^{5}
E10	−8.76	6.58×10^{5}
E11	−8.22	1.86×10^{6}
$N = 17.41$ $s_N = 0.68$		

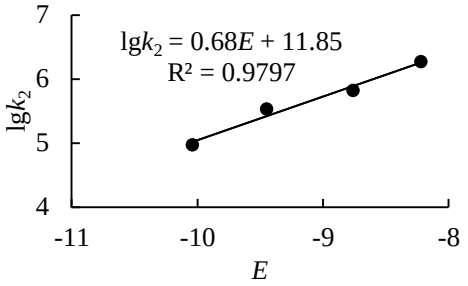

(*S*)-1-(Pyrrolidin-2-ylmethyl)pyrrolidine (A10)

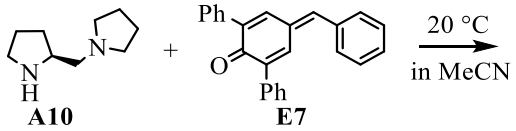

A10 **E7**

Table 59. Kinetics of the reaction of **A10** with **E7** (stopped-flow method, detection at 376 nm)

[**A10**] / M	[**E7**] / M	k_{obs} / s^{-1}
1.66×10^{-4}		1.79
2.49×10^{-4}		2.83
3.32×10^{-4}	1.61×10^{-5}	3.90
4.15×10^{-4}		5.03
4.98×10^{-4}		6.13
$k_2 = 1.31 \times 10^4$ $M^{-1} \cdot s^{-1}$		

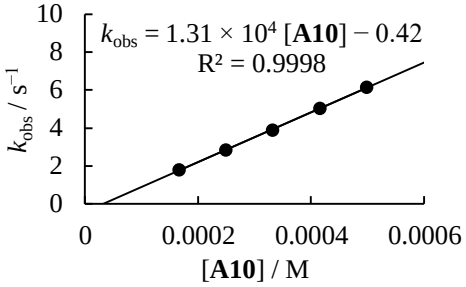

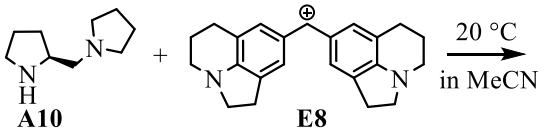

A10 **E8**

Table 60. Kinetics of the reaction of **A10** with **E8** (stopped-flow method, detection at 632 nm)

[**A10**] / M	[**E8**] / M	k_{obs} / s^{-1}
4.98×10^{-5}		7.25
7.47×10^{-5}		1.16×10^1
9.96×10^{-5}	4.89×10^{-6}	1.60×10^1
1.24×10^{-4}		2.01×10^1
1.49×10^{-4}		2.43×10^1
$k_2 = 1.72 \times 10^5$ $M^{-1} \cdot s^{-1}$		

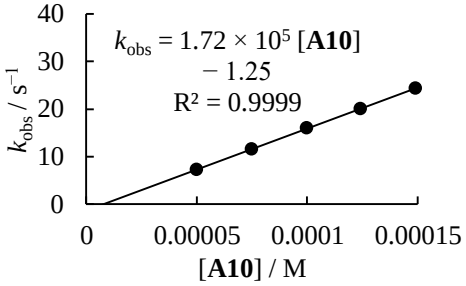

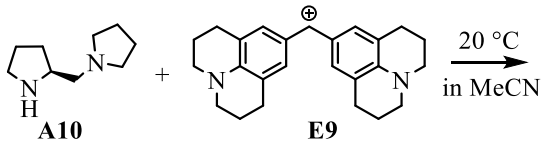

A10 **E9**

Table 61. Kinetics of the reaction of **A10** with **E9** (stopped-flow method, detection at 635 nm)

[**A10**] / M	[**E9**] / M	k_{obs} / s^{-1}
3.32×10^{-5}		1.56×10^1
4.98×10^{-5}		2.43×10^1
6.64×10^{-5}	3.31×10^{-6}	3.27×10^1
8.30×10^{-5}		4.16×10^1
9.96×10^{-5}		5.24×10^1
$k_2 = 5.48 \times 10^5$ $M^{-1} \cdot s^{-1}$		

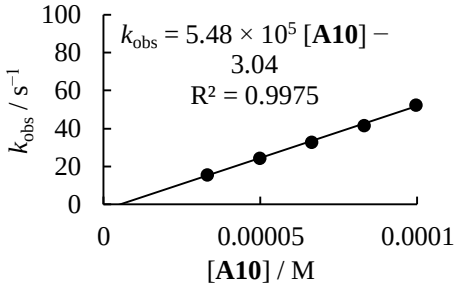

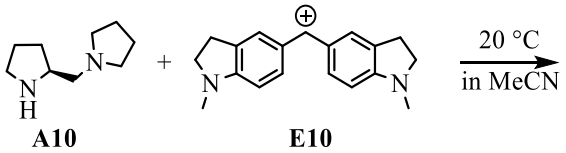

A10 **E10**

Table 62. Kinetics of the reaction of **A10** with **E10** (stopped-flow method, detection at 616 nm)

[**A10**] / M	[**E10**] / M	k_{obs} / s^{-1}
3.32×10^{-5}		2.78×10^{1}
4.98×10^{-5}		4.52×10^{1}
6.64×10^{-5}	3.29×10^{-6}	6.28×10^{1}
8.30×10^{-5}		8.00×10^{1}
9.96×10^{-5}		9.75×10^{1}
$k_2 = 1.05 \times 10^{6}$ $M^{-1} \cdot s^{-1}$		

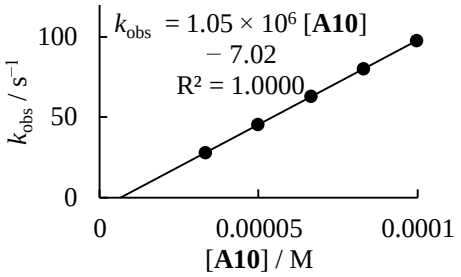

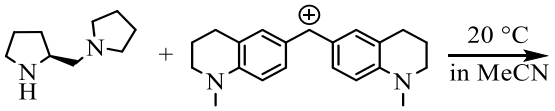

A10 **E11**

Table 63. Kinetics of the reaction of **A10** with **E11** (stopped-flow method, detection at 620 nm)

[**A10**] / M	[**E11**] / M	k_{obs} / s^{-1}
3.32×10^{-5}		7.80×10^{1}
4.98×10^{-5}		1.28×10^{2}
6.64×10^{-5}	3.35×10^{-6}	1.79×10^{2}
8.30×10^{-5}		2.22×10^{2}
9.96×10^{-5}		2.74×10^{2}
$k_2 = 2.93 \times 10^{6}$ $M^{-1} \cdot s^{-1}$		

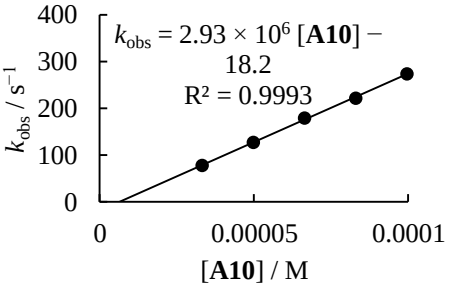

Table 64. Determination of the parameters N and s_N for **A10** in acetonitrile

Electrophile	E	k_2 / $M^{-1} \cdot s^{-1}$
E7	−11.87	1.31×10^{4}
E8	−10.04	1.72×10^{5}
E9	−9.45	5.48×10^{5}
E10	−8.76	1.05×10^{6}
E11	−8.22	2.93×10^{6}
$N = 18.33$ $s_N = 0.64$		

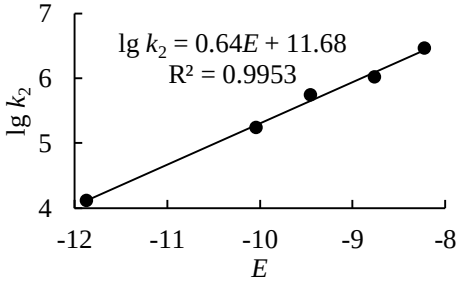

(*S*)-2-(Azidomethyl)pyrrolidine (A11)

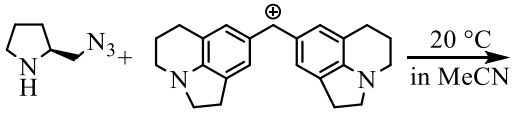

A11 **E8**

Table 65. Kinetics of the reaction of **A11** with **E8** (stopped-flow method, detection at 632 nm)

[**A11**] / M	[**E8**] / M	k_{obs} / s^{-1}
6.08×10^{-5}		5.84×10^{-1}
9.12×10^{-5}		7.97×10^{-1}
1.22×10^{-4}	5.29×10^{-6}	1.02
1.52×10^{-4}		1.27
1.82×10^{-4}		1.49
$k_2 = 7.54 \times 10^3$ $M^{-1} \cdot s^{-1}$		

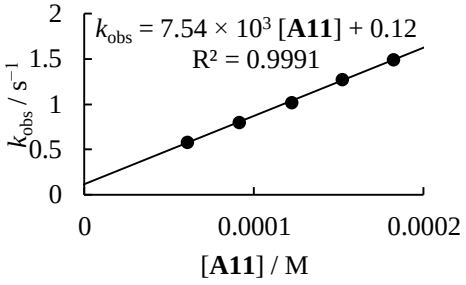

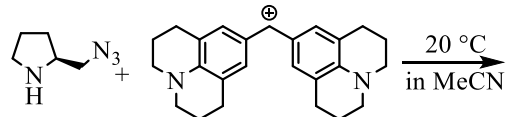

A11 **E9**

Table 66. Kinetics of the reaction of **A11** with **E9** (stopped-flow method, detection at 635 nm)

[**A11**] / M	[**E9**] / M	k_{obs} / s^{-1}
6.08×10^{-5}		2.00
9.12×10^{-5}		2.65
1.22×10^{-4}	5.91×10^{-6}	3.34
1.52×10^{-4}		4.14
1.82×10^{-4}		4.94
$k_2 = 2.43 \times 10^4$ $M^{-1} \cdot s^{-1}$		

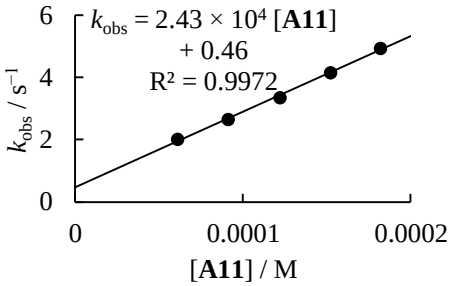

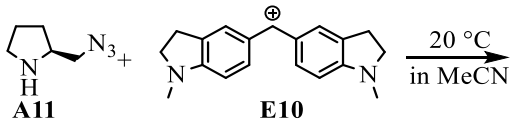

A11 **E10**

Table 67. Kinetics of the reaction of **A11** with **E10** (stopped-flow method, detection at 616 nm)

[**A11**] / M	[**E10**] / M	k_{obs} / s^{-1}
6.08×10^{-5}		3.38
9.12×10^{-5}		5.37
1.22×10^{-4}	5.93×10^{-6}	7.23
1.52×10^{-4}		9.27
1.82×10^{-4}		1.11×10^1
$k_2 = 6.38 \times 10^4$ $M^{-1} \cdot s^{-1}$		

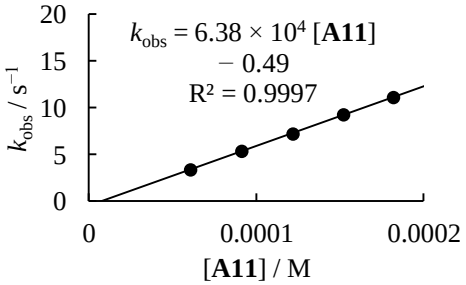

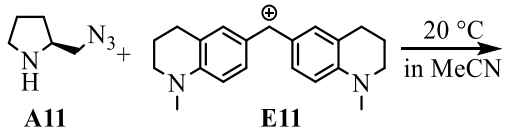

A11 **E11**

Table 68. Kinetics of the reaction of **A11** with **E11** (stopped-flow method, detection at 620 nm)

[**A11**] / M	[**E11**] / M	k_{obs} / s^{-1}
6.08×10^{-5}		1.01×10^{1}
9.12×10^{-5}		1.58×10^{1}
1.22×10^{-4}	5.93×10^{-6}	2.16×10^{1}
1.52×10^{-4}		2.75×10^{1}
1.82×10^{-4}		3.33×10^{1}
$k_2 = 1.92 \times 10^{5}$ $M^{-1} \cdot s^{-1}$		

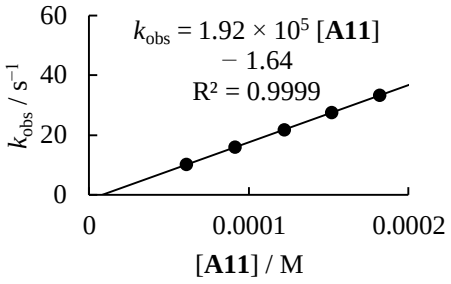

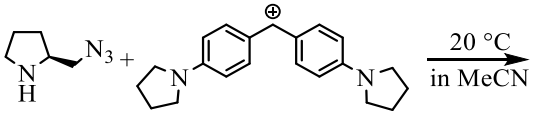

A11 **E12**

Table 69. Kinetics of the reaction of **A11** with **E12** (stopped-flow method, detection at 612 nm)

[**A11**] / M	[**E12**] / M	k_{obs} / s^{-1}
4.05×10^{-5}		1.71×10^{1}
6.08×10^{-5}		2.69×10^{1}
8.11×10^{-5}	3.19×10^{-6}	3.61×10^{1}
1.01×10^{-4}		4.63×10^{1}
1.22×10^{-4}		5.58×10^{1}
$k_2 = 4.76 \times 10^{5}$ $M^{-1} \cdot s^{-1}$		

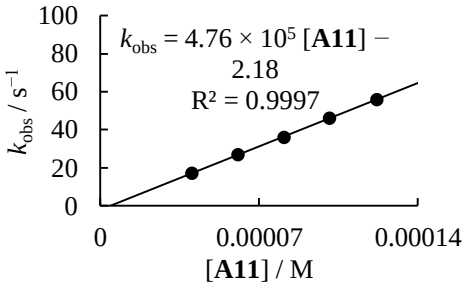

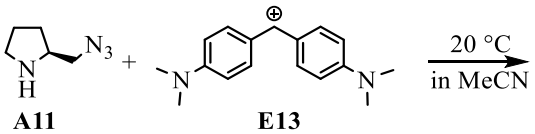

A11 **E13**

Table 70. Kinetics of the reaction of **A11** with **E13** (stopped-flow method, detection at 605 nm)

[**A11**] / M	[**E13**] / M	k_{obs} / s^{-1}
2.03×10^{-5}		1.81×10^{1}
3.04×10^{-5}		2.90×10^{1}
4.05×10^{-5}	2.01×10^{-6}	4.03×10^{1}
5.07×10^{-5}		5.15×10^{1}
6.08×10^{-5}		6.39×10^{1}
$k_2 = 1.13 \times 10^{6}$ $M^{-1} \cdot s^{-1}$		

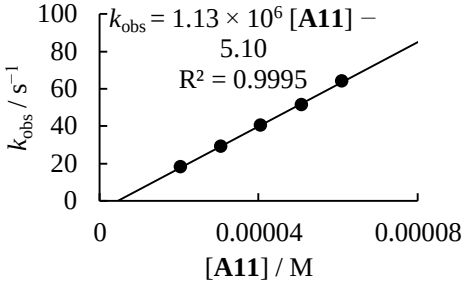

Table 71. Determination of the parameters N and s_N for **A11** in acetonitrile

Electrophile	E	k_2 / $M^{-1} \cdot s^{-1}$
E8	−10.04	7.54×10^3
E9	−9.45	2.43×10^4
E10	−8.76	6.38×10^5
E11	−8.22	1.92×10^5
E12	−7.69	4.76×10^5
E13	−7.02	1.13×10^6
N = 15.43 s_N = 0.73		

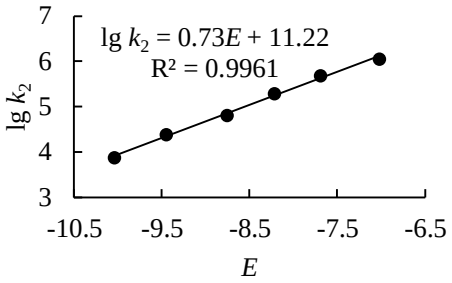

(*S*)-Pyrrolidin-2-ylmethanol (A12)

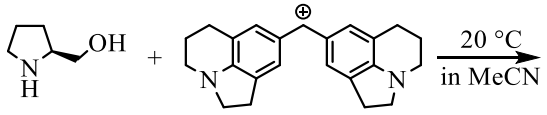

A12 **E8**

Table 72. Kinetics of the reaction of **A12** with **E8** (stopped-flow method, detection at 632 nm)

[**A12**] / M	[**E8**] / M	k_{obs} / s^{-1}
6.29×10^{-5}		1.31
9.43×10^{-5}		2.17
1.26×10^{-4}	5.41×10^{-6}	3.11
1.57×10^{-4}		4.05
1.89×10^{-4}		4.93
$k_2 = 2.90 \times 10^4$ $M^{-1} \cdot s^{-1}$		

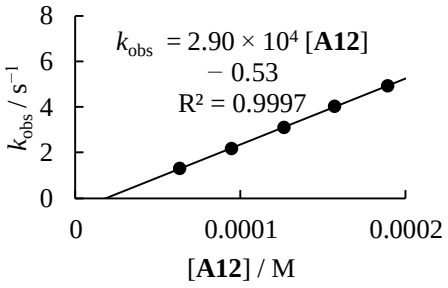

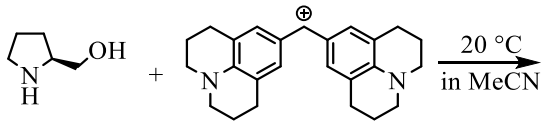

A12 **E9**

Table 73. Kinetics of the reaction of **A12** with **E9** (stopped-flow method, detection at 635 nm)

[**A12**] / M	[**E9**] / M	k_{obs} / s^{-1}
6.29×10^{-5}		4.51
9.43×10^{-5}		6.72
1.26×10^{-4}	5.45×10^{-6}	9.28
1.57×10^{-4}		1.18×10^1
1.89×10^{-4}		1.44×10^1
$k_2 = 7.89 \times 10^4$ $M^{-1} \cdot s^{-1}$		

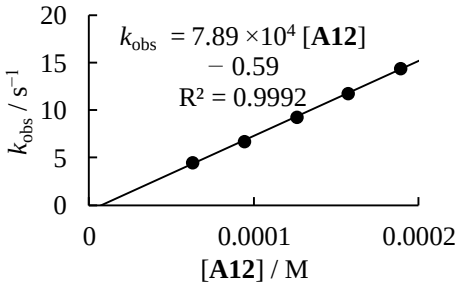

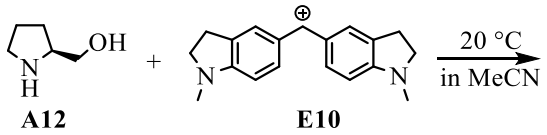

A12 **E10**

Table 74. Kinetics of the reaction of **A12** with **E10** (stopped-flow method, detection at 616 nm)

[**A12**] / M	[**E10**] / M	k_{obs} / s^{-1}
5.24×10^{-5}		8.96
7.34×10^{-5}		1.32×10^1
9.43×10^{-5}	5.00×10^{-6}	1.72×10^1
1.15×10^{-4}		2.20×10^1
1.36×10^{-4}		2.57×10^1
$k_2 = 2.02 \times 10^5$ $M^{-1} \cdot s^{-1}$		

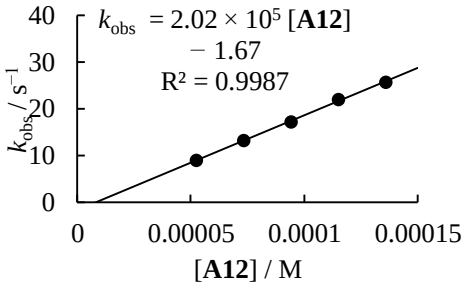

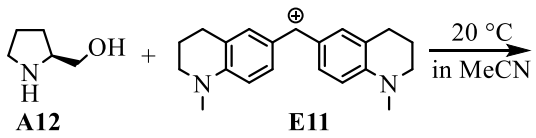

A12 **E11**

Table 75. Kinetics of the reaction of **A12** with **E11** (stopped-flow method, detection at 620 nm)

[**A12**] / M	[**E11**] / M	k_{obs} / s^{-1}
4.19×10^{-5}		1.70×10^{1}
7.34×10^{-5}		2.97×10^{1}
9.43×10^{-5}	4.35×10^{-6}	3.99×10^{1}
1.15×10^{-4}		5.16×10^{1}
1.36×10^{-4}		6.37×10^{1}
$k_2 = 4.98 \times 10^{5}$ $M^{-1} \cdot s^{-1}$		

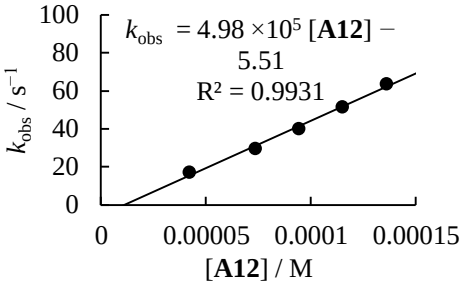

Table 76. Determination of the parameters N and s_N for **A12** in acetonitrile

Electrophile	E	k_2 / $M^{-1} \cdot s^{-1}$
E8	−10.04	2.90×10^{4}
E9	−9.45	7.89×10^{4}
E10	−8.76	2.02×10^{5}
E11	−8.22	4.98×10^{5}
$N = 16.74$ $s_N = 0.67$		

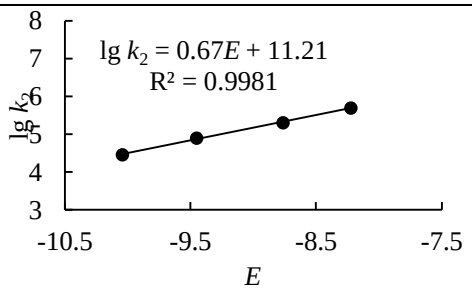

(*S*)-2-(Methoxymethyl)pyrrolidine (A13)

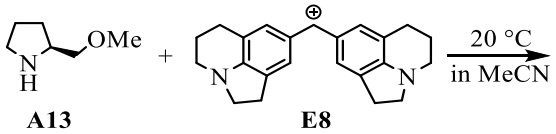

A13 **E8**

Table 77. Kinetics of the reaction of **A13** with **E8** (stopped-flow method, detection at 632 nm)

[**A13**] / M	[**E8**] / M	k_{obs} / s^{-1}
4.49×10^{-5}		1.70
6.74×10^{-5}		2.41
8.99×10^{-5}	4.42×10^{-6}	3.20
1.12×10^{-4}		4.00
1.35×10^{-4}		4.95

$k_2 = 3.60 \times 10^4$ $M^{-1} \cdot s^{-1}$

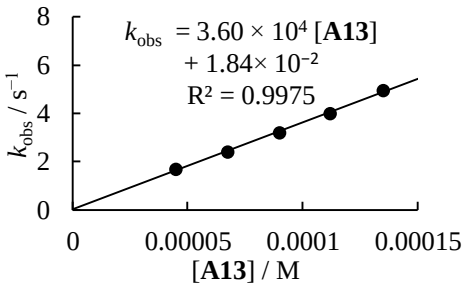

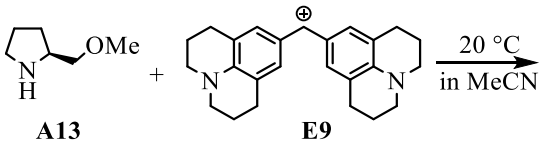

A13 **E9**

Table 78. Kinetics of the reaction of **A13** with **E9** (stopped-flow method, detection at 635 nm)

[**A13**] / M	[**E9**] / M	k_{obs} / s^{-1}
4.49×10^{-5}		5.41
6.74×10^{-5}		7.74
8.99×10^{-5}	4.28×10^{-6}	1.02×10^{1}
1.12×10^{-4}		1.28×10^{1}
1.35×10^{-4}		1.53×10^{1}

$k_2 = 1.10 \times 10^5$ $M^{-1} \cdot s^{-1}$

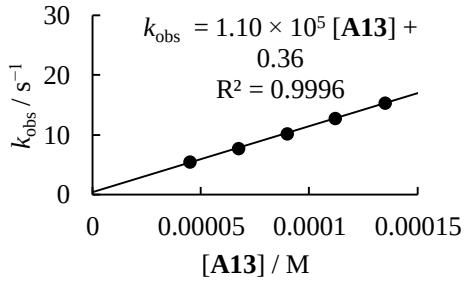

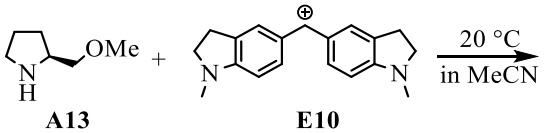

A13 **E10**

Table 79. Kinetics of the reaction of **A13** with **E10** (stopped-flow method, detection at 616 nm)

[**A13**] / M	[**E10**] / M	k_{obs} / s^{-1}
4.49×10^{-5}		1.09×10^{1}
6.74×10^{-5}		1.65×10^{1}
8.99×10^{-5}	4.32×10^{-6}	2.26×10^{1}
1.12×10^{-4}		2.85×10^{1}
1.35×10^{-4}		3.45×10^{1}

$k_2 = 2.63 \times 10^5$ $M^{-1} \cdot s^{-1}$

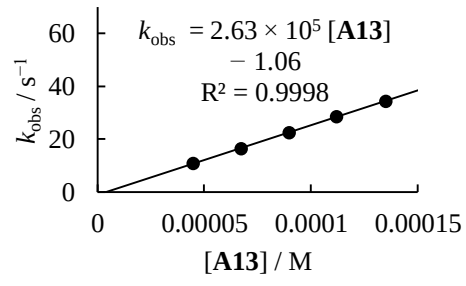

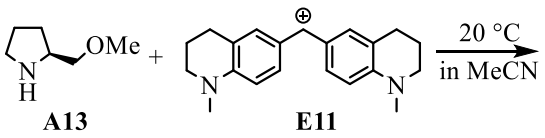

A13 **E11**

Table 80. Kinetics of the reaction of **A13** with **E11** (stopped-flow method, detection at 620 nm)

[**A13**] / M	[**E11**] / M	k_{obs} / s^{-1}
3.59×10^{-5}		2.36×10^{1}
5.39×10^{-5}		3.71×10^{1}
7.19×10^{-5}	3.56×10^{-6}	5.00×10^{1}
8.99×10^{-5}		6.46×10^{1}
1.08×10^{-4}		7.91×10^{1}

$k_2 = 7.69 \times 10^5$ $M^{-1} \cdot s^{-1}$

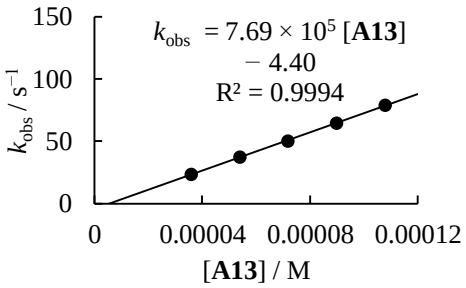

Table 81. Determination of the parameters N and s_N for **A13** in acetonitrile

Electrophile	E	k_2 / $M^{-1} \cdot s^{-1}$
E8	−10.04	3.60×10^4
E9	−9.45	1.10×10^5
E10	−8.76	2.63×10^5
E11	−8.22	7.69×10^5

$N = 16.50$ $s_N = 0.71$

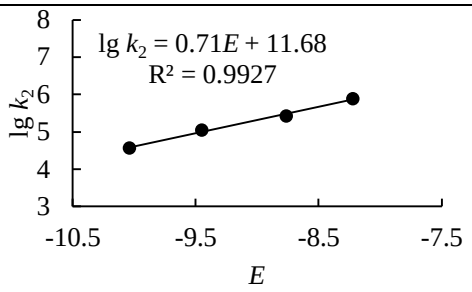

2-(Trifluoromethyl)pyrrolidine (A14)

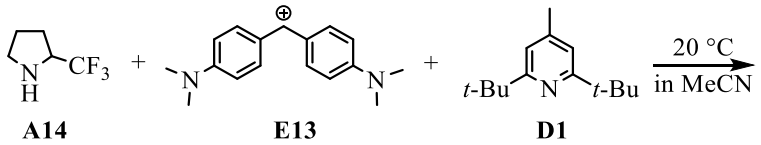

A14 **E13** **D1**

Table 82. Kinetics of the reaction of **A14** with **E13** and **D1** ([**D1**] = 2.46 mM, stopped-flow method, detection at 605 nm)

[**A14**] / M	[**E13**] / M	k_{obs} / s^{-1}
9.33×10^{-5}	4.85×10^{-6}	8.82×10^{-3}
1.87×10^{-4}		1.92×10^{-2}
2.80×10^{-4}		3.72×10^{-2}
3.73×10^{-4}		5.11×10^{-2}
4.67×10^{-4}		7.54×10^{-2}
5.60×10^{-4}		1.00×10^{-1}

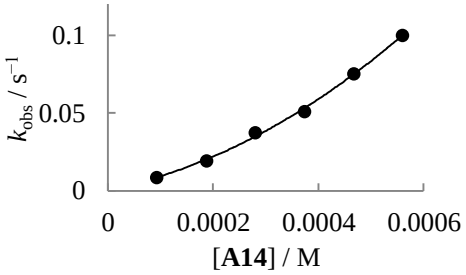

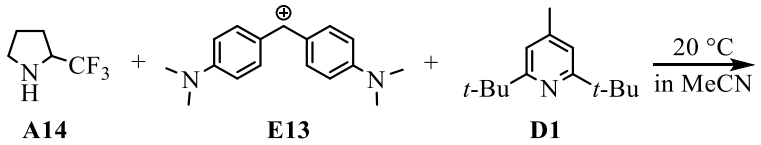

A14 **E13** **D1**

Table 83. Kinetics of the reaction of **A14** with **E13** and **D1** ([**D1**] = 4.92 mM, stopped-flow method, detection at 605 nm)

[**A14**] / M	[**E13**] / M	k_{obs} / s^{-1}
3.39×10^{-4}	4.85×10^{-6}	4.65×10^{-2}
6.79×10^{-4}		1.37×10^{-1}
1.01×10^{-3}		2.82×10^{-1}
1.36×10^{-3}		4.72×10^{-1}
1.70×10^{-3}		6.94×10^{-1}
2.04×10^{-3}		9.73×10^{-1}

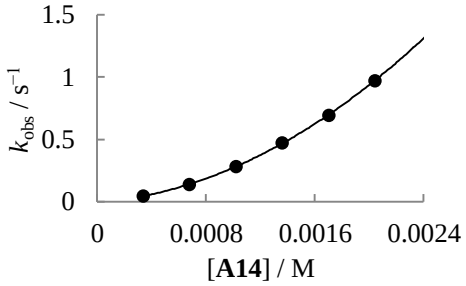

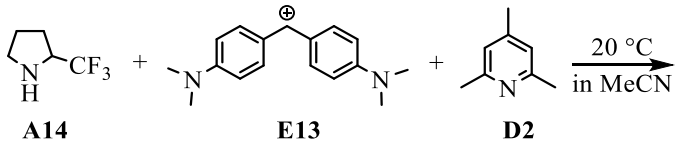

A14 **E13** **D2**

Table 84. Influence of the concentration of the base **D2** on the kinetics of the reaction of **A14** with **E13** ([**A14**] = 2.12 × 10^{-4} M, [**E13**] = 4.85 × 10^{-6} M, stopped-flow method, detection at 605 nm)

Entry	[**D2**] / M
1	1.12 × 10^{-4}
2	2.81 × 10^{-4}
3	5.61 × 10^{-4}
5	2.25 × 10^{-3}
6	4.49 × 10^{-3}

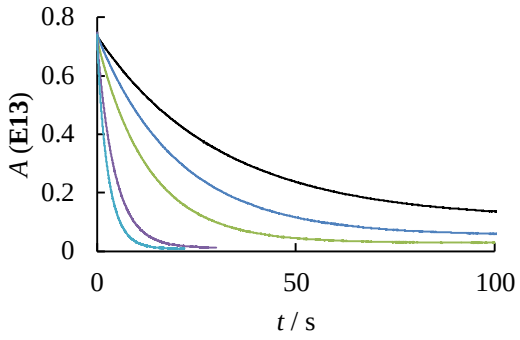

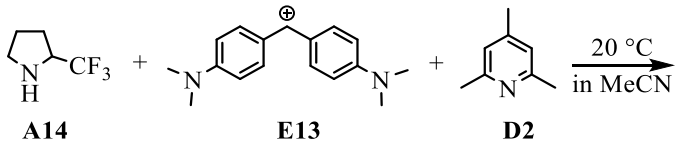

A14 **E13** **D2**

Table 85. Kinetics of the reaction of **A14** with **E13** and **D2** ([**D2**] = 1.12 mM, stopped-flow method, detection at 605 nm)

[**A14**] / M	[**E13**] / M	k_{obs} / s^{-1}
1.70 × 10^{-4}	4.85 × 10^{-6}	8.09 × 10^{-2}
3.39 × 10^{-4}		1.79 × 10^{-1}
5.09 × 10^{-4}		3.13 × 10^{-1}
6.79 × 10^{-4}		4.28 × 10^{-1}
8.48 × 10^{-4}		5.89 × 10^{-1}
1.02 × 10^{-3}		7.19 × 10^{-1}

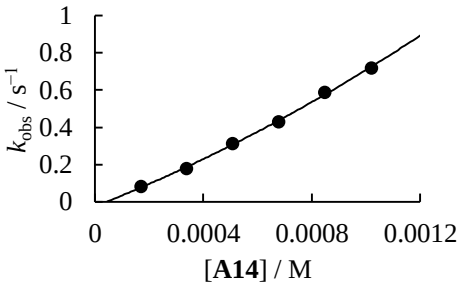

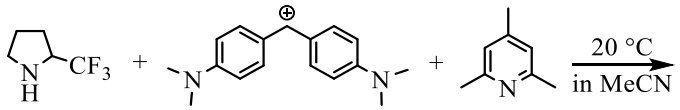

A14 **E13** **D2**

Table 86. Kinetics of the reaction of **A14** with **E13** and **D2** ([**D2**] = 2.25 mM, stopped-flow method, detection at 605 nm)

[**A14**] / M	[**E13**] / M	k_{obs} / s^{-1}
1.70×10^{-4}	4.85×10^{-6}	1.42×10^{-1}
3.39×10^{-4}		2.86×10^{-1}
5.09×10^{-4}		4.58×10^{-1}
6.79×10^{-4}		6.31×10^{-1}
8.48×10^{-4}		8.43×10^{-1}
1.02×10^{-4}		1.13

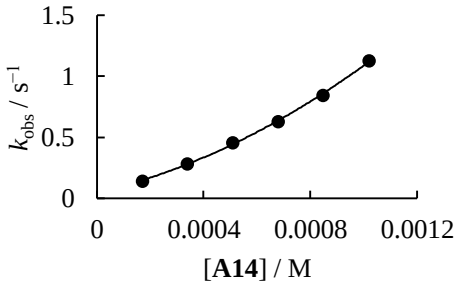

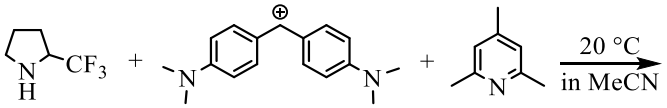

A14 **E13** **D2**

Table 87. Kinetics of the reaction of **A14** with **E13** and **D2** ([**D2**] = 4.49 mM, stopped-flow method, detection at 605 nm)

[**A14**] / M	[**E13**] / M	k_{obs} / s^{-1}
1.70×10^{-4}	4.85×10^{-6}	2.28×10^{-1}
3.39×10^{-4}		4.41×10^{-1}
5.09×10^{-4}		6.95×10^{-1}
6.79×10^{-4}		9.48×10^{-1}
8.48×10^{-4}		1.20
$k_2 = 1.45 \times 10^3$ $M^{-1} \cdot s^{-1}$		

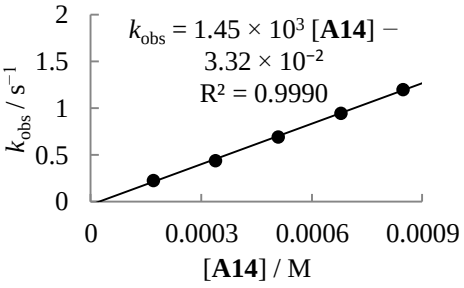

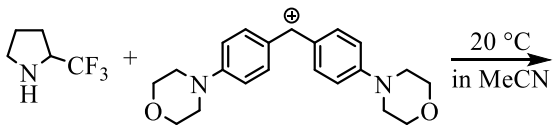

A14 **E15**

Table 88. Kinetics of the reaction of **A14** with **E15** (stopped-flow method, detection at 612 nm)

[**A14**] / M	[**E15**] / M	k_{obs} / s^{-1}
4.76×10^{-5}	4.62×10^{-6}	2.88×10^{-1}
9.33×10^{-5}		6.98×10^{-1}
1.34×10^{-4}		1.03
1.87×10^{-4}		1.69
2.33×10^{-4}		2.27
2.80×10^{-4}		3.37

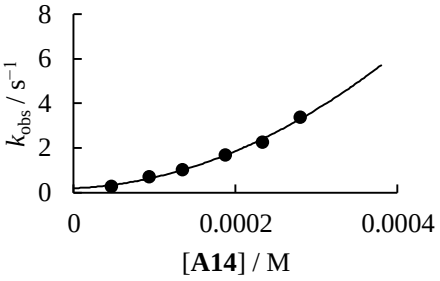

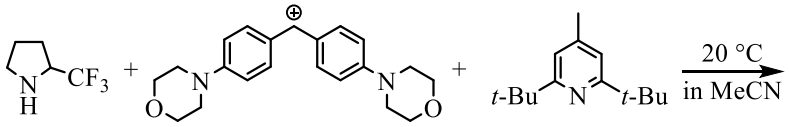

A14 **E15** **D1**

Table 89. Kinetics of the reaction of **A14** with **E15** and **D1** ([**D1**] = 2.46 mM, stopped-flow method, detection at 612 nm)

[**A14**] / M	[**E15**] / M	k_{obs} / s^{-1}
9.33×10^{-5}	4.67×10^{-6}	1.10
1.40×10^{-4}		1.91
1.87×10^{-4}		2.82
2.33×10^{-4}		3.72
2.80×10^{-4}		4.66
$k_2 = 1.91 \times 10^4$ $M^{-1} \cdot s^{-1}$		

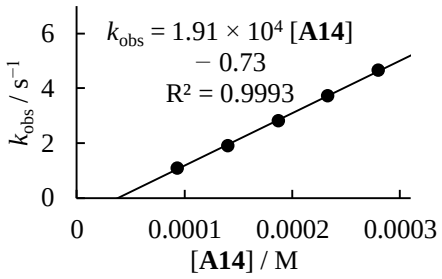

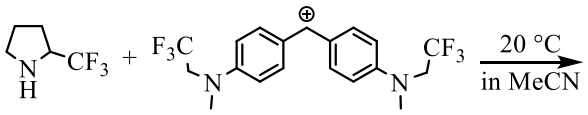

A14 **E17**

Table 90. Kinetics of the reaction of **A14** with **E17** (stopped-flow method, detection at 586 nm)

[**A14**] / M	[**E17**] / M	k_{obs} / s^{-1}
5.60×10^{-5}	5.51×10^{-6}	5.31
8.40×10^{-5}		9.83
1.12×10^{-4}		1.47×10^{1}
1.40×10^{-4}		1.98×10^{1}
1.68×10^{-4}		2.51×10^{1}
1.96×10^{-4}		3.16×10^{1}

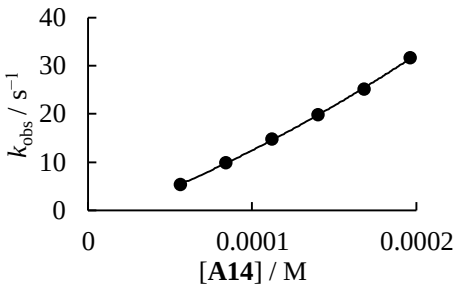

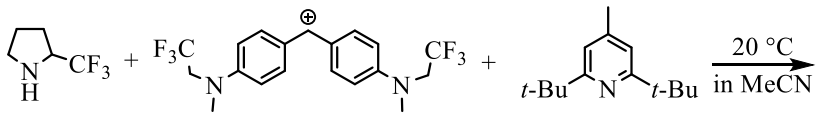

A14 **E17** **D1**

Table 91. Kinetics of the reaction of **A14** with **E17** and **D1** ([**D1**] = 1.23 mM, stopped-flow method, detection at 586 nm)

[**A14**] / M	[**E17**] / M	k_{obs} / s^{-1}
9.33×10^{-5}		1.28×10^{1}
1.40×10^{-4}		2.25×10^{1}
1.87×10^{-4}	4.62×10^{-6}	3.23×10^{1}
2.33×10^{-4}		4.39×10^{1}
2.80×10^{-4}		5.50×10^{1}
$k_2 = 2.27 \times 10^{5}$ $M^{-1} \cdot s^{-1}$		

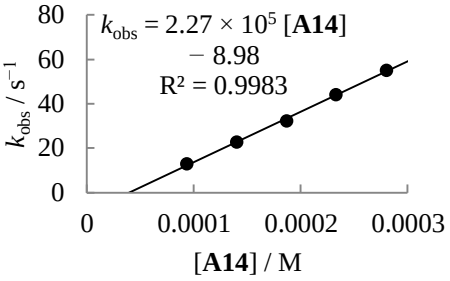

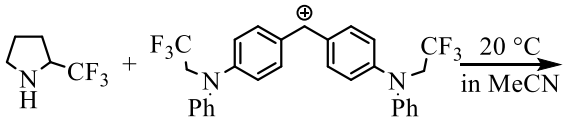

A14 **E18**

Table 92. Kinetics of the reaction of **A14** with **E18** (stopped-flow method, detection at 592 nm)

[**A14**] / M	[**E18**] / M	k_{obs} / s^{-1}
4.66×10^{-5}		4.83×10^{1}
7.00×10^{-5}		8.01×10^{1}
9.33×10^{-5}	4.66×10^{-6}	1.06×10^{2}
1.17×10^{-5}		1.37×10^{2}
1.40×10^{-4}		1.61×10^{2}
$k_2 = 1.21 \times 10^{6}$ $M^{-1} \cdot s^{-1}$		

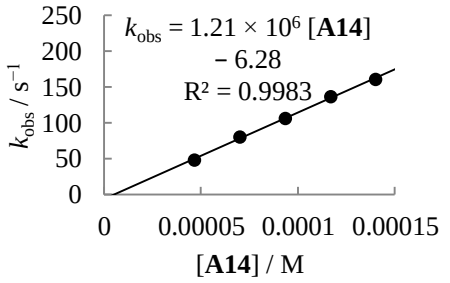

Table 93. Determination of the parameters N and s_N for **A14** in acetonitrile

Electrophile	E	k_2 / $M^{-1} \cdot s^{-1}$
E13	−7.02	1.45×10^{3}
E15	−5.53	1.91×10^{4}
E17	−3.85	2.27×10^{5}
E18	−3.14	1.21×10^{6}
$N = 11.34$ $s_N = 0.73$		

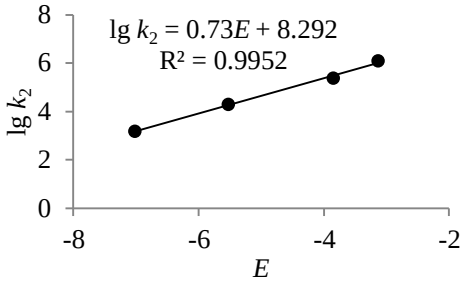

Methyl L-prolinate (A15)

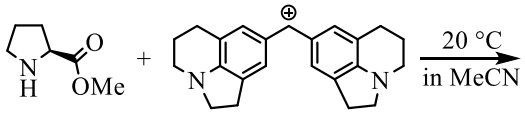

A15 **E8**

Table 94. Kinetics of the reaction of **A15** with **E8** (stopped-flow method, detection at 632 nm)

[**A15**] / M	[**E8**] / M	k_{obs} / s^{-1}
1.34×10^{-4}		2.14
2.67×10^{-4}		2.74
4.01×10^{-4}	1.34×10^{-5}	3.68
5.35×10^{-4}		4.56
6.68×10^{-4}		5.62
$k_2 = 6.57 \times 10^3$ $M^{-1} \cdot s^{-1}$		

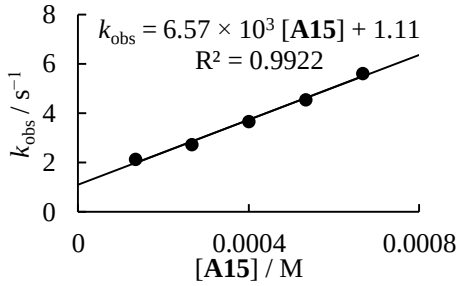

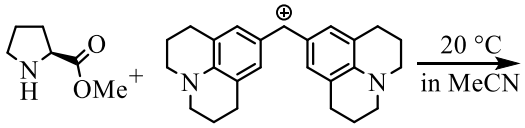

A15 **E9**

Table 95. Kinetics of the reaction of **A15** with **E9** (stopped-flow method, detection at 635 nm)

[**A15**] / M	[**E9**] / M	k_{obs} / s^{-1}
1.34×10^{-4}		7.97
2.67×10^{-4}		1.04×10^1
4.01×10^{-4}	1.35×10^{-5}	1.35×10^1
5.35×10^{-4}		1.70×10^1
6.68×10^{-4}		2.12×10^1
$k_2 = 2.47 \times 10^4$ $M^{-1} \cdot s^{-1}$		

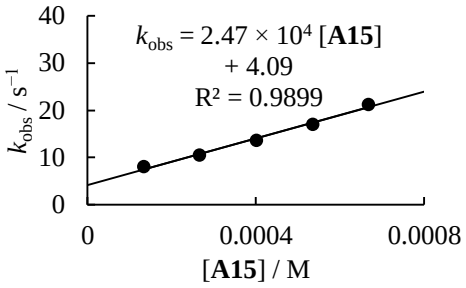

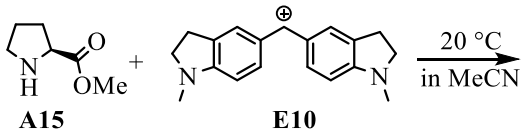

A15 **E10**

Table 96. Kinetics of the reaction of **A15** with **E10** (stopped-flow method, detection at 616 nm)

[**A15**] / M	[**E10**] / M	k_{obs} / s^{-1}
1.34×10^{-4}		8.36
2.67×10^{-4}		1.75×10^1
4.01×10^{-4}	1.34×10^{-5}	2.61×10^1
5.35×10^{-4}		3.59×10^1
6.68×10^{-4}		4.59×10^1
$k_2 = 7.00 \times 10^4$ $M^{-1} \cdot s^{-1}$		

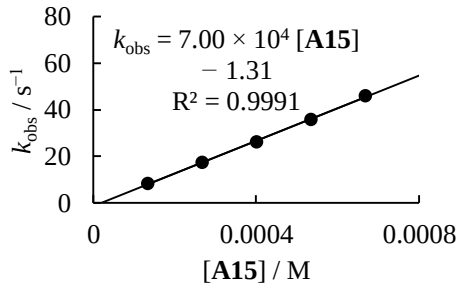

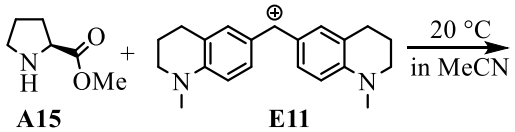

A15 **E11**

Table 97. Kinetics of the reaction of **A15** with **E11** (stopped-flow method, detection at 620 nm)

[**A15**] / M	[**E11**] / M	k_{obs} / s^{-1}
1.34×10^{-4}		2.55×10^{1}
2.67×10^{-4}		5.42×10^{1}
4.01×10^{-4}	1.26×10^{-5}	8.12×10^{1}
5.35×10^{-4}		1.12×10^{2}
6.68×10^{-4}		1.44×10^{2}
$k_2 = 2.21 \times 10^{5}$ $M^{-1} \cdot s^{-1}$		

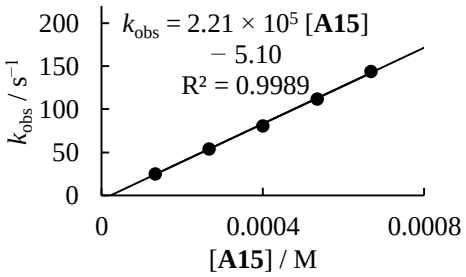

Table 98. Determination of the parameters N and s_N for **A15** in acetonitrile

Electrophile	E	k_2 / $M^{-1} \cdot s^{-1}$
E8	−10.04	6.57×10^{3}
E9	−9.45	2.47×10^{4}
E10	−8.76	7.00×10^{4}
E11	−8.22	2.21×10^{5}
$N = 14.75$ $s_N = 0.82$		

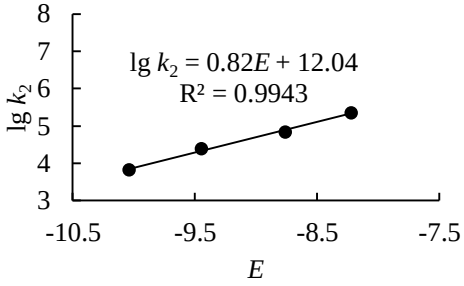

(*S*)-*N*,*N*-Dimethylpyrrolidine-2-carboxamide (A16)

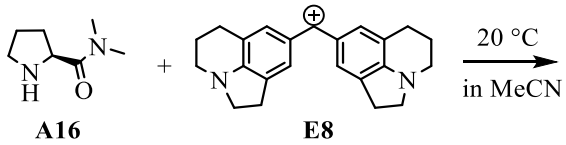

A16 **E8**

Table 99. Kinetics of the reaction of **A16** with **E8** (stopped-flow method, detection at 632 nm)

[**A16**] / M	[**E8**] / M	k_{obs} / s^{-1}
1.08×10^{-4}		1.32×10^{1}
2.16×10^{-4}		2.39×10^{1}
3.24×10^{-4}	8.00×10^{-6}	3.60×10^{1}
4.32×10^{-4}		4.47×10^{1}
5.41×10^{-4}		6.14×10^{1}
$k_2 = 1.08 \times 10^{5}$ $M^{-1} \cdot s^{-1}$		

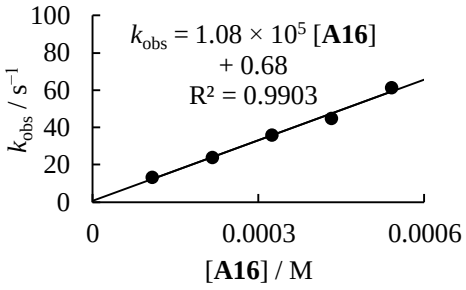

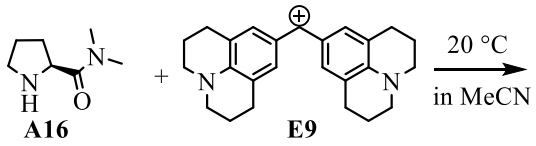

A16 **E9**

Table 100. Kinetics of the reaction of **A16** with **E9** (stopped-flow method, detection at 635 nm)

[**A16**] / M	[**E9**] / M	k_{obs} / s^{-1}
1.08×10^{-4}		4.23×10^{1}
2.16×10^{-4}		7.91×10^{1}
3.24×10^{-4}	5.63×10^{-6}	1.22×10^{2}
4.32×10^{-4}		1.66×10^{2}
5.41×10^{-4}		1.99×10^{2}
$k_2 = 3.70 \times 10^{5}$ $M^{-1} \cdot s^{-1}$		

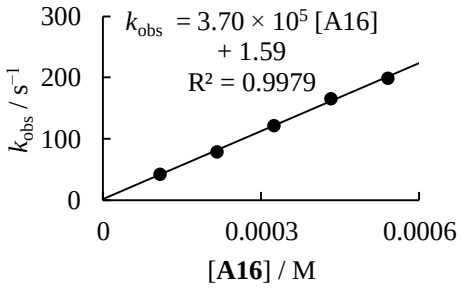

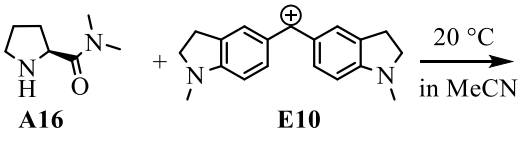

A16 **E10**

Table 101. Kinetics of the reaction of **A16** with **E10** (stopped-flow method, detection at 616 nm)

[**A16**] / M	[**E10**] / M	k_{obs} / s^{-1}
1.08×10^{-4}		5.55×10^{1}
2.16×10^{-4}		1.30×10^{2}
3.24×10^{-4}	8.94×10^{-6}	2.17×10^{2}
4.32×10^{-4}		3.01×10^{2}
5.41×10^{-4}		3.85×10^{2}
$k_2 = 7.67 \times 10^{5}$ $M^{-1} \cdot s^{-1}$		

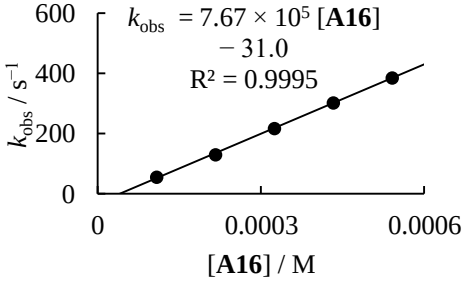

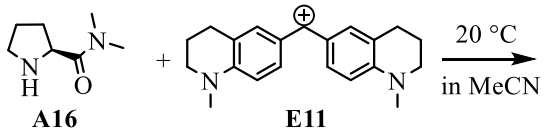

A16 **E11**

Table 102. Kinetics of the reaction of **A16** with **E11** (stopped-flow method, detection at 620 nm)

[**A16**] / M	[**E11**] / M	k_{obs} / s^{-1}
1.08×10^{-4}	9.67×10^{-6}	1.74×10^{2}
2.16×10^{-4}		4.29×10^{2}
3.24×10^{-4}		6.53×10^{2}
4.32×10^{-4}		8.33×10^{2}
$k_2 = 2.04 \times 10^{6}$ $M^{-1} \cdot s^{-1}$		

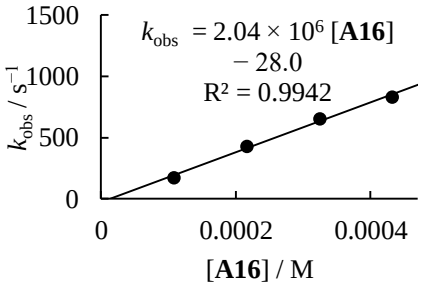

Table 103. Determination of the parameters N and s_N for **A16** in acetonitrile

Electrophile	E	k_2 / $M^{-1} \cdot s^{-1}$
E8	−10.04	1.08×10^{5}
E9	−9.45	3.70×10^{5}
E10	−8.76	7.67×10^{5}
E11	−8.22	2.04×10^{6}
$N = 17.61$ $s_N = 0.67$		

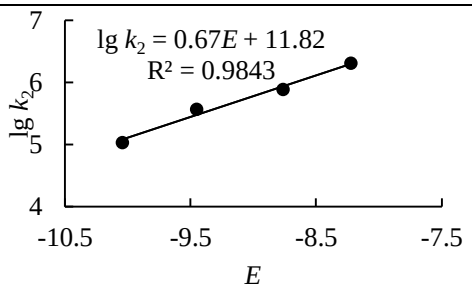

(*S*)-*N*-Propylpyrrolidine-2-carboxamide (A17)

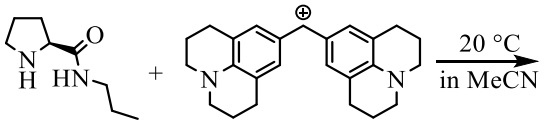

A17 **E9**

Table 104. Kinetics of the reaction of **A17** with **E9** (stopped-flow method, detection at 635 nm)

[**A17**] / M	[**E9**] / M	k_{obs} / s^{-1}
1.20×10^{-4}		3.01
2.39×10^{-4}		4.73
3.59×10^{-4}	1.13×10^{-5}	6.71
4.78×10^{-4}		8.82
5.98×10^{-4}		1.10×10^{1}
$k_2 = 1.68 \times 10^{4}$ $M^{-1} \cdot s^{-1}$		

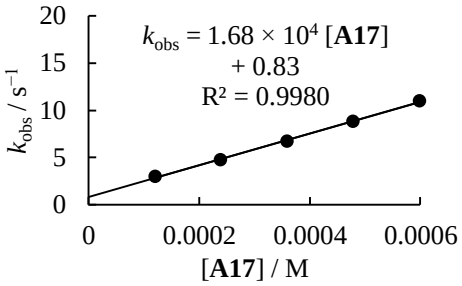

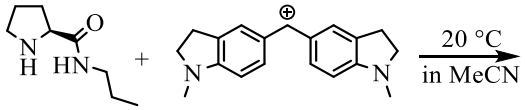

A17 **E10**

Table 105. Kinetics of the reaction of **A17** with **E10** (stopped-flow method, detection at 616 nm)

[**A17**] / M	[**E10**] / M	k_{obs} / s^{-1}
1.20×10^{-4}		3.76
2.39×10^{-4}		8.71
3.59×10^{-4}	8.51×10^{-6}	1.26×10^{1}
4.78×10^{-4}		1.75×10^{1}
5.98×10^{-4}		2.25×10^{1}
$k_2 = 3.87 \times 10^{4}$ $M^{-1} \cdot s^{-1}$		

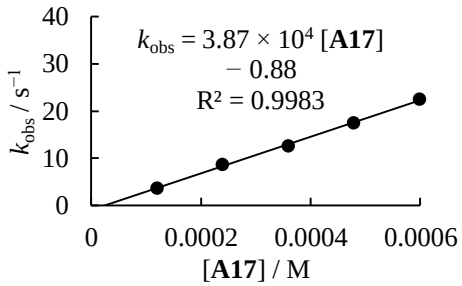

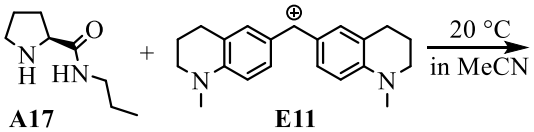

A17 **E11**

Table 106. Kinetics of the reaction of **A17** with **E11** (stopped-flow method, detection at 620 nm)

[**A17**] / M	[**E11**] / M	k_{obs} / s^{-1}
1.20×10^{-4}		1.18×10^{1}
2.39×10^{-4}		2.52×10^{1}
3.59×10^{-4}	1.20×10^{-5}	3.92×10^{1}
4.78×10^{-4}		5.28×10^{1}
5.98×10^{-4}		6.79×10^{1}
$k_2 = 1.17 \times 10^{5}$ $M^{-1} \cdot s^{-1}$		

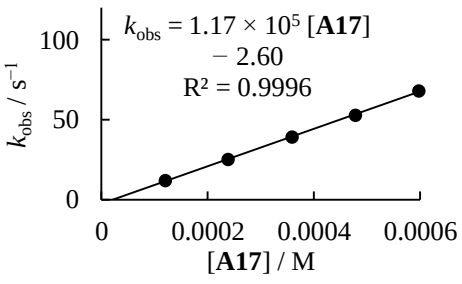

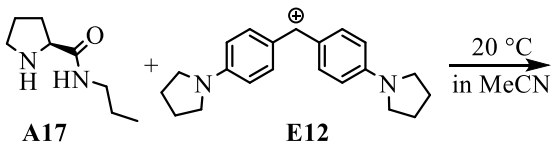

A17 **E12**

Table 107. Kinetics of the reaction of **A17** with **E12** (stopped-flow method, detection at 612 nm)

[**A17**] / M	[**E12**] / M	k_{obs} / s^{-1}
1.20×10^{-4}		2.93×10^{1}
2.39×10^{-4}		6.45×10^{1}
3.59×10^{-4}	1.20×10^{-5}	9.98×10^{1}
4.78×10^{-4}		1.38×10^{2}
5.98×10^{-4}		1.74×10^{2}
$k_2 = 3.04 \times 10^{5}$ $M^{-1} \cdot s^{-1}$		

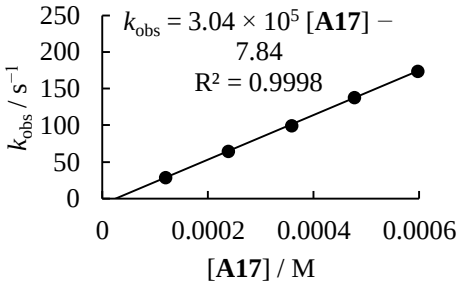

Table 108. Determination of the parameters *N* and s_N for **A17** in acetonitrile

Electrophile	*E*	k_2 / $M^{-1} \cdot s^{-1}$
E9	−9.45	1.68×10^{4}
E10	−8.76	3.87×10^{4}
E11	−8.22	1.17×10^{5}
E12	−7.69	3.04×10^{5}
$N = 15.20$ $s_N = 0.73$		

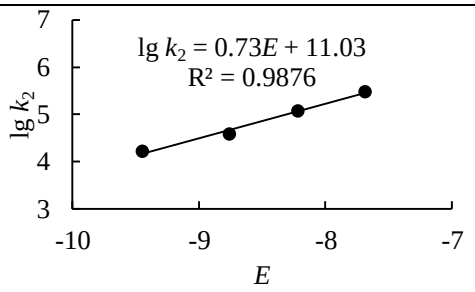

(*S*)-2-(Pyrrolidin-2-ylmethyl)isoindoline-1,3-dione (A18)

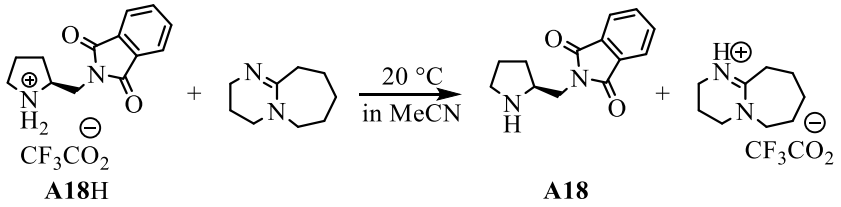

The stock solution of **A18** was achieved by quantitative deprotonation of **A18**H with DBU base ($n_{\mathbf{a11}H}/n_{DBU}$ = 1.15 : 1).

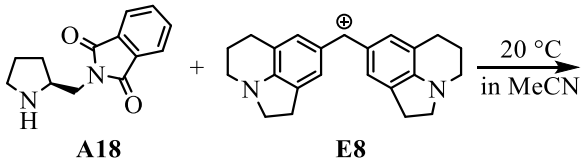

Table 109. Kinetics of the reaction of **A18** with **E8** (stopped-flow method, detection at 632 nm)

[**A18**] / M	[**E8**] / M	k_{obs} / s^{-1}
7.76×10^{-5}	4.88×10^{-6}	3.77
1.03×10^{-4}		4.60
1.29×10^{-4}		5.53
1.55×10^{-4}		6.33

$k_2 = 3.33 \times 10^4$ $M^{-1} \cdot s^{-1}$

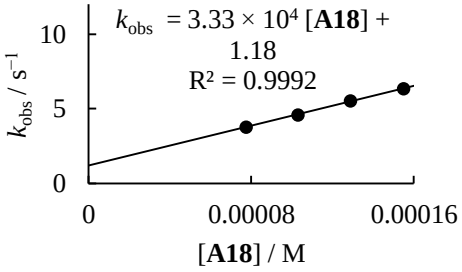

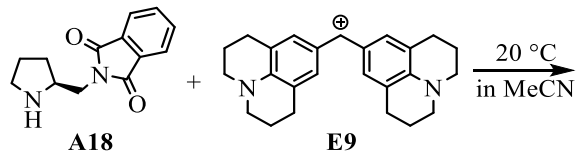

Table 110. Kinetics of the reaction of **A18** with **E9** (stopped-flow method, detection at 635 nm)

[**A18**] / M	[**E9**] / M	k_{obs} / s^{-1}
7.76×10^{-5}	4.83×10^{-6}	1.13×10^1
1.03×10^{-4}		1.33×10^1
1.29×10^{-4}		1.55×10^1
1.55×10^{-4}		1.75×10^1

$k_2 = 8.06 \times 10^4$ $M^{-1} \cdot s^{-1}$

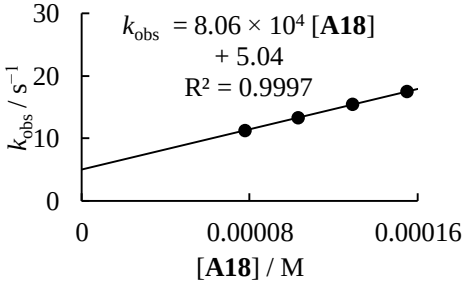

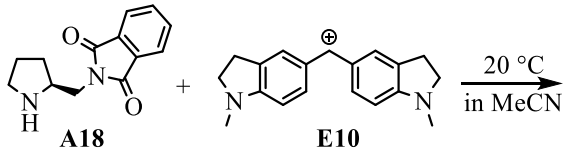

Table 111. Kinetics of the reaction of **A18** with **E10** (stopped-flow method, detection at 616 nm)

[**A18**] / M	[**E10**] / M	k_{obs} / s^{-1}
5.17×10^{-5}	3.79×10^{-6}	1.40×10^{1}
6.47×10^{-5}		1.80×10^{1}
7.76×10^{-5}		2.10×10^{1}
9.05×10^{-5}		2.54×10^{1}
1.03×10^{-4}		2.84×10^{1}
1.16×10^{-4}		3.18×10^{1}
$k_2 = 2.77 \times 10^{5}$ $M^{-1} \cdot s^{-1}$		

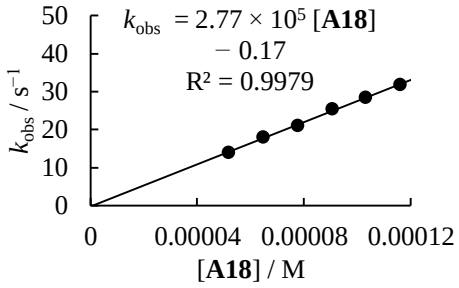

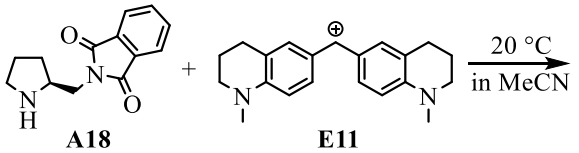

Table 112. Kinetics of the reaction of **A18** with **E11** (stopped-flow method, detection at 620 nm)

[**A18**] / M	[**E11**] / M	k_{obs} / s^{-1}
3.88×10^{-5}	3.88×10^{-6}	2.48×10^{1}
5.17×10^{-5}		3.49×10^{1}
6.47×10^{-5}		4.50×10^{1}
7.76×10^{-5}		5.22×10^{1}
9.05×10^{-5}		6.35×10^{1}
1.03×10^{-4}		7.32×10^{1}
1.16×10^{-4}		8.13×10^{1}
$k_2 = 7.35 \times 10^{5}$ $M^{-1} \cdot s^{-1}$		

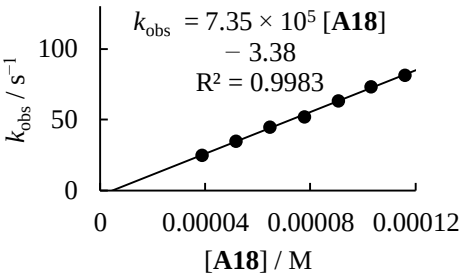

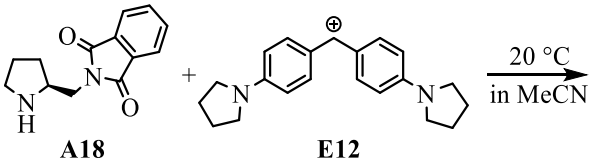

A18 **E12**

Table 113. Kinetics of the reaction of **A18** with **E12** (stopped-flow method, detection at 612 nm)

[**A18**] / M	[**E12**] / M	k_{obs} / s^{-1}
3.88×10^{-5}		6.16×10^{1}
5.17×10^{-5}		9.51×10^{1}
6.47×10^{-5}		1.16×10^{2}
7.76×10^{-5}	3.67×10^{-6}	1.47×10^{2}
9.05×10^{-5}		1.70×10^{2}
1.03×10^{-4}		1.98×10^{2}
1.16×10^{-4}		2.22×10^{2}
$k_2 = 2.06 \times 10^{6}$ $M^{-1} \cdot s^{-1}$		

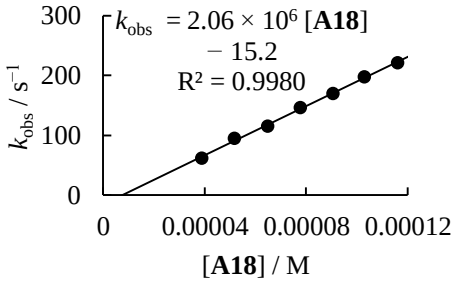

Table 114. Determination of the parameters N and s_N for **A18** in acetonitrile

Electrophile	E	k_2 / $M^{-1} \cdot s^{-1}$
E8	−10.04	3.33×10^{4}
E9	−9.45	8.06×10^{4}
E10	−8.76	2.77×10^{5}
E11	−8.22	7.35×10^{5}
E12	−7.69	2.06×10^{6}
$N = 15.90$ $s_N = 0.77$		

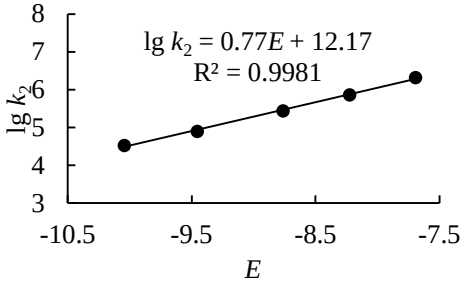

(*S*)-4-Phenyl-1-(pyrrolidin-2-ylmethyl)-1H-1,2,3-triazole (A19)

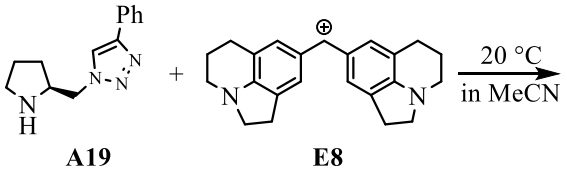

A19 **E8**

Table 115. Kinetics of the reaction of **A19** with **E8** (stopped-flow method, detection at 632 nm)

[**A19**] / M	[**E8**] / M	k_{obs} / s^{-1}
3.89×10^{-5}		4.03×10^{-1}
5.96×10^{-5}		5.26×10^{-1}
7.95×10^{-5}	3.89×10^{-6}	6.53×10^{-1}
9.94×10^{-5}		7.79×10^{-1}
1.19×10^{-4}		8.92×10^{-1}
$k_2 = 6.16 \times 10^3$ $M^{-1} \cdot s^{-1}$		

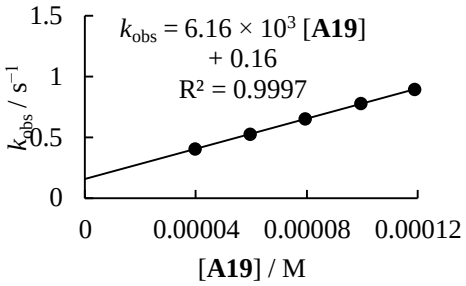

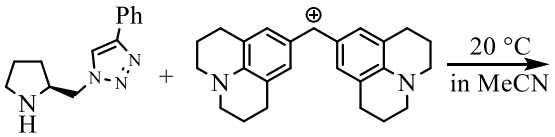

A19 **E9**

Table 116. Kinetics of the reaction of **A19** with **E9** (stopped-flow method, detection at 635 nm)

[**A19**] / M	[E**9**] / M	k_{obs} / s^{-1}
5.30×10^{-5}		1.35
7.95×10^{-5}		1.71
1.06×10^{-4}	3.78×10^{-6}	2.08
1.33×10^{-4}		2.54
1.59×10^{-4}		2.98
$k_2 = 1.54 \times 10^4$ $M^{-1} \cdot s^{-1}$		

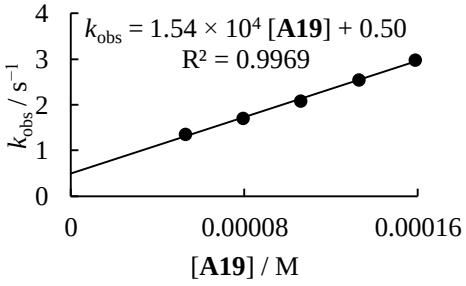

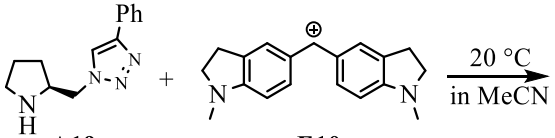

A19 **E10**

Table 117. Kinetics of the reaction of **A19** with **E10** (stopped-flow method, detection at 616 nm)

[**A19**] / M	[**E10**] / M	k_{obs} / s^{-1}
3.98×10^{-5}		1.81
5.96×10^{-5}		2.60
7.95×10^{-5}	3.91×10^{-6}	3.50
9.94×10^{-5}		4.31
1.19×10^{-4}		5.34
$k_2 = 4.42 \times 10^4$ $M^{-1} \cdot s^{-1}$		

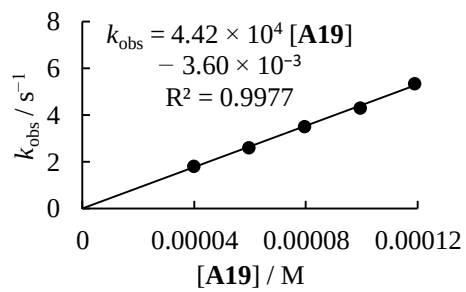

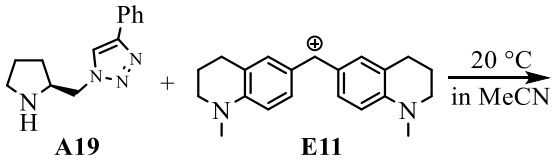

A19 E11

Table 118. Kinetics of the reaction of **A19** with E**11** (stopped-flow method, detection at 620 nm)

[**A19**] / M	[**E11**] / M	k_{obs} / s^{-1}
3.98×10^{-5}		4.75
5.96×10^{-5}		7.23
7.95×10^{-5}	3.81×10^{-6}	9.89
9.94×10^{-5}		1.27×10^{1}
1.19×10^{-4}		1.50×10^{1}
$k_2 = 1.31 \times 10^{5}$ $M^{-1} \cdot s^{-1}$		

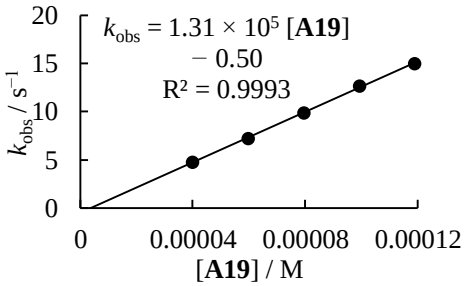

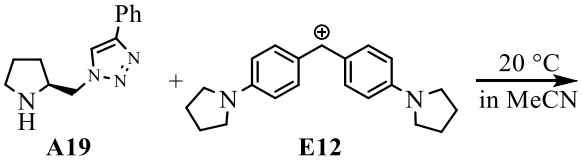

A19 E12

Table 119. Kinetics of the reaction of **A19** with **E12** (stopped-flow method, detection at 612 nm)

[**A19**] / M	[**E12**] / M	k_{obs} / s^{-1}
3.98×10^{-5}		1.22×10^{1}
5.96×10^{-5}		1.84×10^{1}
7.95×10^{-5}	3.81×10^{-6}	2.47×10^{1}
9.94×10^{-5}		3.18×10^{1}
1.19×10^{-4}		3.89×10^{1}
$k_2 = 3.37 \times 10^{5}$ $M^{-1} \cdot s^{-1}$		

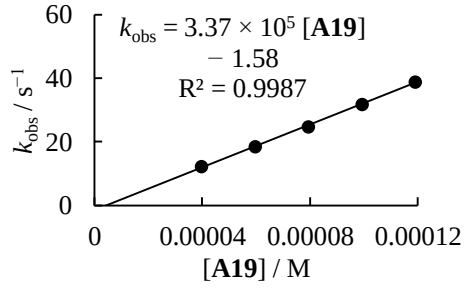

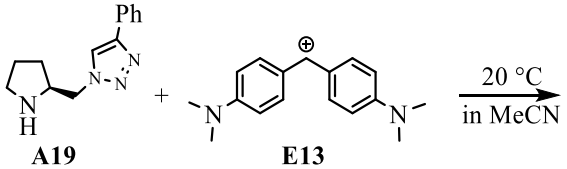

A19 E13

Table 120. Kinetics of the reaction of **A19** with **E13** (stopped-flow method, detection at 605 nm)

[**A19**] / M	[**E13**] / M	k_{obs} / s^{-1}
2.65×10^{-5}		1.89×10^{1}
3.98×10^{-5}		2.87×10^{1}
5.30×10^{-5}	2.62×10^{-6}	3.92×10^{1}
6.63×10^{-5}		5.00×10^{1}
7.95×10^{-5}		6.00×10^{1}
$k_2 = 7.81 \times 10^{5}$ $M^{-1} \cdot s^{-1}$		

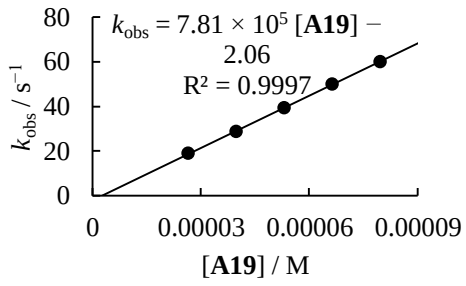

Table 121. Determination of the parameters N and s_N for **A19** in acetonitrile

Electrophile	E	k_2 / $M^{-1} \cdot s^{-1}$
E8	−10.04	6.16×10^3
E9	−9.45	1.54×10^4
E10	−8.76	4.42×10^4
E11	−8.22	1.31×10^5
E12	−7.69	3.37×10^5
E13	−7.02	7.81×10^5
$N = 15.32$ $s_N = 0.72$		

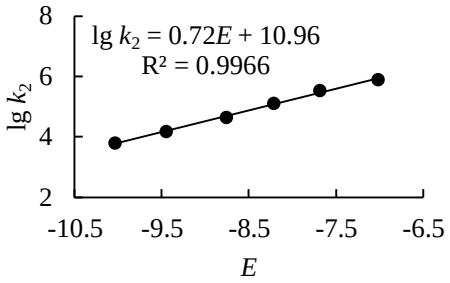

(*S*)-1-(Pyrrolidin-2-ylmethyl)-1H-imidazole (A20)

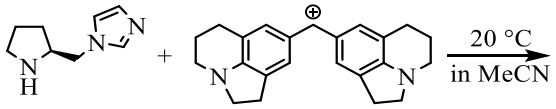

A20 **E8**

Table 122. Kinetics of the reaction of **A20** with **E8** (stopped-flow method, detection at 632 nm)

[**A20**] / M	[**E8**] / M	k_{obs} / s^{-1}
2.35×10^{-4}		1.41
3.52×10^{-4}		2.00
4.70×10^{-4}	6.75×10^{-6}	2.60
5.87×10^{-4}		3.26
7.04×10^{-4}		3.94
$k_2 = 5.39 \times 10^3$ $M^{-1} \cdot s^{-1}$		

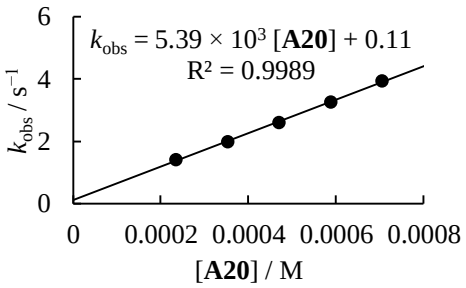

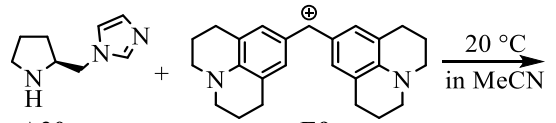

A20 **E9**

Table 123. Kinetics of the reaction of **A20** with **E9** (stopped-flow method, detection at 635 nm)

[**A20**] / M	[**E9**] / M	k_{obs} / s^{-1}
2.35×10^{-4}		4.74
3.52×10^{-4}		6.82
4.70×10^{-4}	5.81×10^{-6}	8.77
5.87×10^{-4}		1.12×10^1
7.04×10^{-4}		1.33×10^1
$k_2 = 1.83 \times 10^4$ $M^{-1} \cdot s^{-1}$		

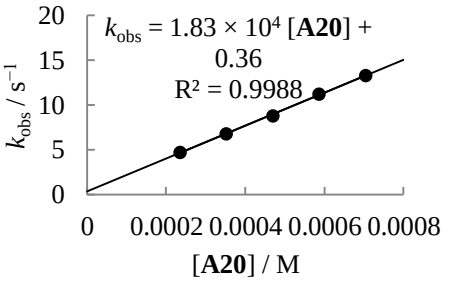

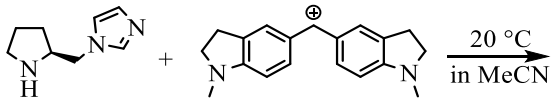

A20 **E10**

Table 124. Kinetics of the reaction of **A20** with **E10** (stopped-flow method, detection at 616 nm)

[**A20**] / M	[**E10**] / M	k_{obs} / s^{-1}
9.39×10^{-5}		3.98
1.41×10^{-4}		5.08
1.88×10^{-4}	8.35×10^{-6}	6.94
2.35×10^{-4}		8.49
2.82×10^{-4}		1.06×10^1
3.29×10^{-4}		1.24×10^1
$k_2 = 3.66 \times 10^4$ $M^{-1} \cdot s^{-1}$		

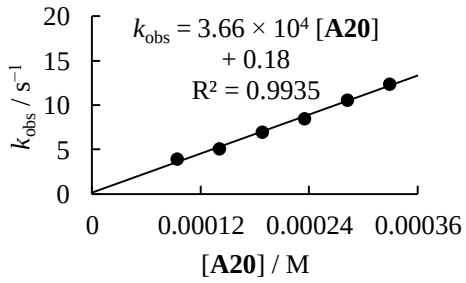

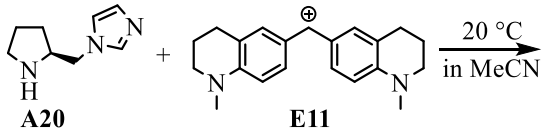

A20 **E11**

Table 125. Kinetics of the reaction of **A20** with **E11** (stopped-flow method, detection at 620 nm)

[**A20**] / M	[**E11**] / M	k_{obs} / s^{-1}
7.04×10^{-5}	6.12×10^{-6}	7.29
1.17×10^{-4}		1.24×10^{1}
1.64×10^{-4}		1.85×10^{1}
2.11×10^{-4}		2.38×10^{1}
2.58×10^{-4}		2.91×10^{1}
3.05×10^{-4}		3.51×10^{1}
$k_2 = 1.18 \times 10^{5}$ $M^{-1} \cdot s^{-1}$		

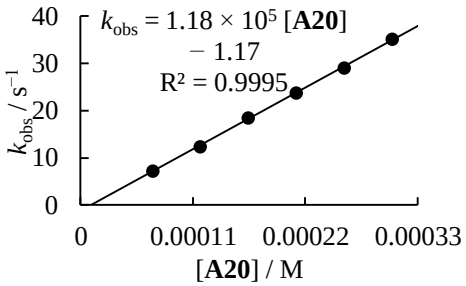

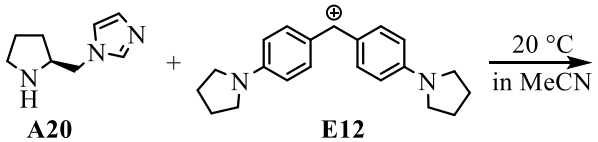

A20 **E12**

Table 126. Kinetics of the reaction of **A20** with **E12** (stopped-flow method, detection at 612 nm)

[**A20**] / M	[**E12**] / M	k_{obs} / s^{-1}
7.04×10^{-5}	5.30×10^{-6}	1.70×10^{1}
1.17×10^{-4}		2.91×10^{1}
1.64×10^{-4}		4.25×10^{1}
2.11×10^{-4}		5.53×10^{1}
2.58×10^{-4}		6.89×10^{1}
3.05×10^{-4}		8.16×10^{1}
$k_2 = 2.77 \times 10^{5}$ $M^{-1} \cdot s^{-1}$		

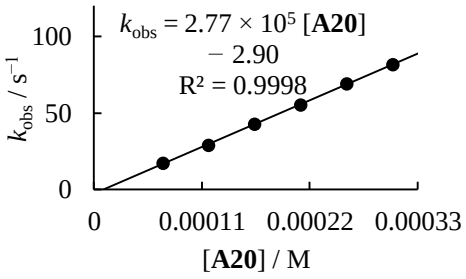

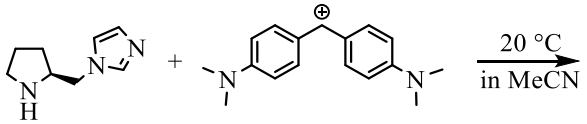

A20 **E13**

Table 127. Kinetics of the reaction of **A20** with **E13** (stopped-flow method, detection at 605 nm)

[**A20**] / M	[**E13**] / M	k_{obs} / s^{-1}
9.39×10^{-5}	8.00×10^{-6}	5.15×10^{1}
1.41×10^{-4}		8.45×10^{1}
1.88×10^{-4}		1.11×10^{2}
2.35×10^{-4}		1.39×10^{2}
2.82×10^{-4}		1.72×10^{2}
$k_2 = 6.28 \times 10^{5}$ $M^{-1} \cdot s^{-1}$		

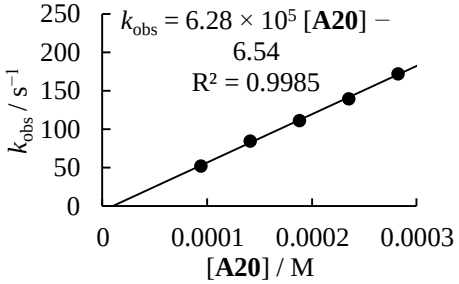

Table 128. Determination of the parameters N and s_N for **A20** in acetonitrile

Electrophile	E	k_2 / $M^{-1} \cdot s^{-1}$
E8	−10.04	5.39×10^3
E9	−9.45	1.83×10^4
E10	−8.76	3.66×10^4
E11	−8.22	1.18×10^5
E12	−7.69	2.77×10^5
E13	−7.02	6.28×10^5
N = 15.55 s_N = 0.69		

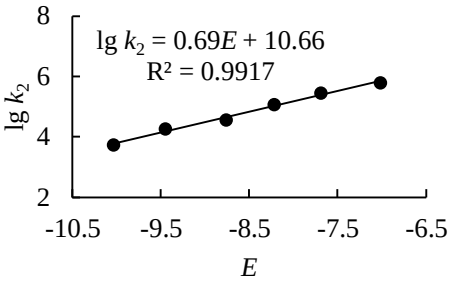

(*S*)-3-Butyl-1-(pyrrolidin-2-ylmethyl)-1H-imidazol-3-ium trifluoromethanesulfonate (A21)

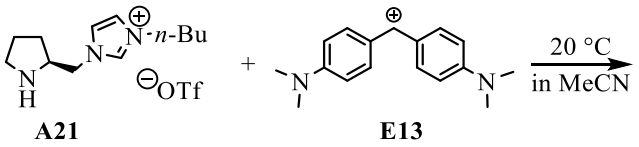

A21 **E13**

Table 129. Kinetics of the reaction of **A21** with **E13** (stopped-flow method, detection at 605 nm)

[**A21**] / M	[**E13**] / M	k_{obs} / s^{-1}
1.75×10^{-4}		4.54×10^{-1}
2.62×10^{-4}		6.69×10^{-1}
3.50×10^{-4}	6.82×10^{-6}	9.21×10^{-1}
4.37×10^{-4}		1.24
5.25×10^{-4}		1.47
$k_2 = 2.97 \times 10^3$ $M^{-1} \cdot s^{-1}$		

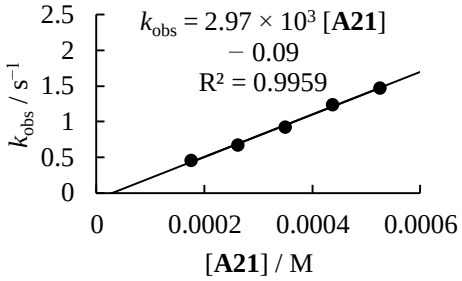

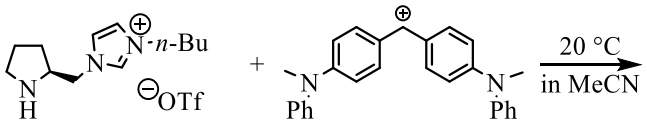

A21 **E14**

Table 130. Kinetics of the reaction of **A21** with **E14** (stopped-flow method, detection at 613 nm)

[**A21**] / M	[**E14**] / M	k_{obs} / s^{-1}
1.05×10^{-4}		1.62
1.57×10^{-4}		2.66
2.10×10^{-4}	1.05×10^{-5}	3.54
2.62×10^{-4}		4.82
6.30×10^{-4}		1.26×10^{1}
$k_2 = 2.11 \times 10^4$ $M^{-1} \cdot s^{-1}$		

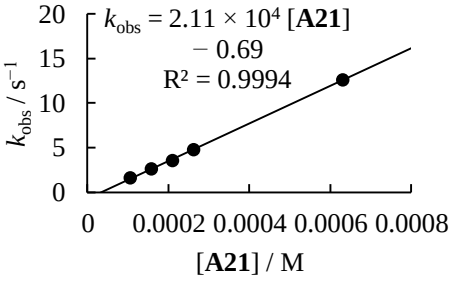

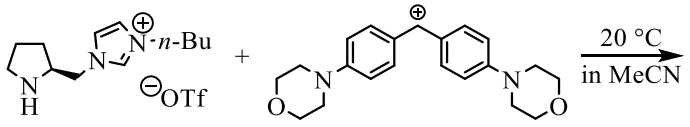

A21 **E15**

Table 131. Kinetics of the reaction of **A21** with **E15** (stopped-flow method, detection at 612 nm)

[**A21**] / M	[**E15**] / M	k_{obs} / s^{-1}
1.05×10^{-4}		1.18
1.57×10^{-4}		2.00
2.10×10^{-4}	9.90×10^{-6}	2.53
2.62×10^{-4}		3.40
3.15×10^{-4}		4.38
$k_2 = 1.49 \times 10^4$ $M^{-1} \cdot s^{-1}$		

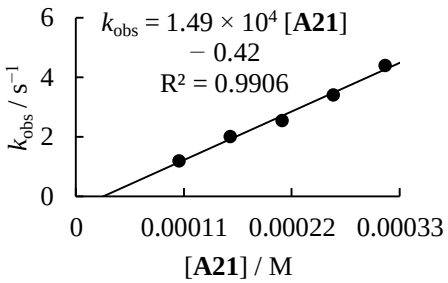

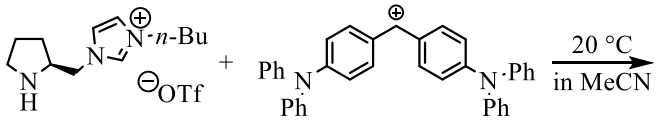

A21 **E16**

Table 132. Kinetics of the reaction of **A21** with **E16** (stopped-flow method, detection at 645 nm)

[**A21**] / M	[**E16**] / M	k_{obs} / s^{-1}
1.75×10^{-4}		1.52×10^{1}
2.62×10^{-4}		2.41×10^{1}
3.50×10^{-4}	8.78×10^{-6}	3.43×10^{1}
4.37×10^{-4}		4.55×10^{1}
5.25×10^{-4}		5.68×10^{1}
$k_2 = 1.20 \times 10^{5}$ $M^{-1} \cdot s^{-1}$		

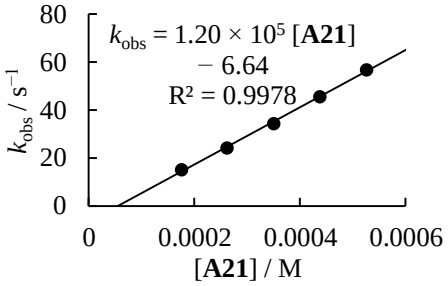

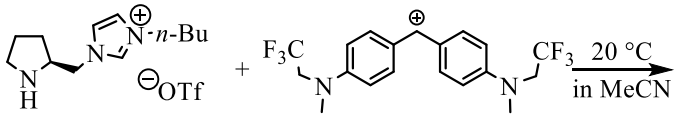

A21 **E17**

Table 133. Kinetics of the reaction of **A21** with **E17** (stopped-flow method, detection at 586 nm)

[**A21**] / M	[**E17**] / M	k_{obs} / s^{-1}
7.00×10^{-5}		7.18
1.05×10^{-4}		1.12×10^{1}
1.40×10^{-4}	4.84×10^{-6}	1.58×10^{1}
1.75×10^{-4}		2.02×10^{1}
2.10×10^{-4}		2.60×10^{1}
$k_2 = 1.33 \times 10^{5}$ $M^{-1} \cdot s^{-1}$		

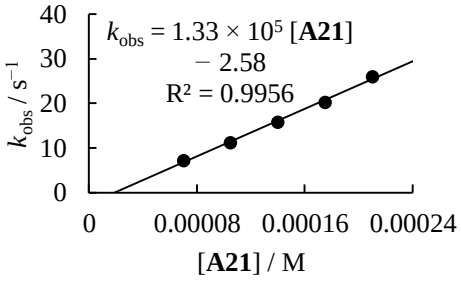

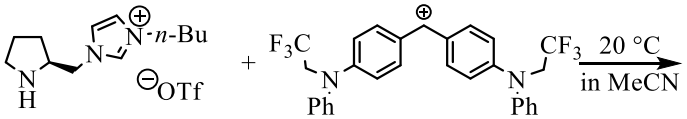

A21 **E18**

Table 134. Kinetics of the reaction of **A21** with **E18** (stopped-flow method, detection at 592 nm)

[**A21**] / M	[**E18**] / M	k_{obs} / s^{-1}
7.00×10^{-5}		1.81×10^{1}
1.05×10^{-4}		2.72×10^{1}
1.40×10^{-4}	7.00×10^{-6}	3.73×10^{1}
1.75×10^{-4}		4.87×10^{1}
2.10×10^{-4}		6.15×10^{1}
$k_2 = 3.09 \times 10^{5}$ $M^{-1} \cdot s^{-1}$		

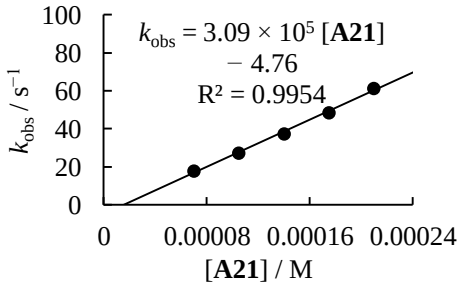

Table 135. Determination of the parameters N and s_N for **A21** in acetonitrile

Electrophile	E	k_2 / $M^{-1} \cdot s^{-1}$
E13	−7.02	2.97×10^3
E14	−5.89	$2.11 \times 10^{4*}$
E15	−5.53	1.49×10^4
E16	−4.72	$1.20 \times 10^{5*}$
E17	−3.85	1.33×10^5
E18	−4.14	3.09×10^5
$N = 13.57$ $s_N = 0.53$		

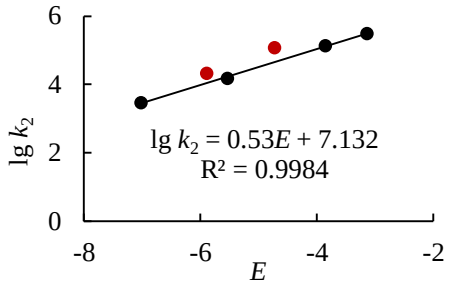

* Second-order rate constants k_2 for the reactions of **A21** with **E14** and **E16** are not used for the determination of the N and s_N parameters.

(*S*)-1-(3,5-Bis(trifluoromethyl)phenyl)-3-(pyrrolidin-2-ylmethyl)thiourea (A22)

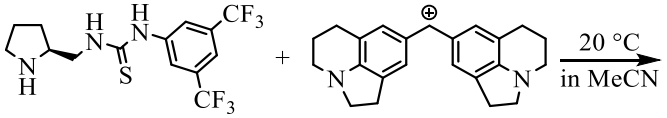

A22 **E8**

Table 136. Kinetics of the reaction of **A22** with **E8** (stopped-flow method, detection at 632 nm)

[**A22**] / M	[**E8**] / M	k_{obs} / s^{-1}
1.11×10^{-4}	5.29×10^{-6}	5.73×10^{-1}
1.66×10^{-4}		6.81×10^{-1}
2.21×10^{-4}		8.26×10^{-1}
2.76×10^{-4}		9.36×10^{-1}
3.31×10^{-4}		1.09
4.42×10^{-4}		1.37
$k_2 = 2.42 \times 10^3$ $M^{-1} \cdot s^{-1}$		

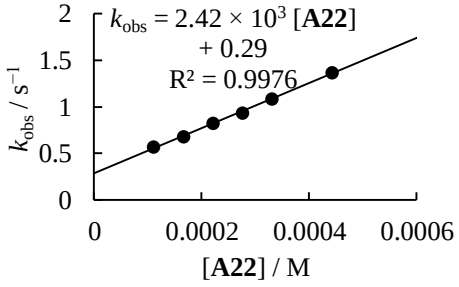

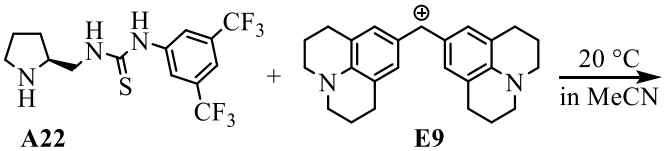

A22 **E9**

Table 137. Kinetics of the reaction of **A22** with **E9** (stopped-flow method, detection at 635 nm)

[**A22**] / M	[**E9**] / M	k_{obs} / s^{-1}
1.66×10^{-4}	6.08×10^{-6}	2.06
2.21×10^{-4}		2.45
2.76×10^{-4}		2.87
3.86×10^{-4}		3.65
$k_2 = 7.25 \times 10^3$ $M^{-1} \cdot s^{-1}$		

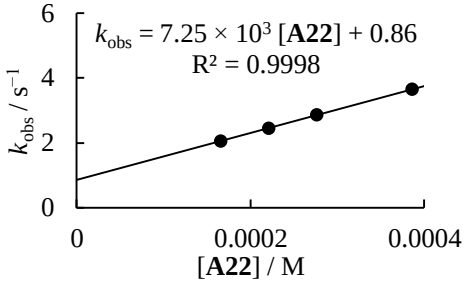

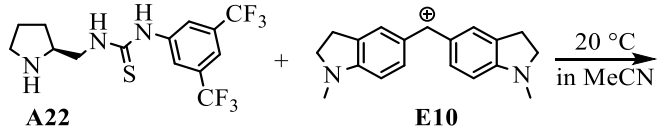

A22 **E10**

Table 138. Kinetics of the reaction of **A22** with **E10** (stopped-flow method, detection at 616 nm)

[**A22**] / M	[**E10**] / M	k_{obs} / s^{-1}
6.62×10^{-5}	4.86×10^{-6}	1.13
9.94×10^{-5}		1.69
1.32×10^{-4}		2.30
1.66×10^{-4}		2.85
1.99×10^{-4}		3.48
$k_2 = 1.76 \times 10^4$ $M^{-1} \cdot s^{-1}$		

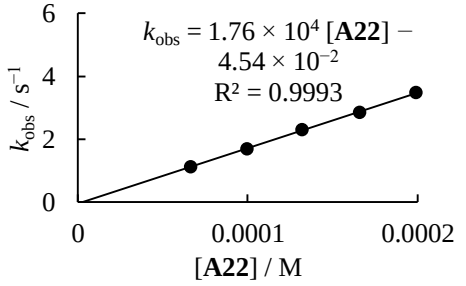

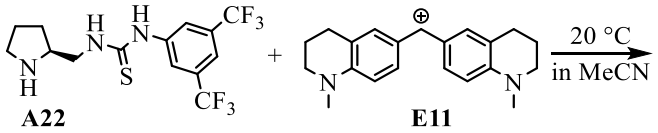

A22 **E11**

Table 139. Kinetics of the reaction of **A22** with **E11** (stopped-flow method, detection at 620 nm)

[**A22**] / M	[**E11**] / M	k_{obs} / s^{-1}
4.42×10^{-5}		2.19
6.62×10^{-5}		3.02
8.83×10^{-5}	4.28×10^{-6}	3.96
1.10×10^{-4}		4.76
1.32×10^{-4}		5.83
$k_2 = 4.11 \times 10^4$ $M^{-1} \cdot s^{-1}$		

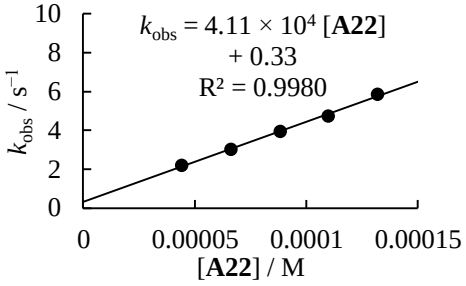

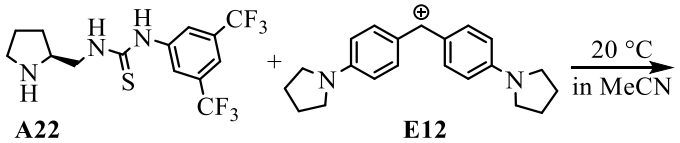

A22 **E12**

Table 140. Kinetics of the reaction of **A22** with **E12** (stopped-flow method, detection at 612 nm)

[**A22**] / M	[**E12**] / M	k_{obs} / s^{-1}
4.42×10^{-5}		4.65
6.62×10^{-5}		7.07
8.83×10^{-5}	4.41×10^{-6}	9.56
1.10×10^{-4}		1.24×10^1
1.32×10^{-4}		1.45×10^1
$k_2 = 1.14 \times 10^5$ $M^{-1} \cdot s^{-1}$		

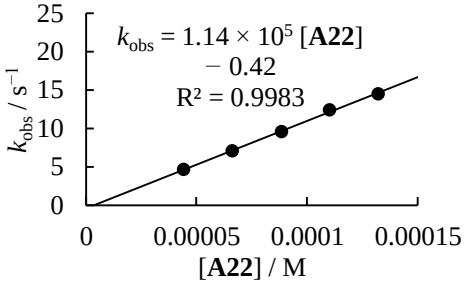

Table 141. Determination of the parameters N and s_N for **A22** in acetonitrile

Electrophile	E	k_2 / $M^{-1} \cdot s^{-1}$
E8	−10.04	2.42×10^3
E9	−9.45	7.25×10^3
E10	−8.76	1.76×10^3
E11	−8.22	4.11×10^4
E12	−7.69	1.14×10^5
$N = 14.97$ $s_N = 0.69$		

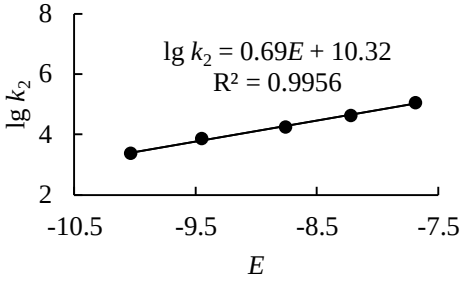

(*S*)-1-(3,5-Bis(trifluoromethyl)phenyl)-3-(pyrrolidin-2-ylmethyl)urea (A23)

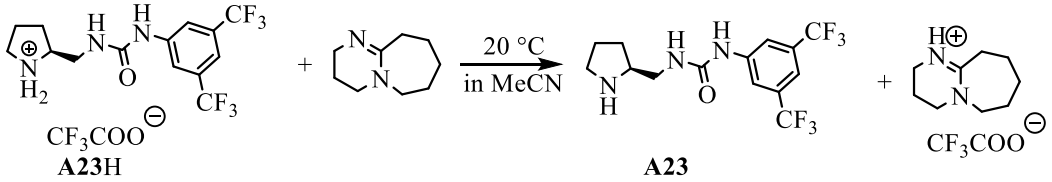

The stock solution of **A23** was prepared by quantitative deprotonation of **A23**H with DBU base ($n_{\mathbf{a13H}}/n_{DBU}$ = 1.2 : 1).

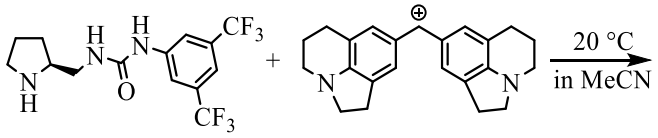

Table 142. Kinetics of the reaction of **A23** with **E8** (stopped-flow method, detection at 632 nm)

[**A23**] / M	[**E8**] / M	k_{obs} / s^{-1}
4.48×10^{-5}		1.69
6.72×10^{-5}		2.67
8.95×10^{-5}	4.32×10^{-6}	3.93
1.12×10^{-4}		5.19
1.34×10^{-4}		6.50
$k_2 = 5.44 \times 10^4$ $M^{-1} \cdot s^{-1}$		

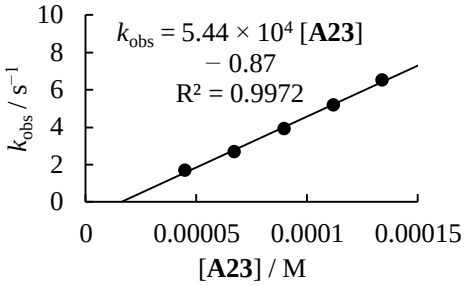

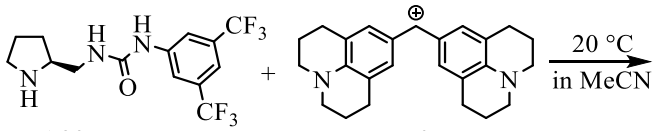

Table 143. Kinetics of the reaction of **A23** with **E9** (stopped-flow method, detection at 635 nm)

[**A23**] / M	[**E9**] / M	k_{obs} / s^{-1}
4.48×10^{-5}		4.88
6.72×10^{-5}	4.28×10^{-6}	7.65
8.95×10^{-5}		1.07×10^1
1.12×10^{-4}		1.47×10^1
$k_2 = 1.45 \times 10^5$ $M^{-1} \cdot s^{-1}$		

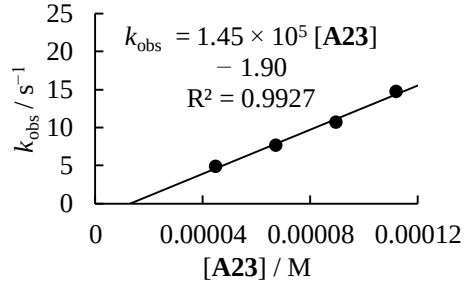

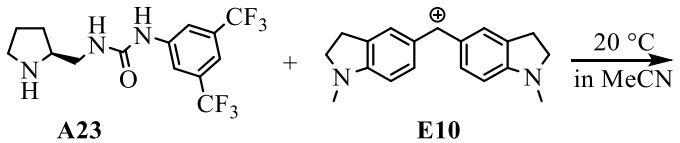

A23 **E10**

Table 144. Kinetics of the reaction of **A23** with **E10** (stopped-flow method, detection at 616 nm)

[**A23**] / M	[**E10**] / M	k_{obs} / s^{-1}
4.48×10^{-5}		9.16
6.72×10^{-5}		1.61×10^{1}
7.84×10^{-5}	4.12×10^{-6}	2.06×10^{1}
8.96×10^{-5}		2.45×10^{1}
1.23×10^{-4}		3.77×10^{1}
$k_2 = 3.68 \times 10^{5}$ $M^{-1} \cdot s^{-1}$		

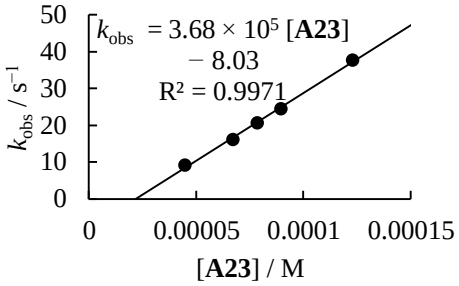

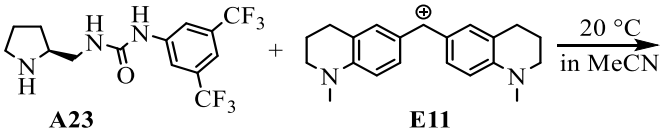

A23 **E11**

Table 145. Kinetics of the reaction of **A23** with **E11** (stopped-flow method, detection at 620 nm)

[**A23**] / M	[**E11**] / M	k_{obs} / s^{-1}
3.36×10^{-5}		1.56×10^{1}
4.48×10^{-5}		2.40×10^{1}
5.60×10^{-5}	3.67×10^{-6}	3.21×10^{1}
6.72×10^{-5}		4.25×10^{1}
8.96×10^{-5}		6.07×10^{1}
$k_2 = 8.11 \times 10^{5}$ $M^{-1} \cdot s^{-1}$		

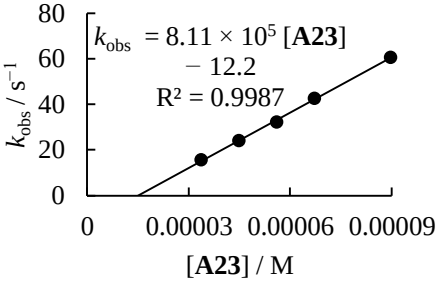

Table 146. Determination of the parameters N and s_N for **A23** in acetonitrile

Electrophile	E	k_2 / $M^{-1} \cdot s^{-1}$
E8	−10.04	5.44×10^{4}
E9	−9.45	1.45×10^{5}
E10	−8.76	3.68×10^{5}
E11	−8.22	8.11×10^{5}
$N = 17.50$ $s_N = 0.64$		

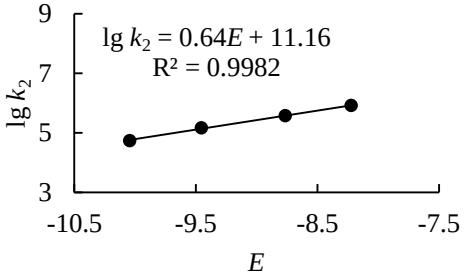

(*S*)-2-Tritylpyrrolidine (A24)

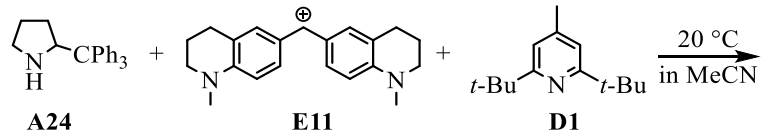

A24 **E11** **D1**

Table 147. Kinetics of the reaction of **A24** with **E11** and **D1** ([**D1**] = 5.83 mmol·L^{-1}, stopped-flow method, detection at 620 nm)

[**A24**] / M	[**E11**] / M	k_{obs} / s^{-1}
3.23×10^{-4}		2.67×10^{-2}
5.02×10^{-4}		2.97×10^{-2}
6.82×10^{-4}	5.61×10^{-6}	3.37×10^{-2}
8.61×10^{-4}		3.71×10^{-2}
1.04×10^{-3}		4.07×10^{-2}
$k_2 = 1.97 \times 10^{1}$ M^{-1}·s^{-1}		

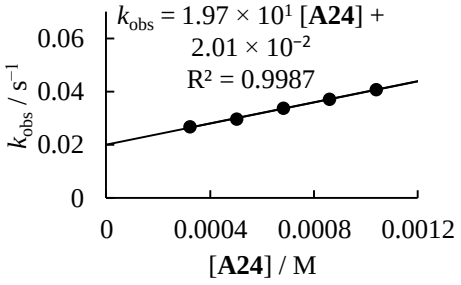

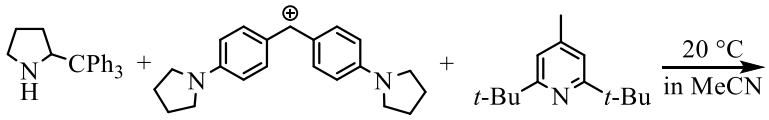

A24 **E12** **D1**

Table 148. Kinetics of the reaction of **A24** with **E12** and **D1** ([**D1**] = 5.83 mmol·L^{-1}, stopped-flow method, detection at 612 nm)

[**A24**] / M	[**E12**] / M	k_{obs} / s^{-1}
2.06×10^{-4}		3.89×10^{-2}
3.43×10^{-4}		5.46×10^{-2}
4.80×10^{-4}	4.59×10^{-6}	7.05×10^{-2}
6.17×10^{-4}		8.86×10^{-2}
7.55×10^{-4}		1.09×10^{-1}
$k_2 = 1.27 \times 10^{2}$ M^{-1}·s^{-1}		

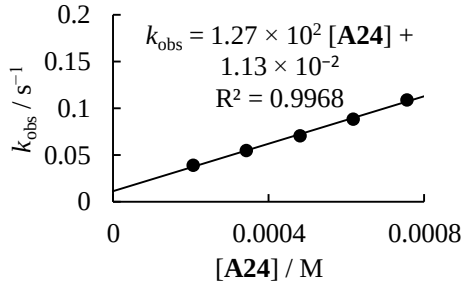

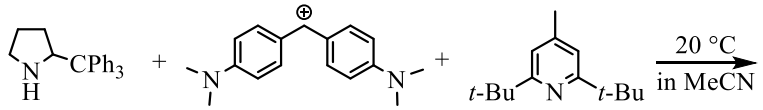

A24 **E13** **D1**

Table 149. Kinetics of the reaction of **A24** with **E13** and **D1** ([**D1**] = 5.83 mmol·L^{-1}, stopped-flow method, detection at 605 nm)

[**A24**] / M	[**E13**] / M	k_{obs} / s^{-1}
1.37×10^{-4}	4.70×10^{-6}	8.80×10^{-2}
2.06×10^{-4}		1.40×10^{-1}
2.74×10^{-4}		1.92×10^{-1}
3.43×10^{-4}		2.50×10^{-1}
4.12×10^{-4}		3.05×10^{-1}
$k_2 = 7.92 \times 10^{2}$ M^{-1}·s^{-1}		

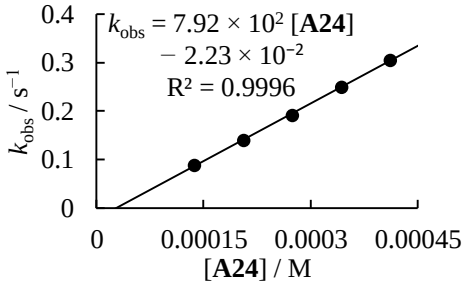

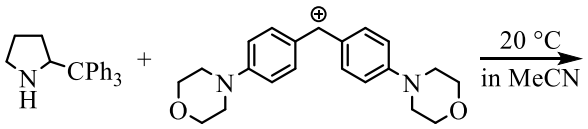

A24 **E15**

Table 150. Kinetics of the reaction of **A24** with **E15** (stopped-flow method, detection at 612 nm)

[**A24**] / M	[**E15**] / M	k_{obs} / s^{-1}
9.97×10^{-5}	9.19×10^{-6}	8.83
1.50×10^{-4}		1.46×10^{1}
1.99×10^{-4}		1.95×10^{1}
2.49×10^{-4}		2.58×10^{1}
2.99×10^{-4}		3.22×10^{1}
3.49×10^{-4}		3.66×10^{1}
$k_2 = 1.14 \times 10^{5}$ M^{-1}·s^{-1}		

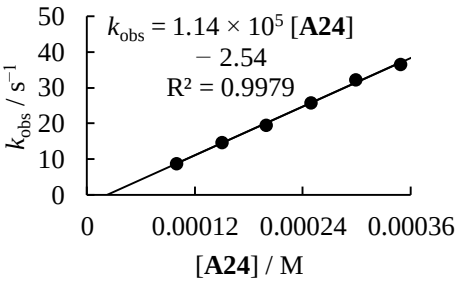

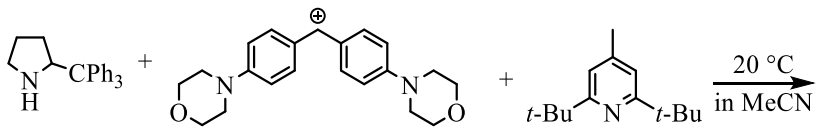

A24 **E15** **D1**

Table 151. Kinetics of the reaction of **A24** with **E15** and **D1** ([**D1**] = 4.66 mmol·L^{-1}, stopped-flow method, detection at 612 nm)

[**A24**] / M	[**E15**] / M	k_{obs} / s^{-1}
4.12×10^{-5}	4.24×10^{-6}	5.04
6.86×10^{-5}		8.10×10^{5}
9.60×10^{-5}		1.10×10^{1}
1.23×10^{-4}		1.42×10^{1}
1.51×10^{-4}		1.76×10^{1}
1.78×10^{-4}		2.10×10^{1}
$k_2 = 1.16 \times 10^{5}$ M^{-1}·s^{-1}		

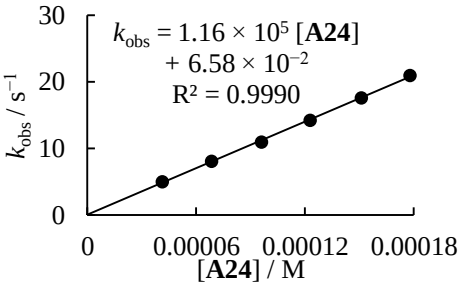

Table 152. Determination of the parameters N and s_N for **A24** in acetonitrile

Electrophile	E	k_2 / M^{-1}·s^{-1}
E11	−8.22	1.97×10^{1}
E12	−7.69	1.27×10^{2}
E13	−7.02	7.92×10^{2}
E15	−5.53	1.16×10^{5}
$N = 9.16$ $s_N = 1.39$		

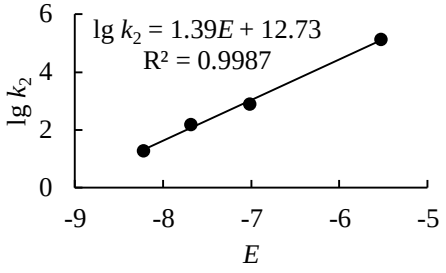

(*S*)-2-(Diphenyl((trimethylsilyl)oxy)methyl)pyrrolidine (A25)

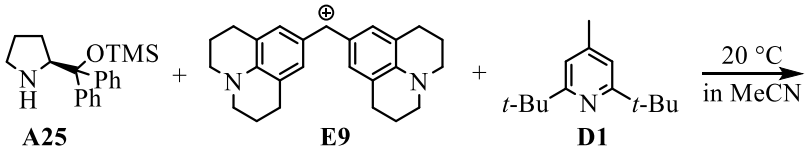

A25 **E9** **D1**

Table 153. Kinetics of the reaction of **A25** with **E9** and **D1** ([**D1**] = 4.86 mmol·L^{-1}, stopped-flow method, detection at 635 nm)

[**A25**] / M	[**E9**] / M	k_{obs} / s^{-1}
5.93×10^{-4}	4.68×10^{-6}	2.07×10^{-1}
8.89×10^{-4}		2.71×10^{-1}
1.19×10^{-3}		3.29×10^{-1}
1.78×10^{-3}		4.57×10^{-1}
2.37×10^{-3}		5.96×10^{-1}
2.96×10^{-3}		7.44×10^{-1}
$k_2 = 2.26 \times 10^2$ M^{-1}·s^{-1}		

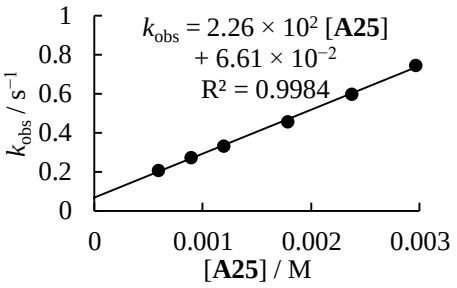

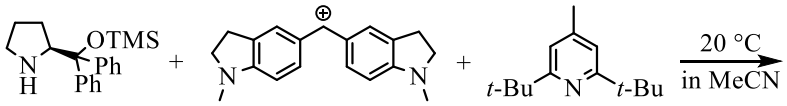

A25 **E10** **D1**

Table 154. Kinetics of the reaction of **A25** with **E10** and **D1** ([**D1**] = 4.86 mmol·L^{-1}, stopped-flow method, detection at 616 nm)

[**A25**] / M	[**E10**] / M	k_{obs} / s^{-1}
3.92×10^{-4}	7.25×10^{-6}	8.98×10^{-1}
5.22×10^{-4}		1.24
6.53×10^{-4}		1.57
7.83×10^{-4}		1.91
1.04×10^{-3}		2.80
1.31×10^{-3}		3.26
$k_2 = 2.67 \times 10^3$ M^{-1}·s^{-1}		

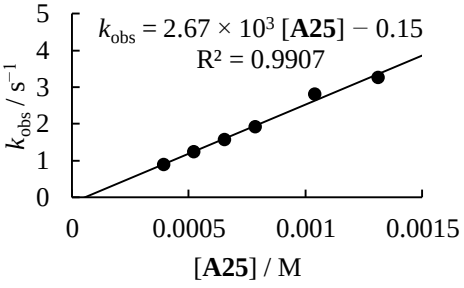

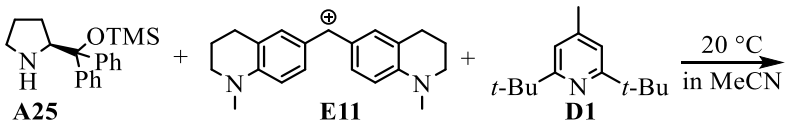

Table 155. Kinetics of the reaction of **A25** with **E11** and **D1** ([**D1**] = 4.86 mmol·L^{-1}, stopped-flow method, detection at 620 nm)

[**A25**] / M	[**E11**] / M	k_{obs} / s^{-1}
2.40×10^{-4}	4.97×10^{-6}	1.44
3.59×10^{-4}		1.93
4.79×10^{-4}		2.52
5.99×10^{-4}		3.13
8.39×10^{-4}		4.35
1.08×10^{-3}		5.91
$k_2 = 5.30 \times 10^3$ M^{-1}·s^{-1}		

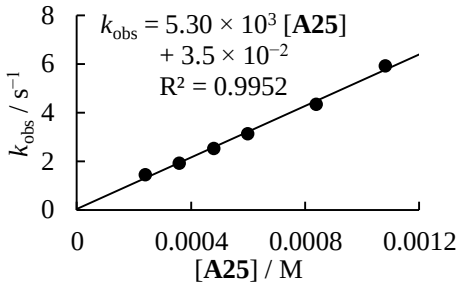

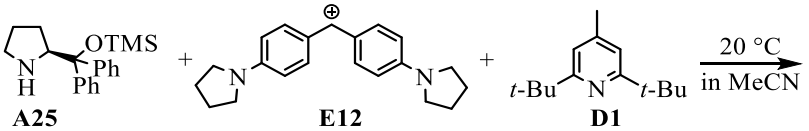

Table 156. Kinetics of the reaction of **A25** with **E12** and **D1** ([**D1**] = 4.86 mmol·L^{-1}, stopped-flow method, detection at 612 nm)

[**A25**] / M	[**E12**] / M	k_{obs} / s^{-1}
1.11×10^{-4}	5.16×10^{-6}	1.31
2.21×10^{-4}		2.92
3.32×10^{-4}		4.87
4.42×10^{-4}		6.50
5.53×10^{-4}		8.39
6.64×10^{-4}		1.03×10^1
$k_2 = 1.63 \times 10^4$ M^{-1}·s^{-1}		

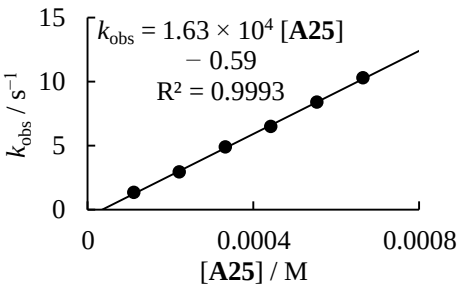

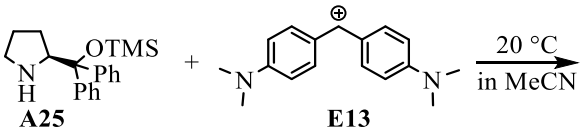

Table 157. . Kinetics of the reaction of **A25** with **E13** (stopped-flow method, detection at 605 nm)

[**A25**] / M	[**E13**] / M	k_{obs} / s^{-1}
1.10×10^{-4}	4.41×10^{-6}	8.32
1.65×10^{-4}		1.32×10^1
2.20×10^{-4}		1.88×10^1
2.75×10^{-4}		2.43×10^1
3.30×10^{-4}		2.93×10^1
$k_2 = 9.65 \times 10^4$ M^{-1}·s^{-1}		

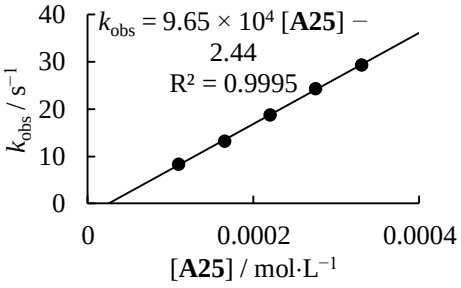

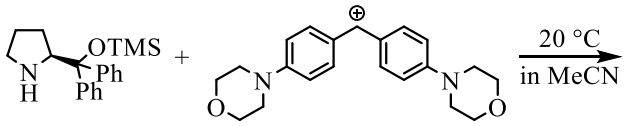

A25 **E15**

Table 158. Kinetics of the reaction of **A25** with **E15** (stopped-flow method, detection at 612 nm)

[**A25**] / M	[**E15**] / M	k_{obs} / s^{-1}
4.40×10^{-5}	4.29×10^{-6}	7.27×10^{1}
6.60×10^{-5}		1.22×10^{2}
8.80×10^{-5}		1.61×10^{2}
1.10×10^{-4}		2.10×10^{2}

$k_2 = 2.05 \times 10^{6}$ $M^{-1} \cdot s^{-1}$

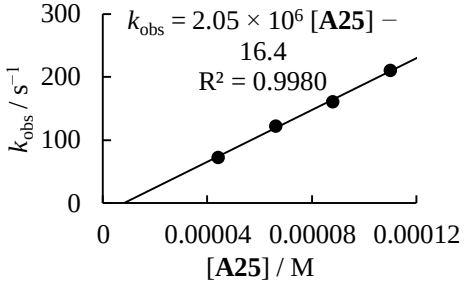

Table 159. Determination of the parameters N and s_N for **A25** in acetonitrile

Electrophile	E	k_2 / $M^{-1} \cdot s^{-1}$
E9	−9.45	2.26×10^{2}
E10	−8.76	2.67×10^{3}
E11	−8.22	5.30×10^{3}
E12	−7.69	1.63×10^{4}
E13	−7.02	9.65×10^{4}
E15	−5.53	2.05×10^{6}

$N = 12.03$ $s_N = 0.98$

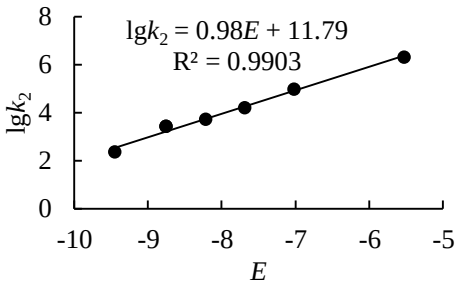

(*S*)-Diphenyl(pyrrolidin-2-yl)methanol (A26)

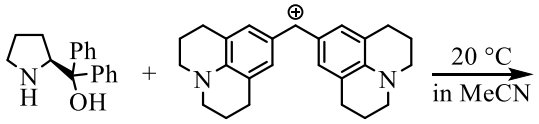

A26 **E9**

Table 160. Kinetics of the reaction of **A26** with **E9** (stopped-flow method, detection at 635 nm)

[**A26**] / M	[**E9**] / M	k_{obs} / s^{-1}
4.42×10^{-4}		5.40
6.63×10^{-4}		6.62
8.84×10^{-4}	4.39×10^{-6}	7.38
1.33×10^{-3}		9.78
1.77×10^{-3}		1.28×10^{1}
$k_2 = 5.48 \times 10^{3}$ $M^{-1} \cdot s^{-1}$		

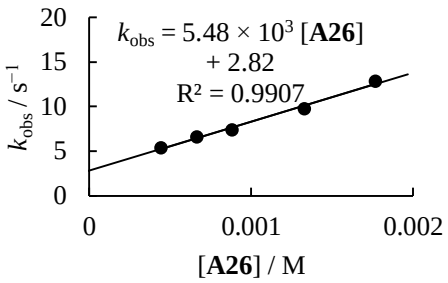

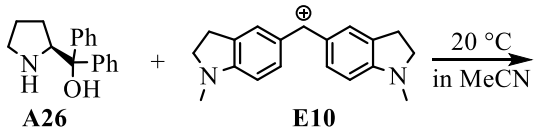

A26 **E10**

Table 161. Kinetics of the reaction of **A26** with **E10** (stopped-flow method, detection at 616 nm)

[**A26**] / M	[**E10**] / M	k_{obs} / s^{-1}
2.31×10^{-4}		2.91
3.46×10^{-4}		4.19
4.62×10^{-4}	4.67×10^{-6}	5.57
6.93×10^{-4}		8.44
9.24×10^{-4}		1.13×10^{1}
$k_2 = 1.22 \times 10^{4}$ $M^{-1} \cdot s^{-1}$		

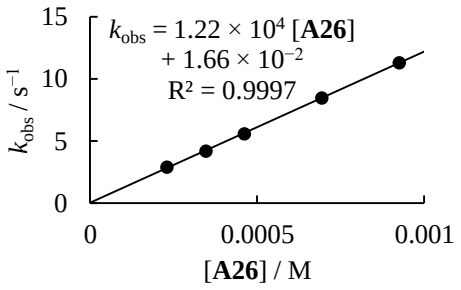

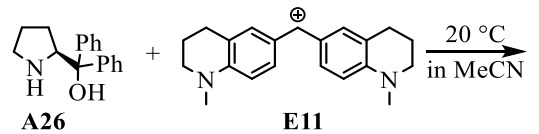

A26 **E11**

Table 162. Kinetics of the reaction of **A26** with **E11** (stopped-flow method, detection at 620 nm)

[**A26**] / M	[**E11**] / M	k_{obs} / s^{-1}
1.15×10^{-4}		4.72
2.31×10^{-4}		8.37
3.46×10^{-4}	3.25×10^{-6}	1.20×10^{1}
4.62×10^{-4}		1.62×10^{1}
6.93×10^{-4}		2.45×10^{1}
9.24×10^{-4}		3.35×10^{1}
$k_2 = 3.57 \times 10^{4}$ $M^{-1} \cdot s^{-1}$		

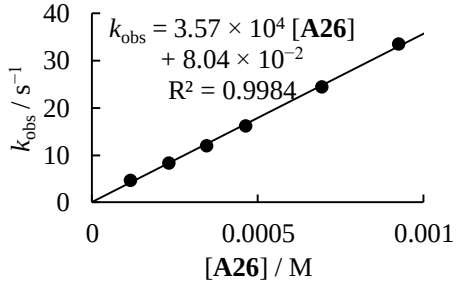

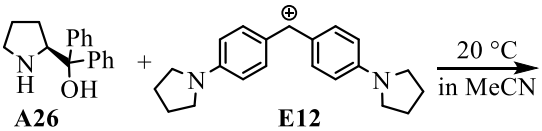

A26 **E12**

Table 163. Kinetics of the reaction of **A26** with **E12** (stopped-flow method, detection at 612 nm)

[**A26**] / M	[**E12**] / M	k_{obs} / s^{-1}
5.77×10^{-5}		4.45
1.15×10^{-4}		7.73
2.31×10^{-4}		1.52×10^{1}
3.46×10^{-4}	4.08×10^{-6}	2.43×10^{1}
4.62×10^{-4}		3.32×10^{1}
6.93×10^{-4}		5.05×10^{1}
9.24×10^{-4}		6.90×10^{1}

$k_2 = 7.50 \times 10^{4}$ $M^{-1} \cdot s^{-1}$

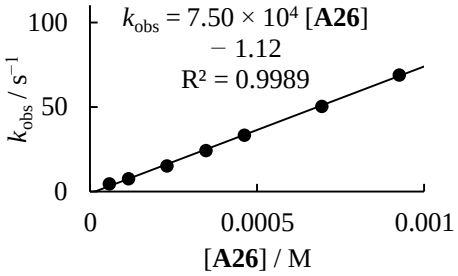

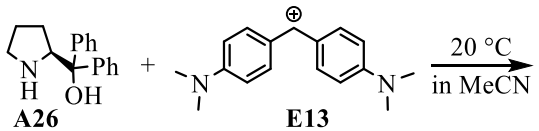

A26 **E13**

Table 164. Kinetics of the reaction of **A26** with **E13** (stopped-flow method, detection at 605 nm)

[**A26**] / M	[**E13**] / M	k_{obs} / s^{-1}
4.62×10^{-5}		6.27
9.24×10^{-5}		1.35×10^{1}
1.39×10^{-4}	4.85×10^{-6}	2.09×10^{1}
1.85×10^{-4}		2.95×10^{1}
2.31×10^{-4}		3.75×10^{1}
2.77×10^{-4}		4.58×10^{1}

$k_2 = 1.72 \times 10^{5}$ $M^{-1} \cdot s^{-1}$

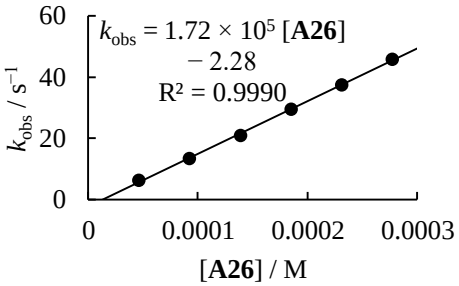

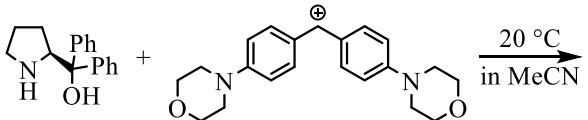

A26 **E15**

Table 165. Kinetics of the reaction of **A26** with **E15** (stopped-flow method, detection at 612 nm)

[**A26**] / M	[**E15**] / M	k_{obs} / s^{-1}
4.04×10^{-5}		2.51×10^{1}
5.77×10^{-5}		3.86×10^{1}
7.50×10^{-5}	3.89×10^{-6}	5.27×10^{1}
9.24×10^{-5}		6.41×10^{1}
1.10×10^{-4}		7.80×10^{1}
1.27×10^{-4}		9.20×10^{1}

$k_2 = 7.64 \times 10^{5}$ $M^{-1} \cdot s^{-1}$

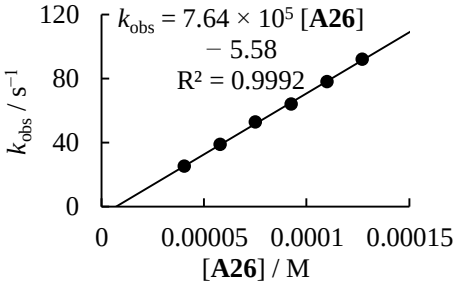

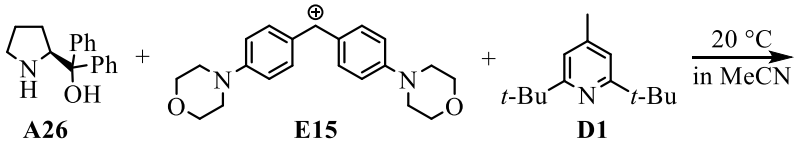

A26 **E15** **D1**

Table 166. Kinetics of the reaction of **A26** with **E15** and **D1** ([**D1**] = 4.66 mM, stopped-flow method, detection at 612 nm)

[**A26**] / M	[**E15**] / M	k_{obs} / s^{-1}
6.41×10^{-5}		4.35×10^{1}
1.28×10^{-4}		9.32×10^{1}
1.92×10^{-4}	3.54×10^{-6}	1.44×10^{2}
2.57×10^{-4}		1.98×10^{2}
3.21×10^{-4}		2.49×10^{2}
$k_2 = 8.02 \times 10^{5}$ $M^{-1} \cdot s^{-1}$		

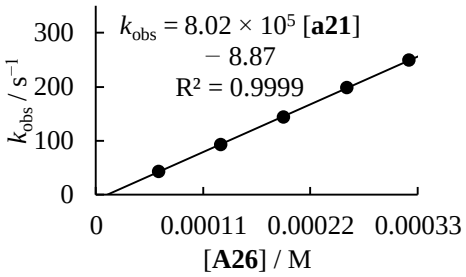

Table 167. Determination of the parameters N and s_N for **A26** in acetonitrile

Electrophile	E	k_2 / $M^{-1} \cdot s^{-1}$
E9	−9.45	5.48×10^{3}
E10	−8.76	1.22×10^{4}
E11	−8.22	3.57×10^{4}
E12	−7.69	7.50×10^{4}
E13	−7.02	1.72×10^{5}
E15	−5.53	8.02×10^{5}
$N = 16.18$ $s_N = 0.56$		

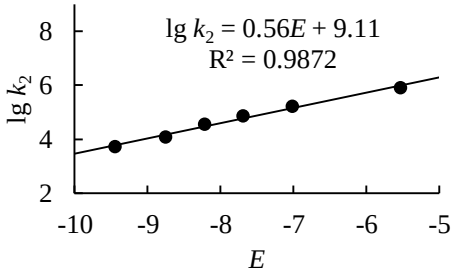

(*S*)-2-(Azidodiphenylmethyl)pyrrolidine (A27)

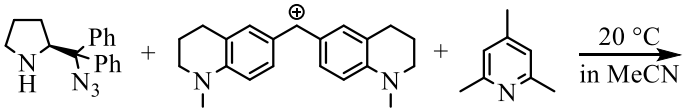

A27 **E11** **D2**

Table 168. Kinetics of the reaction of **A27** with **E11** and **D2** ([**D2**] = 5.08 mM, stopped-flow method, detection at 620 nm)

[**A27**] / M	[**E11**] / M	k_{obs} / s^{-1}
5.39×10^{-4}	5.10×10^{-6}	1.51×10^{-1}
8.08×10^{-4}		1.96×10^{-1}
1.08×10^{-3}		2.25×10^{-1}
1.35×10^{-3}		2.55×10^{-1}
1.62×10^{-3}		2.92×10^{-1}
$k_2 = 1.26 \times 10^2$ $M^{-1} \cdot s^{-1}$		

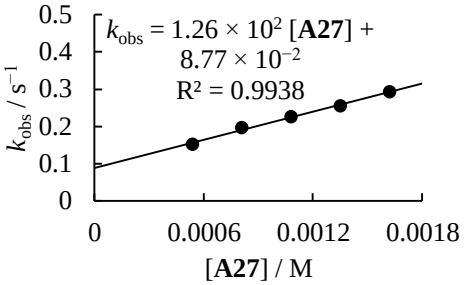

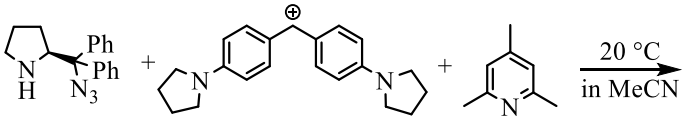

A27 **E12** **D2**

Table 169. Kinetics of the reaction of **A27** with **E12** and **D2** ([**D2**] = 5.08 mM, stopped-flow method, detection at 612 nm)

[**A27**] / M	[**E12**] / M	k_{obs} / s^{-1}
8.98×10^{-5}	4.97×10^{-6}	6.61×10^{-2}
1.80×10^{-4}		9.79×10^{-2}
2.69×10^{-4}		1.31×10^{-1}
3.69×10^{-4}		1.54×10^{-1}
4.49×10^{-4}		1.81×10^{-1}
5.39×10^{-4}		2.19×10^{-1}
$k_2 = 3.29 \times 10^2$ $M^{-1} \cdot s^{-1}$		

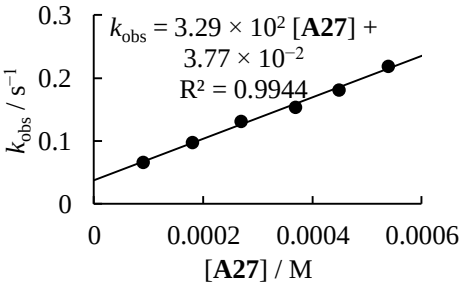

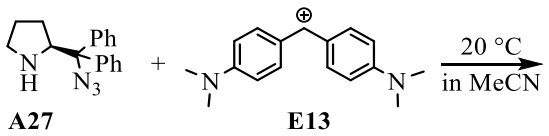

A27 **E13**

Table 170. Kinetics of the reaction of **A27** with **E13** (stopped-flow method, detection at 605 nm)

[**A27**] / M	[**E13**] / M	k_{obs} / s^{-1}
2.12×10^{-5}	2.35×10^{-6}	1.40×10^{-1}
3.18×10^{-5}		2.13×10^{-1}
4.24×10^{-5}		1.98×10^{-1}
5.30×10^{-5}		1.98×10^{-1}
6.36×10^{-5}		2.59×10^{-1}
8.48×10^{-5}		2.92×10^{-1}
1.06×10^{-4}		3.26×10^{-1}
1.59×10^{-4}		5.05×10^{-1}
2.12×10^{-4}		6.44×10^{-1}
3.18×10^{-4}		9.45×10^{-1}
5.30×10^{-3}		2.36
1.06×10^{-2}		5.09

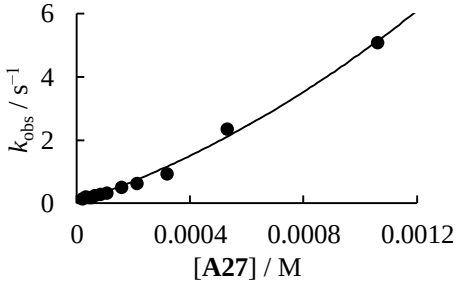

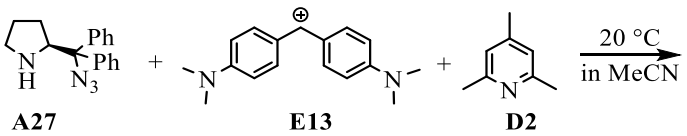

A27 **E13** **D2**

Table 171. Kinetics of the reaction of **A27** with **E13** and **D2** ([**A27**] = 7.67 × 10^{-5} mmol·L^{-1}, ([**E13**] = 7.06 × 10^{-6} mmol·L^{-1}, stopped-flow method, detection at 605 nm)

Entry	[**D2**] / M
1	0
2	1.89 × 10^{-5}
3	3.78 × 10^{-5}
4	7.55 × 10^{-5}
5	1.51 × 10^{-4}
6	3.78 × 10^{-4}
7	1.89 × 10^{-3}
8	3.78 × 10^{-3}
9	7.29 × 10^{-3}
10	1.02 × 10^{-2}
11	2.03 × 10^{-2}
12	3.05 × 10^{-2}
13	4.06 × 10^{-2}

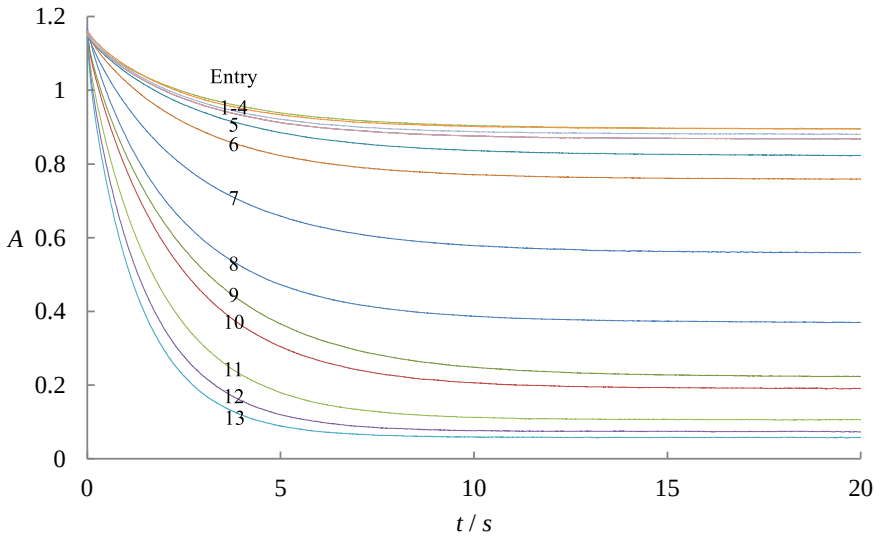

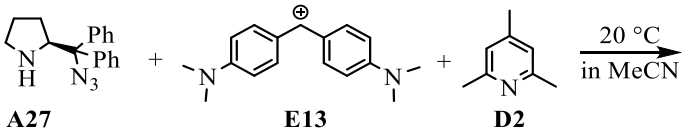

A27 **E13** **D2**

Table 172. Kinetics of the reaction of **A27** with **E13** and **D2** ([**D2**] = 5.08 mM, stopped-flow method, detection at 605 nm)

[**A27**] / M	[**E13**] / M	k_{obs} / s^{-1}
7.67 × 10^{-5}	5.10 × 10^{-6}	3.45 × 10^{-1}
1.53 × 10^{-4}		6.56 × 10^{-1}
2.30 × 10^{-4}		9.87 × 10^{-1}
5.37 × 10^{-4}		2.33

k_2 = 4.33 × 10^3 M^{-1}·s^{-1}

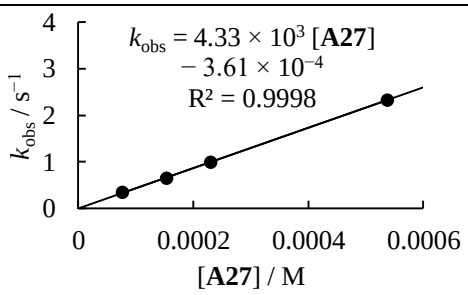

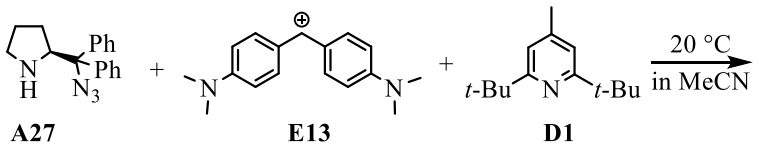

A27 **E13** **D1**

Table 173. Kinetics of the reaction of **A27** with **E13** and **D1** ([**D1**] = 5.13 mmol·L^{-1}, stopped-flow method, detection at 605 nm)

[**A27**] / M	[**E13**] / M	k_{obs} / s^{-1}
1.44×10^{-4}		4.09×10^{-1}
2.87×10^{-4}		9.75×10^{-1}
4.31×10^{-4}	5.29×10^{-6}	1.60
5.75×10^{-4}		2.27
7.18×10^{-4}		2.90
$k_2 = 4.37 \times 10^3$ M^{-1}·s^{-1}		

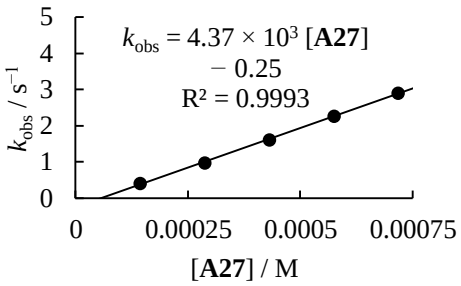

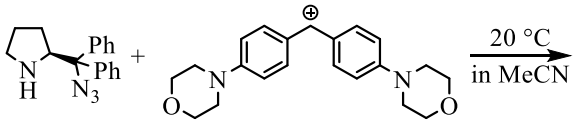

A27 **E15**

Table 174. Kinetics of the reaction of **A27** with **E15** (stopped-flow method, detection at 612 nm)

[**A27**] / M	[**E15**] / M	k_{obs} / s^{-1}
6.36×10^{-5}		8.59
8.48×10^{-5}		1.32×10^1
1.06×10^{-4}	6.13×10^{-6}	1.61×10^1
1.27×10^{-4}		2.03×10^1
1.48×10^{-4}		2.55×10^1
$k_2 = 1.94 \times 10^5$ M^{-1}·s^{-1}		

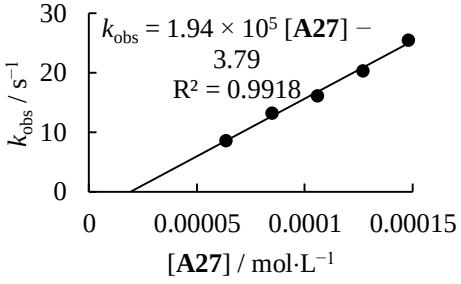

Table 175. Determination of the parameters N and s_N for **A27** in acetonitrile

Electrophile	E	k_2 / M^{-1}·s^{-1}
E11	−8.22	1.26×10^2
E12	−7.69	3.29×10^2
E13	−7.02	4.33×10^3
E15	−5.53	1.94×10^5
N = 9.90 s_N = 1.22		

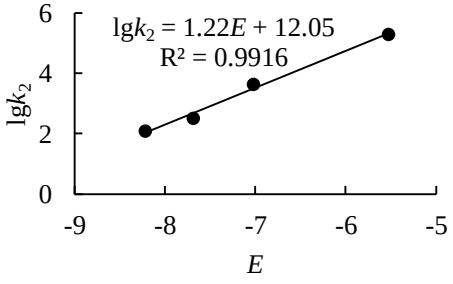

2-(Triphenylsilyl)pyrrolidine (A28)

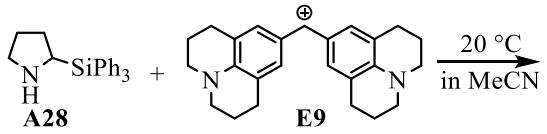

A28 E9

Table 176. Kinetics of the reaction of **A28** with **E9** (stopped-flow method, detection at 635 nm)

[**A28**] / M	[**E9**] / M	k_{obs} / s^{-1}
3.16×10^{-4}	5.18×10^{-6}	2.50
4.73×10^{-4}		2.88
6.31×10^{-4}		3.59
7.89×10^{-4}		4.32
9.47×10^{-4}		5.28
1.03×10^{-3}		6.30

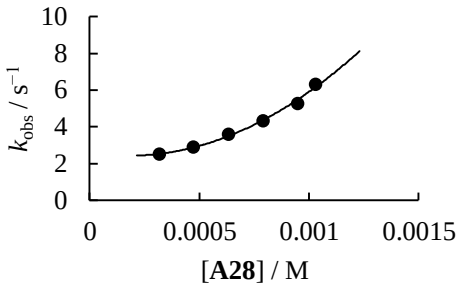

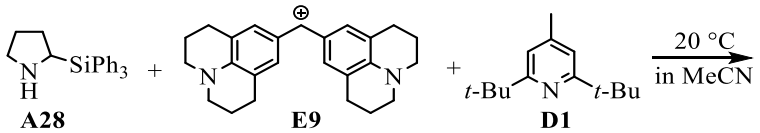

A28 E9 D1

Table 177. Kinetics of the reaction of **A28** with **E9** using **D1** ([**D1**] = 5.13 mM, stopped-flow method, detection at 635 nm)

[**A28**] / M	[**E9**] / M	k_{obs} / s^{-1}
2.09×10^{-4}	4.73×10^{-6}	2.04
4.19×10^{-4}		3.09
5.23×10^{-4}		3.60
6.28×10^{-4}		4.14
7.33×10^{-4}		4.59
$k_2 = 4.90 \times 10^3$ $M^{-1} \cdot s^{-1}$		

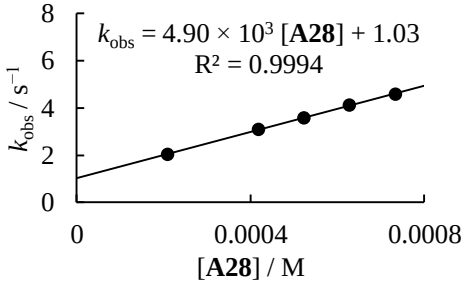

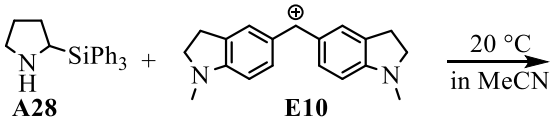

A28 E10

Table 178. Kinetics of the reaction of **A28** with **E10** (stopped-flow method, detection at 616 nm)

[**A28**] / M	[**E10**] / M	k_{obs} / s^{-1}
2.37×10^{-4}	5.77×10^{-6}	10.1
3.55×10^{-4}		14.7
4.73×10^{-4}		19.9
7.10×10^{-4}		2.91
8.28×10^{-4}		3.48
$k_2 = 4.14 \times 10^4$ $M^{-1} \cdot s^{-1}$		

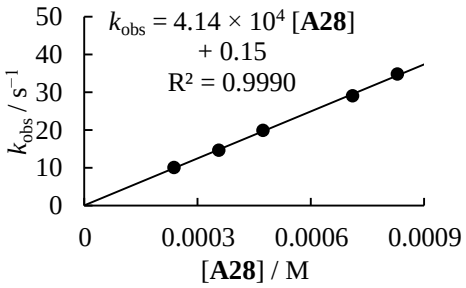

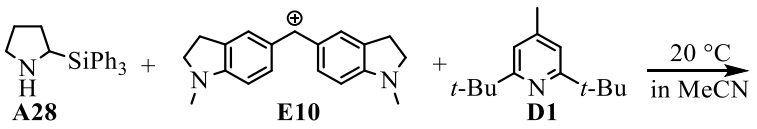

A28 **E10** **D1**

Table 179. Kinetics of the reaction of **A28** with **E10** and **D1** ([**D1**] = 2.57 mmol·L^{-1}, stopped-flow method, detection at 616 nm)

[**A28**] / M	[**E10**] / M	k_{obs} / s^{-1}
6.98×10^{-5}	5.49×10^{-6}	3.11
1.40×10^{-4}		5.34
2.09×10^{-4}		8.50
2.79×10^{-4}		1.10×10^{1}
3.49×10^{-4}		1.41×10^{1}
4.19×10^{-4}		1.67×10^{1}
$k_2 = 3.96 \times 10^{4}$ M^{-1}·s^{-1}		

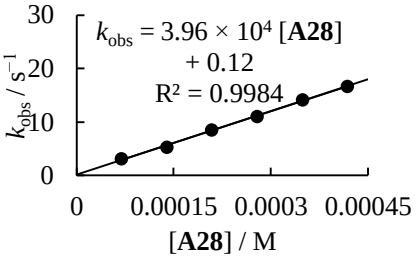

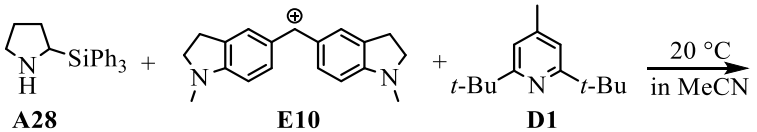

A28 **E10** **D1**

Table 180. Kinetics of the reaction of **A28** with **E10** and **D1** ([**D1**] = 5.13 mmol·L^{-1}, stopped-flow method, detection at 616 nm)

[**A28**] / M	[**E10**] / M	k_{obs} / s^{-1}
6.98×10^{-5}	5.49×10^{-6}	2.67
1.40×10^{-4}		5.26
2.09×10^{-4}		8.34
2.79×10^{-4}		1.10×10^{1}
3.49×10^{-4}		1.37×10^{1}
4.89×10^{-4}		1.95×10^{1}
$k_2 = 4.02 \times 10^{4}$ M^{-1}·s^{-1}		

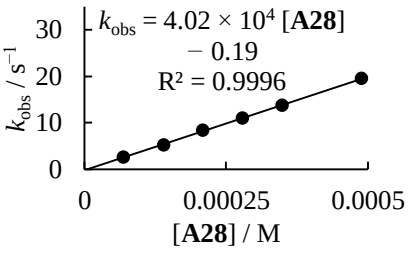

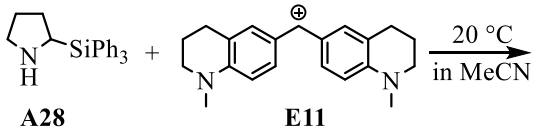

A28 **E11**

Table 181. Kinetics of the reaction of **A28** with **E11** (stopped-flow method, detection at 620 nm)

[**A28**] / M	[**E11**] / M	k_{obs} / s^{-1}
1.49×10^{-4}	5.10×10^{-6}	9.28
2.23×10^{-4}		1.43×10^{1}
2.97×10^{-4}		1.98×10^{1}
3.72×10^{-4}		2.56×10^{1}
4.46×10^{-4}		3.07×10^{1}
$k_2 = 7.29 \times 10^{4}$ M^{-1}·s^{-1}		

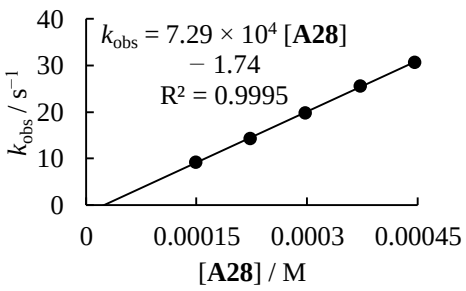

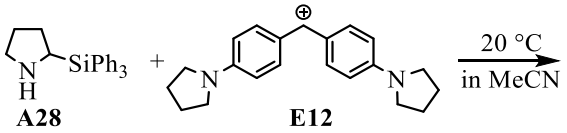

A28 **E12**

Table 182. Kinetics of the reaction of **A28** with **E12** (stopped-flow method, detection at 612 nm)

[**A28**] / M	[**E12**] / M	k_{obs} / s^{-1}
7.44×10^{-5}	5.61×10^{-6}	1.03×10^{1}
1.16×10^{-4}		1.54×10^{1}
1.49×10^{-4}		2.02×10^{1}
1.86×10^{-4}		2.70×10^{1}
2.23×10^{-4}		3.34×10^{1}
2.60×10^{-4}		3.94×10^{1}
$k_2 = 1.60 \times 10^{5}$ $M^{-1} \cdot s^{-1}$		

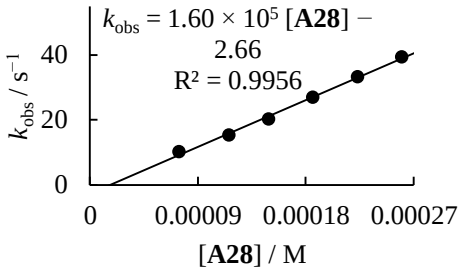

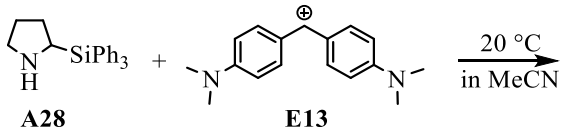

A28 **E13**

Table 183. Kinetics of the reaction of **A28** with **E13** (stopped-flow method, detection at 605 nm)

[**A28**] / M	[**E13**] / M	k_{obs} / s^{-1}
5.95×10^{-5}	5.88×10^{-6}	3.54×10^{1}
8.92×10^{-5}		5.67×10^{1}
1.19×10^{-4}		7.55×10^{1}
1.49×10^{-4}		9.79×10^{1}
1.78×10^{-4}		1.21×10^{2}
2.08×10^{-4}		1.41×10^{2}
$k_2 = 7.15 \times 10^{5}$ $M^{-1} \cdot s^{-1}$		

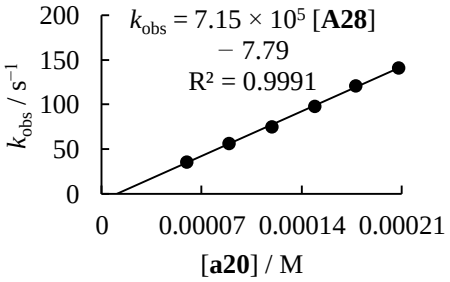

Table 184. Determination of the parameters N and s_N for **A28** in acetonitrile

Electrophile	E	k_2 / $M^{-1} \cdot s^{-1}$
E9	−9.45	4.90×10^{3}
E10	−8.76	3.96×10^{4}
E11	−8.22	7.29×10^{4}
E12	−7.69	1.60×10^{5}
E13	−7.02	7.15×10^{5}
$N = 14.00$ $s_N = 0.84$		

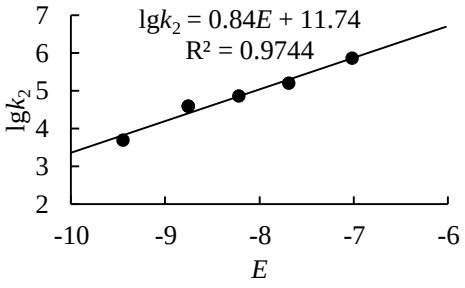

(*S*)-5-Benzyl-2,2,3-trimethylimidazolidin-4-one (A29)

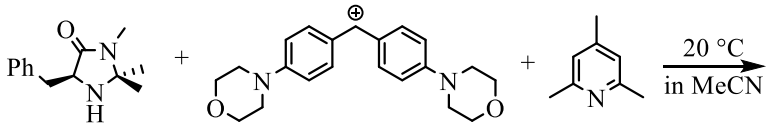

A29 **E15** **D2**

Table 185. Kinetics of the reaction of **A29** with **E15** and **D2** ([**D2**] = 2.80 mM, conventional UV-Vis method, detection at 612 nm)

[**A29**] / M	[**E15**] / M	k_{obs} / s^{-1}
3.03×10^{-4}		2.71×10^{-3}
6.05×10^{-4}		3.47×10^{-3}
9.08×10^{-4}	2.17×10^{-5}	4.42×10^{-3}
1.21×10^{-3}		5.37×10^{-3}
1.51×10^{-3}		6.27×10^{-3}
	$k_2 = 2.99\ M^{-1} \cdot s^{-1}$	

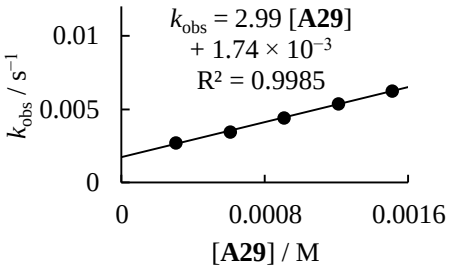

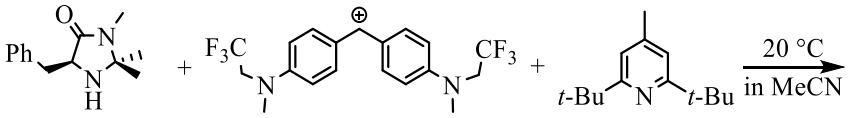

A29 **E17** **D1**

Table 186. Kinetics of the reaction of **A29** with **E17** and **D1** ([**D1**] = 0.966 mM, conventional UV-Vis method, detection at 586 nm)

[**A29**] / M	[**E17**] / M	k_{obs} / s^{-1}
1.24×10^{-4}	1.01×10^{-5}	7.07×10^{-4}
2.48×10^{-4}	1.01×10^{-5}	1.67×10^{-3}
4.96×10^{-4}	1.26×10^{-5}	4.89×10^{-3}
7.42×10^{-4}	1.26×10^{-5}	9.38×10^{-3}
9.91×10^{-4}	1.26×10^{-5}	1.56×10^{-2}
1.24×10^{-3}	1.01×10^{-5}	2.25×10^{-2}

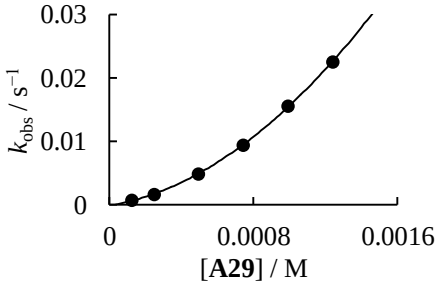

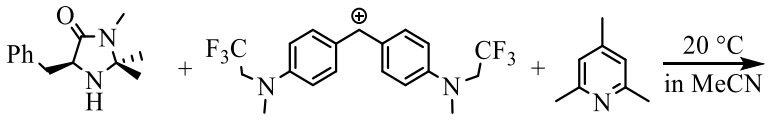

A29 **E17** **D2**

Table 187. Kinetics of the reaction of **A29** with **E17** and **D2** ([**D2**] = 1.18 mM, conventional UV-Vis method, detection at 586 nm)

[**A29**] / M	[**E17**] / M	k_{obs} / s^{-1}
1.44×10^{-4}	1.33×10^{-5}	6.91×10^{-3}
2.87×10^{-4}	1.33×10^{-5}	1.46×10^{-2}
4.31×10^{-4}	1.33×10^{-5}	3.10×10^{-2}
7.19×10^{-4}	1.33×10^{-5}	6.45×10^{-2}

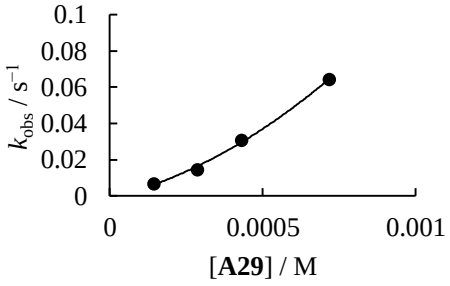

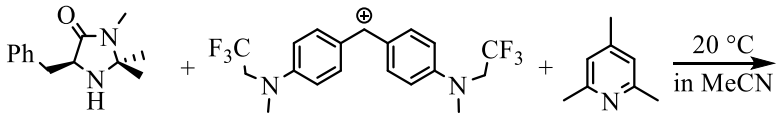

A29 **E17** **D2**

Table 188. Kinetics of the reaction of **A29** with **E17** and **D2** ([**D2**] = 2.33 mM, conventional UV-Vis method, detection at 586 nm)

[**A29**] / M	[**E17**] / M	k_{obs} / s^{-1}
1.42×10^{-4}	1.33×10^{-5}	1.75×10^{-2}
2.85×10^{-4}		3.51×10^{-2}
4.27×10^{-4}		5.05×10^{-2}
5.70×10^{-4}		6.96×10^{-2}
$k_2 = 1.20 \times 10^{2}$ $M^{-1} \cdot s^{-1}$		

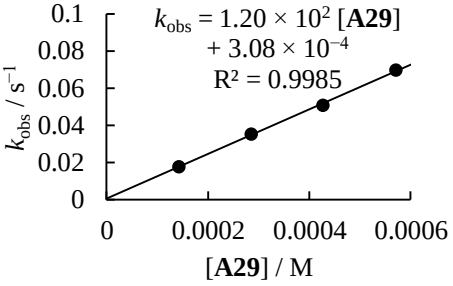

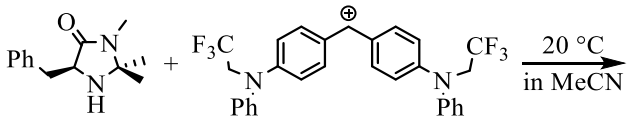

A29 **E18**

Table 189. Kinetics of the reaction of **A29** with **E18** (conventional UV-Vis method, detection at 592 nm)

[**A29**] / M	[**E18**] / M	k_{obs} / s^{-1}
8.99×10^{-5}	8.10×10^{-6}	1.32×10^{-2}
1.33×10^{-4}	7.98×10^{-6}	1.61×10^{-2}
1.77×10^{-4}	7.95×10^{-6}	2.50×10^{-2}
2.18×10^{-4}	7.84×10^{-6}	3.36×10^{-2}
2.60×10^{-4}	7.81×10^{-6}	4.58×10^{-2}
2.97×10^{-4}	1.02×10^{-5}	5.46×10^{-2}

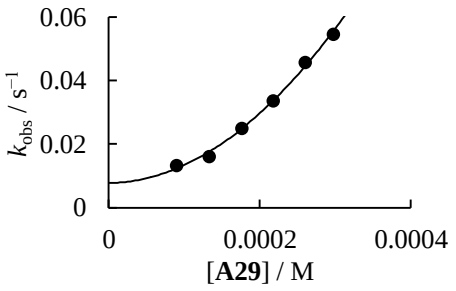

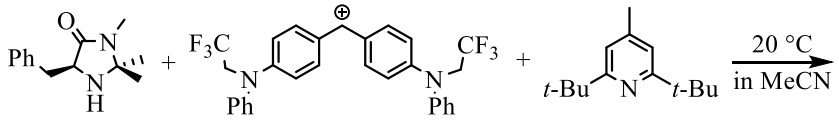

A29 **E18** **D1**

Table 190. Kinetics of the reaction of **A29** with **E18** and **D1** ([**D1**] = 0.99 mM, conventional UV-Vis method, detection at 586 nm)

[**A29**] / M	[**E18**] / M	k_{obs} / s^{-1}
1.29×10^{-4}	1.17×10^{-5}	1.79×10^{-2}
1.95×10^{-4}	1.17×10^{-5}	4.24×10^{-2}
2.60×10^{-4}	1.18×10^{-5}	6.68×10^{-2}
3.24×10^{-4}	1.17×10^{-5}	8.99×10^{-2}
3.89×10^{-4}	1.76×10^{-5}	1.17×10^{-1}

$k_2 = 3.79 \times 10^2$ $M^{-1} \cdot s^{-1}$

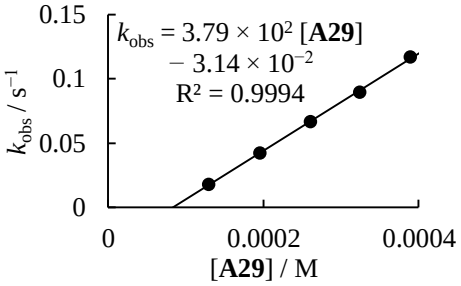

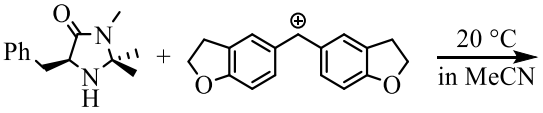

A29 **E19**

Table 191. Kinetics of the reaction of **A29** with **E19** (stopped-flow method, detection at 523 nm)

[**A29**] / M	[**E19**] / M	k_{obs} / s^{-1}
9.62×10^{-4}	9.61×10^{-6}	1.15×10^{1}
1.28×10^{-3}		1.77×10^{1}
1.60×10^{-3}		2.48×10^{1}
1.92×10^{-3}		3.21×10^{1}

$k_2 = 2.16 \times 10^4$ $M^{-1} \cdot s^{-1}$

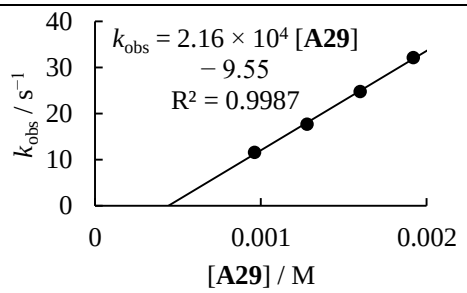

Table 192. Determination of the parameters N and s_N for **A29** in acetonitrile

Electrophile	E	k_2 / $M^{-1} \cdot s^{-1}$
E15	−5.53	2.99
E17	−3.85	1.20×10^2
E18	−3.14	3.79×10^2
E19	−1.36	2.16×10^4

$N = 6.04$ $s_N = 0.92$

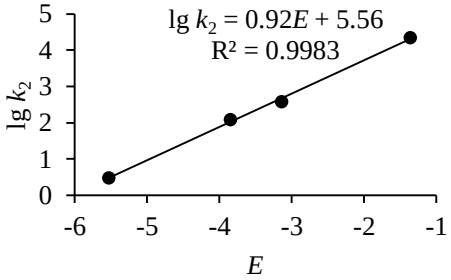

(2*S*,5*S*)-5-Benzyl-2-(tert-butyl)-3-methylimidazolidin-4-one (A30)

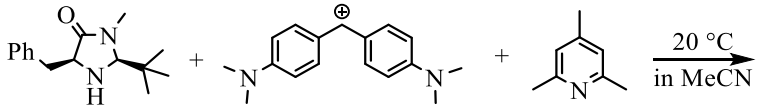

A30 **E13** **D2**

Table 193. Kinetics of the reaction of **A30** with **E13** and **D2** ([**D2**] = 11.4 mmol·L^{-1}, conventional UV-Vis method, detection at 605 nm)

[**A30**] / M	[**E13**] / M	k_{obs} / s^{-1}
3.18×10^{-4}	1.86×10^{-5}	1.44×10^{-5}
5.44×10^{-4}		1.76×10^{-5}
9.13×10^{-4}		2.25×10^{-5}
1.56×10^{-3}		3.10×10^{-5}
$k_2 = 1.33 \times 10^{-2}$ M^{-1}·s^{-1}		

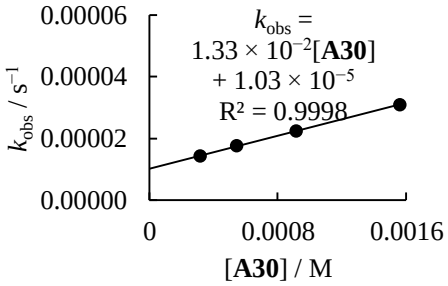

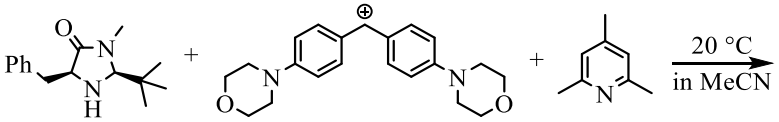

A30 **E15** **D2**

Table 194. Kinetics of the reaction of **A30** with **E15** and **D2** ([**D2**] = 3.25 mmol·L^{-1}, conventional UV-Vis method, detection at 612 nm)

[**A30**] / M	[**E13**] / M	k_{obs} / s^{-1}
1.97×10^{-4}	1.86×10^{-5}	6.42×10^{-4}
3.04×10^{-4}	2.24×10^{-5}	7.74×10^{-4}
3.94×10^{-4}	1.86×10^{-5}	8.95×10^{-4}
7.88×10^{-4}	2.24×10^{-5}	1.45×10^{-3}
$k_2 = 1.38$ M^{-1}·s^{-1}		

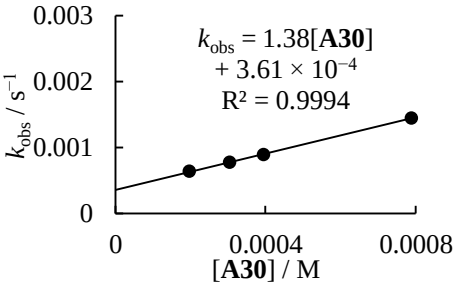

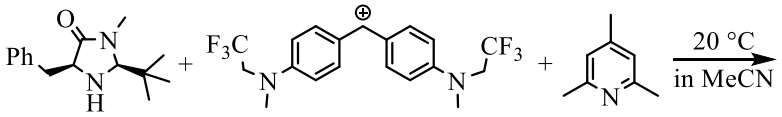

A30 **E17** **D2**

Table 195. Kinetics of the reaction of **A30** with **E17** and **D2** ([**D2**] = 2.71 mmol·L^{-1}, conventional UV-Vis method, detection at 586 nm)

[**A30**] / M	[**E13**] / M	k_{obs} / s^{-1}
1.56×10^{-4}		3.06×10^{-3}
2.35×10^{-4}		5.46×10^{-3}
3.12×10^{-4}	1.53×10^{-5}	9.39×10^{-3}
3.88×10^{-4}		1.19×10^{-2}
6.24×10^{-4}		2.13×10^{-2}
$k_2 = 3.94 \times 10^{1}$ M^{-1}·s^{-1}		

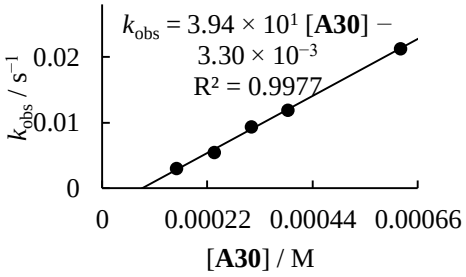

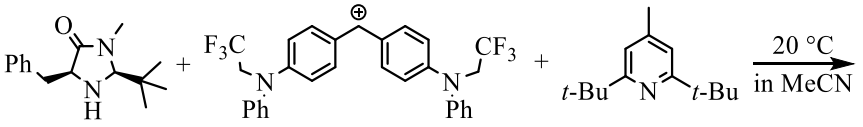

A30 **E18** **D1**

Table 196. . Kinetics of the reaction of **A30** with **E18** and **D1** ([**D1**] = 1.37 mmol·L^{-1}, stopped-flow method, detection at 592 nm)

[**A30**] / M	[**E13**] / M	k_{obs} / s^{-1}
1.36×10^{-4}		4.39×10^{-2}
2.73×10^{-4}		9.28×10^{-2}
4.09×10^{-4}	1.04×10^{-5}	1.46×10^{-1}
5.46×10^{-4}		2.13×10^{-1}
6.82×10^{-4}		2.73×10^{-1}
$k_2 = 4.24 \times 10^{2}$ M^{-1}·s^{-1}		

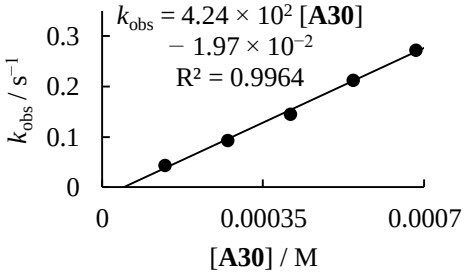

Table 197. Determination of the parameters N and s_N for **A30** in acetonitrile

Electrophile	E	k_2 / M^{-1}·s^{-1}
E13	−7.02	1.33×10^{-2}
E15	−5.53	1.38
E17	−3.85	3.94×10^{1}
E19	−3.14	4.24×10^{2}
$N = 5.44$ $s_N = 1.12$		

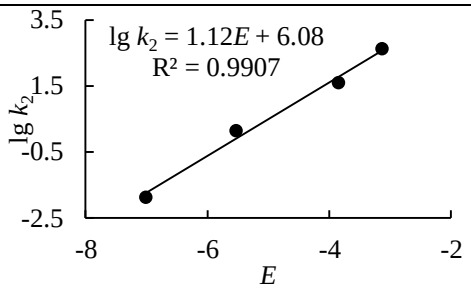

(2*S*,5*S*)-5-Benzyl-3-methyl-2-(5-methylfuran-2-yl)imidazolidin-4-one (A31)

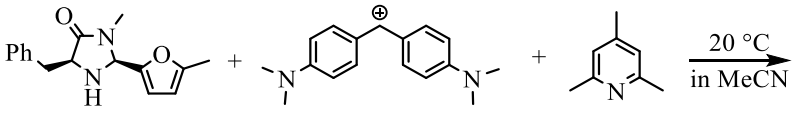

A31 **E13** **D2**

Table 198. Kinetics of the reaction of **A31** with **E13** and **D2** ([**D2**] = 11.3 mM, conventional UV-Vis method, detection at 586 nm)

[**A31**] / M	[**E13**] / M	k_{obs} / s^{-1}
2.07×10^{-4}	1.84×10^{-5}	5.09×10^{-3}
4.15×10^{-4}		9.76×10^{-3}
6.23×10^{-4}		1.60×10^{-2}
8.31×10^{-4}		2.16×10^{-2}
$k_2 = 2.68 \times 10^{1}$ $M^{-1} \cdot s^{-1}$		

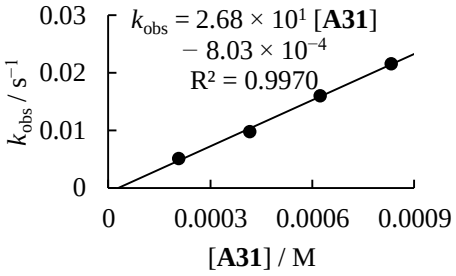

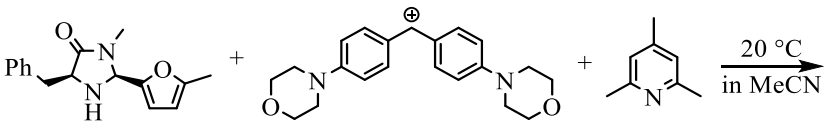

A31 **E15** **D2**

Table 199. Kinetics of the reaction of **A31** with **E15** and **D2** ([**D2**] = 2.99 mM, stopped-flow method, detection at 612 nm)

[**A31**] / M	[**E15**] / M	k_{obs} / s^{-1}
1.47×10^{-4}	9.49×10^{-6}	1.67×10^{-1}
2.94×10^{-4}		3.28×10^{-1}
4.41×10^{-4}		5.05×10^{-1}
5.88×10^{-4}		7.31×10^{-1}
7.35×10^{-4}		9.40×10^{-1}
$k_2 = 1.33 \times 10^{3}$ $M^{-1} \cdot s^{-1}$		

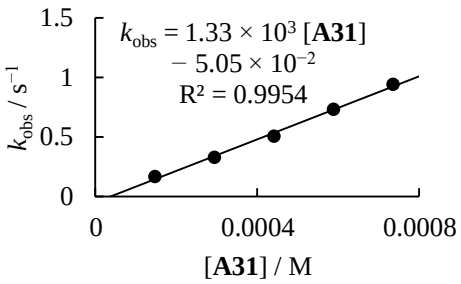

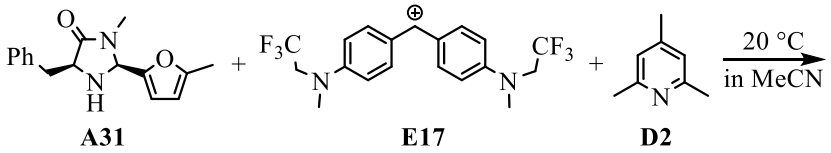

A31 **E17** **D2**

Table 200. Kinetics of the reaction of **A31** with **E17** and **D2** ([**D2**] = 1.98 mM, stopped-flow method, detection at 586 nm)

[**A31**] / M	[**E17**] / M	k_{obs} / s^{-1}
9.80×10^{-5}		1.18
1.96×10^{-4}		2.34
2.94×10^{-4}	9.45×10^{-6}	4.25
3.92×10^{-4}		5.70
4.90×10^{-4}		7.51
$k_2 = 1.63 \times 10^4$ $M^{-1} \cdot s^{-1}$		

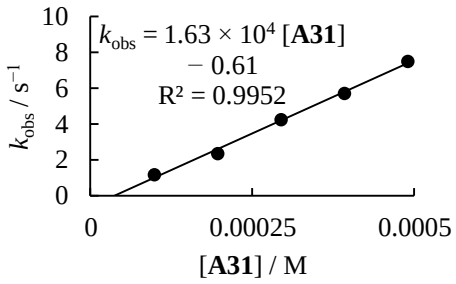

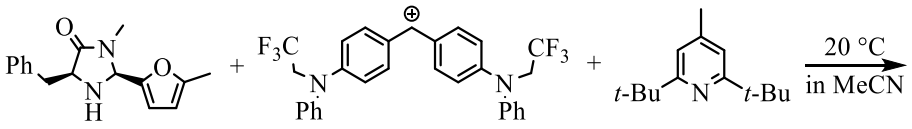

A31 **E18** **D1**

Table 201. Kinetics of the reaction of **A31** with **E18** and **D1** ([**D1**] = 1.21 mM, stopped-flow method, detection at 592 nm)

[**A31**] / M	[**E18**] / M	k_{obs} / s^{-1}
1.11×10^{-4}		1.04×10^1
1.66×10^{-4}		1.96×10^1
2.22×10^{-4}	9.60×10^{-6}	2.32×10^1
3.33×10^{-4}		3.53×10^1
4.44×10^{-4}		4.92×10^1
5.55×10^{-4}		5.99×10^1
$k_2 = 1.10 \times 10^5$ $M^{-1} \cdot s^{-1}$		

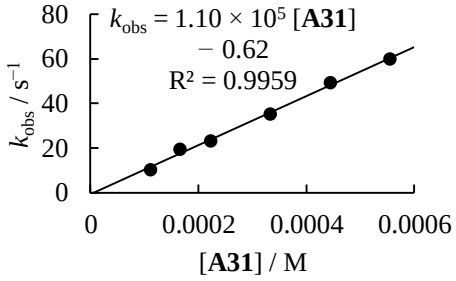

Table 202. Determination of the parameters N and s_N for **A31** in acetonitrile

Electrophile	E	k_2 / $M^{-1} \cdot s^{-1}$
E13	−7.02	2.68×10^1
E15	−5.53	1.33×10^3
E17	−3.85	1.63×10^4
E18	−3.14	1.10×10^5
$N = 8.76$ $s_N = 0.89$		

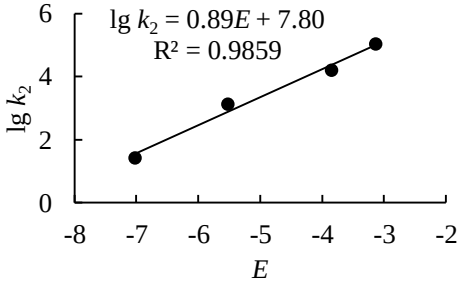

(2*R*,5*S*)-5-Benzyl-3-methyl-2-(5-methylfuran-2-yl)imidazolidin-4-one (A32)

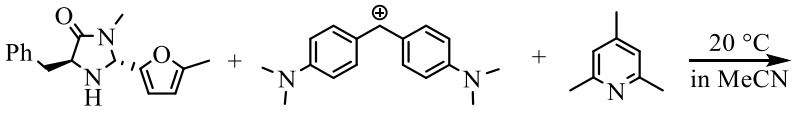

A32 **E13** **D2**

Table 203. Kinetics of the reaction of **A32** with **E13** and **D2** ([**D2**] = 7.68 mM, conventional UV-Vis method, detection at 605 nm)

[**A32**] / M	[**E13**] / M	k_{obs} / s^{-1}
1.98×10^{-4}	1.83×10^{-5}	5.24×10^{-4}
3.97×10^{-4}		7.64×10^{-4}
5.57×10^{-4}		1.17×10^{-3}
7.16×10^{-4}		1.40×10^{-3}
$k_2 = 1.76\ M^{-1} \cdot s^{-1}$		

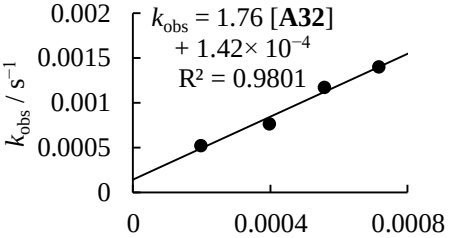

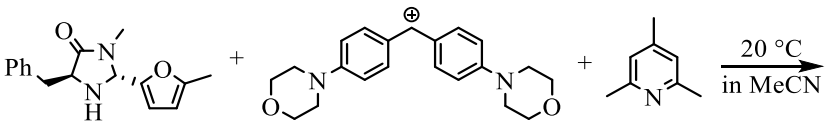

A32 **E15** **D2**

Table 204. Kinetics of the reaction of **A32** with **E15** and **D2** ([**D2**] = 3.01 mM, conventional UV-Vis method, detection at 612 nm)

[**A32**] / M	[**E15**] / M	k_{obs} / s^{-1}
2.15×10^{-4}	2.06×10^{-5}	3.84×10^{-2}
3.59×10^{-4}		5.69×10^{-2}
5.02×10^{-4}		8.09×10^{-2}
6.46×10^{-4}		9.18×10^{-2}
$k_2 = 1.28 \times 10^2\ M^{-1} \cdot s^{-1}$		

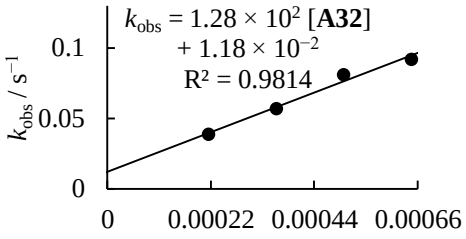

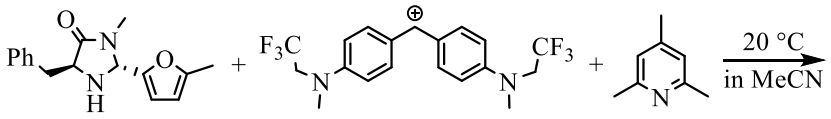

A32 **E17** **D2**

Table 205. Kinetics of the reaction of **A32** with **E17** and **D2** ([**D2**] = 1.98 mM, stopped-flow method, detection at 586 nm)

[**A32**] / M	[**E17**] / M	k_{obs} / s^{-1}
1.97×10^{-4}	1.01×10^{-5}	3.48×10^{-1}
2.75×10^{-4}		4.90×10^{-1}
4.32×10^{-4}		9.14×10^{-1}
5.11×10^{-4}		1.11

$k_2 = 2.48 \times 10^3$ $M^{-1} \cdot s^{-1}$

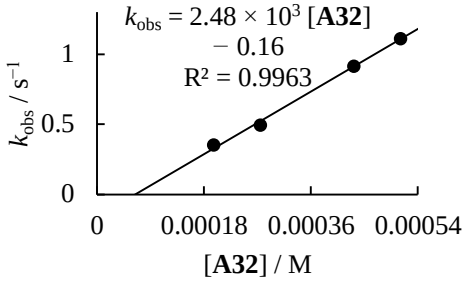

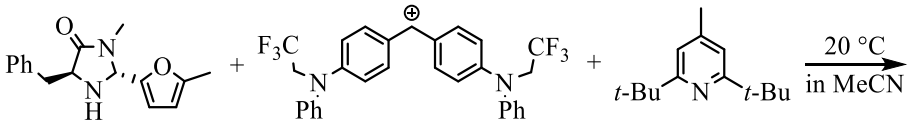

A32 **E18** **D1**

Table 206. Kinetics of the reaction of **A32** with **E18** and **D2** ([**D2**] = 1.33 mM, stopped-flow method, detection at 592 nm)

[**A32**] / M	[**E18**] / M	k_{obs} / s^{-1}
1.18×10^{-4}	1.02×10^{-5}	1.62
1.97×10^{-4}		3.00
2.75×10^{-4}		4.77
3.54×10^{-4}		6.21
4.32×10^{-4}		7.45

$k_2 = 1.89 \times 10^4$ $M^{-1} \cdot s^{-1}$

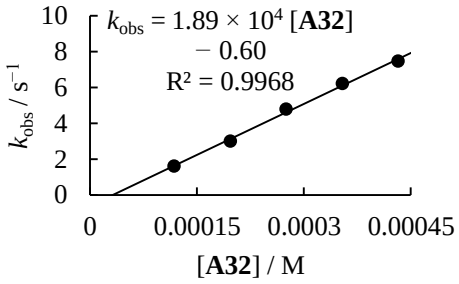

Table 207. Determination of the parameters N and s_N for **A32** in acetonitrile

Electrophile	E	k_2 / $M^{-1} \cdot s^{-1}$
E13	−7.02	1.76
E15	−5.53	1.28×10^2
E17	−3.85	2.48×10^3
E18	−3.14	1.89×10^4

$N = 7.39$ $s_N = 1.00$

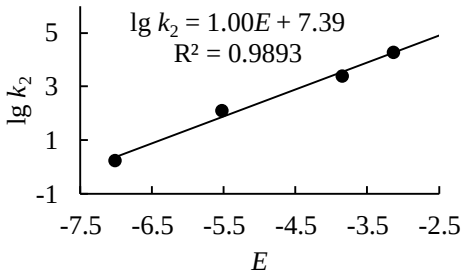

7.2.3 Kinetics in Dichloromethane

Pyrrolidine in CH_2Cl_2 (A2)

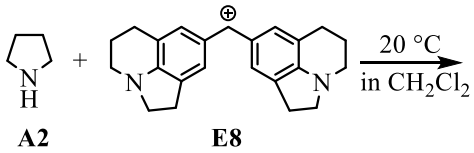

A2 E8

Table 208. Kinetics of the reaction of **A2** with **E8** in dichloromethane (stopped-flow method, detection at 639 nm)

[**A2**] / M	[**E8**] / M	k_{obs} / s^{-1}
8.33×10^{-5}	5.94×10^{-6}	7.16
1.25×10^{-4}		8.17
1.67×10^{-4}		9.43
2.08×10^{-4}		1.07×10^{1}
2.50×10^{-4}		1.28×10^{1}

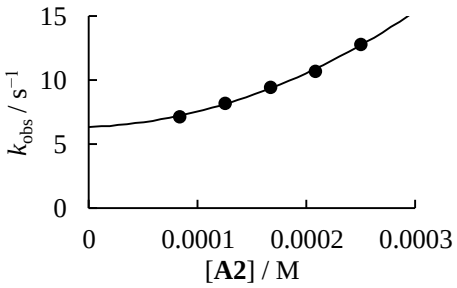

[**A2**]^2 / mol^2· L^{-2}	[**E8**] / M	k_{obs} / s^{-1}
6.34×10^{-9}	5.94×10^{-6}	7.16
1.56×10^{-8}		8.17
2.79×10^{-8}		9.43
4.33×10^{-8}		1.07×10^{1}
6.25×10^{-8}		1.28×10^{1}

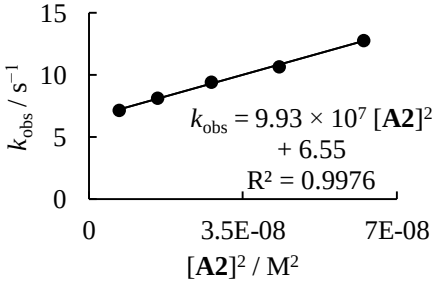

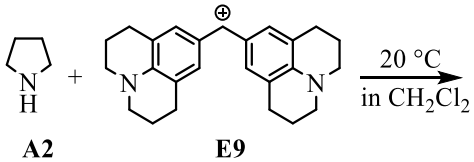

A2 E9

Table 209. Kinetics of the reaction of **A2** with **E9** in dichloromethane (stopped-flow method, detection at 643 nm)

[**A2**] / M	[**E9**] / M	k_{obs} / s^{-1}
8.33×10^{-5}	4.00×10^{-6}	1.42×10^{1}
1.25×10^{-4}		1.70×10^{1}
1.67×10^{-4}		2.14×10^{1}
2.08×10^{-4}		2.64×10^{1}
2.50×10^{-4}		3.32×10^{1}

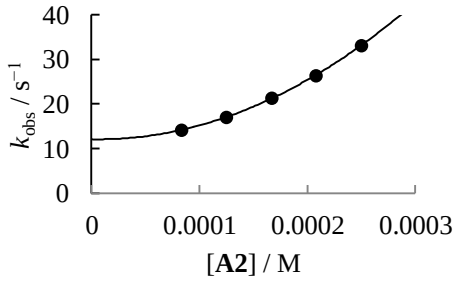

[**A2**]^2 / mol^2· L^{-2}	[**E9**] / M	k_{obs} / s^{-1}
6.34×10^{-9}	4.00×10^{-6}	1.42×10^{1}
1.56×10^{-8}		1.70×10^{1}
2.79×10^{-8}		2.14×10^{1}
4.33×10^{-8}		2.64×10^{1}

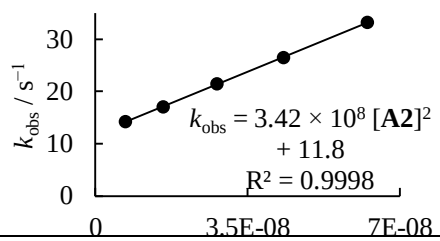

6.25×10^{-8}	3.32×10^{1}	

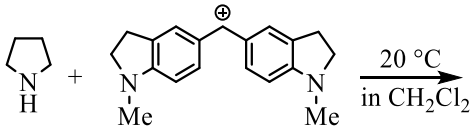

A2 **E10**

Table 210. Kinetics of the reaction of **A2** with **E10** in dichloromethane (stopped-flow method, detection at 625 nm)

[**A2**] / M	[**E9**] / M	k_{obs} / s^{-1}
8.33×10^{-5}	8.19×10^{-6}	2.13×10^{1}
1.25×10^{-4}		3.33×10^{1}
1.67×10^{-4}		4.63×10^{1}
2.08×10^{-4}		5.84×10^{1}
2.50×10^{-4}		7.09×10^{1}

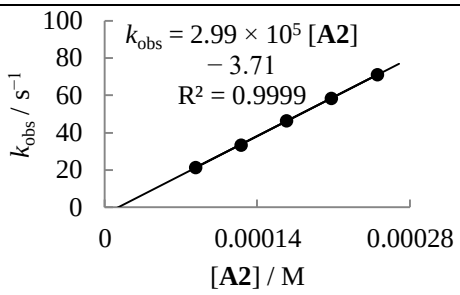

7.3 Experimental Section for pK_{aH} Measurements

General for Titration

The amines **A** and protonated indicators **C**H were stored under an atmosphere of dry argon (glove box). Stock solutions of **A** (or **C**H) were prepared in anhydrous acetonitrile, which was freshly distilled from phosphorus pentoxide.

Diode array spectrophotometers (J&M TIDAS) controlled by Labcontrol Spectacle or TIDASDAQ 3 (v3.8.1) software and connected to Hellma 661.502-QX quartz Suprasil immersion probes (5 mm light path) via fiber optic cables and standard SMA connectors were used for all measurements of equilibrium constants. The temperature of the solutions during the titration was maintained to 20 ± 0.1 °C by using circulating bath cryostats.

For the titrations, a known volume of **C**H stock solutions was injected into a known (by weight) amount of acetonitrile (step 0). Small volumes (V_+) of **A** stock solution were added into the acetonitrile solution to reach the proton transfer equilibrium step by step. In the final step (step f), quantitative deprotonation of **C**H was accomplished by adding an excess amount of DBU dissolved in acetonitrile. TBD was used in step f for the quantitative deprotonation of **C1** (pK_{aH} titration of **A1**) and **A22** (pK_{aH} titration of **A22**$^-$). Pyrrolidine was used in step f for the pK_{aH} titration of **A22**.

During the titrations, the UV-vis spectra of the solutions were recorded. A wavelength, where only the indicator **C**$^-$ absorbs light, was chosen to monitor the reactions by following the changes in the absorbance A of the acetonitrile solutions. The final absorbance A_f was applied to calculate the concentration of the indicator [**C**$^-$] at each step of the titration. Together with known initial concentrations of the amines ([**A**]$_0$) and protonated indicators ([**C**H]$_0$), the equilibrium constants K are described by equation 2 for each step in a titration:

$$K = \frac{[\mathrm{C}^-]^2}{([\mathrm{A}]_0 - [\mathbf{C}^-])([\mathbf{CH}]_0 - [\mathrm{C}^-])} \qquad (2)$$

The pK_{aH} of the colored anion **A22**$^-$ was determined without adding an indicator by direct titration with DBU (pK_{aH} 24.31 in MeCN, from literature[62]). For the pK_{aH} determination of **A18** and **A23**, proton transfer was reversed and solutions of deprotonated indicators [**C3**$^-$] or [**C4**$^-$] and protonated amines [**A18**H$^+$] or [**A23**H$^+$], respectively, were used for the titrations.

Potassium *L*-prolinate (A1)

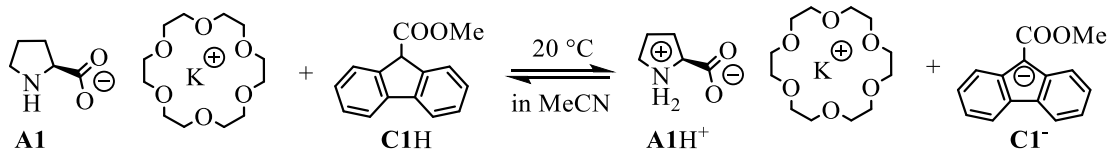

A1 **C1**H **A1**H$^+$ **C1**$^-$

Table 211. Determination of the pK_{aH} for **A1** with **C1**H in acetonitrile at 20 °C (detection at 407 nm). Stock solutions: **A1**K (5.0 mg) and 18-crown-6 (17.3 mg) in 25.0 mL MeCN; **C1**H (13.2 mg) in 10.0 mL MeCN; [TBD] = 6.58×10^{-2} mol L^{-1}. Step 0: 0.900 mL **C1**H stock solution in 19.3 g MeCN.

step	V_+ / mL	V / mL	[**C1**H]$_0$ / M	[**A1**]$_0$ / M	A	[**C1**$^-$] / M	[**C1**H] / M	[**A1**] / M
0	-	25.455	2.08×10^{-4}	0	0	0	2.08×10^{-4}	0
1	0.500	25.955	2.04×10^{-4}	2.51×10^{-5}	0.046	2.48×10^{-5}	1.79×10^{-4}	3.79×10^{-7}
2	1.000	26.455	2.00×10^{-4}	4.93×10^{-5}	0.087	4.66×10^{-5}	1.54×10^{-4}	2.75×10^{-6}
3	1.500	26.955	1.97×10^{-4}	7.26×10^{-5}	0.120	6.45×10^{-5}	1.32×10^{-4}	8.14×10^{-6}
4	2.000	27.455	1.93×10^{-4}	9.51×10^{-5}	0.147	7.92×10^{-5}	1.14×10^{-4}	1.59×10^{-5}
5	2.500	27.955	1.90×10^{-4}	1.17×10^{-4}	0.169	9.08×10^{-5}	9.87×10^{-5}	2.60×10^{-5}
6	3.000	28.455	1.86×10^{-4}	1.38×10^{-4}	0.187	1.01×10^{-4}	8.54×10^{-5}	3.69×10^{-5}
7	3.500	28.955	1.83×10^{-4}	1.58×10^{-4}	0.202	1.09×10^{-4}	7.40×10^{-5}	4.88×10^{-5}
f	-	31.055	1.71×10^{-4}	2.10×10^{-4}	0.317	1.71×10^{-4}	0	2.10×10^{-4}

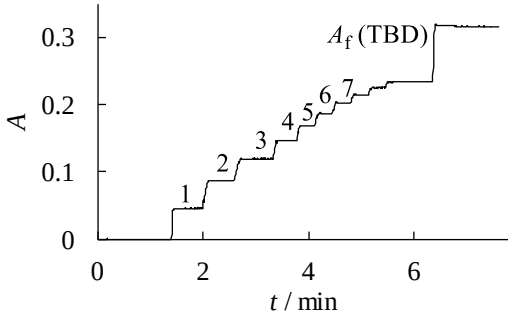

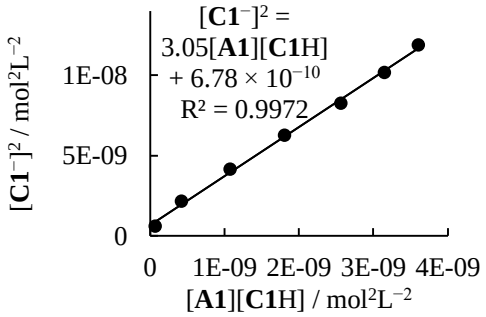

$K = 3.05 \pm 0.07$

Owing to the low solubility of *L*-proline (**A1**H$^+$) in MeCN, only first 7 steps of the titration were used for the determination of the pK_{aH}.

Table 212. Determination of the pK_{aH} for **A1** with **C1**H in acetonitrile at 20 °C (detection at 407 nm). Stock solutions: **A1**K (5.0 mg) and 18-crown-6 (17.3 mg) in 25.0 mL MeCN; **C1**H (13.2 mg) in 10.0 mL MeCN; [TBD] = 6.58×10^{-2} mol L^{-1}. Step 0: 0.700 mL **C1**H stock solution in 19.6 g MeCN.

step	V_+ / mL	V / mL	[**C1**H]$_0$ / M	[**A1**]$_0$ / M	*A*	[**C1**$^-$] / M	[**C1**H] / M	[**A1**] / M
0	-	25.636	1.61×10^{-4}	0	0	0	1.61×10^{-4}	0
1	1.000	26.636	1.55×10^{-4}	4.90×10^{-5}	0.084	4.45×10^{-5}	1.10×10^{-4}	4.53×10^{-6}
2	1.500	27.136	1.52×10^{-4}	7.22×10^{-5}	0.113	6.02×10^{-5}	9.16×10^{-5}	1.19×10^{-5}
3	2.000	27.636	1.49×10^{-4}	9.45×10^{-5}	0.137	7.28×10^{-5}	7.63×10^{-5}	2.17×10^{-5}
4	2.500	28.136	1.46×10^{-4}	1.16×10^{-4}	0.155	8.26×10^{-5}	6.38×10^{-5}	3.33×10^{-5}
5	3.000	28.636	1.44×10^{-4}	1.37×10^{-4}	0.170	9.03×10^{-5}	5.35×10^{-5}	4.64×10^{-5}
f	-	31.136	1.32×10^{-4}	2.10×10^{-4}	0.248	1.32×10^{-4}	0	2.10×10^{-4}

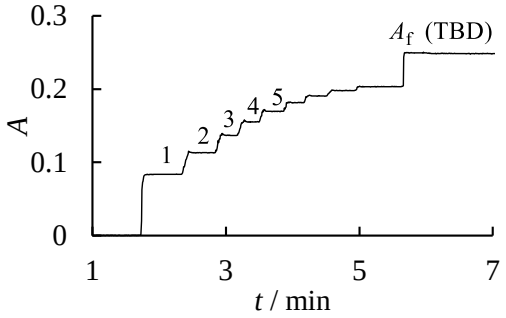

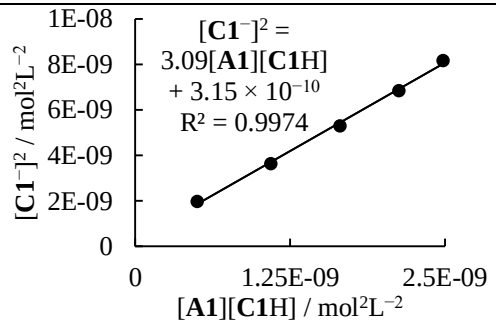

K = 3.09 ± 0.09

Owing to the low solubility of *L*-proline (**A1**H$^+$) in MeCN, only first 5 titrations were used for the determination of the pK_{aH}.

$$\bar{K} = 3.07 \pm 0.02$$

$$pK_{aH}(\mathbf{A1}) = 24.02$$

Pyrrolidine (A2)

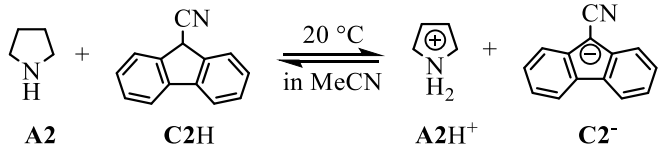

A2 **C2**H $A2H^+$ $C2^-$

Table 213. Determination of the pK_{aH} for **A2** with **C2**H in acetonitrile at 20 °C (detection at 420 nm). Stock solutions: **A2** (16.8 mg) in 10.0 mL MeCN; **C2**H (15.2 mg) in 10.0 mL MeCN; [DBU] = 2.52×10^{-2} mol L^{-1}. Step 0: 0.900 mL **C2**H stock solution in 24.4 g MeCN.

step	V_+ / mL	V / mL	[**C2**H]$_0$ / M	[**A2**]$_0$ / M	*A*	[$\mathbf{C2}^-$] / M	[**C2**H] / M	[**A2**] / M
0	-	31.943	2.24×10^{-4}	0	0.000	0	2.239×10^{-4}	0
1	0.250	32.193	2.22×10^{-4}	1.83×10^{-4}	0.034	3.04×10^{-5}	1.918×10^{-4}	1.53×10^{-4}
2	0.500	32.443	2.21×10^{-4}	3.64×10^{-4}	0.048	4.29×10^{-5}	1.776×10^{-4}	3.21×10^{-4}
3	0.750	32.693	2.19×10^{-4}	5.42×10^{-4}	0.057	5.16×10^{-5}	1.672×10^{-4}	4.90×10^{-4}
4	1.000	32.943	2.17×10^{-4}	7.17×10^{-4}	0.065	5.85×10^{-5}	1.587×10^{-4}	6.59×10^{-4}
5	1.250	33.193	2.16×10^{-4}	8.90×10^{-4}	0.071	6.42×10^{-5}	1.513×10^{-4}	8.25×10^{-4}
6	1.500	33.443	2.14×10^{-4}	1.06×10^{-3}	0.077	6.91×10^{-5}	1.448×10^{-4}	9.90×10^{-4}
f	2.200	34.143	2.10×10^{-4}	1.04×10^{-3}	0.232	2.10×10^{-4}	0	1.04×10^{-3}

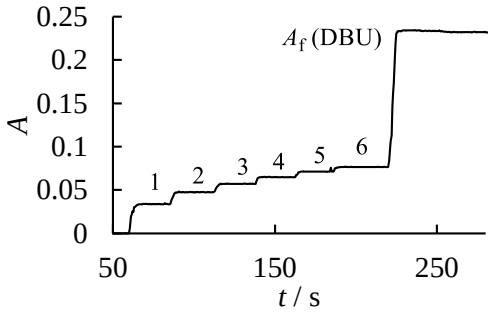

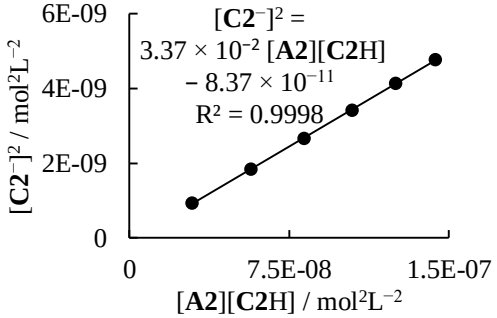

$K = (3.37 \pm 0.02) \times 10^{-2}$

Table 214. Determination of the pK_{aH} for **A2** with **C2**H in acetonitrile at 20 °C (detection at 420 nm). Stock solutions: **A2** (16.8 mg) in 10.0 mL MeCN; **C2**H (15.2 mg) in 10.0 mL MeCN; [DBU] = 2.52 × 10^{-2} mol L^{-1}. Step 0: 0.900 mL **C2**H stock solution in 21.6 g MeCN.

step	V_+ / mL	V / mL	[**C2**H]$_0$ / M	[**A2**]$_0$ / M	*A*	[**C2**$^-$] / M	[**C2**H] / M	[**A2**] / M
0	-	28.381	2.52 × 10^{-4}	0	0	0	2.52 × 10^{-4}	0
1	0.250	28.631	2.50 × 10^{-4}	2.06 × 10^{-4}	0.036	3.38 × 10^{-5}	2.16 × 10^{-4}	1.72 × 10^{-4}
2	0.500	28.881	2.48 × 10^{-4}	4.09 × 10^{-4}	0.051	4.75 × 10^{-5}	2.00 × 10^{-4}	3.61 × 10^{-4}
3	0.750	29.131	2.46 × 10^{-4}	6.08 × 10^{-4}	0.062	5.74 × 10^{-5}	1.88 × 10^{-4}	5.51 × 10^{-4}
4	1.000	29.381	2.43 × 10^{-4}	8.04 × 10^{-4}	0.070	6.51 × 10^{-5}	1.78 × 10^{-4}	7.39 × 10^{-4}
5	1.250	29.631	2.41 × 10^{-4}	9.96 × 10^{-4}	0.077	7.14 × 10^{-5}	1.70 × 10^{-4}	9.25 × 10^{-4}
6	1.500	29.881	2.39 × 10^{-4}	1.19 × 10^{-3}	0.083	7.69 × 10^{-5}	1.62 × 10^{-4}	1.11 × 10^{-3}
f	2.200	30.581	2.34 × 10^{-4}	1.16 × 10^{-3}	0.251	2.34 × 10^{-4}	0	1.16 × 10^{-3}

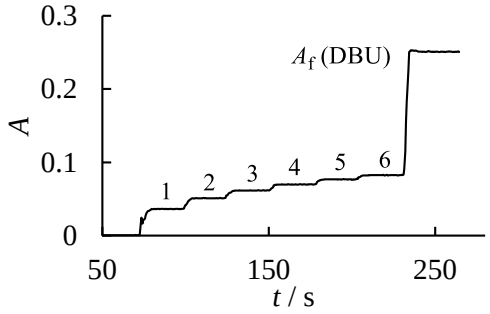

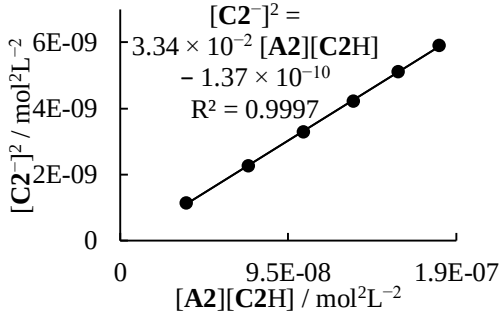

K = (3.34 ± 0.03) × 10^{-2}

$\bar{K}$ = (3.35 ± 0.02) × 10^{-2}

pK_{aH}(**A2**) = 19.89

2-Methylpyrrolidine (A3)

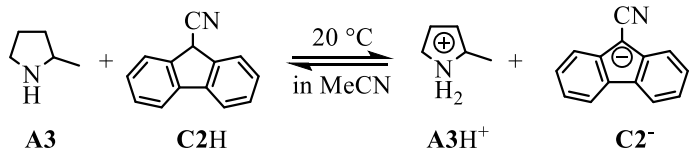

A3 **C2**H **A3**H$^+$ **C2**$^-$

Table 215. Determination of the pK_{aH} for **A3** with **C2**H in acetonitrile at 20 °C (detection at 420 nm). Stock solutions: **A3** (22.0 mg) in 10.0 mL MeCN; **C2**H (11.0 mg) in 10.0 mL MeCN; [DBU] = 4.77×10^{-2} mol L^{-1}. Step 0: 0.900 mL **C2**H stock solution in 20.9 g MeCN.

step	V_+ / mL	V / mL	[**C2**H]$_0$ / M	[**A3**]$_0$ / M	A	[**C2**$^-$] / M	[**C2**H] / M	[**A3**] / M
0	-	27.490	1.88×10^{-4}	0	0	0	1.88×10^{-4}	0
1	0.250	27.740	1.87×10^{-4}	2.33×10^{-4}	0.025	2.29×10^{-5}	1.64×10^{-4}	2.10×10^{-4}
2	0.500	27.990	1.85×10^{-4}	4.62×10^{-4}	0.034	3.20×10^{-5}	1.53×10^{-4}	4.29×10^{-4}
3	0.750	28.240	1.83×10^{-4}	6.86×10^{-4}	0.041	3.85×10^{-5}	1.45×10^{-4}	6.48×10^{-4}
4	1.000	28.490	1.82×10^{-4}	9.07×10^{-4}	0.047	4.35×10^{-5}	1.38×10^{-4}	8.63×10^{-4}
5	1.250	28.740	1.80×10^{-4}	1.12×10^{-3}	0.051	4.75×10^{-5}	1.33×10^{-4}	1.08×10^{-3}
6	1.500	28.990	1.79×10^{-4}	1.34×10^{-3}	0.055	5.08×10^{-5}	1.28×10^{-4}	1.29×10^{-3}
f	1.800	29.290	1.77×10^{-4}	1.32×10^{-3}	0.190	1.77×10^{-4}	0	1.32×10^{-3}

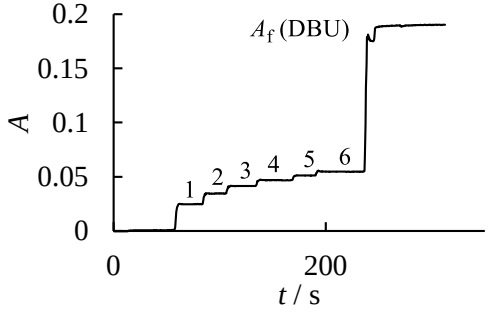

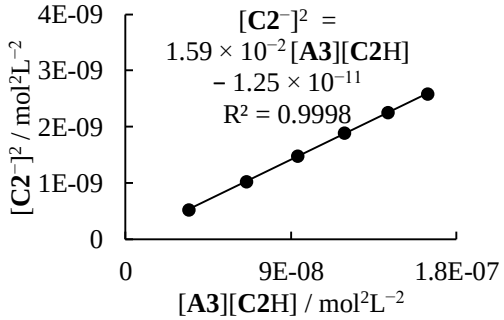

$K = (1.59 \pm 0.01) \times 10^{-2}$

Table 216. Determination of the pK_{aH} for **A3** with **C2**H in acetonitrile at 20 °C (detection at 420 nm). Stock solutions: **A3** (22.0 mg) in 10.0 mL MeCN; **C2**H (11.0 mg) in 10.0 mL MeCN; [DBU] = 4.77×10^{-2} mol L^{-1}. Step 0: 1.000 mL **C2**H stock solution in 22.7 g MeCN.

step	V_+ / mL	V / mL	[**C2**H]$_0$ / M	[**A3**]$_0$ / M	*A*	[**C2**$^-$] / M	[**C2**H] / M	[**A3**] / M
0	-	29.880	1.93×10^{-4}	0	0	0	1.93×10^{-4}	0
1	0.250	30.130	1.91×10^{-4}	2.14×10^{-4}	0.025	2.29×10^{-5}	1.68×10^{-4}	1.91×10^{-4}
2	0.500	30.380	1.89×10^{-4}	4.25×10^{-4}	0.035	3.18×10^{-5}	1.58×10^{-4}	3.93×10^{-4}
3	0.750	30.630	1.88×10^{-4}	6.33×10^{-4}	0.042	3.82×10^{-5}	1.50×10^{-4}	5.94×10^{-4}
4	1.000	30.880	1.86×10^{-4}	8.37×10^{-4}	0.047	4.31×10^{-5}	1.43×10^{-4}	7.94×10^{-4}
5	1.250	31.130	1.85×10^{-4}	1.04×10^{-3}	0.052	4.73×10^{-5}	1.37×10^{-4}	9.90×10^{-4}
6	1.500	31.380	1.83×10^{-4}	1.24×10^{-3}	0.055	5.07×10^{-5}	1.33×10^{-4}	1.18×10^{-3}
f	1.800	31.680	1.82×10^{-4}	1.22×10^{-3}	0.198	1.82×10^{-4}	0	1.22×10^{-3}

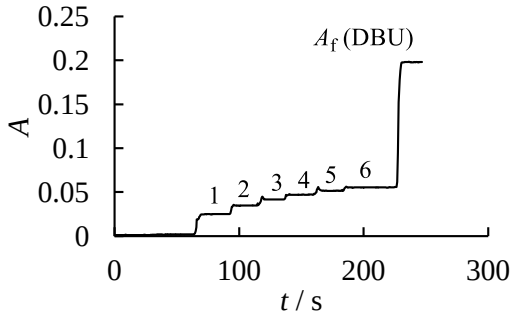

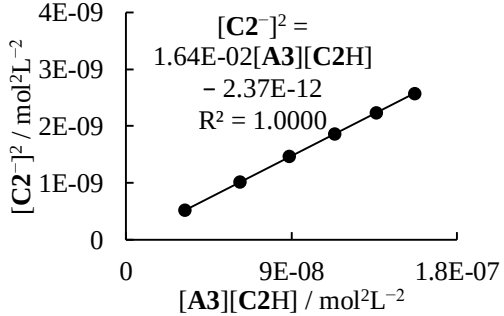

$K = (1.64 \pm 0.00) \times 10^{-2}$

$\bar{K} = (1.62 \pm 0.03) \times 10^{-2}$

pK_{aH}(**A3**) = 19.57

2-Isopropylpyrrolidine (A4)

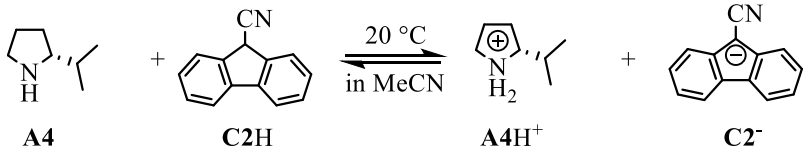

A4 **C2**H $A4H^+$ $C2^-$

Table 217. Determination of the pK_{aH} for **A4** with **C2**H in acetonitrile at 20 °C (detection at 420 nm). Stock solutions: **A4** (17.4 mg) in 10.0 mL MeCN; **C2**H (13.2 mg) in 10.0 mL MeCN; [DBU] = 2.38×10^{-2} mol L^{-1}. Step 0: 0.700 mL **C2**H stock solution in 22.3 g MeCN.

step	V_+ / mL	V / mL	[**C2**H]$_0$ / M	[**A4**]$_0$ / M	*A*	[$\mathbf{C2}^-$] / M	[**C2**H] / M	[**A4**] / M
0	-	29.072	1.66×10^{-4}	0	0	0	1.66×10^{-4}	0
1	0.250	29.322	1.65×10^{-4}	1.31×10^{-4}	0.014	1.24×10^{-5}	1.52×10^{-4}	1.19×10^{-4}
2	0.500	29.572	1.63×10^{-4}	2.60×10^{-4}	0.020	1.75×10^{-5}	1.46×10^{-4}	2.42×10^{-4}
3	0.750	29.822	1.62×10^{-4}	3.87×10^{-4}	0.025	2.12×10^{-5}	1.41×10^{-4}	3.65×10^{-4}
4	1.000	30.072	1.61×10^{-4}	5.11×10^{-4}	0.028	2.42×10^{-5}	1.36×10^{-4}	4.87×10^{-4}
5	1.250	30.322	1.59×10^{-4}	6.34×10^{-4}	0.031	2.67×10^{-5}	1.33×10^{-4}	6.07×10^{-4}
6	1.500	30.572	1.58×10^{-4}	7.54×10^{-4}	0.033	2.88×10^{-5}	1.29×10^{-4}	7.25×10^{-4}
f	1.900	30.972	1.56×10^{-4}	7.44×10^{-4}	0.180	1.56×10^{-4}	0	7.44×10^{-4}

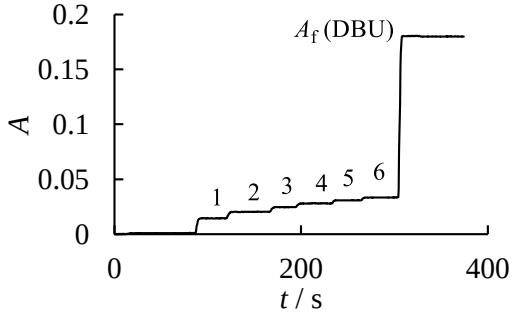

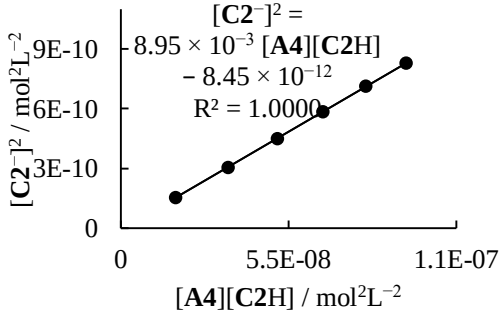

$K = (8.95 \pm 0.02) \times 10^{-3}$

Table 218. Determination of the pK_{aH} for **A4** with **C2**H in acetonitrile at 20 °C (detection at 420 nm). Stock solutions: **A4** (17.4 mg) in 10.0 mL MeCN; **C2**H (13.2 mg) in 10.0 mL MeCN; [DBU] = 2.38×10^{-2} mol L^{-1}. Step 0: 0.800 mL **C2**H stock solution in 22.3 g MeCN.

step	V_+ / mL	V / mL	[**C2**H]$_0$ / M	[**A4**]$_0$ / M	*A*	[**C2**$^-$] / M	[**C2**H] / M	[**A4**] / M
0	-	29.172	1.89×10^{-4}	0	0	0	1.89×10^{-4}	0
1	0.500	29.672	1.86×10^{-4}	2.59×10^{-4}	0.020	1.78×10^{-5}	1.68×10^{-4}	2.41×10^{-4}
2	1.000	30.172	1.83×10^{-4}	5.09×10^{-4}	0.028	2.50×10^{-5}	1.58×10^{-4}	4.84×10^{-4}
3	1.500	30.672	1.80×10^{-4}	7.52×10^{-4}	0.034	3.02×10^{-5}	1.50×10^{-4}	7.21×10^{-4}
4	2.000	31.172	1.77×10^{-4}	9.86×10^{-4}	0.039	3.41×10^{-5}	1.43×10^{-4}	9.52×10^{-4}
5	2.500	31.672	1.74×10^{-4}	1.21×10^{-3}	0.042	3.73×10^{-5}	1.37×10^{-4}	1.18×10^{-3}
f	3.000	32.172	1.72×10^{-4}	1.19×10^{-3}	0.194	1.72×10^{-4}	0	1.19×10^{-3}

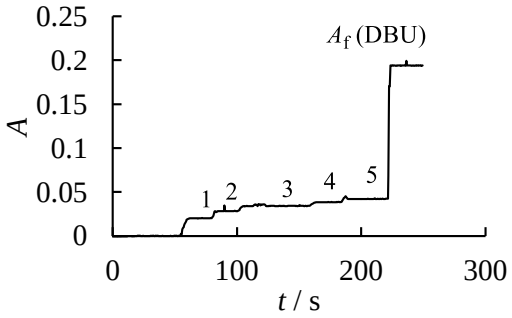

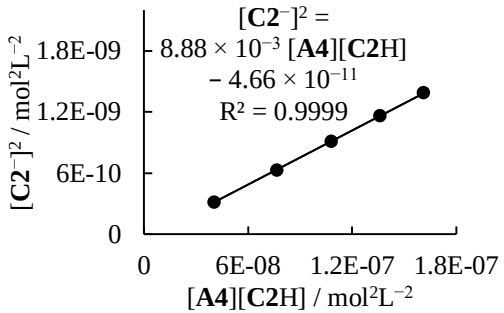

$K = (8.88 \pm 0.05) \times 10^{-3}$

$\bar{K} = (8.92 \pm 0.04) \times 10^{-3}$

pK_{aH}(**A4**) = 19.31

2,2-Dimethylpyrrolidine (A5)

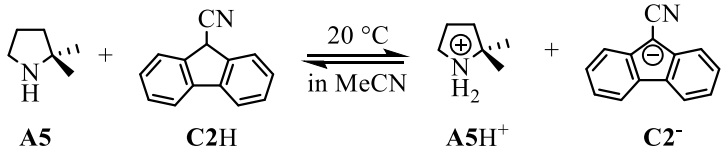

A5 **C2**H **A5**H$^+$ **C2**$^-$

Table 219. Determination of the pK_{aH} for **A5** with **C2**H in acetonitrile at 20 °C (detection at 420 nm). Stock solutions: **A5** (13.4 mg) in 5.0 mL MeCN; **C2**H (11.4 mg) in 10.0 mL MeCN; [DBU] = 3.69×10^{-2} mol L^{-1}. Step 0: 0.800 mL **C2**H stock solution in 20.4 g MeCN.

step	V_+ / mL	V / mL	[**C2**H]$_0$ / M	[**A5**]$_0$ / M	*A*	[**C2**$^-$] / M	[**C2**H] / M	[**A5**] / M
0	-	26.754	1.78×10^{-4}	0	0	0	1.78×10^{-4}	0
1	0.250	27.004	1.77×10^{-4}	2.50×10^{-4}	0.023	2.01×10^{-5}	1.57×10^{-4}	2.30×10^{-4}
2	0.500	27.254	1.75×10^{-4}	4.96×10^{-4}	0.033	2.83×10^{-5}	1.47×10^{-4}	4.67×10^{-4}
3	0.750	27.504	1.73×10^{-4}	7.37×10^{-4}	0.040	3.41×10^{-5}	1.39×10^{-4}	7.03×10^{-4}
4	1.000	27.754	1.72×10^{-4}	9.74×10^{-4}	0.045	3.87×10^{-5}	1.33×10^{-4}	9.35×10^{-4}
5	1.250	28.004	1.70×10^{-4}	1.21×10^{-3}	0.050	4.27×10^{-5}	1.28×10^{-4}	1.16×10^{-3}
6	1.500	28.254	1.69×10^{-4}	1.43×10^{-3}	0.054	4.60×10^{-5}	1.23×10^{-4}	1.39×10^{-3}
f	1.900	28.654	1.66×10^{-4}	1.41×10^{-3}	0.194	1.66×10^{-4}	0	1.41×10^{-3}

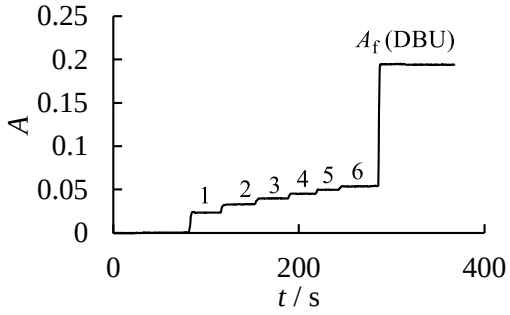

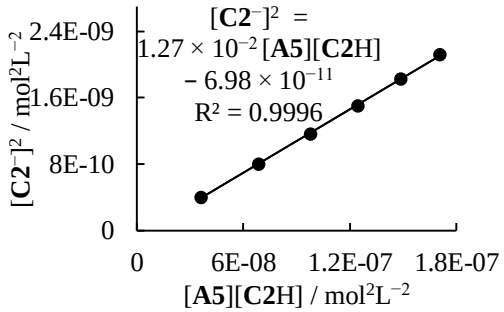

K = (1.27 ± 0.01) × 10^{-2}

Table 220. Determination of the pK_{aH} for **A5** with **C2**H in acetonitrile at 20 °C (detection at 420 nm). Stock solutions: **A5** (13.4) mg in 5.0 mL MeCN; **C2**H (11.4 mg) in 10.0 mL MeCN; [DBU] = 3.69×10^{-2} mol L^{-1}. Step 0: 0.800 mL **C2**H stock solution in 20.8 g MeCN.

step	V_+ / mL	V / mL	[**C2**H]$_0$ / M	[**A5**]$_0$ / M	*A*	[**C2**$^-$] / M	[**C2**H] / M	[**A5**] / M
0	-	27.263	1.75×10^{-4}	0	0	0	1.75×10^{-4}	0
1	0.500	27.763	1.72×10^{-4}	4.87×10^{-4}	0.033	2.76×10^{-5}	1.44×10^{-4}	4.59×10^{-4}
2	1.000	28.263	1.69×10^{-4}	9.56×10^{-4}	0.045	3.78×10^{-5}	1.31×10^{-4}	9.18×10^{-4}
3	1.500	28.763	1.66×10^{-4}	1.41×10^{-3}	0.053	4.49×10^{-5}	1.21×10^{-4}	1.36×10^{-3}
4	2.000	29.263	1.63×10^{-4}	1.85×10^{-3}	0.060	5.04×10^{-5}	1.13×10^{-4}	1.80×10^{-3}
5	2.500	29.763	1.60×10^{-4}	2.27×10^{-3}	0.065	5.48×10^{-5}	1.05×10^{-4}	2.22×10^{-3}
f	2.900	30.163	1.58×10^{-4}	2.24×10^{-3}	0.187	1.58×10^{-4}	0	2.24×10^{-3}

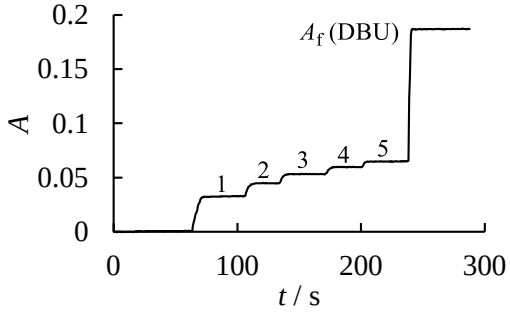

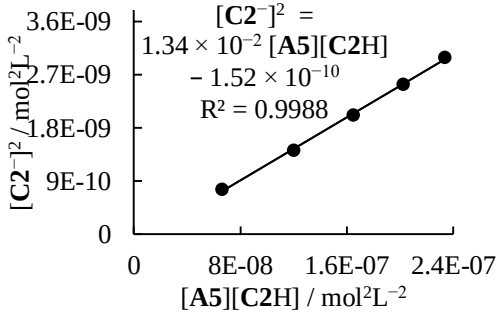

$K = (1.34 \pm 0.03) \times 10^{-2}$

$\bar{K} = (1.30 \pm 0.03) \times 10^{-2}$

pK_{aH}(**A5**) = 19.47

2-Benzylpyrrolidine (A6)

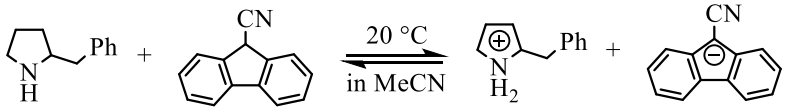

A6 **C2**H **A6**H$^+$ **C2**$^-$

Table 221. Determination of the pK_{aH} for **A6** with **C2**H in acetonitrile at 20 °C (detection at 420 nm). Stock solutions: **A6** (10.3 mg) in 10.0 mL MeCN; **C2**H (12.9 mg) in 10.0 mL MeCN; [DBU] = 3.26×10^{-2} mol L^{-1}. Step 0: 0.800 mL **C2**H stock solution in 20.6 g MeCN.

step	V_+ / mL	V / mL	[**C2**H]$_0$ / M	[**A6**]$_0$ / M	A	[**C2**$^-$] / M	[**C2**H] / M	[**A6**] / M
0	-	27.009	2.00×10^{-4}	0	0	0	2.00×10^{-4}	0
1	0.500	27.509	1.96×10^{-4}	1.16×10^{-4}	0.008	6.55×10^{-6}	1.90×10^{-4}	1.10×10^{-4}
2	1.000	28.009	1.93×10^{-4}	2.28×10^{-4}	0.011	9.13×10^{-6}	1.84×10^{-4}	2.19×10^{-4}
3	1.500	28.509	1.89×10^{-4}	3.36×10^{-4}	0.013	1.10×10^{-5}	1.78×10^{-4}	3.25×10^{-4}
4	2.000	29.009	1.86×10^{-4}	4.40×10^{-4}	0.015	1.24×10^{-5}	1.74×10^{-4}	4.28×10^{-4}
5	2.500	29.509	1.83×10^{-4}	5.41×10^{-4}	0.016	1.36×10^{-5}	1.69×10^{-4}	5.28×10^{-4}
f	3.500	30.509	1.77×10^{-4}	5.23×10^{-4}	0.210	1.77×10^{-4}	0	5.23×10^{-4}

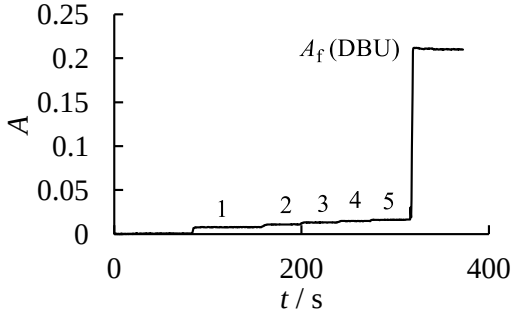

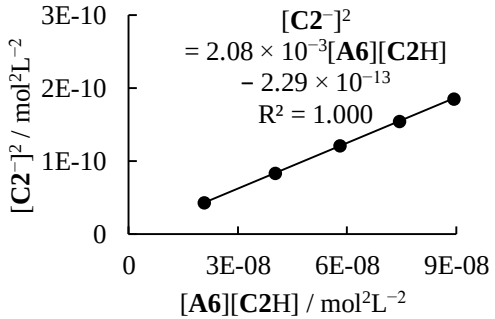

$K = (2.08 \pm 0.00) \times 10^{-3}$

Table 222. Determination of the pK_{aH} for **A6** with **C2**H in acetonitrile at 20 °C (detection at 420 nm). Stock solutions: **A6** (10.3 mg) in 10.0 mL MeCN; **C2**H (12.9 mg) in 10.0 mL MeCN; [DBU] = 3.26×10^{-2} mol L^{-1}. Step 0: 0.800 mL **C2**H stock solution in 21.0 g MeCN.

step	V_+ / mL	V / mL	[**C2**H]$_0$ / M	[**A6**]$_0$ / M	A	[**C2**$^-$] / M	[**C2**H] / M	[**A6**] / M
0	-	27.518	1.96×10^{-4}	0	0	0	1.96×10^{-4}	0
1	0.500	28.018	1.93×10^{-4}	1.14×10^{-4}	0.007	5.93×10^{-6}	1.87×10^{-4}	1.08×10^{-4}
2	1.000	28.518	1.89×10^{-4}	2.24×10^{-4}	0.010	8.52×10^{-6}	1.81×10^{-4}	2.15×10^{-4}
3	2.000	29.518	1.83×10^{-4}	4.33×10^{-4}	0.014	1.17×10^{-5}	1.71×10^{-4}	4.21×10^{-4}
4	3.000	30.518	1.77×10^{-4}	6.28×10^{-4}	0.016	1.39×10^{-5}	1.63×10^{-4}	6.14×10^{-4}
5	4.000	31.518	1.71×10^{-4}	8.11×10^{-4}	0.018	1.56×10^{-5}	1.56×10^{-4}	7.95×10^{-4}
f	4.900	32.418	1.66×10^{-4}	7.88×10^{-4}	0.196	1.66×10^{-4}	0	7.88×10^{-4}

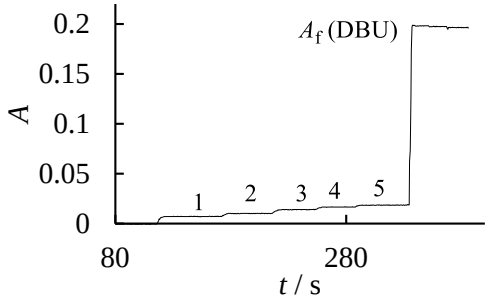

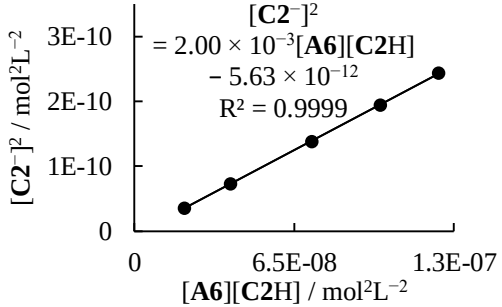

$K = (2.00 \pm 0.01) \times 10^{-3}$

$\bar{K} = (2.04 \pm 0.03) \times 10^{-3}$

pK_{aH}(**A6**) = 18.67

(*S*)-2-Benzhydrylpyrrolidine (A7)

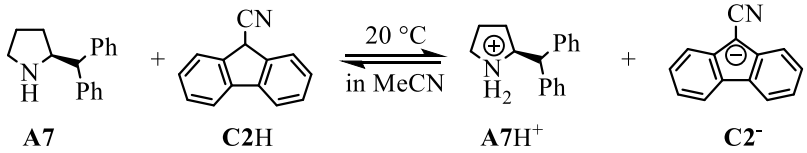

A7 **C2**H $A7H^+$ $C2^-$

Table 223. Determination of the pK_{aH} for **A7** with **C2**H in acetonitrile (detection at 420 nm). Stock solutions: **A7** (14.4 mg) in 10.0 mL MeCN; **C2**H (12.9 mg) in 10.0 mL MeCN; [DBU] = 3.26×10^{-2} mol L^{-1}. Step 0: 0.800 mL **C2**H stock solution in 18.7 g MeCN.

step	V_+ / mL	V / mL	[**C2**H]$_0$ / M	[**A7**]$_0$ / M	*A*	[$\mathbf{C2}^-$] / M	[**C2**H] / M	[**A7**] / M
0	-	24.591	2.19×10^{-4}	0	0	0	2.19×10^{-4}	0
1	0.500	25.091	2.15×10^{-4}	1.21×10^{-4}	0.005	4.06×10^{-6}	2.11×10^{-4}	1.17×10^{-4}
2	1.000	25.591	2.11×10^{-4}	2.37×10^{-4}	0.007	5.51×10^{-6}	2.05×10^{-4}	2.32×10^{-4}
3	2.000	26.591	2.03×10^{-4}	4.56×10^{-4}	0.009	7.25×10^{-6}	1.96×10^{-4}	4.49×10^{-4}
4	3.000	27.591	1.96×10^{-4}	6.60×10^{-4}	0.010	8.40×10^{-6}	1.87×10^{-4}	6.51×10^{-4}
5	4.000	28.591	1.89×10^{-4}	8.49×10^{-4}	0.011	9.36×10^{-6}	1.79×10^{-4}	8.39×10^{-4}
f	4.500	29.091	1.86×10^{-4}	8.34×10^{-4}	0.224	1.86×10^{-4}	0	8.34×10^{-4}

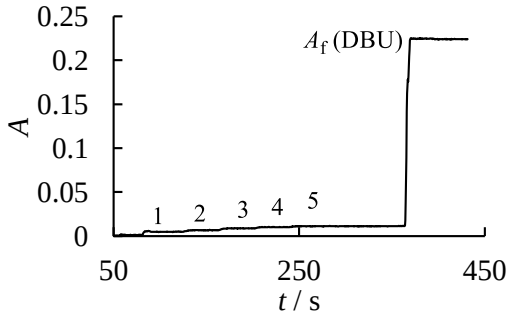

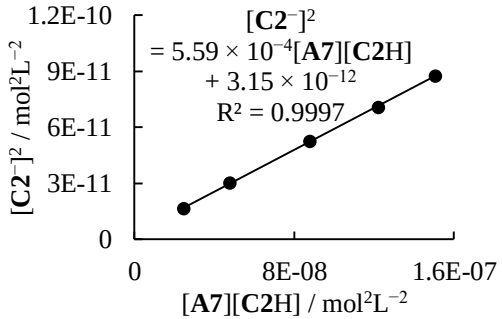

$K = (5.59 \pm 0.06) \times 10^{-4}$

pK_{aH} = 18.11

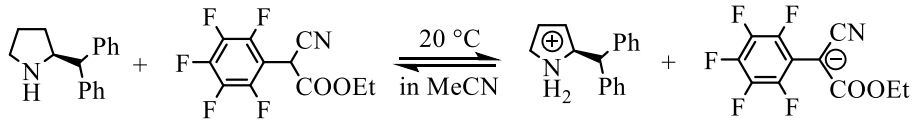

A7 **C3**H $\mathbf{A7}H^+$ $\mathbf{C3}^-$

Table 224. Determination of the pK_{aH} for **A7** with **C3**H in acetonitrile at 20 °C (detection at 333 nm). Stock solutions: **A7** (23.0 mg) in 10.0 mL MeCN, then 1.000 mL solution diluted in 10.0 mL MeCN; **C3**H (11.2 mg) in 10.0 mL MeCN; [DBU] = 4.05×10^{-2} mol· L^{-1}. Step 0: 0.800 mL **C3**H stock solution in 17.8 g MeCN.

step	V_+ / mL	V / mL	[**C3**H]$_0$ / M	[**A7**]$_0$ / M	*A*	[$\mathbf{C3}^-$] / M	[**C3**H] / M	[**A7**] / M
0	-	23.446	1.37×10^{-4}	0	0	0	1.37×10^{-4}	0
1	0.300	23.746	1.35×10^{-4}	2.45×10^{-5}	0.059	2.16×10^{-5}	1.14×10^{-4}	2.93×10^{-6}
2	0.400	23.846	1.35×10^{-4}	3.25×10^{-5}	0.076	2.79×10^{-5}	1.07×10^{-4}	4.66×10^{-6}
3	0.500	23.946	1.34×10^{-4}	4.05×10^{-5}	0.093	3.39×10^{-5}	1.00×10^{-4}	6.57×10^{-6}
4	0.600	24.046	1.33×10^{-4}	4.84×10^{-5}	0.108	3.97×10^{-5}	9.38×10^{-5}	8.70×10^{-6}
5	0.700	24.146	1.33×10^{-4}	5.62×10^{-5}	0.123	4.50×10^{-5}	8.79×10^{-5}	1.12×10^{-5}
f	0.900	24.346	1.32×10^{-4}	5.57×10^{-5}	0.360	1.32×10^{-4}	0	5.57×10^{-5}

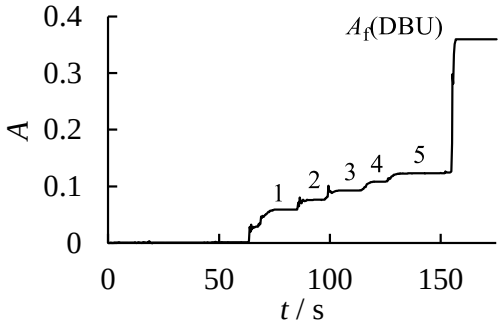

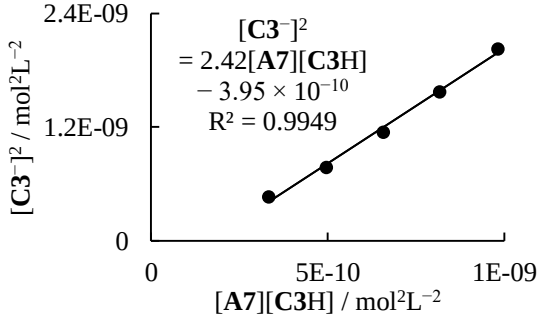

K = 2.42 ± 0.10

Table 225. Determination of the pK_{aH} for **A7** with **C3**H in acetonitrile at 20 °C (detection at 333 nm). Stock solutions: **A7** (23.0 mg) in 10.0 mL MeCN, then 1.000 mL solution diluted in 10.0 mL MeCN; **C3**H (11.2 mg) in 10.0 mL MeCN; [DBU] = 4.05×10^{-2} mol· L^{-1}. Step 0: 0.700 mL **C3**H stock solution in 17.2 g MeCN.

step	V_+ / mL	V / mL	[**C3**H]$_0$ / M	[**A7**]$_0$ / M	*A*	[**C3**$^-$] / M	[**C3**H] / M	[**A7**] / M
0	-	22.583	1.24×10^{-4}	0	0	0	1.24×10^{-4}	0
1	0.300	22.883	1.23×10^{-4}	2.54×10^{-5}	0.061	2.20×10^{-5}	1.01×10^{-4}	3.37×10^{-6}
2	0.400	22.983	1.22×10^{-4}	3.37×10^{-5}	0.078	2.84×10^{-5}	9.38×10^{-5}	5.32×10^{-6}
3	0.500	23.083	1.22×10^{-4}	4.20×10^{-5}	0.095	3.44×10^{-5}	8.72×10^{-5}	7.56×10^{-6}
4	0.600	23.183	1.21×10^{-4}	5.02×10^{-5}	0.110	4.01×10^{-5}	8.11×10^{-5}	1.01×10^{-5}
5	0.700	23.283	1.21×10^{-4}	5.83×10^{-5}	0.125	4.55×10^{-5}	7.52×10^{-5}	1.28×10^{-5}
f	0.900	23.483	1.20×10^{-4}	5.78×10^{-5}	0.328	1.20×10^{-4}	0	5.78×10^{-5}

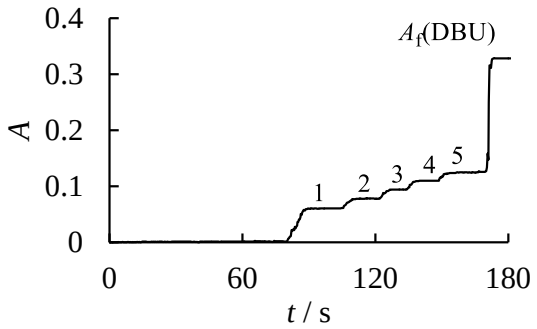

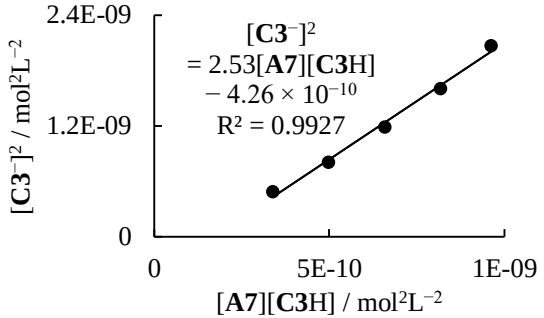

K = 2.53 ± 0.13

For **A7** + **C3**H: $\bar{K}$ = 2.47 ± 0.05

pK_{aH} = 18.14

pK_{aH}(**A7**) = 18.13 (average)

(*S*)-Pyrrolidin-2-ylmethanamine (A8)

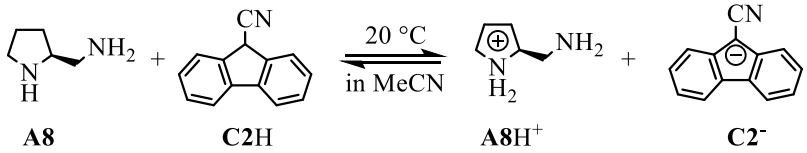

A8 **C2**H **A8**H$^+$ **C2**$^-$

Table 226. Determination of the pK_{aH} for **A8** with **C2**H in acetonitrile at 20 °C (detection at 420 nm). Stock solutions: **A8** (19.3 mg) in 10.0 mL MeCN; **C2**H (15.8 mg) in 10.0 mL MeCN; [DBU] = 8.50×10^{-2} mol L^{-1}. Step 0: 0.800 mL **C2**H stock solution in 21.1 g MeCN.

step	V_+ / mL	V / mL	[**C2**H]$_0$ / M	[**A8**]$_0$ / M	*A*	[**C2**$^-$] / M	[**C2**H] / M	[**A8**] / M
0	-	27.645	2.39×10^{-4}	0	0	0	2.39×10^{-4}	0
1	0.250	27.895	2.37×10^{-4}	1.73×10^{-4}	0.033	2.94×10^{-5}	2.08×10^{-4}	1.43×10^{-4}
2	0.500	28.145	2.35×10^{-4}	3.42×10^{-4}	0.047	4.14×10^{-5}	1.93×10^{-4}	3.01×10^{-4}
3	0.750	28.395	2.33×10^{-4}	5.09×10^{-4}	0.057	5.02×10^{-5}	1.83×10^{-4}	4.59×10^{-4}
4	1.000	28.645	2.31×10^{-4}	6.73×10^{-4}	0.065	5.69×10^{-5}	1.74×10^{-4}	6.16×10^{-4}
5	1.250	28.895	2.29×10^{-4}	8.34×10^{-4}	0.071	6.25×10^{-5}	1.66×10^{-4}	7.71×10^{-4}
6	1.500	29.145	2.27×10^{-4}	9.92×10^{-4}	0.077	6.73×10^{-5}	1.59×10^{-4}	9.24×10^{-4}
f	1.700	29.345	2.25×10^{-4}	9.85×10^{-4}	0.256	2.25×10^{-4}	0	9.85×10^{-4}

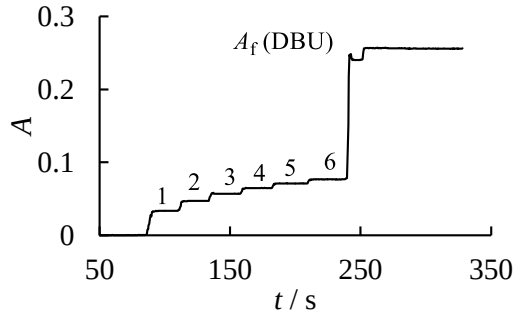

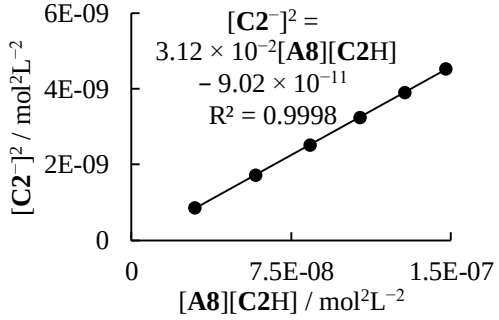

$K = (3.12 \pm 0.02) \times 10^{-2}$

Table 227. Determination of the pK_{aH} for **A8** with **C2**H in acetonitrile at 20 °C (detection at 420 nm). Stock solutions: **A8** (19.3 mg) in 10.0 mL MeCN; **C2**H (15.8 mg) in 10.0 mL MeCN; [DBU] = 8.50×10^{-2} mol L^{-1}. Step 0: 0.900 mL **C2**H stock solution in 21.0 g MeCN.

step	V_+ / mL	V / mL	[**C2**H]$_0$ / M	[**A8**]$_0$ / M	*A*	[**C2**$^-$] / M	[**C2**H] / M	[**A8**] / M
0	-	27.618	2.69×10^{-4}	0	0	0	2.69×10^{-4}	0
1	0.500	28.118	2.64×10^{-4}	3.43×10^{-4}	0.050	4.37×10^{-5}	2.21×10^{-4}	2.99×10^{-4}
2	1.000	28.618	2.60×10^{-4}	6.73×10^{-4}	0.069	6.05×10^{-5}	1.99×10^{-4}	6.13×10^{-4}
3	1.500	29.118	2.55×10^{-4}	9.93×10^{-4}	0.082	7.17×10^{-5}	1.84×10^{-4}	9.21×10^{-4}
4	2.000	29.618	2.51×10^{-4}	1.30×10^{-3}	0.092	8.04×10^{-5}	1.71×10^{-4}	1.22×10^{-3}
5	2.500	30.118	2.47×10^{-4}	1.60×10^{-3}	0.099	8.72×10^{-5}	1.60×10^{-4}	1.51×10^{-3}
6	3.000	30.618	2.43×10^{-4}	1.89×10^{-3}	0.105	9.25×10^{-5}	1.50×10^{-4}	1.80×10^{-3}
f	3.300	30.918	2.41×10^{-4}	1.87×10^{-3}	0.274	2.41×10^{-4}	0	1.87×10^{-3}

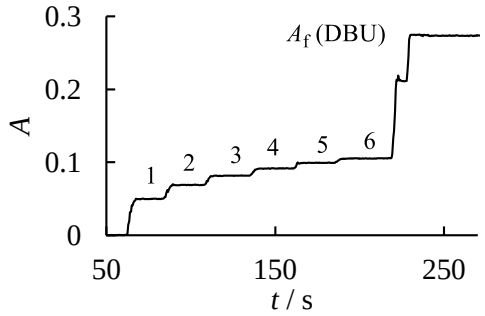

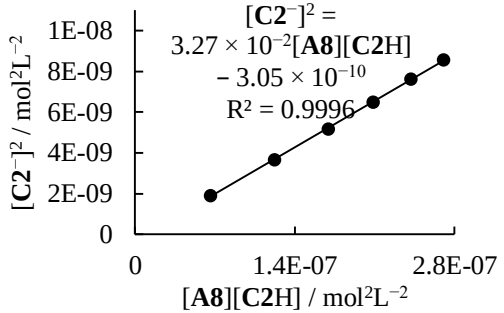

$K = (3.27 \pm 0.03) \times 10^{-2}$

$\bar{K} = (3.19 \pm 0.07) \times 10^{-2}$

pK_{aH}(**A8**) = 19.86

(*S*)-*N*,*N*-Dimethyl-1-(pyrrolidin-2-yl)methanamine (A9)

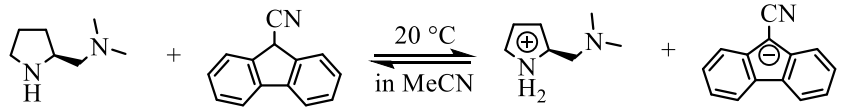

A9 **C2**H $\mathbf{A9}H^+$ $\mathbf{C2}^-$

Table 228. Determination of the pK_{aH} for **A9** with **C2**H in acetonitrile at 20 °C (detection at 420 nm). Stock solutions: **A9** (21.9 mg) in 10.0 mL MeCN; **C2**H (12.9 mg) in 10.0 mL MeCN; [DBU] = 1.75×10^{-2} mol L^{-1}. Step 0: 0.600 mL **C2**H stock solution in 18.6 g MeCN.

step	V_+ / mL	V / mL	[**C2**H]$_0$ / M	[**A9**]$_0$ / M	*A*	[$\mathbf{C2}^-$] / M	[**C2**H] / M	[**A9**] / M
0	-	24.264	1.67×10^{-4}	0	0	0	1.67×10^{-4}	0
1	0.250	24.514	1.65×10^{-4}	1.74×10^{-4}	0.025	2.08×10^{-5}	1.44×10^{-4}	1.53×10^{-4}
2	0.500	24.764	1.63×10^{-4}	3.45×10^{-4}	0.036	3.04×10^{-5}	1.33×10^{-4}	3.14×10^{-4}
3	1.000	25.264	1.60×10^{-4}	6.76×10^{-4}	0.050	4.24×10^{-5}	1.18×10^{-4}	6.34×10^{-4}
4	1.500	25.764	1.57×10^{-4}	9.94×10^{-4}	0.060	5.04×10^{-5}	1.07×10^{-4}	9.44×10^{-4}
5	2.000	26.264	1.54×10^{-4}	1.30×10^{-3}	0.067	5.60×10^{-5}	9.81×10^{-4}	1.24×10^{-3}
f	2.900	27.164	1.49×10^{-4}	1.26×10^{-3}	0.177	1.49×10^{-4}	0	1.26×10^{-3}

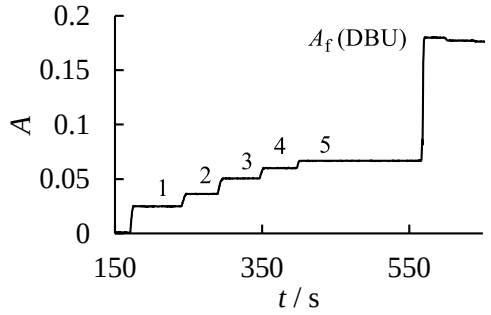

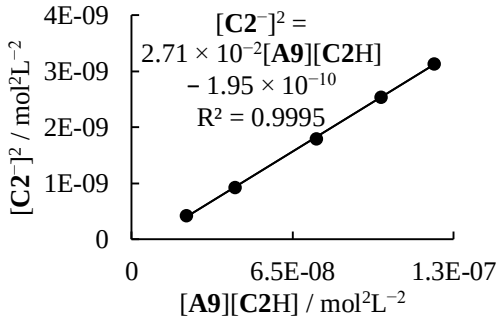

$K = (2.71 \pm 0.03) \times 10^{-2}$

Table 229. Determination of the pK_{aH} for **A9** with **C2**H in acetonitrile at 20 °C (detection at 420 nm). Stock solutions: **A9** (21.9 mg) in 10.0 mL MeCN; **C2**H (12.9 mg) in 10.0 mL MeCN; [DBU] = 1.75×10^{-2} mol L^{-1}. Step 0: 0.800 mL **C2**H stock solution in 18.3 g MeCN.

step	V_+ / mL	V / mL	[**C2**H]$_0$ / M	[**A9**]$_0$ / M	*A*	[**C2**$^-$] / M	[**C2**H] / M	[**A9**] / M
0	-	24.082	2.24×10^{-4}	0	0	0	2.24×10^{-4}	0
1	0.500	24.582	2.20×10^{-4}	3.47×10^{-4}	0.042	3.56×10^{-5}	1.84×10^{-4}	3.12×10^{-4}
2	1.000	25.082	2.15×10^{-4}	6.81×10^{-4}	0.059	5.01×10^{-5}	1.65×10^{-4}	6.31×10^{-4}
3	1.500	25.582	2.11×10^{-4}	1.00×10^{-3}	0.071	6.00×10^{-5}	1.51×10^{-4}	9.41×10^{-4}
4	2.500	26.582	2.03×10^{-4}	1.61×10^{-3}	0.086	7.29×10^{-5}	1.30×10^{-4}	1.53×10^{-3}
5	3.500	27.582	1.96×10^{-4}	2.17×10^{-3}	0.095	8.11×10^{-5}	1.15×10^{-4}	2.09×10^{-3}
f	4.400	28.482	1.89×10^{-4}	2.10×10^{-3}	0.223	1.89×10^{-4}	0	2.10×10^{-3}

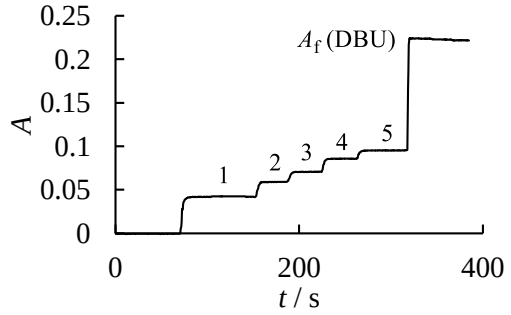

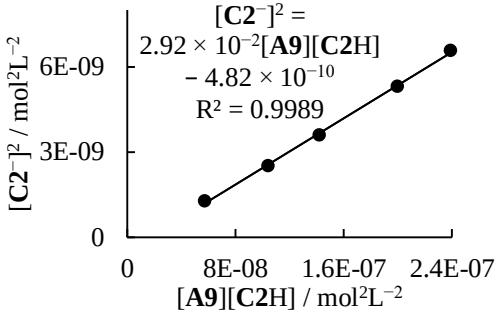

$K = (2.92 \pm 0.06) \times 10^{-2}$

$\bar{K} = (2.82 \pm 0.10) \times 10^{-2}$

pK_{aH}(**A9**) = 19.81

(*S*)-2-((Dimethylamino)methyl)pyrrolidin-1-ium trifluoromethanesulfonate (A9H$^+$)

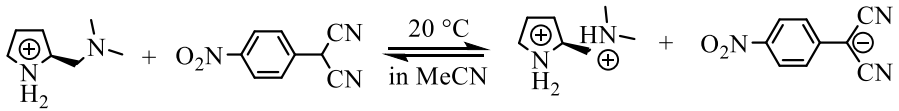

A9H$^+$ **C6**H **A9**H$_2^{2+}$ **C6**$^-$

Table 230. Determination of the pK_{aH} for **A9**H$^+$ with **C6**H in acetonitrile at 20 °C (detection at 478 nm). Stock solutions: **A9**H$^+$ TfO$^-$ (19.8 mg) in 10.0 mL MeCN; **C6**H (8.9 mg) in 10.0 mL MeCN; [DBU] = 1.27 × 10^{-2} mol L^{-1}. Step 0: 0.200 mL **C6**H stock solution in 18.1 g MeCN.

step	V_+ / mL	V / mL	[**C6**H]$_0$ / M	[**A9**H$^+$]$_0$ / M	*A*	[**C6**$^-$] / M	[**C6**H] / M	[**A9**H$^+$] / M
0	-	23.228	4.09 × 10^{-5}	0	0	0	4.09 × 10^{-5}	0
1	0.600	23.828	3.99 × 10^{-5}	1.79 × 10^{-4}	0.029	1.68 × 10^{-6}	3.82 × 10^{-5}	1.77 × 10^{-4}
2	1.100	24.328	3.91 × 10^{-5}	3.22 × 10^{-4}	0.037	2.18 × 10^{-6}	3.69 × 10^{-5}	3.20 × 10^{-4}
3	1.600	24.828	3.83 × 10^{-5}	4.59 × 10^{-4}	0.042	2.48 × 10^{-6}	3.58 × 10^{-5}	4.56 × 10^{-4}
4	2.100	25.328	3.76 × 10^{-5}	5.90 × 10^{-4}	0.047	2.75 × 10^{-6}	3.48 × 10^{-5}	5.87 × 10^{-4}
5	2.600	25.828	3.68 × 10^{-5}	7.16 × 10^{-4}	0.051	2.99 × 10^{-6}	3.38 × 10^{-5}	7.13 × 10^{-4}
f	4.200	27.428	3.47 × 10^{-5}	6.74 × 10^{-4}	0.589	3.47 × 10^{-5}	0	6.74 × 10^{-4}

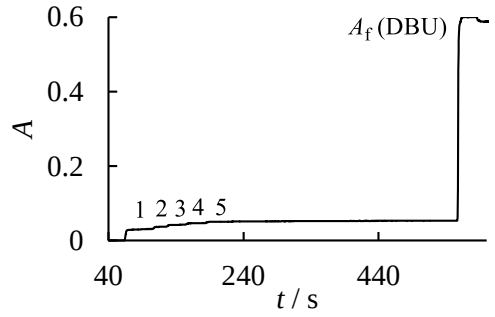

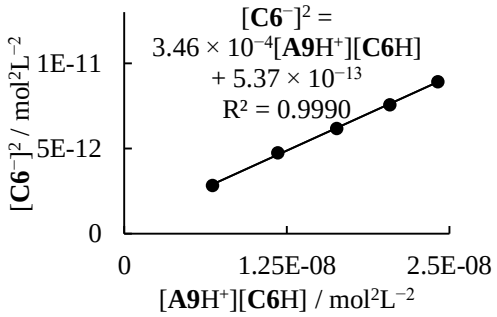

K = (3.46 ± 0.06) × 10^{-4}

pK_{aH} = 8.15

(*S*)-1-(Pyrrolidin-2-ylmethyl)pyrrolidine (A10)

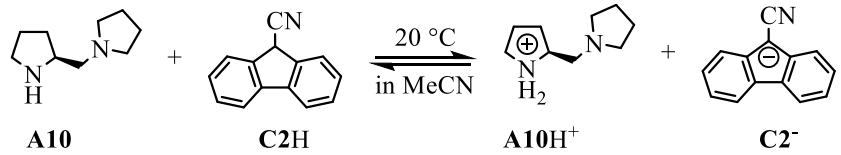

A10 **C2**H **A10**H$^+$ **C2**$^-$

Table 231. Determination of the pK_{aH} for **A10** with **C2**H in acetonitrile at 20 °C (detection at 420 nm). Stock solutions: **A10** (25.6 mg) in 10.0 mL MeCN; **C2**H (11.0 mg) in 10.0 mL MeCN; [DBU] = 4.77 × 10^{-2} mol L^{-1}. Step 0: 0.900 mL **C2**H stock solution in 20.5 g MeCN.

step	V_+ / mL	V / mL	[**C2**H]$_0$ / M	[**A10**]$_0$ / M	*A*	[**C2**$^-$] / M	[**C2**H] / M	[**A10**] / M
0	-	26.981	1.92 × 10^{-4}	0	0	0	1.92 × 10^{-4}	0
1	0.250	27.231	1.90 × 10^{-4}	1.53 × 10^{-4}	0.033	3.23 × 10^{-5}	1.58 × 10^{-4}	1.20 × 10^{-4}
2	0.500	27.481	1.88 × 10^{-4}	3.02 × 10^{-4}	0.046	4.44 × 10^{-5}	1.44 × 10^{-4}	2.58 × 10^{-4}
3	0.750	27.731	1.87 × 10^{-4}	4.49 × 10^{-4}	0.054	5.28 × 10^{-5}	1.34 × 10^{-4}	3.96 × 10^{-4}
4	1.000	27.981	1.85 × 10^{-4}	5.93 × 10^{-4}	0.061	5.91 × 10^{-5}	1.26 × 10^{-4}	5.34 × 10^{-4}
5	1.250	28.231	1.83 × 10^{-4}	7.35 × 10^{-4}	0.066	6.41 × 10^{-5}	1.19 × 10^{-4}	6.71 × 10^{-4}
6	1.500	28.481	1.82 × 10^{-4}	8.74 × 10^{-4}	0.070	6.82 × 10^{-5}	1.14 × 10^{-4}	8.06 × 10^{-4}
f	1.800	28.781	1.80 × 10^{-4}	8.65 × 10^{-4}	0.184	1.80 × 10^{-4}	0	8.65 × 10^{-4}

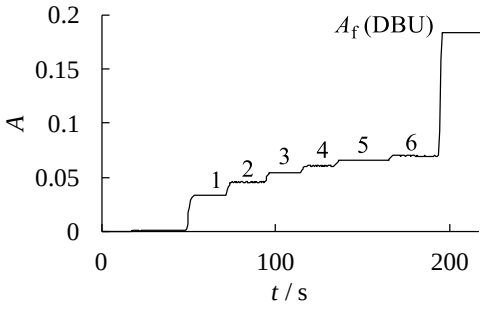

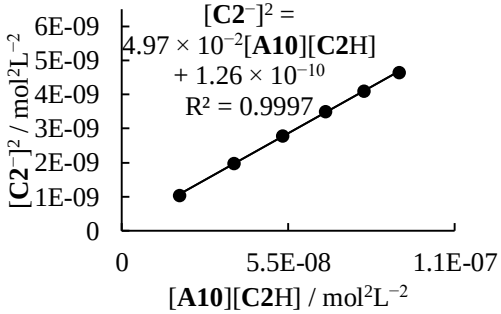

K = (4.97 ± 0.05) × 10^{-2}

Table 232. Determination of the pK_{aH} for **A10** with **C2**H in acetonitrile at 20 °C (detection at 420 nm). Stock solutions: **A10** (25.6 mg) in 10.0 mL MeCN; **C2**H (10.7 mg) in 10.0 mL MeCN; [DBU] = 4.77×10^{-2} mol L^{-1}. Step 0: 0.900 mL **C2**H stock solution in 19.5 g MeCN.

step	V_+ / mL	V / mL	[**C2**H]$_0$ / M	[**A10**]$_0$ / M	*A*	[**C2**$^-$] / M	[**C2**H] / M	[**A10**] / M
0	-	25.709	1.96×10^{-4}	0	0	0	1.96×10^{-4}	0
1	0.250	25.959	1.94×10^{-4}	1.60×10^{-4}	0.035	3.16×10^{-5}	1.62×10^{-4}	1.28×10^{-4}
2	0.500	26.209	1.92×10^{-4}	3.17×10^{-4}	0.048	4.39×10^{-5}	1.48×10^{-4}	2.73×10^{-4}
3	0.750	26.459	1.90×10^{-4}	4.70×10^{-4}	0.058	5.25×10^{-5}	1.38×10^{-4}	4.18×10^{-4}
4	1.000	26.709	1.89×10^{-4}	6.21×10^{-4}	0.065	5.89×10^{-5}	1.30×10^{-4}	5.62×10^{-4}
5	1.250	26.959	1.87×10^{-4}	7.69×10^{-4}	0.070	6.41×10^{-5}	1.23×10^{-4}	7.05×10^{-4}
6	1.500	27.209	1.85×10^{-4}	9.15×10^{-4}	0.075	6.83×10^{-5}	1.17×10^{-4}	8.47×10^{-4}
f	1.800	27.509	1.83×10^{-4}	9.05×10^{-4}	0.201	1.83×10^{-4}	0	9.05×10^{-4}

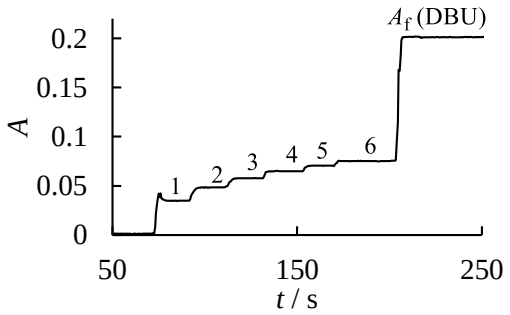

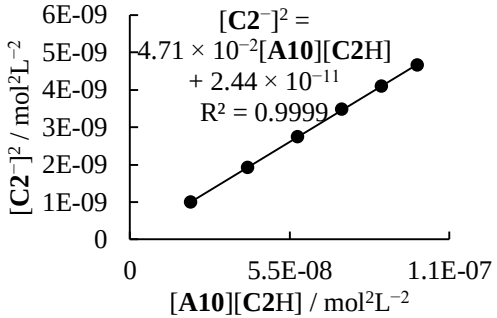

$K = (4.71 \pm 0.02) \times 10^{-2}$

Table 233. Determination of the pK_{aH} for **A10** with **C2**H in acetonitrile at 20 °C (detection at 420 nm). Stock solutions: **A10** (25.6 mg) in 10.0 mL MeCN; **C2**H (10.7 mg) in 10.0 mL MeCN; [DBU] = 4.77×10^{-2} mol L^{-1}. Step 0: 1.000 mL **C2**H stock solution in 19.9 g MeCN.

step	V_+ / mL	V / mL	[**C2**H]$_0$ / M	[**A10**]$_0$ / M	*A*	[**C2**$^-$] / M	[**C2**H] / M	[**A10**] / M
0	-	26.318	2.13×10^{-4}	0	0	0	2.13×10^{-4}	0
1	0.250	26.568	2.11×10^{-4}	1.56×10^{-4}	0.036	3.35×10^{-5}	1.77×10^{-4}	1.23×10^{-4}
2	0.500	26.818	2.09×10^{-4}	3.09×10^{-4}	0.049	4.60×10^{-5}	1.63×10^{-4}	2.63×10^{-4}
3	0.750	27.068	2.07×10^{-4}	4.60×10^{-4}	0.059	5.48×10^{-5}	1.52×10^{-4}	4.05×10^{-4}
4	1.000	27.318	2.05×10^{-4}	6.07×10^{-4}	0.066	6.15×10^{-5}	1.43×10^{-4}	5.46×10^{-4}
5	1.250	27.568	2.03×10^{-4}	7.52×10^{-4}	0.072	6.69×10^{-5}	1.36×10^{-4}	6.86×10^{-4}
6	1.500	27.818	2.01×10^{-4}	8.95×10^{-4}	0.077	7.13×10^{-5}	1.30×10^{-4}	8.24×10^{-4}
f	1.800	28.118	1.99×10^{-4}	8.85×10^{-4}	0.214	1.99×10^{-4}	0	8.85×10^{-4}

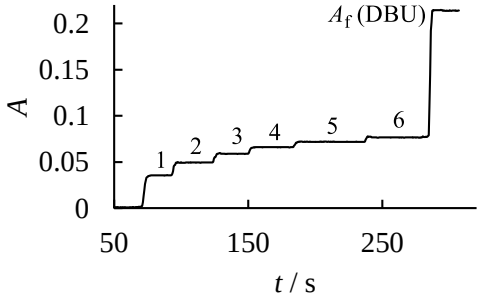

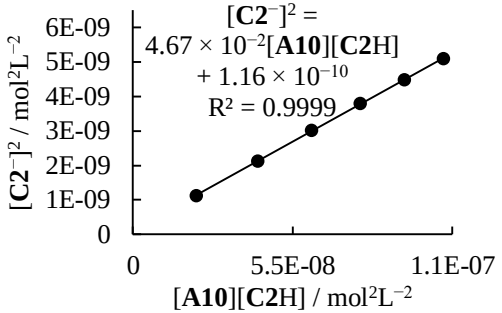

$K = (4.67 \pm 0.02) \times 10^{-2}$

Table 234. Determination of the pK_{aH} for **A10** with **C2**H in acetonitrile at 20 °C (detection at 420 nm). Stock solutions: **A10** (25.6 mg) in 10.0 mL MeCN; **C2**H (10.7 mg) in 10.0 mL MeCN; [DBU] = 4.77×10^{-2} mol L^{-1}. Step 0: 0.900 mL **C2**H stock solution in 20.5 g MeCN.

step	V_+ / mL	V / mL	[**C2**H]$_0$ / M	[**A10**]$_0$ / M	*A*	[**C2**$^-$] / M	[**C2**H] / M	[**A10**] / M
0	-	26.981	1.87×10^{-4}	0	0	0	1.87×10^{-4}	0
1	0.250	27.231	1.85×10^{-4}	1.52×10^{-4}	0.034	3.20×10^{-5}	1.53×10^{-4}	1.20×10^{-4}
2	0.500	27.481	1.83×10^{-4}	3.02×10^{-4}	0.046	4.36×10^{-5}	1.40×10^{-4}	2.58×10^{-4}
3	0.750	27.731	1.82×10^{-4}	4.49×10^{-4}	0.055	5.17×10^{-5}	1.30×10^{-4}	3.97×10^{-4}
4	1.000	27.981	1.80×10^{-4}	5.93×10^{-4}	0.061	5.78×10^{-5}	1.22×10^{-4}	5.35×10^{-4}
5	1.250	28.231	1.78×10^{-4}	7.35×10^{-4}	0.066	6.27×10^{-5}	1.16×10^{-4}	6.72×10^{-4}
6	1.500	28.481	1.77×10^{-4}	8.74×10^{-4}	0.070	6.67×10^{-5}	1.10×10^{-4}	8.07×10^{-4}
f	1.800	28.781	1.75×10^{-4}	8.65×10^{-4}	0.185	1.75×10^{-4}	0	8.65×10^{-4}

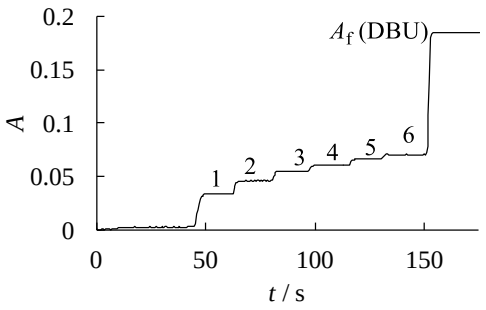

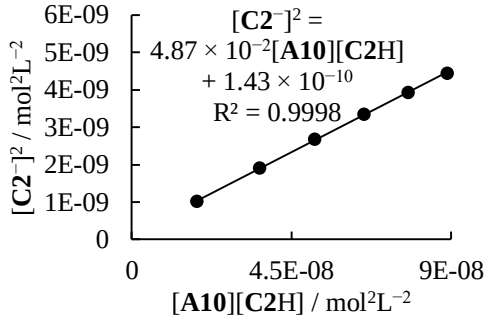

$K = (4.87 \pm 0.03) \times 10^{-2}$

$\bar{K} = (4.81 \pm 0.12) \times 10^{-2}$

pK_{aH}(**A10**) = 20.04

(*S*)-2-(Azidomethyl)pyrrolidine (A11)

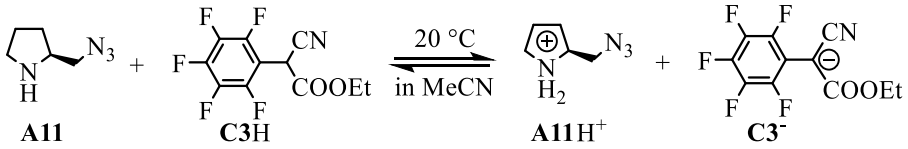

Table 235. Determination of the pK_{aH} for **A11** with **C3**H in acetonitrile at 20 °C (detection at 333 nm). Stock solutions: **A11** (26.1 mg) in 10.0 mL MeCN; **C3**H (25.4 mg) in 10.0 mL MeCN; [DBU] = 8.50×10^{-2} mol L^{-1}. Step 0: 0.500 mL **C3**H stock solution in 21.9 g MeCN.

step	V_+ / mL	V / mL	[**C3**H]$_0$ / M	[**A11**]$_0$ / M	*A*	[**C3**$^-$] / M	[**C3**H] / M	[**A11**] / M
0	-	28.363	1.60×10^{-4}	0	0	0	1.60×10^{-4}	0
1	0.050	28.413	1.60×10^{-4}	3.64×10^{-5}	0.072	2.61×10^{-5}	1.34×10^{-4}	1.03×10^{-5}
2	0.100	28.463	1.60×10^{-4}	7.27×10^{-5}	0.121	4.41×10^{-5}	1.16×10^{-4}	2.86×10^{-5}
3	0.150	28.513	1.60×10^{-4}	1.09×10^{-4}	0.159	5.76×10^{-5}	1.02×10^{-4}	5.12×10^{-5}
4	0.200	28.563	1.59×10^{-4}	1.45×10^{-4}	0.188	6.81×10^{-5}	9.12×10^{-5}	7.68×10^{-5}
5	0.250	28.613	1.59×10^{-4}	1.81×10^{-4}	0.211	7.65×10^{-5}	8.25×10^{-5}	1.04×10^{-4}
6	0.300	28.663	1.59×10^{-4}	2.17×10^{-4}	0.230	8.34×10^{-5}	7.53×10^{-5}	1.33×10^{-4}
7	0.350	28.713	1.58×10^{-4}	2.52×10^{-4}	0.246	8.94×10^{-5}	6.91×10^{-5}	1.63×10^{-4}
8	0.400	28.763	1.58×10^{-4}	2.88×10^{-4}	0.260	9.44×10^{-5}	6.37×10^{-5}	1.93×10^{-4}
9	0.450	28.813	1.58×10^{-4}	3.23×10^{-4}	0.272	9.88×10^{-5}	5.91×10^{-5}	2.24×10^{-4}
10	0.500	28.863	1.58×10^{-4}	3.58×10^{-4}	0.282	1.03×10^{-4}	5.51×10^{-5}	2.56×10^{-4}
f	0.800	29.163	1.56×10^{-4}	3.55×10^{-4}	0.430	1.56×10^{-4}	0	3.55×10^{-4}

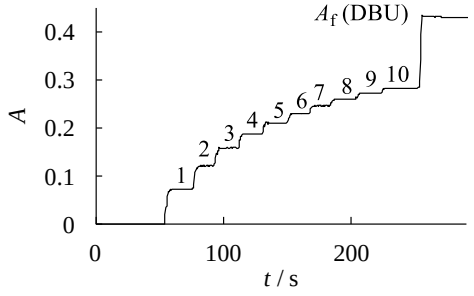

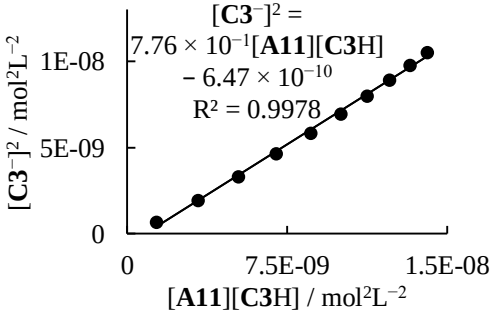

$K = (7.76 \pm 0.13) \times 10^{-1}$

Table 236. Determination of the pK_{aH} for **A11** with **C3**H in acetonitrile at 20 °C (detection at 333 nm). Stock solutions: **A11** (26.1 mg) in 10.0 mL MeCN; **C3**H (25.4 mg) in 10.0 mL MeCN; [DBU] = 8.50×10^{-2} mol L^{-1}. Step 0: 0.500 mL **C3**H stock solution in 21.6 g MeCN.

step	V_+ / mL	V / mL	[**C3**H]$_0$ / M	[**A11**]$_0$ / M	*A*	[**C3**$^-$] / M	[**C3**H] / M	[**A11**] / M
0	-	27.981	1.63×10^{-4}	0	0	0	1.63×10^{-4}	0
1	0.100	28.081	1.62×10^{-4}	7.37×10^{-5}	0.121	4.37×10^{-5}	1.18×10^{-4}	3.00×10^{-5}
2	0.150	28.131	1.62×10^{-4}	1.10×10^{-4}	0.159	5.74×10^{-5}	1.04×10^{-4}	5.29×10^{-5}
3	0.200	28.181	1.61×10^{-4}	1.47×10^{-4}	0.188	6.82×10^{-5}	9.33×10^{-5}	7.87×10^{-5}
4	0.250	28.231	1.61×10^{-4}	1.83×10^{-4}	0.212	7.68×10^{-5}	8.43×10^{-5}	1.06×10^{-4}
5	0.300	28.281	1.61×10^{-4}	2.19×10^{-4}	0.231	8.38×10^{-5}	7.71×10^{-5}	1.36×10^{-4}
6	0.350	28.331	1.61×10^{-4}	2.56×10^{-4}	0.249	8.99×10^{-5}	7.06×10^{-5}	1.66×10^{-4}
f	0.650	28.631	1.59×10^{-4}	2.53×10^{-4}	0.439	1.59×10^{-4}	0	2.53×10^{-4}

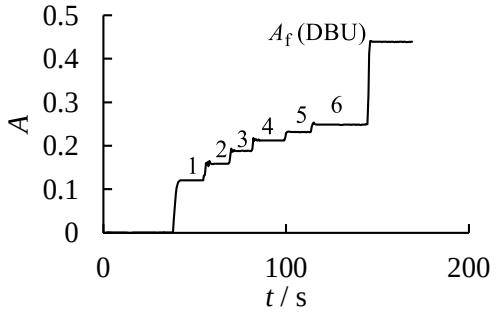

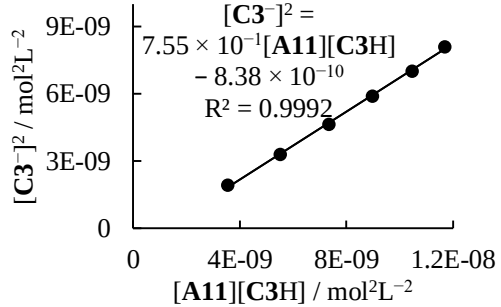

$K = (7.55 \pm 0.11) \times 10^{-1}$

For **A11** + **C3**H: $\bar{K} = (7.65 \pm 0.10) \times 10^{-1}$

pK_{aH}(**A11**) = 17.63

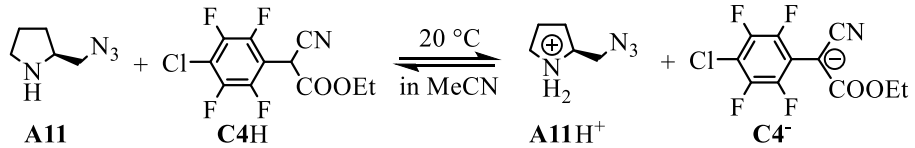

Table 237. Determination of the pK_{aH} for **A11** with **C4**H in acetonitrile at 20 °C (detection at 333 nm). Stock solutions: **A11** (26.1 mg) in 10.0 mL MeCN; **C4**H (15.3 mg) in 10.0 mL MeCN; [DBU] = 8.50×10^{-2} mol L^{-1}. Step 0: 0.500 mL **C4**H stock solution in 24.5 g MeCN.

step	V_+ / mL	V / mL	[**C4**H]$_0$ / M	[**A11**]$_0$ / M	*A*	[**C4**$^-$] / M	[**C4**H] / M	[**A11**] / M
0	-	31.670	8.17×10^{-5}	0	0	0	8.17×10^{-5}	0
1	0.100	31.770	8.15×10^{-5}	6.51×10^{-5}	0.281	3.78×10^{-5}	4.36×10^{-5}	2.73×10^{-5}
2	0.150	31.820	8.13×10^{-5}	9.75×10^{-5}	0.356	4.78×10^{-5}	3.35×10^{-5}	4.97×10^{-5}
3	0.200	31.870	8.12×10^{-5}	1.30×10^{-4}	0.404	5.43×10^{-5}	2.69×10^{-5}	7.55×10^{-5}
4	0.250	31.920	8.11×10^{-5}	1.62×10^{-4}	0.438	5.89×10^{-5}	2.22×10^{-5}	1.03×10^{-4}
5	0.300	31.970	8.09×10^{-5}	1.94×10^{-4}	0.462	6.22×10^{-5}	1.88×10^{-5}	1.32×10^{-4}
6	0.350	32.020	8.08×10^{-5}	2.26×10^{-4}	0.481	6.47×10^{-5}	1.61×10^{-5}	1.61×10^{-4}
f	0.650	32.320	8.01×10^{-5}	2.24×10^{-4}	0.595	8.01×10^{-5}	0	2.24×10^{-4}

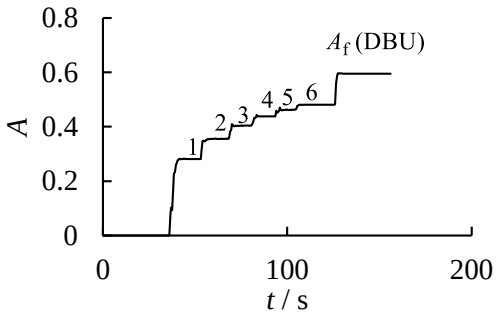

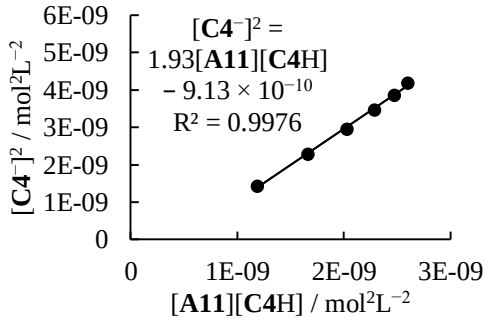

K = 1.93 ± 0.05

pK_{aH}(**A11**) = 17.68

pK_{aH} (**A11**) = 17.66 (average)

(*S*)-Pyrrolidin-2-ylmethanol (A12)

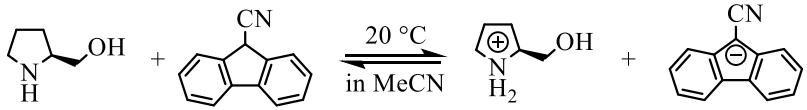

A12 **C2**H **A12**H$^+$ **C2**$^-$

Table 238. Determination of the pK_{aH} for **A12** with **C2**H in acetonitrile at 20 °C (detection at 420 nm). Stock solutions: **A12** (19.2 mg) in 10.0 mL MeCN; **C2**H (13.2 mg) in 10.0 mL MeCN; [DBU] = 2.38 × 10^{-2} mol L^{-1}. Step 0: 0.700 mL **C2**H stock solution in 19.4 g MeCN.

step	V_+ / mL	V / mL	[**C2**H]$_0$ / M	[**A12**]$_0$ / M	*A*	[**C2**$^-$] / M	[**C2**H] / M	[**A12**] / M
0	-	25.382	1.90 × 10^{-4}	0	0.000	0	1.90 × 10^{-4}	0
1	0.250	25.632	1.89 × 10^{-4}	1.85 × 10^{-4}	0.013	1.14 × 10^{-5}	1.77 × 10^{-4}	1.74 × 10^{-4}
2	0.500	25.882	1.87 × 10^{-4}	3.67 × 10^{-4}	0.018	1.58 × 10^{-5}	1.71 × 10^{-4}	3.51 × 10^{-4}
3	0.750	26.132	1.85 × 10^{-4}	5.45 × 10^{-4}	0.022	1.91 × 10^{-5}	1.66 × 10^{-4}	5.26 × 10^{-4}
4	1.000	26.382	1.83 × 10^{-4}	7.20 × 10^{-4}	0.025	2.17 × 10^{-5}	1.61 × 10^{-4}	6.98 × 10^{-4}
5	1.250	26.632	1.81 × 10^{-4}	8.91 × 10^{-4}	0.027	2.39 × 10^{-5}	1.57 × 10^{-4}	8.67 × 10^{-4}
6	1.500	26.882	1.80 × 10^{-4}	1.06 × 10^{-3}	0.029	2.59 × 10^{-5}	1.54 × 10^{-4}	1.03 × 10^{-3}
f	1.900	27.282	1.77 × 10^{-4}	1.04 × 10^{-3}	0.201	1.77 × 10^{-4}	0	1.04 × 10^{-3}

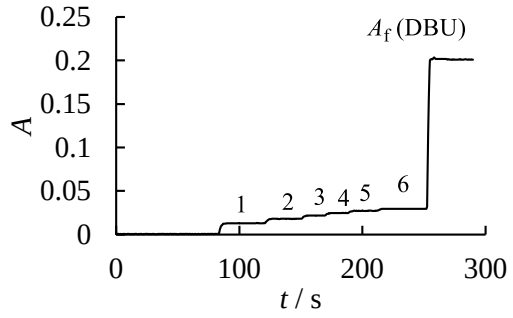

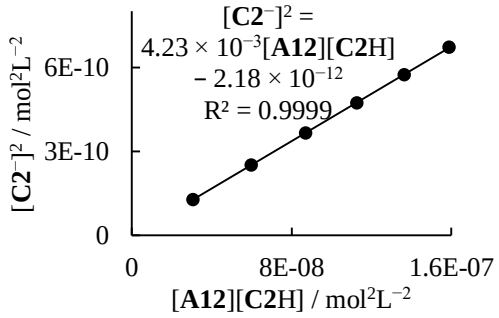

K = (4.23 ± 0.02) × 10^{-3}

Table 239. Determination of the pK_{aH} for **A12** with **C2**H in acetonitrile at 20 °C (detection at 420 nm). Stock solutions: **A12** (19.2 mg) in 10.0 mL MeCN; **C2**H (13.2 mg) in 10.0 mL MeCN; [DBU] = 2.38×10^{-2} mol L^{-1}. Step 0: 0.470 mL **C2**H stock solution in 21.4 g MeCN.

step	V_+ / mL	V / mL	[**C2**H]$_0$ / M	[**A12**]$_0$ / M	*A*	[**C2**$^-$] / M	[**C2**H] / M	[**A12**] / M
0	-	27.696	1.17×10^{-4}	0	0	0	1.17×10^{-4}	0
1	0.250	27.946	1.16×10^{-4}	1.70×10^{-4}	0.010	9.05×10^{-6}	1.07×10^{-4}	1.61×10^{-4}
2	0.500	28.196	1.15×10^{-4}	3.37×10^{-4}	0.014	1.23×10^{-5}	1.03×10^{-4}	3.24×10^{-4}
3	1.000	28.696	1.13×10^{-4}	6.61×10^{-4}	0.019	1.65×10^{-5}	9.66×10^{-5}	6.45×10^{-4}
4	1.500	29.196	1.11×10^{-4}	9.75×10^{-4}	0.023	1.96×10^{-5}	9.15×10^{-5}	9.56×10^{-4}
5	2.000	29.696	1.09×10^{-4}	1.28×10^{-3}	0.025	2.19×10^{-5}	8.73×10^{-5}	1.26×10^{-3}
6	2.500	30.196	1.07×10^{-4}	1.57×10^{-3}	0.027	2.38×10^{-5}	8.36×10^{-5}	1.55×10^{-3}
f	2.900	30.596	1.06×10^{-4}	1.55×10^{-3}	0.122	1.06×10^{-4}	0	1.55×10^{-3}

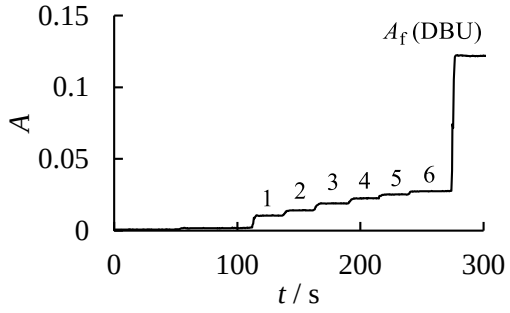

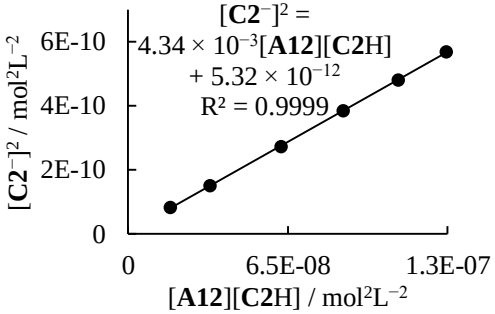

$K = (4.34 \pm 0.02) \times 10^{-3}$

$\bar{K} = (4.28 \pm 0.05) \times 10^{-3}$

pK_{aH}(**A12**) = 18.99

(*S*)-2-(Methoxymethyl)pyrrolidine (A13)

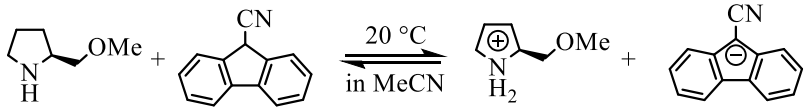

A13 **C2**H **A13**H$^+$ **C2**$^-$

Table 240. Determination of the pK_{aH} for **A13** with **C2**H in acetonitrile at 20 °C (detection at 420 nm). Stock solutions: **A13** (15.7 mg) in 10.0 mL MeCN; **C2**H (11.4 mg) in 10.0 mL MeCN; [DBU] = 3.69×10^{-2} mol L^{-1}. Step 0: 0.800 mL **C2**H stock solution in 20.2 g MeCN.

step	V_+ / mL	V / mL	[**C2**H]$_0$ / M	[**A13**]$_0$ / M	*A*	[**C2**$^-$] / M	[**C2**H] / M	[**A13**] / M
0	-	26.500	1.80×10^{-4}	0	0	0	1.80×10^{-4}	0
1	0.250	26.750	1.78×10^{-4}	1.27×10^{-4}	0.009	7.88×10^{-6}	1.70×10^{-4}	1.20×10^{-4}
2	0.500	27.000	1.77×10^{-4}	2.52×10^{-4}	0.013	1.11×10^{-5}	1.66×10^{-4}	2.41×10^{-4}
3	0.750	27.250	1.75×10^{-4}	3.75×10^{-4}	0.016	1.35×10^{-5}	1.62×10^{-4}	3.62×10^{-4}
4	1.000	27.500	1.73×10^{-4}	4.96×10^{-4}	0.018	1.54×10^{-5}	1.58×10^{-4}	4.80×10^{-4}
5	1.250	27.750	1.72×10^{-4}	6.14×10^{-4}	0.020	1.71×10^{-5}	1.55×10^{-4}	5.97×10^{-4}
6	1.500	28.000	1.70×10^{-4}	7.30×10^{-4}	0.022	1.85×10^{-5}	1.52×10^{-4}	7.12×10^{-4}
f	1.900	28.400	1.68×10^{-4}	7.20×10^{-4}	0.197	1.68×10^{-4}	0	7.20×10^{-4}

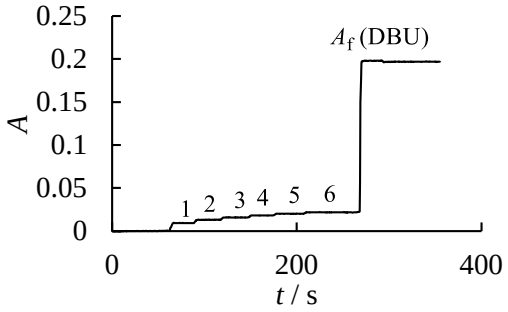

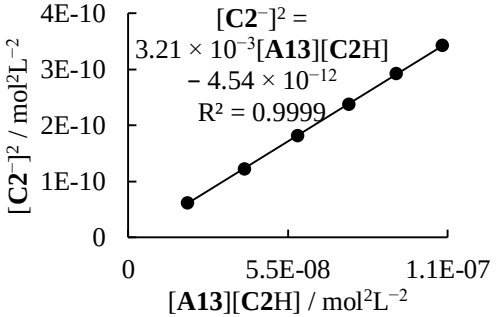

$K = (3.21 \pm 0.01) \times 10^{-3}$

Table 241. Determination of the pK_{aH} for **A13** with **C2**H in acetonitrile at 20 °C (detection at 420 nm). Stock solutions: **A13** (15.7 mg) in 10.0 mL MeCN; **C2**H (11.4 mg) in 10.0 mL MeCN; [DBU] = 3.69×10^{-2} mol L^{-1}. Step 0: 0.800 mL **C2**H stock solution in 19.7 g MeCN.

step	V_+ / mL	V / mL	[**C2**H]$_0$ / M	[**A13**]$_0$ / M	*A*	[**C2**$^-$] / M	[**C2**H] / M	[**A13**] / M
0	-	25.864	1.84×10^{-4}	0	0	0	1.84×10^{-4}	0
1	0.500	26.364	1.81×10^{-4}	2.59×10^{-4}	0.013	1.12×10^{-5}	1.70×10^{-4}	2.47×10^{-4}
2	1.000	26.864	1.78×10^{-4}	5.07×10^{-4}	0.019	1.58×10^{-5}	1.62×10^{-4}	4.92×10^{-4}
3	1.500	27.364	1.74×10^{-4}	7.47×10^{-4}	0.022	1.89×10^{-5}	1.55×10^{-4}	7.28×10^{-4}
4	2.000	27.864	1.71×10^{-4}	9.78×10^{-4}	0.025	2.15×10^{-5}	1.50×10^{-4}	9.57×10^{-4}
5	2.500	28.364	1.68×10^{-4}	1.20×10^{-3}	0.028	2.35×10^{-5}	1.45×10^{-4}	1.18×10^{-3}
6	3.000	28.864	1.65×10^{-4}	1.42×10^{-3}	0.030	2.52×10^{-5}	1.40×10^{-4}	1.39×10^{-3}
f	3.400	29.264	1.63×10^{-4}	1.40×10^{-3}	0.192	1.63×10^{-4}	0	1.40×10^{-3}

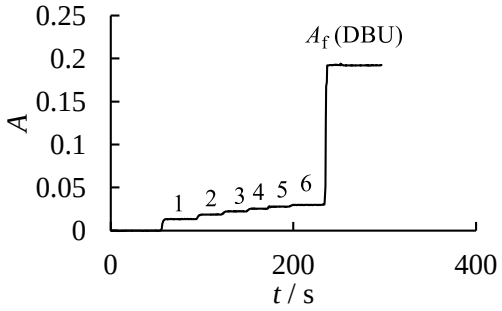

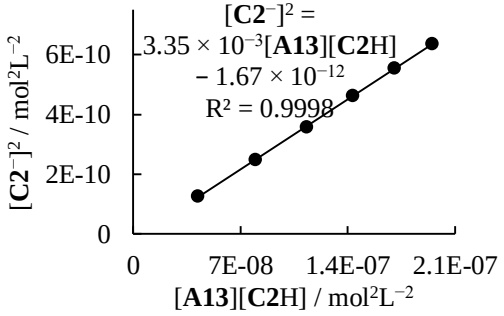

$K = (3.35 \pm 0.02) \times 10^{-3}$

$\bar{K} = (3.28 \pm 0.07) \times 10^{-3}$

pK_{aH}(**A13**) = 18.88

2-(Trifluoromethyl)pyrrolidine (A14)

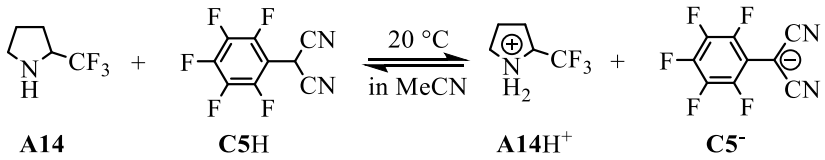

A14 **C5**H $\mathbf{A14}H^+$ $\mathbf{C5}^-$

Table 242. Determination of the pK_{aH} for **A14** with **C5**H in acetonitrile at 20 °C (detection at 330 nm). Stock solutions: **A14** (8.1 mg) in 10.0 mL MeCN; **C5**H (11.8 mg) in 10.0 mL MeCN; [DBU] = 3.99×10^{-2} mol L^{-1}. Step 0: 1.000 mL **C5**H stock solution in 20.8 g MeCN.

step	V_+ / mL	V / mL	[**C5**H]$_0$ / M	[**A14**]$_0$ / M	*A*	[$\mathbf{C5}^-$] / M	[**C5**H] / M	[**A14**] / M
0	-	27.463	1.85×10^{-4}	0	0	0	1.85×10^{-4}	0
1	0.250	27.713	1.83×10^{-4}	5.25×10^{-5}	0.078	2.91×10^{-5}	1.54×10^{-4}	2.34×10^{-5}
2	0.500	27.963	1.82×10^{-4}	1.04×10^{-4}	0.127	4.75×10^{-5}	1.34×10^{-4}	5.66×10^{-5}
3	0.750	28.213	1.80×10^{-4}	1.55×10^{-4}	0.162	6.07×10^{-5}	1.19×10^{-4}	9.40×10^{-5}
4	1.000	28.463	1.79×10^{-4}	2.05×10^{-4}	0.189	7.08×10^{-5}	1.08×10^{-4}	1.34×10^{-4}
5	1.250	28.713	1.77×10^{-4}	2.53×10^{-4}	0.210	7.88×10^{-5}	9.82×10^{-5}	1.75×10^{-4}
6	1.500	28.963	1.76×10^{-4}	3.02×10^{-4}	0.227	8.51×10^{-5}	9.04×10^{-5}	2.16×10^{-4}
7	1.750	29.213	1.74×10^{-4}	3.49×10^{-4}	0.241	9.04×10^{-5}	8.36×10^{-5}	2.58×10^{-4}
8	2.000	29.463	1.73×10^{-4}	3.95×10^{-4}	0.253	9.48×10^{-5}	7.78×10^{-5}	3.00×10^{-4}
f	2.200	29.663	1.71×10^{-4}	3.93×10^{-4}	0.457	1.71×10^{-4}	0	3.93×10^{-4}

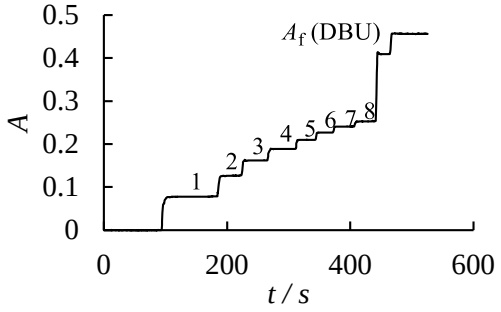

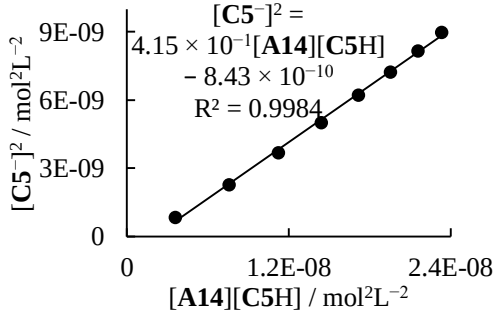

$K = (4.15 \pm 0.07) \times 10^{-1}$

Table 243. Determination of the pK_{aH} for **A14** with **C5**H in acetonitrile at 20 °C (detection at 330 nm). Stock solutions: **A14** (8.1 mg) in 10.0 mL MeCN; **C5**H (11.8 mg) in 10.0 mL MeCN; [DBU] = 3.99 × 10^{-2} mol· L^{-1}. Step 0: 0.800 mL **C5**H stock solution in 18.5 g MeCN.

step	V_+ / mL	V / mL	[**C5**H]$_0$ / M	[**A14**]$_0$ / M	*A*	[**C5**$^-$] / M	[**C5**H] / M	[**A14**] / M
0	-	24.337	1.67 × 10^{-4}	0	0	0	1.67 × 10^{-4}	0
1	0.250	24.587	1.65 × 10^{-4}	5.92 × 10^{-5}	0.082	3.07 × 10^{-5}	1.35 × 10^{-4}	2.85 × 10^{-5}
2	0.500	24.837	1.64 × 10^{-4}	1.17 × 10^{-4}	0.132	4.91 × 10^{-5}	1.15 × 10^{-4}	6.81 × 10^{-5}
3	0.750	25.087	1.62 × 10^{-4}	1.74 × 10^{-4}	0.166	6.19 × 10^{-5}	1.00 × 10^{-4}	1.12 × 10^{-4}
4	1.000	25.337	1.61 × 10^{-4}	2.30 × 10^{-4}	0.191	7.11 × 10^{-5}	8.94 × 10^{-5}	1.59 × 10^{-4}
5	1.250	25.587	1.59 × 10^{-4}	2.84 × 10^{-4}	0.210	7.83 × 10^{-5}	8.07 × 10^{-5}	2.06 × 10^{-4}
6	1.500	25.837	1.57 × 10^{-4}	3.38 × 10^{-4}	0.225	8.39 × 10^{-5}	7.35 × 10^{-5}	2.54 × 10^{-4}
7	1.750	26.087	1.56 × 10^{-4}	3.91 × 10^{-4}	0.238	8.85 × 10^{-5}	6.74 × 10^{-5}	3.02 × 10^{-4}
8	2.000	26.337	1.54 × 10^{-4}	4.42 × 10^{-4}	0.247	9.21 × 10^{-5}	6.23 × 10^{-5}	3.50 × 10^{-4}
f	2.200	26.537	1.53 × 10^{-4}	4.39 × 10^{-4}	0.411	1.53 × 10^{-4}	0	4.39 × 10^{-4}

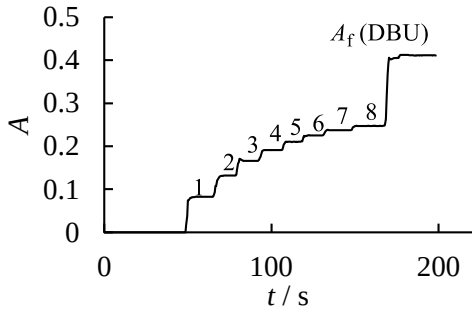

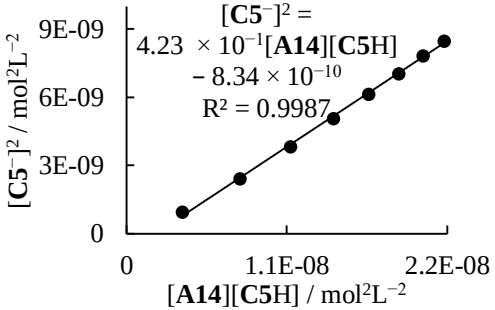

K = (4.23 ± 0.06) × 10^{-1}

Table 244. Determination of the pK_{aH} for **A14** with **C5**H in acetonitrile at 20 °C (detection at 330 nm). Stock solutions: **A14** (8.1 mg) in 10.0 mL MeCN; **C5**H (11.8 mg) in 10.0 mL MeCN; [DBU] = 3.99 × 10^{-2} mol L^{-1}. Step 0: 0.800 mL **C5**H stock solution in 21.3 g MeCN.

step	V_+ / mL	V / mL	[**C5**H]$_0$ / M	[**A14**]$_0$ / M	*A*	[**C5**$^-$] / M	[**C5**H] / M	[**A14**] / M
0	-	27.899	1.46×10^{-4}	0	0	0	1.46×10^{-4}	0
1	0.250	28.149	1.44×10^{-4}	5.17×10^{-5}	0.072	2.67×10^{-5}	1.18×10^{-4}	2.50×10^{-5}
2	0.500	28.399	1.43×10^{-4}	1.03×10^{-4}	0.115	4.29×10^{-5}	1.00×10^{-4}	5.96×10^{-5}
3	0.750	28.649	1.42×10^{-4}	1.52×10^{-4}	0.146	5.43×10^{-5}	8.77×10^{-5}	9.81×10^{-5}
4	1.000	28.899	1.41×10^{-4}	2.01×10^{-4}	0.168	6.24×10^{-5}	7.83×10^{-5}	1.39×10^{-4}
5	1.250	29.149	1.40×10^{-4}	2.50×10^{-4}	0.185	6.88×10^{-5}	7.08×10^{-5}	1.81×10^{-4}
6	1.500	29.399	1.38×10^{-4}	2.97×10^{-4}	0.198	7.38×10^{-5}	6.45×10^{-5}	2.23×10^{-4}
7	1.750	29.649	1.37×10^{-4}	3.44×10^{-4}	0.209	7.80×10^{-5}	5.92×10^{-5}	2.66×10^{-4}
8	2.000	29.899	1.36×10^{-4}	3.89×10^{-4}	0.219	8.14×10^{-5}	5.46×10^{-5}	3.08×10^{-4}
f	2.200	30.099	1.35×10^{-4}	3.87×10^{-4}	0.363	1.35×10^{-4}	0	3.87×10^{-4}

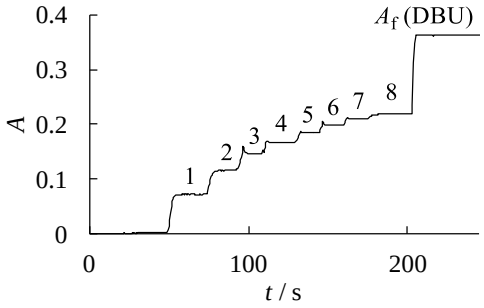

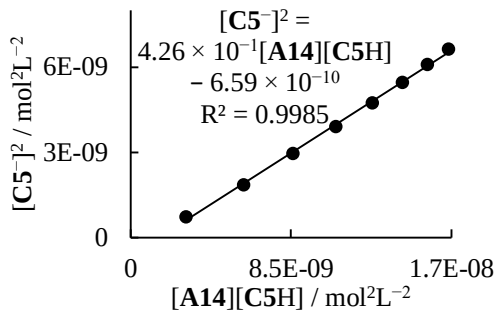

$K = (4.26 \pm 0.07) \times 10^{-1}$

$\bar{K} = (4.21 \pm 0.05) \times 10^{-1}$

pK_{aH}(**A14**) = 12.63

Methyl *L*-prolinate (A15)

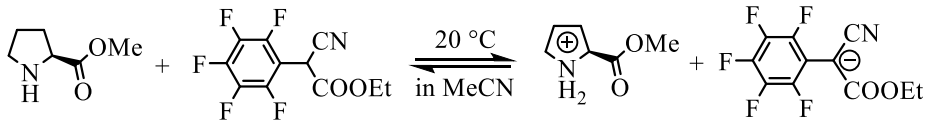

A15 **C3**H **A15**H$^+$ **C3**$^-$

Table 245. Determination of the pK_{aH} for **A15** with **C3**H in acetonitrile at 20 °C (detection at 333 nm). Stock solutions: **A15** (35.6 mg) in 10.0 mL MeCN; **C3**H (18.9 mg) in 10.0 mL MeCN; [DBU] = 3.69×10^{-2} mol L^{-1}. Step 0: 0.500 mL **C3**H stock solution in 20.3 g MeCN.

step	V_+ / mL	V / mL	[**C3**H]$_0$ / M	[**A15**]$_0$ / M	*A*	[**C3**$^-$] / M	[**C3**H] / M	[**A15**] / M
0	-	26.327	1.29×10^{-4}	0	0	0	1.29×10^{-4}	0
1	0.050	26.377	1.28×10^{-4}	5.22×10^{-5}	0.046	1.65×10^{-5}	1.12×10^{-4}	3.57×10^{-5}
2	0.100	26.427	1.28×10^{-4}	1.04×10^{-4}	0.068	2.43×10^{-5}	1.04×10^{-4}	8.00×10^{-5}
3	0.150	26.477	1.28×10^{-4}	1.56×10^{-4}	0.084	2.99×10^{-5}	9.79×10^{-5}	1.26×10^{-4}
4	0.200	26.527	1.28×10^{-4}	2.08×10^{-4}	0.097	3.44×10^{-5}	9.32×10^{-5}	1.73×10^{-4}
5	0.260	26.587	1.27×10^{-4}	2.70×10^{-4}	0.109	3.89×10^{-5}	8.85×10^{-5}	2.31×10^{-4}
6	0.300	26.627	1.27×10^{-4}	3.11×10^{-4}	0.116	4.14×10^{-5}	8.58×10^{-5}	2.69×10^{-4}
7	0.350	26.677	1.27×10^{-4}	3.62×10^{-4}	0.124	4.42×10^{-5}	8.27×10^{-5}	3.17×10^{-4}
8	0.400	26.727	1.27×10^{-4}	4.13×10^{-4}	0.131	4.67×10^{-5}	8.00×10^{-5}	3.66×10^{-4}
f	0.600	26.927	1.26×10^{-4}	4.09×10^{-4}	0.352	1.26×10^{-4}	0	4.09×10^{-4}

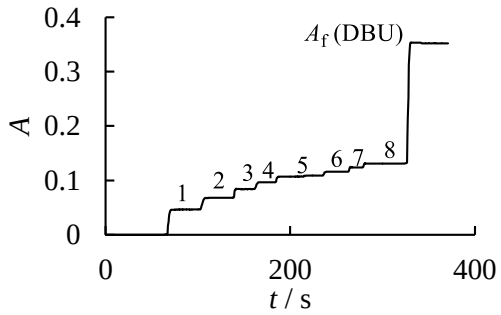

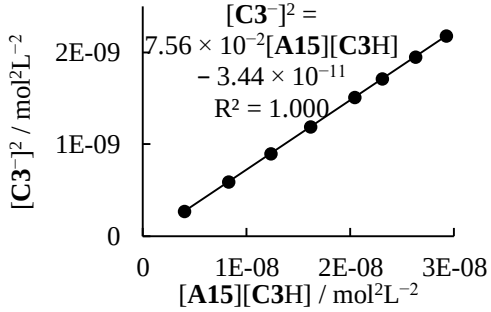

$K = (7.56 \pm 0.01) \times 10^{-2}$

pK_{aH}(**A15**) = 16.63

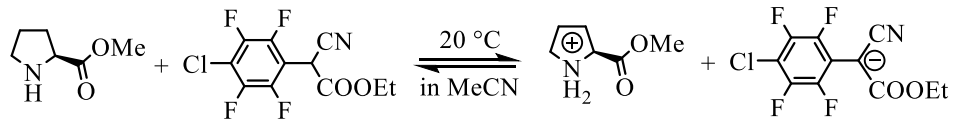

A15 **C4**H **A15**H$^+$ **C4**$^-$

Table 246. Determination of the pK_{aH} for **A15** with **C4**H in acetonitrile at 20 °C (detection at 333 nm). Stock solutions: **A15** (35.6 mg) in 10.0 mL MeCN; **C4**H (13.1 mg) in 10.0 mL MeCN; [DBU] = 2.76 × 10^{-2} mol L^{-1}. Step 0: 0.500 mL **C4**H stock solution in 20.8 g MeCN.

step	V_+ / mL	V / mL	[**C4**H]$_0$ / M	[**A15**]$_0$ / M	*A*	[**C4**$^-$] / M	[**C4**H] / M	[**A15**] / M
0	-	26.963	8.22 × 10^{-5}	0	0	0	8.22 × 10^{-5}	0
1	0.050	27.013	8.20 × 10^{-5}	5.10 × 10^{-5}	0.143	1.87 × 10^{-5}	6.34 × 10^{-5}	3.24 × 10^{-5}
2	0.100	27.063	8.19 × 10^{-5}	1.02 × 10^{-4}	0.203	2.66 × 10^{-5}	5.53 × 10^{-5}	7.53 × 10^{-5}
3	0.150	27.113	8.17 × 10^{-5}	1.52 × 10^{-4}	0.245	3.20 × 10^{-5}	4.97 × 10^{-5}	1.20 × 10^{-4}
4	0.200	27.163	8.16 × 10^{-5}	2.03 × 10^{-4}	0.276	3.60 × 10^{-5}	4.55 × 10^{-5}	1.67 × 10^{-4}
5	0.250	27.213	8.14 × 10^{-5}	2.53 × 10^{-4}	0.300	3.93 × 10^{-5}	4.21 × 10^{-5}	2.14 × 10^{-4}
6	0.300	27.263	8.13 × 10^{-5}	3.03 × 10^{-4}	0.321	4.20 × 10^{-5}	3.93 × 10^{-5}	2.61 × 10^{-4}
f	0.500	27.463	8.07 × 10^{-5}	3.01 × 10^{-4}	0.617	8.07 × 10^{-5}	0	3.01 × 10^{-4}

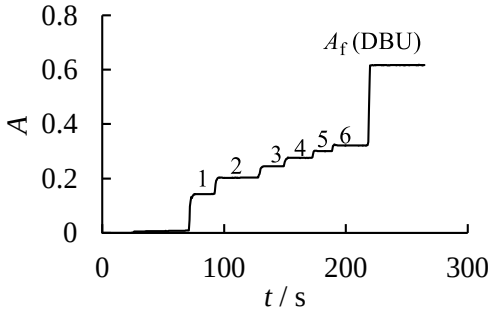

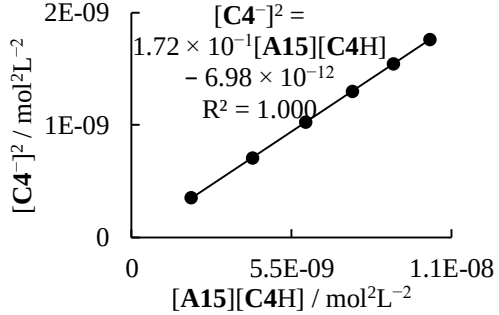

K = (1.72 ± 0.00) × 10^{-1}

pK_{aH}(**A15**) = 16.63

pK_{aH}(**A15**) = 16.63

(*S*)-*N*,*N*-Dimethylpyrrolidine-2-carboxamide (A16)

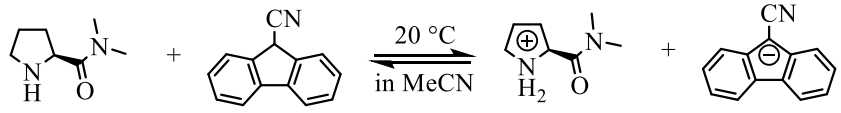

A16 **C2**H **A16**H$^+$ **C2**$^-$

Table 247. Determination of the pK_{aH} for **A16** with **C2**H in acetonitrile at 20 °C (detection at 420 nm). Stock solutions: **A16** (30.3 mg) in 10.0 mL MeCN; **C2**H (12.9 mg) in 10.0 mL MeCN; [DBU] = 1.72×10^{-2} mol L^{-1}. Step 0: 0.600 mL **C2**H stock solution in 18.6 g MeCN.

step	V_+ / mL	V / mL	[**C2**H]$_0$ / M	[**A16**]$_0$ / M	*A*	[**C2**$^-$] / M	[**C2**H] / M	[**A16**] / M
0	-	24.264	1.67×10^{-4}	0	0	0	1.67×10^{-4}	0
1	0.500	24.764	1.63×10^{-4}	4.30×10^{-4}	0.008	6.78×10^{-6}	1.57×10^{-4}	4.23×10^{-4}
2	1.000	25.264	1.60×10^{-4}	8.43×10^{-4}	0.012	1.02×10^{-5}	1.50×10^{-4}	8.33×10^{-4}
3	1.500	25.764	1.57×10^{-4}	1.24×10^{-3}	0.015	1.26×10^{-5}	1.44×10^{-4}	1.23×10^{-3}
4	2.000	26.264	1.54×10^{-4}	1.62×10^{-3}	0.017	1.47×10^{-5}	1.39×10^{-4}	1.61×10^{-3}
5	2.500	26.764	1.51×10^{-4}	1.99×10^{-3}	0.019	1.62×10^{-5}	1.35×10^{-4}	1.97×10^{-3}
f	3.400	27.664	1.46×10^{-4}	1.93×10^{-3}	0.171	1.46×10^{-4}	0	1.93×10^{-3}

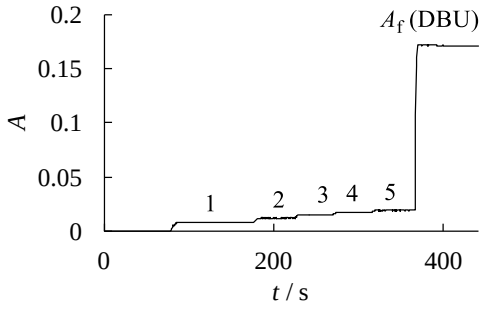

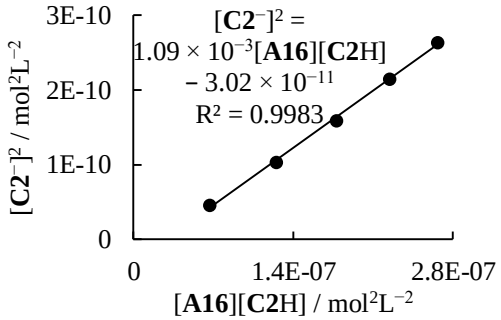

$K = (1.09 \pm 0.03) \times 10^{-3}$

Table 248. Determination of the pK_{aH} for **A16** with **C2**H in acetonitrile at 20 °C (detection at 420 nm). Stock solutions: **A16** (30.3 mg) in 10.0 mL MeCN; **C2**H (12.9 mg) in 10.0 mL MeCN; [DBU] = 1.72×10^{-2} mol L^{-1}. Step 0: 0.600 mL **C2**H stock solution in 18.1 g MeCN.

step	V_+ / mL	V / mL	[**C2**H]$_0$ / M	[**A16**]$_0$ / M	*A*	[**C2**$^-$] / M	[**C2**H] / M	[**A16**] / M
0	-	23.628	1.71×10^{-4}	0	0	0	1.71×10^{-4}	0
1	1.000	24.628	1.64×10^{-4}	8.65×10^{-4}	0.012	9.78×10^{-6}	1.55×10^{-4}	8.55×10^{-4}
2	2.000	25.628	1.58×10^{-4}	1.66×10^{-3}	0.017	1.44×10^{-5}	1.44×10^{-4}	1.65×10^{-3}
3	3.000	26.628	1.52×10^{-4}	2.40×10^{-3}	0.021	1.75×10^{-5}	1.34×10^{-4}	2.38×10^{-3}
4	4.000	27.628	1.46×10^{-4}	3.08×10^{-3}	0.024	1.98×10^{-5}	1.27×10^{-4}	3.07×10^{-3}
5	5.000	28.628	1.41×10^{-4}	3.72×10^{-3}	0.026	2.16×10^{-5}	1.20×10^{-4}	3.70×10^{-3}
f	6.000	29.628	1.37×10^{-4}	3.60×10^{-3}	0.162	1.37×10^{-4}	0	3.60×10^{-3}

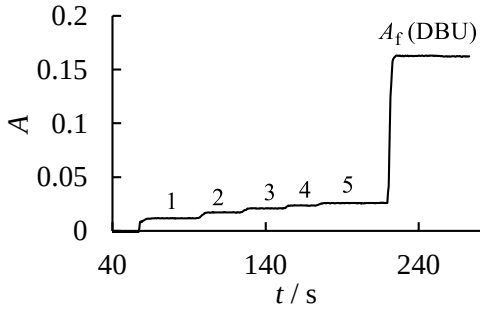

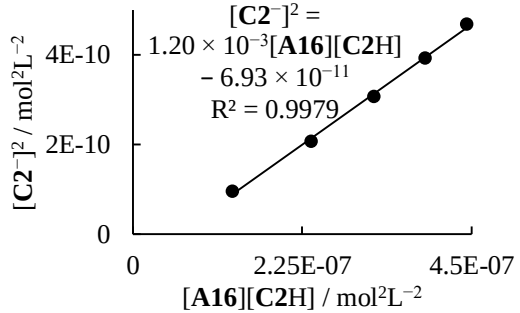

$K = (1.20 \pm 0.03) \times 10^{-3}$

For **A16** + **C2**H: $\bar{K} = (1.14 \pm 0.05) \times 10^{-3}$
pK_{aH} = 18.42

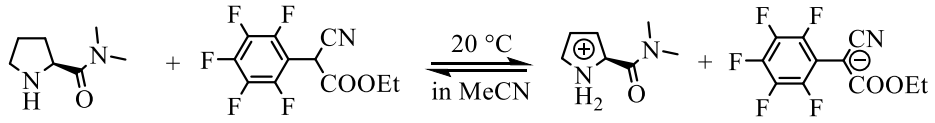

A16 **C3**H **A16**H$^+$ **C3**$^-$

Table 249. Determination of the pK_{aH} for **A16** with **C3**H in acetonitrile at 20 °C (detection at 333 nm). Stock solutions: **A16** (30.3 mg) in 10.0 mL MeCN; **C3**H (12.6 mg) in 10.0 mL MeCN; [DBU] = 1.72×10^{-2} mol L^{-1}. Step 0: 0.600 mL **C3**H stock solution in 19.7 g MeCN.

step	V_+ / mL	V / mL	[**C3**H]$_0$ / M	[**A16**]$_0$ / M	*A*	[**C3**$^-$] / M	[**C3**H] / M	[**A16**] / M
0	-	25.664	1.06×10^{-4}	0	0	0	1.06×10^{-4}	0
1	0.050	25.714	1.05×10^{-4}	4.14×10^{-5}	0.101	3.68×10^{-5}	6.86×10^{-5}	4.67×10^{-6}
2	0.100	25.764	1.05×10^{-4}	8.27×10^{-5}	0.177	6.40×10^{-5}	4.11×10^{-5}	1.87×10^{-5}
3	0.150	25.814	1.05×10^{-4}	1.24×10^{-4}	0.221	8.02×10^{-5}	2.47×10^{-5}	4.36×10^{-5}
4	0.200	25.864	1.05×10^{-4}	1.65×10^{-4}	0.244	8.83×10^{-5}	1.64×10^{-5}	7.65×10^{-5}
5	0.250	25.914	1.05×10^{-4}	2.06×10^{-4}	0.255	9.24×10^{-5}	1.21×10^{-5}	1.13×10^{-4}
6	0.300	25.964	1.04×10^{-4}	2.46×10^{-4}	0.262	9.49×10^{-5}	9.45×10^{-6}	1.51×10^{-4}
7	0.400	26.064	1.04×10^{-4}	3.27×10^{-4}	0.269	9.73×10^{-5}	6.59×10^{-6}	2.30×10^{-4}
8	0.500	26.164	1.04×10^{-4}	4.07×10^{-4}	0.272	9.84×10^{-5}	5.09×10^{-6}	3.09×10^{-4}
f	1.000	26.664	1.02×10^{-4}	4.00×10^{-4}	0.280	1.02×10^{-4}	0	4.00×10^{-4}

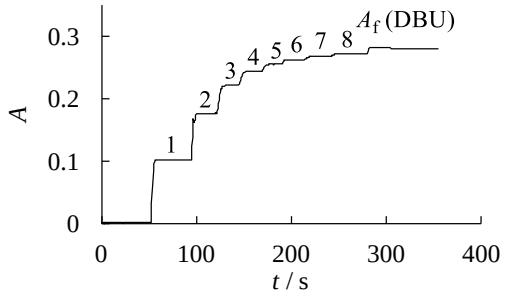

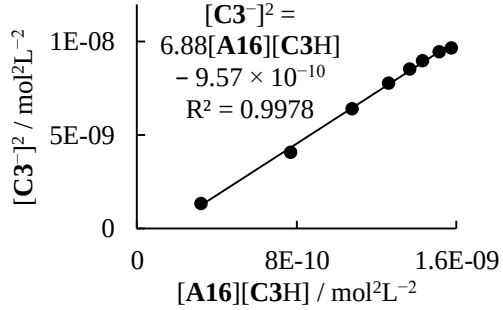

$K = 6.88 \pm 0.13$

Table 250. Determination of the pK_{aH} for **A16** with **C3**H in acetonitrile at 20 °C (detection at 333 nm). Stock solutions: **A16** (30.3 mg) in 10.0 mL MeCN; **C3**H (12.6 mg) in 10.0 mL MeCN; [DBU] = 1.72×10^{-2} mol L^{-1}. Step 0: 0.600 mL **C3**H stock solution in 19.4 g MeCN.

step	V_+ / mL	V / mL	[**C3**H]$_0$ / M	[**A16**]$_0$ / M	*A*	[**C3**$^-$] / M	[**C3**H] / M	[**A16**] / M
0	-	25.282	1.07×10^{-4}	0	0	0	1.07×10^{-4}	0
1	0.020	25.302	1.07×10^{-4}	1.68×10^{-5}	0.043	1.56×10^{-5}	9.14×10^{-5}	1.23×10^{-6}
2	0.040	25.322	1.07×10^{-4}	3.37×10^{-5}	0.082	3.01×10^{-5}	7.69×10^{-5}	3.59×10^{-6}
3	0.060	25.342	1.07×10^{-4}	5.04×10^{-5}	0.117	4.30×10^{-5}	6.39×10^{-5}	7.49×10^{-6}
4	0.080	25.362	1.07×10^{-4}	6.72×10^{-5}	0.149	5.46×10^{-5}	5.21×10^{-5}	1.26×10^{-5}
5	0.100	25.382	1.07×10^{-4}	8.39×10^{-5}	0.175	6.42×10^{-5}	4.25×10^{-5}	1.98×10^{-5}
f	0.600	25.882	1.05×10^{-4}	8.23×10^{-5}	0.286	1.05×10^{-4}	0	8.23×10^{-5}

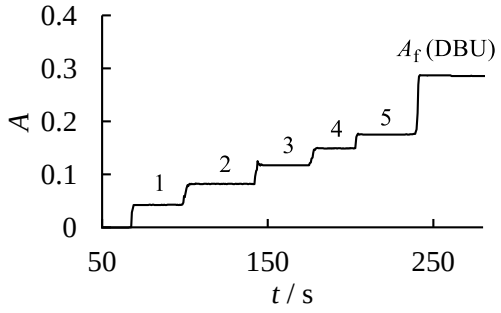

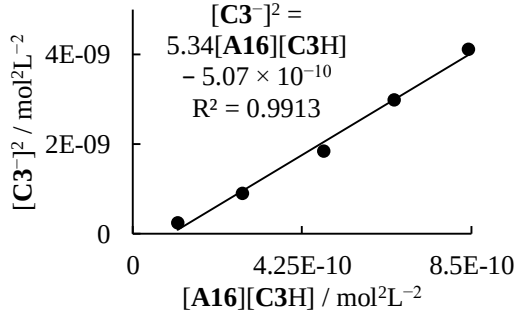

K = 5.34 ± 0.29

For **A16** + **C3**H: $\overline{K}$ = 6.11 ± 0.77

pK_{aH} = 18.34

pK_{aH}(**A16**) = 18.38 (average)

(*S*)-*N*-Propylpyrrolidine-2-carboxamide (A17)

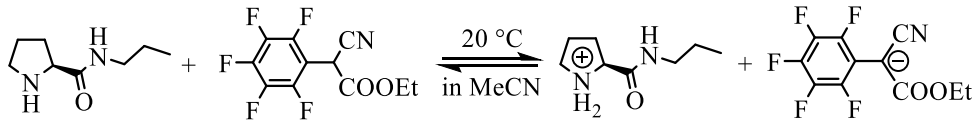

A17 **C3**H **A17**H$^+$ **C3**$^-$

Table 251. Determination of the pK_{aH} for **A17** with **C3**H in acetonitrile at 20 °C (detection at 333 nm). Stock solutions: **A17** (20.6 mg) in 10.0 mL MeCN; **C3**H (12.6 mg) stock solution in 10.0 mL MeCN; [DBU] = 1.75 × 10^{-2} mol L^{-1}. Step 0: 0.600 mL **C3**H stock solution in 19.3 g MeCN.

step	V_+ / mL	V / mL	[**C3**H]$_0$ / M	[**A17**]$_0$ / M	*A*	[**C3**$^-$] / M	[**C3**H] / M	[**A17**] / M
0	-	25.155	1.08 × 10^{-4}	0	0	0	1.08 × 10^{-4}	0
1	0.025	25.180	1.08 × 10^{-4}	1.31 × 10^{-5}	0.026	9.35 × 10^{-6}	9.82 × 10^{-5}	3.74 × 10^{-6}
2	0.050	25.205	1.07 × 10^{-4}	2.62 × 10^{-5}	0.042	1.54 × 10^{-5}	9.20 × 10^{-5}	1.07 × 10^{-5}
3	0.100	25.255	1.07 × 10^{-4}	5.22 × 10^{-5}	0.067	2.44 × 10^{-5}	8.29 × 10^{-5}	2.79 × 10^{-5}
4	0.150	25.305	1.07 × 10^{-4}	7.82 × 10^{-5}	0.085	3.08 × 10^{-5}	7.62 × 10^{-5}	4.74 × 10^{-5}
5	0.200	25.355	1.07 × 10^{-4}	1.04 × 10^{-4}	0.099	3.60 × 10^{-5}	7.09 × 10^{-5}	6.81 × 10^{-5}
6	0.250	25.405	1.07 × 10^{-4}	1.30 × 10^{-4}	0.110	4.00 × 10^{-5}	6.66 × 10^{-5}	8.98 × 10^{-5}
f	0.750	25.905	1.05 × 10^{-4}	1.27 × 10^{-4}	0.287	1.05 × 10^{-4}	0	1.27 × 10^{-4}

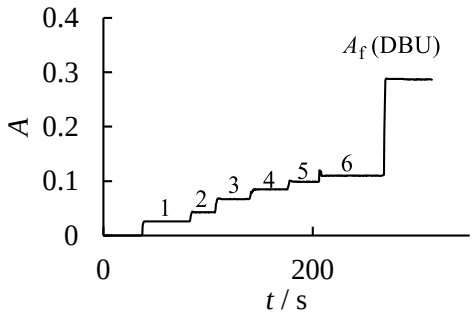

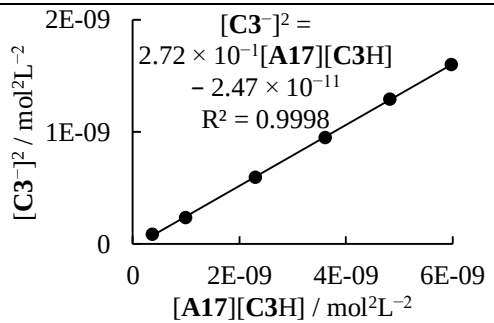

K = (2.72 ± 0.02) × 10^{-1}

pK_{aH} = 17.18

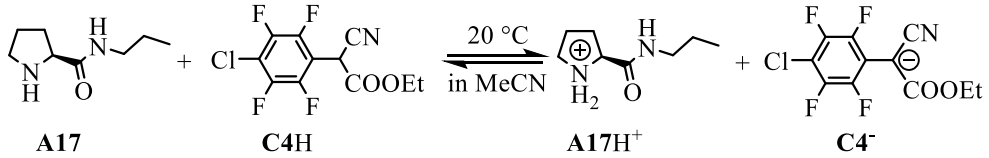

Table 252. Determination of the pK_{aH} for **A17** with **C4**H in acetonitrile at 20 °C (detection at 333 nm). Stock solutions: **A17** (20.6 mg) in 10.0 mL MeCN; **C4**H (10.3 mg) in 10.0 mL MeCN; [DBU] = 1.75 × 10^{-2} mol L^{-1}. Step 0: 0.500 mL **C4**H stock solution in 19.1 g MeCN.

step	V_+ / mL	V / mL	[**C4**H]$_0$ / M	[**A17**]$_0$ / M	*A*	[**C4**$^-$] / M	[**C4**H] / M	[**A17**] / M
0	-	24.800	7.02 × 10^{-5}	0	0	0	7.02 × 10^{-5}	0
1	0.025	24.825	7.02 × 10^{-5}	1.33 × 10^{-5}	0.076	1.02 × 10^{-5}	6.00 × 10^{-5}	3.11 × 10^{-6}
2	0.050	24.850	7.01 × 10^{-5}	2.65 × 10^{-5}	0.126	1.68 × 10^{-5}	5.33 × 10^{-5}	9.68 × 10^{-6}
3	0.075	24.875	7.00 × 10^{-5}	3.98 × 10^{-5}	0.165	2.20 × 10^{-5}	4.80 × 10^{-5}	1.77 × 10^{-5}
4	0.100	24.900	7.00 × 10^{-5}	5.30 × 10^{-5}	0.196	2.62 × 10^{-5}	4.37 × 10^{-5}	2.67 × 10^{-5}
5	0.125	24.925	6.99 × 10^{-5}	6.61 × 10^{-5}	0.222	2.97 × 10^{-5}	4.02 × 10^{-5}	3.64 × 10^{-5}
6	0.150	24.950	6.98 × 10^{-5}	7.93 × 10^{-5}	0.243	3.26 × 10^{-5}	3.73 × 10^{-5}	4.67 × 10^{-5}
f	0.550	25.350	6.87 × 10^{-5}	7.80 × 10^{-5}	0.514	6.87 × 10^{-5}	0	7.80 × 10^{-5}

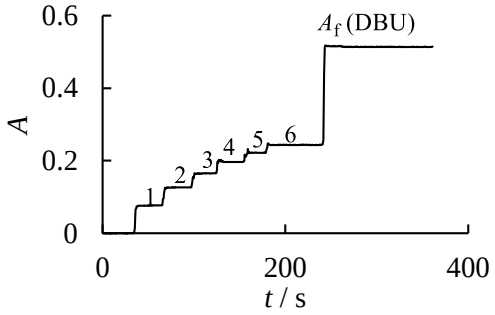

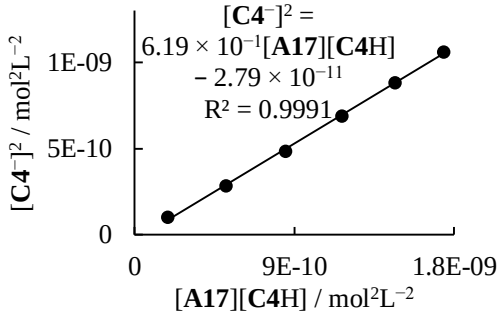

K = (6.19 ± 0.10) × 10^{-1}

pK_{aH} = 17.18

pK_{aH}(**A17**) = 17.18 (average)

(*S*)-2-(Pyrrolidin-2-ylmethyl)isoindoline-1,3-dione (A18)

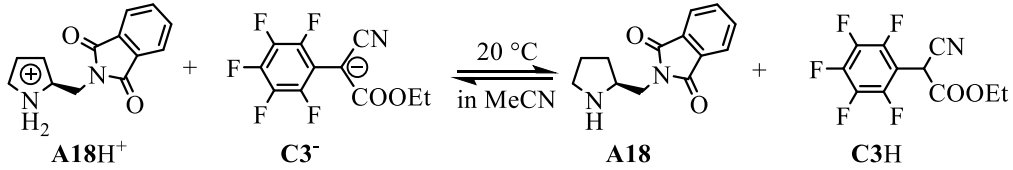

A18H$^+$ **C3**$^-$ **A18** **C3**H

Table 253. Determination of the pK_{aH} for **A18** with **C3**$^-$ in acetonitrile at 20 °C (detection at 333 nm). Stock solutions: **A18**H$^+$CF$_3$CO$_2^-$ (10.3 mg) in 10.0 mL MeCN; **C3**$^-$K$^+$ (5.4 mg) in 25.0 mL MeCN. Step 0: 2.000 mL **C3**$^-$K$^+$ stock solution in 17.7 g MeCN.

step	V_+ / mL	V / mL	[**C3**$^-$]$_0$ / M	[**A18**H$^+$]$_0$ / M	*A*	[**C3**$^-$] / M	[**C3**H] / M	[**A18**H$^+$] / M
0	-	24.519	5.55×10^{-5}	0	0.167	5.55×10^{-5}	0	0
1	0.100	24.619	5.53×10^{-5}	1.22×10^{-5}	0.141	4.69×10^{-5}	8.45×10^{-6}	3.71×10^{-6}
2	0.200	24.719	5.51×10^{-5}	2.42×10^{-5}	0.123	4.11×10^{-5}	1.40×10^{-5}	1.02×10^{-5}
3	0.300	24.819	5.49×10^{-5}	3.62×10^{-5}	0.110	3.67×10^{-5}	1.82×10^{-5}	1.80×10^{-5}
4	0.400	24.919	5.46×10^{-5}	4.80×10^{-5}	0.101	3.36×10^{-5}	2.11×10^{-5}	2.69×10^{-5}
5	0.500	25.019	5.44×10^{-5}	5.98×10^{-5}	0.093	3.10×10^{-5}	2.34×10^{-5}	3.63×10^{-5}
6	0.600	25.119	5.42×10^{-5}	7.15×10^{-5}	0.087	2.90×10^{-5}	2.52×10^{-5}	4.63×10^{-5}
7	0.700	25.219	5.40×10^{-5}	8.30×10^{-5}	0.082	2.73×10^{-5}	2.67×10^{-5}	5.63×10^{-5}
8	0.800	25.319	5.38×10^{-5}	9.45×10^{-5}	0.078	2.58×10^{-5}	2.79×10^{-5}	6.66×10^{-5}
9	0.900	25.419	5.36×10^{-5}	1.06×10^{-4}	0.074	2.46×10^{-5}	2.90×10^{-5}	7.69×10^{-5}
10	1.000	25.519	5.34×10^{-5}	1.17×10^{-4}	0.071	2.35×10^{-5}	2.98×10^{-5}	8.74×10^{-5}

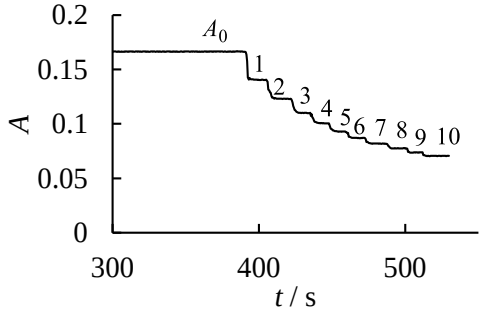

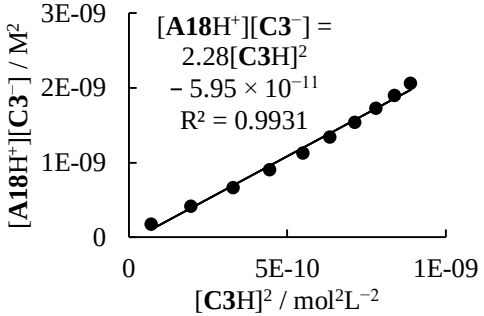

K = 2.28 ± 0.07

pK_{aH} = 18.11

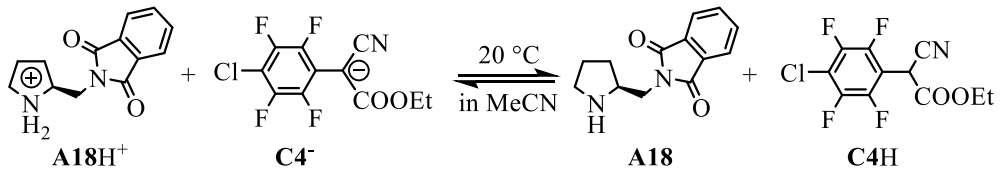

Table 254. Determination of the pK_{aH} for **A18** with **C4**$^-$ in acetonitrile at 20 °C (detection at 333 nm). Stock solutions: **A18**H$^+$CF$_3$CO$_2^-$ (10.3 mg) in 10.0 mL MeCN; **C4**$^-$K$^+$ (5.1 mg) in 25.0 mL MeCN. Step 0: 1.000 mL **C4**$^-$K$^+$ stock solution in 18.8 g MeCN.

step	V_+ / mL	V / mL	[**C4**H]$_0$ / M	[**A18**H$^+$]$_0$ / M	*A*	[**C4**$^-$] / M	[**C4**H] / M	[**A18**H$^+$] / M
0	-	24.919	2.45×10^{-5}	0	0.204	2.45×10^{-5}	0	0
1	0.100	25.019	2.44×10^{-5}	1.20×10^{-5}	0.161	1.93×10^{-5}	5.13×10^{-6}	6.83×10^{-6}
2	0.250	25.169	2.43×10^{-5}	2.97×10^{-5}	0.131	1.57×10^{-5}	8.56×10^{-6}	2.12×10^{-5}
3	0.500	25.419	2.40×10^{-5}	5.88×10^{-5}	0.106	1.27×10^{-5}	1.13×10^{-5}	4.75×10^{-5}
4	0.750	25.669	2.38×10^{-5}	8.74×10^{-5}	0.091	1.10×10^{-5}	1.28×10^{-5}	7.46×10^{-5}
5	1.000	25.919	2.36×10^{-5}	1.15×10^{-4}	0.082	9.82×10^{-6}	1.38×10^{-5}	1.02×10^{-4}
6	1.250	26.169	2.34×10^{-5}	1.43×10^{-4}	0.075	8.95×10^{-6}	1.44×10^{-5}	1.28×10^{-4}

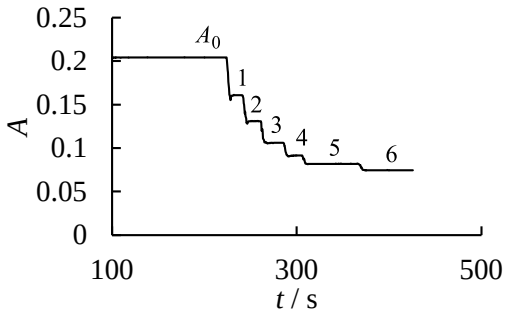

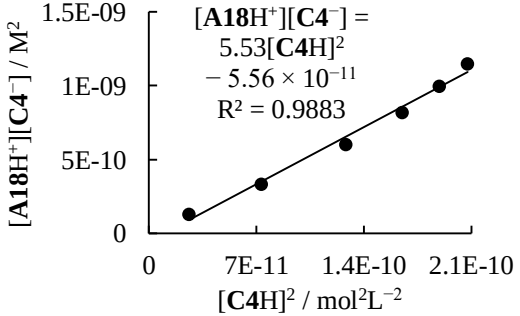

K = 5.53 ± 0.30

pK_{aH} = 18.13

pK_{aH}(**A18**) = 18.12 (average)

(*S*)-4-Phenyl-1-(pyrrolidin-2-ylmethyl)-1H-1,2,3-triazole (A19)

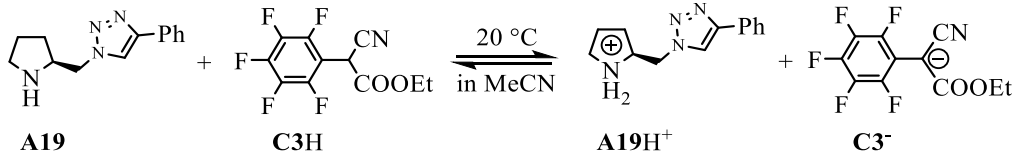

A19 **C3**H **A19**H$^+$ **C3**$^-$

Table 255. Determination of the pK_{aH} for **A19** with **C3**H in acetonitrile at 20 °C (detection at 350 nm). Stock solutions: **A19** (12.1 mg) in 10.0 mL MeCN; **C3**H (25.4 mg) in 10.0 mL MeCN; [DBU] = 8.50 × 10^{-2} mol L^{-1}. Step 0: 0.700 mL **C3**H stock solution in 21.2 g MeCN.

step	V_+ / mL	V / mL	[**C4**H]$_0$ / M	[**A19**]$_0$ / M	*A*	[**C4**$^-$] / M	[**C4**H] / M	[**A19**] / M
0	-	27.672	2.30 × 10^{-4}	0	0	0	2.30 × 10^{-4}	0
1	0.500	28.172	2.26 × 10^{-4}	9.41 × 10^{-5}	0.028	3.17 × 10^{-5}	1.94 × 10^{-4}	6.23 × 10^{-5}
2	0.750	28.422	2.24 × 10^{-4}	1.40 × 10^{-4}	0.038	4.26 × 10^{-5}	1.81 × 10^{-4}	9.72 × 10^{-5}
3	1.000	28.672	2.22 × 10^{-4}	1.85 × 10^{-4}	0.045	5.14 × 10^{-5}	1.71 × 10^{-4}	1.33 × 10^{-4}
4	1.250	28.922	2.20 × 10^{-4}	2.29 × 10^{-4}	0.052	5.89 × 10^{-5}	1.61 × 10^{-4}	1.70 × 10^{-4}
5	1.500	29.172	2.18 × 10^{-4}	2.73 × 10^{-4}	0.058	6.53 × 10^{-5}	1.53 × 10^{-4}	2.07 × 10^{-4}
6	1.750	29.422	2.16 × 10^{-4}	3.15 × 10^{-4}	0.063	7.10 × 10^{-5}	1.45 × 10^{-4}	2.44 × 10^{-4}
f	2.040	29.712	2.14 × 10^{-4}	3.12 × 10^{-4}	0.189	2.14 × 10^{-4}	0	3.12 × 10^{-4}

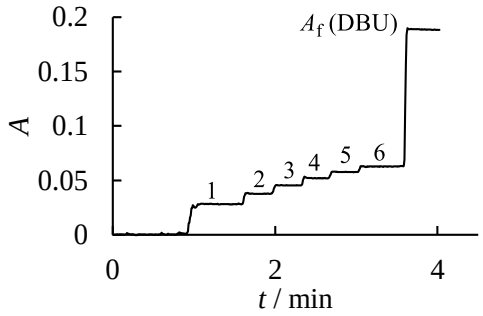

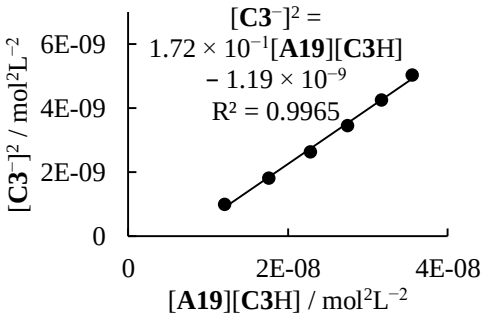

K = (1.72 ± 0.05) × 10^{-1}

pK_{aH} = 16.99

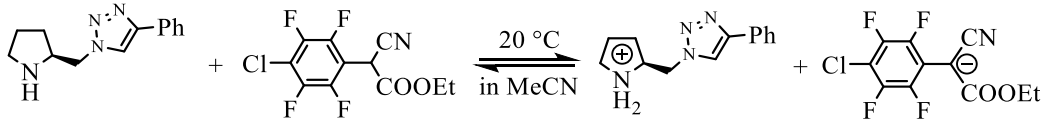

A19 **C4**H **A19**H$^+$ **C4**$^-$

Table 256. Determination of the pK_{aH} for **A19** with **C4**H in acetonitrile at 20 °C (detection at 350 nm). Stock solutions: **A19** (12.1 mg) in 10.0 mL MeCN; **C4**H (15.3 mg) in 10.0 mL MeCN; [DBU] = 8.50 × 10^{-2} mol L^{-1}. Step 0: 0.500 mL **C4**H stock solution in 22.5 g MeCN.

step	V_+ / mL	V / mL	[**C4**H]$_0$ / M	[**A19**]$_0$ / M	*A*	[**C4**$^-$] / M	[**C4**H] / M	[**A19**] / M
0	-	29.126	8.88 × 10^{-5}	0	0	0	8.88 × 10^{-5}	0
1	0.250	29.376	8.81 × 10^{-5}	4.51 × 10^{-5}	0.065	1.42 × 10^{-5}	7.39 × 10^{-5}	3.09 × 10^{-5}
2	0.500	29.626	8.73 × 10^{-5}	8.94 × 10^{-5}	0.119	2.60 × 10^{-5}	6.13 × 10^{-5}	6.34 × 10^{-5}
3	0.750	29.876	8.66 × 10^{-5}	1.33 × 10^{-4}	0.152	3.33 × 10^{-5}	5.34 × 10^{-5}	9.98 × 10^{-5}
4	1.000	30.126	8.59 × 10^{-5}	1.76 × 10^{-4}	0.175	3.85 × 10^{-5}	4.74 × 10^{-5}	1.37 × 10^{-4}
5	1.250	30.376	8.52 × 10^{-5}	2.18 × 10^{-4}	0.194	4.25 × 10^{-5}	4.27 × 10^{-5}	1.76 × 10^{-4}
6	1.500	30.626	8.45 × 10^{-5}	2.60 × 10^{-4}	0.208	4.56 × 10^{-5}	3.89 × 10^{-5}	2.14 × 10^{-4}
f	1.800	30.926	8.37 × 10^{-5}	2.57 × 10^{-4}	0.382	8.37 × 10^{-5}	0	2.57 × 10^{-4}

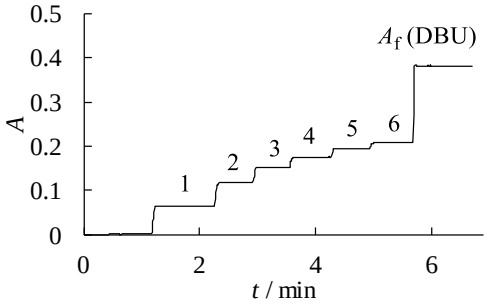

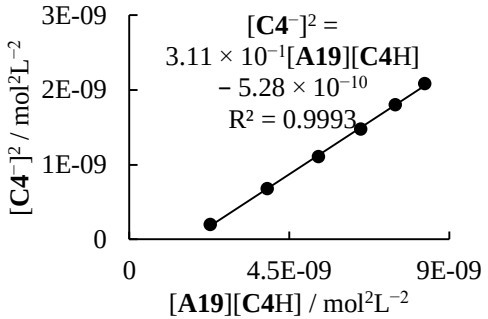

$K = (3.11 \pm 0.04) \times 10^{-1}$

Table 257. Determination of the pK_{aH} for **A19** with **C4**H in acetonitrile at 20 °C (detection at 350 nm). Stock solutions: **A19** (12.1 mg) in 10.0 mL MeCN; **C4**H (15.3 mg) in 10.0 mL MeCN; [DBU] = 8.50×10^{-2} mol L^{-1}. Step 0: 0.500 mL **C4**H stock solution in 23.5 g MeCN.

step	V_+ / mL	V / mL	[**C4**H]$_0$ / M	[**A19**]$_0$ / M	*A*	[**C4**$^-$] / M	[**C4**H] / M	[**A19**] / M
0	-	30.398	8.51×10^{-5}	0	0	0	8.51×10^{-5}	0
1	0.500	30.898	8.38×10^{-5}	8.58×10^{-5}	0.111	2.43×10^{-5}	5.94×10^{-5}	6.15×10^{-5}
2	0.750	31.148	8.31×10^{-5}	1.28×10^{-4}	0.142	3.12×10^{-5}	5.19×10^{-5}	9.64×10^{-5}
3	1.000	31.398	8.24×10^{-5}	1.69×10^{-4}	0.166	3.64×10^{-5}	4.60×10^{-5}	1.32×10^{-4}
4	1.250	31.648	8.18×10^{-5}	2.09×10^{-4}	0.184	4.03×10^{-5}	4.15×10^{-5}	1.69×10^{-4}
5	1.500	31.898	8.11×10^{-5}	2.49×10^{-4}	0.198	4.34×10^{-5}	3.78×10^{-5}	2.06×10^{-4}
f	1.800	32.198	8.04×10^{-5}	2.47×10^{-4}	0.367	8.04×10^{-5}	0	2.47×10^{-4}

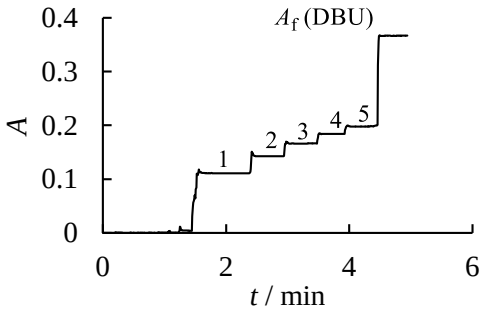

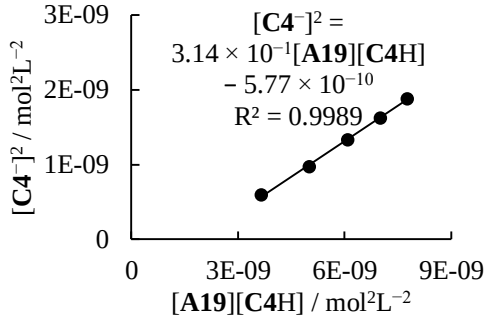

$K = (3.14 \pm 0.06) \times 10^{-1}$

For **A19** + **C4**H: $\bar{K} = (3.13 \pm 0.02) \times 10^{-1}$
pK_{aH} = 16.89

pK_{aH}(**A19**) = 16.94 (average)

(*S*)-1-(Pyrrolidin-2-ylmethyl)-1H-imidazole (A20)

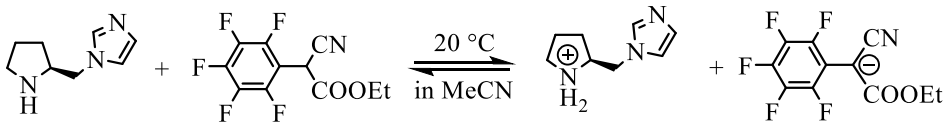

A20 **C3**H **A20**H$^+$ **C3**$^-$

Table 258. Determination of the pK_{aH} for **A20** with **C3**H in acetonitrile at 20 °C (detection at 333 nm). Stock solutions: **A20** (5.3 mg) in 10.0 mL MeCN; **C3**H (11.4 mg) in 10.0 mL MeCN; [DBU] = 4.70×10^{-2} mol L^{-1}. Step 0: 0.700 mL **C3**H stock solution in 19.8 g MeCN.

step	V_+ / mL	V / mL	[**C3**H]$_0$ / M	[**A20**]$_0$ / M	*A*	[**C3**$^-$] / M	[**C3**H] / M	[**A20**] / M
0	-	25.891	1.10×10^{-4}	0	0	0	1.10×10^{-4}	0
1	0.100	25.991	1.10×10^{-4}	1.35×10^{-5}	0.018	6.52×10^{-6}	1.03×10^{-4}	6.96×10^{-6}
2	0.200	26.091	1.10×10^{-4}	2.69×10^{-5}	0.030	1.05×10^{-5}	9.91×10^{-5}	1.64×10^{-5}
3	0.300	26.191	1.09×10^{-4}	4.01×10^{-5}	0.039	1.38×10^{-5}	9.53×10^{-5}	2.63×10^{-5}
4	0.400	26.291	1.09×10^{-4}	5.33×10^{-5}	0.047	1.66×10^{-5}	9.22×10^{-5}	3.68×10^{-5}
5	0.600	26.491	1.08×10^{-4}	7.94×10^{-5}	0.059	2.10×10^{-5}	8.69×10^{-5}	5.84×10^{-5}
6	0.800	26.691	1.07×10^{-4}	1.05×10^{-4}	0.069	2.46×10^{-5}	8.25×10^{-5}	8.05×10^{-5}
7	1.000	26.891	1.06×10^{-4}	1.30×10^{-4}	0.078	2.75×10^{-5}	7.88×10^{-5}	1.03×10^{-4}
f	1.300	27.191	1.05×10^{-4}	1.29×10^{-4}	0.297	1.05×10^{-4}	0	1.29×10^{-4}

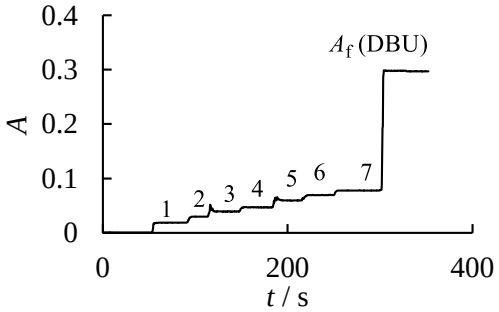

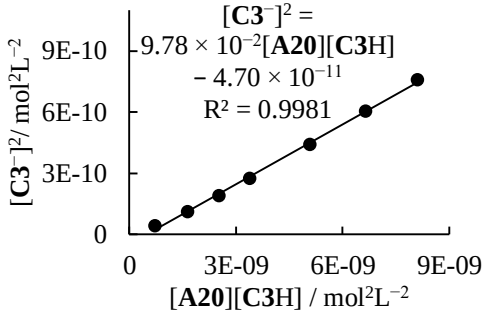

$K = (9.78 \pm 0.19) \times 10^{-2}$

pK_{aH} = 16.74

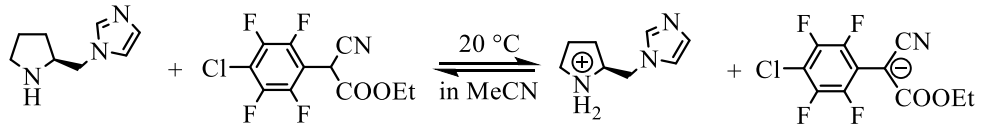

A20 **C4**H $A20H^+$ $C4^-$

Table 259. Determination of the pK_{aH} for **A20** with **C4**H in acetonitrile at 20 °C (detection at 333 nm). Stock solutions: **A20** (5.3 mg) in 10.0 mL MeCN; **C4**H (11.8 mg) in 10.0 mL MeCN; [DBU] = 4.70×10^{-2} mol L^{-1}. Step 0: 0.500 mL **C4**H stock solution in 18.5 g MeCN.

step	V_+ / mL	V / mL	[**C4**H]$_0$ / M	[**A20**]$_0$ / M	*A*	[$C4^-$] / M	[**C4**H] / M	[**A20**] / M
0	-	24.037	8.30×10^{-5}	0	0	0	8.30×10^{-5}	0
1	0.100	24.137	8.27×10^{-5}	1.45×10^{-5}	0.060	7.95×10^{-6}	7.47×10^{-5}	6.57×10^{-6}
2	0.200	24.237	8.23×10^{-5}	2.89×10^{-5}	0.098	1.29×10^{-5}	6.94×10^{-5}	1.60×10^{-5}
3	0.300	24.337	8.20×10^{-5}	4.32×10^{-5}	0.129	1.70×10^{-5}	6.50×10^{-5}	2.62×10^{-5}
4	0.400	24.437	8.17×10^{-5}	5.74×10^{-5}	0.154	2.03×10^{-5}	6.14×10^{-5}	3.70×10^{-5}
5	0.500	24.537	8.13×10^{-5}	7.14×10^{-5}	0.175	2.31×10^{-5}	5.82×10^{-5}	4.83×10^{-5}
6	0.600	24.637	8.10×10^{-5}	8.54×10^{-5}	0.193	2.56×10^{-5}	5.55×10^{-5}	5.98×10^{-5}
7	0.700	24.737	8.07×10^{-5}	9.92×10^{-5}	0.209	2.77×10^{-5}	5.30×10^{-5}	7.15×10^{-5}
8	0.800	24.837	8.04×10^{-5}	1.13×10^{-4}	0.224	2.96×10^{-5}	5.08×10^{-5}	8.33×10^{-5}
9	0.900	24.937	8.00×10^{-5}	1.26×10^{-4}	0.236	3.13×10^{-5}	4.87×10^{-5}	9.52×10^{-5}
10	1.000	25.037	7.97×10^{-5}	1.40×10^{-4}	0.248	3.28×10^{-5}	4.69×10^{-5}	1.07×10^{-4}
f	1.200	25.237	7.91×10^{-5}	1.39×10^{-4}	0.598	7.91×10^{-5}	0	1.39×10^{-4}

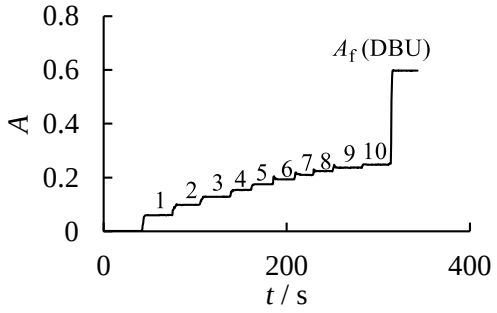

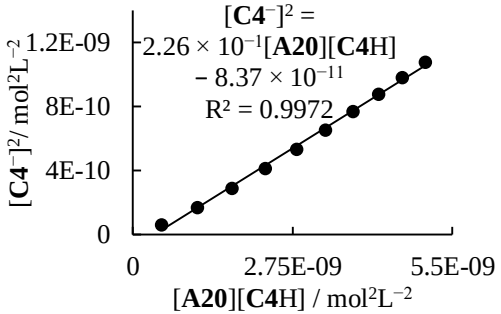

$K = (2.26 \pm 0.04) \times 10^{-1}$

pK_{aH} = 16.75

pK_{aH}(**A20**) = 16.74 (average)

(*S*)-3-Butyl-1-(pyrrolidin-2-ylmethyl)-1H-imidazol-3-ium trifluoromethanesulfonate (A21)

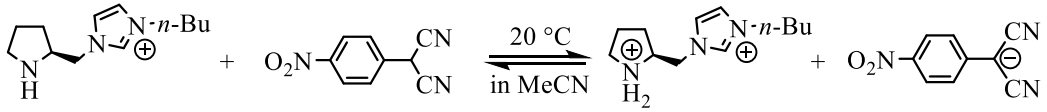

A21 **C6**H **A21**H$^+$ **C6**$^-$

Table 260. Determination of the pK_{aH} for **A21** with **C6**H in acetonitrile at 20 °C (detection at 478 nm). Stock solutions: **A21**TfO$^-$ (4.9 mg) in 25.0 mL MeCN; **C6**H (6.0 mg) in 10.0 mL MeCN; [DBU] = 1.48 × 10^{-2} mol L^{-1}. Step 0: 0.100 mL **C4**H stock solution in 18.6 g MeCN.

step	V_+ / mL	V / mL	[**C6**H]$_0$ / M	[**A21**]$_0$ / M	*A*	[**C6**$^-$] / M	[**C6**H] / M	[**A21**] / M
0	-	23.764	1.35 × 10^{-5}	0	-	-	1.35 × 10^{-5}	0
1	0.200	23.964	1.34 × 10^{-5}	4.58 × 10^{-6}	0.039	2.33 × 10^{-6}	1.11 × 10^{-5}	2.25 × 10^{-6}
2	0.250	24.014	1.33 × 10^{-5}	5.71 × 10^{-6}	0.045	2.69 × 10^{-6}	1.07 × 10^{-5}	3.02 × 10^{-6}
3	0.300	24.064	1.33 × 10^{-5}	6.84 × 10^{-6}	0.051	3.02 × 10^{-6}	1.03 × 10^{-5}	3.81 × 10^{-6}
4	0.350	24.114	1.33 × 10^{-5}	7.96 × 10^{-6}	0.056	3.36 × 10^{-6}	9.93 × 10^{-6}	4.60 × 10^{-6}
5	0.400	24.164	1.33 × 10^{-5}	9.08 × 10^{-6}	0.062	3.70 × 10^{-6}	9.57 × 10^{-6}	5.38 × 10^{-6}
6	0.450	24.214	1.32 × 10^{-5}	1.02 × 10^{-5}	0.067	4.03 × 10^{-6}	9.21 × 10^{-6}	6.16 × 10^{-6}
f	0.550	24.314	1.32 × 10^{-5}	1.01 × 10^{-5}	0.220	1.32 × 10^{-5}	0	1.01 × 10^{-5}

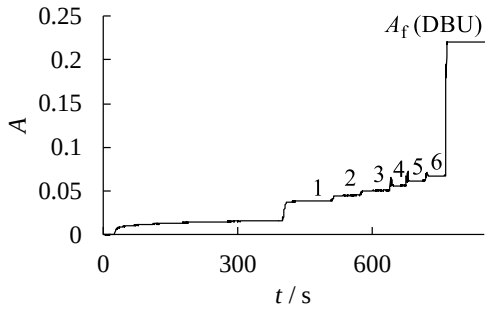

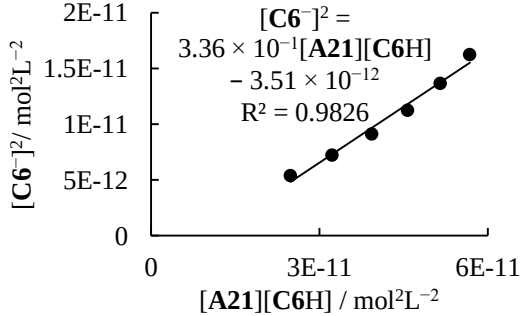

K = (3.36 ± 0.22) × 10^{-1}

Table 261. Determination of the pK_{aH} for **A21** with **C6**H in acetonitrile at 20 °C (detection at 478 nm). Stock solutions: **A21**TfO$^-$ (4.9 mg) in 25.0 mL MeCN; **C6**H (6.0 mg) in 10.0 mL MeCN; [DBU] = 1.48 × 10^{-2} mol L^{-1}. Step 0: 0.100 mL **C4**H stock solution in 18.5 g MeCN.

step	V_+ / mL	V / mL	[**C6**H]$_0$ / M	[**A21**]$_0$ / M	*A*	[**C6**$^-$] / M	[**C6**H] / M	[**A21**] / M
0	-	23.637	1.36 × 10^{-5}	0	-	-	1.36 × 10^{-5}	0
1	0.200	23.837	1.34 × 10^{-5}	4.60 × 10^{-6}	0.039	2.33 × 10^{-6}	1.11 × 10^{-5}	2.28 × 10^{-6}
2	0.250	23.887	1.34 × 10^{-5}	5.74 × 10^{-6}	0.045	2.70 × 10^{-6}	1.07 × 10^{-5}	3.04 × 10^{-6}
3	0.300	23.937	1.34 × 10^{-5}	6.87 × 10^{-6}	0.051	3.03 × 10^{-6}	1.04 × 10^{-5}	3.85 × 10^{-6}
4	0.350	23.987	1.34 × 10^{-5}	8.00 × 10^{-6}	0.056	3.38 × 10^{-6}	9.98 × 10^{-6}	4.62 × 10^{-6}
5	0.400	24.037	1.33 × 10^{-5}	9.13 × 10^{-6}	0.062	3.72 × 10^{-6}	9.61 × 10^{-6}	5.40 × 10^{-6}
6	0.450	24.087	1.33 × 10^{-5}	1.02 × 10^{-5}	0.068	4.05 × 10^{-6}	9.26 × 10^{-6}	6.20 × 10^{-6}
f	0.550	24.187	1.33 × 10^{-5}	1.02 × 10^{-5}	0.221	1.33 × 10^{-5}	0	1.02 × 10^{-5}

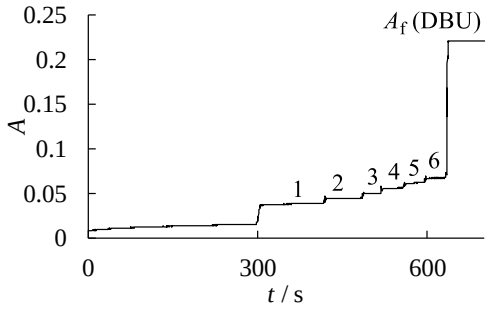

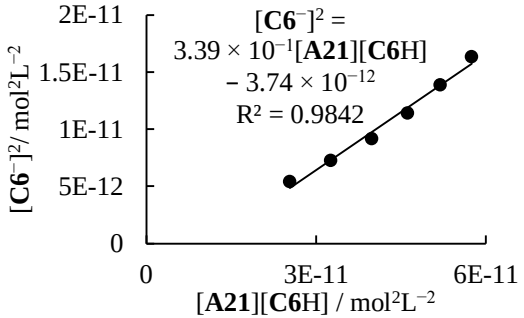

K = (3.39 ± 0.21) × 10^{-1}

$\bar{K}$ = (3.38 ± 0.02) × 10^{-1}

pK_{aH}(**A21**) = 11.14

(*S*)-1-(3,5-Bis(trifluoromethyl)phenyl)-3-(pyrrolidin-2-ylmethyl)thiourea (A22)

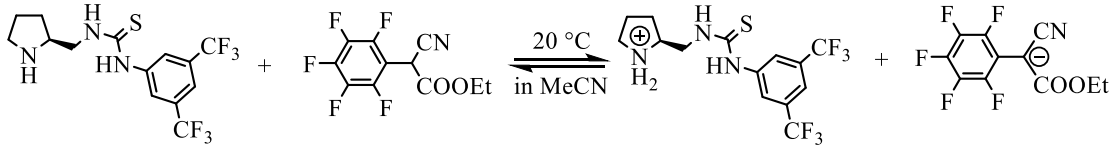

A22 **C3**H **A22**H$^+$ **C3**$^-$

Table 262. Determination of the pK_{aH} for **A22** with **C3**H in acetonitrile at 20 °C (detection at 350 nm); Stock solutions: **A22** (9.3 mg) in 10.0 mL MeCN; **C3**H (12.6 mg) in 10.0 mL MeCN; [pyrrolidine] = 7.02×10^{-2} mol L^{-1}. Step 0: 0.800 mL **C3**H stock solution in 20.7 g MeCN.

step	V_+ / mL	V / mL	[**C3**H]$_0$ / M	[**A22**]$_0$ / M	*A*	[**C3**$^-$] / M	[**C3**H] / M	[**A22**] / M
0	-	27.136	1.33×10^{-4}	0	0	0	1.33×10^{-4}	0
1	1.000	28.136	1.28×10^{-4}	8.90×10^{-5}	0.034	3.72×10^{-5}	9.11×10^{-5}	5.18×10^{-5}
2	1.300	28.436	1.27×10^{-4}	1.14×10^{-4}	0.039	4.30×10^{-5}	8.40×10^{-5}	7.15×10^{-5}
3	1.600	28.736	1.26×10^{-4}	1.39×10^{-4}	0.044	4.79×10^{-5}	7.77×10^{-5}	9.15×10^{-5}
4	1.900	29.036	1.24×10^{-4}	1.64×10^{-4}	0.047	5.20×10^{-5}	7.24×10^{-5}	1.12×10^{-4}
5	2.200	29.336	1.23×10^{-4}	1.88×10^{-4}	0.050	5.53×10^{-5}	6.78×10^{-5}	1.32×10^{-4}
f	2.300	29.436	1.23×10^{-4}	1.87×10^{-4}	0.112	1.23×10^{-4}	0	1.87×10^{-4}

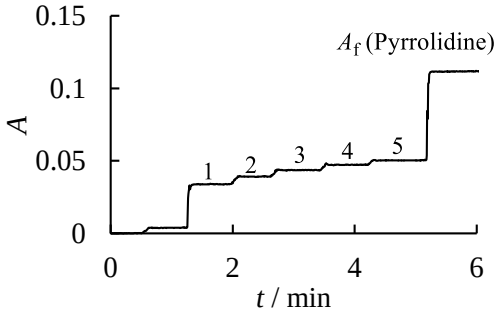

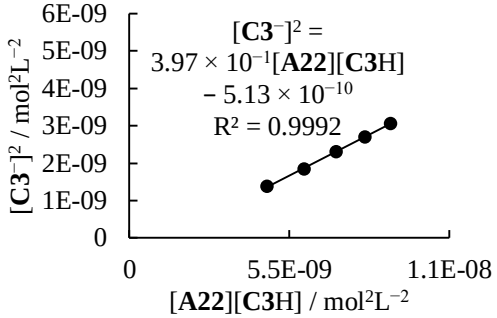

$K = (3.97 \pm 0.07) \times 10^{-1}$

pK_{aH} = 17.35

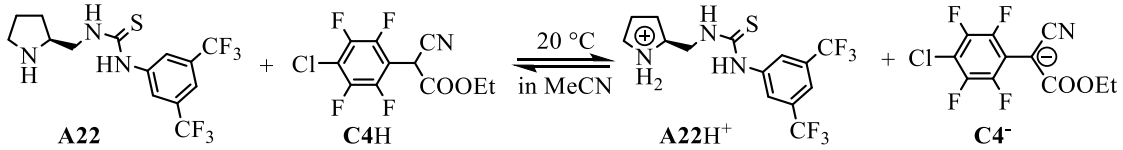

Table 263. Determination of the pK_{aH} for **A22** with **C4**H in acetonitrile at 20 °C (detection at 350 nm). Stock solutions: **A22** (9.3 mg) in 10.0 mL MeCN; **C4**H (11.9 mg) in 10.0 mL MeCN; [pyrrolidine] = 7.02×10^{-2} mol L^{-1}. Step 0: 0.700 mL **C4**H stock solution in 21.1 g MeCN.

step	V_+ / mL	V / mL	[**C4**H]$_0$ / M	[**A22**]$_0$ / M	*A*	[**C4**$^-$] / M	[**C4**H] / M	[**A22**] / M
0	-	27.545	1.02×10^{-4}	0	0	0	1.02×10^{-4}	0
1	1.000	28.545	9.87×10^{-5}	8.77×10^{-5}	0.178	4.39×10^{-5}	5.48×10^{-5}	4.38×10^{-5}
2	1.500	29.045	9.70×10^{-5}	1.29×10^{-4}	0.212	5.23×10^{-5}	4.47×10^{-5}	7.71×10^{-5}
3	2.000	29.545	9.54×10^{-5}	1.70×10^{-4}	0.233	5.75×10^{-5}	3.79×10^{-5}	1.12×10^{-4}
4	2.500	30.045	9.38×10^{-5}	2.08×10^{-4}	0.249	6.13×10^{-5}	3.25×10^{-5}	1.47×10^{-4}
5	3.000	30.545	9.23×10^{-5}	2.46×10^{-4}	0.259	6.38×10^{-5}	2.85×10^{-5}	1.82×10^{-4}
f	3.200	30.745	9.17×10^{-5}	2.44×10^{-4}	0.372	9.17×10^{-5}	0	2.44×10^{-4}

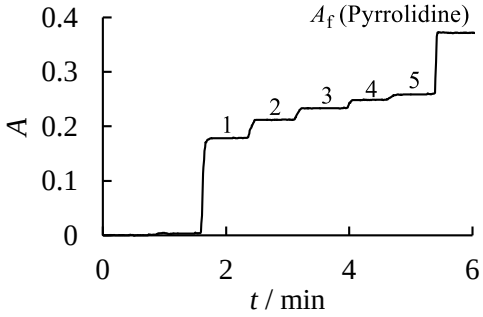

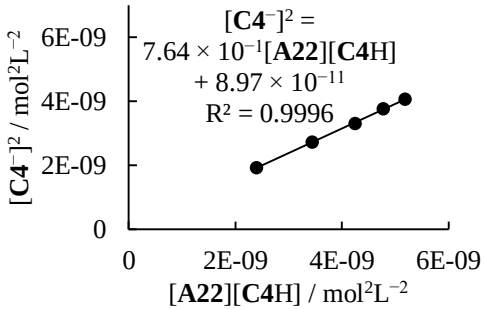

$K = (7.64 \pm 0.09) \times 10^{-1}$

pK_{aH} = 17.27

pK_{aH}(**A22**) = 17.31 (average)

(*S*)-(3,5-Bis(trifluoromethyl)phenyl)((pyrrolidin-2-ylmethyl)carbamothioyl)amide ($A22^-$)

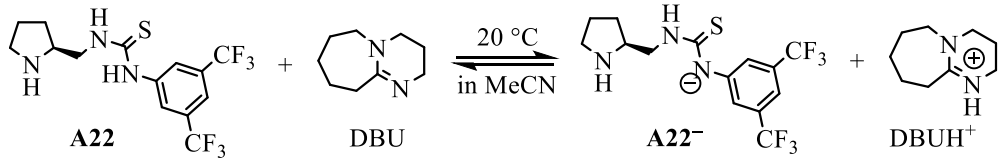

Table 264. Determination of the pK_{aH} for **A22**-H^+ with DBU in acetonitrile at 20 °C (detection at 350 nm); Stock solutions: **A22** (8.0 mg) in 10.0 mL MeCN; DBU (22.5 mg) in 10.0 mL MeCN; [TBD] = 7.33 × 10^{-2} mol· L^{-1}. Step 0: 1.000 mL **A22** stock solution in 18.5 g MeCN.

step	V_+ / mL	V / mL	[**A22**]$_0$ / M	[DBU]$_0$ / M	*A*	[$\mathbf{A22}^-$] / M	[**A22**] / M	[DBU] / M
0	-	24.537	8.78×10^{-5}	0	0	0	8.78×10^{-5}	0
1	0.100	24.637	8.74×10^{-5}	6.00×10^{-5}	0.039	1.82×10^{-5}	6.93×10^{-5}	4.18×10^{-5}
2	0.200	24.737	8.71×10^{-5}	1.19×10^{-4}	0.057	2.66×10^{-5}	6.05×10^{-5}	9.29×10^{-5}
3	0.300	24.837	8.67×10^{-5}	1.79×10^{-4}	0.069	3.25×10^{-5}	5.42×10^{-5}	1.46×10^{-4}
4	0.400	24.937	8.64×10^{-5}	2.37×10^{-4}	0.078	3.68×10^{-5}	4.95×10^{-5}	2.00×10^{-4}
5	0.500	25.037	8.60×10^{-5}	2.95×10^{-4}	0.086	4.03×10^{-5}	4.57×10^{-5}	2.55×10^{-4}
6	0.600	25.137	8.57×10^{-5}	3.53×10^{-4}	0.092	4.31×10^{-5}	4.26×10^{-5}	3.10×10^{-4}
7	0.700	25.237	8.54×10^{-5}	4.10×10^{-4}	0.097	4.53×10^{-5}	4.00×10^{-5}	3.65×10^{-4}
8	0.800	25.337	8.50×10^{-5}	4.67×10^{-4}	0.101	4.72×10^{-5}	3.78×10^{-5}	4.19×10^{-4}
9	0.900	25.437	8.47×10^{-5}	5.23×10^{-4}	0.104	4.89×10^{-5}	3.58×10^{-5}	4.74×10^{-4}
10	1.000	25.537	8.44×10^{-5}	5.79×10^{-4}	0.107	5.03×10^{-5}	3.41×10^{-5}	5.28×10^{-4}
f	1.400	25.937	8.31×10^{-5}	5.70×10^{-4}	0.177	8.31×10^{-5}	0	5.70×10^{-4}

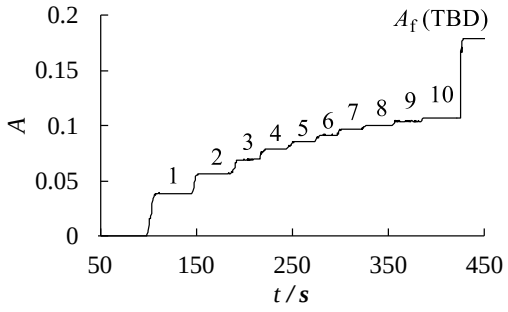

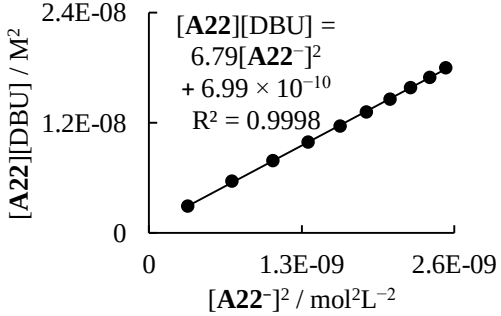

K = 6.79 ± 0.04

Table 265. Determination of the pK_{aH} for **A22**-H$^+$ with DBU in acetonitrile at 20 °C (detection at 350 nm). Stock solutions: **A22** (8.0 mg) in 10.0 mL MeCN; DBU (22.5 mg) in 10.0 mL MeCN; [TBD] = 7.33 × 10^{-2} mol· L^{-1}. Step 0: 1.000 mL **A22** stock solution in 18.3 g MeCN.

step	V_+ / mL	V / mL	[**A22**]$_0$ / M	[DBU]$_0$ / M	*A*	[**A22**$^-$] / M	[**A22**] / M	[DBU] / M
0	-	24.282	8.87×10^{-5}	0	0	0	8.87×10^{-5}	0
1	0.100	24.382	8.84×10^{-5}	6.06×10^{-5}	0.039	1.84×10^{-5}	6.99×10^{-5}	4.22×10^{-5}
2	0.200	24.482	8.80×10^{-5}	1.21×10^{-4}	0.058	2.68×10^{-5}	6.11×10^{-5}	9.39×10^{-5}
3	0.300	24.582	8.76×10^{-5}	1.80×10^{-4}	0.070	3.25×10^{-5}	5.52×10^{-5}	1.48×10^{-4}
4	0.400	24.682	8.73×10^{-5}	2.40×10^{-4}	0.079	3.68×10^{-5}	5.05×10^{-5}	2.03×10^{-4}
5	0.500	24.782	8.69×10^{-5}	2.98×10^{-4}	0.086	4.01×10^{-5}	4.69×10^{-5}	2.58×10^{-4}
6	0.600	24.882	8.66×10^{-5}	3.56×10^{-4}	0.092	4.28×10^{-5}	4.38×10^{-5}	3.14×10^{-4}
7	0.700	24.982	8.62×10^{-5}	4.14×10^{-4}	0.097	4.51×10^{-5}	4.12×10^{-5}	3.69×10^{-4}
8	0.800	25.082	8.59×10^{-5}	4.71×10^{-4}	0.101	4.70×10^{-5}	3.89×10^{-5}	4.24×10^{-4}
9	0.900	25.182	8.55×10^{-5}	5.28×10^{-4}	0.104	4.86×10^{-5}	3.69×10^{-5}	4.80×10^{-4}
10	1.000	25.282	8.52×10^{-5}	5.85×10^{-4}	0.107	5.00×10^{-5}	3.52×10^{-5}	5.35×10^{-4}
f	1.400	25.682	8.39×10^{-5}	5.75×10^{-4}	0.178	8.39×10^{-5}	0	5.75×10^{-4}

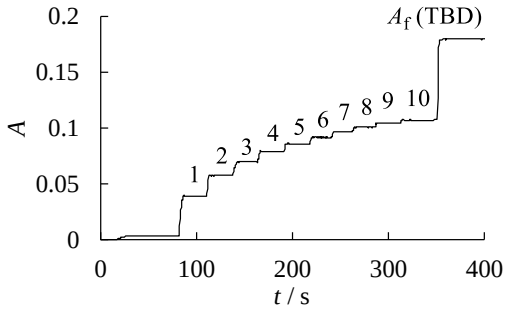

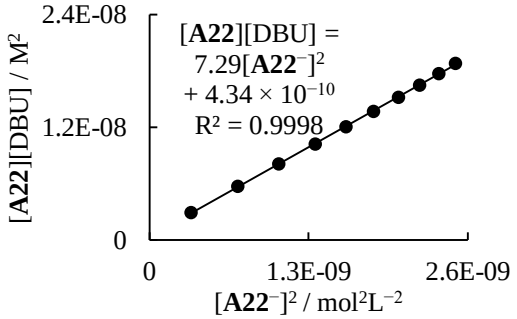

K = 7.29 ± 0.03

$\bar{K}$ = 7.04 ± 0.25

pK_{aH}(**A22**$^-$) = 25.16

(*S*)-1-(3,5-Bis(trifluoromethyl)phenyl)-3-(pyrrolidin-2-ylmethyl)urea (A23)

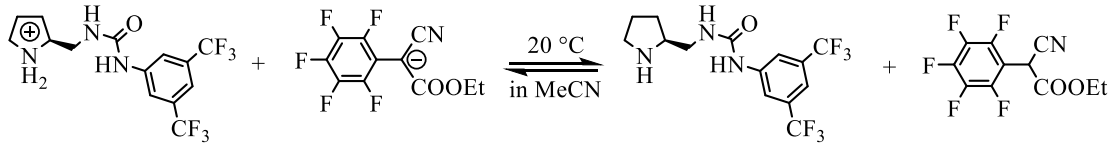

A23H$^+$ **C3**$^-$ **A23** **C3**H

Table 266. Determination of the pK_{aH} for **A23** with **C3**$^-$ in acetonitrile at 20 °C (detection at 333 nm). Stock solutions: **A23**H$^+$CF$_3$CO$_2^-$ (8.4 mg) in 10.0 mL MeCN; **C3**$^-$K$^+$ (5.4 mg) in 25.0 mL MeCN. Step 0: 2.000 mL **C3**$^-$K$^+$ stock solution in 18.0 g MeCN.

step	V_+ / mL	V / mL	[**C3**$^-$]$_0$ / M	[**A23**H$^+$]$_0$ / M	*A*	[**C3**$^-$] / M	[**C3**H] / M	[**A23**H$^+$] / M
0	-	24.901	5.47×10^{-5}	0	0.164	5.47×10^{-5}	0	0
1	0.100	25.001	5.45×10^{-5}	7.16×10^{-6}	0.155	5.15×10^{-5}	3.01×10^{-6}	4.15×10^{-6}
2	0.200	25.101	5.42×10^{-5}	1.43×10^{-5}	0.149	4.94×10^{-5}	4.82×10^{-6}	9.44×10^{-6}
3	0.400	25.301	5.38×10^{-5}	2.83×10^{-5}	0.140	4.67×10^{-5}	7.15×10^{-6}	2.11×10^{-5}
4	0.600	25.501	5.34×10^{-5}	4.21×10^{-5}	0.134	4.47×10^{-5}	8.69×10^{-6}	3.34×10^{-5}
5	0.800	25.701	5.30×10^{-5}	5.57×10^{-5}	0.130	4.32×10^{-5}	9.81×10^{-6}	4.59×10^{-5}
6	1.000	25.901	5.26×10^{-5}	6.91×10^{-5}	0.126	4.19×10^{-5}	1.07×10^{-5}	5.84×10^{-5}

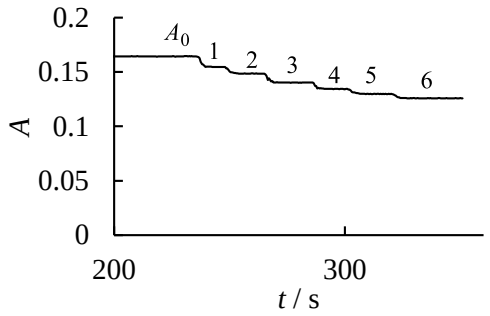

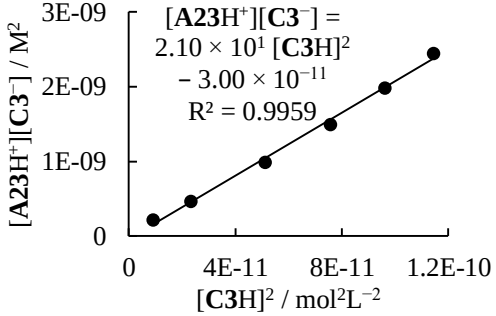

$K = (2.10 \pm 0.08) \times 10^1$

Table 267. Determination of the pK_{aH} for **A23** with **C3**$^-$ in acetonitrile at 20 °C (detection at 333 nm). Stock solutions: **A23**H$^+$$CF_3CO_2^-$ (8.4 mg) in 10.0 mL MeCN; **C3**$^-$$K^+$ (5.4 mg) in 25.0 mL MeCN. Step 0: 2.000 mL **C3**$^-$$K^+$ stock solution in 19.7 g MeCN.

step	V_+ / mL	V / mL	[**C3**$^-$]$_0$ / M	[**A23**H$^+$]$_0$ / M	*A*	[**C3**$^-$] / M	[**C3**H] / M	[**A23**H$^+$] / M
0	-	27.064	5.03×10^{-5}	0	0.149	5.03×10^{-5}	0	0
1	0.200	27.264	4.99×10^{-5}	1.31×10^{-5}	0.135	4.56×10^{-5}	4.33×10^{-6}	8.80×10^{-6}
2	0.400	27.464	4.96×10^{-5}	2.61×10^{-5}	0.127	4.31×10^{-5}	6.47×10^{-6}	1.96×10^{-5}
3	0.600	27.664	4.92×10^{-5}	3.88×10^{-5}	0.122	4.13×10^{-5}	7.88×10^{-6}	3.09×10^{-5}
4	0.800	27.864	4.89×10^{-5}	5.14×10^{-5}	0.118	3.99×10^{-5}	8.98×10^{-6}	4.24×10^{-5}
5	1.000	28.064	4.85×10^{-5}	6.38×10^{-5}	0.114	3.87×10^{-5}	9.81×10^{-6}	5.40×10^{-5}

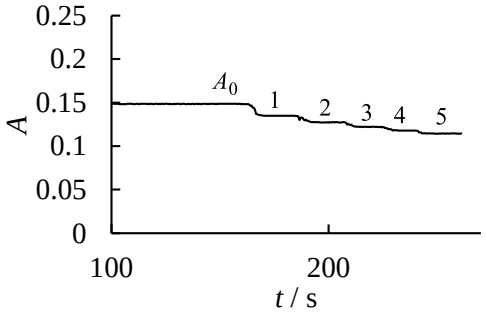

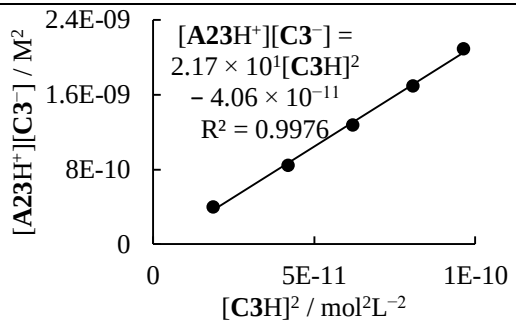

$K = (2.17 \pm 0.06) \times 10^1$

For **A23**H$^+$ + **C3**$^-$: $\bar{K} = (2.14 \pm 0.04) \times 10^1$

pK_{aH} = 19.08

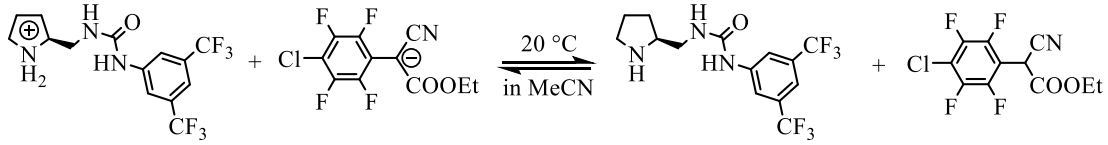

A23H$^+$ **C4**$^-$ **A23** **C4**H

Table 268. Determination of the pK_{aH} for **A23** with **C4**$^-$ in acetonitrile at 20 °C (detection at 333 nm). Stock solutions: **A23**H$^+$$CF_3CO_2^-$ (8.4 mg) in 10.0 mL MeCN; **C4**$^-$$K^+$ (5.1 mg) in 25.0 mL MeCN. Step 0: 1.000 mL **C4**$^-$$K^+$ stock solution in 19.4 g MeCN.

step	V_+ / mL	V / mL	[**C4**$^-$]$_0$ / M	[**A23**H$^+$]$_0$ / M	*A*	[**C4**$^-$] / M	[**C4**H] / M	[**A23**H$^+$] / M
0	-	25.682	2.38×10^{-5}	0	0.198	2.38×10^{-5}	0	0
1	0.250	25.932	2.36×10^{-5}	1.73×10^{-5}	0.175	2.11×10^{-5}	2.50×10^{-6}	1.48×10^{-5}
2	0.500	26.182	2.33×10^{-5}	3.42×10^{-5}	0.165	1.98×10^{-5}	3.53×10^{-6}	3.07×10^{-5}
3	0.750	26.432	2.31×10^{-5}	5.08×10^{-5}	0.158	1.90×10^{-5}	4.15×10^{-6}	4.66×10^{-5}
4	1.000	26.682	2.29×10^{-5}	6.71×10^{-5}	0.152	1.83×10^{-5}	4.61×10^{-6}	6.25×10^{-5}
5	1.250	26.932	2.27×10^{-5}	8.31×10^{-5}	0.147	1.77×10^{-5}	4.96×10^{-6}	7.81×10^{-5}
6	1.500	27.182	2.25×10^{-5}	9.88×10^{-5}	0.143	1.73×10^{-5}	5.24×10^{-6}	9.35×10^{-5}

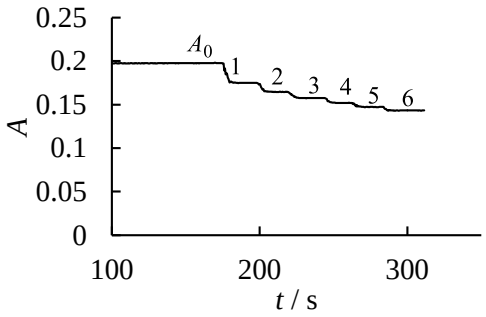

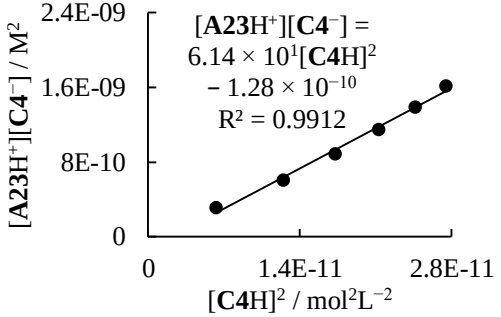

$K = (6.14 \pm 0.29) \times 10^1$

Table 269. Determination of the pK_{aH} for **A23** with **C4**$^-$ in acetonitrile at 20 °C (detection at 333 nm). Stock solutions: **A23**H$^+$$CF_3CO_2^-$ (8.4 mg) in 10.0 mL MeCN; **C4**$^-$$K^+$ (5.1 mg) in 25.0 mL MeCN. Step 0: 1.000 mL **C4**$^-$$K^+$ stock solution in 19.1 g MeCN.

step	V_+ / mL	V / mL	[**C4**$^-$]$_0$ / M	[**A23**H$^+$]$_0$ / M	*A*	[**C4**$^-$] / M	[**C4**H] / M	[**A23**H$^+$] / M
0	-	25.300	2.42×10^{-5}	0	0.199	2.42×10^{-5}	0	0
1	0.250	25.550	2.39×10^{-5}	1.75×10^{-5}	0.177	2.15×10^{-5}	2.43×10^{-6}	1.51×10^{-5}
2	0.500	25.800	2.37×10^{-5}	3.47×10^{-5}	0.167	2.02×10^{-5}	3.46×10^{-6}	3.12×10^{-5}
3	0.750	26.050	2.35×10^{-5}	5.15×10^{-5}	0.160	1.94×10^{-5}	4.08×10^{-6}	4.74×10^{-5}
4	1.000	26.300	2.32×10^{-5}	6.81×10^{-5}	0.154	1.87×10^{-5}	4.55×10^{-6}	6.35×10^{-5}
5	1.250	26.550	2.30×10^{-5}	8.43×10^{-5}	0.149	1.81×10^{-5}	4.92×10^{-6}	7.94×10^{-5}

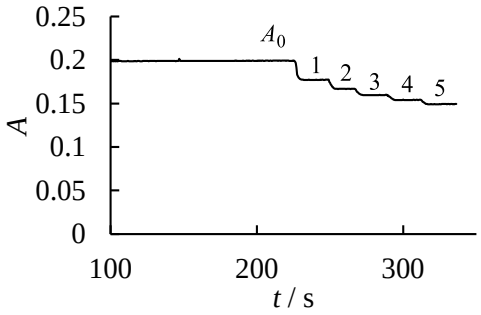

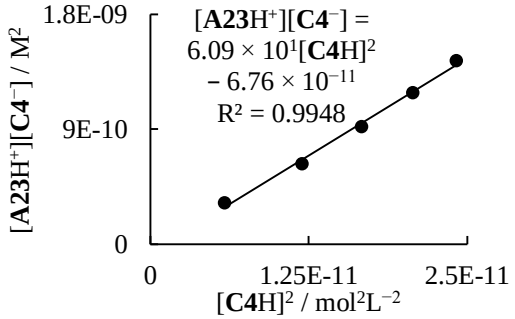

$K = (6.09 \pm 0.25) \times 10^1$

$\bar{K} = (6.12 \pm 0.03) \times 10^1$

pK_{aH} = 19.18

pK_{aH}(**A23**) = 19.13 (average)

(*S*)-2-Tritylpyrrolidine (A24)

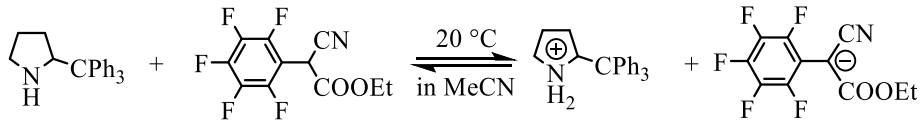

A24 **C3**H **A24**H$^+$ **C3**$^-$

Table 270. Determination of the pK_{aH} for **A24** with **C3**H in acetonitrile at 20 °C (detection at 333 nm). Stock solutions: **A24** (7.1 mg) in 10.0 mL MeCN; **C3**H (11.4 mg) in 10.0 mL MeCN; [DBU] = 3.26×10^{-2} mol L^{-1}. Step 0: 0.700 mL **C3**H stock solution in 18.4 g MeCN.

step	V_+ / mL	V / mL	[**C3**H]$_0$ / M	[**A24**]$_0$ / M	*A*	[**C3**$^-$] / M	[**C3**H] / M	[**A24**] / M
0	-	24.110	1.19×10^{-4}	0	0	0	1.19×10^{-4}	0
1	0.500	24.610	1.16×10^{-4}	4.60×10^{-5}	0.047	1.66×10^{-5}	9.96×10^{-5}	2.94×10^{-5}
2	1.000	25.110	1.14×10^{-4}	9.02×10^{-5}	0.070	2.44×10^{-5}	8.95×10^{-5}	6.58×10^{-5}
3	1.500	25.610	1.12×10^{-4}	1.33×10^{-4}	0.084	2.96×10^{-5}	8.21×10^{-5}	1.03×10^{-4}
4	2.000	26.110	1.09×10^{-4}	1.74×10^{-4}	0.095	3.34×10^{-5}	7.61×10^{-5}	1.40×10^{-4}
5	2.500	26.610	1.07×10^{-4}	2.13×10^{-4}	0.104	3.64×10^{-5}	7.10×10^{-5}	1.76×10^{-4}
6	3.000	27.110	1.05×10^{-4}	2.51×10^{-4}	0.111	3.88×10^{-5}	6.67×10^{-5}	2.12×10^{-4}
7	4.000	28.110	1.02×10^{-4}	3.22×10^{-4}	0.121	4.24×10^{-5}	5.93×10^{-5}	2.80×10^{-4}
8	5.000	29.110	9.82×10^{-5}	3.89×10^{-4}	0.128	4.48×10^{-5}	5.34×10^{-5}	3.44×10^{-4}
f	5.300	29.410	9.72×10^{-5}	3.85×10^{-4}	0.277	9.72×10^{-5}	0	3.85×10^{-4}

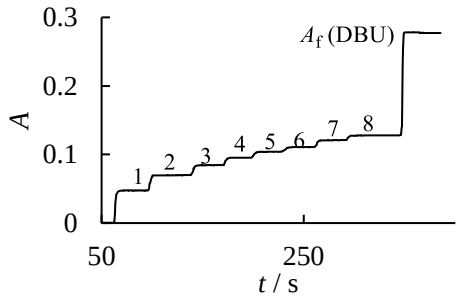

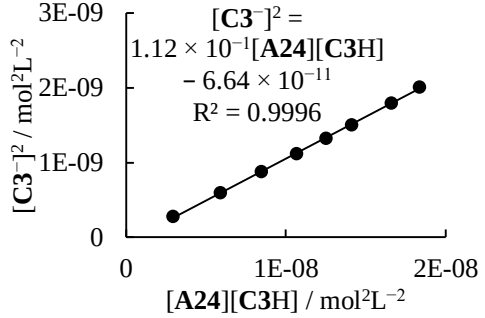

$K = (1.12 \pm 0.01) \times 10^{-1}$

pK_{aH} = 16.80

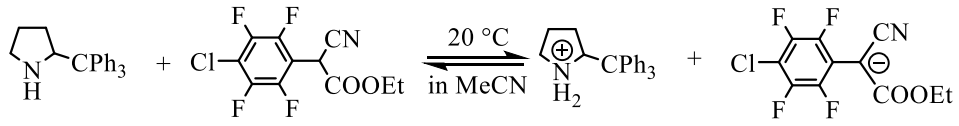

A24 **C4**H **A24**H$^+$ **C4**$^-$

Table 271. Determination of the pK_{aH} for **A24** with **C4**H in acetonitrile at 20 °C (detection at 333 nm). Stock solutions: **A24** (7.1 mg) in 10.0 mL MeCN; **C4**H (11.8 mg) in 10.0 mL MeCN; [DBU] = 3.26 × 10^{-2} mol L^{-1}. Step 0: 0.500 mL **C4**H stock solution in 18.9 g MeCN.

step	V_+ / mL	V / mL	[**C4**H]$_0$ / M	[**A24**]$_0$ / M	*A*	[**C4**$^-$] / M	[**C4**H] / M	[**A24**] / M
0	-	24.546	8.13 × 10^{-5}	0	0	0	8.13 × 10^{-5}	0
1	0.250	24.796	8.05 × 10^{-5}	2.28 × 10^{-5}	0.091	1.20 × 10^{-5}	6.85 × 10^{-5}	1.08 × 10^{-5}
2	0.500	25.046	7.97 × 10^{-5}	4.52 × 10^{-5}	0.143	1.89 × 10^{-5}	6.08 × 10^{-5}	2.63 × 10^{-5}
3	0.750	25.296	7.89 × 10^{-5}	6.72 × 10^{-5}	0.180	2.37 × 10^{-5}	5.52 × 10^{-5}	4.35 × 10^{-5}
4	1.000	25.546	7.81 × 10^{-5}	8.87 × 10^{-5}	0.206	2.72 × 10^{-5}	5.09 × 10^{-5}	6.15 × 10^{-5}
5	1.250	25.796	7.74 × 10^{-5}	1.10 × 10^{-4}	0.227	3.00 × 10^{-5}	4.74 × 10^{-5}	7.98 × 10^{-5}
6	1.500	26.046	7.66 × 10^{-5}	1.30 × 10^{-4}	0.244	3.23 × 10^{-5}	4.44 × 10^{-5}	9.82 × 10^{-5}
7	1.750	26.296	7.59 × 10^{-5}	1.51 × 10^{-4}	0.259	3.41 × 10^{-5}	4.18 × 10^{-5}	1.17 × 10^{-4}
8	2.000	26.546	7.52 × 10^{-5}	1.71 × 10^{-4}	0.271	3.58 × 10^{-5}	3.94 × 10^{-5}	1.35 × 10^{-4}
9	2.500	27.046	7.38 × 10^{-5}	2.09 × 10^{-4}	0.290	3.83 × 10^{-5}	3.55 × 10^{-5}	1.71 × 10^{-4}
f	2.800	27.346	7.30 × 10^{-5}	2.07 × 10^{-4}	0.553	7.30 × 10^{-5}	0	2.07 × 10^{-4}

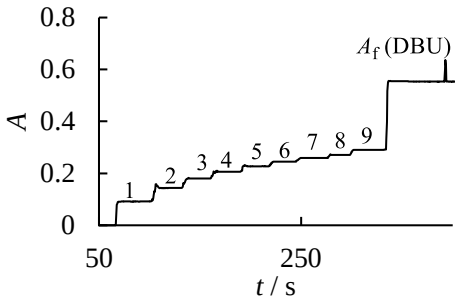

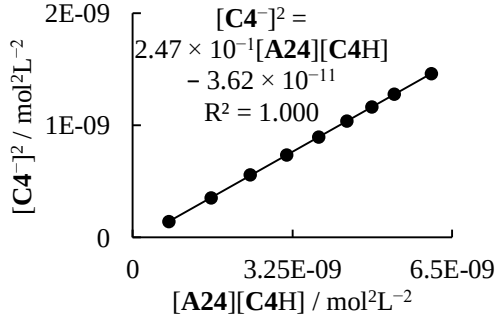

K = (2.47 ± 0.01) × 10^{-1}

pK_{aH} = 16.78

pK_{aH}(**A24**) = 16.79 (average)

(*S*)-2-(Diphenyl((trimethylsilyl)oxy)methyl)pyrrolidine (A25)

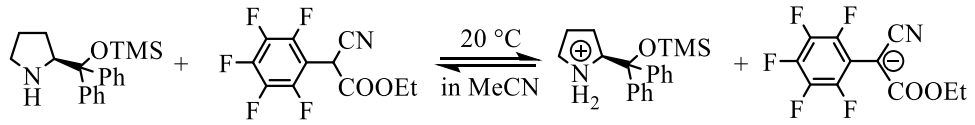

A25 **C3**H **A25**H$^+$ **C3**$^-$

Table 272. Determination of the pK_{aH} for **A25** with **C3**H in acetonitrile at 20 °C (detection at 333 nm). Stock solutions: **A25** (7.1 mg) in 10.0 mL MeCN; **C3**H (11.4 mg) in 10.0 mL MeCN; [DBU] = 3.26×10^{-2} mol L^{-1}. Step 0: 0.700 mL **C3**H stock solution in 19.1 g MeCN.

step	V_+ / mL	V / mL	[**C3**H]$_0$ / M	[**A25**]$_0$ / M	*A*	[**C3**$^-$] / M	[**C3**H] / M	[**A25**] / M
0	-	25.000	1.14×10^{-4}	0	0	0	1.14×10^{-4}	0
1	1.000	26.000	1.10×10^{-4}	8.39×10^{-5}	0.112	3.92×10^{-5}	7.08×10^{-5}	4.47×10^{-5}
2	1.500	26.500	1.08×10^{-4}	1.23×10^{-4}	0.138	4.84×10^{-5}	5.95×10^{-5}	7.51×10^{-5}
3	2.000	27.000	1.06×10^{-4}	1.62×10^{-4}	0.157	5.50×10^{-5}	5.09×10^{-5}	1.07×10^{-4}
4	2.500	27.500	1.04×10^{-4}	1.98×10^{-4}	0.170	5.96×10^{-5}	4.44×10^{-5}	1.39×10^{-4}
5	3.000	28.000	1.02×10^{-4}	2.34×10^{-4}	0.180	6.30×10^{-5}	3.90×10^{-5}	1.71×10^{-4}
6	3.500	28.500	1.00×10^{-4}	2.68×10^{-4}	0.187	6.55×10^{-5}	3.48×10^{-5}	2.02×10^{-4}
7	4.000	29.000	9.86×10^{-5}	3.01×10^{-4}	0.192	6.72×10^{-5}	3.14×10^{-5}	2.34×10^{-4}
f	4.300	29.300	9.76×10^{-5}	2.98×10^{-4}	0.279	9.76×10^{-5}	0	2.98×10^{-4}

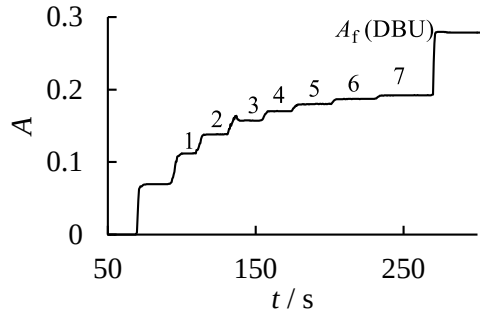

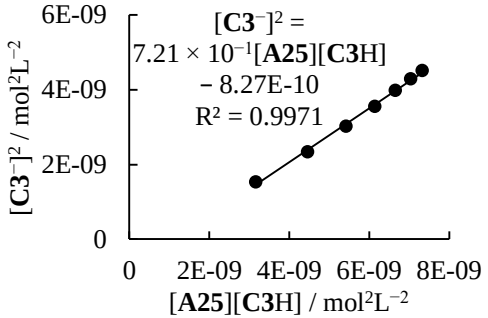

$K = (7.21 \pm 0.17) \times 10^{-1}$

pK_{aH} = 17.61

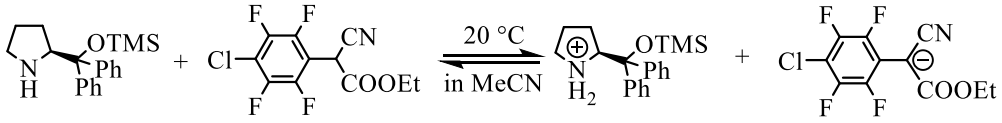

Table 273. Determination of the pK_{aH} for **A25** with **C4**H in acetonitrile at 20 °C (detection at 333 nm). Stock solutions: **A25** (7.1 mg) in 10.0 mL MeCN; **C4**H (11.8 mg) in 10.0 mL MeCN; [DBU] = 3.26×10^{-2} mol L^{-1}. Step 0: 0.500 mL **C4**H stock solution in 19.0 g MeCN.

step	V_+ / mL	V / mL	[**C4**H]$_0$ / M	[**A25**]$_0$ / M	*A*	[**C4**$^-$] / M	[**C4**H] / M	[**A25**] / M
0	-	24.673	8.09×10^{-5}	0	0	0	8.09×10^{-5}	0
1	0.500	25.173	7.93×10^{-5}	4.33×10^{-5}	0.203	2.69×10^{-5}	5.24×10^{-5}	1.64×10^{-5}
2	0.750	25.423	7.85×10^{-5}	6.43×10^{-5}	0.269	3.56×10^{-5}	4.29×10^{-5}	2.87×10^{-5}
3	1.000	25.673	7.77×10^{-5}	8.50×10^{-5}	0.316	4.19×10^{-5}	3.59×10^{-5}	4.31×10^{-5}
4	1.250	25.923	7.70×10^{-5}	1.05×10^{-4}	0.351	4.65×10^{-5}	3.04×10^{-5}	5.86×10^{-5}
5	1.500	26.173	7.63×10^{-5}	1.25×10^{-4}	0.377	5.00×10^{-5}	2.62×10^{-5}	7.50×10^{-5}
6	1.750	26.423	7.55×10^{-5}	1.44×10^{-4}	0.397	5.27×10^{-5}	2.29×10^{-5}	9.18×10^{-5}
7	2.000	26.673	7.48×10^{-5}	1.64×10^{-4}	0.412	5.46×10^{-5}	2.02×10^{-5}	1.09×10^{-4}
f	2.300	26.973	7.40×10^{-5}	1.62×10^{-4}	0.558	7.40×10^{-5}	0	1.62×10^{-4}

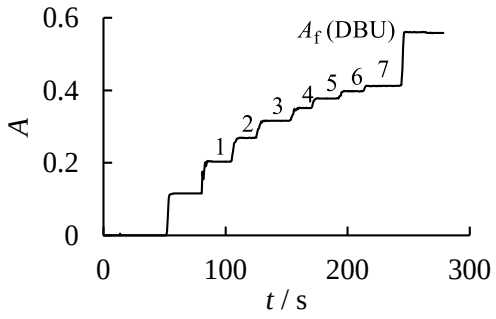

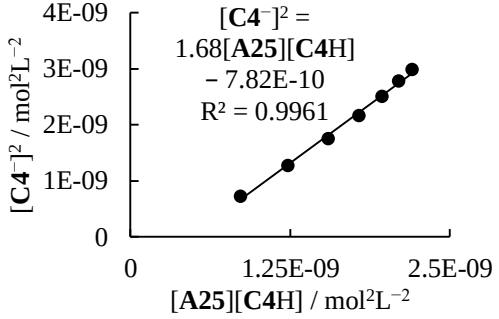

$K = 1.68 \pm 0.05$

p$K_{aH} = 17.62$

pK_{aH}(**A25**) = 17.61 (average)

(*S*)-Diphenyl(pyrrolidin-2-yl)methanol (A26)

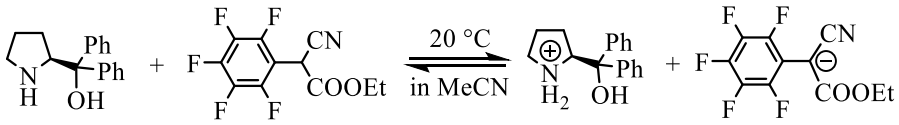

A26 **C3**H **A26**H$^+$ **C3**$^-$

Table 274. Determination of the pK_{aH} for **A26** with **C3**H in acetonitrile at 20 °C (detection at 333 nm). Stock solutions: **A26** (9.7 mg) in 10.0 mL MeCN; **C3**H (11.4 mg) in 10.0 mL MeCN; [DBU] = 3.26×10^{-2} mol L^{-1}. Step 0: 0.700 mL **C3**H stock solution in 20.7 g MeCN.

step	V_+ / mL	V / mL	[**C3**H]$_0$ / M	[**A26**]$_0$ / M	*A*	[**C3**$^-$] / M	[**C3**H] / M	[**A26**] / M
0	-	27.036	1.06×10^{-4}	0	0	0	1.06×10^{-4}	0
1	0.250	27.286	1.05×10^{-4}	3.51×10^{-5}	0.061	2.17×10^{-5}	8.31×10^{-5}	1.34×10^{-5}
2	0.500	27.536	1.04×10^{-4}	6.95×10^{-5}	0.093	3.32×10^{-5}	7.06×10^{-5}	3.63×10^{-5}
3	0.750	27.786	1.03×10^{-4}	1.03×10^{-4}	0.115	4.10×10^{-5}	6.19×10^{-5}	6.23×10^{-5}
4	1.000	28.036	1.02×10^{-4}	1.37×10^{-4}	0.131	4.65×10^{-5}	5.54×10^{-5}	9.00×10^{-5}
5	1.250	28.286	1.01×10^{-4}	1.69×10^{-4}	0.143	5.08×10^{-5}	5.02×10^{-5}	1.18×10^{-4}
6	1.500	28.536	1.00×10^{-4}	2.01×10^{-4}	0.152	5.42×10^{-5}	4.60×10^{-5}	1.47×10^{-4}
7	1.750	28.786	9.93×10^{-5}	2.33×10^{-4}	0.160	5.69×10^{-5}	4.24×10^{-5}	1.76×10^{-4}
8	2.000	29.036	9.84×10^{-5}	2.64×10^{-4}	0.166	5.91×10^{-5}	3.93×10^{-5}	2.05×10^{-4}
f	2.300	29.336	9.74×10^{-5}	2.61×10^{-4}	0.274	9.74×10^{-5}	0	2.61×10^{-4}

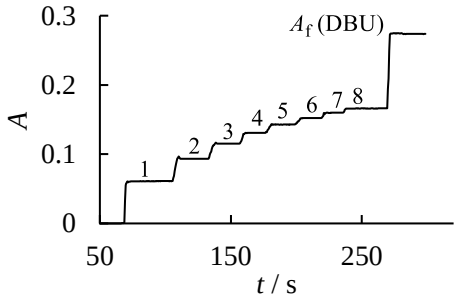

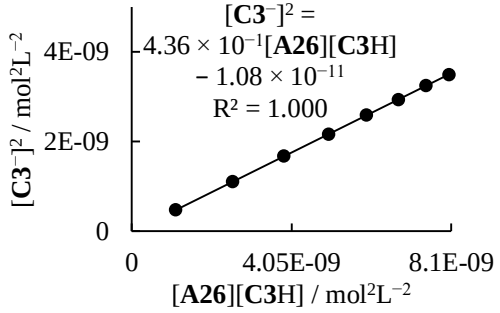

$K = (4.36 \pm 0.01) \times 10^{-1}$

pK_{aH} = 17.39

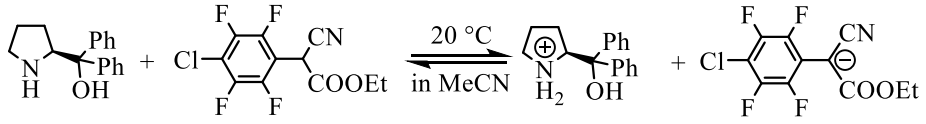

A26 **C4**H **A26**H$^+$ **C4**$^-$

Table 275. Determination of the pK_{aH} for **A26** with **C4**H in acetonitrile at 20 °C (detection at 333 nm). Stock solutions: **A26** (9.7 mg) in 10.0 mL MeCN; **C4**H (11.8 mg) in 10.0 mL MeCN; [DBU] = 3.26 × 10^{-2} mol L^{-1}. Step 0: 0.500 mL **C4**H stock solution in 19.8 g MeCN.

step	V_+ / mL	V / mL	[**C4**H]$_0$ / M	[**A26**]$_0$ / M	*A*	[**C4**$^-$] / M	[**C4**H] / M	[**A26**] / M
0	-	25.691	7.77 × 10^{-5}	0	0	0	7.77 × 10^{-5}	0
1	0.200	25.891	7.71 × 10^{-5}	2.96 × 10^{-5}	0.163	2.14 × 10^{-5}	5.57 × 10^{-5}	8.16 × 10^{-6}
2	0.400	26.091	7.65 × 10^{-5}	5.87 × 10^{-5}	0.255	3.34 × 10^{-5}	4.31 × 10^{-5}	2.53 × 10^{-5}
3	0.600	26.291	7.59 × 10^{-5}	8.74 × 10^{-5}	0.310	4.06 × 10^{-5}	3.53 × 10^{-5}	4.68 × 10^{-5}
4	0.800	26.491	7.53 × 10^{-5}	1.16 × 10^{-4}	0.348	4.57 × 10^{-5}	2.97 × 10^{-5}	7.00 × 10^{-5}
5	1.000	26.691	7.48 × 10^{-5}	1.43 × 10^{-4}	0.375	4.92 × 10^{-5}	2.56 × 10^{-5}	9.43 × 10^{-5}
6	1.250	26.941	7.41 × 10^{-5}	1.78 × 10^{-4}	0.399	5.22 × 10^{-5}	2.19 × 10^{-5}	1.25 × 10^{-4}
7	1.500	27.191	7.34 × 10^{-5}	2.11 × 10^{-4}	0.415	5.44 × 10^{-5}	1.90 × 10^{-5}	1.57 × 10^{-4}
8	1.750	27.441	7.27 × 10^{-5}	2.44 × 10^{-4}	0.427	5.59 × 10^{-5}	1.68 × 10^{-5}	1.88 × 10^{-4}
9	2.000	27.691	7.21 × 10^{-5}	2.77 × 10^{-4}	0.436	5.71 × 10^{-5}	1.50 × 10^{-5}	2.19 × 10^{-4}
f	2.300	27.991	7.13 × 10^{-5}	2.74 × 10^{-4}	0.544	7.13 × 10^{-5}	0	2.74 × 10^{-4}

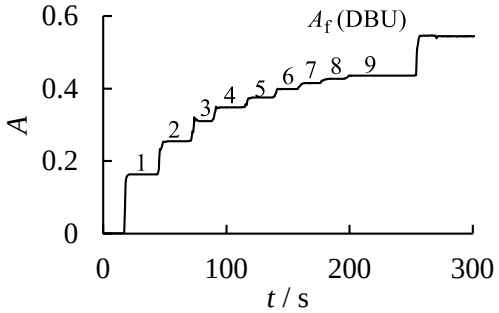

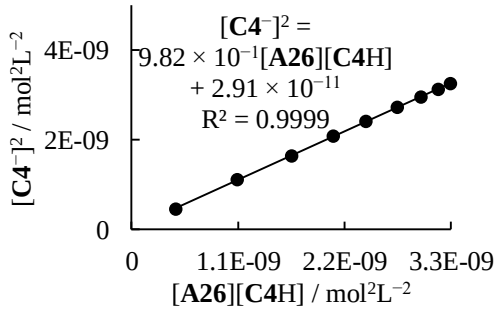

K = (9.82 ± 0.04) × 10^{-1}

pK_{aH} = 17.38

pK_{aH}(**A26**) = 17.39 (average)

(*S*)-2-(Azidodiphenylmethyl)pyrrolidine (A27)

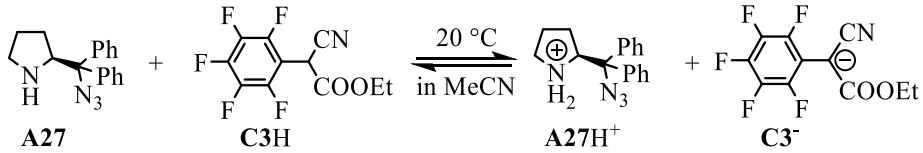

Table 276. Determination of the pK_{aH} for **A27** with **C3**H in acetonitrile at 20 °C (detection at 333 nm). Stock solutions: **A27** (9.6 mg) in 10.0 mL MeCN; **C3**H (11.4 mg) in 10.0 mL MeCN; [DBU] = 3.26×10^{-2} mol L^{-1}. Step 0: 0.700 mL **C3**H stock solution in 20.8 g MeCN.

step	V_+ / mL	V / mL	[**C3**H]$_0$ / M	[**A27**]$_0$ / M	*A*	[**C3**$^-$] / M	[**C3**H] / M	[**A27**] / M
0	-	27.163	1.05×10^{-4}	0	0	0	1.05×10^{-4}	0
1	0.500	27.663	1.03×10^{-4}	6.23×10^{-5}	0.021	7.31×10^{-6}	9.60×10^{-5}	5.50×10^{-5}
2	1.000	28.163	1.01×10^{-4}	1.22×10^{-4}	0.029	1.03×10^{-5}	9.12×10^{-5}	1.12×10^{-4}
3	1.500	28.663	9.97×10^{-5}	1.80×10^{-4}	0.036	1.24×10^{-5}	8.73×10^{-5}	1.68×10^{-4}
4	2.000	29.163	9.80×10^{-5}	2.37×10^{-4}	0.040	1.41×10^{-5}	8.39×10^{-5}	2.22×10^{-4}
5	2.500	29.663	9.64×10^{-5}	2.91×10^{-4}	0.044	1.55×10^{-5}	8.09×10^{-5}	2.75×10^{-4}
6	3.000	30.163	9.48×10^{-5}	3.43×10^{-4}	0.048	1.66×10^{-5}	7.81×10^{-5}	3.26×10^{-4}
7	3.500	30.663	9.32×10^{-5}	3.94×10^{-4}	0.051	1.76×10^{-5}	7.56×10^{-5}	3.76×10^{-4}
8	4.000	31.163	9.17×10^{-5}	4.43×10^{-4}	0.053	1.85×10^{-5}	7.32×10^{-5}	4.24×10^{-4}
9	4.500	31.663	9.03×10^{-5}	4.90×10^{-4}	0.055	1.93×10^{-5}	7.10×10^{-5}	4.71×10^{-4}
10	5.000	32.163	8.89×10^{-5}	5.36×10^{-4}	0.057	2.00×10^{-5}	6.89×10^{-5}	5.16×10^{-4}
f	5.300	32.463	8.81×10^{-5}	5.31×10^{-4}	0.252	8.81×10^{-5}	0	5.31×10^{-4}

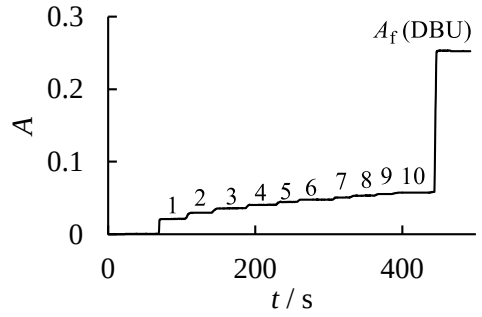

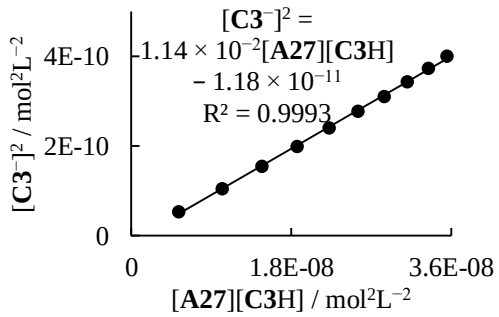

$K = (1.14 \pm 0.01) \times 10^{-2}$

pK_{aH} = 15.81

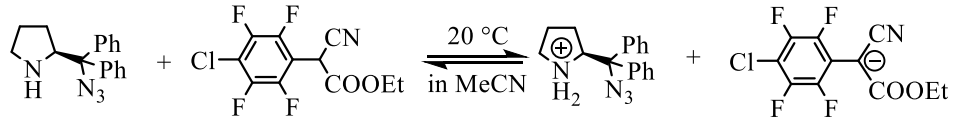

A27 **C4**H **A27**H$^+$ **C4**$^-$

Table 277. Determination of the pK_{aH} for **A27** with **C4**H in acetonitrile at 20 °C (detection at 333 nm). Stock solutions: **A27** (9.6 mg) in 10.0 mL MeCN; **C4**H (11.8 mg) in 10.0 mL MeCN; [DBU] = 3.26×10^{-2} mol L^{-1}. Step 0: 0.500 mL **C4**H stock solution in 20.2 g MeCN.

step	V_+ / mL	V / mL	[**C4**H]$_0$ / M	[**A27**]$_0$ / M	*A*	[**C4**$^-$] / M	[**C4**H] / M	[**A27**] / M
0	-	26.200	7.62×10^{-5}	0	0	0	7.62×10^{-5}	0
1	0.250	26.450	7.55×10^{-5}	3.26×10^{-5}	0.050	6.65×10^{-6}	6.88×10^{-5}	2.59×10^{-5}
2	0.500	26.700	7.48×10^{-5}	6.46×10^{-5}	0.071	9.42×10^{-6}	6.53×10^{-5}	5.52×10^{-5}
3	0.750	26.950	7.41×10^{-5}	9.60×10^{-5}	0.087	1.15×10^{-5}	6.26×10^{-5}	8.45×10^{-5}
4	1.000	27.200	7.34×10^{-5}	1.27×10^{-4}	0.099	1.30×10^{-5}	6.03×10^{-5}	1.14×10^{-4}
5	1.250	27.450	7.27×10^{-5}	1.57×10^{-4}	0.109	1.43×10^{-5}	5.84×10^{-5}	1.43×10^{-4}
6	1.500	27.700	7.21×10^{-5}	1.87×10^{-4}	0.117	1.55×10^{-5}	5.66×10^{-5}	1.71×10^{-4}
7	1.750	27.950	7.14×10^{-5}	2.16×10^{-4}	0.124	1.64×10^{-5}	5.50×10^{-5}	1.99×10^{-4}
8	2.000	28.200	7.08×10^{-5}	2.45×10^{-4}	0.131	1.73×10^{-5}	5.35×10^{-5}	2.27×10^{-4}
9	2.250	28.450	7.02×10^{-5}	2.73×10^{-4}	0.137	1.81×10^{-5}	5.21×10^{-5}	2.55×10^{-4}
10	2.500	28.700	6.95×10^{-5}	3.00×10^{-4}	0.142	1.88×10^{-5}	5.08×10^{-5}	2.82×10^{-4}
f	2.800	29.000	6.88×10^{-5}	2.97×10^{-4}	0.521	6.88×10^{-5}	0	2.97×10^{-4}

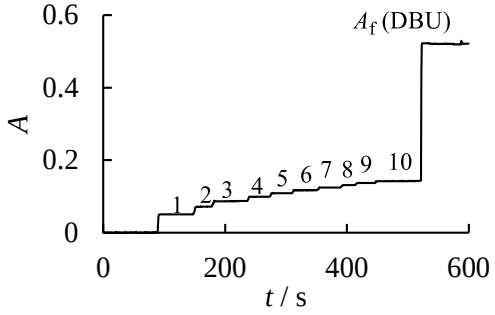

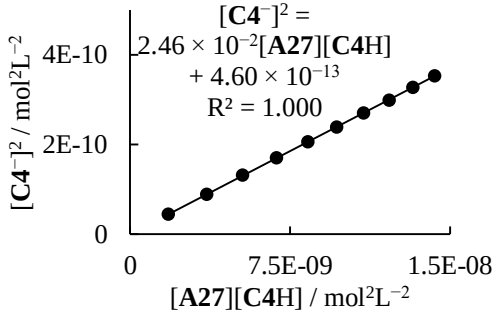

$K = (2.46 \pm 0.00) \times 10^{-2}$

pK_{aH} = 15.78

pK_{aH} (**A27**) = 15.79 (average)

2-(Triphenylsilyl)pyrrolidine (A28)

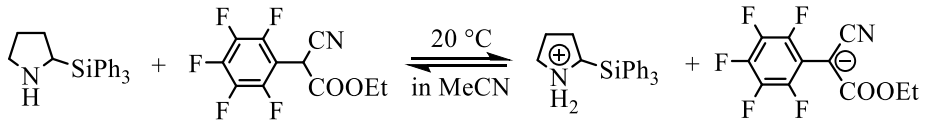

A28 **C3**H **A28**H$^+$ **C3**$^-$

Table 278. Determination of the pK_{aH} for **A28** with **C3**H in acetonitrile at 20 °C (detection at 333 nm). Stock solutions: **A28** (9.9 mg) in 10.0 mL MeCN; **C3**H (11.4 mg) in 10.0 mL MeCN; [DBU] = 3.26×10^{-2} mol L^{-1}. Step 0: 0.700 mL **C3**H stock solution in 18.8 g MeCN.

step	V_+ / mL	V / mL	[**C3**H]$_0$ / M	[**A28**]$_0$ / M	*A*	[**C3**$^-$] / M	[**C3**H] / M	[**A28**] / M
0	-	24.619	1.16×10^{-4}	0	0	0	1.16×10^{-4}	0
1	0.250	24.869	1.15×10^{-4}	3.02×10^{-5}	0.066	2.34×10^{-5}	9.16×10^{-5}	6.82×10^{-6}
2	0.500	25.119	1.14×10^{-4}	5.98×10^{-5}	0.110	3.91×10^{-5}	7.47×10^{-5}	2.08×10^{-5}
3	0.750	25.369	1.13×10^{-4}	8.88×10^{-5}	0.142	5.04×10^{-5}	6.23×10^{-5}	3.84×10^{-5}
4	1.000	25.619	1.12×10^{-4}	1.17×10^{-4}	0.164	5.83×10^{-5}	5.33×10^{-5}	5.90×10^{-5}
5	1.250	25.869	1.11×10^{-4}	1.45×10^{-4}	0.180	6.42×10^{-5}	4.63×10^{-5}	8.10×10^{-5}
6	1.500	26.119	1.09×10^{-4}	1.73×10^{-4}	0.193	6.86×10^{-5}	4.08×10^{-5}	1.04×10^{-4}
7	1.750	26.369	1.08×10^{-4}	1.99×10^{-4}	0.202	7.20×10^{-5}	3.64×10^{-5}	1.27×10^{-4}
8	2.000	26.619	1.07×10^{-4}	2.26×10^{-4}	0.210	7.47×10^{-5}	3.27×10^{-5}	1.51×10^{-4}
f	2.290	26.909	1.06×10^{-4}	2.23×10^{-4}	0.299	1.06×10^{-4}	0	2.23×10^{-4}

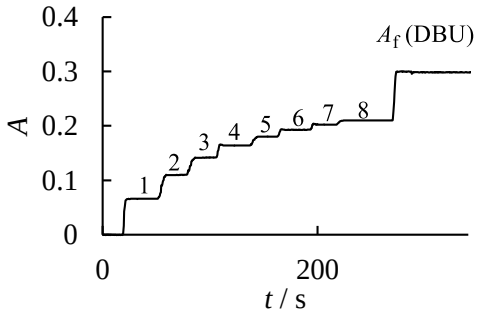

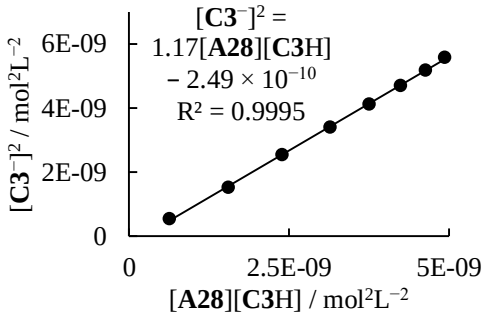

K = 1.17 ± 0.01

pK_{aH} = 17.82

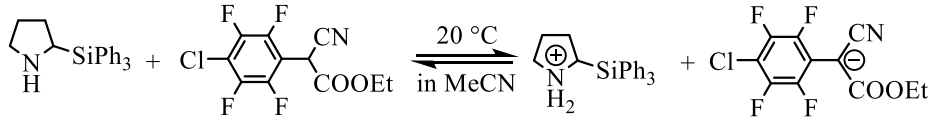

A28 **C4**H $A28H^+$ $C4^-$

Table 279. Determination of the pK_{aH} for **A28** with **C4**H in acetonitrile at 20 °C (detection at 333 nm). Stock solutions: **A28** (9.9 mg) in 10.0 mL MeCN; **C4**H (11.8 mg) in 10.0 mL MeCN; [DBU] = 3.26×10^{-2} mol L^{-1}. Step 0: 0.500 mL **C4**H stock solution in 21.0 g MeCN.

step	V_+ / mL	V / mL	[**C4**H]$_0$ / M	[**A28**]$_0$ / M	*A*	[$\mathbf{C4}^-$] / M	[**C4**H] / M	[**A28**] / M
0	-	27.218	7.33×10^{-5}	0	0	0	7.33×10^{-5}	0
1	0.100	27.318	7.31×10^{-5}	1.10×10^{-5}	0.077	1.01×10^{-5}	6.30×10^{-5}	9.00×10^{-7}
2	0.200	27.418	7.28×10^{-5}	2.19×10^{-5}	0.144	1.88×10^{-5}	5.40×10^{-5}	3.10×10^{-6}
3	0.300	27.518	7.25×10^{-5}	3.28×10^{-5}	0.201	2.63×10^{-5}	4.62×10^{-5}	6.44×10^{-6}
4	0.400	27.618	7.23×10^{-5}	4.35×10^{-5}	0.248	3.24×10^{-5}	3.98×10^{-5}	1.11×10^{-5}
5	0.500	27.718	7.20×10^{-5}	5.42×10^{-5}	0.287	3.75×10^{-5}	3.45×10^{-5}	1.67×10^{-5}
6	0.600	27.818	7.17×10^{-5}	6.48×10^{-5}	0.318	4.16×10^{-5}	3.02×10^{-5}	2.32×10^{-5}
7	0.700	27.918	7.15×10^{-5}	7.53×10^{-5}	0.344	4.49×10^{-5}	2.65×10^{-5}	3.04×10^{-5}
8	0.800	28.018	7.12×10^{-5}	8.58×10^{-5}	0.364	4.76×10^{-5}	2.37×10^{-5}	3.82×10^{-5}
f	1.100	28.318	7.05×10^{-5}	8.49×10^{-5}	0.539	7.05×10^{-5}	0	8.49×10^{-5}

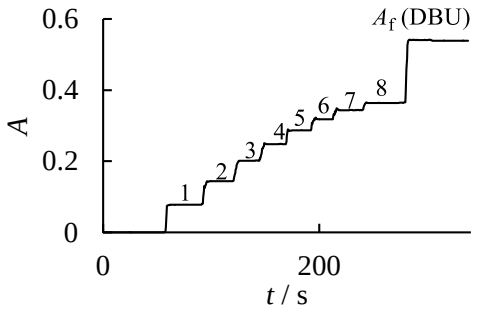

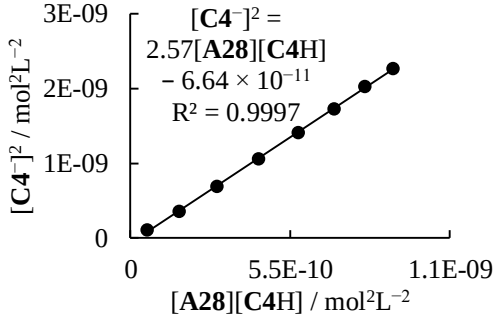

$K = 2.57 \pm 0.02$

pK_{aH} = 17.80

pK_{aH}(**A28**) = 17.81 (average)

(*S*)-5-Benzyl-2,2,3-trimethylimidazolidin-4-one (A29)

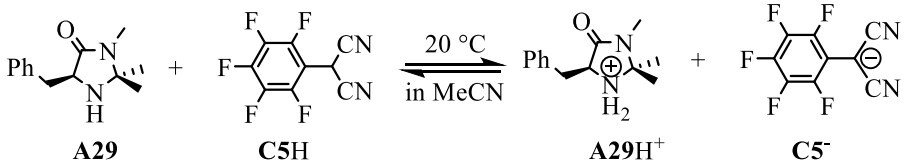

A29 **C5**H **A29**H$^+$ **C5**$^-$

Table 280. Determination of the pK_{aH} for **A29** with **C5**H in acetonitrile at 20 °C (detection at 330 nm). Stock solutions: **A29** (8.2 mg) in 10.0 mL MeCN; **C5**H (20.5 mg) in 10.0 mL MeCN; [DBU] = 4.62×10^{-2} mol L^{-1}. Step 0: 1.000 mL **C5**H stock solution in 21.3 g MeCN.

step	V_+ / mL	V / mL	[**C5**H]$_0$ / M	[**A29**]$_0$ / M	*A*	[**C5**$^-$] / M	[**C5**H] / M	[**A29**] / M
0	-	28.099	3.14×10^{-4}	0	-	-	-	0
1	0.250	28.349	3.12×10^{-4}	3.31×10^{-5}	0.049	1.86×10^{-5}	2.93×10^{-4}	1.45×10^{-5}
2	0.500	28.599	3.09×10^{-4}	6.57×10^{-5}	0.073	2.75×10^{-5}	2.81×10^{-4}	3.82×10^{-5}
3	0.750	28.849	3.06×10^{-4}	9.77×10^{-5}	0.091	3.44×10^{-5}	2.72×10^{-4}	6.33×10^{-5}
4	1.000	29.099	3.04×10^{-4}	1.29×10^{-4}	0.106	4.00×10^{-5}	2.64×10^{-4}	8.91×10^{-5}
5	1.500	29.599	2.98×10^{-4}	1.90×10^{-4}	0.129	4.89×10^{-5}	2.50×10^{-4}	1.42×10^{-4}
6	2.000	30.099	2.93×10^{-4}	2.50×10^{-4}	0.148	5.59×10^{-5}	2.38×10^{-4}	1.94×10^{-4}
f	2.500	30.599	2.89×10^{-4}	2.46×10^{-4}	0.763	2.89×10^{-4}	0	2.46×10^{-4}

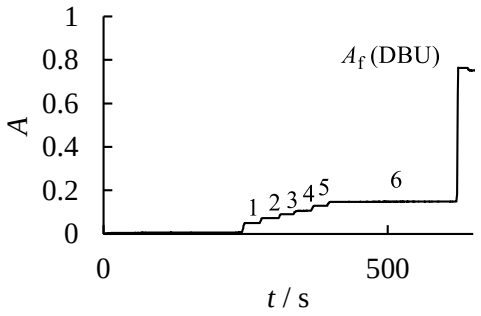

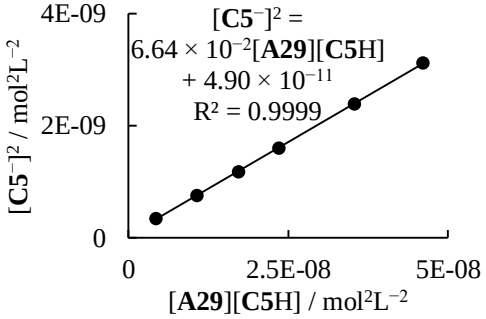

$K = (6.64 \pm 0.04) \times 10^{-2}$

Table 281. Determination of the pK_{aH} for **A29** with **C5**H in acetonitrile at 20 °C (detection at 330 nm). Stock solutions: **A29** (8.2 mg) in 10.0 mL MeCN; **C5**H (20.5 mg) in 10.0 mL MeCN; [DBU] = 4.62×10^{-2} mol L^{-1}. Step 0: 0.600 mL **C5**H stock solution in 18.4 g MeCN.

step	V_+ / mL	V / mL	[**C5**H]$_0$ / M	[**A29**]$_0$ / M	*A*	[**C5**$^-$] / M	[**C5**H] / M	[**A29**] / M
0	-	24.010	2.21×10^{-4}	0	-	-	-	0
1	c	24.510	2.16×10^{-4}	7.66×10^{-5}	0.069	2.64×10^{-5}	1.90×10^{-4}	5.02×10^{-5}
2	1.000	25.010	2.12×10^{-4}	1.50×10^{-4}	0.097	3.71×10^{-5}	1.75×10^{-4}	1.13×10^{-4}
3	1.500	25.510	2.08×10^{-4}	2.21×10^{-4}	0.117	4.46×10^{-5}	1.63×10^{-4}	1.76×10^{-4}
4	2.000	26.010	2.04×10^{-4}	2.89×10^{-4}	0.132	5.02×10^{-5}	1.54×10^{-4}	2.39×10^{-4}
5	2.500	26.510	2.00×10^{-4}	3.54×10^{-4}	0.144	5.48×10^{-5}	1.45×10^{-4}	2.99×10^{-4}
f	2.800	26.810	1.98×10^{-4}	3.50×10^{-4}	0.519	1.98×10^{-4}	0	3.50×10^{-4}

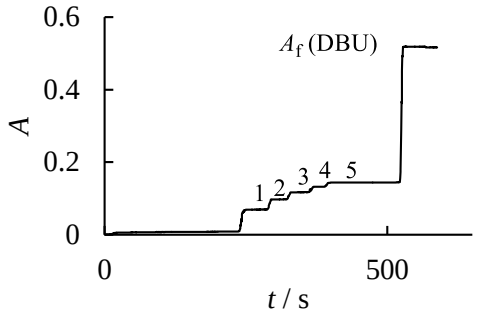

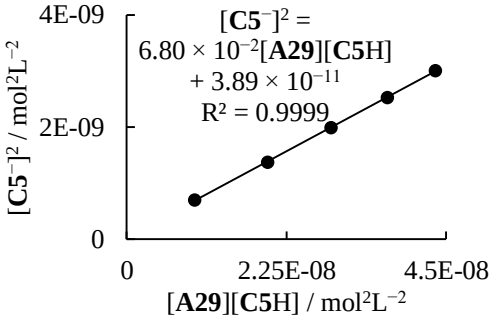

$K = (6.80 \pm 0.04) \times 10^{-2}$

$\bar{K} = (6.72 \pm 0.08) \times 10^{-2}$

pK_{aH} = 11.84

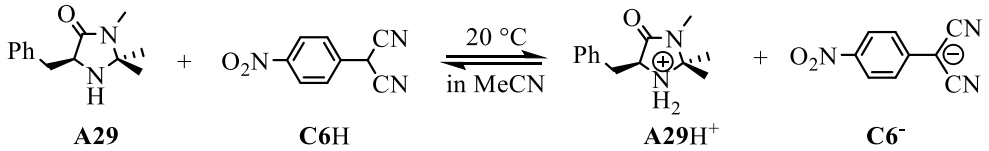

A29 **C6**H **A29**H$^+$ **C6**$^-$

Table 282. Determination of the pK_{aH} for **A29** with **C6**H in acetonitrile at 20 °C (detection at 478 nm). Stock solutions: **A29** (8.2 mg) in 10.0 mL MeCN; **C6**H (9.3 mg) in 10.0 mL MeCN; [DBU] = 4.62×10^{-2} mol L^{-1}. Step 0: 0.200 mL **C6**H stock solution in 19.3 g MeCN.

step	V_+ / mL	V / mL	[**C6**H]$_0$ / M	[**A29**]$_0$ / M	*A*	[**C6**$^-$] / M	[**C6**H] / M	[**A29**] / M
0	-	24.755	4.01×10^{-5}	0	-	-	-	0
1	0.250	25.005	3.97×10^{-5}	3.76×10^{-5}	0.361	2.12×10^{-5}	1.86×10^{-5}	1.64×10^{-5}
2	0.500	25.255	3.94×10^{-5}	7.44×10^{-5}	0.483	2.84×10^{-5}	1.10×10^{-5}	4.60×10^{-5}
3	0.750	25.505	3.90×10^{-5}	1.10×10^{-4}	0.533	3.13×10^{-5}	7.70×10^{-6}	7.92×10^{-5}
4	1.000	25.755	3.86×10^{-5}	1.46×10^{-4}	0.557	3.27×10^{-5}	5.91×10^{-6}	1.13×10^{-4}
5	1.250	26.005	3.82×10^{-5}	1.81×10^{-4}	0.570	3.34×10^{-5}	4.78×10^{-6}	1.47×10^{-4}
6	1.500	26.255	3.79×10^{-5}	2.15×10^{-4}	0.577	3.39×10^{-5}	4.00×10^{-6}	1.81×10^{-4}
7	1.750	26.505	3.75×10^{-5}	2.48×10^{-4}	0.581	3.41×10^{-5}	3.43×10^{-6}	2.14×10^{-4}
8	2.000	26.755	3.71×10^{-5}	2.81×10^{-4}	0.582	3.41×10^{-5}	3.00×10^{-6}	2.47×10^{-4}
f	2.100	26.855	3.70×10^{-5}	2.80×10^{-4}	0.631	3.70×10^{-5}	0	2.80×10^{-4}

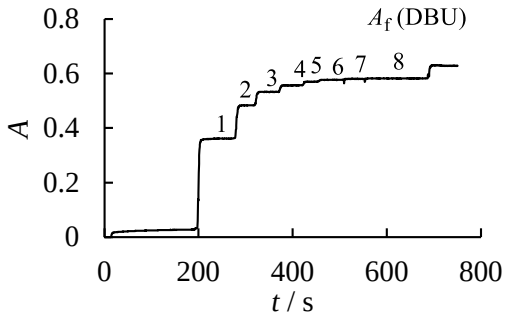

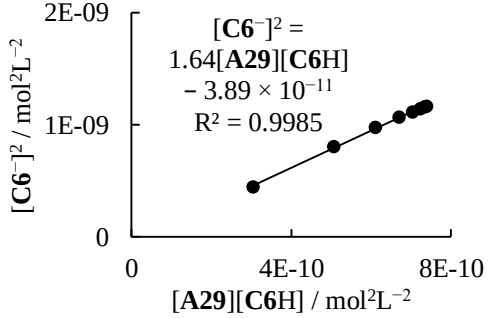

$K = 1.64 \pm 0.03$

p$K_{aH} = 11.83$

pK_{aH}(**A29**) = 11.83 (average)

(2*S*,5*S*)-5-Benzyl-2-(*tert*-butyl)-3-methylimidazolidin-4-one (A30)

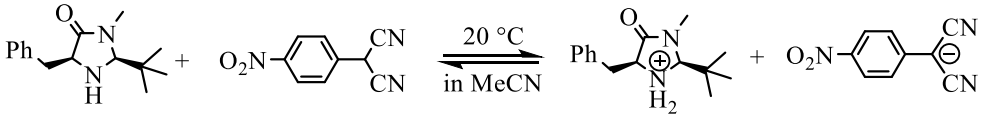

A30 **C6**H **A30**H$^+$ **C6**$^-$

Table 283. Determination of the pK_{aH} for **A30** with **C6**H in acetonitrile at 20 °C (detection at 478 nm). Stock solutions: **A30** (8.4 mg) in 10.0 mL MeCN; **C6**H (9.3 mg) in 10.0 mL MeCN; [DBU] = 4.62×10^{-2} mol L^{-1}. Step 0: 0.200 mL **C6**H stock solution in 21.9 g MeCN.

step	V_+ / mL	V / mL	[**C6**H]$_0$ / M	[**A30**]$_0$ / M	*A*	[**C6**$^-$] / M	[**C6**H] / M	[**A30**] / M
0	-	28.063	3.54×10^{-5}	0	-	-	-	0
1	0.250	28.313	3.51×10^{-5}	3.01×10^{-5}	0.154	9.01×10^{-6}	2.61×10^{-5}	2.11×10^{-5}
2	0.500	28.563	3.48×10^{-5}	5.97×10^{-5}	0.203	1.19×10^{-5}	2.29×10^{-5}	4.78×10^{-5}
3	0.750	28.813	3.45×10^{-5}	8.88×10^{-5}	0.235	1.37×10^{-5}	2.08×10^{-5}	7.50×10^{-5}
4	1.000	29.063	3.42×10^{-5}	1.17×10^{-4}	0.260	1.52×10^{-5}	1.90×10^{-5}	1.02×10^{-4}
5	1.500	29.563	3.36×10^{-5}	1.73×10^{-4}	0.294	1.71×10^{-5}	1.65×10^{-5}	1.56×10^{-4}
6	2.000	30.063	3.31×10^{-5}	2.27×10^{-4}	0.318	1.85×10^{-5}	1.45×10^{-5}	2.08×10^{-4}
f	2.100	30.163	3.29×10^{-5}	2.26×10^{-4}	0.565	3.29×10^{-5}	0	2.26×10^{-4}

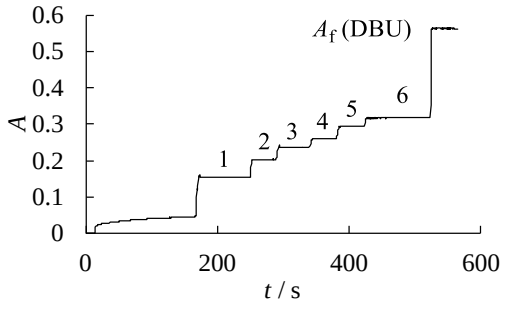

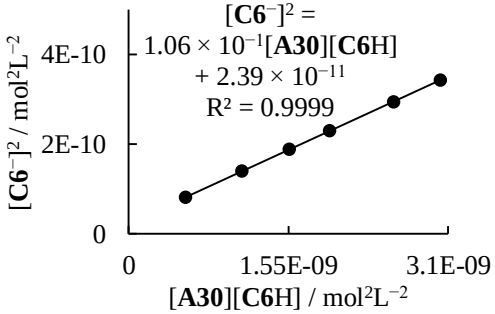

$K = (1.06 \pm 0.00) \times 10^{-1}$

Table 284. Determination of the pK_{aH} for **A30** with **C6**H in acetonitrile at 20 °C (detection at 478 nm). Stock solutions: **A30** (8.4 mg) in 10.0 mL MeCN; **C6**H (9.3 mg) in 10.0 mL MeCN; [DBU] = 4.62×10^{-2} mol L^{-1}. Step 0: 0.200 mL **C6**H stock solution in 20.3 g MeCN.

step	V_+ / mL	V / mL	[**C6**H]$_0$ / M	[**A30**]$_0$ / M	*A*	[**C6**$^-$] / M	[**C6**H] / M	[**A30**] / M
0	-	26.027	3.82×10^{-5}	0	-	-	-	0
1	1.000	27.027	3.68×10^{-5}	1.26×10^{-4}	0.278	1.60×10^{-5}	2.08×10^{-5}	1.10×10^{-4}
2	1.500	27.527	3.61×10^{-5}	1.86×10^{-4}	0.315	1.81×10^{-5}	1.80×10^{-5}	1.68×10^{-4}
3	2.000	28.027	3.55×10^{-5}	2.43×10^{-4}	0.341	1.96×10^{-5}	1.58×10^{-5}	2.24×10^{-4}
4	2.500	28.527	3.48×10^{-5}	2.99×10^{-4}	0.359	2.07×10^{-5}	1.42×10^{-5}	2.78×10^{-4}
5	3.000	29.027	3.42×10^{-5}	3.52×10^{-4}	0.372	2.14×10^{-5}	1.28×10^{-5}	3.31×10^{-4}
f	3.100	29.127	3.41×10^{-5}	3.51×10^{-4}	0.593	3.41×10^{-5}	0	3.51×10^{-4}

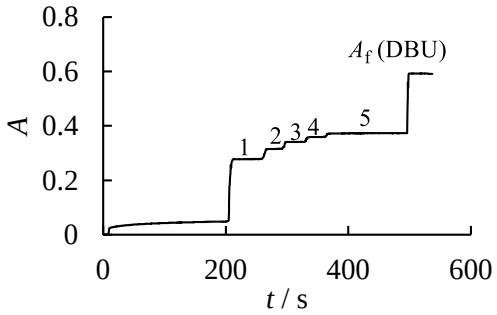

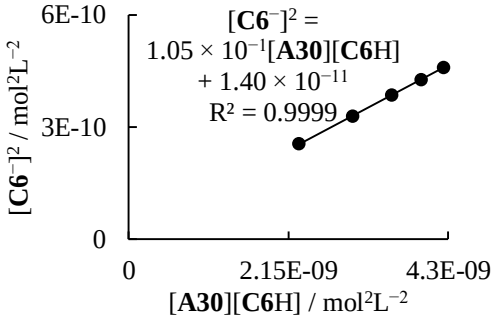

$K = (1.05 \pm 0.01) \times 10^{-1}$

Table 285. Determination of the pK_{aH} for **A30** with **C6**H in acetonitrile at 20 °C (detection at 478 nm). Stock solutions: **A30** (8.4 mg) in 10.0 mL MeCN; **C6**H (9.3 mg) in 10.0 mL MeCN; [DBU] = 4.62×10^{-2} mol L^{-1}. Step 0: 0.200 mL **C6**H stock solution in 19.2 g MeCN.

step	V_+ / mL	V / mL	[**C6**H]$_0$ / M	[**A30**]$_0$ / M	*A*	[**C6**$^-$] / M	[**C6**H] / M	[**A30**] / M
0	-	24.627	4.04×10^{-5}	0	-	-	-	0
1	1.000	25.627	3.88×10^{-5}	1.33×10^{-4}	0.280	1.63×10^{-5}	2.25×10^{-5}	1.17×10^{-4}
2	1.500	26.127	3.80×10^{-5}	1.96×10^{-4}	0.320	1.87×10^{-5}	1.94×10^{-5}	1.77×10^{-4}
3	2.000	26.627	3.73×10^{-5}	2.56×10^{-4}	0.347	2.03×10^{-5}	1.71×10^{-5}	2.36×10^{-4}
4	2.500	27.127	3.66×10^{-5}	3.14×10^{-4}	0.367	2.14×10^{-5}	1.52×10^{-5}	2.93×10^{-4}
5	3.000	27.627	3.60×10^{-5}	3.70×10^{-4}	0.381	2.22×10^{-5}	1.37×10^{-5}	3.48×10^{-4}
f	3.100	27.727	3.58×10^{-5}	3.69×10^{-4}	0.615	3.58×10^{-5}	0	3.69×10^{-4}

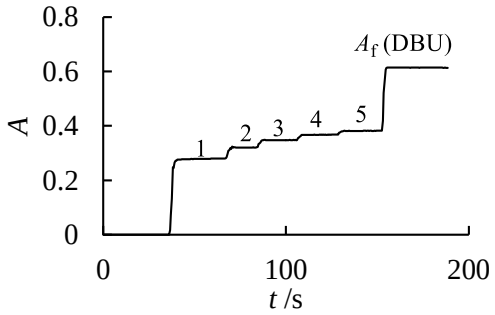

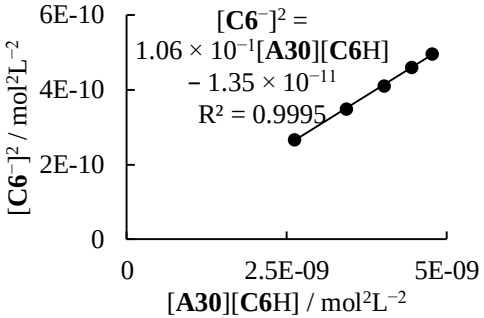

$K = (1.06 \pm 0.01) \times 10^{-1}$

$\bar{K} = (1.06 \pm 0.00) \times 10^{-1}$

pK_{aH}(**A30**) = 10.63

(2*S*,5*S*)-5-Benzyl-3-methyl-2-(5-methylfuran-2-yl)imidazolidin-4-one (A31)

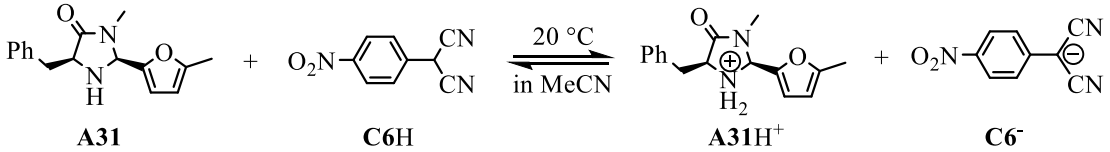

A31 **C6**H **A31**H$^+$ **C6**$^-$

Table 286. Determination of the pK_{aH} for **A31** with **C6**H in acetonitrile at 20°C (detection at 478 nm). Stock solutions: **A31** (13.8 mg) in 10.0 mL MeCN; **C6**H (8.9 mg) in 10.0 mL MeCN; [DBU] = 1.27×10^{-2} mol L^{-1}. Step 0: 0.200 mL **C6**H stock solution in 19.5 g MeCN.

step	V_+ / mL	V / mL	[**C6**H]$_0$ / M	[**A31**]$_0$ / M	*A*	[**C6**$^-$] / M	[**C6**H] / M	[**A31**] / M
0	-	25.009	3.80×10^{-5}	0	-	-	-	0
1	0.500	25.509	3.73×10^{-5}	1.00×10^{-4}	0.231	1.33×10^{-5}	2.40×10^{-5}	8.68×10^{-5}
2	0.750	25.759	3.69×10^{-5}	1.49×10^{-4}	0.270	1.55×10^{-5}	2.14×10^{-5}	1.33×10^{-4}
3	1.000	26.009	3.66×10^{-5}	1.96×10^{-4}	0.299	1.71×10^{-5}	1.95×10^{-5}	1.79×10^{-4}
4	1.250	26.259	3.62×10^{-5}	2.43×10^{-4}	0.320	1.84×10^{-5}	1.79×10^{-5}	2.25×10^{-4}
5	1.500	26.509	3.59×10^{-5}	2.89×10^{-4}	0.338	1.94×10^{-5}	1.65×10^{-5}	2.69×10^{-4}
6	2.000	27.009	3.52×10^{-5}	3.78×10^{-4}	0.365	2.09×10^{-5}	1.43×10^{-5}	3.57×10^{-4}
f	2.200	27.209	3.50×10^{-5}	3.75×10^{-4}	0.610	3.50×10^{-5}	0	3.75×10^{-4}

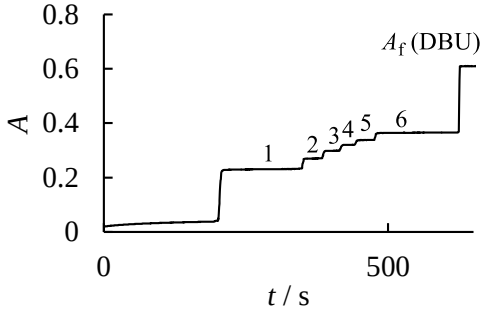

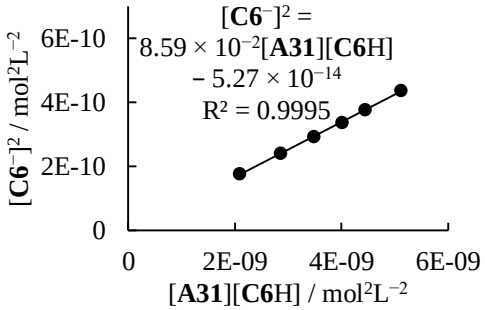

$K = (8.59 \pm 0.09) \times 10^{-2}$

Table 287. Determination of the pK_{aH} for **A31** with **C6**H in acetonitrile at 20°C (detection at 478 nm). Stock solutions: **A31** (13.8 mg) in 10.0 mL MeCN; **C6**H (8.9 mg) in 10.0 mL MeCN; [DBU] = 1.27×10^{-2} mol L^{-1}. Step 0: 0.245 mL **C6**H stock solution in 20.0 g MeCN.

step	V_+ / mL	V / mL	[**C6**H]$_0$ / M	[**A31**]$_0$ / M	*A*	[**C6**$^-$] / M	[**C6**H] / M	[**A31**] / M
0	-	25.690	4.54×10^{-5}	0	-	-	-	0
1	0.500	26.190	4.45×10^{-5}	9.75×10^{-5}	0.253	1.48×10^{-5}	2.97×10^{-5}	8.27×10^{-5}
2	1.000	26.690	4.37×10^{-5}	1.91×10^{-4}	0.326	1.90×10^{-5}	2.46×10^{-5}	1.72×10^{-4}
3	1.500	27.190	4.28×10^{-5}	2.82×10^{-4}	0.371	2.16×10^{-5}	2.12×10^{-5}	2.60×10^{-4}
4	2.000	27.690	4.21×10^{-5}	3.69×10^{-4}	0.402	2.35×10^{-5}	1.86×10^{-5}	3.45×10^{-4}
5	2.500	28.190	4.13×10^{-5}	4.53×10^{-4}	0.426	2.48×10^{-5}	1.65×10^{-5}	4.28×10^{-4}
f	2.750	28.440	4.10×10^{-5}	4.49×10^{-4}	0.702	4.10×10^{-5}	0	4.49×10^{-4}

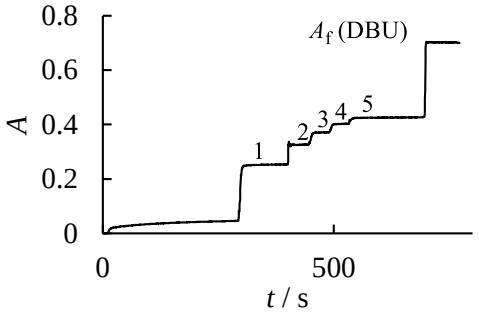

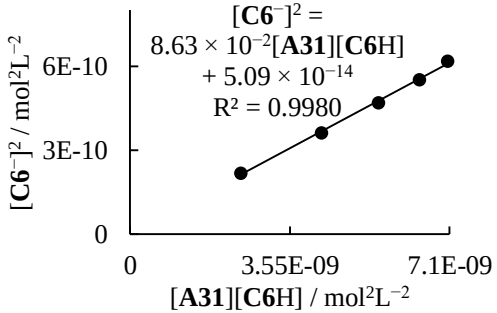

$K = (8.63 \pm 0.22) \times 10^{-2}$

$\bar{K} = (8.61 \pm 0.02) \times 10^{-2}$

pK_{aH}(**A31**) = 10.54

(2*R*,5*S*)-5-Benzyl-3-methyl-2-(5-methylfuran-2-yl)imidazolidin-4-one (A32)

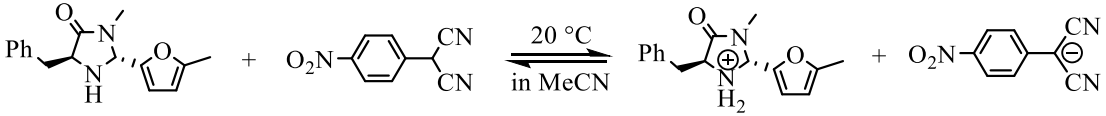

A32 **C6**H $A32H^+$ $C6^-$

Table 288. Determination of the pK_{aH} for **A32** with **C6**H in acetonitrile at 20 °C (detection at 478 nm). Stock solutions: **A32** (9.4 mg) in 10.0 mL MeCN; **C6**H (8.9 mg) in 10.0 mL MeCN; [DBU] = 1.27×10^{-2} mol L^{-1}. Step 0: 0.200 mL **C6**H stock solution in 20.1 g MeCN.

step	V_+ / mL	V / mL	[**C6**H]$_0$ / M	[**A32**]$_0$ / M	*A*	[**C6**$^-$] / M	[**C6**H] / M	[**A32**] / M
0	-	25.773	3.69×10^{-5}	0	-	-	-	0
1	0.500	26.273	3.62×10^{-5}	6.62×10^{-5}	0.223	1.27×10^{-5}	2.35×10^{-5}	5.35×10^{-5}
2	0.750	26.523	3.59×10^{-5}	9.83×10^{-5}	0.261	1.48×10^{-5}	2.10×10^{-5}	8.35×10^{-5}
3	1.000	26.773	3.55×10^{-5}	1.30×10^{-4}	0.288	1.64×10^{-5}	1.91×10^{-5}	1.13×10^{-4}
4	1.500	27.273	3.49×10^{-5}	1.91×10^{-4}	0.327	1.86×10^{-5}	1.63×10^{-5}	1.73×10^{-4}
5	2.000	27.773	3.42×10^{-5}	2.50×10^{-4}	0.352	2.00×10^{-5}	1.42×10^{-5}	2.30×10^{-4}
f	2.200	27.973	3.40×10^{-5}	2.49×10^{-4}	0.598	3.40×10^{-5}	0	2.49×10^{-4}

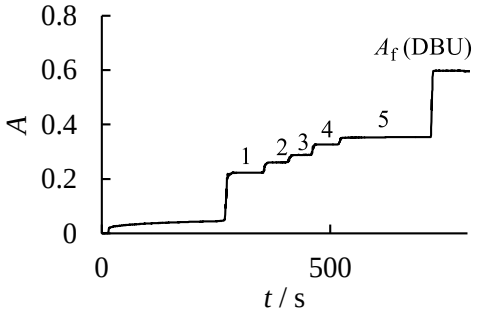

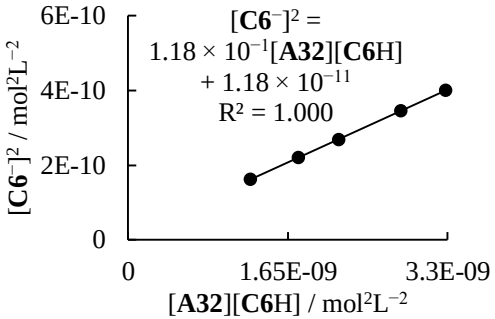

$K = (1.18 \pm 0.00) \times 10^{-1}$

Table 289. Determination of the pK_{aH} for **A32** with **C6**H in acetonitrile at 20 °C (detection at 478 nm). Stock solutions: **A32** (9.4 mg) in 10.0 mL MeCN; **C6**H (8.9 mg) in 10.0 mL MeCN; [DBU] = 1.27×10^{-2} mol L^{-1}. Step 0: 0.250 mL of **C6**H stock solution stock solution in 22.0 g MeCN.

step	V_+ / mL	V / mL	[**C6**H]$_0$ / M	[**A32**]$_0$ / M	*A*	[**C6**$^-$] / M	[**C6**H] / M	[**A32**] / M
0	-	28.240	4.21×10^{-5}	0	-	-	-	0
1	0.500	28.740	4.14×10^{-5}	6.05×10^{-5}	0.215	1.26×10^{-5}	2.88×10^{-5}	4.79×10^{-5}
2	1.000	29.240	4.07×10^{-5}	1.19×10^{-4}	0.288	1.68×10^{-5}	2.38×10^{-5}	1.02×10^{-4}
3	1.500	29.740	4.00×10^{-5}	1.75×10^{-4}	0.333	1.95×10^{-5}	2.05×10^{-5}	1.56×10^{-4}
4	2.000	30.240	3.93×10^{-5}	2.30×10^{-4}	0.364	2.12×10^{-5}	1.81×10^{-5}	2.09×10^{-4}
5	2.500	30.740	3.87×10^{-5}	2.83×10^{-4}	0.387	2.26×10^{-5}	1.61×10^{-5}	2.60×10^{-4}
f	2.750	30.990	3.84×10^{-5}	2.81×10^{-4}	0.657	3.84×10^{-5}	0	2.81×10^{-4}

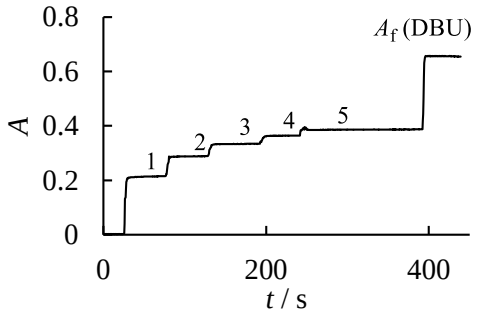

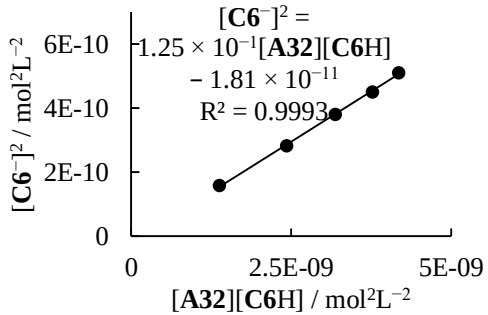

$K = (1.25 \pm 0.02) \times 10^{-1}$

$\bar{K} = (1.22 \pm 0.03) \times 10^{-1}$

pK_{aH}(**A32**) = 10.70

References

[1] (a) Dalko, P. I.; Moisan, L. *Angew. Chem. Int. Ed.* **2001**, *40*, 3726–3748. (b) List, B. *Tetrahedron*, **2002**, *58*, 5573–5590. (c) Notz, W.; Tanaka, F.; Barbas III, C. F. *Acc. Chem. Res.* **2004**, *37*, 580–591. (d) Dalko, P. I.; Moisan, L. *Angew. Chem. Int. Ed.* **2004**, *43*, 5138–5175. (e) Mukherjee, S.; Yang, J. W.; Hoffmann, S.; List, B. *Chem. Rev.* **2007***, 107,* 5471–5569. (f) Erkkilä, A.; Majander, I.; Pihko, P. M. *Chem. Rev.* **2007***, 107,* 5416–5470. (g) Enders, D.; Grondal, C.; Hüttl, M. R. M. *Angew. Chem. Int. Ed.* **2007***, 46,* 1570–1581. (h) Tsogoeva, S. B.; *Eur. J. Org. Chem.* **2007***,* 1701–1716. (i) Dondoni, A.; Massi, A.; *Angew. Chem. Int. Ed.* **2008***, 47,* 4638–4660. (j) Melchiorre, P.; Marigo, M.; Carlone, A.; Bartoli, G. *Angew. Chem. Int. Ed.* **2008***, 47,* 6138–6171.

[2] (a) Stork, G.; Terrell, R. *J. Am. Chem. Soc.* **1954**, *76*, 2029–2030. (b) Stork, G.; Landesman, H. K.; *J. Am. Chem. Soc.* **1956**, *78*, 5128–5129.

[3] (a) Hajos, Z. G.; Parrish, D. R. German Patent DE 2102623 **1971**. (b) Eder, U.; Sauer, G.; Wiechert, R. *Angew. Chem. Internat. Edit.* **1971**, *10*, 496–497.

[4] (a) Yamaguchi, M.; Yokota, N.; Minami, T. *J. Chem. Soc., Chem. Commun.* **1991**, 1088–1089. (b) Yamaguchi, M.; Shiraishi, T.; Hirama, M. *J. Org. Chem.* **1996**, *61*, 3520–3530.

[5] (a) Ahrendt, K. A.; Borths, C. J.; MacMillan, D. W. C.. *J. Am. Chem. Soc.* **2000**, *122*, 4243–4244. (b) Jen, W. S.; Wiener, J. J.; MacMillan, D. W. C. *J. Am. Chem. Soc.* **2000**, *122*, 9874–9875. (c) Northrup, A. B.; MacMillan, D. W. C. *J. Am. Chem. Soc.* **2002**, *124*, 2458–2460. (d) Paras, N. A.; MacMillan, D.W.C. *J. Am. Chem. Soc.* **2002**, *124*, 7894–7895.

[6] (a) Peelen, T. J.; Chi, Y.; Gellman, S. H. *J. Am. Chem. Soc.* **2005**, *127*, 11598–11599. (b) Chia, P. W.; Brennan, S. C.; Slawin, A. M. Z.; Riccardi, D.; O'Hagan, D. *Org. Biomol. Chem.* **2012**, *10*, 7922–7927. (c) Khumsubdee, S.; Zhou, H.; Burgess, K. *J. Org. Chem.* **2013**, *78*, 11948–11955. (d) Srinivas, K.; Singh, N.; Das, D.; Koley, D. *Org. Lett.* **2017**, *19*, 274–277.

[7] (a) Burley, J. C.; Gilmour, R.; Prior, T. J.; Day, G. M. *Acta. Cryst.* **2008**, *C64*, o10–o14. (b) Seebach, D.; Grošelj, U.; Badine, D. M.; Schweizer, W. B.; Beck, A. K. *Helvetica Chimica Acta* **2008**, *91*, 1999–2034. (c) Grošelj, U.; Schweizer, W. B.; Ebert, M. O.; Seebach, D. *Helvetica Chimica Acta* **2009**, *92*, 1–13. (d) Brazier, J. B.; Evans, G.; Gibbs, T. J. K.; Coles, S. J.; Hursthouse, M. B.; Platts, J. A.; Tomkinson, N. C. O. *Org. Lett.* **2009**, *11*, 133–136. (e) Holland, M. C.; Paul, S.; Schweizer, W. B.; Bergander, K.; Mück-Lichtenfeld, C.; Lakhdar, S.; Mayr, H.; Gilmour, R. *Angew. Chem. Int. Ed.* **2013**, *52*, 7967–7971. (f) Grošelj, U.; Beck, A.; Schweizer, W. B.; Seebach, D. *Helvetica Chimica Acta* **2014**, *97*, 751–796.

[8] (a) Devery, Ⅲ, J. J.; Conrad, J. C.; MacMillan, D. W. C.; Flowers, Ⅱ, R. A. *Angew. Chem. Int. Ed.* **2010**, *49*, 6106–6110. (b) Beel, R.; Kobialka, S.; Schmidt, M. L.; Engeser, M. *Chem. Commun.* **2011**, *47*, 3293–3295. (c) Abeykoon, G. A.; Chatterjee, S.; Chen, J. S. *Org. Lett.* **2014**, *16*, 3248–3251. (d) Chem, J. S.; Abeykoon, G. A. *Org. Lett.* **2015**, *17*, 6050–6053.

[9] (a) Lakhdar, S.; Tokuyasu, T.; Mayr, H. *Angew. Chem. Int. Ed.* **2008**, *47*, 8723–8726. (b) Lakhdar, S.; Appel, R.; Mayr, H. *Angew. Chem. Int. Ed.* **2009**, *48*, 5034–5037. (c) Lakhdar, S.; Ammer, J.; Mayr, H. *Angew. Chem. Int. Ed.* **2011**, *50*, 9953–9956. (d) An, F.; Paul, S.; Ammer, J.; Ofial, R.; Mayer, P.; Lakhdar, S.; Mayr, H. *Asian J. Org. Chem.* **2014**, *3*, 550–555.

[10] Brazier, J. B.; Jones, K. M.; Platts, J. A.; Tomkinson, N. C. O. *Angew. Chem. Int. Ed.* **2011**, *50*, 1613–1616.

[11] (a) Marigo, M.; Wabnitz, T. C.; Fielenbach, D.; Jørgwnsen, K. A. *Angew. Chem. Int. Ed.* **2005**, *44*, 794–797. (b) Hayashi, Y.; Gotoh, H.; Hayashi, T.; Shoji, M. *Angew. Chem. Int. Ed.* **2005**, *44*, 4212–4215.

[12] (a) Ibrahem, I.; Córdova, A. *Chem. Commun.* **2006**, 1760–1762. (b) Zhao, G. L.; Ibrahem, I.; Sundén, H.; Córdova, A. *Adv. Synth. Catal.* **2007**, *349*, 1210–1224. (c) Kobayashi, S.; Kinoshita, T.; Uehara, H.; Sudo, T.; Ryu, L. *Org. Lett.* **2009**, *11*, 3934–3937. (d) Patora-Komisarska, K.; Benohoud, M.; Ishikawa, H.; Seebach, D. Hayashi, Y. *Helvetica Chimica Acta* **2011**, *94*, 719–745. (e) Ansari, S.; Raabe, G.; Enders, D. *Monatsh Chem* **2013**, *144*, 641–646.

[13] (a) Sundén, H.; Ibrahem, I.; Córdova, A. *Tetrahedron Letters* **2006**, *47*, 99–103. (b) Chow, S. S.; Nevalainen, M. Evans, C. A. Johannes, C. W. *Tetrahedron Letters* **2007**, *48*, 277–280. (c) Zu, L.; Zhang, S.; Xie, H.; Wang, W. *Org. Lett.* **2009**, *11*, 1627–1630. (d) Luo, S. P.; Li, Z. Bo.; Wang, L. P.; Guo, Y.; Xia, A. B.; Xu, D, Q. *Org. Biomol. Chem.* **2009**, *7*, 4539–4546. (e) Fleischer, I.; Pfaltz, A. *Chem. Eur. J.* **2010**, *16*, 95–99. (f) Tang, J.; Xu, D. D.; Xia, A. B.; Wang, Y. F.; Jiang, J. R.; Luo, S. P.; Xu, Z. Y. *Adv. Synth. Catal.* **2010**, *352*, 2121–2126. (g) Zhang, F.; Wei, M.; Dong, J.; Zhou,

Y.; Lu, D.; Gong, Y.; Yang, X. *Adv. Synth. Catal.* **2010**, *352*, 2875–2880. (h) Xu, F.; Zacuto, M.; Yoshikawa, N.; Desmond, R.; Hoerrner, S.; Itoh, T.; Journet, M.; Humphrey, G. R.; Cowden, C.; Strotman, N.; Devine, P. *J. Org. Chem.* **2010**, *75*, 7829–7841. (i) Shi, Z. H.; Sheng, H.; Yang, K. F.; Jiang, J. X.; Lai, G. Q.; Lu, Y.; Xu, L. W. *Eur. J. Org. Chem.* **2011**, 66–70. (j) Alachraf, M. W.; Handayani, P. P.; Hüttl, M. R. M.; Grondal, C.; Enders, D.; Schrader, W. *Org. Biomol. Chem.* **2011**, *9*, 1047–1053. (k) Lin, S.; Deiana, L.; Zhao, G. L.; Sun, J.; Córdova, A. *Angew. Chem. Int. Ed.* **2011**, *50*, 7624–7630. (l) Shen, H.; Yang, K. F.; Shi, Z. H.; Jiang, J. X.; lai, G. Q.; Xu, L. W. *Eur. J. Org. Chem.* **2011**, 5031–5038. (m) Zhu, H. L.; Ling, J. B.; Xu, P. F. *J. Org. Chem.* **2012**, *77*, 7737–7743. (n) Gupta, V.; Sudhir V., S.; Mandal, T.; Schneider, C. *Angew. Chem. Int. Ed.* **2012**, *51*, 12609–12612. (o) Duan, G. J.; Ling, J. B.; Wang, W. P.; Luo, Y. C.; Xu, P. F. *Chem. Commun.* **2013**, *49*, 4625–4627. (p) jiang, X.; Tan, B.; Barbas III, C. F. *Angew. Chem. Int. Ed.* **2013**, *52*, 9261–9265.

[14] (a) Seebach, D.; Grošelj, U.; Badine, D. M.; Schweizer, W. B.; Beck, A. K. *Helvetica Chimica Acta* **2008**, *91*, 1999–2034. (b) Grošelj, U.; Seebach, D.; Badine, D. M.; Schweizer, W. B.; Beck, A. K. *Helvetica Chimica Acta* **2009**, *92*, 1225–1259.

[15] (a) Orue, A.; Reyes, E.; Vicario, J. L.; Carrillo, L.; Uria, U. *Org. Lett.* **2012**, *14*, 3740–3743. (b) Parra, A.; Reboredo, S.; Alemán, J. *Angew. Chem. Int. Ed.* **2012**, *51*, 9734–9736. (c) Seegerer, A.; Hioe, J.; Hammer, M. M.; Morana, F.; Fuchs, P. J. W.; Gschwind, R. M. *J. Am. Chem. Soc.* **2016**, *138*, 9864–9873.

[16] (a) Jia, Z. J.; Jiang, H.; Li, J. L.; Gschwend, B.; Li, Q. Z.; Yin, X.; Grouleff, J.; Chen, Y. C.; Jørgensen, K. A. *J. Am. Chem. Soc.* **2011**, *133*, 5053–5061. (b) Zhu, K.; Huang, H.; Wu, W; Wei, Y.; Ye, J. *CHem. Commun.* **2013**, *49*, 2157–2159. (c) Zhang, S. J.; Zhang, J.; Zhou, Q. Q.; Dong, L.; Chen, Y. C. *Org. Lett.* **2013**, *15*, 968–971. (d) Jiang, H.; Cruz, D. C.; Li, Y.; Lauridsen, V. H.; Jørgensen, K. A. *J. Am. Chem. Soc.* **2013**, *135*, 5200–5207.

[17] Dell'Amico, L.; Albrecht, L.; Naicker, T.; Poulsen, P. H.; Jørgensen, K. A. *J. Am. Chem. Soc.* **2013**, *135*, 8063–8070.

[18] (a) Lakhdar, S.; Maji, B.; Mayr, H. *Angew. Chem. Int. Ed.* **2012**, *51*, 5739–5742. (b) Erdmann, H.; An, F.; Mayer, P.; Ofial, A. R.; Lakhdar, S.; Mayr, H. *J. Am. Chem. Soc.* **2014**, *136*, 14263–14269.

[19] Halskov, K. S.; Kniep, F.; Lauridsen, V. H.; Iversen, E. H.; Donslund, B. S.; Jørgensen, K. A. *J. Am. Chem. Soc.* **2015**, *137*, 1685–1691.

[20] (a) Schmid, M. B.; Zeitler, K.; Gschwind, R. M. *J. Am. Chem. Soc.* **2011**, *133*, 7065–7074. (b) Burés, J.; Armstrong, A.; Blackmond, D. G. *J. Am. Chem. Soc.* **2011**, *133*, 8822–8825. (c) Burés, J.; Armstrong, A.; Blackmond, D. G. *J. Am. Chem. Soc.* **2012**, *134*, 6741–6750. (d) Sahoo, G.; Rahaman, H.; Madarász, Á.; Pápai, I.; Melarto, M.; Valkonen, A.; Pihko, P. M. *Angew. Chem. Int. Ed.* **2012**, *51*, 13144–13148. (e) Seebach, D.; Sun, X.; Ebert, M. O.; Schweizer, W. B.; Purkayastha, N.; Beck, A. K.; Duschmalé, J.; Wennemers, H. *Helvetica Chimcia Acta* **2013**, *96*, 799–852.

[21] Companyó, X.; Burés, J. *J. Am. Chem. Soc.* **2017**, *139*, 8432–8435.

[22] (a) Khalaf, A.; Grée, D.; Abdallah, H.; Jaber, N.; Hachem, A.; Grée, R. *Eur. J. Org. Chem.* **2013**, 653–657. (b) Wang, Z.; Zhao, K.; Fu, J.; Zhang, J.; Yin, W.; Tang, Y. *Org. Biomol. Chem.* **2013**, *11*, 2093–2097. (c) Veerasamy, N.; Carlson, E. C.; Collett, N. D.; Saha, M.; Carter, R. G.; *J. Org. Chem.* **2013**, *78*, 4779–4800. (d) Caruana, L.; Fochi, M.; Franchini, M. C.; Ranieri, S.; Mazzanti, A.; Bernardi, L. *Chem. Commun.* **2014**, *50*, 445–447. (e) Meng, Z.; Sun, S.; Yuan, H.; Lou, H.; Liu, L. *Angew. Chem. Int. Ed.* **2014**, *53*, 543–547. (f) Du, H.; Rodriguez, J.; Bugaut, X.; Constantieux, T. *Adv. Synth. Catal.* **2014**, *356*, 851–856. (g) Koley, D.; Krishna, Y.; Srinivas, K.; Khan, A. A.; Kant, R. *Angew. Chem. Int. Ed.* **2014**, *53*, 13196–13200. (h) Berti, F.; Malossi, F.; Marchetti, F.; Pineschi, M. *Chem. Commun.* **2015**, *51*, 13694–13697. (i) Buckingham, F. Kirjavainen, A. K.; Forsback, S.; Krzyczmonik, A.; Keller, T.; Newington, I. M.; Glaser, M.; Luthra, S. K.; Solin, O.; Gouverneur, V. *Angew. Chem. Int. Ed.* **2015**, *54*, 13366–13369. (j) Fjelbye, K.; Marigo, M.; Clausen, R. P.; Juhl, K. *Org. Lett.* **2016**, *18*, 1170–1173. (k) Xie, Z.; Zan, X.; Sun, S.; Pan, X.; Liu, L. *Org. Lett.* **2016**, *18*, 3944–3947.

[23] (a) Kano, T.; Mii, H.; Maruoka, K. *J. Am. Chem. Soc.* **2009**, *131*, 3450–3451. (b) Kano, T.; Shirozu, F.; Maruoka, K. *Org. Lett.* **2014**, *16*, 1530–1532. (c) Lang, J. H.; Jones, P. G.; Lindel, T. *Chem. Eur. J.* **2017**, *23*, 12714–12717.

[24] Husmann, R. Jörres, M.; Raabe, G.; Bolm, C. *Chem. Eur. J.* **2010**, *16*, 12549–12552.

[25] Luo, S.; Xu, H.; Mi, X.; Li, J.; Zheng, X.; Cheng, J. P. *J. Org. Chem.* **2006**, *71*, 9244–9247.

[26] Ishii, T.; Fujioka, S.; Sekiguchi, Y.; Kotsuki, H. *J. Am. Chem. Soc.* **2004**, *126*, 9558–9559.

[27] Cao, Y. J.; Lai, Y. Y.; Wang, X.; Li, Y. J.; Xiao, W. J. *Tetrahedron Letters***2007**, *48*, 21–24.

[28] Luo, S.; Mi, X.; Zhang, L.; Liu, S.; Xu, H.; Cheng, J. P. *Angew. Chem. Int. Ed.* **2006**, *45*, 3093–3097.

[29] Albrecht, L.; Dickmeiss, G.; Acosta, C. A.; Rodríguez-Escrich, C.; Davis, R. L.; Jørgensen, K. A. *J. Am. Chem. Soc.***2012**, *134*, 2543–2546.
[30] Brenner, M.; Huber, W. *Helv. Chim. Acta* **1953**, *36*, 1109–1115.
[31] Vogl, O.; Pöhm, M. *Monatsh. Chem.* **1952**, *83*, 541.
[32] Krishna, P. R.; Kannan, V.; Reddy, P. V. N. *Adv. Synth. Catal.* **2004**, *346*, 603–606.
[33] Cao, X. Y.; Zheng, J. C.; Li. Y. X.; Shu, Z. C.; Sun, X. L.; Wang, B. Q. *Tetrahedron* **2010**, *66*, 9703–9707.
[34] Alza, E.; Cambeiro, X. C.; Jimenez, C.; Pericàs. *Org. Lett.* **2007**, *9*, 3717–3720.
[35] Hendrie, S. K.; Leonard, J. *Tetrahedron* **1987**, *43*, 3289–3294.
[36] Dahlin, N.; Bøgevig, A.; Adolfsson, H. *Adv. Synth. Catal.* **2004**, *346*, 1101–1105.
[37] Cao, C. L.; Ye, M. C.; Sun, X. L.; Tang, Y. *Org. Lett.* **2006**, *8*, 2901–2904.
[38] Li, Y.; Tur, F.; Nielsen, R. P.; Jiang, H.; Jensen, F.; Jørgensen, K. A. *Angew. Chem. Int. Ed.* **2016**, *55*, 1020–1024.
[39] Kanth, J. V. B.; Periasamy, M. *Tetrahedron* **1993**, *49*, 5127–5132.
[40] Shi, Z.; Tan, B.; Leong, W. Y.; Zeng, X.; Lu, M.; Zhong, G. *Org. Lett.* **2010**, *12*, 5402–5405.
[41] Claudio, P.; Silvia, V.; Antonia, M.; Enrique, G. B. *Angew. Chem. Int. Ed.* **2006**, *45*, 5984–5987.
[42] Diakos, C. I.; Zhang, M.; Beale, P. J.; Fenton, R. R.; Hambley, T. W.; *Eur. J. Med. Chem.* **2009**, *44*, 2807–2814.
[43] Cicchi, S.; Corsi, M.; Goti, A.; *J. Org. Chem.* **1999**, *64*, 7243–7245.
[44] Mckennon, M. J.; Meyers, A. I. *J. Org. Chem.* **1993**, *58*, 3568–3571.
[45] Tseng, C. C.; Terashima, S.; Yamada, S.; *Chem. Pharm. Bull.* **1977**, *25*, 29–40.
[46] Kerrick, S.; Beak, P. *J. Am. Chem. Soc.* **1991**, *113*, 9708–9710.
[47] Bauer, J. O.; Stiller, J.; Marqués-López, E.; Strohfeldt, K.; Christmann, M.; Strohmann, C. *Chem. Eur. J.* **2010**, *16*, 12553–12558.
[48] Alderson, G. W.; Black, D. S. C.; Clark, V. M.; Todd, L. *J. Chem. Soc. Perkin Trans. 1* **1976**, 1955–1960.
[49] Pou, S.; Rose, G. M.; Wu, Y.; Keana, J. F. W.; *J. Org. Chem.* **1990**, *55*, 4438–4443.
[50] Ali, S. A.; Wazeer, M. I. M. *Tetrahedron* **1993**, *49*, 4339–4354.
[51] Leinisch, F.; Jiang, J.; Deterding, L. J.; Mason, R. P. *Molecules* **2011**, *16*, 8428–8436.
[52] Osby, J. O.; Ganem, B. *Tetrahedron Lett.* **1985**, *26*, 6413–6416.
[53] Moffett, R. B. *Org. Synth.* **1953**, *33*, 32–35.
[54] Procopio, A.; Alcaro, S.; Nino, A. D.; Maiuolo, L.; Ortuso, F.; Sindona, G.; *Bioorg. Med. Chem. Lett.* **2005**, *15*, 545–550.
[55] Schevchenko, N. E.; Balenkova, E. S.; Röschenthaler, G. V.; Nenajdenko, V. G. *Synthesis*, **2010**, 120–126.
[56] Meuresch, M.; Westhues, S.; Leitner, W.; Klankermayer, J.. *Angew. Chem. Int. Ed.* **2016**, *55*, 1392–1395.
[57] Eckert, F.; Leito, I.; Kaljurand, I. A.; Kütt, A.; Klamt, A.; Diedenhofen, M. *J. Comput. Chem.* **2009**, *30*, 799–810.
[58] Kütt, A.; Leito, I.; Kaljurand, I.; Sooväli, L.; Vlasov, V. M.; Yagupolskii, L. M.; Koppel, I. A. *J. Org. Chem.* **2006**, *71*, 2829–2838.
[59] Vlasov, V. M.; Zakharova, O. V. *Zh. Org. Khim.* **1975**, *11*, 778–785.
[60] Hull, R.; Maisey, R. F. British Patent 901880, **1962**.
[61] (a) Suzuki, H.; Koide, H.; Ogawa, T.. *Bull. Chem. Soc. Jpn.* **1988**, *61*, 501–504. (b) Atkins, J. M.; Moteki, S. A.; Dimagno, S. G.; Takacs, J. M. *Org. Lett.* **2006**, *8*, 2759–2762.
[62] Tshepelevitsh, S.; Kütt, A.; Lõkov, M.; Kaljurand, I.; Saame, J.; Heering, A.; Pliger, P. G.; Vianello, R.; Leito, I. *Eur. J. Org. Chem.* DOI: 10.1002/ejoc.201900956.
[63] (a) Mayr, H.; Patz, M. *Angew. Chem.* **1994**, *106*, 990–1010.; *Angew. Chem. Int. Ed. Engl.***1994**, *33*, 938–957. (b) Mayr, H.; Kuhn, O.; Gotta, M. F.; Patz, M. *J. Phys. Org. Chem.* **1998**, *11*, 642–654.
[64] Kanzian, T.; Nigst, T. A.; Maier, A.; Pichl, S.; Mayr, H. *Eur. J. Org. Chem.* **2009**, 6379–6385.
[65] Anne, A.; Moiroux, J.; Savéant, J.-M. *J. Am. Chem. Soc.* **1993**, *115*, 10224–10230.
[66] Bordwell, F. G.; Cripe, T. A.; Hughes, D. L. In *Nucleophilicity;* Harris, J. M.; McManus, S. P., Eds.; American Chemical Society: Washington DC, **1987**; pp 137–153.
[67] (a) Brotzel, F.; Chu, Y. C.; Mayr, H. *J. Org. Chem.* **2007**, *72*, 3679–3688. (b) Brotzel, F.; Mayr, H. *Org. Biomol. Chem.* **2007**, *5*, 3814–3820. (c) Ammer, J.; Baidya, M; Kobayashi, S.; Mayr, H. *J. Phys. Org. Chem.* **2010**, *23*, 1029–1035. (d) Breugst, M.; Tokuyasu, T.; Mayr, H. *J. Org. Chem.* **2010**, *75*, 5250–5258. (e) Nigst, T. A.; Antipova, A.; Mayr, H. *J. Org. Chem.* **2012**, *77*, 8142–8155.

[68] (a) Hansch, C.; Leo, A.; Taft, R. W. *Chem. Rev.* **1991**, *91*, 165–195. (b) Hansch, C.; Leo, A.; Hoekman, D. *Exploring QSAR: Hydrophobic*, *Electronic*, *and Steric Constants.* American Chemical Society: Washington DC, **1995**; pp 219–304.
[69] Shamala, N.; Guru Row, T. N.; Venkatesan, K. *Acta Cryst.* **1976**, *B32*, 3267–3270.
[70] Schaller, H. F.; Tishkov, A. A.; Feng, X.; Mayr, H. *J. Am. Chem. Soc.* **2008**, *130*, 3012–3022.
[71] Gharzaryan, V. V.; Fleck, M.; Petrosyan, A. M.; *Proceedings of SPIE - International Conference on Laser Physics* **2010**, **2011**, 7998, 79980F.
[72] Schnitzer, T.; Wennemers, H. *J. Am Chem. Soc.* **2017**, *139*, 15356–15362.
[73] Zhang, Y. M.; Liu, P.; Zhang, H. L. *J. Chem. Res.* **2010**, 610–612.
[74] Wang, P. A.; Liu, W. M.; Sun, X. L. *Organic Preparations and Procedures International* **2011**, *43*, 477–483.
[75] Stiller, J.; Marqués-López, E.; Herrera, R. P.; Fröhlich, R.; Strohmann, C.; Christmann, M. *Org. Lett.* **2011**, *13*, 70–73.
[76] Seebach, D.; Sun, X.; Sparr, C.; Ebert, M.-O.; Schweizer, W. B.; Beck, A. K. *Helv. Chim. Acta* **2012**, *95*, 1064–1078.
[77] Jentzsch, K. I.; Min, T.; Etcheson, J. I.; Fettinger, J. C.; Franz, A. K. *J. Org. Chem.* **2011**, *76*, 7065–7075.
[78] Burley, J. C.; Gilmour, R.; Prior, T. J.; Day, G. M. *Acta Cryst.* **2008**, *C64*, o10–o14.

Appendix 1 Published work 1

Asian J. Org. Chem. **2014**, *3*, 550–555.

Structures and Reactivities of Iminium Ions Derived from Substituted Cinnamaldehydes and Various Chiral Imidazolidin-4-ones

Feng An,[a] Shyeni Paul,[a] Johannes Ammer,[a] Armin R. Ofial,[a] Peter Mayer,[a] Sami Lakhdar,*[a, b] and Herbert Mayr[a]

Dedicated to Professor François Terrier

Abstract: A series of α,β-unsaturated iminium ions derived from substituted cinnamaldehydes and C2- and C5-substituted chiral imidazolidin-4-ones were isolated and characterized in solution and in the solid state. The kinetics of the reactions of the iminium ions with silyl ketene acetals were determined in dichloromethane at 20 °C. The resulting second-order rate constants were used to estimate the electrophilicity E of the iminium ions according to the linear free energy relationship $\log k_2(20\,^\circ\mathrm{C}) = s_N(N+E)$. The kinetics for the reactions of two of the iminium ions with tributylphosphine were studied by laser flash spectroscopy and their second-order rate constants were found to agree within a factor of 2.2 with those calculated by using the linear free energy relationship above.

Keywords: cinnamaldehydes · imidazolidinones · kinetics · linear free energy relationships · organocatalysis

1. Introduction

Chiral imidazolidinones belong to an important class of heterocycles with numerous applications in organic and bioorganic chemistry. Their use in asymmetric synthesis has been triggered by Seebach and co-workers' discovery that imidazolidinones are excellent chiral auxiliaries for the synthesis of enantiomerically enriched α-amino acids.[1]

In 2000, MacMillan and co-workers showed that the imidazolidinone **1a** and related compounds are effective catalysts in iminium activated processes,[2] e.g., for enantioselective reactions of α,β-unsaturated aldehydes with 1,3-dienes (Diels–Alder reactions),[2] nitrones (1,3-dipolar cycloadditions),[3] and pyrroles (Friedel–Crafts reactions).[4] Subsequently, an impressive number of chiral secondary amines has been used as catalysts in various iminium-activated reactions.[5]

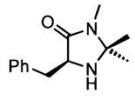

1a

Despite the tremendous efforts devoted to the development of new organocatalytic processes, only a few investigations have studied mechanistic aspects of these reactions,[6] and the identification of the intermediate iminium ions has only recently been reported.[7,8] The kinetics of the reactions of iminium ions derived from cinnamaldehyde with different nucleophiles have been studied, and their electrophilicities have been determined using the linear free energy relationship (1).[7c,9]

$$\lg k\ (20\,^\circ\mathrm{C}) = s_N\ (E + N) \qquad (1)$$

In this equation, electrophiles are characterized by one solvent-independent parameter, E, and nucleophiles by two solvent-dependent parameters, N and s_N.[10]

Previously, we have studied the reactions of cinnamaldehyde-derived iminium ions with various nucleophiles and found that variation of the amines yields iminium ions which cover a reactivity range of 5 orders of magnitude.[7c,9] We now report how substituents at the phenyl ring of cinnamaldehyde and variation of the substituents at the imidazolidinone ring affect the structure and reactivity (electrophilicity) of the iminium ions.

2. Preparation and Structures of the Cinnamaldehyde Derived Iminium Ions

The substituted cinnamaldehydes **2** were synthesized by Heck coupling as shown in Scheme 1 by following a procedure by Pour and co-workers.[11] Only the homocoupling product of the *p*-cyano-substituted iodobenzene was obtained in our initial attempts to synthesize **2c** by this

[a] F. An, S. Paul, Dr. J. Ammer, Dr. A. R. Ofial, Dr. P. Mayer, Dr. S. Lakhdar, Prof. Dr. H. Mayr
Department Chemie
Ludwig-Maximilians-Universität München
Butenandtstrasse 5-13, 81377 München (Germany)

[b] Dr. S. Lakhdar
Laboratoire de Chimie Moléculaire et Thioorganique
UMR CNRS 6507
6 Boulevard Maréchal Juin, 14050 Caen (France)
E-mail: sami.lakhdar@ensicaen.fr

Supporting information for this article is available on the WWW under http://dx.doi.org/10.1002/ajoc.201402009.

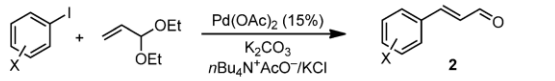

2	X	Yield [%]
2a	4-NO_2	32
2b	3-NO_2	88
2c	4-CN	85
2d	4-Me	99
2e	4-OMe	89

Scheme 1. Preparation of the substituted cinnamaldehydes **2a–e**.[11] DMF = *N*,*N*-dimethylformamide.

method. Finally, **2c** was obtained in high yield when the reaction was carried out in an oxygen atmosphere under otherwise unchanged reaction conditions.

Treatment of the cinnamaldehydes **2** with equimolar amounts of the imidazolidinonium hexafluorophosphate (**1a·HPF$_6$**) in methanol, as described by Tomkinson and co-workers,[7e] gave the iminium ions **3**. While the iminium hexafluorophosphates of **3d**, **3e**, and **3f** formed quantitatively, the iminium salts of **3a**–**c** were obtained as mixtures with the starting materials. Two recrystallizations, first in dichloromethane and then in dichloromethane/diethyl ether yielded pure hexafluorophosphates of **3a**, **3b**, and **3c** (Scheme 2).

The iminium ion **3g** was synthesized analogously but by using perchlorate as the counteranion because **3g·PF$_6$** turned out to be an instable salt (Scheme 3). In agreement with Seebach and co-workers' previous report,[7b] treatment of the ammonium salt **1c·HPF$_6$** with cinnamaldehyde **2i** in the presence of a catalytic amount of triethylamine (5%) in

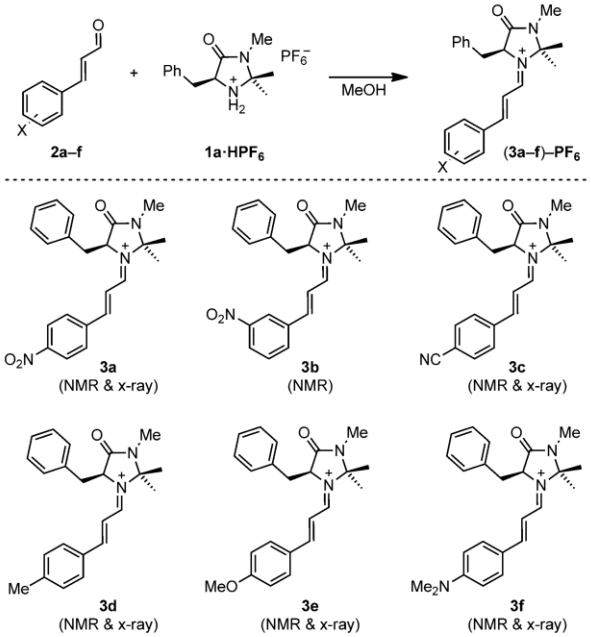

Scheme 2. Preparation of the cinnamaldehyde-derived iminium hexafluorophosphates **3a–f·PF$_6$**.

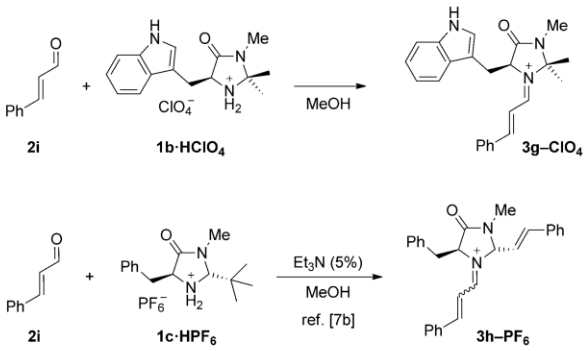

Scheme 3. Preparation of the iminium salts **3g·ClO$_4$** and **3h·PF$_6$**.

methanol led to an exchange of the *tert*.-butyl group and gave the iminium salt **3h·PF$_6$** as a mixture of two isomers (*E*:*Z* = 3:1).

Single crystals suitable for X-ray diffraction were obtained by vapor diffusion of diethyl ether into the acetonitrile solutions of all iminium hexafluorophosphates (**3a–f)·PF$_6$** except **3b·PF$_6$** (Figure 1).[12] As previously described

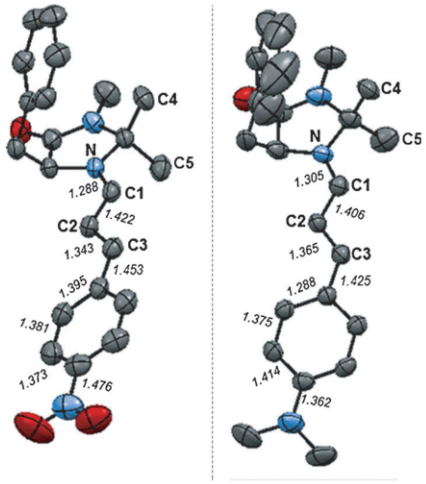

Figure 1. Crystal structures of the iminium ions **3a** (left) and **3f** (right) (Counterion: PF_6^-, only one molecule of the asymmetric unit is presented for **3a**, bond lengths in Å).

for the parent system **3i**,[7b,e] the X-ray structures of the hexafluorophosphates of **3** show that they exist as *E* isomers and adopt the Houk conformation in which the benzylic phenyl group faces the *cis*-Me group (Conformer **A** in Scheme 4).[13] Conformer **B**, in which the phenyl ring resides above the iminium π-system, which was suggested by MacMillan to account for the enantioselectivity, was not detected for any of the crystals investigated.[2,5d,14]

The predominance of conformer **A** over **B**, which is also indicated by the differences of the ^{1}H NMR chemical shifts of the two geminal methyl groups H4 and H5 (Δδ(H4,H5) in Table 1) can be rationalized by London dispersion (ben-

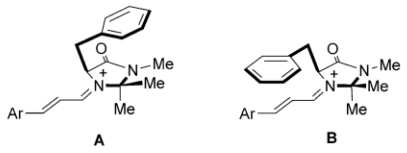

Scheme 4. Different conformations of the iminium ions **3**.

zene ring in contact with the *cis*-methyl group). Table 1 shows that these differences are slightly affected by the nature of the *para* substituent in the iminium ions **3**. Similar observations have been made by Tomkinson and co-workers[7e] and investigated in detail by Seebach et al.[14b]

Table 1. NMR chemical shifts (in ppm, CD_3CN solutions) and bond lengths (in pm, from X-ray structure analysis) of the cinnamaldehyde-derived iminium ions **3**. (For numbering see Figure 1).

3	δ (H3)	δ (C3)	δ (C2)	δ (C1)	Δδ(H4,H5)	*d*(N-C1)	*d*(C1-C2)	*d*(C2-C3)
3a	8.40[a]	164.0[a]	120.1[a]	168.1[a]	0.80[a]	128.8/ 129.2[b]	142.2/ 142.9[b]	134.3/ 134.6[b]
3b	ca. 8.2	162.9	120.8	168.7	0.84	–	–	–
3c	8.12	163.2	121.2	168.6	0.85	129.1	142.0	134.6
3i	8.15	166.7	118.4	168.1	0.89	129.7[c]	142.3[c]	135.1[c]
3d	8.14	166.9	117.4	167.7	0.90	129.4	141.5	135.1
3e	8.09	166.6	115.5	166.6	0.91	129.7/ 130.7[b]	140.5/ 142.2[b]	135.8/ 134.1[b]
3f	7.88	165.2	113.8	161.4	0.92	130.5	140.6	136.5

[a] In CD_2Cl_2; [b] The X-ray structures of **3a**·PF_6 and **3e**·PF_6 revealed two molecules per asymmetric unit; [c] From ref. [7e].

One can see that the substituent at the phenyl ring has a noticeable effect on the C2–C3 bond length of the iminium ions **3** (Table 1). The X-ray structures show that the iminium ions **3a–f** are almost planar (N-C1-C2-C3 ≈ 180°) and the iminium nitrogen atoms are not pyramidalized (Δ(Dunitz) ≈ 0 Å). Only the nitro-substituted phenyl ring of **3a** is out of plane (11°), which indicates the lower importance of phenyl conjugation in this iminium ion.

3. Product from the Reaction of Iminium Salt 3a·PF_6 and the Ketene Acetal 4b

To study the electrophilic reactivity of **3a–h** we chose the silylated ketene acetals **4a** and **4b** as reaction partners, which had previously been shown to be reliable reference nucleophiles for this class of electrophiles.[7c,9] The reaction of **3a** with **4b** served as an example to investigate the product of the reactions that should be studied kinetically. Treatment of **3a** with two equivalents of ketene acetal **4b** in CH_2Cl_2 gave **5**, which instantaneously desilylated to yield **6**. This enamine was not isolated, but hydrolyzed and purified by column chromatography (EtOAc/*n*-pentane, 1:1) to yield the aldehyde **7** (89%) as a mixture of two diastereoisomers in a ratio of 1:5 (Scheme 5). High diastereoselectivity (up to 1:20) were previously obtained by MacMillan and co-workers for the imidazolidinone-catalyzed enantioselective additions of ketene acetals to α,β-unsaturated aldehydes.[15]

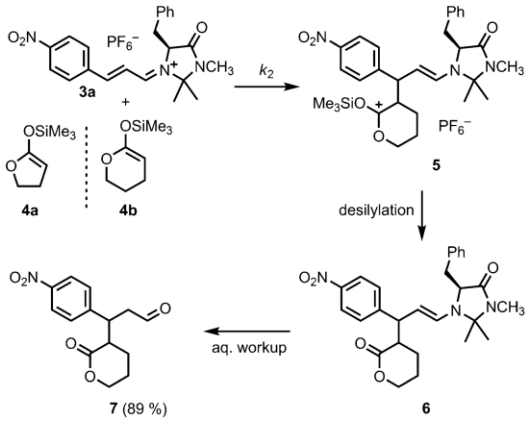

Scheme 5. Reaction of the iminium salt **3a**·PF_6 with the silyl ketene acetal **4b**.

4. Kinetics

As shown in Table 2, the iminium ions **3** have absorption maxima between 343 and 510 nm, the disappearance of which allowed us to study the kinetics of their reactions with nucleophiles photometrically. In the presence of a large excess of the reference nucleophiles **4a** or **4b**, pseudo-first-order kinetics were achieved, and the first-order rate constants k_{obs} (s^{-1}) were derived from the exponential decays of the absorbances of the iminium ions **3** (Figure 2). Plots of k_{obs} (s^{-1}) against the concentrations of the nucleophiles **4** were linear with negligible intercepts as required by the relation $k_{obs} = k_2[\mathbf{4}]$ (see Figure 2). Their slopes correspond to the second-order rate constants k_2 ($M^{-1}s^{-1}$) which are summarized in Table 3.

Table 2. Absorption maxima (λ_{max}) and molar absorption coefficients (ε) of the iminium hexafluorophosphates **3** in dichloromethane at 20 °C.

3	λ_{max} [nm]	ε [$M^{-1}cm^{-1}$]
3a (X = 4-NO_2)	350	1.59×10^4
3b (X = 3-NO_2)	343	1.18×10^4
3c (X = 4-CN)	352	1.57×10^4
3i (X = H)	370[a]	1.62×10^4[a]
3d (X = 4-Me)	388	2.36×10^4
3e (X = 4-OMe)	426	2.66×10^4
3f (X = 4-NMe_2)	510	5.42×10^4
3g[b]	371	1.63×10^4
3h	372	3.62×10^4

[a] Counterion = TfO^-; Tf = trifluoromethanesulfonyl; from ref. [7c]. [b] Counterion = ClO_4^-.

The dihydrofuran **4a** was 11–18 times more reactive than the dihydropyran **4b**, in agreement with previous investiga-

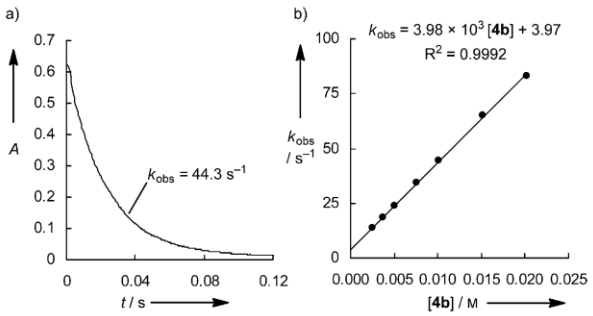

Figure 2. a) Exponential decay of the absorbance at 343 nm during the reaction of **3b** (6.12×10^{-5} M) with **4b** (1.01×10^{-2} M). b) Determination of the second-order rate constant k_2 from the dependence of the first-order rate constant k_{obs} for the reaction of **3b** with **4b** on the concentration of ketene acetal **4b** (20 °C in CH_2Cl_2).

Table 3. Second-order rate constants k_2 for the reactions of the iminium ions **3** with the ketene acetals **4a** and **4b** (20 °C, CH_2Cl_2, counterion = PF_6^-).

3	k_2(**4a**) [M^{-1} s^{-1}]	k_2(**4b**) [M^{-1} s^{-1}]	k_2(**4a**)/k_2(**4b**)	E[a]
3a (X = 4-NO_2)	9.43×10^4	5.72×10^3	16.5	−5.9
3b (X = 3-NO_2)	6.48×10^4	3.98×10^3	16.3	−6.1
3c (X = 4-CN)	7.53×10^4	5.28×10^3	14.3	−6.0
3i (X = H)	9.06×10^3[b]	5.23×10^2[b]	17.3	−7.2[b,c]
3d (X = 4-Me)	9.00×10^3	6.05×10^2	14.9	−7.2
3e (X = 4-OMe)	2.38×10^3	1.45×10^2	16.4	−8.0
3f (X = 4-NMe_2)	2.07×10^1	1.31	15.8	−10.6
3g[d]	6.78×10^3	6.10×10^2	11.1	−7.3
3h	9.71×10^4	5.87×10^3	16.5	−5.9
3j	1.49×10^4[e]	6.78×10^2[e]	22.0	−7.0[e]
3k	8.13×10^4[e]	3.43×10^3[e]	23.7	−6.0[e]

[a] The E parameters for each iminium ion result from a least-squares minimization of $\Delta^2=\Sigma(\log k_2 - s_N(E+N))^2$ which uses the second-order rate constants k_2 (this table) and the nucleophile-specific parameters N and s_N (for **4a**: $N=12.56$, $s_N=0.70$; for **4b**: $N=10.61$, $s_N=0.86$) from ref. [10b]; [b] From ref. [7c]; [c] This value has been slightly revised for a larger data set (Ref. [9b]). For this discussion, we use the original value $E=-7.2$, which reflects the reactivity toward the ketene acetals **4a** and **b**, as the other E values in this table; [d] Counterion = ClO_4^-; data of lower quality, only the first half-life of the reactions followed the monoexponential decay function that was used for the evaluation of k_{obs}; [e] From ref. [8c].

tions.[7b,9b] Substitution of the k_2 values (Table 3) and the known N and s_N parameters of **4a** and **4b** into Equation (1) gave the electrophilicity parameters E for the iminium ions **3** by a least-squares minimization.

Figure 3 shows that the electrophilicities of the iminium ions **3** cover almost five orders of magnitude with $-5.9 > E > -10.6$. The cyano- and nitro-substituted iminium ions **3a**, **3b**, and **3c** have similar reactivities and are ten times more reactive than the iminium ion **3i**, which is derived from the parent cinnamaldehyde.

While the *p*-methyl-substituted iminium ion **3d** has approximately the same electrophilicity as the parent iminium ion **3i**, the *p*-methoxy substituted iminium ion **3e** is about four times, and the dimethylamino-substituted analogue **3f** is about 400 times less reactive than the parent **3i** towards

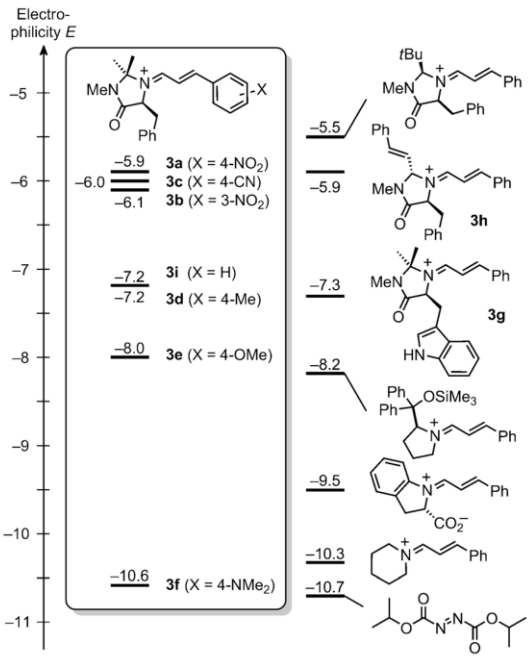

Figure 3. Electrophilicities of iminium ions **3**.

nucleophiles of $s_N \approx 0.8$. This low reactivity of **3f** is due to strong conjugation between the "push" (the dimethylamino group) and the "pull" component (imidazolidinone). The X-ray crystal structure of **3f** depicted in Figure 1 shows that the bond lengths in the iminium π-system and the amino-substituted phenyl ring are highly affected by this conjugation.

Substitution of the gem dimethyl groups at the C2 position of the imidazolidinone ring (**3i**) by a styryl group leads to the 10 times more reactive iminium ion **3h**. An even higher acceleration was previously observed when substituting the gem dimethyl groups (MacMillan first generation) by a *tert*-butyl group (MacMillan second generation).[9b]

Substitution of the phenyl ring of the imidazolidinone in **3i** by an indole ring (→**3g**) does not affect the electrophilicity at all. This result is in line with our recent report with the Gilmour group,[8c] that introduction of three electron-donating methoxy groups into the benzylic phenyl ring of **3i** (→**3j**) had little effect on the electrophilicity (Table 3), whereas perfluorination of the benzylic phenyl group (**3i**→**3k**) increased the reactivity by a factor of 6–9.[8c]

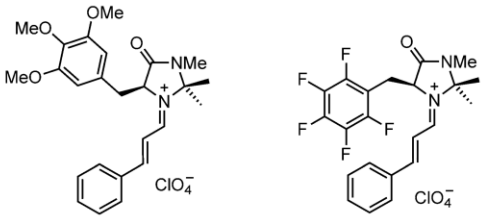

3j **3k**

Figure 4 shows a linear correlation between the electrophilicity parameters E of the iminium ions **3** and Hammett's σ^+ parameters.[16] The slope of 1.80 corresponds to a reaction constant of $\rho = 1.44$ for the reaction with ketene acetals with an averaged s_N of 0.80. According to this ρ value, the electrophilic reactivities of the iminium ions **3** are more affected by the variation of the *para* substituents than the reactivities of the aryl-substituted quinone methides ($\rho = 0.84$).[17]

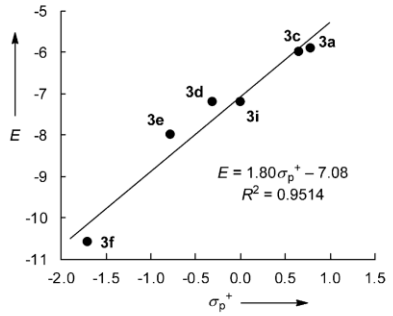

Figure 4. Correlation of the electrophilicity parameter E of the iminium ions **3** with Hammett's σ_p^+ parameters.

To examine the applicability of the electrophilicity parameters of the iminium ions **3** in reactions with other types of nucleophiles, we have studied the kinetics of the reactions of **3d** and **3e** with tributylphosphine (**8**). As these reactions proceed on the microsecond timescale, the recently described laser-flash technique was used.[18] For this purpose, the enamino phosphonium ions **9d** and **9e** were generated by combination of **3d** and **3e**, respectively, with one equivalent of **8** in dichloromethane as illustrated in Scheme 6. Irradiation of these solutions with 7 ns laser pulses (266 nm)[9b] regenerated the iminium ions **3d** and **3e**. In the presence of a large excess of PBu_3, their absorbances decayed monoexponentially to yield the first-order rate constants k_{obs}, which were plotted versus the concentrations of the phosphine **8** to give the second-order rate constants

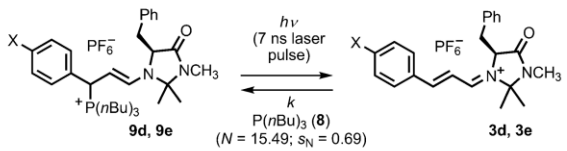

Iminium ions	**3d** (X = Me)	**3e** (X = OMe)
E	–7.2	–8.0
k^{calcd} [M^{-1} s^{-1}]	5.25×10^5	1.47×10^5
k^{exp} [M^{-1} s^{-1}]	2.42×10^5	1.16×10^5
k^{calcd}/k^{exp}	2.2	1.3

Scheme 6. Laser-flash photolytic generation of the iminium ions **3d** and **3e** and comparison of the calculated (by Equation 1) and experimental rate constants for their reactions with tributylphosphine (**8**).

k^{exp} shown in Scheme 6. From the electrophilicity parameters E of **3d** and **3e** (Table 3) and the previously reported nucleophilicity parameters for **8**,[19] one can calculate k^{calcd} for these reactions by Equation (1). Scheme 6 shows remarkably good agreements between the experimental and the calculated second-order rate constants, which indicates the reliability of the iminium electrophilicities listed in Table 3.

5. Conclusions

In conclusion, we have synthesized a series of substituted, cinnamaldehyde-derived iminium ions **3** and studied their structures in the solid and liquid phases. The kinetics of the reactions of **3** with the ketene acetals **4a** and **4b** allowed us to determine their electrophilicities, which cover almost five orders of magnitude, which reflects the strong effect of the substituents at the aromatic ring of the cinnamaldehydes on the electrophilicity of the corresponding iminium ions, which is in line with the substituent effects on the structures of the iminium ions elucidated by the crystal structures. As the rate constants for the reactions of the iminium ions **3d** and **3e** with tributylphosphine (**8**), which are calculated by Equation (1), are in good agreement with the experimentally determined values, we conclude that the electrophilicity parameters for the iminium ions **3**, which are reported in this work, can widely be applied for predicting the reactivities of **3** with nucleophiles.

Experimental Section

*Iminium Salts **3***

Details on the preparation as well as spectroscopic and crystallographic characterization of the iminium salts **3** are given in the Supporting Information and in ref. [12].

Kinetics

Stopped-Flow UV/vis spectroscopy. The kinetics of the reactions of **3** with ketene acetals **4a** and **4b** were followed by UV/vis spectroscopy in CH_2Cl_2 by using a commercial stopped-flow spectrophotometer system (Applied Photophysics SX.18MV-R). The kinetic runs were initiated by mixing equal volumes of dichloromethane solutions of the nucleophiles and the iminium salts. The temperature of the solutions during the kinetic studies was maintained at (20 ± 0.2)°C by using circulating bath cryostats.

Conventional UV/vis spectroscopy: The rates of slow reactions of **4a** and **4b** with **3** ($t_{1/2} > 15$–20 s) were determined by using a J&M TIDAS diode array spectrophotometer controlled by Labcontrol Spectacle software and connected to a Hellma 661.502-QX quartz Suprasil immersion probe (5 mm light path) via fiber optic cables and standard SMA connectors. The temperature of the solutions during the kinetic studies was maintained at (20 ± 0.1)°C by using circulating bath cryostats.

Laser flash photolysis: Solutions of the precursor phosphonium salts **9** with $A_{266\,nm} \approx 0.5$–1.0 (ca. 1×10^{-4} M) were irradiated with a 7 ns pulse (266 nm, 30–60 mJ $pulse^{-1}$) from a quadrupled Nd/YAG laser using a xenon short-arc lamp as probe light. The system was equipped with a fluorescence flow cell and a dosage pump, which allows the sample volume to be completely replaced between subsequent laser pulses. When the iminium ions **3d** and **3e** were generated in presence of a large

excess of phosphane **8**, monoexponential decays of the UV/vis absorbances of the iminium ions at their absorption maxima were detected. Typically, 64 or more individual decay curves were averaged for noise reduction.

Evaluation of the kinetic measurements: Kinetics under first-order conditions were achieved by applying an excess of the nucleophiles relative to the iminium ions, that is, the ratio of [**4** or **8**]$_0$/[**3**]$_0 > 9$, was maintained in all kinetic experiments. As a consequence, a monoexponential decay of the absorbance of the iminium ion **3** was detected, from which the first-order rate constant k_{obs} (s^{-1}) was derived by a least-squares fitting of the function $A_t = A_0 \exp(-k_{obs}t) + C$. According to the relation $k_{obs} = k[\mathrm{Nu}]$, the first-order rate constants k_{obs} depended linearly on the nucleophile concentrations [**4** or **8**], whereby the slopes correspond to the second-order rate constants k_2 ($M^{-1}s^{-1}$). Details of the individual kinetic experiments are given in the Supporting Information.

Acknowledgements

We thank the Deutsche Forschungsgemeinschaft (SFB 749, project B1) and COST CM0905 for support of this work.

[1] a) D. Seebach, A. R. Sting, M. Hoffmann, *Angew. Chem. Int. Ed. Engl.* **1996**, *35*, 2708–2748; *Angew. Chem.* **1996**, *108*, 2881–2921; b) D. Seebach, R. Imwinkelried, T. Weber in *Modern Synthetic Methods 1986* (Ed.: R. Scheffold), Springer, Berlin, **1986**, p. 125; c) D. Seebach, M. Boes, R. Naef, W. B. Schweizer, *J. Am. Chem. Soc.* **1983**, *105*, 5390–5398; d) R. Naef, D. Seebach, *Helv. Chim. Acta* **1985**, *68*, 135–143; e) D. Seebach, R. Naef, G. Calderari, *Tetrahedron* **1984**, *40*, 1313–1324.

[2] K. A. Ahrendt, C. J. Borths, D. W. C. MacMillan, *J. Am. Chem. Soc.* **2000**, *122*, 4243–4244.

[3] W. S. Jen, J. J. M. Wiener, D. W. C. MacMillan, *J. Am. Chem. Soc.* **2000**, *122*, 9874–9875.

[4] N. A. Paras, D. W. C. MacMillan, *J. Am. Chem. Soc.* **2001**, *123*, 4370–4371.

[5] a) P. I. Dalko, L. Moisan, *Angew. Chem. Int. Ed.* **2004**, *43*, 5138–5175; *Angew. Chem.* **2004**, *116*, 5248–5286; b) A. Berkessel, H. Gröger, *Asymmetric Organocatalysis: From Biomimetics Concepts to Applications in Asymmetric Synthesis* Wiley-VCH, Weinheim, **2005**; c) G. Lelais, D. W. C. MacMillan, *Aldrichimica Acta* **2006**, *39*, 79–87; d) G. Lelais, D. W. C. MacMillan, in *New Frontiers in Asymmetric Catalysis* (Eds.: K. Mikami, M. Lautens), Wiley, Hoboken, NJ, **2007**, pp. 313–358; e) S. G. Ouellet, A. M. Walji, D. W. C. MacMillan, *Acc. Chem. Res.* **2007**, *40*, 1327–1339; f) A. M. Walji, D. W. C. MacMillan, *Synlett* **2007**, 1477–1489; g) C. Palomo, A. Mielgo, *Angew. Chem. Int. Ed.* **2006**, *45*, 7876–7880; *Angew. Chem.* **2006**, *118*, 8042–8046; h) P. Melchiorre, M. Marigo, A. Carlone, G. Bartoli, *Angew. Chem.* **2008**, *120*, 6232–6265; *Angew. Chem. Int. Ed.* **2008**, *47*, 6138–6171; i) *Organocatalysis, Ernst Schering Foundation Symposium Proceedings 2007–2* (Eds.: M. T. Reetz, B. List, S. Jaroch, H. Weinmann), Springer, Berlin, **2008**.

[6] a) C. Isart, J. Burés, J. Vilarrasa, *Tetrahedron Lett.* **2008**, *49*, 5414–5418; b) J. Burés, A. Armstrong, D. G. Blackmond, *J. Am. Chem. Soc.* **2012**, *134*, 6741–6750; c) J. Burés, A. Armstrong, D. G. Blackmond, *J. Am. Chem. Soc.* **2011**, *133*, 8822–8825.

[7] a) M. Lemay, W. W. Ogilvie, *J. Org. Chem.* **2006**, *71*, 4463–4666; b) D. Seebach, U. Grošelj, D. M. Badine, W. B. Schweizer, A. K. Beck, *Helv. Chim. Acta* **2008**, *91*, 1999–2034; c) S. Lakhdar, T. Tokuyasu, H. Mayr, *Angew. Chem. Int. Ed.* **2008**, *47*, 8723–8726; *Angew. Chem.* **2008**, *120*, 8851–8854; d) G. Evans, T. J. K. Gibbs, R. L. Jenkins, S. J. Coles, M. B. Hursthouse, J. A. Platts, N. C. O. Tomkinson, *Angew. Chem. Int. Ed.* **2008**, *47*, 2820–2823; *Angew. Chem.* **2008**, *120*, 2862–2865; e) J. B. Brazier, G. Evans, T. J. K. Gibbs, S. J. Coles, M. B. Hursthouse, J. A. Platts, N. C. O. Tomkinson, *Org. Lett.* **2009**, *11*, 133–136; f) U. Grošelj, D. Seebach, D. M. Badine, W. B. Schweizer, A. K. Beck, I. Krossing, P. Klose, Y. Hayashi, T. Uchimaru, *Helv. Chim. Acta* **2009**, *92*, 1225–1259; g) J. B. Brazier, G. P. Hopkins, M. Jirari, S. Mutter, R. Pommereuil, L. Samulis, J. A. Platts, N. C. O. Tomkinson, *Tetrahedron Lett.* **2011**, *52*, 2783–2785.

[8] a) L. E. Zimmer, C. Sparr, R. Gilmour, *Angew. Chem. Int. Ed.* **2011**, *50*, 11860–11871; *Angew. Chem.* **2011**, *123*, 12062–12074; b) C. Sparr, R. Gilmour, *Angew. Chem. Int. Ed.* **2010**, *49*, 6520–6523; *Angew. Chem.* **2010**, *122*, 6670–6673; c) M. C. Holland, S. Paul, W. B. Schweizer, K. Bergander, C. Mück-Lichtenfeld, S. Lakhdar, H. Mayr, R. Gilmour, *Angew. Chem. Int. Ed.* **2013**, *52*, 7967–7971; *Angew. Chem.* **2013**, *125*, 8125–8129.

[9] a) S. Lakhdar, A. R. Ofial, H. Mayr, *J. Phys. Org. Chem.* **2010**, *23*, 886–892; b) S. Lakhdar, J. Ammer, H. Mayr, *Angew. Chem. Int. Ed.* **2011**, *50*, 9953–9956; *Angew. Chem.* **2011**, *123*, 10127–10130; c) H. Mayr, S. Lakhdar, B. Maji, A. R. Ofial, *Beilstein J. Org. Chem.* **2012**, *8*, 1458–1478.

[10] a) H. Mayr, M. Patz, *Angew. Chem. Int. Ed. Engl.* **1994**, *33*, 938–957; *Angew. Chem.* **1994**, *106*, 990–1010; b) H. Mayr, T. Bug, M. F. Gotta, N. Hering, B. Irrgang, B. Janker, B. Kempf, R. Loos, A. R. Ofial, G. Remennikov, H. Schimmel, *J. Am. Chem. Soc.* **2001**, *123*, 9500–9512; c) H. Mayr, A. R. Ofial, *J. Phys. Org. Chem.* **2008**, *21*, 584–595; d) For a comprehensive database of nucleophilicity parameters N and s_N as well as electrophilicity parameters E, see http://www.cup.uni-muenchen.de/oc/mayr/DBintro.html.

[11] L. Tichotová, E. Matoušová, M. Špulák, J. Kuneš, I. Votruba, V. Buchta, M. Pour, *Bioorg. Med. Chem. Lett.* **2011**, *21*, 6062–6066.

[12] CCDC 984518 (**3a**, only one of the two symmetrically independent molecules in the unit cell is depicted in Figure 1), 984519 (**3c**), 984520 (**3d**), 984521 (**3e**), and 984522 (**3f**) contain the supplementary crystallographic data for this paper. These data can be obtained free of charge from The Cambridge Crystallographic Data Centre via http://www.ccdc.cam.ac.uk/data_request/cif.

[13] a) R. Gordillo, K. N. Houk, *J. Am. Chem. Soc.* **2006**, *128*, 3543–3553; b) R. Gordillo, J. Carter, K. N. Houk, *Adv. Synth. Catal.* **2004**, *346*, 1175–1185.

[14] a) U. Grošelj, W. B. Schweizer, M.-O. Ebert, D. Seebach, *Helv. Chim. Acta* **2009**, *92*, 1–13; b) D. Seebach, U. Grošelj, W. B. Schweizer, S. Grimme, C. Mück-Lichtenfeld, *Helv. Chim. Acta* **2010**, *93*, 1–16.

[15] C. J. Borths, D. E. Carrera, D. W. C. MacMillan, *Tetrahedron* **2009**, *65*, 6746–6753.

[16] C. Hansch, A. Leo, R. W. Taft, *Chem. Rev.* **1991**, *91*, 165–195.

[17] D. Richter, N. Hampel, T. Singer, A. R. Ofial, H. Mayr, *Eur. J. Org. Chem.* **2009**, 3203–3211.

[18] a) J. Ammer, C. F. Sailer, E. Riedle, H. Mayr, *J. Am. Chem. Soc.* **2012**, *134*, 11481–11494; b) T. A. Nigst, J. Ammer, H. Mayr, *J. Phys. Chem. A* **2012**, *116*, 8494–8499; c) J. Ammer, C. Nolte, H. Mayr, *J. Am. Chem. Soc.* **2012**, *134*, 13902–13911; d) J. Ammer, H. Mayr, *J. Phys. Org. Chem.* **2013**, *26*, 956–969.

[19] B. Kempf, H. Mayr, *Chem. Eur. J.* **2005**, *11*, 917–927.

–Experimental Section–

Reaction products

Preparation of the iminium hexafluorophosphates 3a–c

To a solution of (*S*)-5-benzyl-2,2,3-trimethylimidazolidin-4-one·HPF_6 (**1b·HPF$_6$**) (364 mg, 1.00 mmol) in methanol (5 mL), cinnamaldehyde **2a** (dissolved in 2 mL of CH_2Cl_2) or **2b**,**c** (1.50 equiv) was added dropwise at ambient temperature. The mixture was stirred for 2 days to obtain the title iminium salts as mixtures with the starting materials. Recrystallizations from first dichloromethane and then MeCN-Et_2O, yielded pure iminium hexafluorophosphates **3a**–**c**.

Preparation of the iminium hexafluorophosphate 3d

To a solution of (*S*)-5-benzyl-2,2,3-trimethylimidazolidin-4-one·HPF_6 (**1b·HPF$_6$**) (364 mg, 1.00 mmol) in methanol (5 mL), aldehyde **2d** (1.05 equiv) was added dropwise at ambient temperature. The mixture was stirred overnight at ambient temperature and the precipitate was isolated by filtration, washed (on the filter) with cold methanol (10 mL), diethylether (10 mL), and dried in the vacuum. Single crystals were obtained by the diffusion method (acetonitrile/diethylether).

Preparation of the iminium hexafluorophosphates 3e,f

To a solution of (*S*)-5-benzyl-2,2,3-trimethylimidazolidin-4-one·HPF_6 (**1b·HPF$_6$**) (364 mg, 1.00 mmol) in methanol (5 mL), aldehyde **2** (1.05 equiv) was added dropwise at ambient temperature. The mixture was stirred overnight at ambient temperature. After evaporation the crude product was recrystallized from dichloromethane/diethyl ether. Single crystals were obtained by the diffusion method (acetonitrile/diethylether).

3a: Yield: 413 mg (0.789 mmol), 79 %. ^{1}H NMR (400 MHz, CD_2Cl_2): δ = 8.87 (dd, *J* = 10.6, 1.8 Hz, 1 H, 1-H), 8.40 (d, *J* = 15.2 Hz, 1 H, 3-H), 8.28 (d, *J* = 8.8 Hz, 2 H, Ar), 7.93 (d, *J* = 8.8 Hz, 2 H, Ar), 7.32–7.22 (m, 3 H, Ar), 7.15 (dd, *J* = 15.2, 10.6 Hz, 1 H, 2-H), 7.07–7.05 (m, 2 H, Ar), 5.20 (br t, *J* = 4–5 Hz, 1 H, 8-H), 3.55 (d, *J* = 4.8 Hz, 2 H, 9-H), 2.84 (s, 3 H, 16-H), 1.76 (s, 3 H, 4-H), 0.96 (s, 3 H, 5-H); ^{13}C NMR (100.6 MHz, CD_2Cl_2): δ = 168.1 (d, C-1), 164.1 (s, C-7), 164.0 (d, C-3), 151.3 (s), 138.7 (s), 133.5 (s), 132.6 (d), 130.4 (d), 130.1 (d), 129.4 (d), 125.0 (d), 120.1 (d, C-2), 87.0 (s), 65.1 (d, C-8), 37.9 (t, C-9), 27.5 (q, C-4), 26.3 (q, C-6), 24.9 (q, C-5); HRMS (ESI+): calcd for $C_{22}H_{24}N_3O_3^+$ [M^+] 378.1812, found 378.1810.

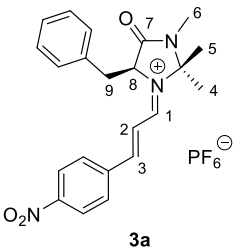

3a

3b: Yield: 366 mg (0.699 mmol), 70 %. ^{1}H NMR (400 MHz, CD_3CN): δ = 8.78 (dd, *J* = 10.5, 2.0 Hz, 1 H, 1-H), 8.73-8.72 (m, 1 H, Ar), 8.47-8.44 (m, 1 H, Ar), 8.21-8.16 (m, 2 H, Ar and 3-H), 7.83 (t, *J* = 8.0 Hz, 1 H, Ar), 7.39–7.22 (m, 5 H, Ar and 2-H), 7.13–7.11 (m, 2 H, Ar), 5.25 (br t, *J* = ca. 5 Hz, 1H, 8-H), 3.60 (dd, *J* = 14.7 Hz, 5.7 Hz, 1 H, 9-H), 3.48 (dd, *J* = 14.7 Hz, 4.2 Hz, 1 H, 9-H), 2.81 (d, *J* = 0.5 Hz, 3 H, 6-H), 1.73 (s, 3 H, 4-H), 0.89 (s, 3 H, 5-H); ^{13}C NMR (100.6 MHz, CD_3CN): δ = 168.7 (d, C-1), 165.0 (s, C-7), 162.9 (d, C-3), 150.0 (s), 138.1 (d), 135.6 (s), 134.7 (s), 131.9 (d), 131.2 (d), 130.2 (d), 129.3 (d), 129.2 (d), 125.8 (d), 120.8 (d, C-2), 87.2 (s), 65.6 (C-8), 37.7 (C-9), 27.5 (C-4), 26.2 (C-6), 24.9 (C-5); HRMS (ESI+): calcd for $C_{22}H_{24}N_3O_3^+$ [M^+] 378.1812, found 378.1810.

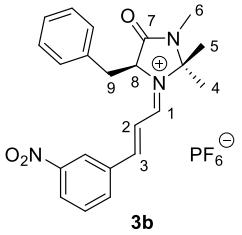

3b

3c: Yield: 258 mg (0.512 mmol), 51 %. ^{1}H NMR (400 MHz, CD_3CN): δ = 8.77 (dd, *J* = 10.5, 2.0 Hz, 1 H, 1-H), 8.12 (d, *J* = 15.2 Hz, 1 H, 3-H), 8.00–7.98 (m, 2 H, Ar), 7.94–7.91 (m, 2 H, Ar), 7.35–7.23 (m, 4 H, Ar and 2-H), 7.11–7.08 (m, 2 H, Ar), 5.22 (br t, *J* = ca. 5 Hz, 1 H, 8-H), 3.57 (dd, *J* = 14.7 Hz, 5.7 Hz, 1 H, 9-H), 3.48 (dd, *J* = 14.7 Hz, 4.1 Hz, 1 H, 9-H), 2.80 (s, 3 H, 16-H), 1.72 (s, 3 H, 4-H), 0.87 (s, 3 H, 5-H); ^{13}C NMR (100.6 MHz, CD_3CN): δ = 168.6 (d, C-1), 165.0 (s, C-7), 163.2 (d, C-3), 137.9 (s), 134.6 (s), 134.2 (d), 132.3 (d), 131.2 (d), 130.2 (d), 129.3 (d), 121.2 (d, C-2), 118.9 (s), 117.6 (s), 87.2 (s), 65.6 (d, C-8), 37.7 (t, C-9), 27.5 (q, C-4), 26.2 (q, C-6), 24.9 (q, C-5); HRMS (ESI+): calcd for $C_{23}H_{24}N_3O^+$ [M^+] 358.1914, found 358.1912.

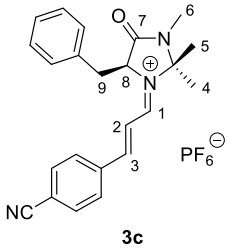

3c

3d: Yield: 477 mg (0.969 mmol), 97 %. ^{1}H NMR (400 MHz, CD_3CN): δ = 8.65 (dd, *J* = 10.8, 1.9 Hz, 1 H, 1-H), 8.14 (d, *J* = 14.9 Hz, 1 H, 3-H), 7.82 (d, *J* = 8.3 Hz, Ar), 7.45 (d, *J* = 8.0 Hz, Ar), 7.33-7.21 (m, 4 H, Ar and 2-H), 7.10–7.07 (m, 2 H, Ar), 5.16 (br t, *J* = ca. 5 Hz, 1 H, 8-H), 3.57 (dd, *J* = 14.7 Hz, 5.6 Hz, 1 H, 9-H), 3.48 (dd, *J* = 14.7 Hz, 3.6 Hz, 1 H, 9-H), 2.78 (s, 3 H, 10-H), 2.47 (s, 3 H, 16-H), 1.69 (s, 3 H, 4–H), 0.79 (s, 3 H, 5–H); ^{13}C NMR (100.6 MHz, CD_3CN): δ = 167.7 (d, C-1), 166.9 (d, C-3), 165.3 (s, C-7), 148.4 (s), 134.9 (s), 132.8 (d), 131.9 (s), 131.5 (d), 131.1 (d), 130.0 (d), 129.2 (d), 117.4 (d, C-2), 86.3 (s), 65.0 (d, C-8), 37.1 (t, C-9), 27.5 (q, C-10), 26.1 (q, C-4), 24.8 (q, C-6), 22.2 (q, C-5); HRMS (ESI+): calcd for $C_{23}H_{27}N_2O^+$ [M^+] 347.2118, found 347.2115.

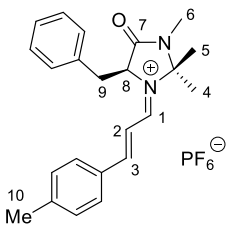

3d

3e: Yield: 508 mg (0.999 mmol), quantitative. ^{1}H NMR (400 MHz, CD_3CN): δ = 8.55 (dd, *J* = 10.9, 1.9 Hz, 1 H, 1-H), 8.09 (d, *J* = 14.7 Hz, 1 H, 3-H), 7.94–7.90 (m, 2 H, Ar), 7.33–7.27 (m, 3 H, Ar), 7.17-7.07 (m, 5 H, Ar and 2-H), 5.11 (br t, *J* = ca. 5 Hz, 1 H, 8-H), 3.95

(s, 3 H, 10-H), 3.57 (dd, *J* = 14.7 Hz, 5.7 Hz, 1 H, 9-H), 3.45 (dd, *J* = 14.7 Hz, 3.5 Hz, 1 H, 9-H), 2.77 (s, 3 H, 10-H), 1.66 (s, 3 H, 4-H), 0.75 (s, 3 H, 5-H); ^{13}C NMR (100.6 MHz, CD_3CN): δ = 167.1 (s), 166.6 (d, C-1 and C-3), 165.5 (s, C-7), 135.6 (d), 135.0 (d), 131.1 (s), 130.0 (d), 129.1 (d), 127.5 (s), 116.5 (d), 115.5 (d, C-2), 85.8 (s), 64.7 (d, C-8), 56.9 (t, C-9), 36.9 (q, C-10), 27.5 (q, C-4), 26.0 (q, C-6), 24.8 (q, C-5); HRMS (ESI+): calcd for $C_{23}H_{27}N_2O_2^+$ [M^+] 363.2067, found 363.2063.

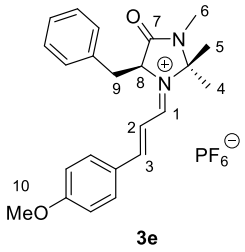

3e

3f: Yield: 521 mg (0.997 mmol), quantitative. ^{1}H NMR (400 MHz, CD_3CN): δ = 8.20 (d, *J* = 11.3 Hz, 1 H, 1-H), 7.88 (d, *J* = 13.9 Hz, 1 H, 3-H), 7.80 (s, 2 H, Ar), 7.31–7.24 (m, 3 H, Ar), 7.08–7.06 (m, 2 H, Ar), 6.89–6.83 (m, 3 H, Ar and 2-H), 4.92 (br s, 1 H, 8-H), 3.56 (dd, *J* = 14.5 Hz, 5.7 Hz, 1 H, 9-H), 3.36 (dd, *J* = 14.5 Hz, 2.9 Hz, 1 H, 9-H), 3.21 (s, 6 H, 10-H), 2.74 (s, 3 H, 6-H), 1.59 (s, 3 H, 4-H), 0.67 (s, 3 H, 5-H); ^{13}C NMR (100.6 MHz, CD_3CN): δ = 166.3 (s, C-7), 165.2 (d, C-3), 161.4 (d, C-1), 157.3 (s), 135.6 (s), 131.1 (d), 129.7 (d), 128.8 (d), 122.8 (s), 113.8 (d, C-2), 110.1 (d), 84.1 (s), 63.6 (C-8), 40.9 (q, C-10), 36.1 (t, C-9), 27.5 (C-4), 25.8 (C-6), 24.7 (C-5); HRMS (ESI+): calcd for $C_{24}H_{30}N_3O^+$ [M^+] 376.2383, found 376.2379.

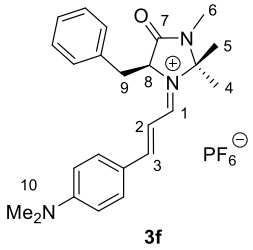

3f

3-(4-Nitrophenyl)-3-(2-oxotetrahydro-2H-pyran-3-yl)propanal (7).

Silyl ketene acetal **4b** (352 mg, 2.04 mmol) was added to a mixture of **3a** (717 mg, 1.37 mmol) in CH_2Cl_2 (20 mL) under nitrogen atmosphere. After stirring for 15 min, the reaction mixture was poured into 20 mL water and extracted with CH_2Cl_2 (2 × 20 mL). The combined organic phases were washed with brine, dried ($MgSO_4$) and filtered. After evaporation of solvent under reduced pressure, components were separated by column chromatography (silica gel, EtOAc/*n*-pentane 50/50 v/v): **7** (338 mg, 89 %); viscous liquid; 5:1 mixture of diastereoisomers.

^{1}H-NMR (300 MHz, $CDCl_3$): δ = 9.71 (major) and 9.67 (minor) (s, 1 H, C*H*O), 8.19–8.14 (m, 2 H, Ar), 7.48–7.43 (m, 2 H, Ar), 4.35-4.07 (m, 2 H), 3.94–3.88 (m, 1 H), 3.34-3.07 (m, 2 H), 2.86–2.93 (m, 1 H), 1.97–1.52 (m, 4 H); ^{13}C-NMR of major diastereomer (75.5 MHz, $CDCl_3$): δ = 200.0 (*C*HO), 172.1, 148.5, 147.2, 129.7, 124.0, 68.9, 45.8, 44.6, 40.3, 22.6), 22.4; HRMS (EI): calcd for $C_{14}H_{15}O_5N$ [M^+] 277.0950, found 227.0952.

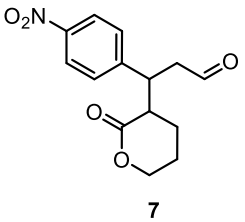

7

Kinetics

Kinetics of the reaction of the iminium triflate 3a with the silyl ketene acetal 4a

(in CH_2Cl_2, 20 °C, stopped-flow method, detection at 350 nm)

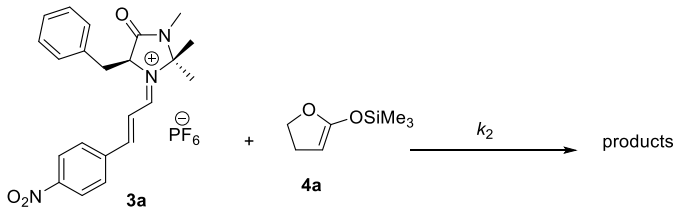

[El] (M)	[Nu] (M)	[Nu]/[El]	k_{obs} (s^{-1})
6.25×10^{-5}	2.20×10^{-3}	35.2	312
6.25×10^{-5}	2.75×10^{-3}	44.0	403
6.25×10^{-5}	4.39×10^{-3}	70.3	529
6.25×10^{-5}	5.49×10^{-3}	87.9	640
6.25×10^{-5}	6.59×10^{-3}	105	726
6.25×10^{-5}	7.69×10^{-3}	123	848
6.25×10^{-5}	8.79×10^{-3}	141	955

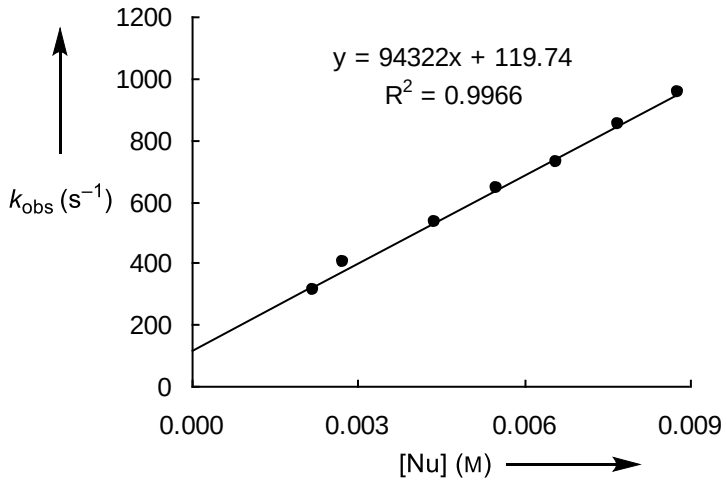

$k_2 = 9.43 \times 10^4\ M^{-1}\ s^{-1}$

Kinetics of the reaction of the iminium triflate 3a with the silyl ketene acetal 4b

(in CH_2Cl_2, 20 °C, stopped-flow method, detection at 350 nm)

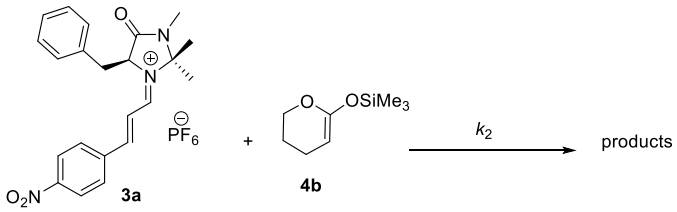

[El] (M)	[Nu] (M)	[Nu]/[El]	k_{obs} (s^{-1})
5.38×10^{-5}	5.54×10^{-4}	10.3	7.45
5.38×10^{-5}	1.11×10^{-3}	20.6	9.65
5.38×10^{-5}	1.66×10^{-3}	30.9	13.1
5.38×10^{-5}	2.21×10^{-3}	41.1	15.8
5.38×10^{-5}	2.77×10^{-3}	51.5	19.7
5.38×10^{-5}	3.22×10^{-3}	61.7	22.8
5.38×10^{-5}	3.88×10^{-3}	72.1	25.7

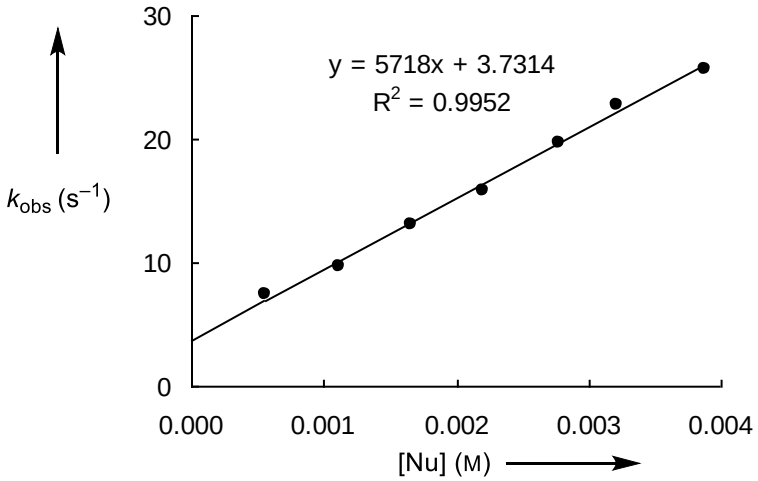

$k_2 = 5.72 \times 10^3\ M^{-1}\ s^{-1}$

Kinetics of the reaction of the iminium triflate 3b with the silyl ketene acetal 4a

(in CH_2Cl_2, 20 °C, stopped-flow method, detection at 343 nm)

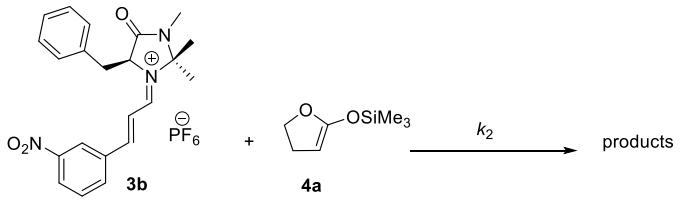

[El] (M)	[Nu] (M)	[Nu]/[El]	k_{obs} (s^{-1})
6.15×10^{-5}	5.11×10^{-4}	8.31	34.3
6.15×10^{-5}	7.67×10^{-4}	12.5	49.1
6.15×10^{-5}	1.02×10^{-3}	16.6	67.3
6.15×10^{-5}	1.53×10^{-3}	24.9	101
6.15×10^{-5}	2.05×10^{-3}	33.3	133

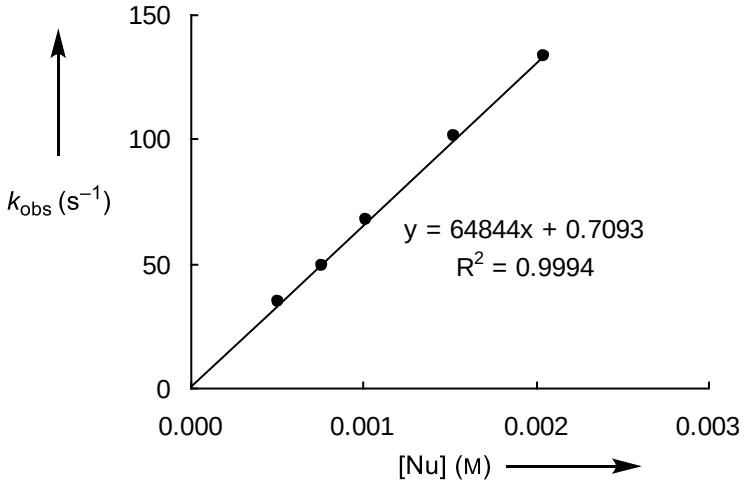

$k_2 = 6.48 \times 10^4\ M^{-1}\ s^{-1}$

Kinetics of the reaction of the iminium triflate 3b with the silyl ketene acetal 4b

(in CH_2Cl_2, 20 °C, stopped-flow method, detection at 343 nm)

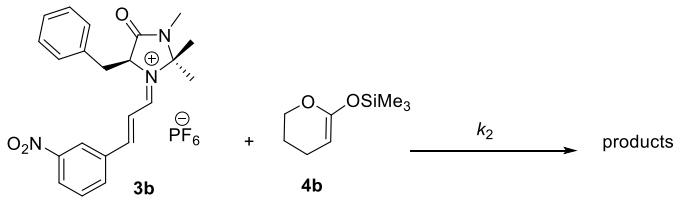

[El] (M)	[Nu] (M)	[Nu]/[El]	k_{obs} (s^{-1})
6.12×10^{-5}	2.52×10^{-3}	41.2	14.0
6.12×10^{-5}	3.78×10^{-3}	61.7	18.3
6.12×10^{-5}	5.04×10^{-3}	82.4	23.9
6.12×10^{-5}	7.56×10^{-3}	124	34.4
6.12×10^{-5}	1.01×10^{-2}	165	44.3
6.12×10^{-5}	1.51×10^{-2}	247	65.2
6.12×10^{-5}	2.02×10^{-2}	330	83.3

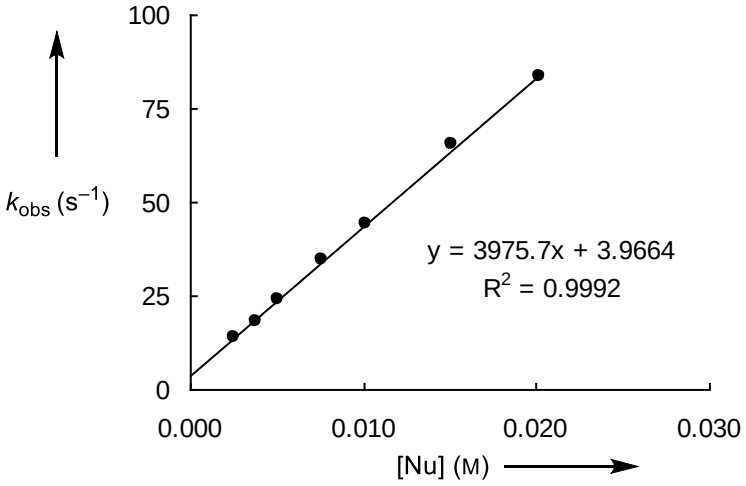

$k_2 = 3.98 \times 10^3\ M^{-1}\ s^{-1}$

Kinetics of the reaction of the iminium triflate 3c with the silyl ketene acetal 4a

(in CH_2Cl_2, 20 °C, stopped-flow method, detection at 352 nm)

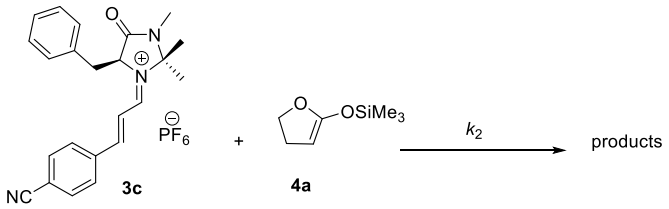

[El] (M)	[Nu] (M)	[Nu]/[El]	k_{obs} (s^{-1})
5.09×10^{-5}	5.11×10^{-4}	10.0	35.5
5.09×10^{-5}	7.67×10^{-4}	15.1	59.0
5.09×10^{-5}	1.02×10^{-3}	20.0	75.9
5.09×10^{-5}	1.53×10^{-3}	30.1	114
5.09×10^{-5}	2.05×10^{-3}	40.3	153

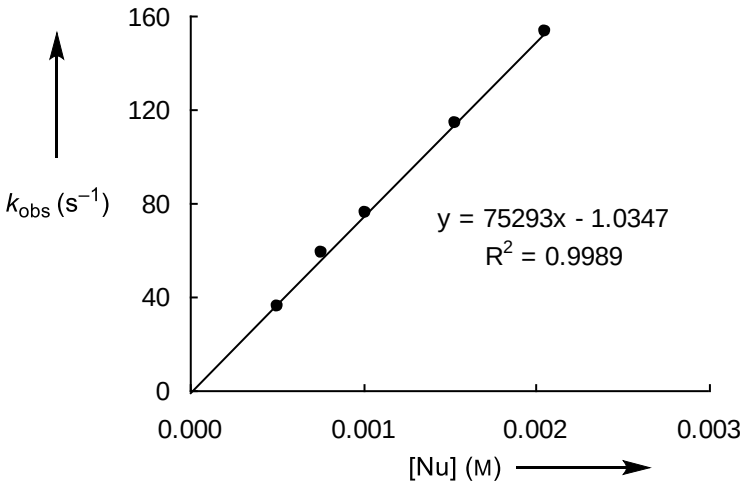

$k_2 = 7.53 \times 10^4\ M^{-1}\ s^{-1}$

Kinetics of the reaction of the iminium triflate 3c with the silyl ketene acetal 4b

(in CH_2Cl_2, 20 °C, stopped-flow method, detection at 352 nm)

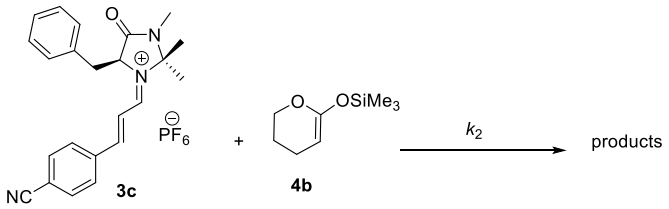

[El] (M)	[Nu] (M)	[Nu]/[El]	k_{obs} (s^{-1})
4.13×10^{-5}	2.04×10^{-3}	49.4	14.3
4.13×10^{-5}	3.06×10^{-3}	74.1	19.6
4.13×10^{-5}	4.08×10^{-3}	98.8	24.8
4.13×10^{-5}	6.12×10^{-3}	148	36.5
4.13×10^{-5}	8.16×10^{-3}	198	47.3
4.13×10^{-5}	1.22×10^{-2}	295	67.9
4.13×10^{-5}	1.60×10^{-2}	387	88.0

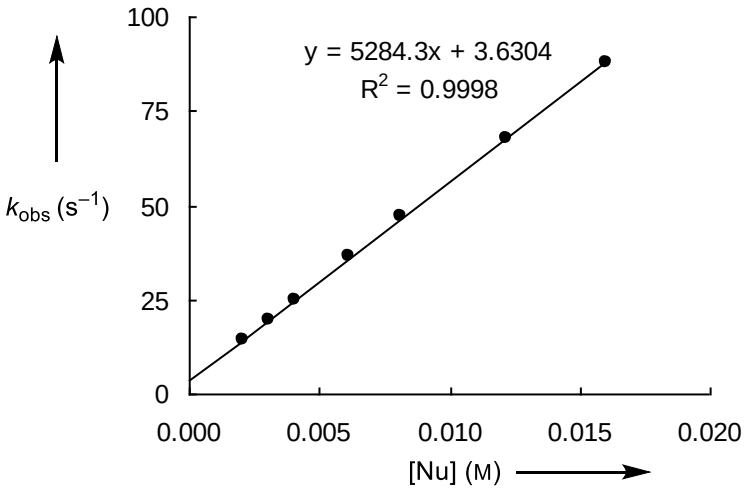

$k_2 = 5.28 \times 10^3\ M^{-1}\ s^{-1}$

Kinetics of the reaction of the iminium triflate 3d with the the silyl ketene acetal 4a

(in CH_2Cl_2, 20 °C, stopped-flow method, detection at 388 nm)

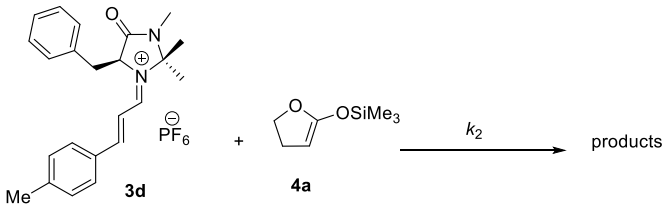

[El] (M)	[Nu] (M)	[Nu]/[El]	k_{obs} (s^{-1})
3.13×10^{-5}	2.38×10^{-3}	76.3	20.9
3.13×10^{-5}	2.98×10^{-3}	95.2	25.7
3.13×10^{-5}	3.58×10^{-3}	114	30.7
3.13×10^{-5}	4.77×10^{-3}	152	41.6
3.13×10^{-5}	5.96×10^{-3}	190	53.0

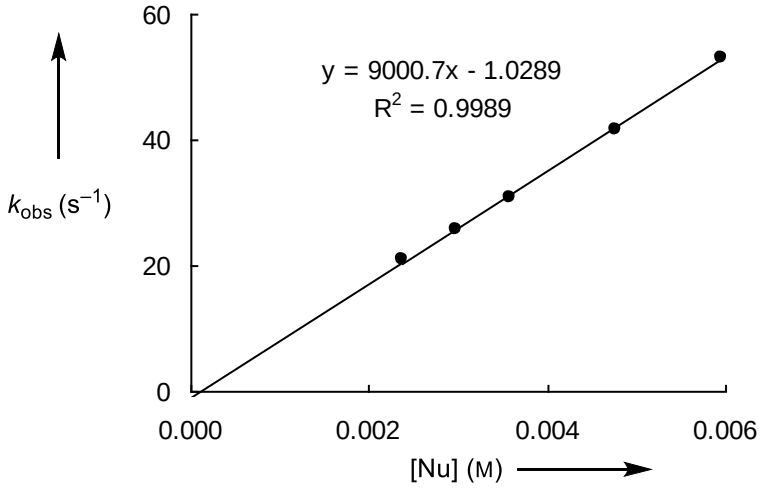

$k_2 = 9.00 \times 10^3\ M^{-1}\ s^{-1}$

Kinetics of the reaction of the iminium triflate 3d with silyl ketene acetal 4b

(in CH_2Cl_2, 20 °C, stopped-flow method, detection at 388 nm)

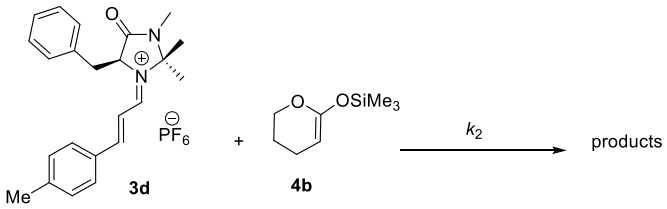

[El] (M)	[Nu] (M)	[Nu]/[El]	k_{obs} (s^{-1})
3.41×10^{-5}	5.92×10^{-3}	174	3.43
3.41×10^{-5}	8.88×10^{-3}	260	5.23
3.41×10^{-5}	1.15×10^{-2}	336	6.77
3.41×10^{-5}	1.81×10^{-2}	532	10.6
3.41×10^{-5}	2.66×10^{-2}	781	16.0

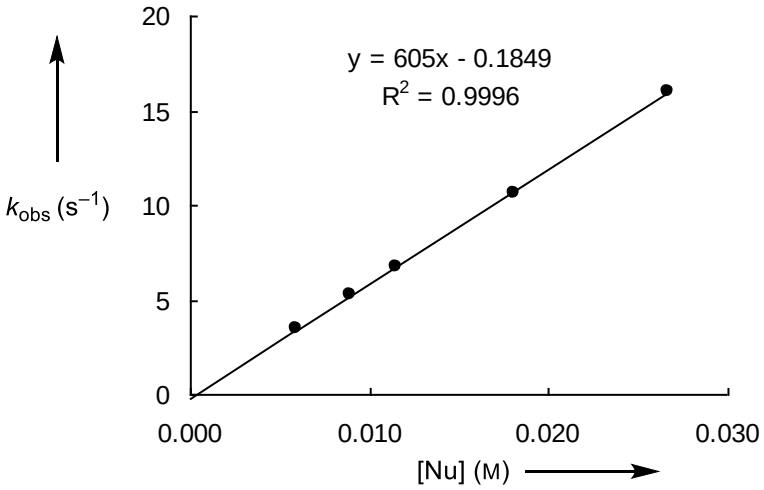

$k_2 = 6.05 \times 10^2\ M^{-1}\ s^{-1}$

Rate constants for the reaction of Tributylphosphine 8 with 3d (precursor: 9d)

(in MeCN, 20 °C, laser flash photolysis, λ = 388 nm)

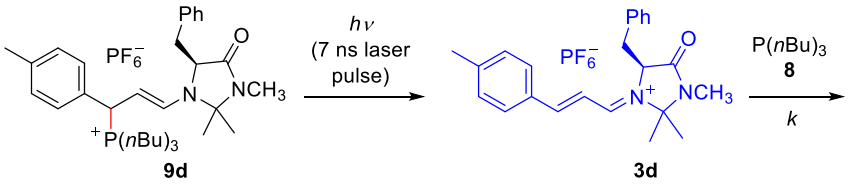

9d 3d

[Nu] (M)	k_{obs} (s^{-1})
1.47×10^{-2}	2.76×10^{3}
3.09×10^{-2}	6.45×10^{3}
4.84×10^{-2}	1.10×10^{4}
6.29×10^{-2}	1.43×10^{4}
8.02×10^{-2}	1.86×10^{4}

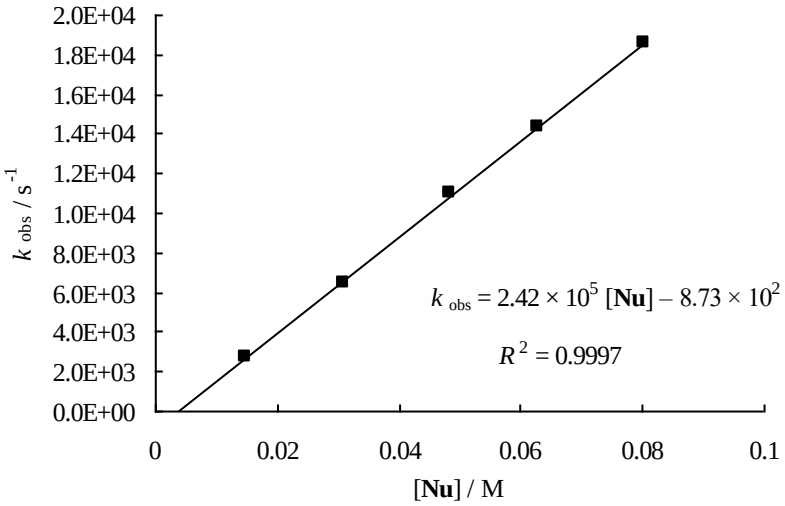

$k_2 = 2.42 \times 10^{5}\ M^{-1}\ s^{-1}$

Kinetics of the reaction of the iminium triflate 3e with the silyl ketene acetal 4a

(in CH_2Cl_2, 20 °C, stopped-flow method, detection at 426 nm)

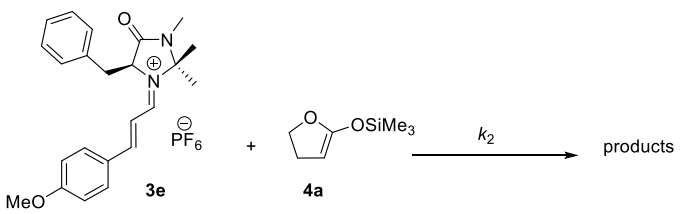

[El] (M)	[Nu] (M)	[Nu]/[El]	k_{obs} (s^{-1})
3.4×10^{-5}	2.38×10^{-3}	70.1	5.58
3.4×10^{-5}	2.98×10^{-3}	87.6	6.85
3.4×10^{-5}	3.58×10^{-3}	105	8.19
3.4×10^{-5}	4.77×10^{-3}	140	10.7
3.4×10^{-5}	5.96×10^{-3}	175	14.1
3.4×10^{-5}	7.15×10^{-3}	210	16.7
3.4×10^{-5}	8.94×10^{-3}	262	21.1

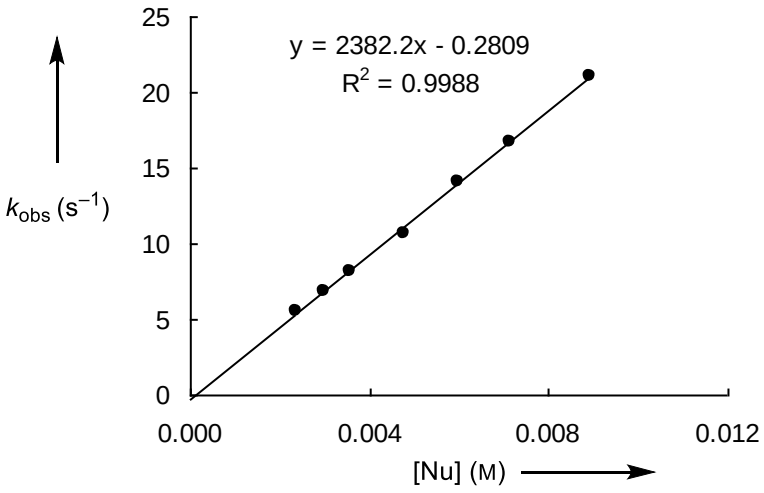

$k_2 = 2.38 \times 10^3\ M^{-1}\ s^{-1}$

Kinetics of the reaction of the iminium triflate 3e with the silyl ketene acetal 4b

(in CH_2Cl_2, 20 °C, conventional UV–Vis method, detection at 426 nm)

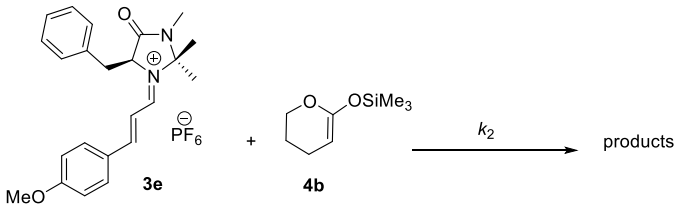

[El] (M)	[Nu] (M)	[Nu]/[El]	k_{obs} (s^{-1})
2.48×10^{-5}	4.36×10^{-3}	176	6.51×10^{-1}
2.48×10^{-5}	6.55×10^{-3}	264	9.23×10^{-1}
2.48×10^{-5}	8.73×10^{-3}	352	1.24
2.48×10^{-5}	1.09×10^{-2}	440	1.57
2.48×10^{-5}	1.36×10^{-2}	548	1.98

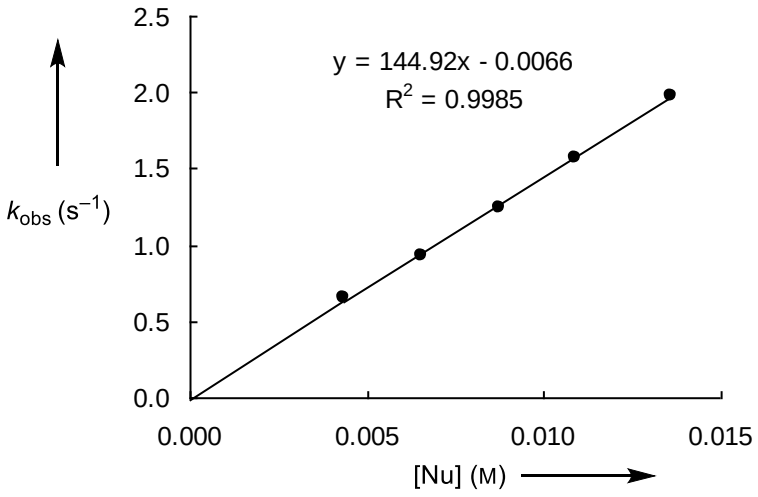

$k_2 = 1.45 \times 10^2\ M^{-1}\ s^{-1}$

Rate constants for the reaction of Tributylphosphine 8 with 3e (precursor: 9e)

(in MeCN, 20 °C, laser flash photolysis, λ = 426 nm)

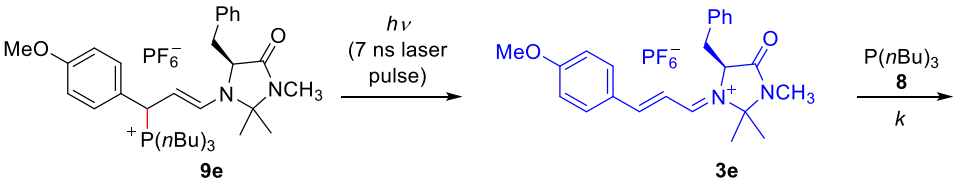

[Nu] (M)	k_{obs} (s^{-1})
1.85×10^{-2}	1.55×10^{3}
3.03×10^{-2}	2.46×10^{3}
4.54×10^{-2}	4.45×10^{3}
6.49×10^{-2}	6.76×10^{3}
8.07×10^{-2}	8.59×10^{3}

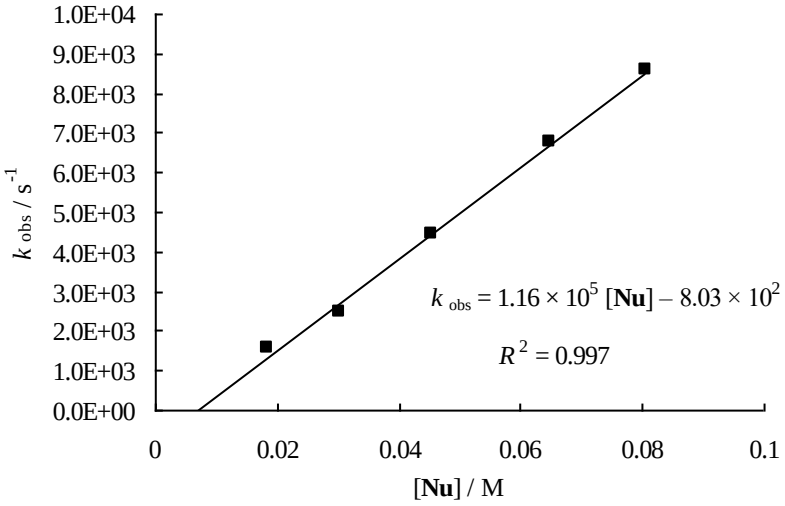

$k_2 = 1.16 \times 10^{5}\ M^{-1}\ s^{-1}$

Kinetics of the reaction of the iminium triflate 3fwith silyl ketene acetal 4a

(in CH_2Cl_2, 20 °C, conventional UV–Vis method, detection at 510 nm)

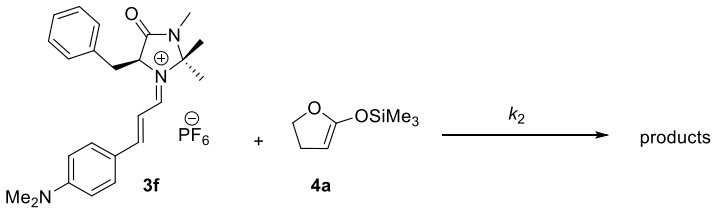

[El] (M)	[Nu] (M)	[Nu]/[El]	k_{obs} (s^{-1})
1.08×10^{-5}	8.25×10^{-4}	76.1	3.89×10^{-2}
1.07×10^{-5}	1.09×10^{-3}	102	4.46×10^{-2}
1.04×10^{-5}	1.58×10^{-3}	152	5.31×10^{-2}
1.01×10^{-5}	2.05×10^{-3}	203	6.44×10^{-2}
1.00×10^{-5}	2.55×10^{-3}	255	7.47×10^{-2}

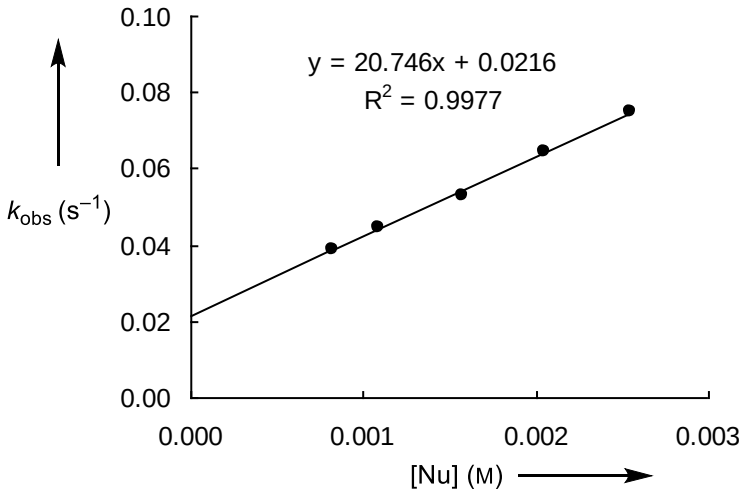

$k_2 = 2.07 \times 10^1\ M^{-1}\ s^{-1}$

Kinetics of the reaction of the iminium triflate 3f with silyl ketene acetal 4b

(in CH_2Cl_2, 20 °C, stopped-flow method, detection at 510 nm)

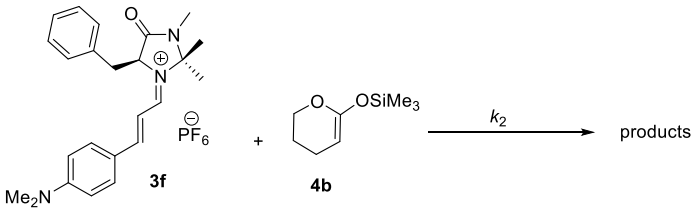

[El] (M)	[Nu] (M)	[Nu]/[El]	k_{obs} (s^{-1})
1.09×10^{-5}	2.22×10^{-3}	204	3.71×10^{-3}
1.06×10^{-5}	2.59×10^{-3}	245	4.27×10^{-3}
1.05×10^{-5}	3.44×10^{-3}	326	5.26×10^{-3}
1.06×10^{-5}	4.33×10^{-3}	407	6.29×10^{-3}
1.07×10^{-5}	5.28×10^{-3}	489	7.69×10^{-3}
1.02×10^{-5}	6.23×10^{-3}	611	9.03×10^{-3}

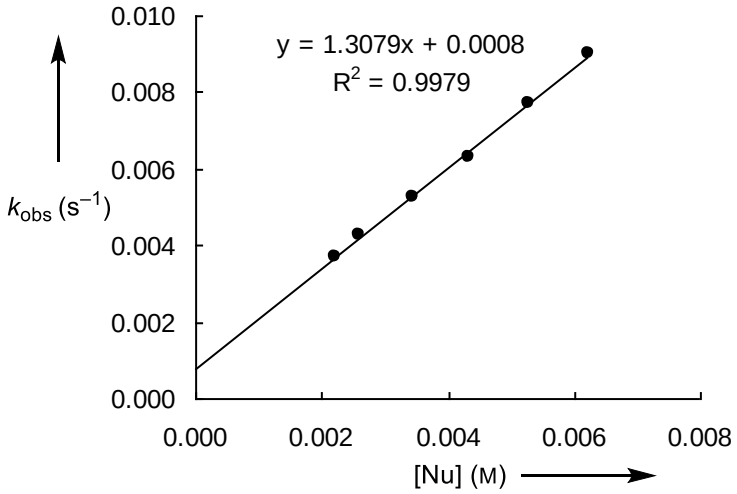

$k_2 = 1.31\ M^{-1}\ s^{-1}$

Appendix 2 Published work 2

J. Am. Chem. Soc. **2014**, *136*, 14263–14269.

Structures and Reactivities of 2-Trityl- and 2-(Triphenylsilyl)pyrrolidine-Derived Enamines: Evidence for Negative Hyperconjugation with the Trityl Group

Hannes Erdmann,[†] Feng An,[†] Peter Mayer,[†] Armin R. Ofial,[†] Sami Lakhdar,*[,†,‡] and Herbert Mayr*[,†]

[†]Department Chemie, Ludwig-Maximilians-Universität München, Butenandtstrasse 5-13, 81377 München, Germany

[‡]Laboratoire de Chimie Moléculaire et Thio-organique, UMR CNRS 6507, 6 Boulevard Maréchal Juin, 14050 Caen, France

Supporting Information

ABSTRACT: X-ray structures of enamines and iminium ions derived from 2-tritylpyrrolidine (Maruoka catalyst) and 2-(triphenylsilyl)pyrrolidine (Bolm–Christmann–Strohmann catalyst) have been determined. Kinetic investigations showed that enamines derived from phenylacetaldehyde and pyrrolidine (R = H) or 2-(triphenylsilyl)pyrrolidine (R = $SiPh_3$) have similar reactivities toward benzhydryl cations Ar_2CH^+ (reference electrophiles), while the corresponding enamine derived from 2-tritylpyrrolidine (R = CPh_3) is 26 times less reactive. The rationalization of this phenomenon by negative hyperconjugative interaction of the trityl group with the lone pair of the enamine nitrogen is supported by the finding that the trityl group in the 2-position of the pyrrolidine increases the electrophilic reactivity of iminium ions derived from cinnamaldehyde by a factor of 14. The consequences of these observations for the rationalization of the reactivity of the Jørgensen–Hayashi catalyst (diphenylprolinol trimethylsilyl ether) are discussed.

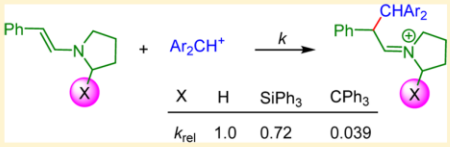

INTRODUCTION

Enamine formation has emerged as a powerful mode of activation in organocatalysis. This methodology is based on the use of chiral secondary amines as catalysts to transform achiral carbonyl derivatives into chiral enamines, which subsequently react with electrophiles to yield enantioenriched α-functionalized carbonyl compounds.[1] The design of effective catalysts for enamine activation has commonly been based on two factors: hydrogen bonding and steric shielding.[1,2]

The first factor, i.e., hydrogen bonding, was probed by List, Barbas, and Lerner for proline-catalyzed enantioselective intermolecular aldol reactions.[3] In this process, as well as in many other proline-catalyzed reactions, the carboxylic proton activates the electrophile through hydrogen bonding and directs the electrophile to the *Re* face of the enamine (Scheme 1).

Scheme 1. Hydrogen Bonding and Steric Control in Enamine Activated Reactions

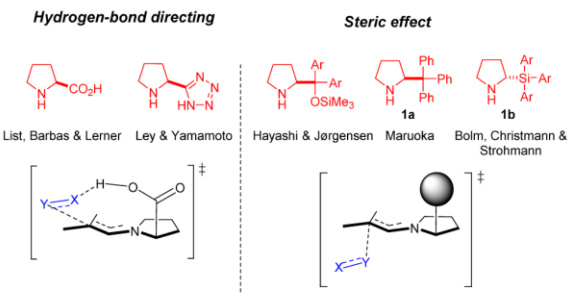

The corresponding transition state was proposed by List and Houk to rationalize the enantioselectivity in proline-catalyzed reactions.[4] Inspired by this work, researchers have developed a large number of bifunctional catalysts, which were expected to operate by a mechanism similar to that for proline.[5]

The second factor, which has been employed for the development of other generations of organocatalysts, is the steric effect, and various pyrrolidines bearing a bulky substituent at the 2-position were used for enamine-activated reactions. Diphenylprolinol trimethylsilyl ether, for instance, also known as the Jørgensen–Hayashi catalyst, has been shown to be a powerful catalyst in enamine-activated reactions as well as in many other modes of activation (Scheme 1).[1b,g−i,6]

Substitution of the trimethylsiloxy group in the Jørgensen–Hayashi catalyst by a phenyl ring yields Maruoka's catalyst **1a**, which showed high efficiency in enamine-activated asymmetric benzoyloxylations and hydroxyaminations of aldehydes[7] but gave only moderate yields and diastereoselectivities in Michael additions of aldehydes to nitroolefins (Scheme 2).[8a]

Better yields and diastereoselectivities have been reported simultaneously by Bolm et al. as well as by Christmann, Strohmann, et al., when 2-silyl-substituted pyrrolidines were used.[8] In particular, 2-(triphenylsilyl)pyrrolidine (**1b**) and 2-(*tert*-butyldiphenylsilyl)pyrrolidine provided high diastereo- and enantioselectivities.[8a,c]

Christmann et al. have attributed the higher efficiency of **1b** compared with **1a** to the larger steric effect (C–Si longer than

Scheme 2. Michael Addition of Propionaldehyde to Nitrostyrene Catalyzed by the Pyrrolidines 1a,b[8a]

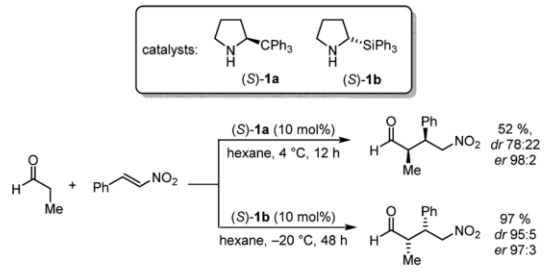

C−C) and higher polarization of the C−Si bond in comparison to the C−C bond.[8a] MP2 calculations by Mersmann, Raabe, and Bolm showed that β-trimethylsilyl-substituted iminium ions, analogues to those formed from **1b** and aldehydes (Scheme 3), are stabilized by the interaction of the Si−C σ bond with the π^* orbital of the C═N double bond.[9]

Scheme 3. Resonance Structures of β-Silyl-Substituted Iminium Ion

We now report on structural and kinetic investigations of the role of trityl and triphenylsilyl substituents on the catalytic activities of the corresponding pyrrolidine derivatives.

In previous work, we have shown that the reactivities of benzhydrylium ions (Table 1), quinone methides, Michael

Table 1. Benzhydrylium Ions 4a−g Employed in This Work and Their Electrophilicity Parameters *E*

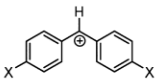

Benzhydrylium Ion		E[a]
4a	X = NPh_2	−4.72
4b	X = $N(CH_2CH_2)_2O$	−5.53
4c	X = N(Ph)(Me)	−5.89
4d	X = NMe_2	−7.02
4e	X = $N(CH_2)_4$	−7.69
4f (n = 2)	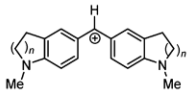	−8.22
4g (n = 1)		−8.76

[a]Electrophilicities E were taken from ref 10b.

acceptors, and iminium ions with n, σ, and π nucleophiles can be described by the linear free energy relationship (1), where s_N and N are solvent-dependent nucleophile-specific parameters and E is an electrophilicity parameter.[10]

$$\log k_2(20^\circ\,\mathrm{C}) = s_N(E + N) \quad (1)$$

By studying the rates of various electrophile−nucleophile combinations, we have been able to establish comprehensive reactivity scales for electrophiles and nucleophiles covering more than 35 orders of magnitude.[11] This methodology has now been employed to characterize the nucleophilicities of the enamines **3** derived from phenylacetaldehyde (**2**) and the pyrrolidines **1a,b** and to compare them with that of the corresponding enamine derived from the Jørgensen−Hayashi catalyst.

RESULTS AND DISCUSSION

Synthesis of the Enamines 3a−c. The enamines **3a,b** were obtained as colorless crystals by condensation of the racemic amines **1a,b** and phenylacetaldehyde **2** in dry toluene in the presence of molecular sieves (4 Å), as shown in Scheme 4.[12]

Scheme 4. Synthesis of the Enamines 3a,b

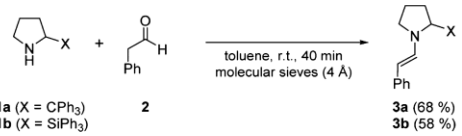

Single crystals suitable for X-ray diffraction were grown by vapor diffusion of n-pentane into dichloromethane solutions of **3a,b**.[13] Enamines **3a,b** both have E-configured double bonds and adopt the *s-trans* conformation, as shown in Figure 1.

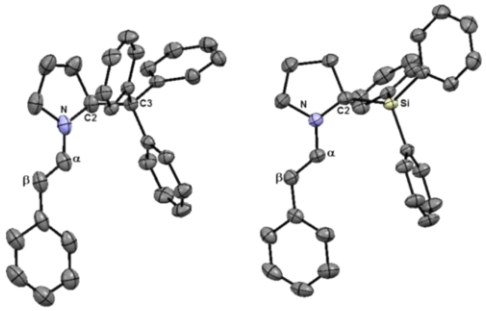

Figure 1. X-ray structures of the enamines **3a** (left) and **3b** (right).

The olefinic bonds (C^α=C^β) of both enamines **3a,b** have comparable bond lengths, 1.347 and 1.339 Å, respectively, showing that the substituents at the 2-position of the pyrrolidine ring do not significantly affect the structures of the enamines. Accordingly, the Dunitz parameters[14] for the enamine nitrogen, which is defined as the distance between the nitrogen and the center of the plane defined by the three nitrogen ligands, were measured to be 0.04 and 0.09 Å, respectively, indicating that both enamines **3a,b** are almost planar.

The NOESY spectra of **3a,b** (in $CDCl_3$) reveal strong interactions between α-H and the 2-H as well as between β-H and 5-H (see numbering in Table 2) and thus confirm that the *s-trans* conformations observed in the crystals also dominate in solution.

Though correlations between ^{13}C NMR chemical shifts and charge densities have to be interpreted with caution, the distance between the substituents X in the 2-position and C^β is so large that the increased shielding of C^β in the order **3a** < **3c** < **3b** might be assigned to the relative electron densities on C^β.

Table 2. NMR Chemical Shifts for the Enamines 3a−c (in $CDCl_3$) and the Corresponding Iminium Ions 5a−c (in CD_3CN)

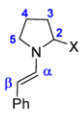

3a–c

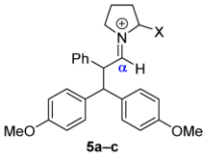

5a–c

compd	X	$\delta(C^{\alpha},3)$	$\delta(C^{\beta},3)$	$\delta(C^{\alpha},5)$
3a or **5a**	CPh_3	136.9	98.0	178.0
3b or **5b**	$SiPh_3$	136.9	97.1	174.0
3c or **5c**	H	135.8[a]	97.4[a]	176.6

[a]From ref 12.

The differences are so small, however, that ground state effects in enamines **3a−c** cannot explain the different catalytic activities of the corresponding pyrrolidines.

Products of the Reactions of the Enamines 3a,b with Benzhydrylium Ions. Combination of the enamines **3a−c** with the dimethoxybenzhydrylium tetrafluoroborate **4h-BF$_4$** in dichloromethane at 20 °C resulted in quantitative formation of iminium salts (**5a−c**)-**BF$_4$** (Scheme 5), which crystallized from a mixture of dichloromethane and *n*-pentane or acetone, yielding crystals suitable for X-ray diffraction analyses (Figure 2).[15]

Scheme 5. Reactions of the Enamines 3a−c with the Electrophiles 4d,h,i

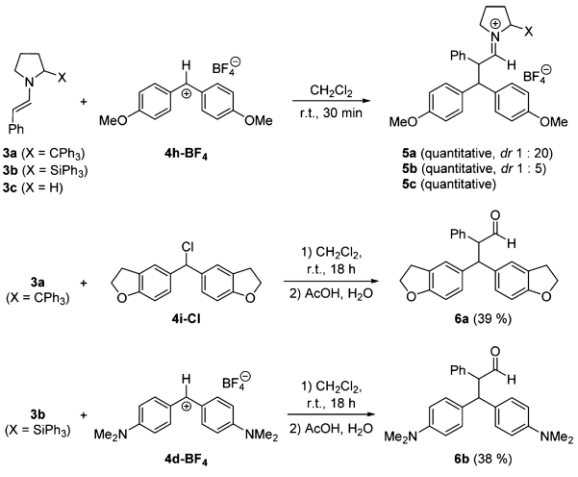

The iminium ions formed analogously from **3a** and the benzhydryl chloride **4i-Cl** and from the combination of **3b** and the benzhydrylium tetrafluoroborate **4d-BF$_4$** were not isolated but hydrolyzed with aqueous acetic acid to give the corresponding aldehydes **6a,b** (Scheme 5).

The X-ray structures depicted in Figure 2 show that the major diastereoisomers of the iminium ions **5a,b** have a *syn* configuration and an *E* configuration about the C═N bond. While lengthening of the C−Si bond from 1.889 Å in enamine **3b** to 1.924 Å in iminium **5b** can be explained by the interaction of the C−Si σ bond with π^* of the C═N bond in **5b** (see above), the expected complementary lengthening of the C═N bond in **5b** due to electron donation into the π^*_{CN} orbital is not observed, as the C═N bond lengths are almost the same in **5a** (1.273 Å), **5b** (1.278 and 1.272 Å), and **5c** (1.271 Å).

Further evidence for the interaction of σ_{C-Si} with π^*_{CN} can be derived from the ^{13}C NMR chemical shifts of C^{α} of the iminium ions **5** (Table 2). While $\delta(C^{\alpha})$ is exactly the same in enamines **3a,b**, C^{α} is shifted to high field by 4 ppm in the silyl-substituted iminium ion **5b** in comparison to the trityl-substituted analogue **5a**. As the nitrogen atoms are coordinated in a trigonal-planar fashion in enamines **3** (Figure 1) and in the iminium ions **5** (Figure 2), geometrical differences cannot account for the differences in chemical shifts. The observation that $\delta(C^{\alpha})$ is more shielded in **5b** than in **5a,c** can thus be assigned to the electron-donating effect of the σ_{C-Si} bond.[9]

Kinetics. All kinetic investigations were carried out in dichloromethane at 20 °C by following the disappearance of the colored benzhydrylium ions **4a−g** in the presence of more than 10 equiv of the enamines **3a−c** (first-order conditions). The first-order rate constants k_{obs} were obtained by least-squares fitting of the single exponential $A_t = A_0 \exp(-k_{obs}\, t)$ to the decays of the UV−vis absorbances of the electrophiles.

Plots of k_{obs} (s^{-1}) against the concentrations of the nucleophiles **3a−c** were linear, as exemplified for the reaction of **3a** with **4c** in Figure 3. Negligible intercepts for these plots were found for the reactions which proceeded quantitatively, while positive intercepts were found for the reactions which led to an equilibrium (for details see the Supporting Information). In both cases, the second-order rate constants k_2 were extracted from the slopes of the plots of k_{obs} against $[\mathbf{3}]_0$ (Table 3).

Figure 4 shows linear correlations between the logarithms of the second-order rate constants (log k_2) and the previously published electrophilicity parameters *E* of the benzhydrylium ions, as required by eq 1. The slopes of the correlation lines yield the nucleophile-specific sensitivity parameters s_N, and the intercepts on the abscissa give the nucleophilicity parameters *N*, which are given in Table 3.

The similar values of the slopes ($0.93 < s_N < 1.06$) of the correlation lines imply that the relative nucleophilicities of the enamines **3a−c** are only slightly affected by the reactivities of the electrophilic reaction partner.

Lewis Basicities of the Enamines 3a−c. As the reactions of the enamines **3a−c** with some benzhydrylium ions proceeded incompletely, we have also studied the corresponding equilibrium constants by UV−vis spectroscopy.

Assuming proportionality between the absorbances and the concentrations of the benzhydrylium ions, the equilibrium constants for the reactions (eq 2) can be determined from the initial absorbances (A_0) of the benzhydrylium ions and the absorbances at equilibrium (*A*) according to eq 3 and are given in Table 4.

$$Ar_2CH^+ + Nu \underset{CH_2Cl_2}{\overset{K}{\rightleftharpoons}} Ar_2CH\text{-}Nu^+ \qquad (2)$$

$$K = \frac{[Ar_2CH\text{-}Nu^+]}{[Ar_2CH^+][Nu]} = \frac{A_0 - A}{A[Nu]} \qquad (3)$$

Equilibrium constants for the reactions of **3b** with the benzhydrylium ions **4e−g** could be determined in this way, and the ratio of the equilibrium constants for the reactions of **3b** with **4e** and **4g** ($K_{4e}/K_{4g} = 3.70$; $\log(K_{4e}/K_{4g}) = 0.57$) was in good agreement with that derived from a statistical treatment of the equilibrium constants for the reactions of these two

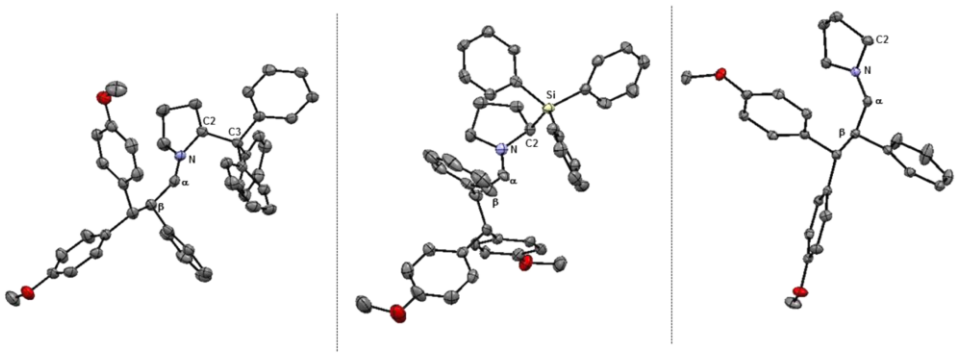

Figure 2. X-ray structures for the iminium ions **5a** (left), **5b** (center), and **5c** (right). Hydrogens and the counterion BF_4^- are omitted for clarity.

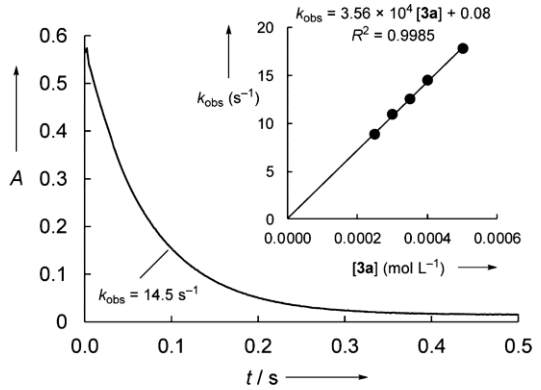

Figure 3. Exponential decay of the absorbance A at 613 nm during the reaction of **4c** (1.12×10^{-5} M) with **3a** (4.01×10^{-4} M). Inset: plot of the rate constant k_{obs} versus [**3a**] (20 °C in CH_2Cl_2).

Table 3. Second-Order Rate Constants k_2 for the Reactions of the Benzhydrylium Salts 4a–g with the Enamines 3a–c in CH_2Cl_2 at 20 °C

enamine	electrophile	$k_2/M^{-1}\ s^{-1}$	N, s_N
3a (X = CPh_3)	**4a**	7.66×10^5	10.19, 1.06
	4b	6.40×10^4	
	4c	3.56×10^4	
	4d	2.56×10^3	
3b (X = $SiPh_3$)	**4d**	4.71×10^4	11.77, 0.98
	4e	8.97×10^3	
	4f	3.25×10^3	
	4g	8.77×10^2	
3c (X = H)	**4c**	8.48×10^5 [a]	12.26, 0.93
	4d	6.60×10^4	
	4e	1.86×10^4	

[a]This value was determined under second-order conditions (small excess of **3c**).

benzhydrylium with a large number of Lewis bases (ΔLA = 0.70; see Table 4). For that reason, the difference of the Lewis acidities of **4e** and **4d** (ΔLA = 1.16) could also be used to calculate the equilibrium constant for the reaction of **3b** with **4d** (8.02×10^4 M^{-1}), which is too large to be directly measured.

From the ratio of the equilibrium constants for the reactions of **3a**,**b** with **4d**, we can now derive that the triphenylsilyl-substituted enamine **3b** is a 76 times stronger Lewis base than

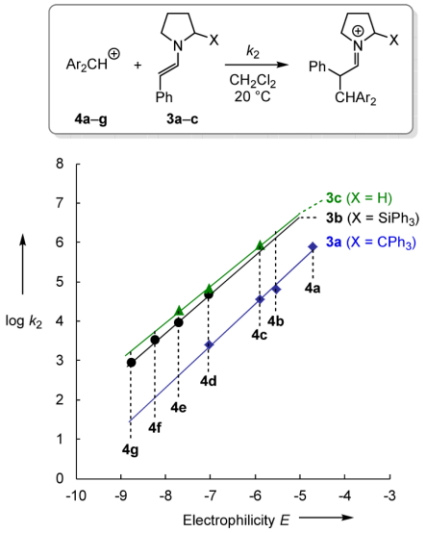

Figure 4. Plots of log k_2 for the reactions of the enamines **3a–c** with the benzhydrylium ions **4a–g** versus their electrophilicity parameters E in CH_2Cl_2 at 20 °C.

Table 4. Equilibrium Constants K (M^{-1}) and Reaction Free Energies $\Delta G°$ (kJ mol^{-1}) for the Reactions of the Enamines 3a–c with the Benzhydrylium Ions 4 in CH_2Cl_2 at 20 °C

enamine	Ar_2CH^+	LA[a]	K	$\Delta G°$
3a (X = CPh_3)	**4d**	−9.30	1.05×10^3	−17.0
3b (X = $SiPh_3$)	**4d**	−9.30	$(8.02 \times 10^4)^b$	(−27.5)
	4e	−10.46	5.55×10^3	−21.0
	4f	−10.92	1.63×10^3	−18.0
	4g	−11.16	1.50×10^3	−17.8
3c (X = H)	**4e**	−10.46	1.87×10^3	−18.4

[a]LA = Lewis acidity derived from equilibrium constants for the reactions of *p*- and *m*-substituted benzhydrylium ions with a variety of Lewis bases (pyridines, phosphines, etc.). ΔLA values equal Δ(log K) in dichloromethane at 20 °C.[16] [b]Calculated as described in the text.

the trityl-substituted enamine **3a**. The thermodynamic effect of the triphenylsilyl stabilization is thus 4 times larger than the kinetic effect derived from the relative rates of the reactions with **4d** (k_{3b}/k_{3a} = 18, Table 3).

While the reaction of **4e** with the triphenylsilyl-substituted enamine **3b** is 2 times slower than the corresponding reaction

with the parent **3c** (Table 3), the equilibrium constants for these reactions showed that the triphenylsilyl-substituted enamine **3b** is an about 3 times stronger Lewis base than the parent enamine **3c** (Table 4), indicating that the hyperconjugative stabilization of the triphenylsilyl-substituted iminium ion is not yet effective in the transition state of the electrophilic additions to **3b**.

Origin of the Trityl Effect. Why is the trityl-substituted enamine **3a** approximately 26 times less reactive than the parent enamine **3c**? Since the planar arrangement of the nitrogen substituents in **3a** was shown by X-ray analysis (Figure 1), we can exclude perturbation of the enamine resonance as the origin of the low reactivity of **3a**. Shielding will block one face of the enamine **3a** and can account for a reduction of the nucleophilic reactivity by a factor of 2.

In order to rationalize the remaining effect, we must conclude that the trityl group acts as an electron acceptor in **3a**. However, when standard reactions to determine Hammett constants had been employed, i.e., reactions of substituted benzoic acids with diphenyldiazomethane or alkylation of phenolates with iodoethane, Hammett σ constants close to 0 were found (Table 5).[17] Consequently, the trityl group was considered to be an electronically neutral substituent, comparable to H.

Table 5. Determination of the Hammett σ Constant for the Trityl Group[a]

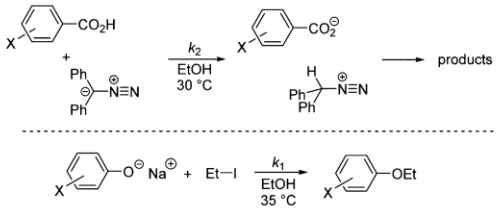

X	$k_2/M^{-1}\ s^{-1}$	k_1/s^{-1}
m-CH_3	1.54×10^{-2}	7.70×10^{-4}
H	1.83×10^{-2}	6.48×10^{-4}
m-Ph_3C	1.85×10^{-2}	7.65×10^{-4}
p-Ph_3C	2.01×10^{-2}	7.43×10^{-4}
p-Cl	3.12×10^{-2}	
p-Br	3.21×10^{-2}	3.63×10^{-4}
m-Cl		2.90×10^{-4}
p-NO_2	8.80×10^{-2}	5.08×10^{-5}

[a]Data from ref 17.

If, on the other hand, the trityl group really acted as an electron acceptor in enamine **3a**, and thus would be the major reason for the reduced nucleophilicity of **3a**, the opposite effect should be operating in iminium ions: i.e., iminium ions derived from 2-tritylpyrrolidine would be expected to be more electrophilic than the corresponding iminium ions derived from the parent pyrrolidine.

Unfortunately, we have not been able to synthesize a persistent iminium ion from **1b** and phenylacetaldehyde. It was possible, however, to prepare the cinnamaldehyde-derived iminium ion **7a** in analogy to a procedure described by Gilmour and co-workers.[18] The reaction of **7a-PF$_6$** with the cyclic ketene acetal **8a** gave 71% of the conjugate addition product **11** after aqueous workup (Scheme 6), in analogy to our earlier studies with other cinnamaldehyde-derived iminium ions.[19]

Scheme 6. Reaction of the Trityl-Substituted Iminium Ion 7a with the Silyl Ketene Acetal 8a in Dichloromethane at 20 °C

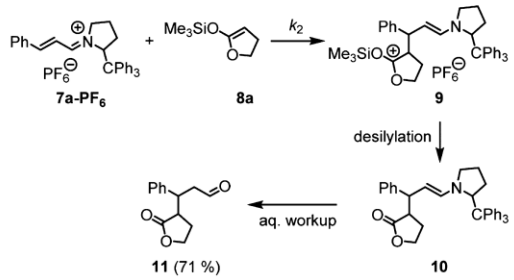

Kinetic investigations of the reactions of **7a** with the ketene acetals **8a,b**, following the previously described procedure,[19a] showed that **7a** is indeed about 10 times more reactive than the iminium ion **7c** (Table 6).

Table 6. Comparison of the Electrophilic Reactivities of the Iminium Ions 7a,c ($k_2/M^{-1}\ s^{-1}$, in CH_2Cl_2 at 20 °C)

Iminium Ions	Nucleophiles	
	Me$_3$SiO, O **8a**	Me$_3$SiO, O **8b**
7a	1.00×10^3	4.81×10^1
7c	$1.30 \times 10^{2\,a}$	3.49^a

[a]From ref 19a.

These observations prompted us to rationalize the low nucleophilic reactivity of the trityl-substituted enamine **3a** by a negative hyperconjugative effect, as depicted in Scheme 7.[20]

Scheme 7. Negative Hyperconjugation in the Trityl-Substituted Enamine 3a

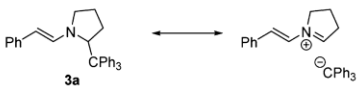

This interaction, which reduces the nucleophilic reactivity of **3a**, is on the other hand a product-stabilizing factor in the formation of the enamine **9** by nucleophilic attack at the iminium ion **7a** (Scheme 6) and thus explains the increase of iminium reactivity by trityl substitution in the pyrrolidine.

Our postulate of a negative hyperconjugative effect of the trityl group is not supported by geometrical parameters, as the distance of the trityl group from the pyrrolidine ring (C3−C2 in Figures 1 and 2) is almost the same in the enamine **3a** (1.574 Å) as in the iminium ion **5a** (1.577 Å). Probably, the negative hyperconjugative effect, which may explain the approximately 5 kJ mol^{-1} difference in activation energies, is too small to be visible in geometrical changes.

These observations have an important consequence for the interpretation of the reactivities of iminium ions and enamines derived from the Jørgensen−Hayashi catalyst.[12,19] As shown in Table 7, the $CPh_2(OSiMe_3)$ substituent of the Jørgensen−

Table 7. Comparison of the Effects of the $CPh_2(OSiMe_3)$ Substituent (Jørgensen–Hayashi Catalyst) and CPh_3 (Maruoka Catalyst) on the Nucleophilicities of Enamines and Electrophilicities of Iminium Ions (k_{rel} in CH_2Cl_2 at 20 °C)

Reaction	X = H	CPh_3	$CPh_2(OSiMe_3)$
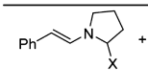 + **4d**	1.0	1/26	1/28 [a]
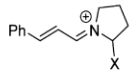 + **8b**	1.0	12	19 [b]

[a]Calculated from $k = 2.33 \times 10^3$ M^{-1} s^{-1} for the reaction of the 2-($CPh_2(OSiMe_3)$)-substituted enamine with **4d** in MeCN.[12] [b]Calculated from $k = 67.0$ M^{-1} s^{-1} for the reaction of the 2-($CPh_2(OSiMe_3)$)-substituted iminium ion with **8b**.[19a]

Hayashi catalyst deactivates the enamine only slightly more than the CPh_3 substituent in the Maruoka catalyst. Vice versa, the $CPh_2(OSiMe_3)$ group has only a slightly larger activating effect on the iminium ion than the trityl group.

For these reasons our earlier explanation of the $CPh_2(OSiMe_3)$ effect by the electronegativity of oxygen[12] can only account for a minor fraction of the effect and we now suggest that negative hyperconjugation of the $CPh_2(OSiMe_3)$ group also accounts for the reactivities of the intermediates of "Jørgensen–Hayashi catalyzed" reactions.

■ CONCLUSION

The X-ray structures of the enamines **3a**,**b** derived from the reactions of phenylacetaldehyde with 2-tritylpyrrolidine (**1a**) and 2-(triphenylsilyl)pyrrolidine (**1b**), respectively, indicate almost perfect planarity of the enamine nitrogen and closely resemble that previously reported[21] for the analogous enamine derived from the Jørgensen–Hayashi catalyst.

Equilibrium measurements showed that the hyperconjugative interaction of σ_{C-Si} with π^*_{CN} increases the Lewis basicity of enamine **3b** by a factor of 3 relative to that of the parent compound **3c**, corresponding to a factor of 6 if the reduced symmetry (two faces accessible in **3c**) is taken into account. This interaction is not yet effective in the transition states of the electrophilic additions, as the silylated enamine **3b** reacts with the same rate as one face of the enamine **3c** (Figure 5).

Though the trityl group had previously been reported to be an electronically neutral substituent with a Hammett substituent constant of $\sigma \approx 0$,[17] the trityl group behaves as an electron-withdrawing substituent at the 2-position of pyrrolidine, which we explain by negative hyperconjugation. This effect rationalizes why the trityl-substituted enamine **3a** is 26 times less nucleophilic than the parent analogue **3c** and the trityl substituted iminium ion **7a** is 8–14 times more electrophilic than the parent analogue **7c**.

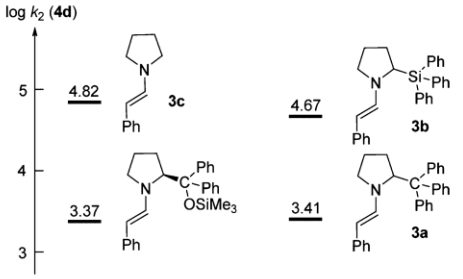

Figure 5. Reactivities of the enamines **3a**–**c** toward **4d** (data from Table 3 and ref 12).

Comparison of the reactivities of the 2-tritylpyrrolidine-derived enamine **3a** and the 2-tritylpyrrolidine-derived iminium ion **7a** with the corresponding Jørgensen–Hayashi pyrrolidine-derived analogues (Table 7) indicates that the CPh_3 group and the CPh_2OSiMe_3 group exert similar electronic effects on the enamine and iminium intermediates of organocatalytic reactions. This similarity rules out specific interactions between the $OSiMe_3$ group and the π system of the intermediate enamines or iminium ions.

For that reason, the high stereoselectivity observed in reactions catalyzed by the Jørgensen–Hayashi pyrrolidine can be entirely assigned to a steric effect. Seebach and co-workers have demonstrated that the enamines and iminium ions derived from 2-(CPh_2OSiR_3)-substituted pyrrolidines preferred synclinal-exo conformations, in which the silyloxy substituent shields one face of the trigonal reaction center.[21a,b] Thus, steric effects can also explain why even higher stereoselectivities have been observed when the $OSiMe_3$ substituent was replaced by the $OSiPh_2Me$ group.[21b,e,22] While 2-tritylpyrrolidine (**1a**) catalyzed stereoselective additions of aldehydes to nitrostyrenes less efficiently than the Jørgensen–Hayashi catalyst,[8c] high enantioselectivities for **1a**-catalyzed reactions have so far only been reported for α-benzoyloxylations and hydroxyaminations of aldehydes.[7] It is not clear whether the small number of reports using **1a** as an organocatalyst[7,8a,c,23] is due to its less convenient accessibility[7a,24] or its poorer performance in comparison to the Jørgensen–Hayashi catalyst in other enamine activated reactions.

■ ASSOCIATED CONTENT

Supporting Information

Text, figures, tables, and CIF files giving experimental procedures, product characterization, kinetic experiments, all NMR spectra, and crystallographic data. This material is available free of charge via the Internet at http://pubs.acs.org.

■ AUTHOR INFORMATION

Corresponding Authors

*E-mail for S.L.: Sami.lakhdar@ensicaen.fr.

*E-mail for H.M.: Herbert.mayr@cup.uni-muenchen.de.

Notes

The authors declare no competing financial interest.

■ ACKNOWLEDGMENTS

We thank the Deutsche Forschungsgemeinschaft (SFB 749, project B1) and the CMST COST Action CM0905 for support of this work. H.E. is grateful to the German National Foundation (Studienstiftung des Deutschen Volkes e.V.) for a fellowship. S.L. thanks the CNRS and Labex Synorg (ANR-11-LABX-0029) for their support. The authors thank Prof. Dr. D. Seebach and Dr. D. W. Lupton for stimulating comments. This paper is dedicated to Professor Shinjiro Kobayashi on the occasion of his 75th birthday.

■ REFERENCES

(1) (a) *Enantioselective Organocatalysis*; Dalko, P. I., Ed.; Wiley: Weinheim, Germany, 2006. (b) Mukherjee, S.; Yang, J. W.; Hoffmann,

S.; List, B. *Chem. Rev.* **2007**, *107*, 5471−5569. (c) Melchiorre, P.; Marigo, M.; Carlone, A.; Bartoli, G. *Angew. Chem., Int. Ed.* **2008**, *47*, 6138−6171. (d) MacMillan, D. W. C. *Nature* **2008**, *455*, 304−308. (e) *Asymmetric Organocatalysis*; List, B., Ed.; Springer: New York, 2009; Topics in Current Chemistry Vol. *291*. (f) Bertelsen, S.; Jørgensen, K. A. *Chem. Soc. Rev.* **2009**, *38*, 2178−2189. (g) Melchiorre, P. *Angew. Chem,. Int. Ed.* **2009**, *48*, 1360−1363. (h) Cheong, P. H.-Y.; Legault, C. Y.; Um, J. M.; Çelebi-Ölçüm, N.; Houk, K. N. *Chem. Rev.* **2011**, *111*, 5042−5137. (i) *Science of Synthesis: Asymmetric Organocatalysis*; List, B., Maruoka, K., Eds.; Thieme: Stuttgart, Germany, 2012.

(2) Nielsen, M.; Worgull, D.; Zweifel, T.; Gschwend, B.; Bertelsen, S.; Jørgensen, K. A. *Chem. Commun.* **2011**, *47*, 632−649.

(3) List, B.; Lerner, R. A.; Barbas, C. F., III *J. Am. Chem. Soc.* **2000**, *122*, 2395−2396.

(4) (a) Bahmanyar, S.; Houk, K. N. *J. Am. Chem. Soc.* **2001**, *123*, 11273−11283. (b) Bahmanyar, S.; Houk, K. N.; Martin, H. J.; List, B. *J. Am. Chem. Soc.* **2003**, *125*, 2475−2479. (c) Hoang, L.; Bahmanyar, S.; Houk, K. N.; List, B. *J. Am. Chem. Soc.* **2003**, *125*, 16−17. (d) List, B.; Hoang, L.; Martin, H. J. *Proc. Natl. Acad. Sci. U.S.A.* **2004**, *101*, 5839−5842. (e) Bock, D. A.; Lehmann, C. W.; List, B. *Proc. Natl. Acad. Sci. U.S.A.* **2010**, *107*, 20636−20641.

(5) (a) Sakthivel, K.; Notz, W.; Bui, T.; Barbas, C. F., III *J. Am. Chem. Soc.* **2001**, *123*, 5260−5267. (b) Martin, H. J.; List, B. *Synlett* **2003**, 1901−1902. (c) Saito, S.; Yamamoto, H. *Acc. Chem. Res.* **2004**, *37*, 570−579. (d) Dahlin, N.; Bøgevig, A.; Adolfsson, H. *Adv. Synth. Catal.* **2004**, *346*, 1101−1105. (e) Berkessel, A.; Koch, B.; Lex, J. *Adv. Synth. Catal.* **2004**, *346*, 1141−1146. (f) Momiyama, N.; Torii, H.; Saito, S.; Yamamoto, H. *Proc. Natl. Acad. Sci. U.S.A.* **2004**, *101*, 5374−5378. (g) Cobb, A. J. A.; Shaw, D. M.; Ley, S. V. *Synlett* **2004**, 558−560. (h) Duschmalé, J.; Wiest, J.; Wiesner, M.; Wennemers, H. *Chem. Sci.* **2013**, *4*, 1312−1318.

(6) (a) Melgo, A.; Palomo, C. *Chem. Asian J.* **2008**, *3*, 922−948. (b) Jensen, K. L.; Dickmeiss, G.; Jiang, H.; Albrecht, Ł.; Jørgensen, K. A. *Acc. Chem. Res.* **2012**, *45*, 248−264.

(7) (a) Kano, T.; Mii, H.; Maruoka, K. *J. Am. Chem. Soc.* **2009**, *131*, 3450−3451. (b) Kano, T.; Shirozu, F.; Maruoka, K. *Org. Lett.* **2014**, *16*, 1530−1532.

(8) (a) Bauer, J. O.; Stiller, J.; Marqués-López, E.; Strohfeldt, K.; Christmann, M.; Strohmann, C. *Chem. Eur. J.* **2010**, *16*, 12553−12558. (b) Husmann, R.; Jörres, M.; Raabe, G.; Bolm, C. *Chem. Eur. J.* **2010**, *16*, 12549−12552. See also: (c) Jentzsch, K. I.; Min, T.; Etcheson, J. I.; Fettinger, J. C.; Franz, A. K. *J. Org. Chem.* **2011**, *76*, 7065−7075.

(9) Mersmann, S.; Raabe, G.; Bolm, C. *Tetrahedron Lett.* **2011**, *52*, 5425−5426.

(10) (a) Mayr, H.; Patz, M. *Angew. Chem., Int. Ed. Engl.* **1994**, *33*, 938−957. (b) Mayr, H.; Bug, T.; Gotta, M. F.; Hering, N.; Irrgang, B.; Janker, B.; Kempf, B.; Loos, R.; Ofial, A. R.; Remennikov, G.; Schimmel, H. *J. Am. Chem. Soc.* **2001**, *123*, 9500−9512. (c) Lucius, R.; Loos, R.; Mayr, H. *Angew. Chem., Int. Ed.* **2002**, *41*, 91−95. (d) Mayr, H.; Kempf, B.; Ofial, A. R. *Acc. Chem. Res.* **2003**, *36*, 66−77. (e) Mayr, H.; Ofial, A. R. *Pure Appl. Chem.* **2005**, 1807−1821. (f) Mayr, H.; Ofial, A. R. *J. Phys. Org. Chem.* **2008**, *21*, 584−595. (g) Mayr, H.; Lakhdar, S.; Maji, B.; Ofial, A. R. *Beilstein J. Org. Chem.* **2012**, *8*, 1458−1478.

(11) For a comprehensive database of nucleophilicity parameters N and s_N as well as electrophilicity parameters E, see: http://www.cup.lmu.de/oc/mayr/DBintro.html.

(12) Lakhdar, S.; Maji, B.; Mayr, H. *Angew. Chem., Int. Ed.* **2012**, *51*, 5739−5742.

(13) CCDC numbers: compound **3a**, 1016097; compound **3b**, 1016098. These supplementary crystallographic data can be obtained free of charge from The Cambridge Crystallographic Data Centre via www.ccdc.cam.ac.uk/data_request/cif.

(14) Dunitz, J. D. *X-Ray Analysis and the Structure of Organic Molecules*; Cornell University Press: London, 1979.

(15) CCDC numbers: for compound **5a**, 1016100; for compound **5b**, 1016099; for compound **5c**, 1017314. These supplementary crystallographic data can be obtained free of charge from The Cambridge Crystallographic Data Centre via www.ccdc.cam.ac.uk/data_request/cif.

(16) Lewis acidities LA were evaluated from statistical analysis of a large number of equilibrium constants for the reactions of benzhydrylium ions with pyridines, phosphines, and related Lewis bases (characterized by their Lewis basicities LB) using the correlation $\log K = \mathrm{LA} + \mathrm{LB}$ with the definition LA = 0 for $(4\text{-MeOC}_6\mathrm{H}_4)_2\mathrm{CH}^+$ in $\mathrm{CH}_2\mathrm{Cl}_2$; unpublished work.

(17) Benkeser, R. A.; Gosnell, R. B. *J. Org. Chem.* **1957**, *22*, 327−329.

(18) (a) Sparr, C.; Schweizer, W. B.; Senn, H. M.; Gilmour, R. *Angew. Chem., Int. Ed.* **2009**, *48*, 3065−3068. (b) Tanzer, E.-M.; Zimmer, L. E.; Schweizer, W. B.; Gilmour, R. *Chem. Eur. J.* **2012**, *18*, 11334−11342.

(19) (a) Lakhdar, S.; Tokuyasu, T.; Mayr, H. *Angew. Chem., Int. Ed.* **2008**, *47*, 8723−8726. (b) Lakhdar, S.; Ammer, J.; Mayr, H. *Angew. Chem., Int. Ed.* **2011**, *50*, 9953−9956.

(20) (a) Kirby, A. J. *Stereoelectronic Effects*; Oxford University Press: Oxford, U.K., 1996. (b) Kirby, A. J. *The Anomeric Effect and Related Stereoelectronic Effects at Oxygen*; Hafner, K., Rees, C. W., Trost, B. M., Lehn, J.-M., Schleyer, P. v. R., Zahradnik, R.; Eds.; Springer Verlag: Berlin, Germany, 1983; Reactivity and Structure Concepts in Organic Chemistry Vol. *15*. (c) Graczyk, P. P.; Mikołajczyk, M. In *Anomeric Effect: Origin and Consequences*; Eliel, E. L., Wilen, S. H., Eds.; Wiley: Hoboken, NJ, 1994; Topics in Stereochemistry Vol. *21*, pp 159−350.

(21) (a) Seebach, D.; Grošelj, U.; Badine, D. M.; Schweizer, W. B.; Beck, A. K. *Helv. Chim. Acta* **2008**, *91*, 1999−2034. (b) Grošelj, U.; Seebach, D.; Badine, D. M.; Schweizer, W. B.; Beck, A. K.; Krossing, I.; Klose, P.; Hayashi, Y.; Uchimaru, T. *Helv. Chim. Acta* **2009**, *92*, 1225−1259. (c) Schmid, M. B.; Zeitler, K.; Gschwind, R. M. *Angew. Chem., Int. Ed.* **2010**, *49*, 4997−5003. (d) Schmid, M. B.; Zeitler, K.; Gschwind, R. M. *Chem. Sci.* **2011**, *2*, 1793−1803. (e) Seebach, D.; Sun, X.; Ebert, M.-O.; Schweizer, W. B.; Purkayastha, N.; Beck, A. K.; Duschmalé, J.; Wennemers, H.; Mukaiyama, T.; Benohoud, M.; Hayashi, Y.; Reiher, M. *Helv. Chim. Acta* **2013**, *96*, 799−852. (f) Carneros, M.; Sánchez, M.; Vilarrasa, J. *Org. Lett.* **2014**, *16*, 2900−2903.

(22) (a) Kemppainen, E. K.; Sahoo, G.; Valkonen, A.; Pihko, P. M. *Org. Lett.* **2012**, *14*, 1086−1089. (b) Hayashi, Y.; Okamura, D.; Umemiya, S.; Uchimaru, T. *ChemCatChem* **2012**, *4*, 959−962. (c) Silvi, M.; Cassani, C.; Moran, A.; Melchiorre, P. *Helv. Chim. Acta* **2012**, *95*, 1985−2006. (d) Cassani, C.; Melchiorre, P. *Org. Lett.* **2012**, *14*, 5590−5593. (e) Mukaiyama, T.; Ishikawa, H.; Koshino, H.; Hayashi, Y. *Chem. Eur. J.* **2013**, *19*, 17789−17800. (f) Kemppainen, E. K.; Sahoo, G.; Piisola, A.; Hamza, A.; Kótai, B.; Pápai, I.; Pihko, P. M. *Chem. Eur. J.* **2014**, *20*, 5983−5993.

(23) (a) Kano, T.; Mii, H.; Maruoka, K. *Angew. Chem., Int. Ed.* **2010**, *49*, 6638−6641. (b) Stiller, J.; Marqués-López, E.; Herrera, R. P.; Fröhlich, R.; Strohmann, C.; Christmann, M. *Org. Lett.* **2011**, *13*, 70−73. (c) Hermange, P.; Portalier, F.; Thomassigny, C.; Greck, C. *Tetrahedron Lett.* **2013**, *54*, 1052−1055.

(24) Klumpp, D. A.; Aguirre, S. L.; Sanchez, G. V., Jr.; de Leon, S. J. *Org. Lett.* **2001**, *3*, 2781−2784.

– Experimental Section–

Reaction products

(*E*)-1-((*E*)-3-phenylallylidene)-2-tritylpyrrolidin-1-ium hexafluorophosphate (*rac*-7a-PF_6)

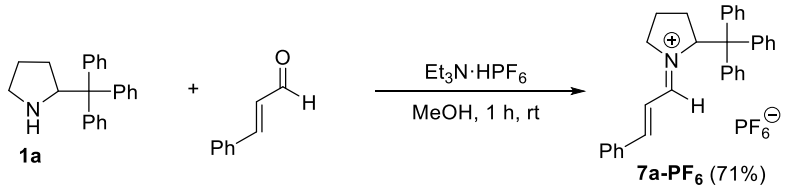

The amine *rac*-**1a** (332 mg, 1.06 mmol) and triethylammonium hexafluorophosphate (0.26 g, 1.1 mmol) were dissolved in anhydrous methanol (3 mL), then cinnamaldehyde (0.15 mL, 1.2 mmol) was added. After stirring the resulting mixture for 1 h at ambient temperature the precipitated powder was filtrated, washed with diethyl ether and dried in the vacuum to give **7a**-$\mathbf{PF_6}$ (430 mg, 0.750 mmol, 71 %) as a pale yellow powder.

^{1}H NMR (400 MHz, CD_3CN): δ 8.09 (d, J = 10.0 Hz, 1 H), 7.75–7.78 (m, 2 H), 7.60–7.65 (m, 1 H), 7.51–7.55 (m, 2 H), 7.47 (d, J = 15.3 Hz, 1 H), 7.32–7.43 (m, 15 H), 7.06 (dd, J = 15.2 Hz, J = 10.5 Hz, 1 H), 6.11 (d, J = 8.6 Hz, 1 H), 3.79–3.87 (m, 1 H), 3.30–3.38 (m, 1 H), 2.65–2.76 (m, 1 H), 2.25–2.32 (m, 1 H), 1.67–1.77 (m, 1 H), 0.34–0.46 (m, 1 H).

^{13}C NMR (100.6 MHz, CD_3CN): δ 168.1 (d), 162.8 (d), 143.3 (s), 135.2 (s), 134.5 (d), 131.6 (d), 131.1 (d), 130.5 (d), 129.7 (d), 128.4 (d), 119.3 (d), 73.5 (d), 64.0 (s), 55.9 (t), 29.9 (t), 22.3 (t).

HRMS (ESI): *m*/*z* calculated for $C_{32}H_{30}N^+$ (**7a**): 428.2373; found: 428.2379.

3-(2-Oxotetrahydrofuran-3-yl)-3-phenylpropanal (11)

The iminium salt *rac*-**7a-PF_6** (50.0 mg, 87.2 µmol) was dissolved in anhydrous dichloromethane (5 mL) under inert gas atmosphere, then the silyl ketene acetal **8a** (20.0 mg, 126 µmol) was added. After stirring the resulting mixture over night at ambient temperature, deionized water was added. The organic layer was separated and the aqueous one extracted with dichloromethane. The organic layers were combined, dried (Na_2SO_4), the volatiles were evaporated and the residue was purified by flash column chromatography on silica gel (pentane/ethyl acetate 10:1→2:1) to give *rac*-**11** (13.5 mg, 61.9 µmol, 71 %) as a viscous yellow liquid in a mixture of two diastereomers in the ratio of 1:1.

^{1}H NMR (400 MHz, $CDCl_3$): δ (9.73–9.74, 9.67–9.68) (m, 1 H), 7.21–7.34 (m, 5 H), (4.01–4.16, 3.47–3.79) (m, 2 H), 3.59–3.69 (m, 1 H), (3.34–3.46, 2.81–3.09) (m, 3 H), (2.25–2.33, 1.99–2.11, 1.83–1.93) (m, 2 H).

^{13}C NMR (100.6 MHz, $CDCl_3$): δ 200.8, 200.4, 177.9, 177.8, 140.7, 140.0, 129.2, 129.1, 128.4, 128.2, 127.8, 127.7, 66.7, 66.4, 47.7, 45.8, 43.9, 43.5, 39.9, 39.5, 27.3, 26.2.

HRMS (EI): *m*/*z* calculated for $C_{13}H_{14}O_3^{\bullet+}$ ($M^{\bullet+}$): 218.0937; found: 218.0947

Kinetics

Kinetics of the reaction of the enamine **3c** with **4c**-$\mathbf{BF_4}$

(CH_2Cl_2, 20°C, stopped-flow, detection at 622 nm)

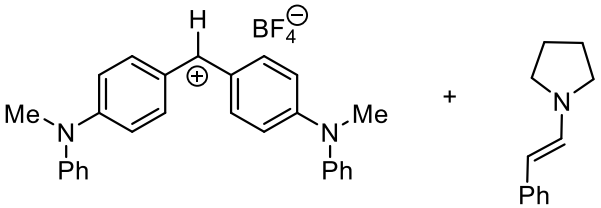

4c-$\mathbf{BF_4}$ **3c**

Experiment	[**3c**]$_0$ (mol L^{-1})	[**4c**]$_0$ (mol L^{-1})	k_2 (L mol^{-1} s^{-1})
A	3.13×10^{-5}	1.18×10^{-5}	8.37×10^{5}
B	3.66×10^{-5}	1.19×10^{-5}	8.45×10^{5}
C	4.18×10^{-5}	1.17×10^{-5}	8.30×10^{5}
D	4.70×10^{-5}	1.22×10^{-5}	8.55×10^{5}
E	1.04×10^{-4}	1.18×10^{-5}	8.71×10^{5}

$k_2 = 8.48 \times 10^{5}$ M^{-1} s^{-1}

All kinetic measurements of the reaction of **3c** with **4c** were performed under second-order conditions. $[\mathbf{4c}]_t$ was derived from the absorbance at 622 nm assuming the validity of the Lambert-Beer law according to the relation $[\mathbf{4c}]_t = A/(\varepsilon d)$ with $\varepsilon(\mathbf{4c}\text{-}BF_4)$ **=**1.42×10^5 L mol^{-1} cm^{-1} and d = 0.5 cm.

A

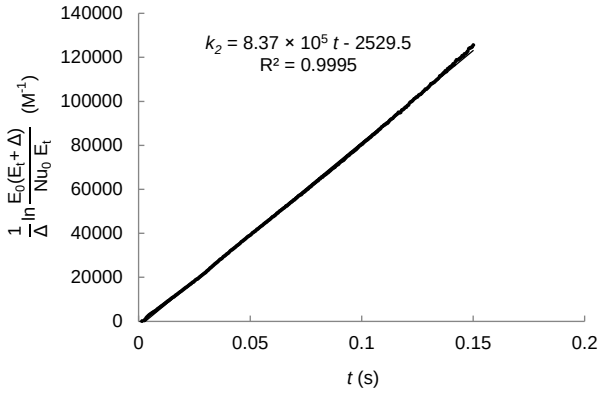

B

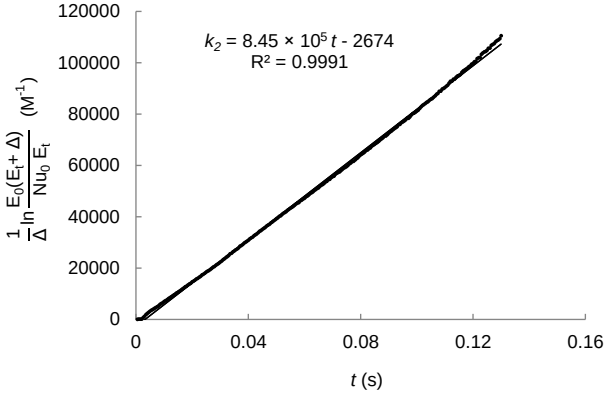

C

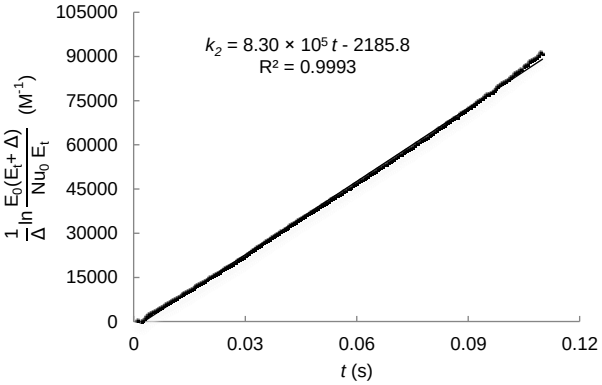

D

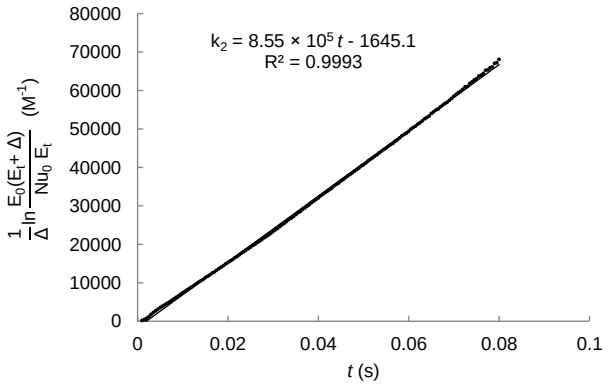

E

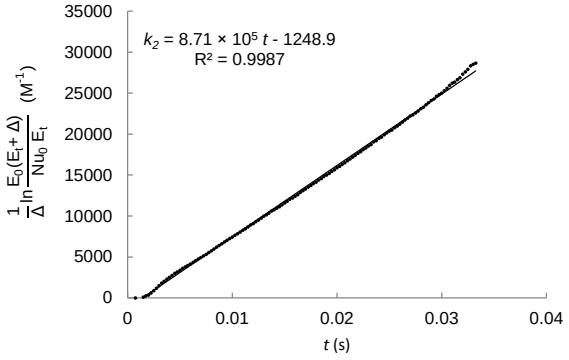

Kinetics of the reaction of the iminium salt **7a-PF$_6$** with the ketene acetal **8a** (CH_2Cl_2, 20°C, stopped-flow, λ = 359 nm)

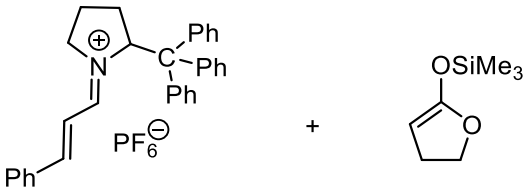

7a-PF$_6$ **8a**

[**7a**] (mol L^{-1})	[**8a**] (mol L^{-1})	[**7a**]/[**8a**]	k_{obs} (s^{-1})
3.33 × 10^{-5}	1.22 × 10^{-3}	36.6	1.40
3.33 × 10^{-5}	1.46 × 10^{-3}	43.8	1.63
3.33 × 10^{-5}	1.94 × 10^{-3}	58.3	2.11
3.33 × 10^{-5}	2.44 × 10^{-3}	37.2	2.62

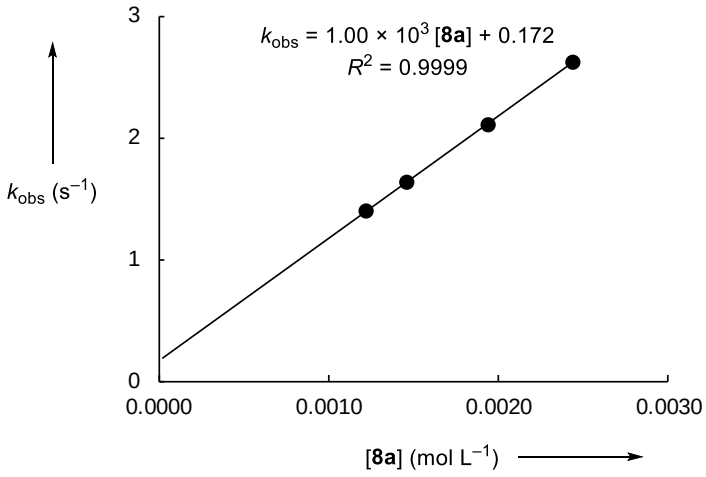

k_2 = 1.00 × 10^3 M^{-1} s^{-1}

Kinetics of the reaction of the iminium salt **7a-**PF_6 with the ketene acetal **8b** (CH_2Cl_2, 20°C, stopped-flow, λ = 359 nm)

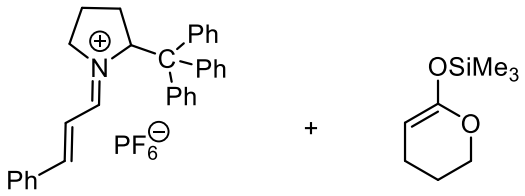

7a-PF_6 **8b**

[**7a**] (mol L^{-1})	[**8b**] (mol L^{-1})	[**7a**]/[**8b**]	k_{obs} (s^{-1})
3.33×10^{-5}	4.97×10^{-4}	14.9	2.82×10^{-2}
3.33×10^{-5}	7.45×10^{-4}	22.4	3.99×10^{-2}
3.33×10^{-5}	9.94×10^{-4}	29.8	5.15×10^{-2}
3.33×10^{-5}	1.24×10^{-3}	37.2	6.39×10^{-2}
3.33×10^{-5}	1.49×10^{-3}	44.7	7.56×10^{-2}
3.33×10^{-5}	1.73×10^{-3}	52.0	8.75×10^{-2}
3.33×10^{-5}	1.99×10^{-3}	59.8	9.97×10^{-2}

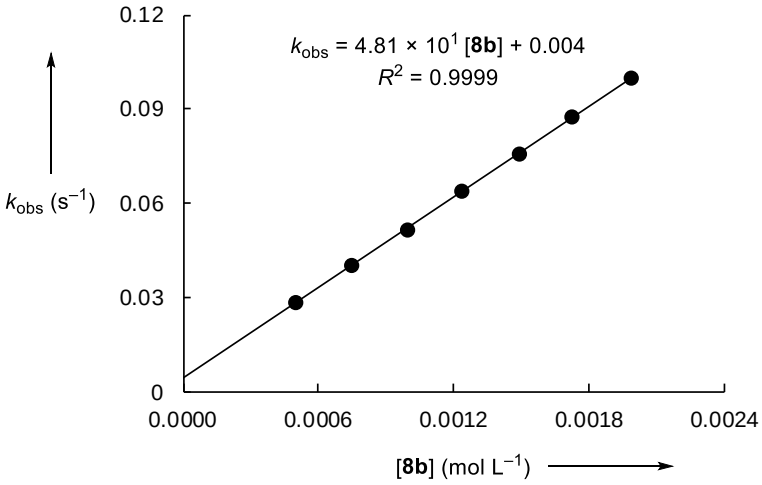

$k_2 = 48.1\ M^{-1}\ s^{-1}$

UV/vis spectrum of the iminium hexafluorophosphate 7a-PF_6

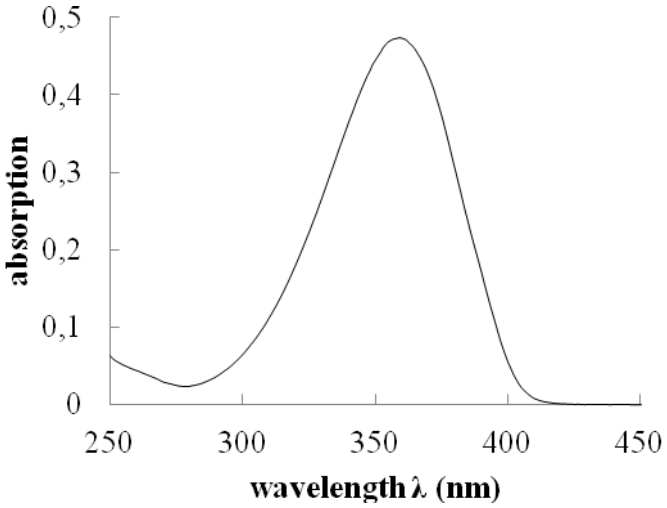

Table S14. Determination of the absorption coefficient of **7a-PF_6**

(5 mm light path, CH_2Cl_2, 20 °C).

[**7a**] (mol L^{-1})	*A*	λ_{max} = 359 nm
1.12×10^{-5}	0.24	
2.23×10^{-5}	0.48	
3.32×10^{-5}	0.69	
4.41×10^{-5}	0.90	
5.49×10^{-5}	1.10	

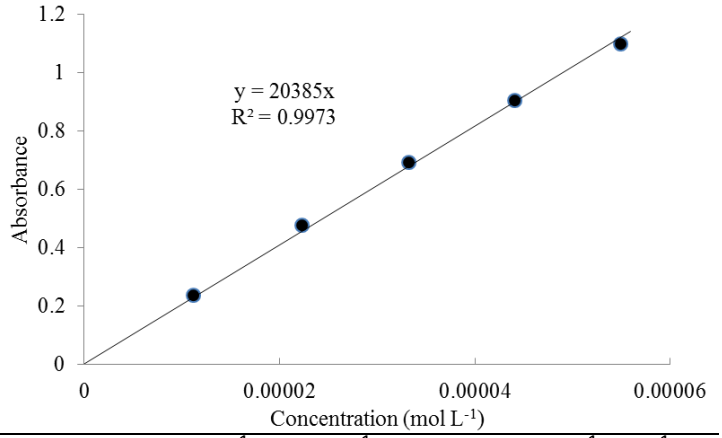

ε = 20385 L mol^{-1}/0.5 cm^{-1} = 40770 L mol^{-1} cm^{-1}

Appendix 3 Published work 3

Org. Lett. **2016**, *18*, 3566–3569.

Influence of the N-Substituents on the Nucleophilicity and Lewis Basicity of N-Heterocyclic Carbenes

Alison Levens,[†] Feng An,[‡] Martin Breugst,[§] Herbert Mayr,[‡] and David W. Lupton*[,†]

[†]School of Chemistry, Monash University, Clayton, Victoria 3800, Australia

[‡]Department Chemie, Ludwig-Maximilians-Universität München, Butenandtstraße 5-13 (Haus F), 81377 München, Germany

[§]Department für Chemie, Universität zu Köln, Greinstraße 4, 50939 Köln, Germany

Supporting Information

ABSTRACT: The ability to modulate the nucleophilicity and Lewis basicity of N-heterocyclic carbenes is pivotal to their application as organocatalysts. Herein we examine the impact of the N-substituent on the nucleophilicity and Lewis basicity. Four N-substituents popular in NHC organocatalysis, namely, the *N*-2,6-$(CH_3O)_2C_6H_3$, *N*-Mes, *N*-4-$CH_3OC_6H_4$, and *N*-*tert*-butyl groups, have been examined and found to strongly affect the nucleophilicity. Thus, the *N*-2,6-$(CH_3O)_2C_6H_3$ group provides the most nucleophilic imidazolylidene NHC reported and the *N*-*tert*-butyl group one of the least. This difference in nucleophilicity is reflected in the catalyst efficiency, as observed with a recently reported trienyl ester rearrangement.

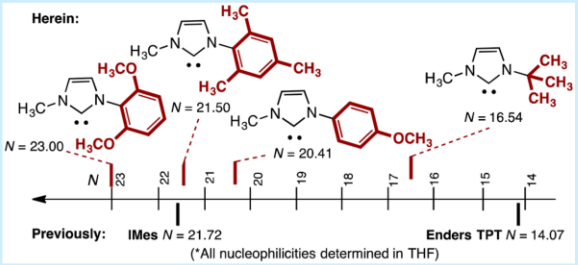

N-Heterocyclic carbene (NHC) catalysis provides access to a diverse range of intermediates for reaction discovery.[1] Among others, the acyl anion equivalent,[2] homoenolates,[3] acyl azoliums[4] and acyl azolium enols/enolates[5] are now routinely exploited in increasingly sophisticated reaction designs. While other Lewis base catalysts can access some of these classes of intermediates, few access all.[6] Although the versatility of NHC organocatalysis is striking, practical application requires highly judicious catalyst selection. This can involve variation of the heterocycle, with imidazole, triazole, and thiazole NHC catalysts being common, although increasingly prevalent is N-substituent modification to deliver optimal catalytic activity for a given reaction design.[7] In the context of acyl anion-mediated reactions, the role of the N-substituent has been investigated.[7b,c,8] In contrast, an examination of NHC nucleophilicity as a function of the N-substituent, to our knowledge, is yet to be reported. Hence, catalyst design remains largely empirical.

Since 2009 we have reported a series of transformations involving enol esters and enolic anhydrides.[9] In these studies, and those from others using ester substrates, it is clear that the required NHC catalysts are distinct from those suited to acyl anion-mediated reactions.[1g,10,11] While Tolman electronic parameters (TEPs), pK_a values, and ^{13}C NMR studies give information that is useful for catalyst selection,[12] measures of nucleophilicity are more scarce. Recently, as part of our studies on reactivity scales for nucleophiles and electrophiles, we reported the nucleophilicities of three common NHCs (SIMes, IMes, and TPT; Figure 1).[13,14] While this study addressed the role of the heterocycle in nucleophilicity, the impact of the N-substituent was not addressed. Herein, the dependence of the nucleophilicity on the N-substituent is examined, with the

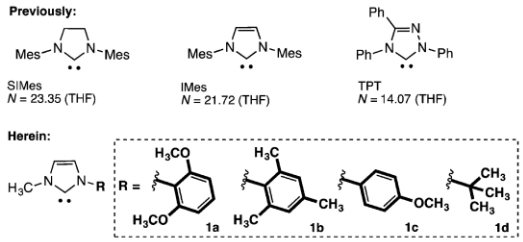

Figure 1. Overview of the study.

nucleophilicity, as well as the Lewis basicity, of NHCs bearing the *N*-2,6-$(CH_3O)_2C_6H_3$ (**1a**), *N*-Mes (**1b**), *N*-4-$CH_3OC_6H_4$ (**1c**), and *N*-*tert*-butyl groups (**1d**) determined. These N-substituents have been exploited in recent discoveries in NHC catalysis,[9h,15−18] particularly using ester substrates. The studies herein demonstrate that the N-substituent plays a significant role in defining the catalyst nucleophilicity, with 3 orders of magnitude rate difference between **1a** and **1d**. Thus, the impact of the N-substituent is at least as significant as the nature of the azolium moiety in determining NHC nucleophilicity.

A series of *p*-quinone methide electrophiles (i.e., **2**, **3**, and **4**) were previously used to determine the nucleophilicity parameters (N) of SIMes, IMes, and TPT (Figure 1). This was achieved by exploiting the observation that the rate of addition of nucleophiles to Michael acceptors or carbocations can be predicted by eq 1:[19]

$$\log k_{20^\circ C} = s_N(N + E) \quad (1)$$

In this equation, nucleophiles are characterized by a solvent-dependent nucleophilicity parameter N and a sensitivity parameter s_N, while electrophiles are characterized by a solvent-independent electrophilicity parameter E. To date, this relationship has been used to examine 1039 nucleophiles and 272 electrophiles.[20a]

To determine the effect of the N-substituent on the nucleophilicity, studies began with the preparation of the required NHCs by deprotonation of the corresponding imidazolium salts **1a–d**·HI with KO*t*-Bu. Although triazolylidenes are more commonly exploited in NHC catalysis, the impact on the nucleophilicity of changing between a triazolylidene and an imidazolylidene has been previously studied (vide supra), thus allowing trends to be extrapolated. Since the nucleophilicities of the four new NHCs **1a–d** are likely to be within the range of those already reported, the reference electrophiles **2a–c**, **3a–d**, and **4** used previously were employed in this study (Table 1). These references are easily handled, have absorption maxima monitorable in the presence of various NHCs, and cover a suitable range of electrophilicities.

Table 1. Reference *p*-Quinone Methides 2–4

electrophile (E)		R	E^a
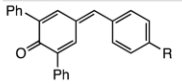	**2a**	H	−11.87
	b	OCH_3	−12.18
	c	$N(CH_3)_2$	−13.39
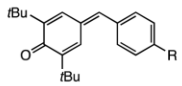	**3a**	NO_2	−14.36
	b	CH_3	−15.83
	c	OCH_3	−16.11
	d	$N(CH_3)_2$	−17.29
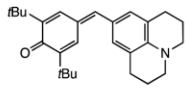	**4**	-	−17.90

[a]Electrophilicity parameters for **2–4** from refs 20b and 20c.

To demonstrate that the outcome of the reaction of NHCs **1a–d** with the reference electrophiles are the expected Michael adducts (i.e., **5a–d**), preparatory studies were undertaken (Scheme 1). Paralleling earlier reports, the reactions of NHCs **1a–d** with *p*-quinone methide **3b** gave the adducts **5a–d** in high yields as the only isolable products. Structural confirmation was obtained through regular spectroscopic methods as well as with single-crystal X-ray diffraction for **5d**. Having confirmed the formation of the expected adducts, attention was directed toward the rates of these reactions.

Scheme 1. Synthesis of 5a–d and X-ray Structure of 5d

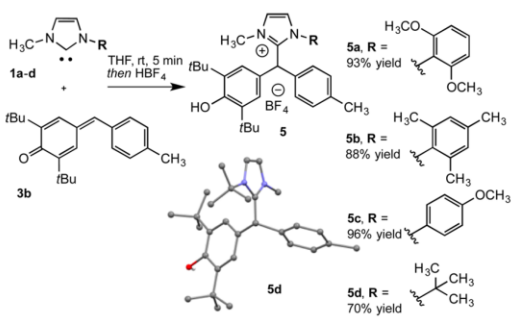

The reactions of NHCs **1a–d** with the reference *p*-quinone methides **2–4** were studied in THF at 20 °C by photometric monitoring of the disappearance of the colored quinone methides in the presence of a large excess of the NHC to achieve pseudo-first-order conditions. Least-squares fitting of the exponential function $A = A_0 \exp(-k_{obs}t) + C$ to the observed time-dependent absorbances A of the quinone methide provided the first-order rate constants k_{obs}. The slopes of the linear correlations between k_{obs} and the concentrations of **1** correspond to the second-order rate constants k_2 listed in Table 2. The rate constants k_2 were then used in association with the electrophilicity parameters of **2–4** to construct correlation lines for the four NHCs (Figure 2). As can be seen, in all cases good fits were obtained, which allowed the nucleophilicity parameters to be accurately determined.

Table 2. Second-Order Rate Constants and Nucleophilicity Parameters for the Reactions of NHCs 1a–d with Reference Electrophiles 2–4 in THF at 20 °C

NHC **1a-d**	E	k_2 [L mol^{-1} s^{-1}]	N, (s_N)
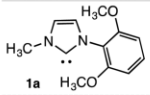 **1a**	**2b**	1.16×10^5	23.00
	2c	2.11×10^4	(0.46)
	3c	1.62×10^3	
	4	2.27×10^2	
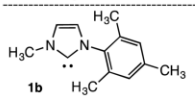 **1b**	**2a**	3.46×10^4	21.50
	2b	1.52×10^4	(0.45)
	2c	3.02×10^3	
	3a	5.62×10^3	
	3b	5.01×10^2	
	3c	3.15×10^2	
	3d	6.34×10^1	
	4	5.86×10^1	
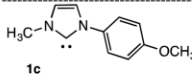 **1c**	**2b**	6.70×10^3	20.41
	2c	1.37×10^3	(0.46)
	4	1.41×10^1	
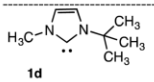 **1d**	**2b**	1.46×10^2	16.54
	2c	2.42×10^1	(0.47)
	3c	3.10	
	4	2.10×10^{-1}	

The nucleophilicities of these newly characterized carbenes can be compared with those of other NHCs and nucleophilic

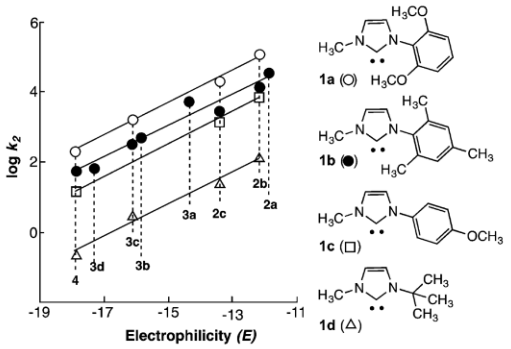

Figure 2. Correlations of log k_2 vs electrophilicity parameters for the reactions of NHCs **1a–d** with *p*-quinone methides **2–4**.

catalysts (Figure 3). From this comparison, it is clear that the nucleophilicity is heavily influenced by the nature of the N-

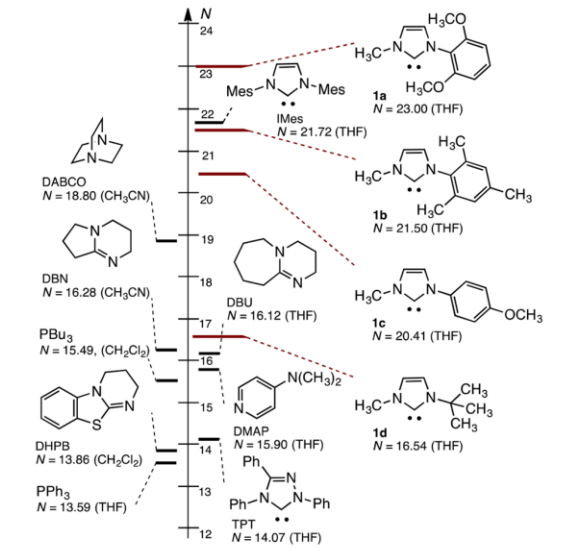

Figure 3. Nucleophilicities of **1a–d** and other catalysts.

substituent. Thus, the most nucleophilic of the NHCs bears an *N*-2,6-$(CH_3O)_2C_6H_3$ substituent (i.e., **1a**) and is more nucleophilic than IMes. The least nucleophilic is the *N*-*tert*-butyl NHC **1d**, which is only moderately more nucleophilic than the Enders carbene (TPT) and DBU. Interestingly, replacing a single mesityl substituent with a methyl group has little impact on the nucleophilicity of the catalyst (IMes, cf. **1b**). Finally, a *para* electron-donating substituent gives an NHC that is less nucleophilic than either the *N*-Mes NHC **1b** or the *N*-2,6-$(CH_3O)_2C_6H_3$ NHC **1a**.

In previous studies, the Lewis basicities of NHCs have been studied computationally because of an inability to determine equilibrium constants from their interactions with *p*-quinone methides. This is a result of their exceptionally high Lewis basicity. To allow Lewis basicity to be determined in this study, methyl cation affinities (MCAs), as defined in Figure 4, have been calculated for NHCs **1a–d** employing MP2/6-31+G-(2d,p)//B86/6-31G(d), a method previously shown to result in reliable MCAs.[13,21]

Most strikingly, we found that the *N*-2,6-$(CH_3O)_2C_6H_3$ substituent in **1a** led to the most Lewis basic catalyst, with an MCA some 28 kJ mol^{-1} higher than that of the variant bearing a single mesityl group (**1b**). Interestingly, the MCA of **1b** was 23 kJ mol^{-1} lower than that of IMes (MCA = 767 kJ mol^{-1}),[13] indicating that replacement of a mesityl group with a methyl

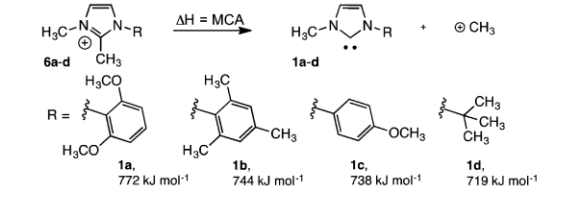

Figure 4. Gas-phase methyl cation affinities (MCAs) calculated at the MP2/6-31+G(2d,p)//B98/6-31G(d) level of theory.

group decreases the Lewis basicity while having little bearing on the nucleophilicity. In contrast, switching from a methyl substituent to a *tert*-butyl substituent has very little impact on the Lewis basicity (719 kJ mol^{-1} vs 718 kJ mol^{-1} for R = CH_3; Figure 4).[13] The dihedral angle between the imidazole and the aromatic N-substituent indicates significant twisting out of plane in both carbenes **1a** and **1b** (80.5° and 83.7°) and methyl imidazoles **6a** and **6b** (69.5° and 88.9°). While some planarization (**1a** → **6a**) is observed, it is not sufficient to allow through-space interactions of the *ortho* group and the azolium.

Studies from our group on NHC-catalyzed (4 + 2) annulations show significant sensitivity to the N-substituent.[9d–f] To further examine this sensitivity, the conversion of triene **7** to cycloadduct **8** was monitored over time using NHCs bearing the four N-substituents examined herein (Figure 5). Preliminary studies on

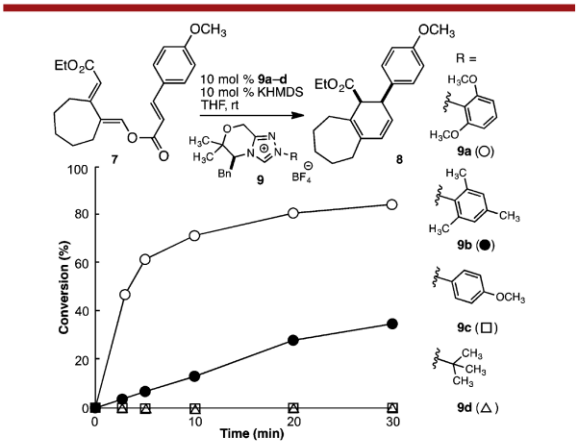

Figure 5. Conversion of ester **7** to diene **8** with catalysts **9a–d**.

imidazolium-derived NHCs were hampered by kinetic difficulties due to very high reaction rates. In contrast, monitoring with the triazolium series of NHCs demonstrated that the reaction is successful with the most nucleophilic triazolium-derived catalysts **9a** and **9b** and fails with N-substituents associated with the least nucleophilic NHCs. These results are consistent with our observations that NHC addition to esters is significantly more challenging than that to aldehydes. The success or failure of this reaction is correlated with the catalyst nucleophilicity and not its Lewis basicity, with catalyst **9b** likely to display similar Lewis basicity to **9c** but giving a significantly different reaction outcome.

The capacity of NHCs to enable reactions that are unattainable with other nucleophilic catalysts is associated with their unique Lewis basicity and nucleophilicity profiles. As applications of NHCs in organocatalysis develop, the capacity to modulate these properties takes on increasing importance. In recent years, the N-substituents examined in this report have allowed new discoveries in NHC catalysis. Herein we report that the *N*-2,6-$(CH_3O)_2C_6H_3$ substituent gives one of the most nucleophilic and Lewis basic NHC catalysts, while the impact of remote electron-donating groups on the NHC properties is modest. Finally, hindered alkyl groups give one of the least nucleophilic and Lewis basic NHCs.

The studies reported herein demonstrate that the N-substituent plays a significant role in defining catalyst nucleophilicity. Together with the known role of heterocycle selection in nucleophilicity,[13] these studies demonstrate that

significant variation in catalyst properties is possible by manipulation of these two parameters.

■ ASSOCIATED CONTENT

Supporting Information

The Supporting Information is available free of charge on the ACS Publications website at DOI: 10.1021/acs.orglett.6b01525.

Procedures and additional data (PDF)

■ AUTHOR INFORMATION

Corresponding Author

*E-mail: david.lupton@monash.edu.

Notes

The authors declare no competing financial interest.

■ ACKNOWLEDGMENTS

The authors acknowledge financial support from the Australian Research Council (DP150101522 and FT110100319), the Deutsche Forschungsgemeinschaft (SFB 749, Project B1), the Fonds der Chemischen Industrie (Liebig Scholarship to M.B.), and the Alexander von Humboldt Foundation (Ludwig Leichardt Memorial Fellowship to D.W.L.). We are grateful to Ms. Nathalie Hampel (LMU) for synthesizing the reference electrophiles and Dr. Peter Mayer (LMU) for the X-ray analysis. This work used the DFG-funded Cologne High Efficiency Operating Platform for Sciences (CHEOPS).

■ REFERENCES

(1) For selected recent reviews of NHC catalysis, see: (a) Enders, D.; Niemeier, O.; Henseler, A. *Chem. Rev.* **2007**, *107*, 5606. (b) Douglas, J.; Churchill, G.; Smith, A. D. *Synthesis* **2012**, *44*, 2295. (c) Bugaut, X.; Glorius, F. *Chem. Soc. Rev.* **2012**, *41*, 3511. (d) Izquierdo, J.; Hutson, G. E.; Cohen, D. T.; Scheidt, K. A. *Angew. Chem., Int. Ed.* **2012**, *51*, 11686. (e) Ryan, S. J.; Candish, L.; Lupton, D. W. *Chem. Soc. Rev.* **2013**, *42*, 4906. (f) Hopkinson, M. N.; Richter, C.; Schedler, M.; Glorius, F. *Nature* **2014**, *510*, 485. (g) Chauhan, P.; Enders, D. *Angew. Chem., Int. Ed.* **2014**, *53*, 1485. (h) Flanigan, D. M.; Romanov-Michailidis; White, N. A.; Rovis, T. *Chem. Rev.* **2015**, *115*, 9307.

(2) For the seminal contributions of Breslow and Ukai, see: Breslow, R. *J. Am. Chem. Soc.* **1958**, *80*, 3719 and references therein.

(3) Early examples of homolenolate chemistry: (a) Sohn, S. S.; Rosen, E. L.; Bode, J. W. *J. Am. Chem. Soc.* **2004**, *126*, 14370. (b) Burstein, C.; Glorius, F. *Angew. Chem., Int. Ed.* **2004**, *43*, 6205.

(4) Early examples of unsaturated acyl azolium chemistry: (a) Zeitler, K. *Org. Lett.* **2006**, *8*, 637. (b) Maki, B. E.; Chan, A.; Phillips, E. M.; Scheidt, K. A. *Org. Lett.* **2007**, *9*, 371. (c) Ryan, S. J.; Candish, L.; Lupton, D. W. *J. Am. Chem. Soc.* **2009**, *131*, 14176. (d) De Sarkar, S.; Studer, A. *Angew. Chem., Int. Ed.* **2010**, *49*, 9266.

(5) Early acyl azolium enolate/enol chemistry: (a) Chow, K. Y.-K.; Bode, J. W. *J. Am. Chem. Soc.* **2004**, *126*, 8126. (b) Reynolds, N. T.; Read de Alaniz, J.; Rovis, T. *J. Am. Chem. Soc.* **2004**, *126*, 9518.

(6) For reaction design with different nucleophilic catalysts, see: Candish, L.; Nakano, Y.; Lupton, D. W. *Synthesis* **2014**, *46*, 1823.

(7) (a) Rovis, T. *Chem. Lett.* **2008**, *37*, 2. (b) Mahatthananchai, J.; Bode, J. W. *Chem. Sci.* **2012**, *3*, 192. (c) Collett, C. J.; Massey, R. S.; Maguire, O. R.; Batsanov, A. S.; O'Donoghue, A. C.; Smith, A. D. *Chem. Sci.* **2013**, *4*, 1514. (d) Collett, C. J.; Massey, R. S.; Taylor, J. E.; Maguire, O. R.; O'Donoghue, A. C.; Smith, A. D. *Angew. Chem., Int. Ed.* **2015**, *54*, 6887.

(8) For selected mechanistic contributions to the field, see: (a) Paul, M.; Breugst, M.; Neudörfl, J.-M.; Sunoj, R. B.; Berkessel, A. *J. Am. Chem. Soc.* **2016**, *138*, 5044. (b) Yatham, V. R.; Neudörfl, J.-M.; Schlörer, N. E.; Berkessel, A. *Chem. Sci.* **2015**, *6*, 3706. (c) Berkessel, A.; Yatham, V. R.; Elfert, S.; Neudörfl, J.-M. *Angew. Chem., Int. Ed.* **2013**, *52*, 11158. (d) Berkessel, A.; Elfert, S.; Etzenbach-Effers, K.; Teles, J. H. *Angew. Chem., Int. Ed.* **2010**, *49*, 7120. (e) Zhao, X.; Glover, G. S.; Oberg, K. M.; Dalton, D. M.; Rovis, T. *Synlett* **2013**, *24*, 1229. (f) Moore, J. L.; Silvestri, A. P.; Read de Alaniz, J.; DiRocco, D. A.; Rovis, T. *Org. Lett.* **2011**, *13*, 1742. (g) Cohen, D. T.; Johnston, R. C.; Rosson, N. T.; Cheong, P. H.-Y.; Scheidt, K. A. *Chem. Commun.* **2015**, *51*, 2690. (h) Johnston, R. C.; Cohen, D. T.; Eichman, C. C.; Scheidt, K. A.; Cheong, P. H.-Y. *Chem. Sci.* **2014**, *5*, 1974. (i) Samanta, R. C.; Maji, B.; De Sarkar, S.; Bergander, K.; Fröhlich, R.; Mück-Lichtenfeld, C.; Mayr, H.; Studer, A. *Angew. Chem., Int. Ed.* **2012**, *51*, 5234. (j) Ryan, S. J.; Stasch, A.; Paddon-Row, M. N.; Lupton, D. W. *J. Org. Chem.* **2012**, *77*, 1113.

(9) For selected studies with esters from our group, see: (a) Reference 4c. (b) Kowalczyk, M.; Lupton, D. W. *Angew. Chem., Int. Ed.* **2014**, *53*, 5314. (c) Candish, L.; Levens, A.; Lupton, D. W. *J. Am. Chem. Soc.* **2014**, *136*, 14397. (d) Candish, L.; Levens, A.; Lupton, D. W. *Chem. Sci.* **2015**, *6*, 2366. (e) Levens, A.; Zhang, C.; Candish, L.; Forsyth, C. M.; Lupton, D. W. *Org. Lett.* **2015**, *17*, 5332. For selected studies using activated acids, see: (f) Ryan, S. J.; Candish, L.; Lupton, D. W. *J. Am. Chem. Soc.* **2011**, *133*, 4694. (g) Candish, L.; Lupton, D. W. *J. Am. Chem. Soc.* **2013**, *135*, 58. (h) Candish, L.; Forsyth, C. M.; Lupton, D. W. *Angew. Chem., Int. Ed.* **2013**, *52*, 9149.

(10) For examples from Chi's group that demonstrate sensitivity to the N-substituent, see: (a) Hao, L.; Chen, S.; Xu, J.; Tiwari, B.; Fu, Z.; Li, T.; Lim, J.; Chi, Y. R. *Org. Lett.* **2013**, *15*, 4956. (b) Xu, J.; Jin, Z.; Chi, Y. R. *Org. Lett.* **2013**, *15*, 5028. (c) Chen, S.; Hao, L.; Zhang, Y.; Tiwari, B.; Chi, Y. R. *Org. Lett.* **2013**, *15*, 5822.

(11) For recent reports on NHC catalysis via anhydrides, see: (a) Lee, A.; Younai, A.; Price, C. K.; Izquierdo, J.; Mishra, R. K.; Scheidt, K. A. *J. Am. Chem. Soc.* **2014**, *136*, 10589. (b) Chen, X.-Y.; Gao, Z.-H.; Song, C.-Y.; Zhang, C.-L.; Wang, Z.-X.; Ye, S. *Angew. Chem., Int. Ed.* **2014**, *53*, 11611. (c) Jin, Z.; Chen, S.; Wang, Y.; Zheng, P.; Yang, S.; Chi, Y. R. *Angew. Chem., Int. Ed.* **2014**, *53*, 13506.

(12) For a review of NHC properties, see: (a) Dröge, T.; Glorius, F. *Angew. Chem., Int. Ed.* **2010**, *49*, 6940. For computational studies on π-acidity, see: (b) Andrada, D. M.; Holzmann, N.; Hamadi, T.; Frenking, G. *Beilstein J. Org. Chem.* **2015**, *11*, 2727 and references therein..

(13) Maji, B.; Breugst, M.; Mayr, H. *Angew. Chem., Int. Ed.* **2011**, *50*, 6915.

(14) For a review of the use of this scale in organocatalysis, see: Mayr, H.; Lakhdar, S.; Maji, B.; Ofial, A. R. *Beilstein J. Org. Chem.* **2012**, *8*, 1458.

(15) For the *N*-2,6-$(CH_3O)_2C_6H_3$ group, see: Liu, F.; Bugaut, X.; Schedler, M.; Fröhlich, R.; Glorius, F. *Angew. Chem., Int. Ed.* **2011**, *50*, 12626.

(16) For the *N*-2,4,6-$(CH_3)_3C_6H_2$ group in enantioselective NHC organocatalysis, see: He, M.; Struble, J. R.; Bode, J. W. *J. Am. Chem. Soc.* **2006**, *128*, 8418.

(17) For the *N*-4-$CH_3OC_6H_4$ group in enantioselective catalysis, see: Nakano, Y.; Lupton, D. W. *Angew. Chem., Int. Ed.* **2016**, *55*, 3135.

(18) The *N*-C_6F_5 group, which is exploited extensively in acyl anion chemistry, was also examined, but difficulties in preparing the carbene in high purity precluded its inclusion in this study.

(19) (a) Mayr, H.; Patz, M. *Angew. Chem., Int. Ed. Engl.* **1994**, *33*, 938. (b) Mayr, H.; Bug, T.; Gotta, M. F.; Hering, N.; Irrgang, B.; Janker, B.; Kempf, B.; Loos, R.; Ofial, A. R.; Remennikov, G.; Schimmel, H. *J. Am. Chem. Soc.* **2001**, *123*, 9500. (c) Mayr, H.; Ofial, A. R. *J. Phys. Org. Chem.* **2008**, *21*, 584.

(20) (a) Access to all constants is provided at: Mayr, H. Database of Nucleophilicties and Electrophilicities. http://www.cup.uni-muenchen.de/oc/mayr/DBintro.html (accessed July 3, 2016). (b) For quinone methides **2b–c**, **3b–d** and **4**, see: Lucius, R.; Loos, R.; Mayr, H. *Angew. Chem., Int. Ed.* **2002**, *41*, 91. (c) For quinone methides **2a** and **3a**, see: Richter, D.; Hampel, N.; Singer, T.; Ofial, A. R.; Mayr, H. *Eur. J. Org. Chem.* **2009**, *2009*, 3203.

(21) (a) Wei, Y.; Sastry, G. N.; Zipse, H. *J. Am. Chem. Soc.* **2008**, *130*, 3473. (b) Wei, Y.; Singer, T.; Mayr, H.; Sastry, G. N.; Zipse, H. *J. Comput. Chem.* **2008**, *29*, 291. (c) Lindner, C.; Maryasin, B.; Richter, F.; Zipse, H. *J. Phys. Org. Chem.* **2010**, *23*, 1036.

– Experimental Section–

Kinetics

Kinetics of the reaction of **1a** with **4** at 20°C in THF (diode array, λ = 492 nm)

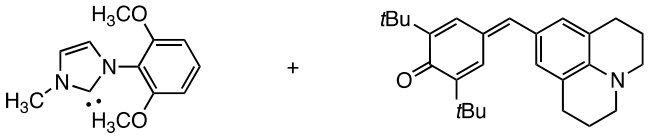

[**1a**] (mol L^{-1})	[**4**] (mol L^{-1})	k_{obs} (s^{-1})
5.90×10^{-4}	3.67×10^{-5}	1.05×10^{-1}
8.84×10^{-4}	3.67×10^{-5}	1.64×10^{-1}
1.20×10^{-3}	3.64×10^{-5}	2.51×10^{-1}
1.78×10^{-3}	3.58×10^{-5}	3.71×10^{-1}

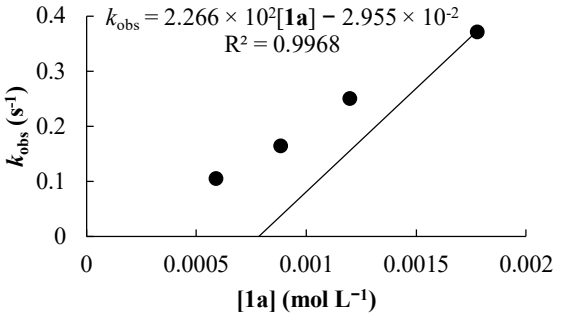

$k_2 = 2.27 \times 10^2$ L mol^{-1} s^{-1}

Kinetics of the reaction of **1a** with **3c** at 20°C in THF (stopped-flow, λ = 430 nm)

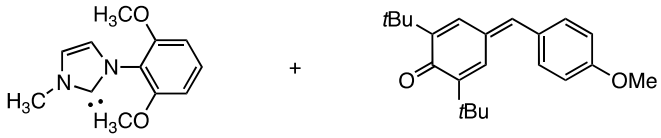

[**1a**] (mol L^{-1})	[**3c**] (mol L^{-1})	k_{obs} (s^{-1})
9.11×10^{-4}	9.55×10^{-5}	1.15
1.21×10^{-3}	9.55×10^{-5}	1.71
1.82×10^{-3}	9.55×10^{-5}	2.77
2.13×10^{-3}	9.55×10^{-5}	3.11
2.43×10^{-3}	9.55×10^{-5}	3.65

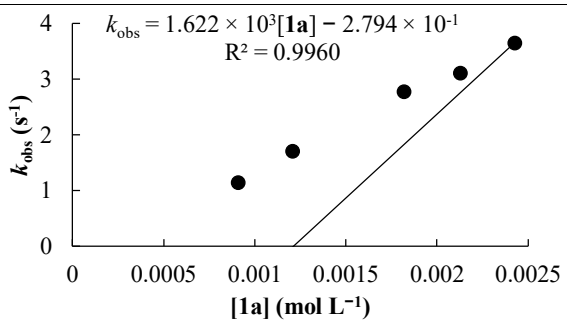

$k_2 = 1.62 \times 10^3$ L mol^{-1} s^{-1}

Kinetics of the reaction of **1a** with **2c** at 20°C in THF (stopped-flow, λ = 499 nm)

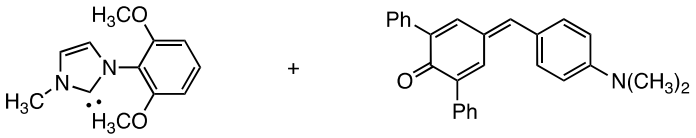

[**1a**] (mol L^{-1})	[**2c**] (mol L^{-1})	k_{obs} (s^{-1})
4.79×10^{-4}	2.74×10^{-5}	5.71
7.19×10^{-4}	2.74×10^{-5}	1.06×10^{1}
9.58×10^{-4}	2.74×10^{-5}	1.60×10^{1}
1.20×10^{-3}	2.74×10^{-5}	2.22×10^{1}
1.68×10^{-3}	2.74×10^{-5}	3.06×10^{1}

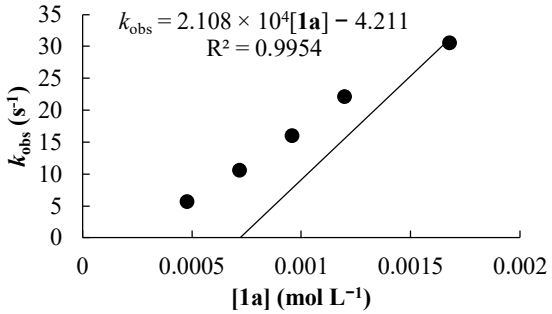

k_2 = 2.11 × 10^4 L mol^{-1} s^{-1}

Kinetics of the reaction of **1a** with **2b** at 20°C in THF (stopped-flow, λ = 450 nm)

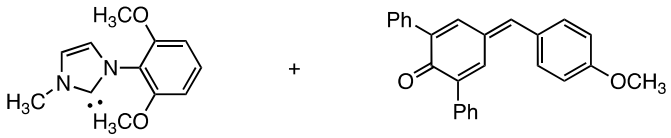

[**1a**] (mol L^{-1})	[**2b**] (mol L^{-1})	k_{obs} (s^{-1})
6.02×10^{-4}	5.30×10^{-5}	5.28×10^{1}
9.02×10^{-4}	5.30×10^{-5}	8.79×10^{1}
1.50×10^{-3}	5.30×10^{-5}	1.47×10^{2}
1.80×10^{-3}	5.30×10^{-5}	1.94×10^{2}
2.11×10^{-3}	5.30×10^{-5}	2.29×10^{2}

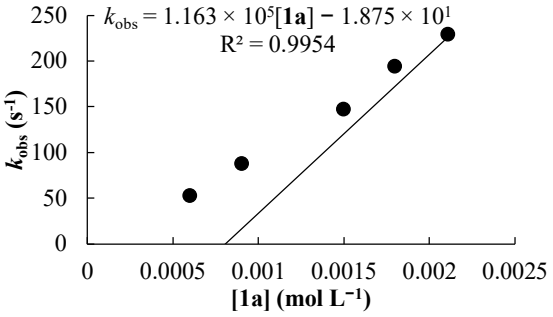

k_2 = 1.16 × 10^5 L mol^{-1} s^{-1}

Determination of the parameters *N* and s_N for **1a** in THF

Electrophile	*E*	k_2 (L mol^{-1} s^{-1})
2b	–12.18	1.16×10^{5}
2c	–13.39	2.11×10^{4}
3c	–16.11	1.62×10^{3}
4	–17.90	2.27×10^{2}

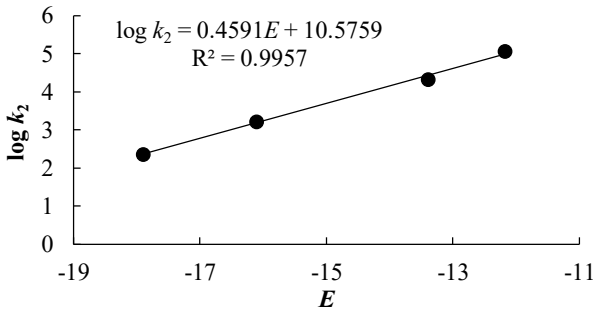

***N* = 23.00**

s_N = 0.46

Kinetics of the reaction of **1b** with **4** at 20°C in THF (diode array, λ = 490 nm)

[**1b**] (mol L^{-1})	[**4**] (mol L^{-1})	k_{obs} (s^{-1})
6.53×10^{-4}	5.49×10^{-5}	3.52×10^{-2}
8.00×10^{-4}	4.48×10^{-5}	4.25×10^{-2}
1.04×10^{-3}	4.37×10^{-5}	5.63×10^{-2}
1.47×10^{-3}	4.94×10^{-5}	8.61×10^{-2}
1.71×10^{-3}	4.80×10^{-5}	9.44×10^{-2}

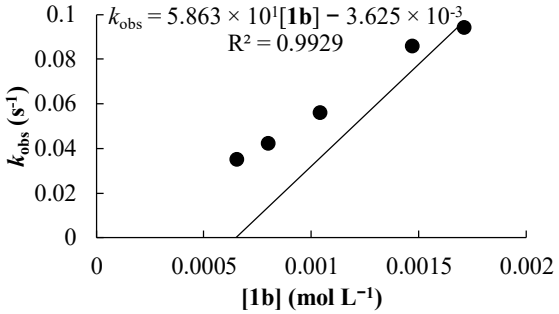

$k_2 = 5.86 \times 10^1$ L mol^{-1} s^{-1}

Kinetics of the reaction of **1b** with **3d** at 20°C in THF (stopped-flow, λ = 486 nm)

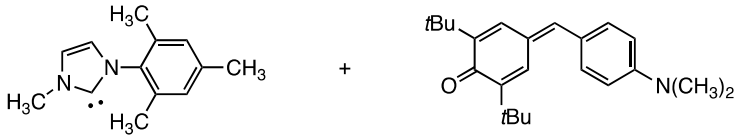

[**1b**] (mol L^{-1})	[**3d**] (mol L^{-1})	k_{obs} (s^{-1})
2.43×10^{-3}	6.32×10^{-5}	1.31×10^{-1}
3.65×10^{-3}	6.32×10^{-5}	2.28×10^{-1}
4.86×10^{-3}	6.32×10^{-5}	3.04×10^{-1}
6.08×10^{-3}	6.32×10^{-5}	3.76×10^{-1}
7.29×10^{-3}	6.32×10^{-5}	4.42×10^{-1}

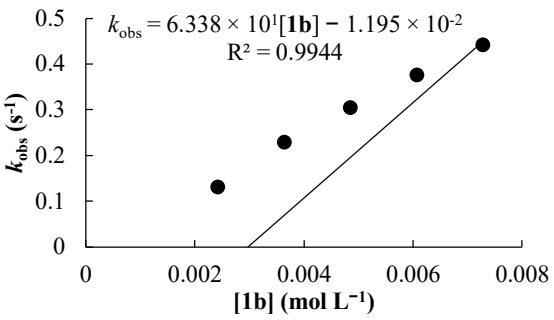

$k_2 = 6.34 \times 10^1$ L mol^{-1} s^{-1}

Kinetics of the reaction of **1b** with **3c** at 20°C in THF (stopped-flow, λ = 390 nm)

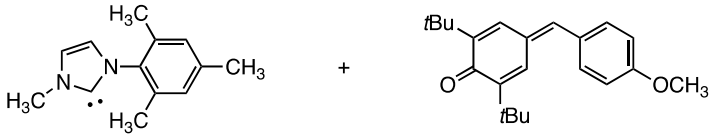

[**1b**] (mol L^{-1})	[**3c**] (mol L^{-1})	k_{obs} (s^{-1})
1.70×10^{-3}	6.90×10^{-5}	4.85×10^{-1}
2.55×10^{-3}	6.90×10^{-5}	7.61×10^{-1}
3.41×10^{-3}	6.90×10^{-5}	1.03×10^{-1}
4.26×10^{-3}	6.90×10^{-5}	1.30×10^{-1}
5.11×10^{-3}	6.90×10^{-5}	1.56×10^{-1}

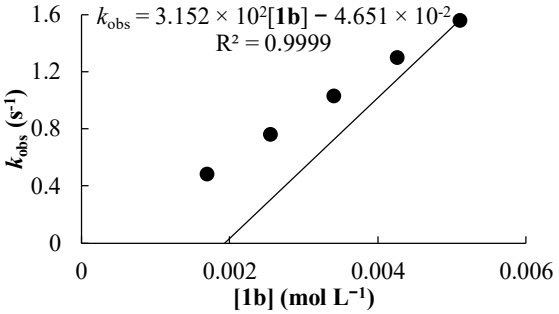

$k_2 = 3.15 \times 10^2$ L mol^{-1} s^{-1}

Kinetics of the reaction of **1b** with **3b** at 20°C in THF (stopped-flow, λ = 375 nm)

[**1b**] (mol L^{-1})	[**3b**] (mol L^{-1})	k_{obs} (s^{-1})
1.32×10^{-3}	7.56×10^{-5}	5.92×10^{-1}
1.98×10^{-3}	7.56×10^{-5}	8.85×10^{-1}
2.65×10^{-3}	7.56×10^{-5}	1.25
3.31×10^{-3}	7.56×10^{-5}	1.58

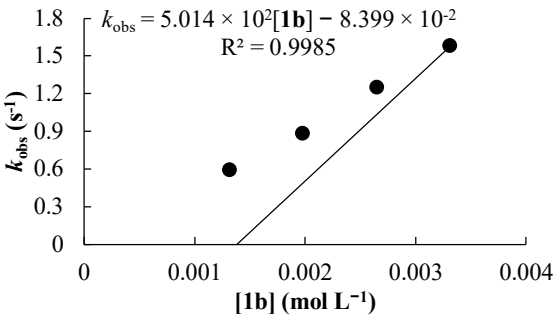

$k_2 = 5.01 \times 10^2$ L mol^{-1} s^{-1}

Kinetics of the reaction of **1b** with **3a** at 20°C in THF (stopped-flow, λ = 375 nm)

[**1b**] (mol L^{-1})	[**3a**] (mol L^{-1})	k_{obs} (s^{-1})
9.79×10^{-4}	9.43×10^{-5}	4.89
1.47×10^{-3}	9.43×10^{-5}	7.68
1.96×10^{-3}	9.43×10^{-5}	10.3
2.45×10^{-3}	9.43×10^{-5}	13.4
2.94×10^{-3}	9.43×10^{-5}	15.8

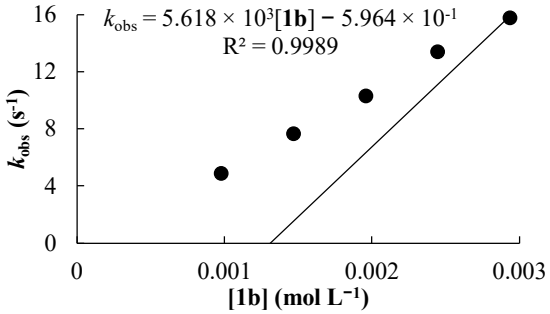

$k_2 = 5.62 \times 10^3$ L mol^{-1} s^{-1}

Kinetics of the reaction of **1b** with **2c** at 20°C in THF (stopped-flow, λ = 499 nm)

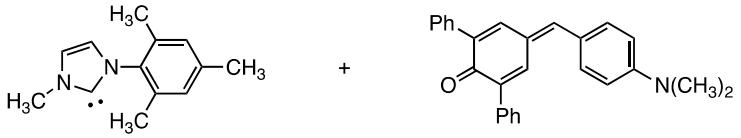

[**1b**] (mol L^{-1})	[**2c**] (mol L^{-1})	k_{obs} (s^{-1})
9.74×10^{-4}	5.51×10^{-5}	2.47
1.46×10^{-3}	5.51×10^{-5}	4.04
1.95×10^{-3}	5.51×10^{-5}	5.46
2.43×10^{-3}	5.51×10^{-5}	6.93
2.92×10^{-3}	5.51×10^{-5}	8.37

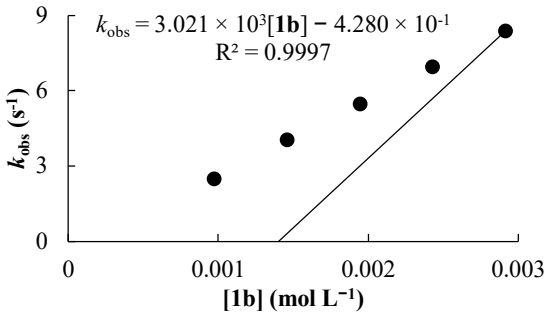

$k_2 = 3.02 \times 10^3$ L mol^{-1} s^{-1}

Kinetics of the reaction of **1b** with **2b** at 20°C in THF (stopped-flow, λ = 411 nm)

[**1b**] (mol L^{-1})	[**2b**] (mol L^{-1})	k_{obs} (s^{-1})
7.99×10^{-4}	6.86×10^{-5}	1.10×10^{1}
1.20×10^{-3}	6.86×10^{-5}	1.74×10^{1}
1.60×10^{-3}	6.86×10^{-5}	2.32×10^{1}
2.00×10^{-3}	6.86×10^{-5}	2.92×10^{1}
2.40×10^{-3}	6.86×10^{-5}	3.55×10^{1}

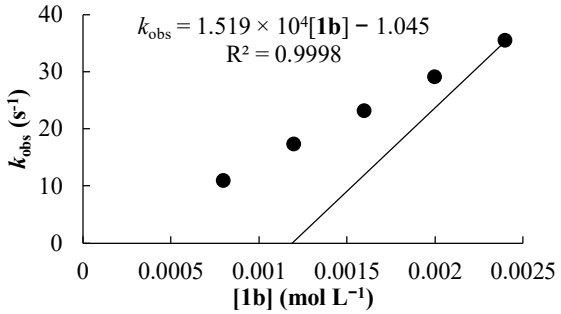

$k_2 = 1.52 \times 10^4$ L mol^{-1} s^{-1}

Kinetics of the reaction of **1b** with **2a** at 20°C in THF (stopped-flow, λ = 375 nm)

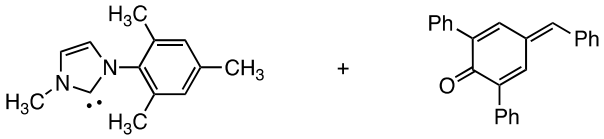

[**1b**] (mol L^{-1})	[**2a**] (mol L^{-1})	k_{obs} (s^{-1})
6.04×10^{-4}	6.44×10^{-5}	1.98×10^{1}
9.06×10^{-4}	6.44×10^{-5}	3.11×10^{1}
1.21×10^{-3}	6.44×10^{-5}	4.18×10^{1}
1.51×10^{-3}	6.44×10^{-5}	5.27×10^{1}
1.81×10^{-3}	6.44×10^{-5}	6.11×10^{1}

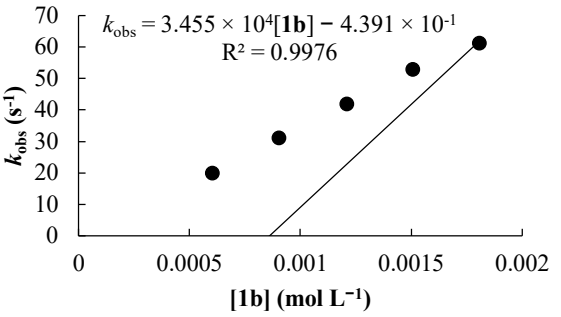

$k_2 = 3.46 \times 10^4$ L mol^{-1} s^{-1}

Determination of the parameters N and s_N for **1b** in THF

Electrophile	E	k_2 (L mol^{-1} s^{-1})
2a	–11.87	3.46×10^4
2b	–12.18	1.52×10^4
2c	–13.39	3.02×10^3
3a	–14.36	5.62×10^3
3b	–15.83	5.01×10^2
3c	–16.11	3.15×10^2
3d	–17.29	6.34×10^1
4	–17.90	5.86×10^1

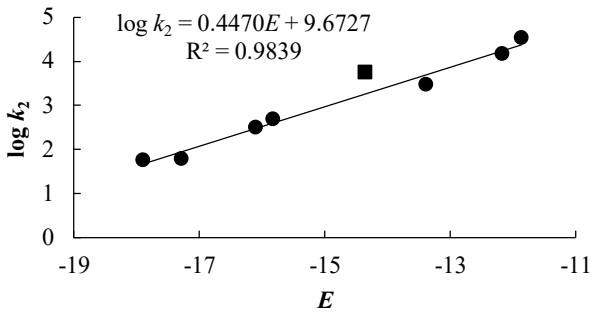

N = 21.50

s_N = 0.45

Kinetics of the reaction of **1c** with **4** at 20°C in THF (diode array, λ = 492 nm)

[**1c**] (mol L^{-1})	[**4**] (mol L^{-1})	k_{obs} (s^{-1})
6.57×10^{-4}	3.58×10^{-5}	9.02×10^{-3}
9.86×10^{-4}	3.52×10^{-5}	1.39×10^{-2}
1.41×10^{-3}	3.54×10^{-5}	1.91×10^{-2}
2.11×10^{-3}	3.49×10^{-5}	2.93×10^{-2}
2.62×10^{-3}	3.54×10^{-5}	3.68×10^{-2}

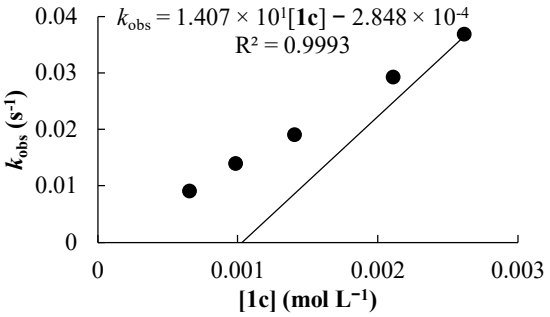

k_2 = 1.41 × 10^1 L mol^{-1} s^{-1}

Kinetics of the reaction of **1c** with **2c** at 20°C in THF (stopped-flow, λ = 499 nm)

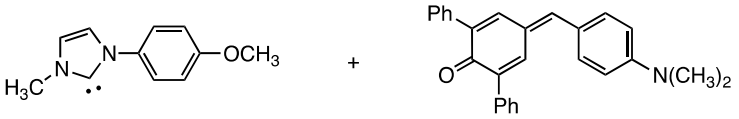

[**1c**] (mol L^{-1})	[**2c**] (mol L^{-1})	k_{obs} (s^{-1})
6.08×10^{-4}	3.86×10^{-5}	5.56×10^{-1}
9.12×10^{-4}	3.86×10^{-5}	9.25×10^{-1}
1.22×10^{-3}	3.86×10^{-5}	1.29
1.52×10^{-3}	3.86×10^{-5}	1.78
1.82×10^{-3}	3.86×10^{-5}	2.21
2.13×10^{-3}	3.86×10^{-5}	2.85

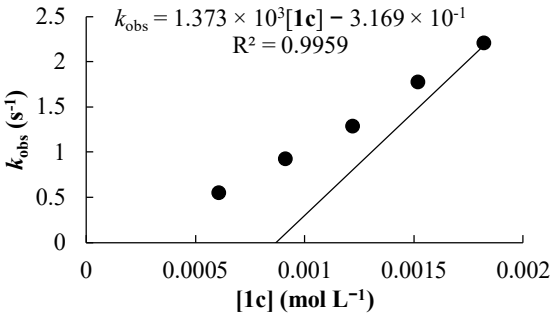

k_2 = 1.37 × 10^3 L mol^{-1} s^{-1}

Kinetics of the reaction of **1c** with **2b** at 20°C in THF (stopped-flow, λ = 411 nm)

[**1c**] (mol L^{-1})	[**2b**] (mol L^{-1})	k_{obs} (s^{-1})
5.92×10^{-4}	2.34×10^{-5}	1.99
8.89×10^{-4}	2.34×10^{-5}	3.57
1.18×10^{-3}	2.34×10^{-5}	5.70
1.48×10^{-3}	2.34×10^{-5}	7.41
1.78×10^{-3}	2.34×10^{-5}	1.00×10^1
2.07×10^{-3}	2.34×10^{-5}	1.30×10^1

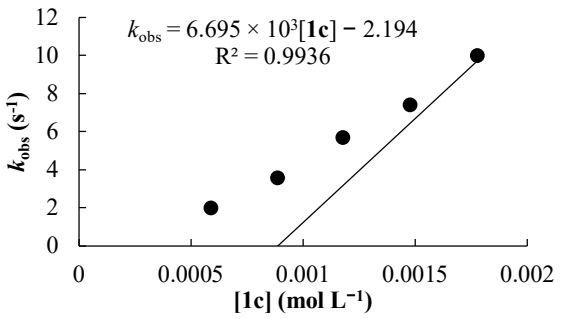

k_2 = 6.70 × 10^3 L mol^{-1} s^{-1}

Determination of the parameters *N* and s_N for **1c** in THF

Electrophile	*E*	k_2 (L mol^{-1} s^{-1})
2b	–12.18	6.70×10^3
2c	–13.39	1.37×10^3
4	–17.90	1.41×10^1

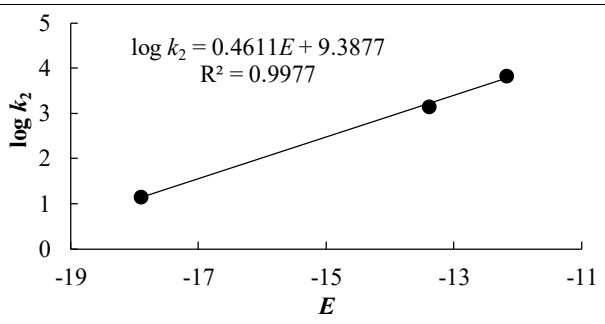

***N* = 20.41**

s_N = 0.46

Kinetics of the reaction of **1d** with **4** at 20°C in THF (diode array, λ = 492 nm)

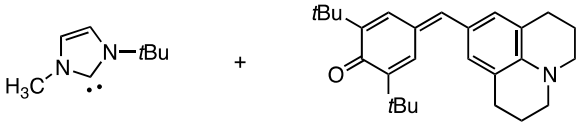

[**1d**] (mol L^{-1})	[**4**] (mol L^{-1})	k_{obs} (s^{-1})
3.86×10^{-3}	5.04×10^{-5}	8.05×10^{-4}
5.97×10^{-3}	8.18×10^{-5}	1.21×10^{-3}
6.87×10^{-3}	5.44×10^{-5}	1.35×10^{-3}
8.47×10^{-3}	5.82×10^{-5}	1.79×10^{-3}

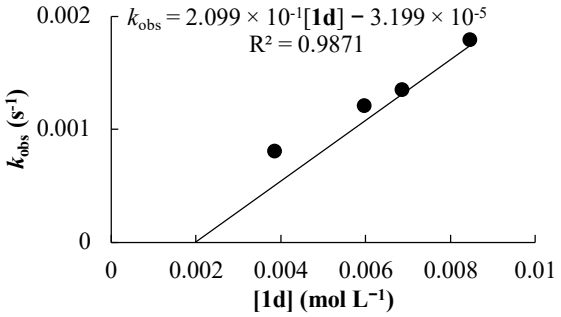

k_2 = 2.10 × 10^{-1} L mol^{-1} s^{-1}

Kinetics of the reaction of **1d** with **3c** at 20°C in THF (diode array, λ = 384 nm)

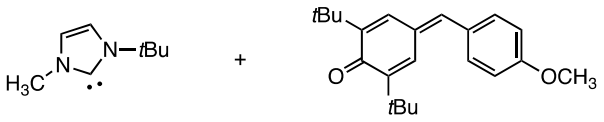

[**1d**] (mol L^{-1})	[**3c**] (mol L^{-1})	k_{obs} (s^{-1})
3.50×10^{-4}	4.08×10^{-5}	1.16×10^{-3}
9.51×10^{-4}	6.79×10^{-5}	2.97×10^{-3}
1.40×10^{-3}	6.66×10^{-5}	4.50×10^{-3}
1.77×10^{-3}	5.79×10^{-5}	5.52×10^{-3}

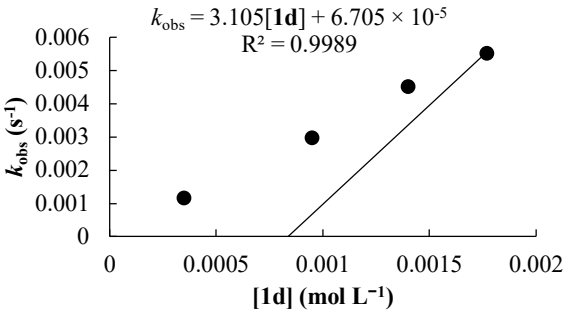

k_2 = 3.10 L mol^{-1} s^{-1}

Kinetics of the reaction of **1d** with **2c** at 20°C in THF (diode array, λ = 499 nm)

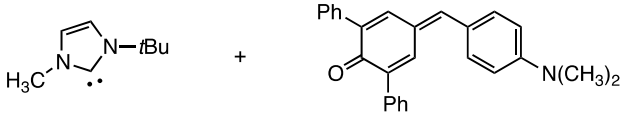

[**1d**] (mol L^{-1})	[**2c**] (mol L^{-1})	k_{obs} (s^{-1})
7.30×10^{-4}	4.48×10^{-5}	1.68×10^{-2}
1.02×10^{-3}	5.38×10^{-5}	2.04×10^{-2}
1.24×10^{-3}	4.91×10^{-5}	2.98×10^{-2}
1.84×10^{-3}	5.80×10^{-5}	4.39×10^{-2}
1.99×10^{-3}	5.25×10^{-5}	4.73×10^{-2}

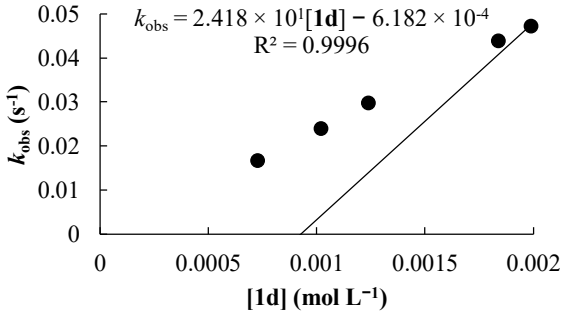

k_2 = 2.42 × 10^{1} L mol^{-1} s^{-1}

Kinetics of the reaction of **1d** with **2b** at 20°C in THF (stopped-flow, λ = 411 nm)

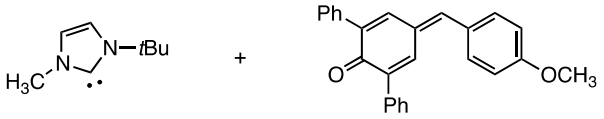

[**1d**] (mol L^{-1})	[**2b**] (mol L^{-1})	k_{obs} (s^{-1})
7.49×10^{-4}	4.46×10^{-5}	6.94×10^{-2}
1.12×10^{-3}	4.46×10^{-5}	1.30×10^{-1}
1.50×10^{-3}	4.46×10^{-5}	1.77×10^{-1}
1.87×10^{-3}	4.46×10^{-5}	2.45×10^{-1}
2.25×10^{-3}	4.46×10^{-5}	2.91×10^{-1}
2.62×10^{-3}	4.46×10^{-5}	3.42×10^{-1}

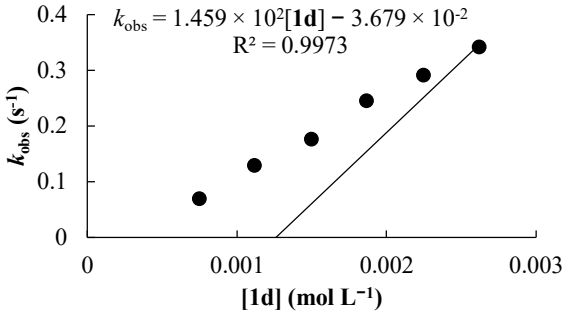

k_2 = 1.46 × 10^2 L mol^{-1} s^{-1}

Determination of the parameters *N* and s_N for **1d** in THF

Electrophile	*E*	k_2 (L mol^{-1} s^{-1})
2b	–12.18	1.46×10^2
2c	–13.39	2.42×10^1
3c	–16.11	3.10
4	–17.90	2.10×10^{-1}

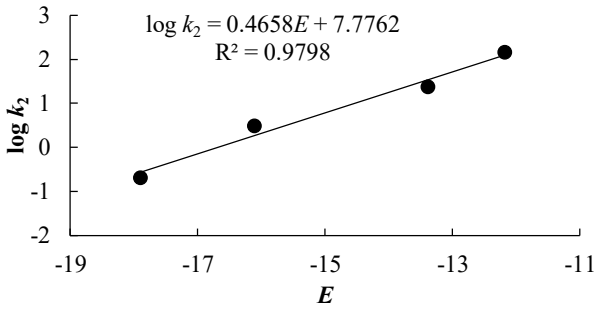

***N* = 16.54**

s_N = 0.47

Appendix 4 Published work 4

Top. Catal. **2018**, *61*, 585–590.

Quantification of the Michael-Acceptor Reactivity of *α,β*-Unsaturated Acyl Azolium Ions

Alison Levens[1] · Feng An[2] · Jared E. M. Fernando[1] · Armin R. Ofial[2] · David W. Lupton[1] · Herbert Mayr[2]

Published online: 9 April 2018

Abstract
2-Cinnamoylimidazolium ions **4** have been synthesized by treatment of 2-cinnamoylimidazoles **8** with methyl triflate. They were characterised by NMR and mass spectroscopy, in one case (**4f**) also by X-ray analysis. The kinetics of their reactions [and also those of cinnamoyl fluoride (**1**)] with stabilised carbanions **9a–e** and silyl ketene acetal **9f** (reference nucleophiles) were measured photometrically. The correlation log $k(20\ °C) = s_N\,(E + N)$ was used to calculate the electrophilicity parameters E of the cinnamoyl azolium ions **4** from the resulting second-order rate constants k and the previously reported N and s_N parameters of the reference nucleophiles **9**. All 2-cinnamoylimidazolium ions **4** were found to be 2–4 orders of magnitude more electrophilic than cinnamoyl fluoride (**1**) showing that the direct attack of nucleophiles at **1** can be avoided if sufficient concentrations of **4** are produced in the NHC-catalysed reactions of **1** with nucleophiles. From the range of electrophilicity($-12 < E < -10$) for the cinnamoylimidazolium ions **4** one can derive that only nucleophiles stronger than $N \approx 7$ will react with **4** at 20 °C in reasonable time, suggesting that in NHC-catalysed reactions of cinnamoyl fluoride (**1**) with silyl enol ethers (typically $4 < N < 7$), enolate ions, produced by fluoride-induced desilylation of silyl enol ethers, are the active nucleophiles.

Keywords Kinetics · Organocatalysis · Nucleophilic carbenes · Reactivity · Electrophilicity

1 Introduction

N-Heterocyclic carbenes (NHCs) have been used as catalysts for numerous C–C bond forming reactions [1–17]. Several of these transformations proceed via intermediate acyl azolium ions, a field of great current interest [13, 14, 18–45]. In 2009, Lupton et al. reported the N-heterocyclic carbene (NHC) catalysed annulation of α,β-unsaturated acyl fluorides (**1**) with trialkylsilyl enol ethers (**2**) to afford dihydropyranones (**3**) (Scheme 1) [18].

In addition to defining a new approach to α,β-unsaturated acyl azoliums (**4**), these studies allowed the first β-additions to these intermediates [18–24]. Subsequent studies by the Monash group and others have uncovered annulations of the α,β-unsaturated acyl azolium with alternate *di*-nucleophiles or bifunctional partners ([18–24]; for selected annulations with bifunctional partners, [25–32]).

A plausible mechanism for this reaction is depicted in Scheme 1. The reaction of the NHC with the acyl fluoride **1** yields the acyl azolium ion **4** and fluoride ion (*Step 1*), which desilylates the silyl enol ether **2**. The resulting enolate ion **5** combines with the acyl azolium ion **4** to generate **6** (*Step 2*) [19, 33–36]. Subsequent tautomerisation yields the acyl azolium ion **6′** (*Step 3*), which cyclises with formation of the dihydropyranone **3** and regeneration of the NHC catalyst (*Step 4*). While this mechanism is reasonable, alternate scenarios can be envisioned that give rise to the same outcome (for selected mechanistic contributions to the field of

Dedicated to the memory of George A. Olah, creator of a new access to organic reactivity.

Alison Levens and Feng An contributed equally to this work.

Electronic supplementary material The online version of this article (https://doi.org/10.1007/s11244-018-0914-5) contains supplementary material, which is available to authorized users.

✉ David W. Lupton
david.lupton@monash.edu

✉ Herbert Mayr
herbert.mayr@cup.uni-muenchen.de

[1] School of Chemistry, Monash University, Clayton 3800, Australia

[2] Department Chemie, Ludwig-Maximilians-Universität München, Butenandtstraße 5-13 (Haus F), 81377 Munich, Germany

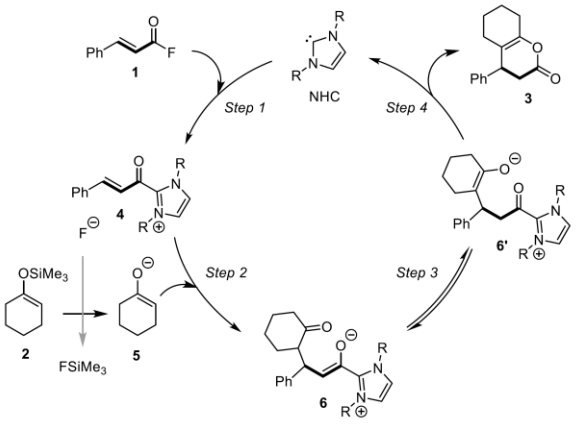

Scheme 1 Plausible catalytic cycle for the NHC-catalysed reaction of acyl fluoride **1** with 1-(trimethylsiloxy)-cyclohexene (**2**)

NHC catalysis [36–45]). To test the viability of the proposed mechanism and to explore the scope of this reaction principle we have addressed the following questions:

(1) Which NHCs are nucleophilic enough to react with acyl fluorides?
(2) Are α,β-unsaturated acyl azolium ions generally more electrophilic than the corresponding α,β-unsaturated acyl fluoride, i.e., can background reactions be suppressed?
(3) Which types of nucleophiles are able to attack at the unsaturated acyl azoliums? Specifically, is the silyl enol ether **2** or the desilylated enolate **5** the nucleophile in this reaction?

In previous work, we had already reported the influence of the substituents R on the nucleophilic reactivities of the NHCs ([46, 47]; for studies on the impact of the N-substituent in NHC organocatalysis see [48–51]). Furthermore, the electrophilicity of the α,β-unsaturated acyl azolium ion **4a** (R = Me) has been determined in collaboration with Studer et al. [36]. Building upon these studies, we now report a kinetic analysis of the electrophilicities of a series of α,β-unsaturated acyl azolium ions (**4b–f**) and of acyl fluoride **1** which allows the above questions to be answered.

2 Synthesis of the Acyl Imidazolium Triflates

Cinnamoylimidazolium triflates **4b–f** were prepared in analogy to the previously reported synthesis of **4a** [36]: Treatment of the imidazoles **7b–f** with n-butyl lithium and methyl cinnamate gave the cinnamoyl-imdazoles **8b–f**, which were methylated with methyl triflate in diethyl ether at ambient

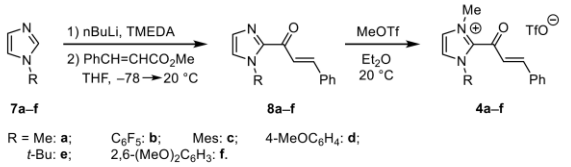

Scheme 2 Synthesis of the cinnamoylimidazolium triflates **4b–f** (for **4a**, see [36])

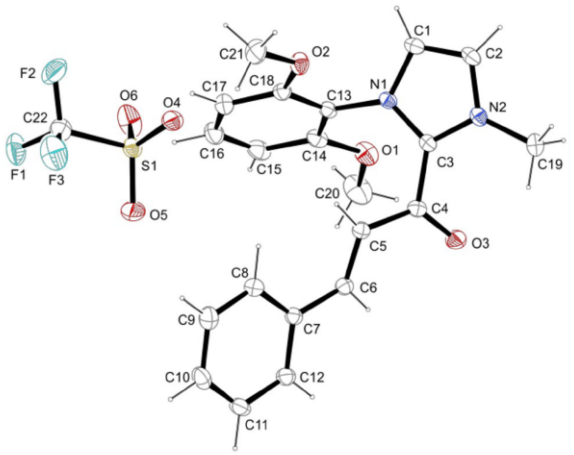

Fig. 1 ORTEP plot of the single crystal X-ray structure of **4f** (represented by 50% thermal ellipsoids) [see Footnote 1]

temperature to give the acyl imidazolium triflates **4b–f** (Scheme 2).

Cinnamoylimidazolium triflate **4f** was crystallised at room temperature by vapour diffusion of pentane into a saturated solution of **4f** in dichloromethane and subsequently analysed by single crystal X-ray crystallography (Fig. 1).[1] The dihedral angle of 11° (O3–C4–C5–C6) in the X-ray structure of **4f** in Fig. 1 shows that the coplanarity of the CC double bond and the carbonyl group is not significantly disturbed by the bulky 2,6-dimethoxy-substituted phenyl ring attached to N1 of the imidazolium ring. In this conformation, the carbonyl group can activate the conjugated CC double bond for 1,4-additions almost as efficiently as in the previously investigated acyl imidazolium electrophile **4a** [36], which showed a dihedral angle of 6° for the Michael-acceptor unit. The plane of the imidazolium group in crystals

[1] CCDC 1532919 contains the supplementary crystallographic data for this paper. These data are provided free of charge by The Cambridge Crystallographic Data Centre (for details on the isolation and characterisation of **4f** see Supporting Information).

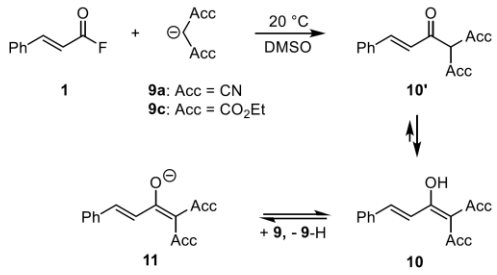

Scheme 3 Reactions of cinnamoyl fluoride (**1**) with the carbanions **9a** and **9c**

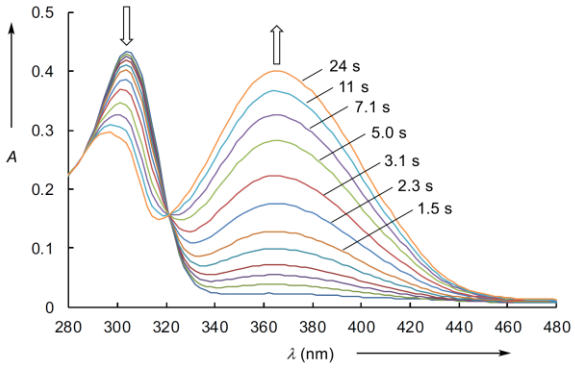

Fig. 2 UV–Vis spectra (stopped-flow method) during the reaction of **1** (5.08×10^{-5} M) with **9c** (3.11×10^{-3} M) in DMSO at 20 °C

of **4f** is twisted by 40° relative to the adjacent carbonyl group, similar to the corresponding twist in **4a** (35°) [36].

3 Determination of the Electrophilicity of the Acyl Fluoride 1

The reactions of the acyl fluoride **1** with the carbanions **9a** and **9c** initially gave the unsaturated ketone **10′**. It is not clear whether this substitution proceeds through tetrahedral intermediates or whether fluoride departs before the new C–C bond is fully established. Tautomerisation of **10′** gave the enols **10**, which were characterised by NMR spectroscopy (Scheme 3). Under the conditions of the kinetic experiments (**9a** and **9c** were used in high excess over **1** to achieve pseudo-first-order conditions) subsequent deprotonation yielded the highly delocalised weakly basic enolate ions **11**.

An isosbestic point was observed when **1** was combined with 61 equivalents of **9c** indicating that **10** does not accumulate in the course of the reaction (Fig. 2). The fact that the absorbance at λ = 312 nm (reactant **1**) decreases 24% more slowly than the λ = 364 nm absorbance increases (product **11**) is due to the fact that the absorption band of **1** overlaps

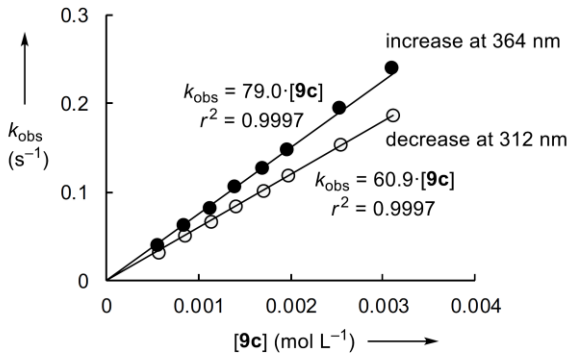

Fig. 3 Plot of the first-order rate constants k_{obs} versus the concentration of **9c** for the reaction of **1** with **9c** in DMSO at 20 °C

Table 1 Reference nucleophiles and their N and s_N parameters in DMSO (data from Footnote 2)

	9a	**9b**	**9c**	**9d**	**9e**	**9f**
N (s_N)	19.36 (0.67)	17.64 (0.73)	20.22 (0.65)	16.27 (0.77)	13.91 (0.86)	10.52 (0.78) in MeCN

with the signal of the developing product, in line with the hypsochromic shift of the 312 nm maximum during the reaction. The monoexponential increase of the concentration of **11** indicates the first-order dependence of the rate on the concentration of **1**, and the linear increase of the first-order rate constants with the concentration of the carbanion **9** (Fig. 3) shows that CC-bond formation and not the subsequent proton transfer to give **11** is rate-determining. The reaction thus follows second-order kinetics, first order in **1** and first order in **9**.

4 Determination of the Electrophilicities of the Acyl Azolium Ions 4b–f

In order to quantify the electrophilicities of the acyl azolium ions we have studied the kinetics of their reactions with the carbanions **9a–e** and the ketene acetal **9f** (reference nucleophiles, Table 1).[2]

As representative examples for the course of the reactions of the acyl azolium ions with carbanions, we have investigated the reactions of **4b** and **4f** with different potassium

[2] Access to all reactivity parameters at http://www.cup.lmu.de/oc/mayr/DBintro.html.

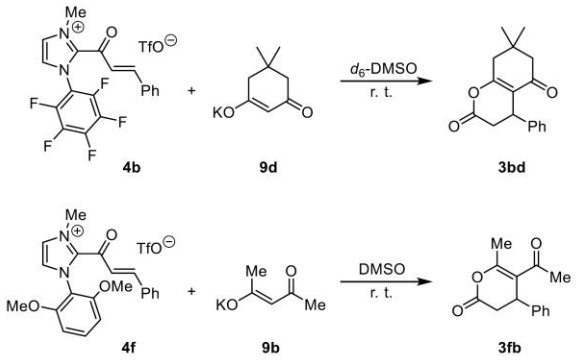

Scheme 4 Formation of dihydropyranones **3** by the reactions of cinnamoyl azolium ions with carbanions

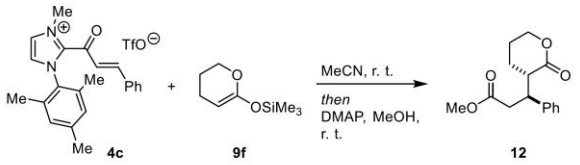

Scheme 5 Conjugate addition of the ketene acetal **9f** to the acyl azolium ion **4c**

give the lactone analogue of intermediate **6**. As this reaction was not carried out under basic conditions as the reactions in Scheme 4, deprotonation of the lactone fragment does not occur. As a consequence, cyclisation does not take place and the reaction stops at the stage of **6**. Methanolic workup converts the corresponding acyl azolium ion into the methyl ester **12** (Scheme 5).

As the acyl azolium ions **4b–f** (the analogous reaction of **4a** has previously been reported [36]) have UV-maxima between 320 and 355 nm, the kinetics of their reactions with the nucleophiles **9a–f** could be followed photometrically in DMSO solution (**9a–e**) or acetonitrile (**9f**, Fig 4a) using conventional UV–Vis spectrometers with fiber optics or stopped-flow instruments as described previously [36]. By using more than 10 equivalents of the nucleophiles, pseudo-first order conditions were achieved as shown by the monoexponential decays of the absorbances of **4**, which is illustrated for the reaction of **4f** with **9f** in Fig. 4b. Figure 4c furthermore shows exemplarily that k_{obs} increases linearly with the concentration of the nucleophiles **9**, and the slopes of these correlations correspond to the second-order rate constants k_2 listed in Table 2.

In numerous kinetic investigations we have shown that the rate constants for the reactions of nucleophiles with carbenium ions and electron-deficient π-systems can be expressed by Eq. (1), where nucleophiles are characterised by two solvent-

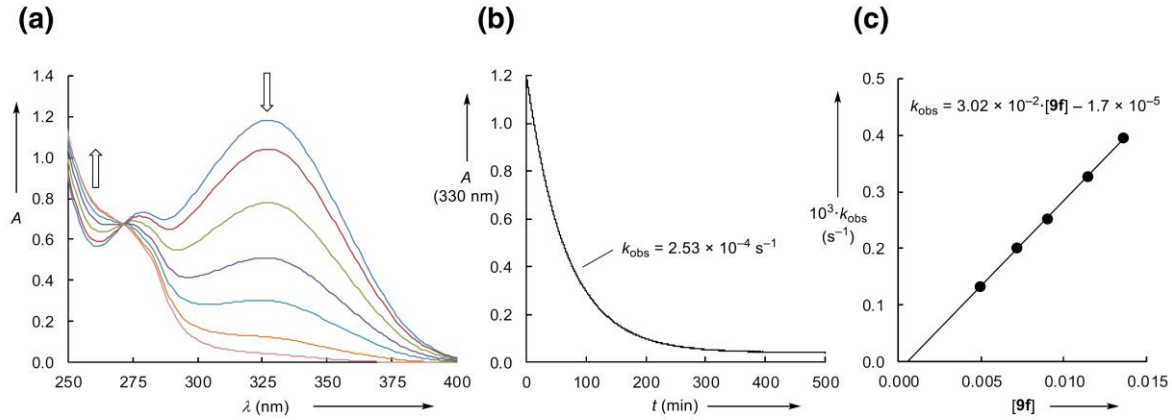

Fig. 4 **a** UV–Vis spectra during the reaction of **4f** (1.24×10^{-4} mol L^{-1}) with **9f** (9.04×10^{-3} mol L^{-1}) in acetonitrile at 20 °C; **b** determination of the first-order rate constant k_{obs} from the decay of the absorbance A at 330 nm with time; **c** determination of the second-order rate constant k_2 from the linear correlation of k_{obs} with [**9f**]

salts as shown in Scheme 4. The mechanism of these reactions corresponds to Steps 2–4 of Scheme 1.

A different type of product was observed in the reaction of **4c**-OTf with the ketene acetal **9f** (Scheme 5). Since fluoride ions are absent when a pregenerated acyl azolium triflate **4**-OTf is used, we can assume that **9f**, which is considerably more nucleophilic (N = 10.52, Table 1) than the enol ether **2** (N = 5.21 [52]), directly attacks the acyl azolium ion **4c** to

dependent parameters, N and s_N, and electrophiles are characterised by the electrophilicity parameter E (for development of this relationship see [52–54] and Footnote 2).

$$\log k(20\ ^\circ\mathrm{C}) = s_N(E + N) \quad (1)$$

As shown in Fig. 5 for the reactions of **4b, 4c**, and **4f** (and for all other acyl azolium ions in the Supporting

Table 2 Second-order rate constants for the reactions of acyl fluoride **1** and acyl azolium ions **4a–f** with nucleophiles **9a–f** in DMSO at 20 °C and the resulting electrophilicity parameters *E*

Electrophiles	Nuc	k_2 (L mol^{-1} s^{-1})	*E*
1	**9a**	4.25×10^{2}	(−15.4)[a]
	9c	7.90×10^{1}	(−17.3)[a]
4a (R = Me)[b]	**9a**	2.29×10^{5} [b]	−11.52[b]
	9b	5.84×10^{4} [b]	
	9d	9.03×10^{3} [b]	
	9e	2.75×10^{2} [b]	
	9f[c]	6.19×10^{-2} [b,c]	
4b (R = C_6F_5)	**9d**	1.50×10^{5}	−10.09
	9e	2.44×10^{3}	
	9f[c]	6.34×10^{-1} [c]	
4c (R = Mes)	**9a**	2.12×10^{5}	−11.48
	9b	3.15×10^{4}	
	9d	7.78×10^{3}	
	9e	1.61×10^{2}	
	9f[c]	7.39×10^{-2} [c]	
4d (R = 4-MeOC_6H_4)	**9a**	8.97×10^{4}	−11.79
	9b	1.78×10^{4}	
	9d	5.87×10^{3}	
	9e	1.22×10^{2}	
	9f[c]	3.47×10^{-2} [c]	
4e (R = *t*-Bu)	**9a**	8.23×10^{4}	−11.80
	9b	1.64×10^{4}	
	9d	5.60×10^{3}	
	9e	1.74×10^{2}	
	9f[c]	2.56×10^{-2} [c]	
4f (R = 2,6-$(MeO)_2C_6H_3$)	**9a**	8.28×10^{4}	−12.02
	9b	1.12×10^{4}	
	9d	3.70×10^{3}	
	9e	5.25×10^{1}	
	9f[c]	3.02×10^{-2} [c]	

[a]Eq. (1) unreliable, see text

[b]Data for **4a** from [36]

[c]In acetonitrile

Information) all plots of (log *k*)/s_N versus *N* are linear with slopes close to 1.0. The fact, that the deviations from the correlation lines in Fig. 5, where the slope of 1.0 was enforced, are negligible, indicates that all reactions follow Eq. (1), i.e., the negative intercepts on the abscissa (log *k* = 0) correspond to the electrophilicity parameters *E* for the acyl azolium ions **4**, which are listed in the last column of Table 2.

In accordance with unpublished work of the München group, Eq. (1) does not work well for the reactions of nucleophiles with acyl halides. The different electrophilicity parameters *E* of **1**, derived from its reactions with **9a** and **9c** (first two entries in Table 2) also illustrate the limitations of Eq. (1). Nevertheless, these numbers give an estimate for

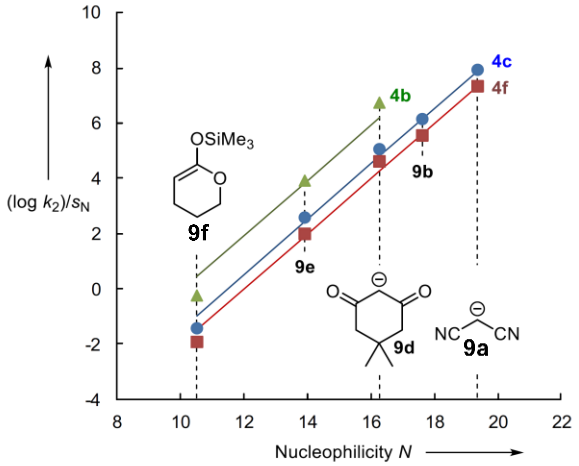

Fig. 5 Plot of (log *k*)/s_N versus *N* for the reactions of **4b, 4c**, and **4f** with the reference nuceophiles **9**; slopes of the correlations are fixed to 1.0, as required by Eq. (1)

the electrophilic reactivity of cinnamoyl fluoride **1** and allow us to answer the key questions raised above.

5 Conclusions

(1) Though Eq. (1) is not suitable for accurately predicting rate constants for the reactions of acyl halides with nucleophiles, the estimated *E* value for **1** in Table 2 suggests that **1** will react with all common imidazole- and triazole-derived NHCs ($14 < N < 23$) (see Footnote 2), though the reactions with triazole-derived carbenes are expected to be slow.

(2) Comparison of the electrophilicities of **4a–f** ($-12 < E < -10$) with the approximate reactivity parameter of **1** ($E \approx -16$) shows that acyl azolium ions **4a–f** are considerably more reactive than **1**, which can also be derived from the directly measured rate constants for their reactions with the malononitrile anion **9a** (Table 2). As a consequence, background reactions, i.e., the direct attack of nucleophiles at **1** will not take place as long as sufficient concentrations of **4** are produced.

(3) From the electrophilicity parameters *E* of **4a–f** one can derive that direct reactions of ordinary silyl enol ethers, such as **2**, with the acyl azolium ions **4a–f** are unlikely to occur at ambient temperature. From $N = 5.21$ (and $s_N = 1.0$) for enol ether **2** [52] and $-12 < E < -10$ for the acyl imidazolium ions **4a–f** (Table 2) one can calculate (Eq. 1) that the direct attack of **2** at **4a–f** would lead to 50% conversion within 1–70 days in 1 M solutions

of the reactants at 20 °C. This calculation supports the previously suggested mechanism for the NHC-catalysed reaction of **1** with siloxycyclohexene **2** through the enolate **5** (Scheme 1). As shown in Scheme 5, the 10^5 times more nucleophilic ketene acetal **9f** ($N = 10.52$) (see Footnote 2) can directly attack at acyl azolium ions, however, and does not require a prior fluoride-induced desilylation. Thus, nucleophiles with $N \approx 10$, including suitably substituted enamines and methylated pyrroles (see Footnote 2), can be expected to be reactive enough to rapidly attack at acyl azolium ions but too sluggish to undergo fast reactions with acyl fluorides and are, therefore, considered promising candidates for further NHC-catalysed reactions with acyl fluorides.

Acknowledgements The authors thank the Australian Research Council (Discovery Program DP120101315) and the Deutsche Forschungsgemeinschaft (SFB 749, Project B1) for financial support and Dr. Peter Mayer for the X-ray analysis of **4f**. DWL is grateful to the Alexander von Humboldt Foundation for the Ludwig-Leichardt Award.

References

1. Enders D, Niemeier O, Henseler A (2007) Chem Rev 107:5606–5655
2. Campbell CD, Ling KB, Smith AD (2011) In: Cazin CSJ (ed) N-heterocyclic carbenes in transition metal catalysis and organocatalysis. Springer, Dordrecht, pp 263–297
3. Chiang PC, Díez-González S, Bode JW (2017) In: Díez-González S (ed) N-heterocyclic carbenes: from laboratory curiositities to efficient synthetic tools, 2nd edn. The Royal Society of Chemistry, Cambridge, pp 534–566 (RSC catalysis series No. 27)
4. Nair V, Menon RS, Biju AT, Sinu CR, Paul RR, Jose A, Sreekumar V (2011) Chem Soc Rev 40:5336–5346
5. Menon RS, Biju AT, Nair V (2016) Beilstein J Org Chem 12:444–461
6. Vora HU, Wheeler P, Rovis T (2012) Adv Synth Catal 354:1617–1639
7. Douglas J, Churchill G, Smith AD (2012) Synthesis 44:2295–2309
8. Grossmann A, Enders D (2012) Angew Chem Int Ed 51:314–325
9. Bugaut X, Glorius F (2012) Chem Soc Rev 41:3511–3522
10. Izquierdo J, Hutson GE, Cohen DT, Scheidt KA (2012) Angew Chem Int Ed 51:11686–11698
11. Ryan SJ, Candish L, Lupton DW (2013) Chem Soc Rev 42:4906–4917
12. De Sarkar S, Biswas A, Samanta RC, Studer A (2013) Chem Eur J 19:4664–4678
13. Zhang C, Hooper JF, Lupton DW (2017) ACS Catal 7:2583–2596
14. Mahatthananchai J, Bode JW (2014) Acc Chem Res 47:696–707
15. Chauhan P, Enders D (2014) Angew Chem Int Ed 53:1485–1487
16. Hopkinson MN, Richter C, Schedler M, Glorius F (2014) Nature 510:485–496
17. Flanigan DM, Romanov-Michailidis F, White NA, Rovis T (2015) Chem Rev 115:9307–9387
18. Ryan SJ, Candish L, Lupton DW (2009) J Am Chem Soc 131:14176–14177
19. De Sarkar S, Studer A (2010) Angew Chem Int Ed 49:9266–9269
20. Kaeobamrung J, Mahatthananchai J, Zheng P, Bode JW (2010) J Am Chem Soc 132:8810–8812
21. Sun FG, Sun LH, Ye S (2011) Adv Synth Catal 353:3134–3138
22. Mo J, Shen L, Chi YR (2013) Angew Chem Int Ed 52:8588–8591
23. Wu X, Liu B, Zhang Y, Jeret M, Wang H, Zheng P, Yang S, Song BA, Chi YR (2016) Angew Chem Int Ed 55:12280–12284
24. Yetra SR, Mondal S, Mukherjee S, Gonnade RG, Biju AT (2016) Angew Chem Int Ed 55:268–272
25. Ryan SJ, Candish L, Lupton DW (2011) J Am Chem Soc 133:4694–4697
26. Candish L, Lupton DW (2013) J Am Chem Soc 135:58–61
27. Candish L, Levens A, Lupton DW (2014) J Am Chem Soc 136:14397–14400
28. Bera S, Samanta RC, Daniliuc CG, Studer A (2014) Angew Chem Int Ed 53:9622–9626
29. Mondal S, Yetra SR, Patra A, Kunte SS, Gonnade RG, Biju AT (2014) Chem Commun 50:14539–14542
30. Bera S, Daniliuc CG, Studer A (2015) Org Lett 17:4940–4943
31. Liang ZQ, Wang DL, Zhang HM, Ye S (2015) Org Lett 17:5140–5143
32. Zhang G, Xu W, Liu J, Das DK, Yang S, Perveen S, Zhang H, Li X, Fang X (2017) Chem Commun 53:13336–13339
33. Mahatthananchai J, Kaeobamrung J, Bode JW (2012) ACS Catal 2:494–503
34. Lyngvi E, Bode JW, Schoenebeck F (2012) Chem Sci 3:2346–2350
35. Candish L, Lupton DW (2011) Org Biomol Chem 9:8182–8189
36. Samanta RC, Maji B, De Sarkar S, Bergander K, Fröhlich R, Mück-Lichtenfeld C, Mayr H, Studer A (2012) Angew Chem Int Ed 51:5234–5238
37. Paul M, Breugst M, Neudörfl JM, Sunoj RB, Berkessel A (2016) J Am Chem Soc 138:5044–5051
38. Yatham VR, Neudörfl JM, Schlörer NE, Berkessel A (2015) Chem Sci 6:3706–3711
39. Berkessel A, Yatham VR, Elfert S, Neudörfl JM (2013) Angew Chem Int Ed 52:11158–11162
40. Berkessel A, Elfert S, Etzenbach-Effers K, Teles JH (2010) Angew Chem Int Ed 49:7120–7124
41. Zhao X, Glover GS, Oberg KM, Dalton DM, Rovis T (2013) Synlett 24:1229–1232
42. Moore JL, Silvestri AP, de Alaniz JR, DiRocco DA, Rovis T (2011) Org Lett 13:1742–1745
43. Cohen DT, Johnston RC, Rosson NT, Cheong PHY, Scheidt KA (2015) Chem Commun 51:2690–2693
44. Johnston RC, Cohen DT, Eichman CC, Scheidt KA, Cheong PHY (2014) Chem Sci 5:1974–1982
45. Ryan SJ, Stasch A, Paddon-Row MN, Lupton DW (2012) J Org Chem 77:1113–1124
46. Maji B, Breugst M, Mayr H (2011) Angew Chem Int Ed 50:6915–6919
47. Levens A, An F, Breugst M, Mayr H, Lupton DW (2016) Org Lett 18:3566–3569
48. Rovis T (2008) Chem Lett 37:2–7
49. Mahatthananchai J, Bode JW (2012) Chem Sci 3:192–197
50. Collett CJ, Massey RS, Maguire OR, Batsanov AS, O'Donoghue AC, Smith AD (2013) Chem Sci 4:1514–1522
51. Collett CJ, Massey RS, Taylor JE, Maguire OR, O'Donoghue AC, Smith AD (2015) Angew Chem Int Ed 54:6887–6892
52. Mayr H, Bug T, Gotta MF, Hering N, Irrgang B, Janker B, Kempf B, Loos R, Ofial AR, Remennikov G, Schimmel H (2001) J Am Chem Soc 123:9500–9512
53. Mayr H, Patz M (1994) Angew Chem Int Ed Engl 33:938–957
54. Mayr H, Ofial AR (2008) J Phys Org Chem 21:584–595

– Experimental Section–

Reaction Products

(*E*)-2-(1-Hydroxy-3-phenylallylidene)malononitrile (10a)

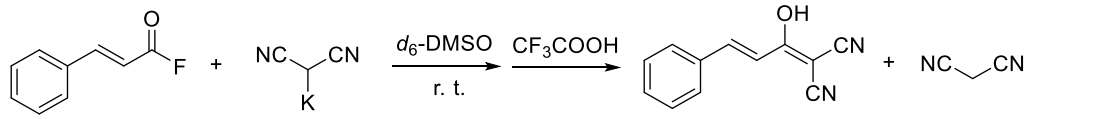

1 (1 equiv) **9a** (2 equiv) **10a** (1 equiv) **9a-H** (1 equiv)

Acyl fluoride **1** (10 mg, 0.067 mmol) and malodinitrile potassium salt **9a** (14 mg, 0.13 mmol) were mixed in d_6-DMSO (0.6 mL) at room temperature. Trifluoroacetic acid (20 mg, 0.18 mmol) was added to the mixture. The ^{1}H and ^{13}C NMR spectra showed the formation of **10a** and **9a-H**.

10a: ^{1}H NMR (400 MHz, d_6-DMSO) δ 7.56–7.54 (m, 2 H), 7.41–7.32 (m, 4 H), 7.00 (d, J = 15.6 Hz, 1 H). ^{13}C NMR (100 MHz, d_6-DMSO) δ 181.7, 136.9, 135.3, 129.3, 129.0, 127.6, 121.5, 120.3, 120.0, 50.7.

9a-H: ^{1}H NMR (400 MHz, d_6-DMSO) δ 4.44 (s, 2 H). ^{13}C NMR (100 MHz, d_6-DMSO) δ 112.1, 8.5.

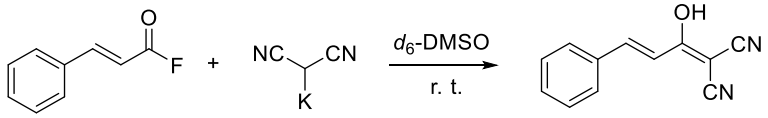

1 (1 equiv) **9a** (3 equiv) **10a** (1 equiv)

Acyl fluoride **1** (10 mg, 0.067 mmol) and malodinitrile potassium salt **9a** (20.8 mg, 0.2 mmol) were mixed in d_6-DMSO (0.6 mL) at room temperature. The ^{1}H NMR and ^{13}C-NMR spectra showed the formation of **10a**.

^{1}H NMR (400 MHz, d_6-DMSO) δ 7.55–7.53 (m, 2 H), 7.41–7.32 (m, 3 H), 7.29 (d, J = 15.6 Hz, 1 H), 6.99 (d, J = 15.6 Hz, 1 H). ^{13}C NMR (100 MHz, d_6-DMSO) δ 181.7, 136.1, 135.4, 129.1, 128.9, 127.5, 123.9, 122.2, 121.0, 49.3.

Potassium (*E*)-5-ethoxy-4-(ethoxycarbonyl)-5-oxo-1-phenylpenta-1,3-dien-3-olate (11c-K)

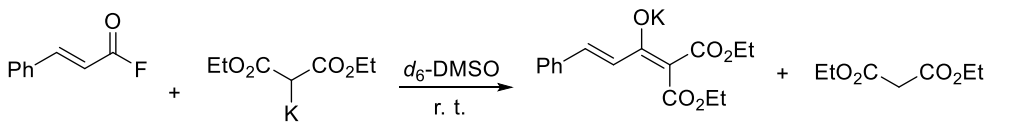

1 (1 equiv) **9c** (2 equiv) **11c-K** (1 equiv) **9c-H** (1 equiv)

Acyl fluoride **1** (10 mg, 0.067 mmol) and diethylmalonate potassium salt (26 mg, 0.13 mmol) were mixed in d_6-DMSO (6 mL) at room temperature. The ^{1}H and ^{13}C NMR spectra showed the formation of compounds **10c-K** and **9c-H**.

10c-K: ^{1}H NMR (400 MHz, d_6-DMSO) δ 7.82 (d, J = 15.7 Hz, 1 H), 7.47–7.45 (m, 2 H), 7.37–7.33 (m, 2 H), 7.28–7.24 (m, 1 H), 7.14 (d, J = 15.7 Hz, 1 H), 3.94 (q, J = 7.1 Hz, 4 H), 1.13 (t, J = 7.1 Hz, 6 H). ^{13}C-NMR (101 MHz, d_6-DMSO) δ 178.2, 169.4, 137.2, 132.4, 130.0, 128.6, 127.8, 126.9, 95.6, 57.4, 14.6.

9c-H: ^{1}H NMR (400 MHz, d_6-DMSO) δ 4.11 (q, J = 7.1 Hz, 4 H), 3.47 (s, 2 H), 1.19 (t, J = 7.1 Hz, 6 H). ^{13}C NMR (101 MHz, d_6-DMSO) δ 166.5, 60.8, 41.2, 13.9.

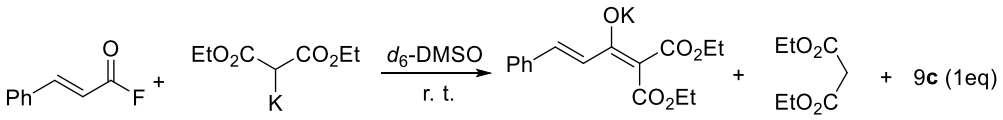

1 (1 equiv) **9c** (3 equiv) **10c-K** (1 equiv) **9c-H** (1equiv)

Acyl fluoride **1** (10 mg, 0.067 mmol) and diethylmalonate potassium salt **9c** (40 mg, 0.20 mmol) were mixed in d_6-DMSO (6 mL) at room temperature, The ^{1}H and ^{13}C NMR spectra showed the formation of compounds **10c-K**, **9c-H** and the remaining **9c**.

10c-K: ^{1}H NMR (400 MHz, d_6-DMSO) δ 7.81 (d, J = 15.7 Hz, 1 H), 7.46–7.44 (m, 2 H), 7.36–7.32 (m, 2 H), 7.27–7.23 (m, 1 H), 7.13 (d, J = 15.7 Hz, 1 H), 3.93 (q, J = 7.1 Hz, 4 H), 1.13 (t, J = 7.1 Hz, 6 H). ^{13}C-NMR (101 MHz, d_6-DMSO) δ 178.7, 169.6, 137.3, 132.3, 130.4, 128.7, 127.7, 126.9, 95.4, 57.3, 14.6.

9c-H: ^{1}H NMR (400 MHz, d_6-DMSO) δ 4.11 (q, J = 7.1 Hz, 4 H), 3.47 (s, 2 H), 1.19 (t, J = 7.1 Hz, 6 H). ^{13}C NMR (101 MHz, d_6-DMSO) δ 166.6, 60.8, 41.2, 13.9.

9c: ^{1}H NMR (400 MHz, d_6-DMSO) δ 3.76 (q, J = 7.1 Hz, 4 H), 3.54 (s, 1 H), 1.04 (t, J = 7.1 Hz, 6 H). ^{13}C NMR (101 MHz, d_6-DMSO) δ 169.5, 61.2, 55.1, 15.4.

Kinetics

Kinetics of the reactions of acyl fluoride **1** with nucleophiles **9a,c** in DMSO

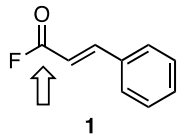

1

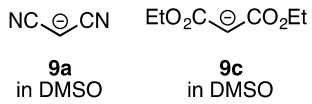

9a in DMSO

9c in DMSO

[**1**] / mol·L^{-1}	[**9a**] / mol·L^{-1}	k_{obs} / s^{-1}
	1.25×10^{-3}	4.68×10^{-1}
7.06×10^{-5}	1.87×10^{-3}	7.07×10^{-1}
	2.50×10^{-3}	9.72×10^{-1}
	3.12×10^{-2}	1.24
	3.75×10^{-2}	1.53

$k_2 = 4.25 \times 10^{2}$ L·mol^{-1}·s^{-1}

λ = 348 nm

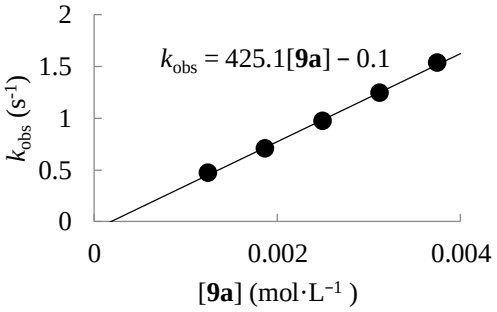

[**1**] / mol·L^{-1}	[**9c**] / mol·L^{-1}	k_{obs} / s^{-1}
	5.65×10^{-4}	3.75×10^{-2}
	8.47×10^{-4}	6.08×10^{-2}
	1.13×10^{-3}	7.98×10^{-2}
5.08×10^{-5}	1.41×10^{-3}	1.04×10^{-1}
	1.70×10^{-3}	1.26×10^{-1}
	1.98×10^{-3}	1.47×10^{-1}
	2.54×10^{-3}	1.93×10^{-1}
	3.11×10^{-3}	2.39×10^{-1}

$k_2 = 7.9 \times 10^{1}$ L·mol^{-1}·s^{-1}

λ = 364 nm

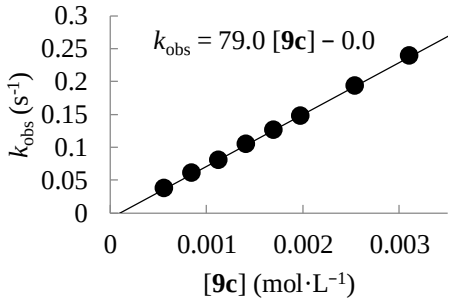

[**1**] / mol·L^{-1}	[**9c**] / M	k_{obs} / s^{-1}
	5.65×10^{-4}	3.21×10^{-2}
	8.47×10^{-4}	5.03×10^{-2}
	1.13×10^{-3}	6.57×10^{-2}
5.08×10^{-5}	1.41×10^{-3}	8.32×10^{-2}
	1.70×10^{-3}	1.01×10^{-1}
	1.98×10^{-3}	1.19×10^{-1}
	2.54×10^{-3}	1.54×10^{-1}
	3.11×10^{-3}	1.86×10^{-1}

λ = 312 nm

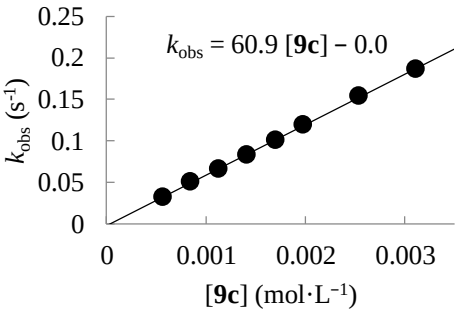

Kinetics of the reactions of acyl azoliums **4b** with nucleophiles **9d–f**

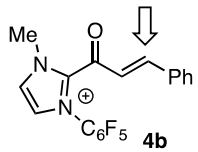

4b

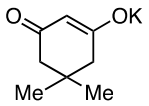

9d
in DMSO

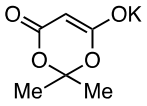

9e
in DMSO

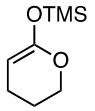

9f
in MeCN

[**4b**] / mol·L^{-1}	[**9d**] / mol·L^{-1}	k_{obs} / s^{-1}
1.38 × 10^{-4}	1.44 × 10^{-3}	2.66 × 10^{2}
	1.92 × 10^{-3}	3.09 × 10^{2}
	2.40 × 10^{-3}	3.71 × 10^{2}
	2.88 × 10^{-3}	4.69 × 10^{2}
	3.36 × 10^{-3}	5.23 × 10^{2}
	3.84 × 10^{-3}	6.22 × 10^{2}

k_2 = 1.5 × 10^{5} L·mol^{-1}·s^{-1}

λ = 350 nm

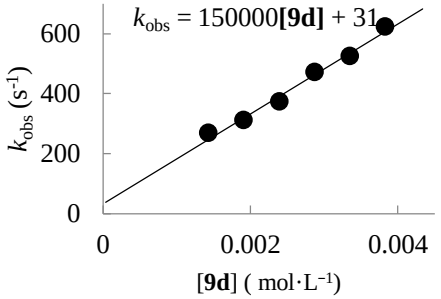

[**4b**] / mol·L^{-1}	[**9e**] / mol·L^{-1}	k_{obs} / s^{-1}
1.25 × 10^{-4}	1.77 × 10^{-3}	4.61
	2.65 × 10^{-3}	6.96
	3.53 × 10^{-3}	9.55
	4.42 × 10^{-3}	1.12 × 10^{1}
	5.30 × 10^{-3}	1.32 × 10^{1}
	6.18 × 10^{-3}	1.56 × 10^{1}

k_2 = 2.44 × 10^{3} L·mol^{-1}·s^{-1}

λ = 350 nm

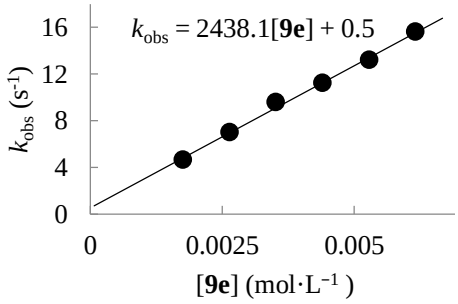

[**4b**] / mol·L^{-1}	[**9f**] / mol·L^{-1}	k_{obs} / s^{-1}
1.13 × 10^{-4}	1.88 × 10^{-3}	1.15 × 10^{-3}
1.12 × 10^{-4}	2.81 × 10^{-3}	1.82 × 10^{-3}
1.11 × 10^{-4}	3.71 × 10^{-3}	2.29 × 10^{-3}
1.10 × 10^{-4}	4.59 × 10^{-2}	2.84 × 10^{-3}
1.07 × 10^{-4}	5.37 × 10^{-2}	3.42 × 10^{-3}

k_2 = 6.34 × 10^{-1} L·mol^{-1}·s^{-1}

λ = 335 nm

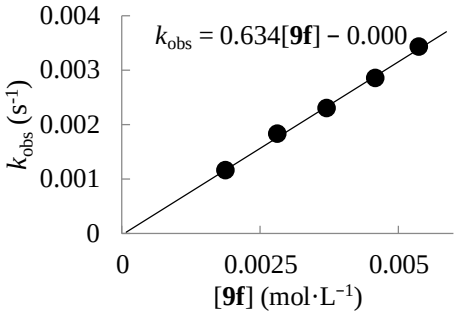

Determination of *E* of azolium **4b**

Electrophiles	*N* (s_N)	k_2 / L·mol^{-1}·s^{-1}	(lg k_2)/s_N
9f	10.52 (0.78)	6.34×10^{-1}	-2.54×10^{-1}
9e	13.91 (0.86)	2.44×10^{3}	3.94
9d	16.27 (0.77)	1.50×10^{5}	6.72

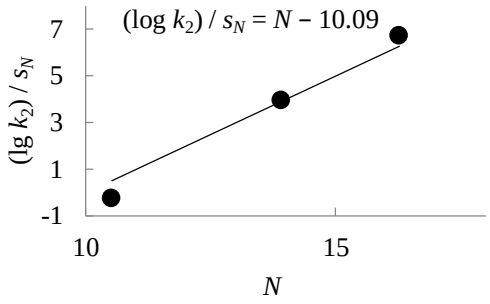

E = –10.09

Kinetics of the reactions of acyl azoliums **4c** with nucleophiles **9a,b,d–f**

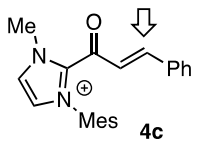

4c

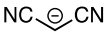

9a in DMSO

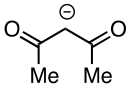

9b in DMSO

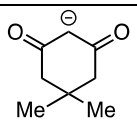

9d in DMSO

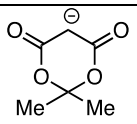

9e in DMSO

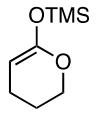

9f in MeCN

[**4c**] / mol·L^{-1}	[**9a**] / mol·L^{-1}	k_{obs} / s^{-1}
1.47 × 10^{-4}	1.64 × 10^{-3}	3.16 × 10^{2}
	2.19 × 10^{-3}	4.31 × 10^{2}
	2.74 × 10^{-3}	5.51 × 10^{2}
	3.28 × 10^{-3}	6.62 × 10^{2}

k_2 = 2.12 × 10^{5} L mol^{-1}·s^{-1}

λ = 350 nm

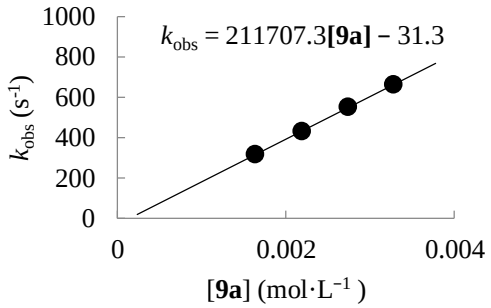

[**4c**] / mol·L^{-1}	[**9b**] / mol·L^{-1}	k_{obs} / s^{-1}
1.63 × 10^{-4}	1.76 × 10^{-3}	5.81 × 10^{1}
	2.65 × 10^{-3}	9.27 × 10^{1}
	3.63 × 10^{-3}	1.20 × 10^{2}
	4.41 × 10^{-3}	1.50 × 10^{2}
	5.30 × 10^{-3}	1.74 × 10^{2}
	6.18 × 10^{-3}	1.98 × 10^{2}

k_2 = 3.15 × 10^{4} L mol^{-1}·s^{-1}

λ = 350 nm

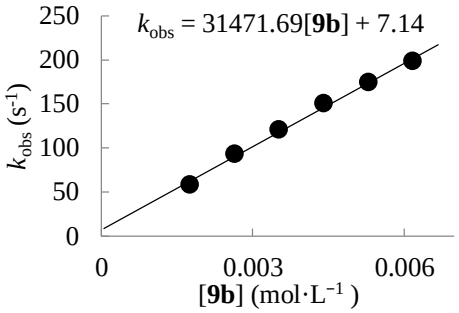

[**4c**] / mol·L^{-1}	[**9d**] / mol·L^{-1}	k_{obs} / s^{-1}
1.63 × 10^{-4}	2.14 × 10^{-3}	1.88 × 10^{1}
	3.21 × 10^{-3}	2.89 × 10^{1}
	4.27 × 10^{-3}	3.81 × 10^{1}
	5.34 × 10^{-3}	4.52 × 10^{1}
	6.41 × 10^{-3}	5.39 × 10^{1}
	7.48 × 10^{-3}	6.05 × 10^{1}

k_2 = 7.78 × 10^{3} L mol^{-1}·s^{-1}

λ = 350 nm

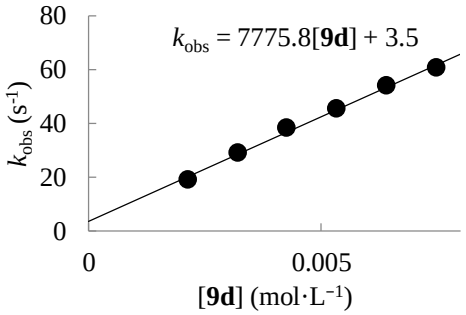

[**4c**] / mol·L^{-1}	[**9e**] / mol·L^{-1}	k_{obs} / s^{-1}
	2.00×10^{-3}	3.48×10^{-1}
	3.01×10^{-3}	5.30×10^{-1}
1.47×10^{-4}	4.01×10^{-3}	6.91×10^{-1}
	5.01×10^{-3}	8.53×10^{-1}
	6.01×10^{-3}	9.94×10^{-1}

$k_2 = 1.61 \times 10^2$ L mol^{-1}·s^{-1}

λ = 350 nm

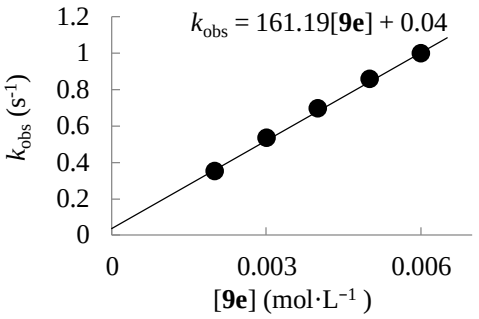

[**4c**] / mol·L^{-1}	[**9f**] / mol·L^{-1}	k_{obs} / s^{-1}
1.52×10^{-4}	2.72×10^{-3}	2.18×10^{-4}
1.83×10^{-4}	4.03×10^{-3}	2.95×10^{-4}
1.73×10^{-4}	5.38×10^{-3}	4.07×10^{-4}
1.70×10^{-4}	6.60×10^{-3}	5.12×10^{-4}
1.58×10^{-4}	7.85×10^{-3}	5.90×10^{-4}
1.55×10^{-4}	8.96×10^{-3}	6.68×10^{-4}

$k_2 = 7.39 \times 10^{-2}$ L mol^{-1}·s^{-1}

λ = 350 nm

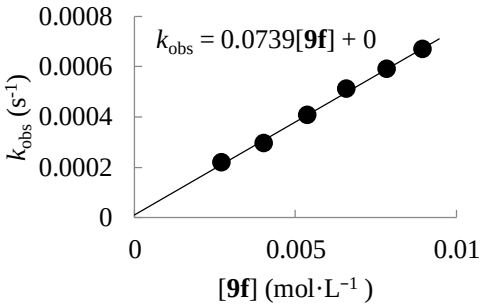

Determination of *E* of azolium **4c**

Nucleophiles	*N* (s_N)	k_2 / L· mol^{-1}·s^{-1}	(log k_2)/s_N
9f	10.52 (0.78)	7.39×10^{-2}	–1.45
9e	13.91 (0.86)	1.61×10^{2}	2.57
9d	16.27 (0.77)	7.78×10^{3}	5.05
9b	17.64 (0.73)	3.15×10^{4}	6.16
9a	19.36 (0.67)	2.12×10^{5}	7.95

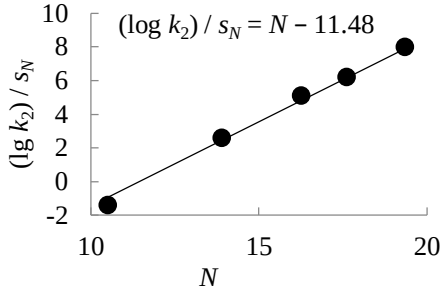

E = –11.48

Kinetics of the reactions of acyl azoliums **4d** with nucleophiles **9a,b,d-f**

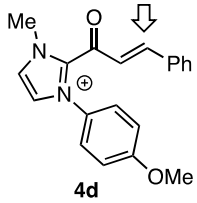

4d

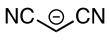

9a in DMSO

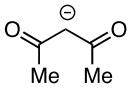

9b in DMSO

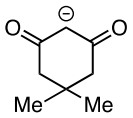

9d in DMSO

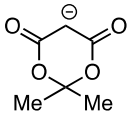

9e in DMSO

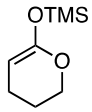

9f in MeCN

[**4d**] / mol·L^{-1}	[**9a**] / mol·L^{-1}	k_{obs} / s^{-1}
1.54 × 10^{-4}	1.53 × 10^{-3}	1.55 × 10^{2}
	2.05 × 10^{-3}	2.07 × 10^{2}
	2.56 × 10^{-3}	2.58 × 10^{2}
	3.07 × 10^{-3}	2.96 × 10^{2}
	3.58 × 10^{-3}	3.38 × 10^{2}
	4.09 × 10^{-3}	3.90 × 10^{2}

k_2 = 8.97 × 10^{4} L mol^{-1}·s^{-1}

λ = 355 nm

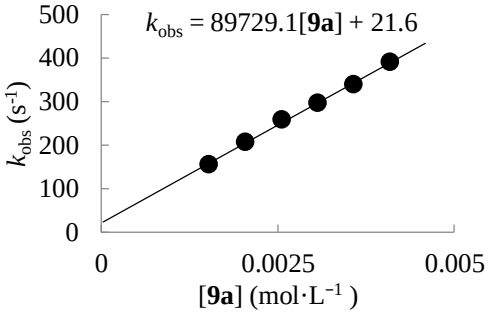

[**4d**] / mol·L^{-1}	[**9b**] / mol·L^{-1}	k_{obs} / s^{-1}
2.28 × 10^{-4}	1.92 × 10^{-3}	4.81 × 10^{1}
	2.89 × 10^{-3}	6.10 × 10^{1}
	3.85 × 10^{-3}	7.94 × 10^{1}
	4.81 × 10^{-3}	9.53 × 10^{1}
	5.77 × 10^{-3}	1.14 × 10^{2}
	6.74 × 10^{-3}	1.27 × 10^{2}

k_2 = 1.78 × 10^{4} L mol^{-1}·s^{-1}

λ = 355 nm

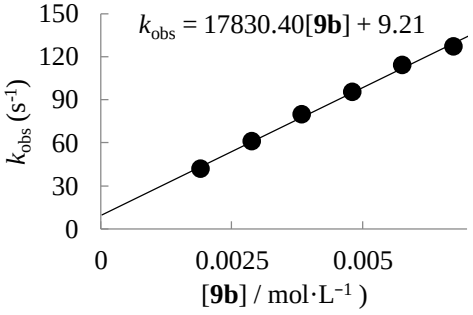

[**4d**] / mol·L^{-1}	[**9d**] / mol·L^{-1}	k_{obs} / s^{-1}
1.37 × 10^{-4}	1.75 × 10^{-3}	1.20 × 10^{1}
	2.63 × 10^{-3}	1.73 × 10^{1}
	3.50 × 10^{-3}	2.35 × 10^{1}
	4.38 × 10^{-3}	2.82 × 10^{1}
	5.25 × 10^{-3}	3.32 × 10^{1}
	6.13 × 10^{-3}	3.75 × 10^{1}

k_2 = 5.87 × 10^{3} L mol^{-1}·s^{-1}

λ = 355 nm

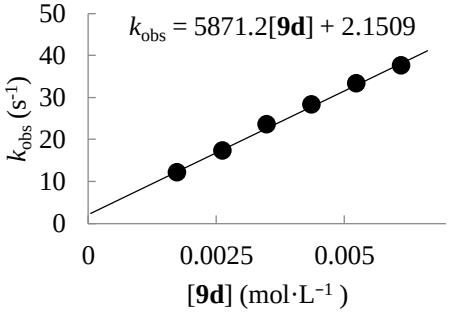

[**4d**] / mol·L^{-1}	[**9e**] / mol·L^{-1}	k_{obs} / s^{-1}
1.54 × 10^{-4}	1.94 × 10^{-3}	2.69 × 10^{-1}
	2.91 × 10^{-3}	3.95 × 10^{-1}
	3.87 × 10^{-3}	5.26 × 10^{-1}
	4.84 × 10^{-3}	6.28 × 10^{-1}
	5.81 × 10^{-3}	7.42 × 10^{-1}
k_2 = 1.22 × 10^2 L mol^{-1}·s^{-1}		

λ = 330 nm

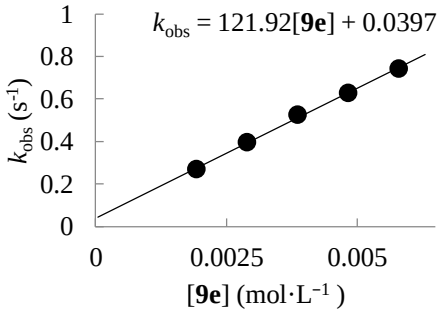

[**4d**] / mol·L^{-1}	[**9f**] / mol·L^{-1}	k_{obs} / s^{-1}
1.14 × 10^{-4}	5.10 × 10^{-3}	1.98 × 10^{-4}
1.14 × 10^{-4}	6.34 × 10^{-3}	2.40 × 10^{-4}
1.14 × 10^{-4}	7.61 × 10^{-3}	2.65 × 10^{-4}
1.11 × 10^{-4}	8.71 × 10^{-3}	3.23 × 10^{-4}
1.10 × 10^{-4}	9.86 × 10^{-3}	3.63 × 10^{-4}
k_2 = 3.47 × 10^{-2} L mol^{-1}·s^{-1}		

λ = 325 nm

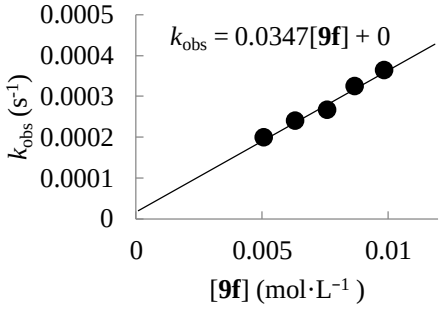

Determination of *E* of azolium **4d**

Nucleophiles	*N* (s_N)	k_2 / L mol^{-1}·s^{-1}	(log k_2)/s_N
9f	10.52 (0.78)	3.47 × 10^{-2}	–1.87
9e	13.91 (0.86)	1.22 × 10^2	2.43
9d	16.27 (0.77)	5.87 × 10^3	4.89
9b	17.64 (0.73)	1.78 × 10^4	5.82
9a	19.36 (0.67)	8.97 × 10^4	7.39

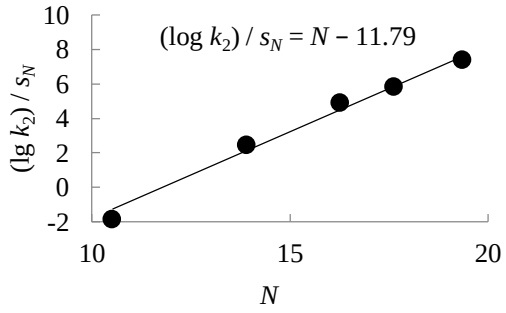

E = –11.79

Kinetics of the reactions of acyl azoliums **4e** with nucleophiles **9a,b,d–f**

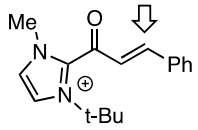

4e

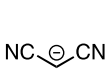

9a in DMSO

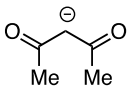

9b in DMSO

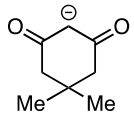

9d in DMSO

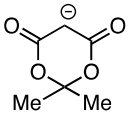

9e in DMSO

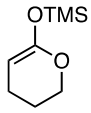

9f in MeCN

[**4e**] / mol·L^{-1}	[**9a**] / mol·L^{-1}	k_{obs} / s^{-1}
1.64 × 10^{-4}	1.52 × 10^{-3}	1.16 × 10^{2}
	2.03 × 10^{-3}	1.52 × 10^{2}
	2.53 × 10^{-3}	2.08 × 10^{2}
	3.04 × 10^{-3}	2.50 × 10^{2}
	3.55 × 10^{-3}	2.81 × 10^{2}
	4.05 × 10^{-3}	3.22 × 10^{2}

k_2 = 8.23 × 10^{4} L mol^{-1}·s^{-1}

λ = 345 nm

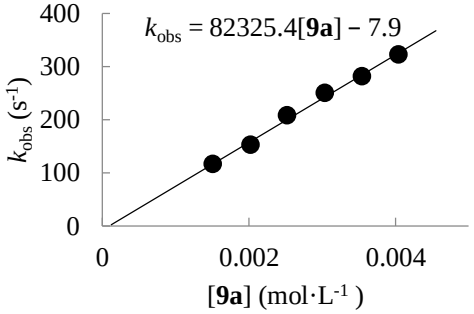

[**4e**] / mol·L^{-1}	[**9b**] / mol·L^{-1}	k_{obs} / s^{-1}
1.68 × 10^{-4}	2.03 × 10^{-3}	3.98 × 10^{1}
	3.04 × 10^{-3}	5.66 × 10^{1}
	4.05 × 10^{-3}	7.48 × 10^{1}
	5.06 × 10^{-3}	9.20 × 10^{1}
	6.08 × 10^{-3}	1.07 × 10^{2}
	7.09 × 10^{-3}	1.22 × 10^{2}

k_2 = 1.64 × 10^{4} L mol^{-1}·s^{-1}

λ = 345 nm

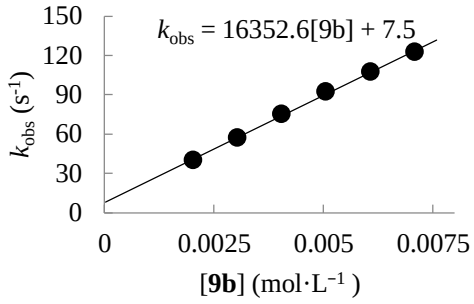

[**4e**] / mol·L^{-1}	[**9d**] / mol·L^{-1}	k_{obs} / s^{-1}
1.68 × 10^{-4}	1.87 × 10^{-3}	1.19 × 10^{1}
	2.81 × 10^{-3}	1.74 × 10^{1}
	3.75 × 10^{-3}	2.33 × 10^{1}
	4.68 × 10^{-3}	2.79 × 10^{1}
	5.62 × 10^{-3}	3.31 × 10^{1}
	6.56 × 10^{-3}	3.83 × 10^{1}

k_2 = 5.60 × 10^{3} L mol^{-1}·s^{-1}

λ = 345 nm

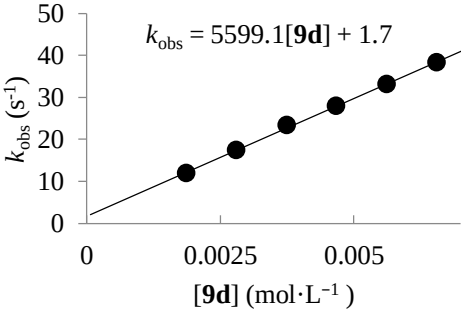

[**4e**] / mol·L^{-1}	[**9e**] / mol·L^{-1}	k_{obs} / s^{-1}
	1.77×10^{-3}	3.42×10^{-1}
	2.65×10^{-3}	5.27×10^{-1}
1.64×10^{-4}	3.53×10^{-3}	6.72×10^{-1}
	4.42×10^{-3}	8.33×10^{-1}
	5.30×10^{-3}	9.89×10^{-1}
	6.18×10^{-3}	1.11

$k_2 = 1.74 \times 10^2$ L mol^{-1}·s^{-1}

λ = 345 nm

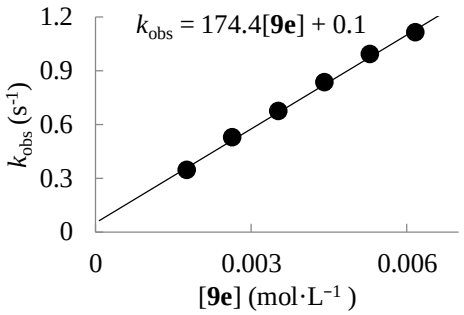

[**4e**] / mol·L^{-1}	[**9f**] / mol·L^{-1}	k_{obs} / s^{-1}
8.70×10^{-5}	3.29×10^{-3}	8.59×10^{-5}
8.79×10^{-5}	4.34×10^{-3}	1.17×10^{-4}
8.62×10^{-5}	5.37×10^{-3}	1.41×10^{-4}
8.34×10^{-5}	6.64×10^{-3}	1.69×10^{-4}
9.27×10^{-5}	7.85×10^{-3}	2.06×10^{-4}

$k_2 = 2.56 \times 10^{-2}$ L·mol^{-1}·s^{-1}

λ = 320 nm

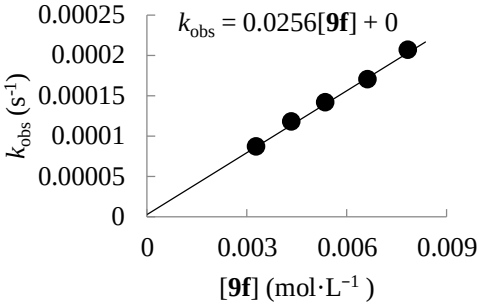

Determination of *E* of azolium **4e**

Nucleophiles	*N* (s_N)	k_2 / L· mol^{-1}·s^{-1}	(log k_2)/s_N
9f	10.52 (0.78)	2.56×10^{-2}	–2.04
9e	13.91 (0.86)	1.74×10^{2}	2.61
9d	16.27 (0.77)	5.60×10^{3}	4.87
9b	17.64 (0.73)	1.64×10^{4}	5.77
9a	19.36 (0.67)	8.23×10^{4}	7.34

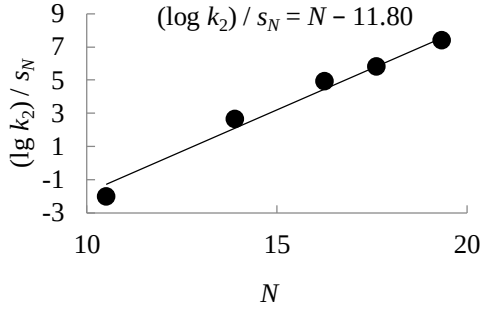

E = –11.80

Kinetics of the reactions of acyl azoliums **4f** with nucleophiles **9a, b, d–f**

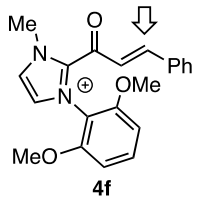

4f

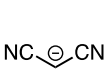

9a
in DMSO

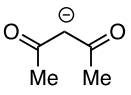

9b
in DMSO

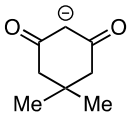

9d
in DMSO

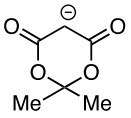

9e
in DMSO

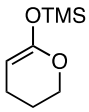

9f
in MeCN

[**4f**] / mol·L^{-1}	[**9a**] / mol·L^{-1}	k_{obs} / s^{-1}
1.70 × 10^{-4}	1.77 × 10^{-3}	1.41 × 10^{2}
	2.36 × 10^{-3}	1.95 × 10^{2}
	2.95 × 10^{-3}	2.37 × 10^{2}
	3.54 × 10^{-3}	2.91 × 10^{2}
	4.13 × 10^{-3}	3.35 × 10^{2}
	4.72 × 10^{-3}	3.88 × 10^{2}

k_2 = 8.28 × 10^{4} L mol^{-1}·s^{-1}

λ = 345 nm

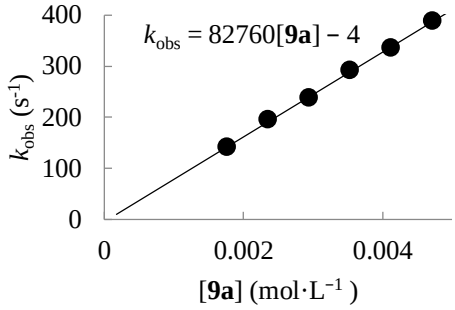

[**4f**] / mol·L^{-1}	[**9b**] / mol·L^{-1}	k_{obs} / s^{-1}
1.69 × 10^{-4}	1.98 × 10^{-3}	2.85 × 10^{1}
	2.97 × 10^{-3}	4.15 × 10^{1}
	3.96 × 10^{-3}	5.18 × 10^{1}
	4.96 × 10^{-3}	6.32 × 10^{1}
	5.95 × 10^{-3}	7.28 × 10^{1}
	6.94 × 10^{-3}	8.53 × 10^{1}

k_2 = 1.12 × 10^{4} L mol^{-1}·s^{-1}

λ = 345 nm

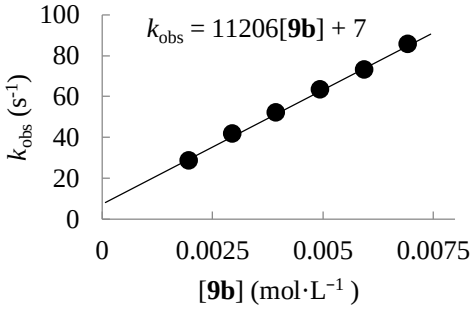

[**4f**] / mol·L^{-1}	[**9d**] / mol·L^{-1}	k_{obs} / s^{-1}
1.69 × 10^{-4}	1.76 × 10^{-3}	7.25
	2.63 × 10^{-3}	1.08 × 10^{1}
	3.51 × 10^{-3}	1.36 × 10^{1}
	4.39 × 10^{-3}	1.74 × 10^{1}
	5.27 × 10^{-3}	2.05 × 10^{1}
	6.15 × 10^{-3}	2.34 × 10^{1}

k_2 = 3.70 × 10^{3} L mol^{-1}·s^{-1}

λ = 345 nm

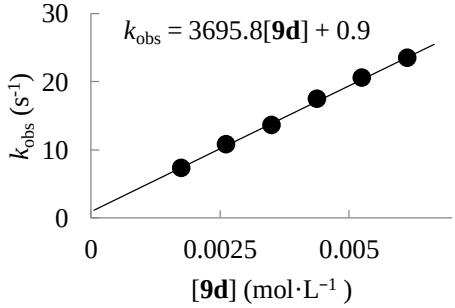

[**4f**] / mol·L^{-1}	[**9e**] / mol·L^{-1}	k_{obs} / s^{-1}
1.70 × 10^{-4}	1.88 × 10^{-3}	1.01 × 10^{-1}
	2.82 × 10^{-3}	1.57 × 10^{-1}
	3.76 × 10^{-3}	2.09 × 10^{-1}
	4.71 × 10^{-3}	2.50 × 10^{-1}
	5.65 × 10^{-3}	3.01 × 10^{-1}
	6.59 × 10^{-3}	3.53 × 10^{-1}
k_2 = 5.25 × 10^{1} L mol^{-1}·s^{-1}		

λ = 345 nm

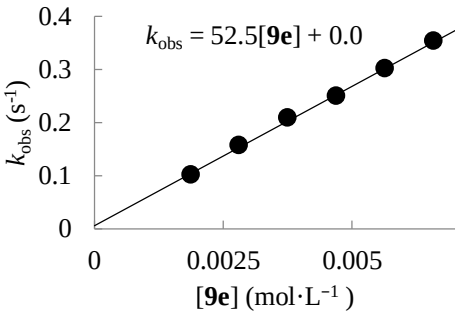

[**4f**] / mol·L^{-1}	[**9f**] / mol·L^{-1}	k_{obs} / s^{-1}
1.46 × 10^{-4}	4.96 × 10^{-3}	1.33 × 10^{-4}
1.33 × 10^{-4}	7.20 × 10^{-3}	2.02 × 10^{-4}
1.24 × 10^{-4}	9.04 × 10^{-3}	2.53 × 10^{-4}
1.45 × 10^{-4}	1.15 × 10^{-2}	3.27 × 10^{-4}
1.33 × 10^{-4}	1.36 × 10^{-2}	3.96 × 10^{-4}
k_2 = 3.02 × 10^{-2} L mol^{-1}·s^{-1}		

λ = 330 nm

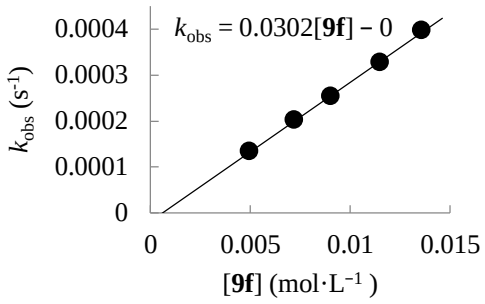

Determination of *E* of azolium **4f**

Nucleophiles	*N* (s_N)	k_2 / L· mol^{-1}·s^{-1}	(log k_2)/s_N
9f	10.52 (0.78)	3.02 × 10^{-2}	–1.95
9e	13.91 (0.86)	5.25 × 10^{1}	2.00
9d	16.27 (0.77)	3.70 × 10^{3}	4.63
9b	17.64 (0.73)	1.12 × 10^{4}	5.55
9a	19.36 (0.67)	8.28 × 10^{4}	7.34

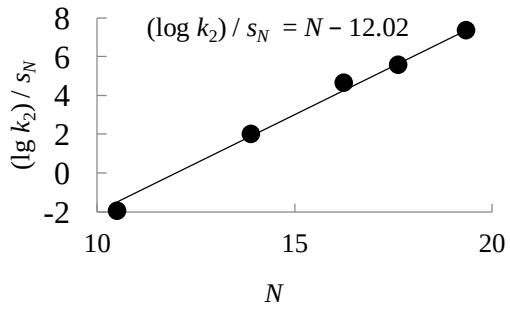

E = –12.02

Appendix 5 Correlation between the change of activation energy and free energy change

Equation (4) and equation (5)[†] are two empirical equations which are developed based on numerous kinetic and equilibrium measurements at 20 °C.

$$\lg k_2(20\ °\mathrm{C}) = s_N(N + E) \quad (4)$$

$$\lg K\ (20\ °\mathrm{C}) = LB + LA \quad (5)$$

The rate constant *k* and equilibrium constant *K* can be described with equation (6) and equation (6).

$$k = \frac{\kappa k_\mathrm{B} T}{h} e^{\frac{-\Delta G^{\ddagger}}{\mathrm{RT}}} \quad (6)$$

$$K = e^{-\frac{\Delta G^0}{\mathrm{RT}}} \quad (7)$$

If we transform equation (6) and (7) into common logarithm form, we get equation (8) and equation (9).

$$\lg k = -\frac{\Delta G^{\ddagger}}{2.303\mathrm{RT}} + \lg\frac{\kappa k_\mathrm{B} T}{h} \quad (8)$$

$$\lg K = -\frac{\Delta G^0}{2.303\mathrm{RT}} \quad (9)$$

If we apply equation (8) for the reactions following second order kinetic and combine with equation (4), we get equation (10).

$$\Delta G^{\ddagger} = -2.303\mathrm{RT}s_N(N + E) + 2.303\mathrm{RT}\lg\frac{\kappa k_\mathrm{B} T}{h} \quad (10)$$

[†] Mayr, H.; Ammer, J.; Baidya, M.; Maji, B.; Nigst, T. A.; Ofial, A, R.; Singer, T. *J. Am. Chem. Soc.* **2015**, *137*, 2580–2599.

If we apply equation (9) for the reactions following second order kinetic and combine with equation (5), we get equation (11).

$$\Delta G^0 = -2.303\mathrm{RT}(LB + LA) \quad (11)$$

The Gibbs energy diagram for the reactions of a certain nucleophile Nu with different electrophiles E_1 and E_2 is shown in figure App. 5-1.

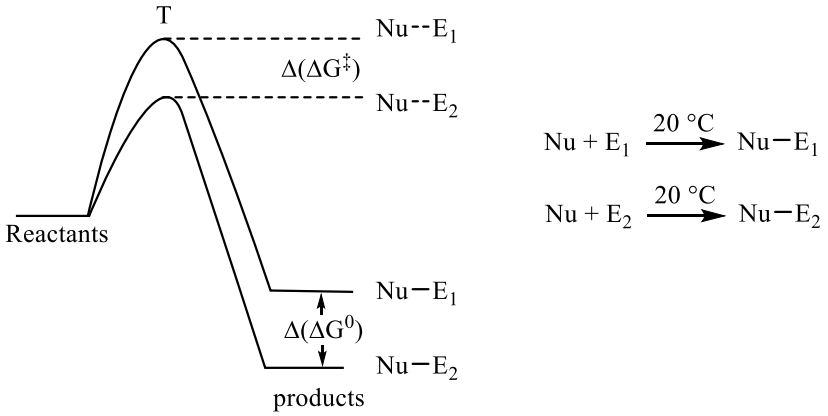

Figure App. 5-1. Gibbs free energy diagram of the comparison for the reactions of one nucleophile Nu_1 with different electrophiles E_1 and E_2

According to equation (10):

$$\Delta(\Delta G^{\ddagger}) = -2.303\mathrm{RT}s_N(E_1 - E_2) \quad (12)$$

According to equation (11):

$$\Delta(\Delta G^0) = -2.303\mathrm{RT}(LA_1 - LA_2) \quad (13)$$

Equation (12) divided by equation (13):

$$\frac{d\Delta G^{\ddagger}}{d\Delta G^0} = s_N \frac{dE}{dLA} \quad (14)$$

Because $\Delta E/\Delta LA$ is constant for the reactions with different nucleophiles, s_N reveals the relative change between the Gibbs energy of activation and Gibbs energy of reaction when a certain nucleophile reacts with different electrophiles. Because the change of Gibbs energy of reaction between any nucleophile with two certain electrophiles keeps constant according to equation (20), s_N indicates also the change of Gibbs energy of activation when a certain nucleophile reacts with different electrophiles.

The correlation between the electrophilicity parameter and the Lewis acidity parameter of benzhydrylium ions **E8** to **E18** is depicted in Figure App. 5-2.

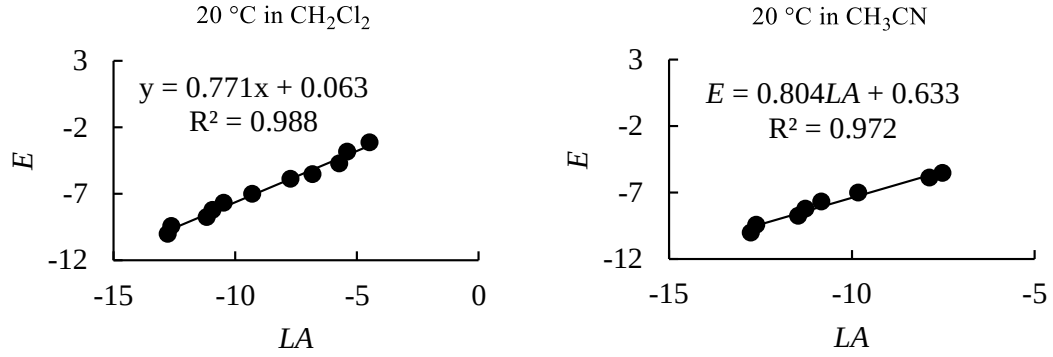

Figure App. 5-2. Correlation between the electrophilicity parameter and the Lewis acidity parameter of benzhydrylium ions **E8** to **E18**

The slope of the correlations of the electrophilicity versus Lewis acidity of benzhydrylium ions in acetonitrile at 20 °C is around 0.8. On average, the change of the Gibbs free energy of activation is about half of the change of the the Gibbs free energy of reaction when sN parameter is about 0.65 and the change of the Gibbs free energy of activation approximately equals the change of the Gibbs free energy of reaction when s_N parameter is 1.2.